

國立交通大學

機械工程學系

碩士論文

數值模擬冷藏垂直開放櫃之氣簾對其動量及熱質傳特



**Effects of Air Curtains on Momentum, Heat and Mass Transfer in an
Open Vertical Refrigerated Display Cabinet- Numerical Simulation**

研究生： 林君達

指導教授： 林清發博士

中華民國九十五年六月

數值模擬冷藏垂直開放櫃之氣簾對其動量及熱質傳特性影響研究

Effects of Air Curtains on Momentum, Heat and Mass Transfer in an Open Vertical Refrigerated Display Cabinet- Numerical Simulation

研究生：林君達

Student : Chun-Ta Lin

指導教授：林清發

Advisor : Tsing-Fa Lin

國立交通大學

機械工程學系



Submitted to Institute of Mechanical Engineering

Collage of Engineering

National Chiao Tung University

In Partial Fulfillment of the Requirements

For the degree of

Master of Science

In

Mechanical Engineering

November 2005

Hsinchu, Taiwan, Republic of China

中華民國九十五年六月

國立交通大學

博碩士論文全文電子檔著作權授權書

(提供授權人裝訂於紙本論文書名頁之次頁用)

本授權書所授權之學位論文，為本人於國立交通大學機械工程系所
熱流組，94學年度第二學期取得碩士學位之論文。

論文題目：數值模擬冷藏垂直開放櫃之氣簾對其動量及熱質傳特性
影響研究
指導教授：林清發

■ 同意

本人茲將本著作，以非專屬、無償授權國立交通大學與台灣聯合大學系統圖書館；基於推動讀者間「資源共享、互惠合作」之理念，與回饋社會與學術研究之目的，國立交通大學及台灣聯合大學系統圖書館得不限地域、時間與次數，以紙本、光碟或數位化等各種方法收錄、重製與利用；於著作權法合理使用範圍內，讀者得進行線上檢索、閱覽、下載或列印。

論文全文上載網路公開之範圍及時間：

本校及台灣聯合大學系統區域 網路	<input checked="" type="checkbox"/> 立即公開
校外網際網路	<input checked="" type="checkbox"/> 中華民國 96 年 6 月 22 日 公開

■ 全文電子檔送交國家圖書館

授權人：林君達

親筆簽名：林君達

中華民國 95 年 6 月 22 日

國立交通大學

博碩士紙本論文著作權授權書

(提供授權人裝訂於全文電子檔授權書之次頁用)

本授權書所授權之學位論文，為本人於國立交通大學機械工程系所
熱流組，94學年度第二學期取得碩士學位之論文。

論文題目：數值模擬冷藏垂直開放櫃之氣簾對其動量及熱質傳特性
影響研究

指導教授：林清發

■ 同意

本人茲將本著作，以非專屬、無償授權國立交通大學，基於推動讀者間「資源共享、互惠合作」之理念，與回饋社會與學術研究之目的，國立交通大學圖書館得以紙本收錄、重製與利用；於著作權法合理使用範圍內，讀者得進行閱覽或列印。

本論文為本人向經濟部智慧局申請專利(未申請者本條款請不予理會)的附件之一，申請文號為：_____，請將論文延至____年____月____日再公開。

授權人：林君達

親筆簽名：林君達

中華民國 95 年 6 月 22 日

國家圖書館 博碩士論文電子檔案上網授權書

(提供授權人裝訂於紙本論文本校授權書之後)

ID:GT009314558

本授權書所授權之論文為授權人在國立交通大學機械工程系所 94 學年度第二學期取得碩士學位之論文。

論文題目：數值模擬冷藏垂直開放櫃之氣簾對其動量及熱質傳特性影響研究

指導教授：林清發

茲同意將授權人擁有著作權之上列論文全文(含摘要)，非專屬、無償授權國家圖書館，不限地域、時間與次數，以微縮、光碟或其他各種數位化方式將上列論文重製，並得將數位化之上列論文及論文電子檔以上載網路方式，提供讀者基於個人非營利性質之線上檢索、閱覽、下載或列印。



※ 讀者基於非營利性質之線上檢索、閱覽、下載或列印上列論文，應依著作權法相關規定辦理。

授權人：林君達

親筆簽名：林君達

民國95年 6月 22日

國立交通大學

論文口試委員會審定書

本校 機械工程 學系碩士班 林君達 君

所提論文(中文) 數值模擬冷藏垂直開放櫃之氣簾對其動量及熱質傳特性影響研究

(英文) Effects of air curtains on momentum, heat and mass transfer in an open vertical refrigerated display cabinet -numerical simulation

合於碩士資格水準、業經本委員會評審認可。

口試委員：

洪英祥

何清波

潘欽

指導教授：

林清波

系主任：

傅武雄

教授

中華民國 95 年 6 月 9 日

誌 謝

時光飛逝，回首在新竹這幾年來的點點滴滴，與當年隻身到交大求學的我相比，在交大這充滿學術氣息的环境下似乎讓我在知識上成長茁壯許多。本論文之所以可以順利完成，首先要感謝的是指導老師 林清發 教授嚴謹及殷切的指導，使學生能培養出獨立思考、釐清並自行解決問題的能力；更在學生撰寫論文時，不辭辛勞逐字斧正文稿，在此獻上最高謝意。在研究所期間，要特別感謝工研院 謝文德 博士與 趙令裕 研究員及 PHOENICS 范乃文 先生在 PHOENICS 軟體上的協助指導，亦要感謝博士班 郭威伸、賴佑民、陳尚緯、謝汎鈞、張文瑞 等博士班學長在生活及課業上指導與建議，使我受益匪淺，謝謝你們。

建安、義祥、宇歆 這群不只是求學中的同學，更是生活上的好朋友。研究所之所以能在緊湊忙碌又充滿歡樂中的氣氛中度過，即是靠這些同學兼好友的夥伴們相互協助幫忙，令我永生難忘。另外也要感謝 奎銘、凱文、峻樟、政陞 等一群努力的學弟妹幫忙及合作，希望你們能繼續保持實驗室優良傳統，並帶著實驗室進步。

最後更要感謝父母及姊姊對於我無怨無悔付出及支持，使我可以無後顧之憂的專注於研究，並且可無憂無慮過求學生活。並特別要感謝女友 佩諭 的陪伴與體恤，生活最精采的部分是妳陪我渡過，不管在課業上或生活上的關心與支持使我有勇氣面對一切的困難挑戰。能與妳相處是我這輩子最大的幸福。

最後，僅以本文獻給我所關心的人和所有關心我的人。

今日我以交大為榮 願他日交大以我為榮

君達 謹致

2006/6/30 于風城交大

數值模擬冷藏垂直開放櫃之氣簾之動量及熱質傳特性研究

研究生：林 君 達

指導老師：林 清 發 博士

國立交通大學 機械工程學系

中文摘要

本篇論文利用二維穩態數值模擬方法探討一之氣簾穿過一垂直開放展示櫃之溫度與溼度濃度特性影響研究；以商用套裝計算流體力學軟體 PHOENICS 對流體的統馭方程式進行求解，論文著重確認由相對溼度對流場的溫溼度濃度影響；針對不同氣簾出口寬度 5.0，7.0，10.0 及 12.0 cm，及氣簾長度 1.20 m 與展示櫃深度 0.57m，及出口流速 0.25 至 3.0 m/s，之冷卻氣簾包含兩種不同渦流結構之穩態開放櫃流場研究。其中氣簾出口與環境溫度分別為 5.0 及 25.0°C，溫度差為 20°C。氣簾出口及環境的相對溼度分別為 90% 與 60%。結果指出在沒有加入溫度差及濃度差的效應下，展示櫃內為單一的 flow recirculation。當加入溫度及濃度的浮力效應時，氣簾將會改變方向，向展示櫃內 bending，且環境的濕暖空氣將滲入展示櫃內。當熱傳與質傳的浮慣比大到一個程度時，氣簾的 bending 將會碰到展示櫃內壁面，形成兩個不同方向旋轉的 flow recirculations。除此之外縮小氣簾出口寬度將會減緩氣簾的 bending。而進一步將氣簾出口環境方向偏移一個角度以及展示櫃內的垂直壁面 perforation 出風，也更有效的減緩氣簾的 bending 現象。

在雙氣簾的設計中，氣簾的 bending 現象及環境的暖濕空氣可藉由內外氣簾分別使用較小及較大的出口寬度。除此之外內外氣簾的相對出口雷諾數再展示

櫃的效應有非單一的影響。並且在外氣簾偏移一個角度後也將有效的改善展示櫃的整體效能。



Effects of Air Curtains on Momentum, Heat and Mass Transfer in an Open Vertical Refrigerated Display Cabinet- Numerical Simulation

Student: Chun-Ta Lin

Advisor: Prof. Tsing-Fa Lin

Department of Mechanical Engineering

National Chiao Tung University

ABSTRACT

A steady two-dimensional numerical simulation is conducted in the present study to investigate the momentum, heat and mass transfer resulting from cold air curtain discharge over the open surface of a vertical open cavity, simulating that in a vertical refrigerated display cabinet. The commercial computational fluid dynamics software PHOENICS [25] is employed to solve the problem. Attention is focused on how the parameters associated with the air curtain affect the characteristics of the flow in the cabinet. Computations are performed for the jet speed at the air discharge grille varying from 0.25 to 3.0 m/s and injection slot width ranging from 0.05 to 0.12 m for the air discharge-to-return grille separation distance fixed at 1.20 m and for the cabinet depth of 0.57 m. The temperature difference between the air discharge and ambient is 20 °C, corresponding to $T_j = 5\text{ °C}$ and $T_{\text{amb}} = 25\text{ °C}$. The relative humidities at the air discharge and ambient are respectively fixed at 90% and 60%. Effects of various parameters on the flow, thermal and solutal characteristics in the cabinet are examined in detail. The results indicate that for the limiting case in the absence of the buoyancy force the cabinet is dominated by a single large flow recirculation. But when the Richardson numbers (buoyancy-to

-inertia ratios) exceed certain levels, the bending of the air curtain toward the cabinet core and the intrusion of the warm moist air from the ambient into the cabinet become significant. At high Ri_t and Ri_m the air curtain bending can be large enough to induce two counter-rotating flow recirculations in the cabinet. Besides, a reduction in the injection slot width is found to result in a milder air curtain bending and warm air intrusion. Similar effects can be obtained by inclining the air curtain at the discharge grille slightly toward the ambient and by injecting the air flow into the cabinet from the back panel perforations.

In a two air-curtain design, the air curtain bending and warm air intrusion can be reduced by a larger inner jet width and a smaller outer jet width at the discharge grille for a fixed total width of the two jets. Besides, the relative magnitudes of the inner and outer jet Reynolds numbers are noted to produce nonmonotonic influence on the performance of the cabinet. Moreover, it is found that inclining the outer air jet toward the ambient with the inner jet still in the vertically downward direction can improve the cabinet performance.

CONTENTS

ABSTRACT	i
CONTENTS	iii
LIST OF FIGURES	v
LIST OF TABLES	xxxiii
NOMENCLATURE	xxxiv
CHAPTER 1	1
INTRODUCTION	1
<i>1.1 Motivation</i>	<i>1</i>
<i>1.2 Literature Review</i>	<i>2</i>
<i>1.3 Objective of Present Study</i>	<i>7</i>
CHAPTER 2	9
MATHEMATICAL FORMULATION	9
<i>2.1 Physical Model</i>	<i>9</i>
<i>2.2 Assumptions and Governing Equations</i>	<i>10</i>
CHAPTER 3	23
SOLUTION METHOD	23
<i>3.1 Numerical Scheme and Solution Procedures</i>	<i>23</i>
<i>3.2 Verification of Numerical Scheme</i>	<i>26</i>
<i>3.2.1 Grid Test</i>	<i>26</i>
<i>3.2.2 Domain Size Test</i>	<i>27</i>
<i>3.2.3 Verification with Published Results</i>	<i>28</i>
CHAPTER 4	47

RESULTS AND DISCUSSION.....	47
<i>4.1 Inertia-Driven Recirculating Flow Patterns for Un-cooled Air Curtain</i>	48
<i>4.2 Buoyancy-Driven Recirculating Flow Patterns for Cold Air Curtain</i>	49
<i>4.3 Effects of Air Curtain Reynolds Number</i>	49
<i>4.4 Effects of Richardson Numbers</i>	50
<i>4.5 Effects of H / b_j Ratio</i>	51
<i>4.6 Effects of the Air Discharge with an Inclined Angle</i>	52
<i>4.7 The Entrainment Factor</i>	52
<i>4.8 Effect of Air Discharge with Double Air Curtain Design</i>	53
<i>4.9 Effect of Back Panel Perforation</i>	56
CHAPTER 5.....	216
CONCLUDING REMARKS	216
REFERENCES.....	218



LIST OF FIGURES

Fig. 1.1	Schematic diagram of a multi-deck open refrigerated display case -----	8
Fig. 2.1	Physical model for a vertical refrigerated display case.-----	21
Fig. 2.2	Schematic diagram illustrating the geometry and some boundary conditions.-----	22
Fig. 3.1	The locations of the centred node P in a typical cell and centred node N in the neighbor cell. -----	29
Fig. 3.2	The upwind differencing with node labeling for flux discretization. -----	30
Fig. 3.3	Flow chart for the simulation procedures. -----	31
Fig. 3.4	The mesh distribution for the entire computational domain. -----	32
Fig. 3.5	The horizontal variations of the steady velocity magnitude at the selected locations on the line $z = 1.7$ m predicted from three different grids for $b_j = 0.1$ m, $V_j = 1.5$ m/s, $\Delta T = 20$ °C and $N = 0$.-----	33
Fig. 3.6	Velocity vector maps at steady state for $b_j = 0.1$ m, $Re_b = 9,548$, $Gr_t = 4.61 \times 10^9$, and $Gr_m = 2.94 \times 10^8$ predicted from the grids with (a) 8,550 cells, (b) 21,315 cells and (c) 16,764 cells. -----	34
Fig. 3.7	Isotherms at steady state for $b_j = 0.1$ m, $Re_b = 9,548$, $Gr_t = 4.61 \times 10^9$, and $Gr_m = 2.94 \times 10^8$ predicted from the grids with (a) 8,550 cells, (b) 21,315 cells and (c) 16,764 cells. -----	35
Fig. 3.8	Iso-concentration lines at steady state for $b_j = 0.1$ m, $Re_b = 9,548$, $Gr_t = 4.61 \times 10^9$, and $Gr_m = 2.94 \times 10^8$ predicted from the grids with (a) 8,550 cells, (b) 21,315 cells and (c) 16,764 cells. -----	36
Fig. 3.9	Conduction heat flux at $x = 0.52$ m at steady state for $b_j = 0.1$ m, $Re_b = 9,548$, $Gr_t = 4.61 \times 10^9$, and $Gr_m = 2.94 \times 10^8$ predicted from the grids with (a) 8,550 cells, (b) 21,315 cells and (c) 16,764 cells.-----	37
Fig. 3.10	Convection heat flux at $x = 0.52$ m at steady state for $b_j = 0.1$ m, $Re_b =$	

9,548, $Gr_t = 4.61 \times 10^9$, and $Gr_m = 2.94 \times 10^8$ predicted from the grids with
 (a) 8,550 cells, (b) 21,315 cells and (c) 16,764 cells.----- 38

Fig. 3.11 Velocity vector maps at steady state for $b_j = 0.1$ m, $Re_b = 9,548$, $Gr_t = 4.61$
 $\times 10^9$, and $Gr_m = 2.94 \times 10^8$ predicted with the domain size of (a) 3×2.5
 m^2 , (b) $6 \times 4.5 m^2$ and (c) $4.61 \times 3.3 m^2$. ----- 39

Fig. 3.12 Isotherms at steady state for $b_j = 0.1$ m, $Re_b = 9,548$, $Gr_t = 4.61 \times 10^9$, and
 $Gr_m = 2.94 \times 10^8$ predicted with the domain size of (a) $3 \times 2.5 m^2$, (b) $6 \times$
 $4.5 m^2$ and (c) $4.61 \times 3.3 m^2$. ----- 40

Fig. 3.13 Iso-concentration lines at steady state for $b_j = 0.1$ m, $Re_b = 9,548$, $Gr_t =$
 4.61×10^9 , and $Gr_m = 2.94 \times 10^8$ predicted with the domain size of (a) $3 \times$
 $2.5 m^2$, (b) $6 \times 4.5 m^2$ and (c) $4.61 \times 3.3 m^2$. ----- 41

Fig. 3.14 Vector velocity maps in the steady cavity flow for the case with $b_j = 0.1$ m,
 $H = 2.0$ m, $Re_b = 18,371$, $Gr_t = 2.7 \times 10^{10}$, $Pr = 0.71$ and $N = 0$ predicted
 from (a) Chen & Yuan (2005) and (b) present study.----- 42

Fig. 3.15 Isotherms in the steady cavity flow for the case with $b_j = 0.1$ m, $H = 2.0$ m,
 $Re_b = 18,371$, $Gr_t = 2.7 \times 10^{10}$, $Pr = 0.71$ and $N = 0$ predicted from (a) Chen
 & Yuan (2005) and (b) present study. ----- 43

Fig. 3.16 Streamlines in the steady square cavity flow for the case with $H = L = 0.02$
 m, $Gr_t = 10^3$, $Gr_m = 1.43 \times 10^3$, $Pr = 0.71$ predicted from (a) Lai (1989) and
 (b) present study. ----- 44

Fig. 3.17 Isotherms in the steady square cavity flow for the case with $H = L = 0.02$ m,
 $Gr_t = 10^3$, $Gr_m = 1.43 \times 10^3$, $Pr = 0.71$ predicted from (a) Lai (1989) and (b)
 present study. ----- 45

Fig. 3.18 Iso-concentration lines in the steady square cavity flow for the case with H
 $= L = 0.02$ m, $Gr_t = 10^3$, $Gr_m = 1.43 \times 10^3$, $Pr = 0.71$ predicted from (a) Lai
 (1989) and (b) present study. ----- 46

Fig. 4.1 Velocity vector maps for steady cavity flow for $b_j = 0.1$ m, $Gr_t = 0$ ($\Delta T = 0$ °C) and $N = 0$ for $Re_b =$ (a) 9,548 ($V_j = 1.5$ m/s), (b) 6,365 ($V_j = 1.0$ m/s), (c) 5,092 ($V_j = 0.8$ m/s), (d) 3,183 ($V_j = 0.5$ m/s) and (e) 1,910 ($V_j = 0.3$ m/s).

----- 59

Fig. 4.2 Velocity vector maps for steady cavity flow for $b_j = 0.07$ m, $Gr_t = 0$ ($\Delta T = 0$ °C), and $N = 0$ for $Re_b =$ (a) 9,548 ($V_j = 2.143$ m/s), (b) 6,365 ($V_j = 1.428$ m/s), (c) 5,092 ($V_j = 1.143$ m/s), (d) 3,183 ($V_j = 0.714$ m/s) and (e) 1,910 ($V_j = 0.428$ m/s).

----- 60

Fig. 4.3 Steady recirculating flow pattern from Chen & Yuan [10] for $H / b_j = 20$, $Gr_t = 2.7 \times 10^{10}$ and $N = 0$ for (a) $Ri_t = 0.2$ and (b) $Ri_t = 0.32$.

----- 61

Fig. 4.4 Velocity vector maps for steady cavity flow for $b_j = 0.1$ m, $Gr_t = 4.61 \times 10^9$ ($\Delta T = 20$ °C), and $N = 6.37 \times 10^{-2}$ for $Re_b =$ (a) 9,548 ($V_j = 1.5$ m/s), (b) 8,275 ($V_j = 1.3$ m/s), (c) 6,365 ($V_j = 1.0$ m/s), (d) 5,092 ($V_j = 0.8$ m/s), (e) 3,183 ($V_j = 0.5$ m/s) and (f) 1,910 ($V_j = 0.3$ m/s).

----- 62

Fig. 4.5 Isotherms in the cavity for steady cavity flow for $b_j = 0.1$ m, $Gr_t = 4.61 \times 10^9$ ($\Delta T = 20$ °C), and $N = 6.37 \times 10^{-2}$ for $Re_b =$ (a) 9,548 ($V_j = 1.5$ m/s), (b) 8,275 ($V_j = 1.3$ m/s), (c) 6,365 ($V_j = 1.0$ m/s), (d) 5,092 ($V_j = 0.8$ m/s), (e) 3,183 ($V_j = 0.5$ m/s) and (f) 1,910 ($V_j = 0.3$ m/s).

----- 63

Fig. 4.6 Iso-concentration lines in the cavity for steady cavity flow for $b_j = 0.1$ m, $Gr_t = 4.61 \times 10^9$ ($\Delta T = 20$ °C), and $N = 6.37 \times 10^{-2}$ for $Re_b =$ (a) 9,548 ($V_j = 1.5$ m/s), (b) 8,275 ($V_j = 1.3$ m/s), (c) 6,365 ($V_j = 1.0$ m/s), (d) 5,092 ($V_j = 0.8$ m/s), (e) 3,183 ($V_j = 0.5$ m/s) and (f) 1,910 ($V_j = 0.3$ m/s).

----- 64

Fig. 4.7 Velocity vector maps for steady cavity flow for $b_j = 0.07$ m, $Gr_t = 4.61 \times 10^9$ ($\Delta T = 20$ °C), and $N = 6.37 \times 10^{-2}$ for $Re_b =$ (a) 9,548 ($V_j = 2.143$ m/s), (b) 8,275 ($V_j = 1.857$ m/s), (c) 6,365 ($V_j = 1.428$ m/s), (d) 5,092 ($V_j = 1.143$ m/s), (e) 3,183 ($V_j = 0.714$ m/s) and (f) 1,910 ($V_j = 0.428$ m/s).

-- 65

Fig. 4.8 Isotherms in the cavity for steady cavity flow for $b = 0.07$ m, $Gr_t = 4.61 \times 10^9$ ($\Delta T = 20^\circ C$), and $N = 6.37 \times 10^{-2}$ for $Re_b =$ (a) 9,548 ($V_j = 2.143$ m/s), (b) 8,275 ($V_j = 1.857$ m/s), (c) 6,365 ($V_j = 1.428$ m/s), (d) 5,092 ($V_j = 1.143$ m/s), (e) 3,183 ($V_j = 0.714$ m/s) and (f) 1,910 ($V_j = 0.428$ m/s).-- 66

Fig. 4.9 Iso-concentration lines in the cavity for steady cavity flow for $b = 0.07$ m, $Gr_t = 4.61 \times 10^9$ ($\Delta T = 20^\circ C$), and $N = 6.37 \times 10^{-2}$ for $Re_b =$ (a) 9,548 ($V_j = 2.143$ m/s), (b) 8,275 ($V_j = 1.857$ m/s), (c) 6,365 ($V_j = 1.428$ m/s), (d) 5,092 ($V_j = 1.143$ m/s), (e) 3,183 ($V_j = 0.714$ m/s) and (f) 1,910 ($V_j = 0.428$ m/s). ----- 67

Fig. 4.10 Velocity vector maps for steady cavity flow for $b_j = 0.05$ m, $Gr_t = 4.61 \times 10^9$ ($\Delta T = 20^\circ C$), and $N = 6.37 \times 10^{-2}$ for $Re_b =$ (a) 9,548 ($V_j = 3$ m/s), (b) 8,275 ($V_j = 2.6$ m/s), (c) 6,365 ($V_j = 2.0$ m/s), (d) 5,092 ($V_j = 1.6$ m/s), (e) 3,183 ($V_j = 1.0$ m/s) and (f) 1,910 ($V_j = 0.6$ m/s).----- 68

Fig. 4.11 Isotherms in the cavity for steady cavity flow for $b_j = 0.05$ m, $Gr_t = 4.61 \times 10^9$ ($\Delta T = 20^\circ C$), and $N = 6.37 \times 10^{-2}$ for $Re_b =$ (a) 9,548 ($V_j = 3$ m/s), (b) 8,275 ($V_j = 2.6$ m/s), (c) 6,365 ($V_j = 2.0$ m/s), (d) 5,092 ($V_j = 1.6$ m/s), (e) 3,183 ($V_j = 1.0$ m/s) and (f) 1,910 ($V_j = 0.6$ m/s).----- 69

Fig. 4.12 Iso-concentration lines in the cavity for steady cavity flow for $b_j = 0.05$ m, $Gr_t = 4.61 \times 10^9$ ($\Delta T = 20^\circ C$), and $N = 6.37 \times 10^{-2}$ for $Re_b =$ (a) 9,548 ($V_j = 3$ m/s), (b) 8,275 ($V_j = 2.6$ m/s), (c) 6,365 ($V_j = 2.0$ m/s), (d) 5,092 ($V_j = 1.6$ m/s), (e) 3,183 ($V_j = 1.0$ m/s) and (f) 1,910 ($V_j = 0.6$ m/s).----- 70

Fig. 4.13 Velocity vector maps for steady cavity flow for $b_j = 0.1$ m, $Gr_t = 4.61 \times 10^9$ ($\Delta T = 20^\circ C$), and $N = 6.37 \times 10^{-2}$ with a jet inclined angle of 5° for $Re_b =$ (a) 9,548 ($V_j = 1.5$ m/s), (b) 8,275 ($V_j = 1.3$ m/s), (c) 6,365 ($V_j = 1.0$ m/s), (d) 5,092 ($V_j = 0.8$ m/s), (e) 3,183 ($V_j = 0.5$ m/s) and (f) 1,910 ($V_j = 0.3$ m/s).----- 71

Fig. 4.14 Isotherms for steady cavity flow for $b_j = 0.1$ m, $Gr_t = 4.61 \times 10^9$ ($\Delta T = 20$ °C), and $N = 6.37 \times 10^{-2}$ with a jet inclined angle of 5° for $Re_b =$ (a) 9,548 ($V_j = 1.5$ m/s), (b) 8,275 ($V_j = 1.3$ m/s), (c) 6,365 ($V_j = 1.0$ m/s), (d) 5,092 ($V_j = 0.8$ m/s), (e) 3,183 ($V_j = 0.5$ m/s) and (f) 1,910 ($V_j = 0.3$ m/s). --- 72

Fig. 4.15 Iso-concentration lines for steady cavity flow for $b_j = 0.1$ m, $Gr_t = 4.61 \times 10^9$ ($\Delta T = 20$ °C), and $N = 6.37 \times 10^{-2}$ with a jet inclined angle of 5° for $Re_b =$ (a) 9,548 ($V_j = 1.5$ m/s), (b) 8,275 ($V_j = 1.3$ m/s), (c) 6,365 ($V_j = 1.0$ m/s), (d) 5,092 ($V_j = 0.8$ m/s), (e) 3,183 ($V_j = 0.5$ m/s) and (f) 1,910 ($V_j = 0.3$ m/s). ----- 73

Fig. 4.16 Velocity vector maps for steady cavity flow for $b_j = 0.1$ m, $Gr_t = 4.61 \times 10^9$ ($\Delta T = 20$ °C), and $N = 6.37 \times 10^{-2}$ with a jet inclined angle of 15° for $Re_b =$ (a) 9,548 ($V_j = 1.5$ m/s), (b) 8,275 ($V_j = 1.3$ m/s), (c) 6,365 ($V_j = 1.0$ m/s), (d) 5,092 ($V_j = 0.8$ m/s), (e) 3,183 ($V_j = 0.5$ m/s) and (f) 1,910 ($V_j = 0.3$ m/s).----- 74

Fig. 4.17 Isotherms for steady cavity flow for $b_j = 0.1$ m, $Gr_t = 4.61 \times 10^9$ ($\Delta T = 20$ °C), and $N = 6.37 \times 10^{-2}$ with a jet inclined angle of 15° for $Re_b =$ (a) 9,548 ($V_j = 1.5$ m/s), (b) 8,275 ($V_j = 1.3$ m/s), (c) 6,365 ($V_j = 1.0$ m/s), (d) 5,092 ($V_j = 0.8$ m/s), (e) 3,183 ($V_j = 0.5$ m/s) and (f) 1,910 ($V_j = 0.3$ m/s). --- 75

Fig. 4.18 Iso-concentration lines for steady cavity flow for $b_j = 0.1$ m, $Gr_t = 4.61 \times 10^9$ ($\Delta T = 20$ °C), and $N = 6.37 \times 10^{-2}$ with a jet inclined angle of 15° for $Re_b =$ (a) 9,548 ($V_j = 1.5$ m/s), (b) 8,275 ($V_j = 1.3$ m/s), (c) 6,365 ($V_j = 1.0$ m/s), (d) 5,092 ($V_j = 0.8$ m/s), (e) 3,183 ($V_j = 0.5$ m/s) and (f) 1,910 ($V_j = 0.3$ m/s). ----- 76

Fig. 4.19 Velocity vector maps for steady cavity flow for $b_j = 0.1$ m, $Gr_t = 4.61 \times 10^9$ ($\Delta T = 20$ °C), and $N = 6.37 \times 10^{-2}$ with a jet inclined angle of 25° for $Re_b =$ (a) 9,548 ($V_j = 1.5$ m/s), (b) 8,275 ($V_j = 1.3$ m/s), (c) 6,365 ($V_j = 1.0$ m/s),

(d) 5,092 ($V_j = 0.8$ m/s), (e) 3,183 ($V_j = 0.5$ m/s) and (f) 1,910 ($V_j = 0.3$ m/s).----- 77

Fig. 4.20 Isotherms for steady cavity flow for $b_j = 0.1$ m, $Gr_t = 4.61 \times 10^9$ ($\Delta T = 20$ °C), and $N = 6.37 \times 10^{-2}$ with a jet inclined angle of 25° for $Re_b =$ (a) 9,548 ($V_j = 1.5$ m/s), (b) 8,275 ($V_j = 1.3$ m/s), (c) 6,365 ($V_j = 1.0$ m/s), (d) 5,092 ($V_j = 0.8$ m/s), (e) 3,183 ($V_j = 0.5$ m/s) and (f) 1,910 ($V_j = 0.3$ m/s). --- 78

Fig. 4.21 Iso-concentration lines for steady cavity flow for $b_j = 0.1$ m, $Gr_t = 4.61 \times 10^9$ ($\Delta T = 20^\circ C$), and $N = 6.37 \times 10^{-2}$ with a jet inclined angle of 25° for $Re_b =$ (a) 9,548 ($V_j = 1.5$ m/s), (b) 8,275 ($V_j = 1.3$ m/s), (c) 6,365 ($V_j = 1.0$ m/s), (d) 5,092 ($V_j = 0.8$ m/s), (e) 3,183 ($V_j = 0.5$ m/s) and (f) 1,910 ($V_j = 0.3$ m/s). ----- 79

Fig. 4.22 Velocity vector maps for steady cavity flow for $b_j = 0.07$ m, $Gr_t = 4.61 \times 10^9$ ($\Delta T = 20^\circ C$), and $N = 6.37 \times 10^{-2}$ with a jet inclined angle of 5° for $Re_b =$ (a) 9,548 ($V_j = 2.143$ m/s), (b) 8,275 ($V_j = 1.857$ m/s), (c) 6,365 ($V_j = 1.428$ m/s), (d) 5,092 ($V_j = 1.143$ m/s), (e) 3,183 ($V_j = 0.714$ m/s) and (f) 1,910 ($V_j = 0.428$ m/s). ----- 80

Fig. 4.23 Isotherms for steady cavity flow for $b_j = 0.07$ m, $Gr_t = 4.61 \times 10^9$ ($\Delta T = 20$ °C), and $N = 6.37 \times 10^{-2}$ with a jet inclined angle of 5° for $Re_b =$ (a) 9,548 ($V_j = 2.143$ m/s), (b) 6,365 ($V_j = 1.428$ m/s), (c) 5,092 ($V_j = 1.143$ m/s), (d) 3,183 ($V_j = 0.714$ m/s) and (e) 1,910 ($V_j = 0.428$ m/s). ----- 81

Fig. 4.24 Iso-concentration lines for steady cavity flow for $b_j = 0.07$ m, $Gr_t = 4.61 \times 10^9$ ($\Delta T = 20^\circ C$), and $N = 6.37 \times 10^{-2}$ with a jet inclined angle of 5° for $Re_b =$ (a) 9,548 ($V_j = 2.143$ m/s), (b) 6,365 ($V_j = 1.428$ m/s), (c) 5,092 ($V_j = 1.143$ m/s), (d) 3,183 ($V_j = 0.714$ m/s) and (e) 1,910 ($V_j = 0.428$ m/s)-- 82

Fig. 4.25 Velocity vector maps for steady cavity flow for $b_j = 0.07$ m, $Gr_t = 4.61 \times 10^9$ ($\Delta T = 20^\circ C$), and $N = 6.37 \times 10^{-2}$ with a jet inclined angle of 15° for Re_b

= (a) 9,548 ($V_j = 2.142$ m/s), (b) 8,275 ($V_j = 1.857$ m/s), (c) 6,365 ($V_j = 1.428$ m/s), (d) 5,092 ($V_j = 1.142$ m/s), (e) 3,183 ($V_j = 0.714$ m/s) and (f) 1,910 ($V_j = 0.428$ m/s). ----- 83

Fig. 4.26 Isotherms for steady cavity flow for $b_j = 0.07$ m, $Gr_t = 4.61 \times 10^9$ ($\Delta T = 20$ °C), and $N = 6.37 \times 10^{-2}$ with a jet inclined angle of 15° for $Re_b =$ (a) 9,548 ($V_j = 2.142$ m/s), (b) 8,275 ($V_j = 1.857$ m/s), (c) 6,365 ($V_j = 1.428$ m/s), (d) 5,092 ($V_j = 1.142$ m/s), (e) 3,183 ($V_j = 0.714$ m/s) and (f) 1,910 ($V_j = 0.428$ m/s). ----- 84

Fig. 4.27 Iso-concentration lines for steady cavity flow for $b_j = 0.07$ m, $Gr_t = 4.61 \times 10^9$ ($\Delta T = 20^\circ C$), and $N = 6.37 \times 10^{-2}$ with a jet inclined angle of 15° for $Re_b =$ (a) 9,548 ($V_j = 2.142$ m/s), (b) 8,275 ($V_j = 1.857$ m/s), (c) 6,365 ($V_j = 1.428$ m/s), (d) 5,092 ($V_j = 1.142$ m/s), (e) 3,183 ($V_j = 0.714$ m/s) and (f) 1,910 ($V_j = 0.428$ m/s). ----- 85

Fig. 4.28 Velocity vector maps for steady cavity flow for $b_j = 0.07$ m, $Gr_t = 4.61 \times 10^9$ ($\Delta T = 20^\circ C$), and $N = 6.37 \times 10^{-2}$ with a jet inclined angle of 25° for $Re_b =$ (a) 9,548 ($V_j = 2.142$ m/s), (b) 8,275 ($V_j = 1.857$ m/s), (c) 6,365 ($V_j = 1.428$ m/s), (d) 5,092 ($V_j = 1.142$ m/s), (e) 3,183 ($V_j = 0.714$ m/s) and (f) 1,910 ($V_j = 0.428$ m/s). ----- 86

Fig. 4.29 Isotherms for steady cavity flow for $b_j = 0.07$ m, $Gr_t = 4.61 \times 10^9$ ($\Delta T = 20$ °C), and $N = 6.37 \times 10^{-2}$ with a jet inclined angle of 25° for $Re_b =$ (a) 9,548 ($V_j = 2.142$ m/s), (b) 8,275 ($V_j = 1.857$ m/s), (c) 6,365 ($V_j = 1.428$ m/s), (d) 5,092 ($V_j = 1.142$ m/s), (e) 3,183 ($V_j = 0.714$ m/s) and (f) 1,910 ($V_j = 0.428$ m/s). ----- 87

Fig. 4.30 Iso-concentration lines for steady cavity flow for $b_j = 0.07$ m, $Gr_t = 4.61 \times 10^9$ ($\Delta T = 20^\circ C$), and $N = 6.37 \times 10^{-2}$ with a jet inclined angle of 25° for $Re_b =$ (a) 9,548 ($V_j = 2.142$ m/s), (b) 8,275 ($V_j = 1.857$ m/s), (c) 6,365 ($V_j = 1.428$ m/s), (d) 5,092 ($V_j = 1.142$ m/s), (e) 3,183 ($V_j = 0.714$ m/s) and (f) 1,910 ($V_j = 0.428$ m/s). ----- 88

= 1.428 m/s), (d) 5,092 ($V_j = 1.142$ m/s), (e) 3,183 ($V_j = 0.714$ m/s) and (f) 1,910 ($V_j = 0.428$ m/s). ----- 88

Fig. 4.31 Velocity vector maps for steady cavity flow for $b_j = 0.05$ m, $Gr_t = 4.61 \times 10^9$ ($\Delta T = 20^\circ C$), and $N = 6.37 \times 10^{-2}$ with a jet inclined angle of 5° for $Re_b =$ (a) 9,548 ($V_j = 3$ m/s), (b) 8,275 ($V_j = 2.6$ m/s), (c) 6,365 ($V_j = 2.0$ m/s), (d) 5,092 ($V_j = 1.6$ m/s), (e) 3,183 ($V_j = 1.0$ m/s) and (f) 1,910 ($V_j = 0.6$ m/s).----- 89

Fig. 4.32 Isotherms for steady cavity flow for $b_j = 0.05$ m, $Gr_t = 4.61 \times 10^9$ ($\Delta T = 20^\circ C$), and $N = 6.37 \times 10^{-2}$ with a jet inclined angle of 5° for $Re_b =$ (a) 9,548 ($V_j = 3$ m/s), (b) 8,275 ($V_j = 2.6$ m/s), (c) 6,365 ($V_j = 2.0$ m/s), (d) 5,092 ($V_j = 1.6$ m/s), (e) 3,183 ($V_j = 1.0$ m/s) and (f) 1,910 ($V_j = 0.6$ m/s). --- 90

Fig. 4.33 Iso-concentration lines for steady cavity flow for $b_j = 0.05$ m, $Gr_t = 4.61 \times 10^9$ ($\Delta T = 20^\circ C$), and $N = 6.37 \times 10^{-2}$ with a jet inclined angle of 5° for $Re_b =$ (a) 9,548 ($V_j = 3$ m/s), (b) 8,275 ($V_j = 2.6$ m/s), (c) 6,365 ($V_j = 2.0$ m/s), (d) 5,092 ($V_j = 1.6$ m/s), (e) 3,183 ($V_j = 1.0$ m/s) and (f) 1,910 ($V_j = 0.6$ m/s).----- 91

Fig. 4.34 Velocity vector maps for steady cavity flow for $b_j = 0.05$ m, $Gr_t = 4.61 \times 10^9$ ($\Delta T = 20^\circ C$), and $N = 6.37 \times 10^{-2}$ with a jet inclined angle of 15° for $Re_b =$ (a) 9,548 ($V_j = 3$ m/s), (b) 8,275 ($V_j = 2.6$ m/s), (c) 6,365 ($V_j = 2.0$ m/s), (d) 5,092 ($V_j = 1.6$ m/s), (e) 3,183 ($V_j = 1.0$ m/s) and (f) 1,910 ($V_j = 0.6$ m/s).----- 92

Fig. 4.35 Isotherms for steady cavity flow for $b_j = 0.05$ m, $Gr_t = 4.61 \times 10^9$ ($\Delta T = 20^\circ C$), and $N = 6.37 \times 10^{-2}$ with a jet inclined angle of 15° for $Re_b =$ (a) 9,548 ($V_j = 3$ m/s), (b) 8,275 ($V_j = 2.6$ m/s), (c) 6,365 ($V_j = 2.0$ m/s), (d) 5,092 ($V_j = 1.6$ m/s), (e) 3,183 ($V_j = 1.0$ m/s) and (f) 1,910 ($V_j = 0.6$ m/s). --- 93

Fig. 4.36 Iso-concentration lines for steady cavity flow for $b_j = 0.05$ m, $Gr_t = 4.61 \times$

10^9 ($\Delta T = 20^\circ\text{C}$), and $N = 6.37 \times 10^{-2}$ with a jet inclined angle of 15° for $Re_b =$ (a) 9,548 ($V_j = 3$ m/s), (b) 8,275 ($V_j = 2.6$ m/s), (c) 6,365 ($V_j = 2.0$ m/s), (d) 5,092 ($V_j = 1.6$ m/s), (e) 3,183 ($V_j = 1.0$ m/s) and (f) 1,910 ($V_j = 0.6$ m/s). ----- 94

Fig. 4.37 Velocity vector maps for steady cavity flow for $b_j = 0.05$ m, $Gr_t = 4.61 \times 10^9$ ($\Delta T = 20^\circ\text{C}$), and $N = 6.37 \times 10^{-2}$ with a jet inclined angle of 25° for $Re_b =$ (a) 9,548 ($V_j = 3$ m/s), (b) 8,275 ($V_j = 2.6$ m/s), (c) 6,365 ($V_j = 2.0$ m/s), (d) 5,092 ($V_j = 1.6$ m/s), (e) 3,183 ($V_j = 1.0$ m/s) and (f) 1,910 ($V_j = 0.6$ m/s).----- 95

Fig. 4.38 Isotherms for steady cavity flow for $b_j = 0.05$ m, $Gr_t = 4.61 \times 10^9$ ($\Delta T = 20^\circ\text{C}$), and $N = 6.37 \times 10^{-2}$ with a jet inclined angle of 25° for $Re_b =$ (a) 9,548 ($V_j = 3$ m/s), (b) 8,275 ($V_j = 2.6$ m/s), (c) 6,365 ($V_j = 2.0$ m/s), (d) 5,092 ($V_j = 1.6$ m/s), (e) 3,183 ($V_j = 1.0$ m/s) and (f) 1,910 ($V_j = 0.6$ m/s). --- 96

Fig. 4.39 Iso-concentration lines for steady cavity flow for $b_j = 0.05$ m, $Gr_t = 4.61 \times 10^9$ ($\Delta T = 20^\circ\text{C}$), and $N = 6.37 \times 10^{-2}$ with a jet inclined angle of 25° for $Re_b =$ (a) 9,548 ($V_j = 3$ m/s), (b) 8,275 ($V_j = 2.6$ m/s), (c) 6,365 ($V_j = 2.0$ m/s), (d) 5,092 ($V_j = 1.6$ m/s), (e) 3,183 ($V_j = 1.0$ m/s) and (f) 1,910 ($V_j = 0.6$ m/s). ----- 97

Fig. 4.40 Velocity vector maps for steady cavity flow for a double air curtain design with $b_i = 0.03$ m, $b_o = 0.07$ m, $Gr_t = 4.61 \times 10^9$ ($\Delta T = 20^\circ\text{C}$), and $N = 6.37 \times 10^{-2}$ for $Re_{ci} = 1,910$ and $Re_{co} =$ (a) 1,910, (b) 3,183, (c) 5,092, (d) 6,365 and (e) 7,638. ----- 98

Fig. 4.41 Isotherms for steady cavity flow for a double air curtain design with $b_i = 0.03$ m, $b_o = 0.07$ m, $Gr_t = 4.61 \times 10^9$ ($\Delta T = 20^\circ\text{C}$), and $N = 6.37 \times 10^{-2}$ for $Re_{ci} = 1,910$ and $Re_{co} =$ (a) 1,910, (b) 3,183, (c) 5,092, (d) 6,365 and (e) 7,638. ----- 99

Fig. 4.42 Iso-concentration lines for steady cavity flow for a double air curtain design with $b_i = 0.03$ m, $b_o = 0.07$ m, $Gr_t = 4.61 \times 10^9$ ($\Delta T = 20^\circ\text{C}$), and $N = 6.37 \times 10^{-2}$ for $Re_{ci} = 1,910$ and $Re_{co} =$ (a) 1,910, (b) 3,183, (c) 5,092, (d) 6,365 and (e) 7,638. -----100

Fig. 4.43 Velocity vector maps for steady cavity flow for a double air curtain design with $b_i = 0.03$ m, $b_o = 0.07$ m, $Gr_t = 4.61 \times 10^9$ ($\Delta T = 20^\circ\text{C}$), and $N = 6.37 \times 10^{-2}$ for $Re_{ci} = 3,183$ and $Re_{co} =$ (a) 1,910, (b) 3,183, (c) 5,092, and (d) 6,365. -----101

Fig. 4.44 Isotherms for steady cavity flow for a double air curtain design with $b_i = 0.03$ m, $b_o = 0.07$ m, $Gr_t = 4.61 \times 10^9$ ($\Delta T = 20^\circ\text{C}$), and $N = 6.37 \times 10^{-2}$ for $Re_{ci} = 3,183$ and $Re_{co} =$ (a) 1,910, (b) 3,183, (c) 5,092, and (d) 6,365. --102

Fig. 4.45 Iso-concentration lines for steady cavity flow for a double air curtain design with $b_i = 0.03$ m, $b_o = 0.07$ m, $Gr_t = 4.61 \times 10^9$ ($\Delta T = 20^\circ\text{C}$), and $N = 6.37 \times 10^{-2}$ for $Re_{ci} = 3,183$ and $Re_{co} =$ (a) 1,910, (b) 3,183, (c) 5,092, and (d) 6,365. -----103

Fig. 4.46 Velocity vector maps for steady cavity flow for a double air curtain design with $b_i = 0.03$ m, $b_o = 0.07$ m, $Gr_t = 4.61 \times 10^9$ ($\Delta T = 20^\circ\text{C}$), and $N = 6.37 \times 10^{-2}$ for (a) $Re_{ci} = 1,910$ and $Re_{co} = 7,638$, (b) $Re_{ci} = 3,183$ and $Re_{co} = 6,365$, (c) $Re_{ci} = 5,092$ and $Re_{co} = 4,456$, (d) $Re_{ci} = 6,365$ and $Re_{co} = 3,183$, (e) $Re_{ci} = 7,638$ and $Re_{co} = 1,910$. -----104

Fig. 4.47 Isotherms for steady cavity flow for a double air curtain design with $b_i = 0.03$ m, $b_o = 0.07$ m, $Gr_t = 4.61 \times 10^9$ ($\Delta T = 20^\circ\text{C}$), and $N = 6.37 \times 10^{-2}$ for (a) $Re_{ci} = 1,910$ and $Re_{co} = 7,638$, (b) $Re_{ci} = 3,183$ and $Re_{co} = 6,365$, (c) $Re_{ci} = 5,092$ and $Re_{co} = 4,456$, (d) $Re_{ci} = 6,365$ and $Re_{co} = 3,183$, (e) $Re_{ci} = 7,638$ and $Re_{co} = 1,910$. -----105

Fig. 4.48 Iso-concentration lines for steady cavity flow for a double air curtain

design with $b_i = 0.03$ m, $b_o = 0.07$ m, $Gr_t = 4.61 \times 10^9$ ($\Delta T = 20^\circ\text{C}$), and $N = 6.37 \times 10^{-2}$ for (a) $Re_{ci} = 1,910$ and $Re_{co} = 7,638$, (b) $Re_{ci} = 3,183$ and $Re_{co} = 6,365$, (c) $Re_{ci} = 5,092$ and $Re_{co} = 4,456$, (d) $Re_{ci} = 6,365$ and $Re_{co} = 3,183$, (e) $Re_{ci} = 7,638$ and $Re_{co} = 1,910$. -----106

Fig. 4.49 Velocity vector maps for steady cavity flow for a double air curtain design with $b_i = 0.05$ m, $b_o = 0.05$ m, $Gr_t = 4.61 \times 10^9$ ($\Delta T = 20^\circ\text{C}$), and $N = 6.37 \times 10^{-2}$ for $Re_{ci} = 1,910$ and $Re_{co} =$ (a) 1,910, (b) 3,183, (c) 5,092, (d) 6,365 and (e) 7,638. -----107

Fig. 4.50 Isotherms for steady cavity flow for a double air curtain design with $b_i = 0.05$ m, $b_o = 0.05$ m, $Gr_t = 4.61 \times 10^9$ ($\Delta T = 20^\circ\text{C}$), and $N = 6.37 \times 10^{-2}$ for $Re_{ci} = 1,910$ and $Re_{co} =$ (a) 1,910, (b) 3,183, (c) 5,092, (d) 6,365 and (e) 7,638. -----108

Fig. 4.51 Iso-concentration lines for steady cavity flow for a double air curtain design with $b_i = 0.05$ m, $b_o = 0.05$ m, $Gr_t = 4.61 \times 10^9$ ($\Delta T = 20^\circ\text{C}$), and $N = 6.37 \times 10^{-2}$ for $Re_{ci} = 1,910$ and $Re_{co} =$ (a) 1,910, (b) 3,183, (c) 5,092, (d) 6,365 and (e) 7,638. -----109

Fig. 4.52 Velocity vector maps for steady cavity flow for a double air curtain design with $b_i = 0.05$ m, $b_o = 0.05$ m, $Gr_t = 4.61 \times 10^9$ ($\Delta T = 20^\circ\text{C}$), and $N = 6.37 \times 10^{-2}$ for $Re_{ci} = 3,183$ and $Re_{co} =$ (a) 1,910, (b) 3,183, (c) 5,092, and (d) 6,365. -----110

Fig. 4.53 Isotherms for steady cavity flow for a double air curtain design with $b_i = 0.05$ m, $b_o = 0.05$ m, $Gr_t = 4.61 \times 10^9$ ($\Delta T = 20^\circ\text{C}$), and $N = 6.37 \times 10^{-2}$ for $Re_{ci} = 3,183$ and $Re_{co} =$ (a) 1,910, (b) 3,183, (c) 5,092, and (d) 6,365. --111

Fig. 4.54 Iso-concentration lines for steady cavity flow for a double air curtain design with $b_i = 0.05$ m, $b_o = 0.05$ m, $Gr_t = 4.61 \times 10^9$ ($\Delta T = 20^\circ\text{C}$), and $N = 6.37 \times 10^{-2}$ for $Re_{ci} = 3,183$ and $Re_{co} =$ (a) 1,910, (b) 3,183, (c) 5,092, and

(d) 6,365. ----- 112

Fig. 4.55 Velocity vector maps for steady cavity flow for a double air curtain design with $b_i = 0.05$ m, $b_o = 0.05$ m, $Gr_t = 4.61 \times 10^9$ ($\Delta T = 20^\circ\text{C}$), and $N = 6.37 \times 10^{-2}$ for (a) $Re_{ci} = 1,910$ and $Re_{co} = 7,638$, (b) $Re_{ci} = 3,183$ and $Re_{co} = 6,365$, (c) $Re_{ci} = 5,092$ and $Re_{co} = 4,456$, (d) $Re_{ci} = 6,365$ and $Re_{co} = 3,183$, (e) $Re_{ci} = 7,638$ and $Re_{co} = 1,910$. ----- 113

Fig. 4.56 Isotherms for steady cavity flow for a double air curtain design with $b_i = 0.05$ m, $b_o = 0.05$ m, $Gr_t = 4.61 \times 10^9$ ($\Delta T = 20^\circ\text{C}$), and $N = 6.37 \times 10^{-2}$ for (a) $Re_{ci} = 1,910$ and $Re_{co} = 7,638$, (b) $Re_{ci} = 3,183$ and $Re_{co} = 6,365$, (c) $Re_{ci} = 5,092$ and $Re_{co} = 4,456$, (d) $Re_{ci} = 6,365$ and $Re_{co} = 3,183$, (e) $Re_{ci} = 7,638$ and $Re_{co} = 1,910$. ----- 114

Fig. 4.57 Iso-concentration lines for steady cavity flow for a double air curtain design with $b_i = 0.05$ m, $b_o = 0.05$ m, $Gr_t = 4.61 \times 10^9$ ($\Delta T = 20^\circ\text{C}$), and $N = 6.37 \times 10^{-2}$ for (a) $Re_{ci} = 1,910$ and $Re_{co} = 7,638$, (b) $Re_{ci} = 3,183$ and $Re_{co} = 6,365$, (c) $Re_{ci} = 5,092$ and $Re_{co} = 4,456$, (d) $Re_{ci} = 6,365$ and $Re_{co} = 3,183$, (e) $Re_{ci} = 7,638$ and $Re_{co} = 1,910$. ----- 115

Fig. 4.58 Velocity vector maps for steady cavity flow for a double air curtain design with $b_i = 0.07$ m, $b_o = 0.03$ m, $Gr_t = 4.61 \times 10^9$ ($\Delta T = 20^\circ\text{C}$), and $N = 6.37 \times 10^{-2}$ for $Re_{ci} = 1,910$ and $Re_{co} =$ (a) 1,910, (b) 3,183, (c) 5,092, (d) 6,365 and (e) 7,638. ----- 116

Fig. 4.59 Isotherms for steady cavity flow for a double air curtain design with $b_i = 0.07$ m, $b_o = 0.03$ m, $Gr_t = 4.61 \times 10^9$ ($\Delta T = 20^\circ\text{C}$), and $N = 6.37 \times 10^{-2}$ for $Re_{ci} = 1,910$ and $Re_{co} =$ (a) 1,910, (b) 3,183, (c) 5,092, (d) 6,365 and (e) 7,638. ----- 117

Fig. 4.60 Iso-concentration lines for steady cavity flow for a double air curtain design with $b_i = 0.07$ m, $b_o = 0.03$ m, $Gr_t = 4.61 \times 10^9$ ($\Delta T = 20^\circ\text{C}$), and N

= 6.37×10^{-2} for $Re_{ci} = 1,910$ and $Re_{co} =$ (a) 1,910, (b) 3,183, (c) 5,092, (d) 6,365 and (e) 7,638. ----- 118

Fig. 4.61 Velocity vector maps for steady cavity flow for a double air curtain design with $b_i = 0.07$ m, $b_o = 0.03$ m, $Gr_t = 4.61 \times 10^9$ ($\Delta T = 20^\circ C$), and $N = 6.37 \times 10^{-2}$ for $Re_{ci} = 3,183$ and $Re_{co} =$ (a) 1,910, (b) 3,183, (c) 5,092, and (d) 6,365. ----- 119

Fig. 4.62 Isotherms for steady cavity flow for a double air curtain design with $b_i = 0.07$ m, $b_o = 0.03$ m, $Gr_t = 4.61 \times 10^9$ ($\Delta T = 20^\circ C$), and $N = 6.37 \times 10^{-2}$ for $Re_{ci} = 3,183$ and $Re_{co} =$ (a) 1,910, (b) 3,183, (c) 5,092, and (d) 6,365. --120

Fig. 4.63 Iso-concentration lines for steady cavity flow for a double air curtain design with $b_i = 0.07$ m, $b_o = 0.03$ m, $Gr_t = 4.61 \times 10^9$ ($\Delta T = 20^\circ C$), and $N = 6.37 \times 10^{-2}$ for $Re_{ci} = 3,183$ and $Re_{co} =$ (a) 1,910, (b) 3,183, (c) 5,092, and (d) 6,365. -----121

Fig. 4.64 Velocity vector maps for steady cavity flow for a double air curtain design with $b_i = 0.07$ m, $b_o = 0.03$ m, $Gr_t = 4.61 \times 10^9$ ($\Delta T = 20^\circ C$), and $N = 6.37 \times 10^{-2}$ for (a) $Re_{ci} = 1,910$ and $Re_{co} = 7,638$, (b) $Re_{ci} = 3,183$ and $Re_{co} = 6,365$, (c) $Re_{ci} = 5,092$ and $Re_{co} = 4,456$, (d) $Re_{ci} = 6,365$ and $Re_{co} = 3,183$, (e) $Re_{ci} = 7,638$ and $Re_{co} = 1,910$. -----122

Fig. 4.65 Isotherms for steady cavity flow for a double air curtain design with $b_i = 0.07$ m, $b_o = 0.03$ m, $Gr_t = 4.61 \times 10^9$ ($\Delta T = 20^\circ C$), and $N = 6.37 \times 10^{-2}$ for (a) $Re_{ci} = 1,910$ and $Re_{co} = 7,638$, (b) $Re_{ci} = 3,183$ and $Re_{co} = 6,365$, (c) $Re_{ci} = 5,092$ and $Re_{co} = 4,456$, (d) $Re_{ci} = 6,365$ and $Re_{co} = 3,183$, (e) $Re_{ci} = 7,638$ and $Re_{co} = 1,910$. -----123

Fig. 4.66 Iso-concentration lines for steady cavity flow for a double air curtain design with $b_i = 0.07$ m, $b_o = 0.03$ m, $Gr_t = 4.61 \times 10^9$ ($\Delta T = 20^\circ C$), and $N = 6.37 \times 10^{-2}$ for (a) $Re_{ci} = 1,910$ and $Re_{co} = 7,638$, (b) $Re_{ci} = 3,183$ and

$Re_{co} = 6,365$, (c) $Re_{ci} = 5,092$ and $Re_{co} = 4,456$, (d) $Re_{ci} = 6,365$ and $Re_{co} = 3,183$, (e) $Re_{ci} = 7,638$ and $Re_{co} = 1,910$. -----124

Fig. 4.67 Velocity vector maps for steady cavity flow for a double air curtain design with $b_i = 0.03$ m, $b_o = 0.09$ m, $Gr_t = 4.61 \times 10^9$ ($\Delta T = 20^\circ C$), and $N = 6.37 \times 10^{-2}$ for $Re_{ci} = 1,910$ and $Re_{co} =$ (a) 1,910, (b) 3,183, (c) 5,092, (d) 6,365 and (e) 7,638. -----125

Fig. 4.68 Isotherms for steady cavity flow for a double air curtain design with $b_i = 0.03$ m, $b_o = 0.09$ m, $Gr_t = 4.61 \times 10^9$ ($\Delta T = 20^\circ C$), and $N = 6.37 \times 10^{-2}$ for $Re_{ci} = 1,910$ and $Re_{co} =$ (a) 1,910, (b) 3,183, (c) 5,092, (d) 6,365 and (e) 7,638. -----126

Fig. 4.69 Iso-concentration lines for steady cavity flow for a double air curtain design with $b_i = 0.03$ m, $b_o = 0.09$ m, $Gr_t = 4.61 \times 10^9$ ($\Delta T = 20^\circ C$), and $N = 6.37 \times 10^{-2}$ for $Re_{ci} = 1,910$ and $Re_{co} =$ (a) 1,910, (b) 3,183, (c) 5,092, (d) 6,365 and (e) 7,638. -----127

Fig. 4.70 Velocity vector maps for steady cavity flow for a double air curtain design with $b_i = 0.03$ m, $b_o = 0.09$ m, $Gr_t = 4.61 \times 10^9$ ($\Delta T = 20^\circ C$), and $N = 6.37 \times 10^{-2}$ for $Re_{ci} = 3,183$ and $Re_{co} =$ (a) 1,910, (b) 3,183, (c) 5,092, and (d) 6,365. -----128

Fig. 4.71 Isotherms for steady cavity flow for a double air curtain design with $b_i = 0.03$ m, $b_o = 0.09$ m, $Gr_t = 4.61 \times 10^9$ ($\Delta T = 20^\circ C$), and $N = 6.37 \times 10^{-2}$ for $Re_{ci} = 3,183$ and $Re_{co} =$ (a) 1,910, (b) 3,183, (c) 5,092, and (d) 6,365. --129

Fig. 4.72 Iso-concentration lines for steady cavity flow for a double air curtain design with $b_i = 0.03$ m, $b_o = 0.09$ m, $Gr_t = 4.61 \times 10^9$ ($\Delta T = 20^\circ C$), and $N = 6.37 \times 10^{-2}$ for $Re_{ci} = 3,183$ and $Re_{co} =$ (a) 1,910, (b) 3,183, (c) 5,092, and (d) 6,365. -----130

Fig. 4.73 Velocity vector maps for steady cavity flow for a double air curtain design

with $b_i = 0.03$ m, $b_o = 0.09$ m, $Gr_t = 4.61 \times 10^9$ ($\Delta T = 20^\circ\text{C}$), and $N = 6.37 \times 10^{-2}$ for (a) $Re_{ci} = 1,910$ and $Re_{co} = 7,638$, (b) $Re_{ci} = 3,183$ and $Re_{co} = 6,365$, (c) $Re_{ci} = 5,092$ and $Re_{co} = 4,456$, (d) $Re_{ci} = 6,365$ and $Re_{co} = 3,183$, (e) $Re_{ci} = 7,638$ and $Re_{co} = 1,910$. -----131

Fig. 4.74 Isotherms for steady cavity flow for a double air curtain design with $b_i = 0.03$ m, $b_o = 0.09$ m, $Gr_t = 4.61 \times 10^9$ ($\Delta T = 20^\circ\text{C}$), and $N = 6.37 \times 10^{-2}$ for (a) $Re_{ci} = 1,910$ and $Re_{co} = 7,638$, (b) $Re_{ci} = 3,183$ and $Re_{co} = 6,365$, (c) $Re_{ci} = 5,092$ and $Re_{co} = 4,456$, (d) $Re_{ci} = 6,365$ and $Re_{co} = 3,183$, (e) $Re_{ci} = 7,638$ and $Re_{co} = 1,910$. -----132

Fig. 4.75 Iso-concentration lines for steady cavity flow for a double air curtain design with $b_i = 0.03$ m, $b_o = 0.09$ m, $Gr_t = 4.61 \times 10^9$ ($\Delta T = 20^\circ\text{C}$), and $N = 6.37 \times 10^{-2}$ for (a) $Re_{ci} = 1,910$ and $Re_{co} = 7,638$, (b) $Re_{ci} = 3,183$ and $Re_{co} = 6,365$, (c) $Re_{ci} = 5,092$ and $Re_{co} = 4,456$, (d) $Re_{ci} = 6,365$ and $Re_{co} = 3,183$, (e) $Re_{ci} = 7,638$ and $Re_{co} = 1,910$. -----133

Fig. 4.76 Velocity vector maps for steady cavity flow for a double air curtain design with $b_i = 0.09$ m, $b_o = 0.03$ m, $Gr_t = 4.61 \times 10^9$ ($\Delta T = 20^\circ\text{C}$), and $N = 6.37 \times 10^{-2}$ for $Re_{ci} = 1,910$ and $Re_{co} =$ (a) 1,910, (b) 3,183, (c) 5,092, (d) 6,365 and (e) 7,638. -----134

Fig. 4.77 Isotherms for steady cavity flow for a double air curtain design with $b_i = 0.09$ m, $b_o = 0.03$ m, $Gr_t = 4.61 \times 10^9$ ($\Delta T = 20^\circ\text{C}$), and $N = 6.37 \times 10^{-2}$ for $Re_{ci} = 1,910$ and $Re_{co} =$ (a) 1,910, (b) 3,183, (c) 5,092, (d) 6,365 and (e) 7,638. -----135

Fig. 4.78 Iso-concentration lines for steady cavity flow for a double air curtain design with $b_i = 0.09$ m, $b_o = 0.03$ m, $Gr_t = 4.61 \times 10^9$ ($\Delta T = 20^\circ\text{C}$), and $N = 6.37 \times 10^{-2}$ for $Re_{ci} = 1,910$ and $Re_{co} =$ (a) 1,910, (b) 3,183, (c) 5,092, (d) 6,365 and (e) 7,638. -----136

Fig. 4.79 Velocity vector maps for steady cavity flow for a double air curtain design with $b_i = 0.09$ m, $b_o = 0.03$ m, $Gr_t = 4.61 \times 10^9$ ($\Delta T = 20^\circ\text{C}$), and $N = 6.37 \times 10^{-2}$ for $Re_{ci} = 3,183$ and $Re_{co} =$ (a) 1,910, (b) 3,183, (c) 5,092, and (d) 6,365. -----137

Fig. 4.80 Isotherms for steady cavity flow for a double air curtain design with $b_i = 0.09$ m, $b_o = 0.03$ m, $Gr_t = 4.61 \times 10^9$ ($\Delta T = 20^\circ\text{C}$), and $N = 6.37 \times 10^{-2}$ for $Re_{ci} = 3,183$ and $Re_{co} =$ (a) 1,910, (b) 3,183, (c) 5,092, and (d) 6,365. --138

Fig. 4.81 Iso-concentration lines for steady cavity flow for a double air curtain design with $b_i = 0.09$ m, $b_o = 0.03$ m, $Gr_t = 4.61 \times 10^9$ ($\Delta T = 20^\circ\text{C}$), and $N = 6.37 \times 10^{-2}$ for $Re_{ci} = 3,183$ and $Re_{co} =$ (a) 1,910, (b) 3,183, (c) 5,092, and (d) 6,365. -----139

Fig. 4.82 Velocity vector maps for steady cavity flow for a double air curtain design with $b_i = 0.09$ m, $b_o = 0.03$ m, $Gr_t = 4.61 \times 10^9$ ($\Delta T = 20^\circ\text{C}$), and $N = 6.37 \times 10^{-2}$ for (a) $Re_{ci} = 1,910$ and $Re_{co} = 7,638$, (b) $Re_{ci} = 3,183$ and $Re_{co} = 6,365$, (c) $Re_{ci} = 5,092$ and $Re_{co} = 4,456$, (d) $Re_{ci} = 6,365$ and $Re_{co} = 3,183$, (e) $Re_{ci} = 7,638$ and $Re_{co} = 1,910$. -----140

Fig. 4.83 Isotherms for steady cavity flow for a double air curtain design with $b_i = 0.09$ m, $b_o = 0.03$ m, $Gr_t = 4.61 \times 10^9$ ($\Delta T = 20^\circ\text{C}$), and $N = 6.37 \times 10^{-2}$ for (a) $Re_{ci} = 1,910$ and $Re_{co} = 7,638$, (b) $Re_{ci} = 3,183$ and $Re_{co} = 6,365$, (c) $Re_{ci} = 5,092$ and $Re_{co} = 4,456$, (d) $Re_{ci} = 6,365$ and $Re_{co} = 3,183$, (e) $Re_{ci} = 7,638$ and $Re_{co} = 1,910$. -----141

Fig. 4.84 Iso-concentration lines for steady cavity flow for a double air curtain design with $b_i = 0.09$ m, $b_o = 0.03$ m, $Gr_t = 4.61 \times 10^9$ ($\Delta T = 20^\circ\text{C}$), and $N = 6.37 \times 10^{-2}$ for (a) $Re_{ci} = 1,910$ and $Re_{co} = 7,638$, (b) $Re_{ci} = 3,183$ and $Re_{co} = 6,365$, (c) $Re_{ci} = 5,092$ and $Re_{co} = 4,456$, (d) $Re_{ci} = 6,365$ and $Re_{co} = 3,183$, (e) $Re_{ci} = 7,638$ and $Re_{co} = 1,910$. -----142

Fig. 4.85 Velocity vector maps for steady cavity flow for a double air curtain design with $b_i = 0.05$ m, $b_o = 0.07$ m, $Gr_t = 4.61 \times 10^9$ ($\Delta T = 20^\circ\text{C}$), and $N = 6.37 \times 10^{-2}$ for $Re_{ci} = 1,910$ and $Re_{co} =$ (a) 1,910, (b) 3,183, (c) 5,092, (d) 6,365 and (e) 7,638. -----143

Fig. 4.86 Isotherms for steady cavity flow for a double air curtain design with $b_i = 0.05$ m, $b_o = 0.07$ m, $Gr_t = 4.61 \times 10^9$ ($\Delta T = 20^\circ\text{C}$), and $N = 6.37 \times 10^{-2}$ for $Re_{ci} = 1,910$ and $Re_{co} =$ (a) 1,910, (b) 3,183, (c) 5,092, (d) 6,365 and (e) 7,638. -----144

Fig. 4.87 Iso-concentration lines for steady cavity flow for a double air curtain design with $b_i = 0.05$ m, $b_o = 0.07$ m, $Gr_t = 4.61 \times 10^9$ ($\Delta T = 20^\circ\text{C}$), and $N = 6.37 \times 10^{-2}$ for $Re_{ci} = 1,910$ and $Re_{co} =$ (a) 1,910, (b) 3,183, (c) 5,092, (d) 6,365 and (e) 7,638. -----145

Fig. 4.88 Velocity vector maps for steady cavity flow for a double air curtain design with $b_i = 0.05$ m, $b_o = 0.07$ m, $Gr_t = 4.61 \times 10^9$ ($\Delta T = 20^\circ\text{C}$), and $N = 6.37 \times 10^{-2}$ for $Re_{ci} = 3,183$ and $Re_{co} =$ (a) 1,910, (b) 3,183, (c) 5,092, and (d) 6,365. -----146

Fig. 4.89 Isotherms for steady cavity flow for a double air curtain design with $b_i = 0.05$ m, $b_o = 0.07$ m, $Gr_t = 4.61 \times 10^9$ ($\Delta T = 20^\circ\text{C}$), and $N = 6.37 \times 10^{-2}$ for $Re_{ci} = 3,183$ and $Re_{co} =$ (a) 1,910, (b) 3,183, (c) 5,092, and (d) 6,365. --147

Fig. 4.90 Iso-concentration lines for steady cavity flow for a double air curtain design with $b_i = 0.05$ m, $b_o = 0.07$ m, $Gr_t = 4.61 \times 10^9$ ($\Delta T = 20^\circ\text{C}$), and $N = 6.37 \times 10^{-2}$ for $Re_{ci} = 3,183$ and $Re_{co} =$ (a) 1,910, (b) 3,183, (c) 5,092, and (d) 6,365. -----148

Fig. 4.91 Velocity vector maps for steady cavity flow for a double air curtain design with $b_i = 0.05$ m, $b_o = 0.07$ m, $Gr_t = 4.61 \times 10^9$ ($\Delta T = 20^\circ\text{C}$), and $N = 6.37 \times 10^{-2}$ for (a) $Re_{ci} = 1,910$ and $Re_{co} = 7,638$, (b) $Re_{ci} = 3,183$ and $Re_{co} =$

6,365, (c) $Re_{ci} = 5,092$ and $Re_{co} = 4,456$, (d) $Re_{ci} = 6,365$ and $Re_{co} = 3,183$,
 (e) $Re_{ci} = 7,638$ and $Re_{co} = 1,910$. -----149

Fig. 4.92 Isotherms for steady cavity flow for a double air curtain design with $b_i = 0.05$ m, $b_o = 0.07$ m, $Gr_t = 4.61 \times 10^9$ ($\Delta T = 20^\circ C$), and $N = 6.37 \times 10^{-2}$ for (a) $Re_{ci} = 1,910$ and $Re_{co} = 7,638$, (b) $Re_{ci} = 3,183$ and $Re_{co} = 6,365$, (c) $Re_{ci} = 5,092$ and $Re_{co} = 4,456$, (d) $Re_{ci} = 6,365$ and $Re_{co} = 3,183$, (e) $Re_{ci} = 7,638$ and $Re_{co} = 1,910$. -----150

Fig. 4.93 Iso-concentration lines for steady cavity flow for a double air curtain design with $b_i = 0.05$ m, $b_o = 0.07$ m, $Gr_t = 4.61 \times 10^9$ ($\Delta T = 20^\circ C$), and $N = 6.37 \times 10^{-2}$ for (a) $Re_{ci} = 1,910$ and $Re_{co} = 7,638$, (b) $Re_{ci} = 3,183$ and $Re_{co} = 6,365$, (c) $Re_{ci} = 5,092$ and $Re_{co} = 4,456$, (d) $Re_{ci} = 6,365$ and $Re_{co} = 3,183$, (e) $Re_{ci} = 7,638$ and $Re_{co} = 1,910$. -----151

Fig. 4.94 Velocity vector maps for steady cavity flow for a double air curtain design with $b_i = 0.07$ m, $b_o = 0.05$ m, $Gr_t = 4.61 \times 10^9$ ($\Delta T = 20^\circ C$), and $N = 6.37 \times 10^{-2}$ for $Re_{ci} = 1,910$ and $Re_{co} =$ (a) 1,910, (b) 3,183, (c) 5,092, (d) 6,365 and (e) 7,638. -----152

Fig. 4.95 Isotherms for steady cavity flow for a double air curtain design with $b_i = 0.07$ m, $b_o = 0.05$ m, $Gr_t = 4.61 \times 10^9$ ($\Delta T = 20^\circ C$), and $N = 6.37 \times 10^{-2}$ for $Re_{ci} = 1,910$ and $Re_{co} =$ (a) 1,910, (b) 3,183, (c) 5,092, (d) 6,365 and (e) 7,638. -----153

Fig. 4.96 Iso-concentration lines for steady cavity flow for a double air curtain design with $b_i = 0.07$ m, $b_o = 0.05$ m, $Gr_t = 4.61 \times 10^9$ ($\Delta T = 20^\circ C$), and $N = 6.37 \times 10^{-2}$ for $Re_{ci} = 1,910$ and $Re_{co} =$ (a) 1,910, (b) 3,183, (c) 5,092, (d) 6,365 and (e) 7,638. -----154

Fig. 4.97 Velocity vector maps for steady cavity flow for a double air curtain design with $b_i = 0.07$ m, $b_o = 0.05$ m, $Gr_t = 4.61 \times 10^9$ ($\Delta T = 20^\circ C$), and $N = 6.37$

$\times 10^{-2}$ for $Re_{ci} = 3,183$ and $Re_{co} =$ (a) 1,910, (b) 3,183, (c) 5,092, and (d) 6,365. -----155

Fig. 4.98 Isotherms for steady cavity flow for a double air curtain design with $b_i = 0.07$ m, $b_o = 0.05$ m, $Gr_t = 4.61 \times 10^9$ ($\Delta T = 20^\circ C$), and $N = 6.37 \times 10^{-2}$ for $Re_{ci} = 3,183$ and $Re_{co} =$ (a) 1,910, (b) 3,183, (c) 5,092, and (d) 6,365. --156

Fig. 4.99 Iso-concentration lines for steady cavity flow for a double air curtain design with $b_i = 0.07$ m, $b_o = 0.05$ m, $Gr_t = 4.61 \times 10^9$ ($\Delta T = 20^\circ C$), and $N = 6.37 \times 10^{-2}$ for $Re_{ci} = 3,183$ and $Re_{co} =$ (a) 1,910, (b) 3,183, (c) 5,092, and (d) 6,365. -----157

Fig. 4.100 Velocity vector maps for steady cavity flow for a double air curtain design with $b_i = 0.07$ m, $b_o = 0.05$ m, $Gr_t = 4.61 \times 10^9$ ($\Delta T = 20^\circ C$), and $N = 6.37 \times 10^{-2}$ for (a) $Re_{ci} = 1,910$ and $Re_{co} = 7,638$, (b) $Re_{ci} = 3,183$ and $Re_{co} = 6,365$, (c) $Re_{ci} = 5,092$ and $Re_{co} = 4,456$, (d) $Re_{ci} = 6,365$ and $Re_{co} = 3,183$, (e) $Re_{ci} = 7,638$ and $Re_{co} = 1,910$. -----158

Fig. 4.101 Isotherms for steady cavity flow for a double air curtain design with $b_i = 0.07$ m, $b_o = 0.05$ m, $Gr_t = 4.61 \times 10^9$ ($\Delta T = 20^\circ C$), and $N = 6.37 \times 10^{-2}$ for (a) $Re_{ci} = 1,910$ and $Re_{co} = 7,638$, (b) $Re_{ci} = 3,183$ and $Re_{co} = 6,365$, (c) $Re_{ci} = 5,092$ and $Re_{co} = 4,456$, (d) $Re_{ci} = 6,365$ and $Re_{co} = 3,183$, (e) $Re_{ci} = 7,638$ and $Re_{co} = 1,910$. -----159

Fig. 4.102 Iso-concentration lines for steady cavity flow for a double air curtain design with $b_i = 0.07$ m, $b_o = 0.05$ m, $Gr_t = 4.61 \times 10^9$ ($\Delta T = 20^\circ C$), and $N = 6.37 \times 10^{-2}$ for (a) $Re_{ci} = 1,910$ and $Re_{co} = 7,638$, (b) $Re_{ci} = 3,183$ and $Re_{co} = 6,365$, (c) $Re_{ci} = 5,092$ and $Re_{co} = 4,456$, (d) $Re_{ci} = 6,365$ and $Re_{co} = 3,183$, (e) $Re_{ci} = 7,638$ and $Re_{co} = 1,910$. -----160

Fig. 4.103 Velocity vector maps for steady cavity flow for a double air curtain design with $b_i = 0.03$ m, $b_o = 0.04$ m, $Gr_t = 4.61 \times 10^9$ ($\Delta T = 20^\circ C$), and $N = 6.37$

$\times 10^{-2}$ for $Re_{ci} = 1,910$ and $Re_{co} =$ (a) 1,910, (b) 3,183, (c) 5,092, (d) 6,365 and (e) 7,638. -----161

Fig. 4.104 Isotherms for steady cavity flow for a double air curtain design with $b_i = 0.03$ m, $b_o = 0.04$ m, $Gr_t = 4.61 \times 10^9$ ($\Delta T = 20^\circ C$), and $N = 6.37 \times 10^{-2}$ for $Re_{ci} = 1,910$ and $Re_{co} =$ (a) 1,910, (b) 3,183, (c) 5,092, (d) 6,365 and (e) 7,638. -----162

Fig. 4.105 Iso-concentration lines for steady cavity flow for a double air curtain design with $b_i = 0.03$ m, $b_o = 0.04$ m, $Gr_t = 4.61 \times 10^9$ ($\Delta T = 20^\circ C$), and $N = 6.37 \times 10^{-2}$ for $Re_{ci} = 1,910$ and $Re_{co} =$ (a) 1,910, (b) 3,183, (c) 5,092, (d) 6,365 and (e) 7,638. -----163

Fig. 4.106 Velocity vector maps for steady cavity flow for a double air curtain design with $b_i = 0.03$ m, $b_o = 0.04$ m, $Gr_t = 4.61 \times 10^9$ ($\Delta T = 20^\circ C$), and $N = 6.37 \times 10^{-2}$ for $Re_{ci} = 3,183$ and $Re_{co} =$ (a) 1,910, (b) 3,183, (c) 5,092, and (d) 6,365. -----164

Fig. 4.107 Isotherms for steady cavity flow for a double air curtain design with $b_i = 0.03$ m, $b_o = 0.04$ m, $Gr_t = 4.61 \times 10^9$ ($\Delta T = 20^\circ C$), and $N = 6.37 \times 10^{-2}$ for $Re_{ci} = 3,183$ and $Re_{co} =$ (a) 1,910, (b) 3,183, (c) 5,092, and (d) 6,365. --165

Fig. 4.108 Iso-concentration lines for steady cavity flow for a double air curtain design with $b_i = 0.03$ m, $b_o = 0.04$ m, $Gr_t = 4.61 \times 10^9$ ($\Delta T = 20^\circ C$), and $N = 6.37 \times 10^{-2}$ for $Re_{ci} = 3,183$ and $Re_{co} =$ (a) 1,910, (b) 3,183, (c) 5,092, and (d) 6,365. -----166

Fig. 4.109 Velocity vector maps for steady cavity flow for a double air curtain design with $b_i = 0.03$ m, $b_o = 0.04$ m, $Gr_t = 4.61 \times 10^9$ ($\Delta T = 20^\circ C$), and $N = 6.37 \times 10^{-2}$ for (a) $Re_{ci} = 1,910$ and $Re_{co} = 7,638$, (b) $Re_{ci} = 3,183$ and $Re_{co} = 6,365$, (c) $Re_{ci} = 5,092$ and $Re_{co} = 4,456$, (d) $Re_{ci} = 6,365$ and $Re_{co} = 3,183$, (e) $Re_{ci} = 7,638$ and $Re_{co} = 1,910$. -----167

Fig. 4.110 Isotherms for steady cavity flow for a double air curtain design with $b_i = 0.03$ m, $b_o = 0.04$ m, $Gr_t = 4.61 \times 10^9$ ($\Delta T = 20^\circ\text{C}$), and $N = 6.37 \times 10^{-2}$ for (a) $Re_{ci} = 1,910$ and $Re_{co} = 7,638$, (b) $Re_{ci} = 3,183$ and $Re_{co} = 6,365$, (c) $Re_{ci} = 5,092$ and $Re_{co} = 4,456$, (d) $Re_{ci} = 6,365$ and $Re_{co} = 3,183$, (e) $Re_{ci} = 7,638$ and $Re_{co} = 1,910$. -----168

Fig. 4.111 Iso-concentration lines for steady cavity flow for a double air curtain design with $b_i = 0.03$ m, $b_o = 0.04$ m, $Gr_t = 4.61 \times 10^9$ ($\Delta T = 20^\circ\text{C}$), and $N = 6.37 \times 10^{-2}$ for (a) $Re_{ci} = 1,910$ and $Re_{co} = 7,638$, (b) $Re_{ci} = 3,183$ and $Re_{co} = 6,365$, (c) $Re_{ci} = 5,092$ and $Re_{co} = 4,456$, (d) $Re_{ci} = 6,365$ and $Re_{co} = 3,183$, (e) $Re_{ci} = 7,638$ and $Re_{co} = 1,910$. -----169

Fig. 4.112 Velocity vector maps for steady cavity flow for a double air curtain design with $b_i = 0.04$ m, $b_o = 0.03$ m, $Gr_t = 4.61 \times 10^9$ ($\Delta T = 20^\circ\text{C}$), and $N = 6.37 \times 10^{-2}$ for $Re_{ci} = 1,910$ and $Re_{co} =$ (a) 1,910, (b) 3,183, (c) 5,092, (d) 6,365 and (e) 7,638. -----170

Fig. 4.113 Isotherms for steady cavity flow for a double air curtain design with $b_i = 0.04$ m, $b_o = 0.03$ m, $Gr_t = 4.61 \times 10^9$ ($\Delta T = 20^\circ\text{C}$), and $N = 6.37 \times 10^{-2}$ for $Re_{ci} = 1,910$ and $Re_{co} =$ (a) 1,910, (b) 3,183, (c) 5,092, (d) 6,365 and (e) 7,638. -----171

Fig. 4.114 Iso-concentration lines for steady cavity flow for a double air curtain design with $b_i = 0.04$ m, $b_o = 0.03$ m, $Gr_t = 4.61 \times 10^9$ ($\Delta T = 20^\circ\text{C}$), and $N = 6.37 \times 10^{-2}$ for $Re_{ci} = 1,910$ and $Re_{co} =$ (a) 1,910, (b) 3,183, (c) 5,092, (d) 6,365 and (e) 7,638. -----172

Fig. 4.115 Velocity vector maps for steady cavity flow for a double air curtain design with $b_i = 0.04$ m, $b_o = 0.03$ m, $Gr_t = 4.61 \times 10^9$ ($\Delta T = 20^\circ\text{C}$), and $N = 6.37 \times 10^{-2}$ for $Re_{ci} = 3,183$ and $Re_{co} =$ (a) 1,910, (b) 3,183, (c) 5,092, and (d) 6,365. -----173

Fig. 4.116 Isotherms for steady cavity flow for a double air curtain design with $b_i = 0.04$ m, $b_o = 0.03$ m, $Gr_t = 4.61 \times 10^9$ ($\Delta T = 20^\circ\text{C}$), and $N = 6.37 \times 10^{-2}$ for $Re_{ci} = 3,183$ and $Re_{co} =$ (a) 1,910, (b) 3,183, (c) 5,092, and (d) 6,365. --174

Fig. 4.117 Iso-concentration lines for steady cavity flow for a double air curtain design with $b_i = 0.04$ m, $b_o = 0.03$ m, $Gr_t = 4.61 \times 10^9$ ($\Delta T = 20^\circ\text{C}$), and $N = 6.37 \times 10^{-2}$ for $Re_{ci} = 3,183$ and $Re_{co} =$ (a) 1,910, (b) 3,183, (c) 5,092, and (d) 6,365. -----175

Fig. 4.118 Velocity vector maps for steady cavity flow for a double air curtain design with $b_i = 0.04$ m, $b_o = 0.03$ m, $Gr_t = 4.61 \times 10^9$ ($\Delta T = 20^\circ\text{C}$), and $N = 6.37 \times 10^{-2}$ for (a) $Re_{ci} = 1,910$ and $Re_{co} = 7,638$, (b) $Re_{ci} = 3,183$ and $Re_{co} = 6,365$, (c) $Re_{ci} = 5,092$ and $Re_{co} = 4,456$, (d) $Re_{ci} = 6,365$ and $Re_{co} = 3,183$, (e) $Re_{ci} = 7,638$ and $Re_{co} = 1,910$. -----176

Fig. 4.119 Isotherms for steady cavity flow for a double air curtain design with $b_i = 0.04$ m, $b_o = 0.03$ m, $Gr_t = 4.61 \times 10^9$ ($\Delta T = 20^\circ\text{C}$), and $N = 6.37 \times 10^{-2}$ for (a) $Re_{ci} = 1,910$ and $Re_{co} = 7,638$, (b) $Re_{ci} = 3,183$ and $Re_{co} = 6,365$, (c) $Re_{ci} = 5,092$ and $Re_{co} = 4,456$, (d) $Re_{ci} = 6,365$ and $Re_{co} = 3,183$, (e) $Re_{ci} = 7,638$ and $Re_{co} = 1,910$. -----177

Fig. 4.120 Iso-concentration lines for steady cavity flow for a double air curtain design with $b_i = 0.04$ m, $b_o = 0.03$ m, $Gr_t = 4.61 \times 10^9$ ($\Delta T = 20^\circ\text{C}$), and $N = 6.37 \times 10^{-2}$ for (a) $Re_{ci} = 1,910$ and $Re_{co} = 7,638$, (b) $Re_{ci} = 3,183$ and $Re_{co} = 6,365$, (c) $Re_{ci} = 5,092$ and $Re_{co} = 4,456$, (d) $Re_{ci} = 6,365$ and $Re_{co} = 3,183$, (e) $Re_{ci} = 7,638$ and $Re_{co} = 1,910$. -----178

Fig. 4.121 Velocity vector maps for steady cavity flow for a double air curtain design with $b_i = 0.05$ m, and $b_o = 0.05$ m, $Gr_t = 4.61 \times 10^9$ ($\Delta T = 20^\circ\text{C}$), and $N = 6.37 \times 10^{-2}$ with a outer curtain inclined angle of 25° for $Re_{ci} = 1,910$ and $Re_{co} =$ (a) 1,910, (b) 3,183, (c) 5,092, (d) 6,365 and (e) 7,638. -----179

Fig. 4.122 Isotherms for steady cavity flow for a double air curtain design with $b_i = 0.05$ m, and $b_o = 0.05$ m, $Gr_t = 4.61 \times 10^9$ ($\Delta T = 20^\circ\text{C}$), and $N = 6.37 \times 10^{-2}$ with a outer curtain inclined angle of 25° for $Re_{ci} = 1,910$ and $Re_{co} =$ (a) 1,910, (b) 3,183, (c) 5,092, (d) 6,365 and (e) 7,638.-----180

Fig. 4.123 Iso-concentration lines for steady cavity flow for a double air curtain design with $b_i = 0.05$ m, and $b_o = 0.05$ m, $Gr_t = 4.61 \times 10^9$ ($\Delta T = 20^\circ\text{C}$), and $N = 6.37 \times 10^{-2}$ with a outer curtain inclined angle of 25° for $Re_{ci} = 3,183$ and $Re_{co} =$ (a) 1,910, (b) 3,183, (c) 5,092, (d) 6,365 and (e) 7,638. ----181

Fig. 4.124 Velocity vector maps for steady cavity flow for a double air curtain design with $b_i = 0.05$ m, and $b_o = 0.05$ m, $Gr_t = 4.61 \times 10^9$ ($\Delta T = 20^\circ\text{C}$), and $N = 6.37 \times 10^{-2}$ with a outer curtain inclined angle of 25° for $Re_{ci} = 3,183$ and $Re_{co} =$ (a) 1,910, (b) 3,183, (c) 5,092, and (d) 6,365.-----182

Fig. 4.125 Isotherms for steady cavity flow for a double air curtain design with $b_i = 0.05$ m, and $b_o = 0.05$ m, $Gr_t = 4.61 \times 10^9$ ($\Delta T = 20^\circ\text{C}$), and $N = 6.37 \times 10^{-2}$ with a outer curtain inclined angle of 25° for $Re_{ci} = 3,183$ and $Re_{co} =$ (a) 1,910, (b) 3,183, (c) 5,092, and (d) 6,365.-----183

Fig. 4.126 Iso-concentration lines for steady cavity flow for a double air curtain design with $b_i = 0.05$ m, and $b_o = 0.05$ m, $Gr_t = 4.61 \times 10^9$ ($\Delta T = 20^\circ\text{C}$), and $N = 6.37 \times 10^{-2}$ with a outer curtain inclined angle of 25° for $Re_{ci} = 3,183$ and $Re_{co} =$ (a) 1,910, (b) 3,183, (c) 5,092, and (d) 6,365.-----184

Fig. 4.127 Velocity vector maps for steady cavity flow for a double air curtain design with $b_i = 0.05$ m, and $b_o = 0.05$ m, $Gr_t = 4.61 \times 10^9$ ($\Delta T = 20^\circ\text{C}$), and $N = 6.37 \times 10^{-2}$ with a outer curtain inclined angle of 25° for (a) $Re_{ci} = 1,910$ and $Re_{co} = 7,638$, (b) $Re_{ci} = 3,183$ and $Re_{co} = 6,365$, (c) $Re_{ci} = 5,092$ and $Re_{co} = 4,456$, (d) $Re_{ci} = 6,365$ and $Re_{co} = 3,183$, (e) $Re_{ci} = 7,638$ and $Re_{co} = 1,910$.-----185

Fig. 4.128 Isotherms for steady cavity flow for a double air curtain design with $b_i = 0.05$ m, and $b_o = 0.05$ m, $Gr_t = 4.61 \times 10^9$ ($\Delta T = 20^\circ\text{C}$), and $N = 6.37 \times 10^{-2}$ with a outer curtain inclined angle of 25° for (a) $Re_{ci} = 1,910$ and $Re_{co} = 7,638$, (b) $Re_{ci} = 3,183$ and $Re_{co} = 6,365$, (c) $Re_{ci} = 5,092$ and $Re_{co} = 4,456$, (d) $Re_{ci} = 6,365$ and $Re_{co} = 3,183$, (e) $Re_{ci} = 7,638$ and $Re_{co} = 1,910$. ---186

Fig. 4.129 Iso-concentration lines for steady cavity flow for a double air curtain design with $b_i = 0.05$ m, and $b_o = 0.05$ m, $Gr_t = 4.61 \times 10^9$ ($\Delta T = 20^\circ\text{C}$), and $N = 6.37 \times 10^{-2}$ with a outer curtain inclined angle of 25° for (a) $Re_{ci} = 1,910$ and $Re_{co} = 7,638$, (b) $Re_{ci} = 3,183$ and $Re_{co} = 6,365$, (c) $Re_{ci} = 5,092$ and $Re_{co} = 4,456$, (d) $Re_{ci} = 6,365$ and $Re_{co} = 3,183$, (e) $Re_{ci} = 7,638$ and $Re_{co} = 1,910$.-----187

Fig. 4.130 Schematic diagram of an open vertical cavity with back panel perforation. -----188

Fig. 4.131 Velocity vector maps for steady cavity flow for a single air curtain design with perforation density of 35% for $b_j = 0.1$ m, $Gr_t = 4.61 \times 10^9$ ($\Delta T = 20^\circ\text{C}$), and $N = 6.37 \times 10^{-2}$ for $Re_p = 1,910$ and $Re_b =$ (a) 1,910, (b) 3,183, (c) 5,092, (d) 6,365, and (e) 9,548. -----189

Fig. 4.132 Isotherms for steady cavity flow for a single air curtain design with perforation density of 35% for $b_j = 0.1$ m, $Gr_t = 4.61 \times 10^9$ ($\Delta T = 20^\circ\text{C}$), and $N = 6.37 \times 10^{-2}$ for $Re_p = 1,910$ and $Re_b =$ (a) 1,910, (b) 3,183, (c) 5,092, (d) 6,365, and (e) 9,548. -----190

Fig. 4.133 Iso-concentration lines for steady cavity flow for a single air curtain design with perforation density of 35% for $b_j = 0.1$ m, $Gr_t = 4.61 \times 10^9$ ($\Delta T = 20^\circ\text{C}$), and $N = 6.37 \times 10^{-2}$ for $Re_p = 1,910$ and $Re_b =$ (a) 1,910, (b) 3,183, (c) 5,092, (d) 6,365, and (e) 9,548. -----191

Fig. 4.134 Velocity vector maps for steady cavity flow for a single air curtain design

with perforation density of 35% for $b_j = 0.1$ m, $Gr_t = 4.61 \times 10^9$ ($\Delta T = 20$ °C), and $N = 6.37 \times 10^{-2}$ for $Re_p = 3,183$ and $Re_b =$ (a) 1,910, (b) 3,183, (c) 5,092, (d) 6,365, and (e) 9,548. -----192

Fig. 4.135 Isotherms for steady cavity flow for a single air curtain design with perforation density of 35% for $b_j = 0.1$ m, $Gr_t = 4.61 \times 10^9$ ($\Delta T = 20$ °C), and $N = 6.37 \times 10^{-2}$ for $Re_p = 3,183$ and $Re_b =$ (a) 1,910 (b) 3,183, (c) 5,092, (d) 6,365, and (e) 9,548.-----193

Fig. 4.136 Iso-concentration lines for steady cavity flow for a single air curtain design with perforation density of 35% for $b_j = 0.1$ m, $Gr_t = 4.61 \times 10^9$ ($\Delta T = 20$ °C), and $N = 6.37 \times 10^{-2}$ for $Re_p = 3,183$ and $Re_b =$ (a) 1,910, (b) 3,183, (c) 5,092, (d) 6,365, and (e) 9,548. -----194

Fig. 4.137 Velocity vector maps for steady cavity flow for a single air curtain design with perforation density of 35% for $b_j = 0.1$ m, $Gr_t = 4.61 \times 10^9$ ($\Delta T = 20$ °C), and $N = 6.37 \times 10^{-2}$ for $Re_p = 5,092$ and $Re_b =$ (a) 1,910, (b) 3,183, (c) 5,092, (d) 6,365, and (e) 9,548. -----195

Fig. 4.138 Isotherms for steady cavity flow for a single air curtain design with perforation density of 35% for $b_j = 0.1$ m, $Gr_t = 4.61 \times 10^9$ ($\Delta T = 20$ °C), and $N = 6.37 \times 10^{-2}$ for $Re_p = 5,092$ and $Re_b =$ (a) 1,910 (b) 3,183, (c) 5,092, (d) 6,365, and (e) 9,548.-----196

Fig. 4.139 Iso-concentration lines for steady cavity flow for a single air curtain design with perforation density of 35% for $b_j = 0.1$ m, $Gr_t = 4.61 \times 10^9$ ($\Delta T = 20$ °C), and $N = 6.37 \times 10^{-2}$ for $Re_p = 5,092$ and $Re_b =$ (a) 1,910, (b) 3,183, (c) 5,092, (d) 6,365, and (e) 9,548. -----197

Fig. 4.140 Velocity vector maps for steady cavity flow for a single air curtain design with perforation density of 25% for $b_j = 0.1$ m, $Gr_t = 4.61 \times 10^9$ ($\Delta T = 20$ °C), and $N = 6.37 \times 10^{-2}$ for $Re_p = 1,910$ and $Re_b =$ (a) 1,910, (b) 3,183, (c)

5,092, (d) 6,365, and (e) 9,548. -----198

Fig. 4.141 Isotherms for steady cavity flow for a single air curtain design with perforation density of 25% for $b_j = 0.1$ m, $Gr_t = 4.61 \times 10^9$ ($\Delta T = 20^\circ C$), and $N = 6.37 \times 10^{-2}$ for $Re_p = 1,910$ and $Re_b =$ (a) 1,910, (b) 3,183, (c) 5,092, (d) 6,365, and (e) 9,548. -----199

Fig. 4.142 Iso-concentration lines for steady cavity flow for a single air curtain design with perforation density of 25% for $b_j = 0.1$ m, $Gr_t = 4.61 \times 10^9$ ($\Delta T = 20^\circ C$), and $N = 6.37 \times 10^{-2}$ for $Re_p = 1,910$ and $Re_b =$ (a) 1,910, (b) 3,183, (c) 5,092, (d) 6,365, and (e) 9,548. -----200

Fig. 4.143 Velocity vector maps for steady cavity flow for a single air curtain design with perforation density of 25% for $b_j = 0.1$ m, $Gr_t = 4.61 \times 10^9$ ($\Delta T = 20^\circ C$), and $N = 6.37 \times 10^{-2}$ for $Re_p = 3,183$ and $Re_b =$ (a) 1,910, (b) 3,183, (c) 5,092, (d) 6,365, and (e) 9,548. -----201

Fig. 4.144 Isotherms for steady cavity flow for a single air curtain design with perforation density of 25% for $b_j = 0.1$ m, $Gr_t = 4.61 \times 10^9$ ($\Delta T = 20^\circ C$), and $N = 6.37 \times 10^{-2}$ for $Re_p = 3,183$ and $Re_b =$ (a) 1,910 (b) 3,183, (c) 5,092, (d) 6,365, and (e) 9,548. -----202

Fig. 4.145 Iso-concentration lines for steady cavity flow for a single air curtain design with perforation density of 25% for $b_j = 0.1$ m, $Gr_t = 4.61 \times 10^9$ ($\Delta T = 20^\circ C$), and $N = 6.37 \times 10^{-2}$ for $Re_p = 3,183$ and $Re_b =$ (a) 1,910, (b) 3,183, (c) 5,092, (d) 6,365, and (e) 9,548. -----203

Fig. 4.146 Velocity vector maps for steady cavity flow for a single air curtain design with perforation density of 25% for $b_j = 0.1$ m, $Gr_t = 4.61 \times 10^9$ ($\Delta T = 20^\circ C$), and $N = 6.37 \times 10^{-2}$ for $Re_p = 5,092$ and $Re_b =$ (a) 1,910, (b) 3,183, (c) 5,092, (d) 6,365, and (e) 9,548. -----204

Fig. 4.147 Isotherms for steady cavity flow for a single air curtain design with

perforation density of 25% for $b_j = 0.1$ m, $Gr_t = 4.61 \times 10^9$ ($\Delta T = 20^\circ C$), and $N = 6.37 \times 10^{-2}$ for $Re_p = 5,092$ and $Re_b =$ (a) 1,910 (b) 3,183, (c) 5,092, (d) 6,365, and (e) 9,548.-----205

Fig. 4.148 Iso-concentration lines for steady cavity flow for a single air curtain design with perforation density of 25% for $b_j = 0.1$ m, $Gr_t = 4.61 \times 10^9$ ($\Delta T = 20^\circ C$), and $N = 6.37 \times 10^{-2}$ for $Re_p = 5,092$ and $Re_b =$ (a) 1,910, (b) 3,183, (c) 5,092, (d) 6,365, and (e) 9,548. -----206

Fig. 4.149 Velocity vector maps for steady cavity flow for a single air curtain design with perforation density of 15% for $b_j = 0.1$ m, $Gr_t = 4.61 \times 10^9$ ($\Delta T = 20^\circ C$), and $N = 6.37 \times 10^{-2}$ for $Re_p = 1,910$ and $Re_b =$ (a) 1,910, (b) 3,183, (c) 5,092, (d) 6,365, and (e) 9,548. -----207

Fig. 4.150 Isotherms for steady cavity flow for a single air curtain design with perforation density of 15% for $b_j = 0.1$ m, $Gr_t = 4.61 \times 10^9$ ($\Delta T = 20^\circ C$), and $N = 6.37 \times 10^{-2}$ for $Re_p = 1,910$ and $Re_b =$ (a) 1,910, (b) 3,183, (c) 5,092, (d) 6,365, and (e) 9,548. -----208

Fig. 4.151 Iso-concentration lines for steady cavity flow for a single air curtain design with perforation density of 15% for $b_j = 0.1$ m, $Gr_t = 4.61 \times 10^9$ ($\Delta T = 20^\circ C$), and $N = 6.37 \times 10^{-2}$ for $Re_p = 1,910$ and $Re_b =$ (a) 1,910, (b) 3,183, (c) 5,092, (d) 6,365, and (e) 9,548. -----209

Fig. 4.152 Velocity vector maps for steady cavity flow for a single air curtain design with perforation density of 15% for $b_j = 0.1$ m, $Gr_t = 4.61 \times 10^9$ ($\Delta T = 20^\circ C$), and $N = 6.37 \times 10^{-2}$ for $Re_p = 3,183$ and $Re_b =$ (a) 1,910, (b) 3,183, (c) 5,092, (d) 6,365, and (e) 9,548. -----210

Fig. 4.153 Isotherms for steady cavity flow for a single air curtain design with perforation density of 15% for $b_j = 0.1$ m, $Gr_t = 4.61 \times 10^9$ ($\Delta T = 20^\circ C$), and $N = 6.37 \times 10^{-2}$ for $Re_p = 3,183$ and $Re_b =$ (a) 1,910 (b) 3,183, (c) 5,092,

(d) 6,365, and (e) 9,548.-----211

Fig. 4.154 Iso-concentration lines for steady cavity flow for a single air curtain design with perforation density of 15% for $b_j = 0.1$ m, $Gr_t = 4.61 \times 10^9$ ($\Delta T = 20^\circ C$), and $N = 6.37 \times 10^{-2}$ for $Re_p = 3,183$ and $Re_b =$ (a) 1,910, (b) 3,183, (c) 5,092, (d) 6,365, and (e) 9,548. -----212

Fig. 4.155 Velocity vector maps for steady cavity flow for a single air curtain design with perforation density of 15% for $b_j = 0.1$ m, $Gr_t = 4.61 \times 10^9$ ($\Delta T = 20^\circ C$), and $N = 6.37 \times 10^{-2}$ for $Re_p = 5,092$ and $Re_b =$ (a) 1,910, (b) 3,183, (c) 5,092, (d) 6,365, and (e) 9,548. -----213

Fig. 4.156 Isotherms for steady cavity flow for a single air curtain design with perforation density of 15% for $b_j = 0.1$ m, $Gr_t = 4.61 \times 10^9$ ($\Delta T = 20^\circ C$), and $N = 6.37 \times 10^{-2}$ for $Re_p = 5,092$ and $Re_b =$ (a) 1,910 (b) 3,183, (c) 5,092, (d) 6,365, and (e) 9,548.-----214

Fig. 4.157 Iso-concentration lines for steady cavity flow for a single air curtain design with perforation density of 15% for $b_j = 0.1$ m, $Gr_t = 4.61 \times 10^9$ ($\Delta T = 20^\circ C$), and $N = 6.37 \times 10^{-2}$ for $Re_p = 5,092$ and $Re_b =$ (a) 1,910, (b) 3,183, (c) 5,092, (d) 6,365, and (e) 9,548. -----215

LIST OF TABLES

Table 4.1 Variations of Richardson numbers with the jet Reynolds number. ----- 57

Table 4.2 Entrainment factors for selected cases with a single air curtain design. -- 58



NOMENCLATURE

A	Ratio of the discharge to return grille distance to the discharge width $A = H / b_j$
b_j	Jet width at the air curtain discharge (m)
B	Upper and bottom plates of the cavity, B_b (bottom) and B_c (ceiling)
c_p	Specific heat at constant pressure, $J/(kg \cdot K)$
D	Solutal diffusivity, m^2/s
d_p	Back panel perforation density
g	Gravitational acceleration (m/s^2)
Gr	Grashof number, $Gr_t = g \beta_t \Delta T H^3 / \nu^2$, $Gr_m = g \beta_m \Delta w_1 H^3 / \nu^2$
Gr/Re_H^2	Ratio of thermal buoyancy-to-inertia force, Richardson number
H	Distance between the discharge grilles to return grilles (m)
k	Thermal conductivity
K	Instantaneous value of turbulence kinetic energy, $u'_i u'_i / 2$ (m^2/s^2)
\bar{K}	Average value of turbulence kinetic energy, $\overline{u'_i u'_i} / 2$ (m^2/s^2)
Le	Lewis number, $Le = \nu / \alpha$
M_a, M_v	Molecular weights of air and water vapor, respectively
N	Buoyancy ratio, $\beta_m (w_{1a} - w_j) / \beta_t (T_{amb} - T_j)$
P	Non-dimensional pressure
p_{amb}	Pressure of the ambient, 101325 Pa
p_m	Motion pressure
Pr	Prandtl number, $Pr = \nu / \alpha$, $Pr_t = \mu_t C_p / k_t$
p	Dimensional pressure (Pa)

Ra	Rayleigh numbers, $Ra_t = g\beta\Delta TH^3/\alpha\nu$, $Ra_m = g\beta\Delta w_1 H^3/\alpha\nu$
Re	Reynolds numbers, $Re_b = \bar{V}_j b_j / \nu$, $Re_H = \bar{V}_j H / \nu$, $Re_p = \bar{V}_p H d_p / \nu$
Ri	Richardson number, $Ri_t = Gr_t / Re_H^2$, $Ri_m = Gr_t / Re_H^2$
Sc	Schmidt numbers, $Sc = \nu / D$, $Sc_t = \mu_t / \rho D$
T	Temperature
T _C	Temperature of the inner cold plate (°C)
T _j	Temperature of air at the discharge grille (°C)
T _{amb}	Temperature of the ambient surrounding (°C)
t, τ	Dimensional (sec.) and dimensionless times
u, w	Dimensional velocity components
U, W	Dimensionless velocity components
\bar{V}_j	Uniform velocity of the air jet at the discharge grille inlet (m/s)
\bar{V}_p	Average air speed at perforations (m/s)
w_1	Mass fraction of moisture
w_{1a}	Mass fraction of moisture of the ambient
w_{1j}	Mass fraction of moisture of the air discharge
x, z	Dimensional Cartesian coordinates
Y^+	Non-dimensional distance from wall in wall coordinates
X, Z	Dimensionless Cartesian coordinates, $x/H, z/H$

Greek symbols

α	Thermal diffusivity of the mixture (cm ² /s)
α_e	Thermal entrainment factor
γ	Jet inclined angle (degree)

ΔT	Temperature difference between the ambient and the air discharge ($^{\circ}\text{C}$)
Θ	Nondimensional temperature, $(\bar{T} - T_C)/(T_{amb} - T_C)$
β_t	Thermal expansion coefficient, $(1/T_0)$
β_m	Concentration expansion coefficient, $(M_a/M_v - 1)$
ν	Kinematic viscosity of the mixture (m^2/s)
ρ	Mass density of the mixture
ε	Turbulence dissipation rate, $\text{N}/(\text{sm}^2)$
ϕ	Relative humidity
γ_ρ	Ratio of density, ρ/ρ_0
γ_μ	Ratio of dynamic viscosity, μ/μ_0
γ_{cp}	Ratio of specific heat at constant pressure, C_p/C_{p0}
λ_k	Ratio of thermal conductivity, k/k_0
λ_D	Ratio of mass diffusivity, D/D_0



Subscripts

0	At reference condition
a	of air
amb	at ambient condition
j	At air curtain discharge
v	of water vapor
b	Parameters based on air discharge width
H	Parameters based on distance between air discharge to return grilles
i	Inner curtain of double curtain design
o	Outer curtain of double curtain design
p	of back panel

c of inner cold vertical plate



CHAPTER 1

INTRODUCTION

1.1 Motivation

In view of the recent significant improvement in the standard of living, refrigerated display cases are extensively used in today's supermarkets and grocery stores. To save precious floor-space and provide a large selling area, vertical display cabinets are the better choice than the horizontal ones [1]. Moreover, to attract consumers and hence increase sales, manufacturers developed open type display cases, as schematically shown in Fig. 1.1, with no obstacle between the products and customers [1-4]. In these display cases a cold air curtain is often used to produce an artificial barrier between the outside warm air in the ambient and inside cold air in the cabinets. The air curtain is essentially a two-dimensional cool air jet. Usually the air curtain is supplied from the top of a display case through a discharge honeycomb, flows over the open surface of the cabinet, and finally reaches a return air grille at the case bottom. In reality, an open display case is operated in a store environment and it exchanges heat and moisture with the surrounding air in the store. Besides, the outside warm and moist air can be entrained into the display case by the air curtain, which in turn can substantially lower the performance of the case. Note that the entrained warm and moist air into the cabinet becomes sensible and latent energy loads to the unit since it needs to be cooled and the moisture in it needs to be removed. Therefore a detailed understanding of the heat and mass transfer processes in open refrigerated display cases are needed to improve the performance of the systems. Especially, how the momentum, energy and moisture transports in the

cabinets are affected by the moist air entrained into the flow and buoyancy forces in the flow requires an in-depth investigation.

1.2 Literature Review

The literature relevant to the present study is reviewed in the following.

1.2.1 Cooling loads

The total cooling loads of a refrigerated display cabinet consists of sensible and latent components. The sensible portion includes heat conduction through physical envelopes of the cabinet, thermal radiation from the ambient to the cabinet, sensible infiltration, and heat gains from fan motors, anti-sweat heater and defrost. The latent portion comes from the entrainment of the moisture in the ambient into the cabinet through the air curtains. Ge and Tassou [5] used an implicit numerical method to simulate flow and heat transfer in a vertical display case and developed an correlation for the total heat transfer across an air curtain in terms of the ambient air enthalpy, initial dry-bulb temperature of air jet, temperature difference between the air inside the cabinet and injected air, and some air curtain properties such as the jet initial velocity, jet mass flow rate and jet length. Jet thickness is not directly included, but has some relationship with the jet velocity and mass flow rate. They also proposed a correlation for the return air temperature based on air temperature at the injection grille and ambient and on the air curtain length. The efficiency of the air curtain ε was defined by Cortella [1, 6] as $\varepsilon = \frac{\text{heat flow rate from the load}}{\text{total refrigerating capacity}}$ according to the results from a numerical simulation by using a LES turbulence model. It was pointed out by Faramarzi [7, 8] that the infiltration of the moist air from the ambient into the cabinet was the largest constituent of the case cooling load. The infiltration load can be further divided into the sensible and latent parts. The sensible portion results from the temperature difference between the ambient and cabinet air. The

latent portion, however, results from the difference in the water vapor concentration between the air in the ambient and cabinet. Hence determining the infiltration load is considered as the most challenging aspect of the display case cooling load analysis.

1.2.2 Thermal entrainment factor

Entrainment of the ambient warm air into a display cabinet was found to increase the temperature of the products and the temperature near the return grille [8, 9]. Recently Chen & Yuan [4, 10] and Bhattacharjee & Loth [11] defined a thermal entrainment factor as $\alpha = \frac{i_r - i_s}{i_{amb} - i_s}$ = (enthalpy difference between the return and supply air) / (enthalpy difference between the ambient and supply air). If the air curtain does not cause any air entrainment, α will be equal to zero. On the contrary, the enthalpy of return air and α increase if the moist air entrainment increases. In practical situation α would be between zero and unity. Similarly, Navaz et al. [3] introduced a parameter to characterize the portion of air mass spillage to the outside and infiltration into the case. Navaz et al. [3] and Bhattacharjee and Loth [11] also estimated the volumetric infiltration rate by integrating the negative horizontal velocity from the bottom edge of the opening at the air return grille to a location where $U=0$. Chen & Yuan [4, 10] investigated how the thermal entrainment factor was affected by the Reynolds number (based on the jet length H) and Richardson number (based on the jet length H and temperature difference between the ambient and injection air, $Ri_t = Gr_t / Re_H^2$). They found that when the Richardson number decreased to 0.14, the infiltration rate arrived at a minimum. For a further reduction in Ri_t the infiltration rate would increase slightly due to the excessive mixing. They suggested that there existed a critical Richardson number to ensure the insulation of the air curtain at a given Grashof number. For increases in Re and Ri_t the thermal entrainment factor increases slightly, signifying that the momentum force would

promote the thermal entrainment but the buoyant force would suppress it.

1.2.3 Importance of ambient temperature and relative humidity

In a numerical prediction Cortella [6] showed that the indoor environment in which display cases operated significantly affected the performance of air curtain. Faramarzi and Kemp [12] experimentally tested several the refrigerated display cabinets subject to different relative humidities and noted that the higher indoor temperature and relative humidity yielded an increase in the case cooling loads for the display cases. In a combined CFD & experimental DPIV study, Navaz et al. [2] found that the discharge average temperature exhibited a relatively slight effect on the flowfield structure in the cabinet. Combined experimental measurement and numerical prediction carried out by Howell et al. [13] showed that the sensible heat transfer was directly proportional to the temperature difference across the air curtain. Recently, Chen & Yuan [4] experimentally demonstrated that the air temperature rise between the discharge and return grilles was slightly affected by the change in the relative humidity of the ambient air. As the ambient temperature increases at a constant relative humidity, the air humidity ratio also increases and hence the latent heat transfer across the air curtain increases with infiltration. Howell [14] developed a numerical procedure to evaluate the effects of relative humidity on the energy performance of refrigerated display cabinets and showed that a decrease in the store relative humidity from 55% to 35% would reduce the open display case energy consumption by 29%.

1.2.4 Effects of discharge air velocity

The total heat transfer through an air curtain was found to be directly proportional to the initial jet velocity [11, 15]. By comparing the CFD and experimental results, Navaz et al. [2] noted that a small air discharge velocity still could entrain the ambient air and a less stable air curtain would break up before

reaching the bottom section of the cabinet. Cortella et al. [1] used a Large Eddy Simulation (LES) turbulence model to predict a two-curtain display case. They found that the most stable flow configuration in the cabinet was obtained when the inner air curtain had a lower velocity. Besides, in combined CFD prediction and experimental measurement Navaz et al. [3] noted that the entrained air flow rate was a function of the turbulence intensity and Reynolds number of the air flow at the discharge grille (based on the discharge grille width). For a high Re at DAG (discharge air grille) the air entrainment rate increased with the turbulence intensity at the DAG. When Re is between 3,200 and 3,400 a minimum entrainment rate is obtained, and at this Re range the air curtain momentum stays nearly intact. Cui & Wang [16] used a commercial software FLUENT to predict the transport processes in a cabinet and introduced a parameter, UI , to describe the uniformity of the air velocity distribution at the discharge grille. A low inlet UI value is preferred in air energy-efficient design for a display case. Chen & Yuan [4] found that when Re was raised from 4100 to 4500 experimentally, the temperature inside the cabinet decreased roughly 1-1.5 °C, and the cabinet temperature was more uniform. Besides, the temperature difference between the discharge and return air is smaller.

Axell and Fahlen [17] carried out experimental measurement and numerical simulation and argued that a relatively small discharge velocity should be recommended in designing the air curtain of a display case. However, a small discharge velocity would possess insufficient initial momentum to prevent the invading of the warm moist air from the outside.

1.2.5 Effects of air flow from the perforated back panels

It was suggested by Navaz et al. [3] and Chen and Yuan [4] that the air flow from the perforated back panels not only provided air curtain stability by reducing the entrained warm ambient air, but also helped the air temperature in the case to

immediately stabilize after any intrusion. Navaz et al. [3] indicated that any intrusion could cause the warm air to penetrate into the lower shelves and became stagnant there. In an experimental investigation Chen & Yuan [4] tested different perforation densities and found that the heat load dropped slightly for an increase in the perforation density.

1.2.6 Effects of discharge width and length of air curtain and jet turbulence intensity

The ratio of the opening height H of a cabinet to the width b_j of the discharge jet was also noted to be an important factor in influencing the performance of air curtains [10, 18, 19]. Chen & Yuan [4] and Besbes et al. [19] showed that as the H/b_j ratio was decreased, the higher energy efficiency was obtained and the critical Richardson number was higher. The flow pattern and heat transfer characteristics of the air curtain could be affected significantly by the value of the H/b_j ratio [4, 10, 21, 22]. Axell & Fahlen [17] manifested that the air flow in the air curtain could be divided into a transition, a fully developed and a recovery regions. Besides, the flow rate was constant in the transition region. In the fully developed region, the air flow slows down. While in the recovery region, the air velocity profile and flow rate depend on the design of the return grille. Loerke and Nagib [20] used a honeycomb to reduce the turbulence intensity. A largely unidirectional flow at the discharge was obtained by using a honeycomb to reduce the transverse fluctuating velocity. Howell et al. [13] noted that the initial turbulence intensity ranging from 0% to 7% exhibited strongest effects on the heat transfer. However, for the turbulence intensity exceeding 8 to 10%, the initial turbulence shows little influence on the total heat transfer through the air curtain. Navaz et al. [3] indicated that the turbulence intensity at the air discharge, measured by DPIV and laser Doppler velocimetry (LDV), reached a maximum at the boundary between the static ambient air and air

curtain and the interfaces between the inner curtain and outer curtain. Besides, the increasing turbulence kinetic energy could subsequently increase the turbulence intensity and entrainment rate. Van and Howell [18] also showed that the air curtain length y_l was dependent on the initial turbulent intensity T_i . They proposed a relation $y_l = (5.39 - 0.266T_i) b_j$. Moreover, the length of the initial region of the air curtain decreases with an increase in the turbulence intensity due to the increasing mixing.

1.3 Objective of Present Study

The above literature review clearly indicates that a better design of refrigerated display cabinets is still an important goal to the refrigeration industry. Minimizing the infiltration of the warm and humid outside air into the cabinets through improving the performance of air curtains is therefore essential in this design. In the present study a two-dimensional numerical simulation will be conducted to explore the detailed momentum, heat and mass transfer processes in an open vertical refrigerated display case. Attention will be focused on how the parameters associated the air curtain affect the transport processes in the display case and hence the performance of the cabinet.

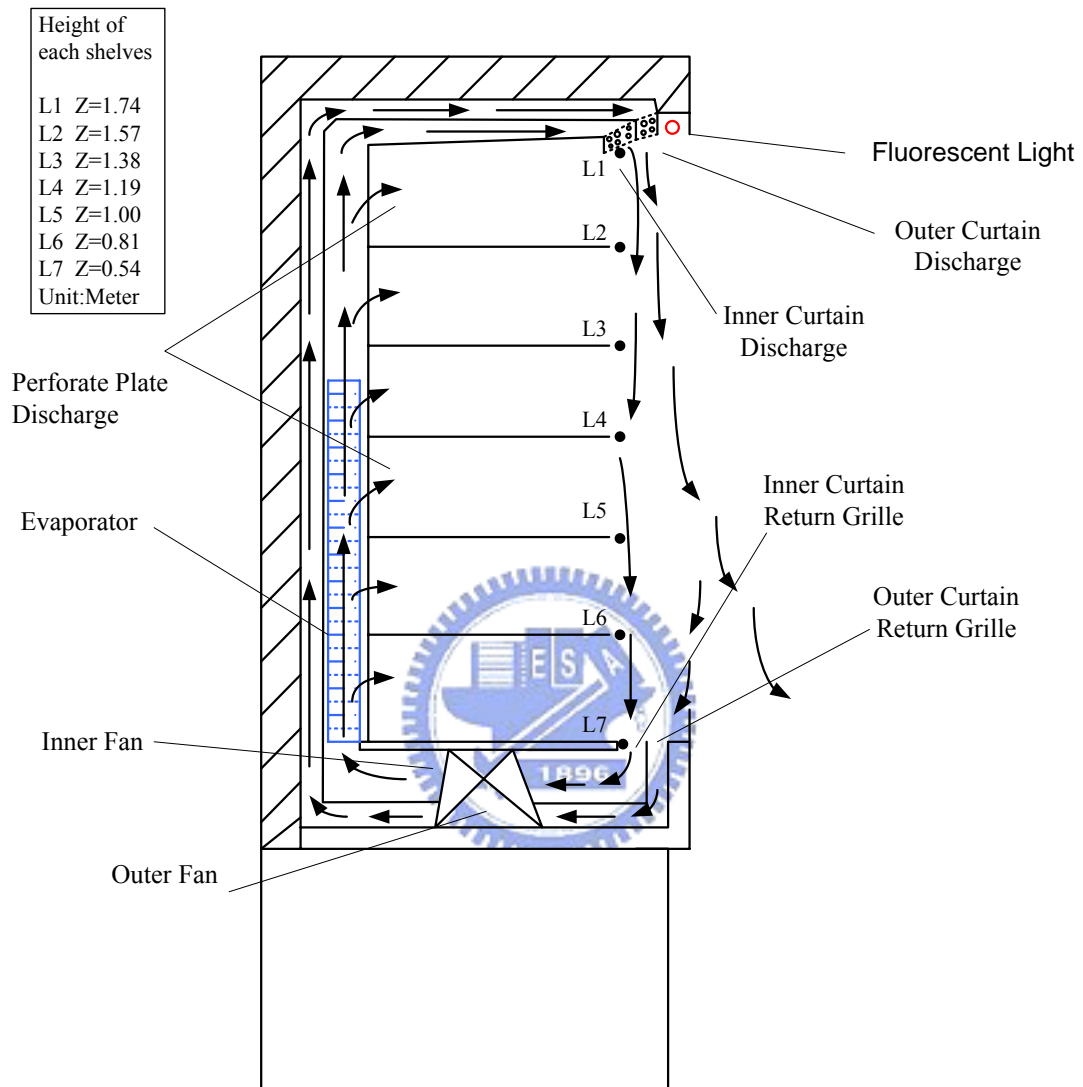


Fig. 1.1 Schematic diagram of a multi-deck open refrigerated display case

CHAPTER 2

MATHEMATICAL FORMULATION

The physical model adopted here and the governing equations used to numerically predict the transport processes in a vertical refrigerated display case are described in this chapter.

2.1 Physical Model

The simplifying physical model for momentum, heat and mass transfer in a vertical refrigerated display case adopted here is a two-dimensional vertical downward cold air jet flowing over the open surface of a vertical open cavity standing in a store, as schematically shown in Fig. 2.1. In order to avoid the boundary conditions in the surrounding to affect our numerical results, the upper and left ambient surroundings are respectively placed at $z = 3.30$ m and $x = 4.61$ m, far from the open cavity. At the top and bottom of the cavity there are discharge and return air zones adjacent to the ambient. Initially, the flows in the case and surrounding are assumed to be stationary, isothermal at the same temperature T_{amb} and iso-solutal at the same water vapor concentration w_{1a} . Then at time $t \geq 0$ a cold air jet is introduced from the discharge grille of the cabinet and injects vertically downwards over the open cavity. At the air discharge the jet flow is assumed to be at a uniform speed V_j and at a lower uniform temperature T_j and uniform relative humidity ϕ_j . The width of the jet is b_j . Meanwhile, at time $t = 0$ we assume that the temperature of the inner vertical plate of the case is suddenly lowered to a uniform value T_c and maintained at this level thereafter. In the mean time, the upper plate and bottom plate of the cavity is kept adiabatic for $t \geq 0$, except at the discharge and return grilles of the cavity. In the present computation we assume $T_j =$

T_c . The air flow at the steady state long after the jet discharged into the cavity is numerically predicted. In this study the size of the cavity is chosen to be 1.2-m in height and 0.57-m in depth. Note that in the present numerical simulation the computation domain surrounding the cavity is chosen to be large enough to reduce the effects of the store size on the flow in the cavity. The ambient is assumed at a uniform temperature T_{amb} and uniform relative humidity ϕ_{amb} for $t \geq 0$.

2.2 Assumptions and Governing Equations

To simplify the computation, the following assumptions are made:

- (1) Flow is two-dimensional, turbulent and incompressible.
- (2) Thermal radiation is neglected.
- (3) Heat conduction in the wall of the cavity and grilles are neglected in the computation. Besides, heat capacity effects associated with the cavity wall and the grilles are negligible.
- (4) The thickness of the cavity wall is very small compared with the cavity height and depth.
- (5) Neglect the viscous dissipation effect.
- (6) $g_x = 0$, $g_z = -g$
- (7) The pressure gradient and body force terms in the momentum equations are:

$$-\partial \bar{p} / \partial z - \rho g .$$

By using the equation of state for ideal gas mixture and assuming a small temperature difference and a low level of water vapor concentration in the flow, the density variation in the air flow can be approximated by Boussinesq approximation as

$$\frac{(\rho_0 - \rho)}{\rho} = \frac{(T - T_0)}{T_0} + \left(\frac{M_a}{M_v} - 1 \right) (w_1 - w_{1_0}) . \quad (2.1)$$

Where ρ_0 is the mixture density evaluated at the referenced temperature T_0 and concentration w_{10} , and the referenced conditions are referred to the air surrounding. Moreover, M_a and M_v are the molecular weights of air and water vapor, respectively.

With a dynamic pressure \bar{p}_m defined as $\bar{p}_m = \bar{p} - \rho g z$, the pressure gradient and body force can be combined so that $-\partial\bar{p}/\partial z - \rho g$ is rewritten as $-\partial\bar{p}_m/\partial z + \beta_t(T - T_{amb}) + \beta_m(w_1 - w_{1_{amb}})$. Here β_t and β_m are respectively the volumetric coefficients of thermal and solutal expansion,

$$\beta_t \equiv -\frac{1}{\rho_0} \left(\frac{\partial \rho}{\partial T} \right)_{w_1, p} \quad (2.2)$$

$$\beta_m \equiv -\frac{1}{\rho_0} \left(\frac{\partial \rho}{\partial w_1} \right)_{T, p} = \left[\frac{M_a}{M_v} - 1 \right] \quad (2.3)$$

The concentration buoyancy force needs to be taken into account here due to the presence of the density variation with the non-uniform species concentration in the flow. Note that the buoyancy force resulting from the concentration difference may assist or oppose the thermal buoyancy force resulting from the temperature variation in the fluid depending on that the concentration expansion coefficient β_m is positive or negative. In the present study, we have an adding buoyancy force for the open cavity flow since $M_a > M_v$ (i.e. the buoyancy ratio $N > 0$). Note that both the thermal and solutal buoyancies tend to induce a counterclockwise flow recirculation in the cavity, which is stronger than the pure thermal buoyancy driven flow. A combined Grashof number $GR = Gr_t + (Pr/Sc)^{1/2} Gr_m$ was proposed to character the combined buoyancy effect [23]. But the air jet from the discharge grille can entrain

the air in the cavity to move in a clockwise direction through the viscous shearing effect.

According to Boussinesq's proposition (1877), the Reynolds stress in a turbulent flow can be approximately related to the gradients of the mean flow and turbulent kinetic energy as

$$\tau_{ij} = -\rho \overline{u'_i u'_j} = \rho \nu_t \left(\frac{\partial \bar{u}_i}{\partial x_j} + \frac{\partial \bar{u}_j}{\partial x_i} \right) - \frac{2}{3} \rho \bar{K} \cdot \delta_{ij} \quad (2.4)$$

where ν_t is called the turbulent or eddy viscosity, \bar{K} is called the kinetic energy of the turbulence $\bar{K} = \frac{1}{2}(\overline{u^2} + \overline{v^2} + \overline{w^2})$ and $\delta_{ij} = 0$ if $i \neq j$. When adopting the two-equation $\bar{K} - \varepsilon$ model, the turbulent eddy viscosity for momentum can be expressed by \bar{K} and ε as $\nu_t = C_\mu \bar{K}^2 / \varepsilon$. The turbulent Prandtl number and turbulent Schmidt number are chosen to be $Pr_t = \rho \nu_t C_p / k_t = 1$ and $Sc_t = \nu_t / D_t = 1$.

Under these assumptions the basic equations describing the time-average turbulent flow in the open cavity are

Continuity equation-

$$\frac{\partial(\rho \bar{u})}{\partial x} + \frac{\partial(\rho \bar{w})}{\partial z} = 0 \quad (2.5)$$

x - momentum equation-

$$\rho \left[\bar{u} \frac{\partial \bar{u}}{\partial x} + \bar{w} \frac{\partial \bar{u}}{\partial z} \right] = -\frac{\partial \bar{p}_m}{\partial x} + \left[\frac{\partial}{\partial x} \left((\mu + \mu_t) \frac{\partial \bar{u}}{\partial x} \right) + \frac{\partial}{\partial z} \left((\mu + \mu_t) \frac{\partial \bar{u}}{\partial z} \right) \right] \quad (2.6)$$

z - momentum equation-

$$\rho \left[\bar{u} \frac{\partial \bar{w}}{\partial x} + \bar{w} \frac{\partial \bar{w}}{\partial z} \right] = -\frac{\partial \bar{p}_m}{\partial z} + \left[\frac{\partial}{\partial x} \left((\mu + \mu_t) \frac{\partial \bar{w}}{\partial x} \right) + \frac{\partial}{\partial z} \left((\mu + \mu_t) \frac{\partial \bar{w}}{\partial z} \right) \right] + \rho_0 g \beta_t (T - T_0) + \rho_0 g \beta_m (w_1 - w_{10}) \quad (2.7)$$

Energy equation-

$$\rho c_p \left[\bar{u} \frac{\partial \bar{T}}{\partial x} + \bar{w} \frac{\partial \bar{T}}{\partial z} \right] = \left[\frac{\partial}{\partial x} \left((k + k_t) \frac{\partial \bar{T}}{\partial x} \right) + \frac{\partial}{\partial z} \left((k + k_t) \frac{\partial \bar{T}}{\partial z} \right) \right] \quad (2.8)$$

Species diffusion equation-

$$\rho \left(\bar{u} \frac{\partial \bar{w}_1}{\partial x} + \bar{w} \frac{\partial \bar{w}_1}{\partial z} \right) = \left[\frac{\partial}{\partial x} \left(\rho(D + D_t) \frac{\partial \bar{w}_1}{\partial x} \right) + \frac{\partial}{\partial z} \left(\rho(D + D_t) \frac{\partial \bar{w}_1}{\partial z} \right) \right] \quad (2.9)$$

The above equations are subjected to the following boundary conditions:

Boundary I-air discharge grille. At the air jet discharge, flow is at uniform speed V_j , temperature T_j , and water vapor concentration w_{1j}

$$\bar{u} = 0, \bar{w} = -V_j, \bar{T} = T_j - T_c, \bar{w}_1 = w_{1j} \text{ at } z = H+B_0=1.74 \text{ m}; \quad (2.10)$$

Boundary II- inner vertical plate of the cavity. At the inner vertical plate with perforation density $d_p = 0$ we have no-slip condition and an isothermal condition is imposed. Besides, the plate is impermeable. Thus

$$\bar{u} = \bar{w} = 0, \bar{T} = T_c, \frac{\partial \bar{w}_1}{\partial x} = 0 \text{ at } x = 0; \quad (2.11)$$

For the inner vertical plate with perforation, flow is at perforation density d_p , uniform velocity V_p , temperature T_c and water vapor concentration w_{1c}

$$\bar{u} = V_p, \bar{w} = 0, \bar{T} = T_c, \bar{w}_1 = w_{1c} \text{ at } x = 0; \quad (2.12)$$

Boundary III- upper and bottom plates of the cavity. At the upper and bottom

plates of the cavity we have adiabatic and no-slip conditions. The plates are also impermeable. Hence

$$\bar{u} = \bar{w} = 0, \frac{\partial \bar{T}}{\partial z} = 0, \frac{\partial \bar{w}_1}{\partial z} = 0 \text{ at } z = B_b = 0.54 \text{ m and } z = B_c = 1.74 \text{ m}; \quad (2.13)$$

Boundary IV- return grille of the air curtain. At the return grille of the air curtain, the velocity, temperature and concentration gradients are assumed to be very small,

$$\bar{u} = 0, \frac{\partial \bar{w}}{\partial z} = \frac{\partial \bar{T}}{\partial z} = \frac{\partial \bar{w}_1}{\partial z} = 0 \text{ at } z = B_b = 0.54 \text{ m}; \quad (2.14)$$

Boundary V- surrounding boundary I- At the upper boundary of the surrounding, the gradient of the air velocity is very small and the air is at ambient temperature and concentration,

$$\frac{\partial \bar{u}}{\partial z} = \frac{\partial \bar{w}}{\partial z} = 0, \bar{T} = T_{amb}, \bar{w}_1 = \bar{w}_{1a} \text{ at } z \rightarrow \infty; \quad (2.15)$$

Boundary VI- surrounding boundary II- At the outer surrounding horizontally far from the cavity the gradient of the velocity is very small, and the pressure and temperature are assumed at the ambient values,

$$\frac{\partial \bar{u}}{\partial x} = \frac{\partial \bar{w}}{\partial x} = 0, \bar{p} = P_{amb}, \bar{T} = T_{amb}, \bar{w}_1 = w_{1a}, \text{ at } x \rightarrow \infty; \quad (2.16)$$

Boundary VII- ground boundary- At the ground the flow is subjected to the adiabatic, impermeable and no-slip conditions,

$$\bar{u} = \bar{w} = 0, \frac{\partial \bar{T}}{\partial z} = 0, \frac{\partial \bar{w}_1}{\partial z} = 0 \text{ at } z=0 \text{ for } x \geq L = 0.57 \text{ m}; \quad (2.17)$$

Boundary VIII- other solid boundary- At the other solid boundary the flow is subjected to the adiabatic, impermeable and no-slip conditions,

Region 1- vertical solid surface


$$\bar{u} = \bar{w} = 0, \frac{\partial \bar{T}}{\partial x} = 0, \frac{\partial \bar{w}_1}{\partial x} = 0 \text{ at } \begin{cases} x = L, \text{ for } 0 \leq z \leq B_b \\ x = L, \text{ for } (H + B_b) \leq z \leq (H + B_b + B_c) \\ x = 0m, \text{ for } z \geq (H + B_b + B_c) \end{cases}; \quad (2.18)$$

Region 2- horizontal solid surface

$$\bar{u} = \bar{w} = 0, \frac{\partial \bar{T}}{\partial z} = 0, \frac{\partial \bar{w}_1}{\partial z} = 0 \text{ at } z = H + B_b + B_c, \text{ for } 0 \leq x \leq L; \quad (2.19)$$

These hydrodynamic and thermal boundary conditions are specified in Fig. 2.2.

Using the following non-dimensional variables

$X = \frac{x}{H}$		$U = \frac{\bar{u}}{V_j}$
$P = \frac{\bar{p}_m}{\rho_o \cdot V_j^2}$		$\Theta = \frac{\bar{T} - T_C}{T_{amb} - T_C}$
$W_1 = \frac{w_{1a} - \bar{w}_1}{w_{1a} - w_{1j}}$	$Pr = \frac{\nu_0}{\alpha_0} = \frac{C_{p0} \mu_0}{k_0}$	$Gr_t = \frac{g \beta_t (T_{amb} - T_j) H^3}{\nu_0^2}$
$Re_b = \frac{V_j b_j}{\nu_0}$	$Sc = \frac{\nu_0}{D_0}$	$N = \frac{\beta_m (w_{1a} - w_{1j})}{\beta_t (T_{amb} - T_j)}$
$A = \frac{H}{b_j}$	$\lambda_\rho = \frac{\rho}{\rho_0}$	$\lambda_\mu = \frac{\mu}{\mu_0}$
$\lambda_{cp} = \frac{C_p}{C_{p0}}$	$\lambda_k = \frac{k}{k_0}$	$\lambda_D = \frac{D}{D_0}$
$\lambda_{\mu_t} = \frac{\mu_t}{\mu_0}$	$\lambda_{k_t} = \frac{k_t}{k_0}$	$\lambda_{D_t} = \frac{D_t}{D_0}$
$Pr_t = \frac{\mu_t C_p}{k_t}$	$Sc_t = \frac{\mu_t}{\rho D_t}$	$Gr_m = \frac{g \beta_m (\bar{w}_{1a} - \bar{w}_j) H^3}{\nu_0^2}$

The basic flow equations can be written in dimensionless form as

Continuity equation-

$$\frac{\partial(\lambda_\rho U)}{\partial X} + \frac{\partial(\lambda_\rho W)}{\partial Z} = 0 \quad (2.20)$$

x- momentum equation-

$$\begin{aligned} & \lambda_\rho \left(U \frac{\partial U}{\partial X} + W \frac{\partial U}{\partial Z} \right) \\ &= -\frac{\partial P}{\partial X} + \frac{1}{Re_b A} \left[\frac{\partial}{\partial X} \left((\lambda_\mu + \lambda_{\mu_i}) \frac{\partial U}{\partial X} \right) + \frac{\partial}{\partial Z} \left((\lambda_\mu + \lambda_{\mu_i}) \frac{\partial U}{\partial Z} \right) \right] \end{aligned} \quad (2.21)$$

z- momentum equation-

$$\begin{aligned} & \lambda_\rho \left(U \frac{\partial W}{\partial X} + W \frac{\partial W}{\partial Z} \right) \\ &= -\frac{\partial P}{\partial Z} + \frac{1}{Re_b A} \left[\frac{\partial}{\partial X} \left((\lambda_\mu + \lambda_{\mu_i}) \frac{\partial W}{\partial X} \right) + \frac{\partial}{\partial Z} \left((\lambda_\mu + \lambda_{\mu_i}) \frac{\partial W}{\partial Z} \right) \right] \\ &+ \frac{1}{(Re_b)^2 \cdot A^2} \cdot Gr \cdot (\Theta + NW_1) \end{aligned} \quad (2.22)$$

Energy equation-

$$\begin{aligned} & \lambda_\rho \lambda_{cp} \left(U \frac{\partial \Theta}{\partial X} + W \frac{\partial \Theta}{\partial Z} \right) \\ &= \frac{1}{Pr Re_b A} \left[\frac{\partial}{\partial X} \left((\lambda_k + \lambda_{k_i}) \frac{\partial \Theta}{\partial X} \right) + \frac{\partial}{\partial Z} \left((\lambda_k + \lambda_{k_i}) \frac{\partial \Theta}{\partial Z} \right) \right] \end{aligned} \quad (2.23)$$

Species diffusion equation

$$\begin{aligned} & \lambda_\rho \left(U \frac{\partial W_1}{\partial X} + W \frac{\partial W_1}{\partial Z} \right) \\ &= \frac{1}{Re_b Sc A} \left[\frac{\partial}{\partial X} \left(\lambda_\rho (\lambda_D + \lambda_{D_i}) \frac{\partial W_1}{\partial X} \right) + \frac{\partial}{\partial Z} \left(\lambda_\rho (\lambda_D + \lambda_{D_i}) \frac{\partial W_1}{\partial Z} \right) \right] \end{aligned} \quad (2.24)$$

The above non-dimensional governing equations are subjected to the following

boundary conditions:

Boundary I-air discharge grille. At the air jet discharge, flow is at uniform speed V_j , temperature T_j , and concentration W_{1j}

$$U = 0, W = -1, \Theta = 0, \text{ and } W_1 = 1 \text{ at } Z = (H+B_b) / H = 1.45; \quad (2.25)$$

Boundary II- inner vertical plate of the cavity. At the inner vertical plate with perforation density $d_p = 0$

$$U = W = 0, \Theta = 0, \frac{\partial W_1}{\partial X} = 0 \text{ at } X=0; \quad (2.26)$$

For the condition with perforation density d_p

$$U = V_p/V_j, W = 0, \Theta = 0, W_1 = 1 \text{ at } X=0 \quad (2.27)$$

Boundary III- upper and bottom plates of the cavity. At the upper and bottom plates of the cavity

$$U = W = 0, \frac{\partial \Theta}{\partial Z} = 0, \frac{\partial W_1}{\partial Z} = 0 \text{ at } Z = \frac{B_b}{H} \text{ and } \frac{H+B_b}{H}; \quad (2.28)$$

Boundary IV- return grilles of the air curtain. At the return grille of the air curtain, the velocity, temperature and concentration gradients are assumed to be very small,

$$U = 0, \frac{\partial W}{\partial Z} = \frac{\partial \Theta}{\partial Z} = \frac{\partial W_1}{\partial Z} = 0 \text{ at } Z = \frac{B_b}{H} \quad (2.29)$$

Boundary V- surrounding boundary I- At the upper boundary of the outer surrounding

$$\frac{\partial U}{\partial Z} = \frac{\partial W}{\partial Z} = 0, \Theta = 1, W_1 = 0 \text{ at } Z \rightarrow \infty; \quad (2.30)$$

Boundary VI- surrounding boundary II- At the outer surrounding horizontally far from the cavity

$$P = 0, \Theta = 1, W_1 = 0, \frac{\partial U}{\partial X} = \frac{\partial W}{\partial X} = 0 \text{ at } X \rightarrow \infty; \quad (2.31)$$

Boundary VII- ground boundary- at the ground boundary we have adiabatic and no-slip conditions,

$$U = W = 0, \frac{\partial \Theta}{\partial Z} = 0, \frac{\partial W_1}{\partial Z} = 0 \text{ at } Z=0 \text{ for } X \geq \frac{L}{H}; \quad (2.32)$$

Boundary VIII- other solid boundary- at the other solid boundary the flow is subjected to the adiabatic, impermeable and no-slip conditions,

Region 1- vertical solid surface

$$U = W = 0, \frac{\partial \Theta}{\partial X} = 0, \frac{\partial W_1}{\partial X} = 0 \text{ at } \begin{cases} X = \frac{L}{H}, \text{ for } 0 \leq Z \leq \frac{B_b}{H} \\ X = \frac{L}{H}, \text{ for } \frac{H + B_b}{H} \leq Z \leq \frac{H + B_b + B_c}{H} \\ X = 0, \text{ for } Z \geq \frac{H + B_b + B_c}{H} \end{cases}; \quad (2.33)$$

Region 2- horizontal solid surface

$$U = W = 0, \frac{\partial \Theta}{\partial Z} = 0, \frac{\partial W_1}{\partial Z} = 0 \text{ at } Z = \frac{H + B_b + B_c}{H}, \text{ for } 0 \leq X \leq \frac{L}{H}; \quad (2.34)$$

The transport equations for k and ε employed in the present study are

Turbulence kinetic energy equation-

$$\begin{aligned}
& \bar{u} \frac{\partial \bar{K}}{\partial x} + \bar{v} \frac{\partial \bar{K}}{\partial z} - \frac{\partial}{\partial x} \left[\frac{\nu_t}{\sigma_k} \frac{\partial \bar{K}}{\partial x} \right] - \frac{\partial}{\partial z} \left[\frac{\nu_t}{\sigma_k} \frac{\partial \bar{K}}{\partial z} \right] \\
& = \nu_t \left[\left(\frac{\partial \bar{u}}{\partial z} \right)^2 + \left(\frac{\partial \bar{u}}{\partial x} \cdot \frac{\partial \bar{u}}{\partial z} \right) + \left(\frac{\partial \bar{w}}{\partial x} \cdot \frac{\partial \bar{w}}{\partial z} \right) + \left(\frac{\partial \bar{w}}{\partial x} \right)^2 \right] - \varepsilon
\end{aligned} \tag{2.35}$$

where ε and ν_t are respectively the dissipation rate of the turbulent kinetic energy and momentum eddy diffusivity.

Turbulent dissipation equation-

$$\begin{aligned}
& \bar{u} \frac{\partial \varepsilon}{\partial x} + \bar{v} \frac{\partial \varepsilon}{\partial y} - \frac{\partial}{\partial y} \left[\frac{\nu_t}{\sigma_\varepsilon} \frac{\partial \varepsilon}{\partial y} \right] - \frac{\partial}{\partial x} \left[\frac{\nu_t}{\sigma_\varepsilon} \frac{\partial \varepsilon}{\partial x} \right] \\
& = \nu_t C_{1\varepsilon} \frac{\varepsilon}{\bar{K}} \left[\left(\frac{\partial \bar{u}}{\partial z} \right)^2 + \left(\frac{\partial \bar{u}}{\partial x} \cdot \frac{\partial \bar{u}}{\partial z} \right) + \left(\frac{\partial \bar{w}}{\partial x} \cdot \frac{\partial \bar{w}}{\partial z} \right) + \left(\frac{\partial \bar{w}}{\partial x} \right)^2 \right] - C_{2\varepsilon} \frac{\varepsilon^2}{\bar{K}}
\end{aligned} \tag{2.36}$$

where $C_\mu, C_{1\varepsilon}, C_{2\varepsilon}, \sigma_k$ and σ_ε are five dimensionless empirical constants. The recommended values [23] for these empirical constants are $C_\mu = 0.09, C_{1\varepsilon} = 1.44, C_{2\varepsilon} = 1.92, \sigma_k = 1.0,$ and $\sigma_\varepsilon = 1.3$. The initial and boundary conditions for the above two equations require some discussion.

Since there is no-slip condition at the solid surface, physically we have $\bar{K} = 0$ and $\varepsilon = 0$ at all solid boundaries. At the air curtain discharge, a 5 % turbulence intensity is chosen to represent the disturbance due to a uniform flow through a rectified honeycomb structure. For the air return grille, the small vertical gradients for \bar{K} and ε are assumed, $\partial \bar{K} / \partial z = \partial \varepsilon / \partial z = 0$. Small gradients in the vertical and horizontal directions are imposed at the upper surrounding and outer surrounding, which are $\partial \bar{K} / \partial z = \partial \varepsilon / \partial z = 0$ and $\partial \bar{K} / \partial x = \partial \varepsilon / \partial x = 0$, respectively. It is a well-known fact that in the near-wall region using the no-slip condition in the $K - \varepsilon$ model adopted here provides unsatisfactory results. An alternative and widely employed way to overcome this deficiency is to introduce the damping

effects through the wall functions. The wall function model can be used only in the near wall region and it uses the empirical laws to approach the velocity profile near wall. In the present prediction, the modified wall functions are employed to replace the direct computation of \bar{K} and ε from the transport equations given in Equations (2.31) and (2.32) near the solid boundaries.

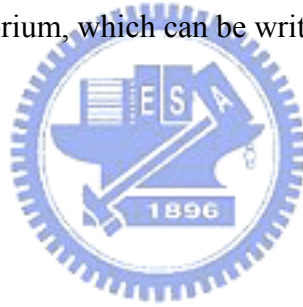
Strictly speaking, it is supposed to be applied to a point up to the dimensionless distance Y^+ ranging from 30 to 130 where $Y^+ = (u_\tau y) / \nu$. The exact Y^+ range in which the wall function is used is automatically determined by the software PHOENICS [25] during the computation. Note that u_τ is the resultant friction velocity, $u_\tau = \sqrt{\tau_0 / \rho}$. Specifically, the following wall functions are employed to a near-wall layer in local equilibrium, which can be written as follows [25]:

$$\frac{U^+}{u_\tau} = \frac{\ln(EY^+)}{\kappa} \quad (2.37)$$

$$K = \frac{u_\tau^2}{\sqrt{C_\mu}} \quad (2.38)$$

$$\varepsilon = \frac{C_\mu^{0.75} \bar{K}^{-1.5}}{\kappa y} \quad (2.39)$$

where U^+ is the non-dimensional centerline velocity, κ is the log-law constant (≈ 0.41), and E is a roughness parameter.



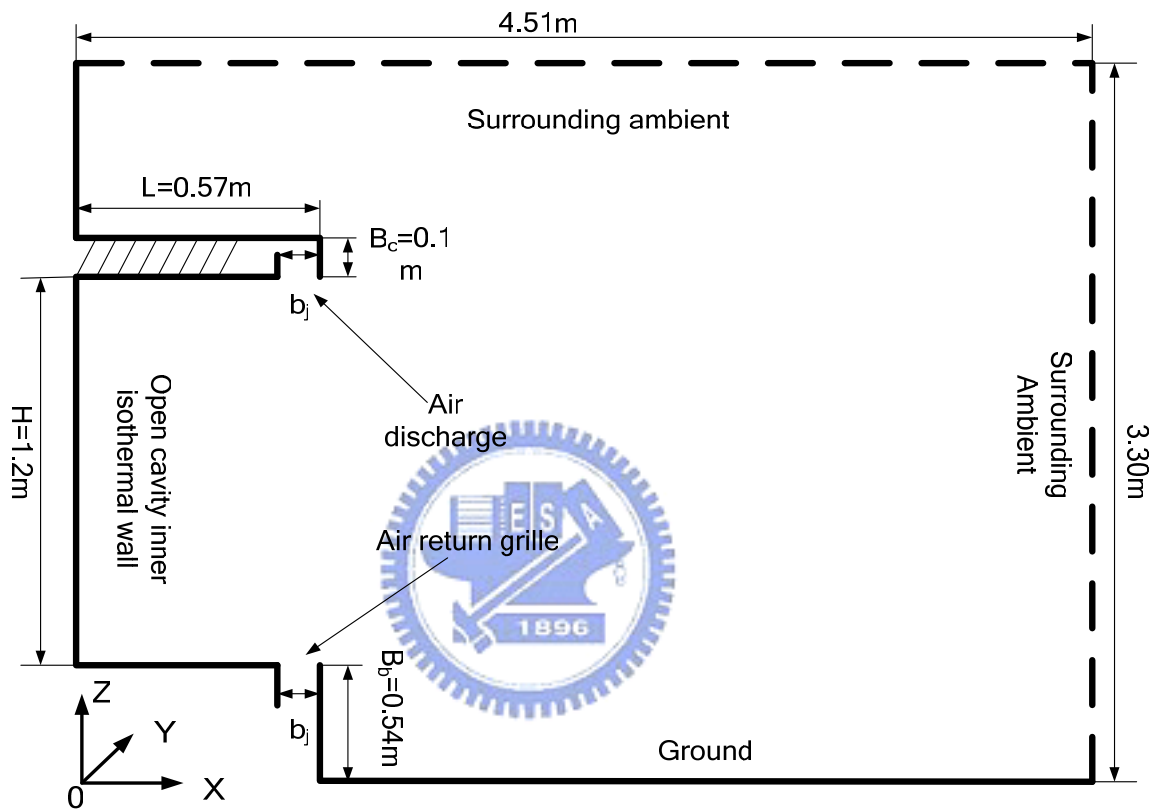


Fig. 2.1 Physical model for a vertical refrigerated display case.

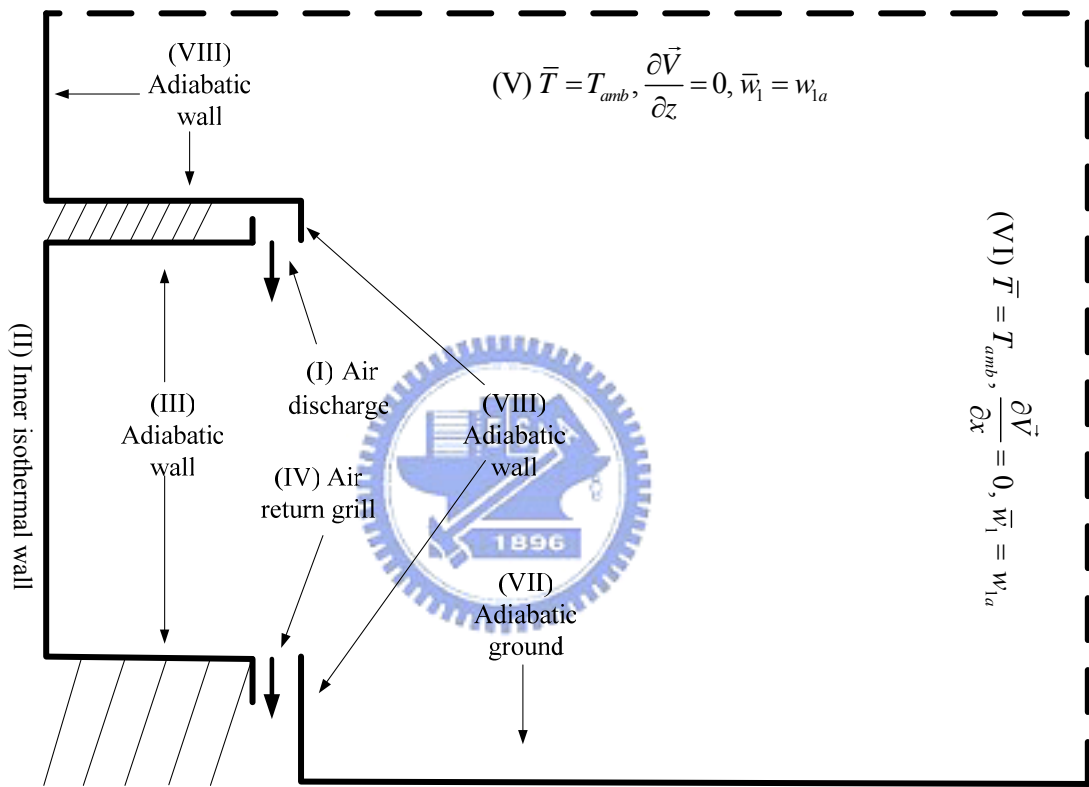


Fig. 2.2 Schematic diagram illustrating the geometry and some boundary conditions.

CHAPTER 3

SOLUTION METHOD

The solution method to be used in the present study and the verification of its applicability to predict the transport processes in the open cavity flow considered here are detailed in this chapter. The grid distribution in the computing domain for this numeral scheme is also verified by comparing the predicted results with the open literature.

3.1 Numerical Scheme and Solution Procedures

The governing differential equations described in Chapter 2 are discretized by the SIMPLE algorithm [24] which applies the finite volume (FV) method to the partial differential equations. In this study, these discretized equations are solved by the commercial software PHOENICS [25], which implements the scheme of SIMPLE with an interactive Windows environment. More specifically, the differential equations are integrated over the chosen individual computational cells during a finite time increment in the present transient formulation. The values of the dependent physical variables are approximated by the hybrid difference method. The thermal and transport properties located at the central node are calculated by means of central average for each cell in the computation domain. For convenience, the general conservation equations are expressed as

$$\frac{1}{\sqrt{g}} \frac{\partial}{\partial t} (\sqrt{g} \rho \phi) + \text{div}(\rho \bar{u} \phi - \Gamma_{\phi} \text{grad} \phi) = s_{\phi} \quad (3.1)$$

where \bar{u} represents u, v or w; ϕ could express any of the dependent variables, like u, w, T and w_1 ; Γ_{ϕ} and s_{ϕ} are respectively the associated diffusion and source

coefficients. Here \sqrt{g} is a metric tensor.

Now Eq. (3.1) can be integrated over a closed surface S valid for an arbitrary control volume \forall to give

$$\frac{d}{dt} \int_{\forall} \rho \phi dV + \int_S (\rho \bar{u} \phi - \Gamma_{\phi} \text{grad} \phi) \cdot d\vec{S} = \int_{\forall} s_{\phi} dV \quad (3.2)$$

where \vec{S} is the surface vector. If \forall and S are respectively taken to be the volume V_p and discrete faces $S_j (j = 1, N_f)$ of a computational cell as that in Fig. 3.1, Eq.

(3.2) becomes

$$\frac{d}{dt} \int_{V_p} \rho \phi dV + \sum_j \int_{S_j} (\rho \bar{u} \phi - \Gamma_{\phi} \text{grad} \phi) \cdot d\vec{S} = \int_{V_p} s_{\phi} dV \quad (3.3)$$

For convenient discussion, the first and second terms on the left hand side of Eq. (3.3) are represented by T_1 and T_2 , respectively. And T_3 represents the right-hand side of Eq. (3.3). Here T_1 is discretised as

$$T_1 \approx \frac{(\rho \phi V)_P^n - (\rho \phi V)_P^o}{\delta t} \quad (3.4)$$

where the subscript ‘‘P’’ in Eq. (3.4) means the node P, and the superscripts ‘‘n’’ and ‘‘o’’ denote the new value and old value, respectively.

The second term T_2 can be separated into convection and diffusion terms by the separate contributions C_j and E_j , respectively. Thus T_2 can be approximated by the average value over each face of the cell as

$$T_2 \approx \sum_j (\rho \bar{u} \phi \cdot \vec{S})_j - \sum_j (\Gamma_\phi \text{grad} \phi \cdot \vec{S})_j \equiv \sum_j C_j - \sum_j E_j \quad (3.5)$$

Upwind differencing is used to approximate the convection term C_j as shown in Fig.

3.2:

$$C_j \equiv (\rho \bar{u} \cdot \vec{S})_j \cdot \phi_p, \quad \text{for } F_j \geq 0 \quad (3.6)$$

$$C_j \equiv (\rho \bar{u} \cdot \vec{S})_j \cdot \phi_{N+}, \quad \text{for } F_j < 0 \quad (3.7)$$

where F_j is defined as $F_j = \rho \bar{u}_j \cdot \vec{S}_j$. And the diffusion term E_j is represented by the face-centred expressions as

$$E_j \approx \Gamma_{\phi,j} \left\{ f'_j (\phi_N - \phi_P) + \left[\bar{\nabla} \phi \cdot \vec{S} - f'_j \bar{\nabla} \phi \cdot \vec{d}_{PN} \right]_j \right\} \quad (3.8)$$

where f'_j is a geometry factor, \vec{d}_{PN} is the vector from P to N, $\Gamma_{\phi,j}$ is the diffusion coefficient at the surface.

Finally, T_3 can be expressed as

$$T_3 \approx s_1 - s_2 \phi_p \quad (3.9)$$

Substitution of the results in Eqs. (3.4)-(3.9) into Eq. (3.3) gives

$$\frac{(\rho \phi V)^n - (\rho \phi V)^o}{\delta t} + \sum \rho \bar{u}_j \cdot \vec{S}_j = 0 \quad (3.10)$$

which can be put in a more compact form as

$$A_p \phi_p^n = \sum_m A_m \phi_m^n + s_1 + B_p \phi_p^o \quad (3.11)$$

where A_m represents the effects of the convection and diffusion and \sum denotes the effects of the overall neighbor nodes shown in Fig. 3.2 for the flux discretisation. Besides, A_p is defined as $\sum_m A_m + s_2 + B_p$ and B_p is equal to $(\rho V)^o / \delta t$.

When implementing the above solution method, the convergence criterion is chosen as

$$C_\phi^k = \sum \left(|B_p^n \phi_p^n| - |B_p^o \phi_p^o| \right) < \text{conservative value} \quad (3.12)$$

We set the conservative values of velocity, pressure and temperature fields all at 0.001 in this study. The simulation procedures are briefly illustrated by a flow chart in Fig. 3.3.

3.2 Verification of Numerical Scheme

The computation domain includes the entire air curtain, cavity and ambient. The above solution method is verified by two typical ways: the grid independence test and comparison with the published computational results.

3.2.1 Grid Test

The grid distribution is frequently an important issue in numerical computation. It affects the efficiency and accuracy of a thermofluid analysis. The grid distribution for numerical simulation of the transport processes in the display cabinet investigated here is shown in Fig. 3.4. The grid number for the jet region is 12×55 and in the space of the display cabinet we place 30×55 grids. We place 132×40 grids for the surrounding region with $x \geq 0$ and $z \geq 1.84$ meters and 90×87 grids for the surrounding region with $x \geq 0.57$ and $0 \leq z \leq 1.84$ meters. For the upper regions with $0 \leq x \leq 0.57$ m and $1.74 \text{ m} \leq z \leq 1.84 \text{ m}$ and bottom region with $0 \leq x \leq 0.57 \text{ m}$ and $0 \leq z \leq 0.54 \text{ m}$ we have 42×7 and 42×25 grids, respectively. Hence a total of

16,764 cells are used in the computation. It should be pointed out that in each region uniform grids are placed. For the cases with $b_j = 0.1$ m, $V_j = 0.3-1.5$ m/s, and $\Delta T = T_{\text{amb}} - T_c = 20$ °C in the absence of mass transfer effects, the computed results using this grid distribution are compared with results computed from the 8,550 and 21,315 cells. Selected results to compare the magnitude of the velocity calculated from these three different grids are shown in Fig. 3.5 at steady state. It is noted that the results from the 16,764 and 21,315 cells are in good agreement. The relative differences in the magnitude of velocity computed from these two grid distributions are less than 1.0%. Besides, we compare the flow pattern, isotherms and iso-concentration lines computed from these three grid distributions in Figs. 3.6, 3.7 and 3.8 for another case with the presence of mass transfer. The predicted vortex flow pattern revealed from the velocity vector maps, isothermal and iso-concentration lines from the 16,764 and 21,315 cells are also in good agreement. Finally, the conduction heat flux and convection heat flux at a chosen vertical line for the same case computed from the three grids are compared in Figs. 3.9 and 3.10. The agreement is also good for the results calculated from the grids with 16,764 and 21,315 cells. Thus the computation model with the 16,764 cells is considered to be suitable in predicting the transport processes in the vertical display cabinet in the present study. Hence the grid distribution with the 16, 764 cells is used in the subsequent computation.

3.2.2 Domain Size Test

The domain size will sometimes affect the numerical results and needs to be tested in the present study. Selected results from the present domain size test are shown in Figs. 3.11-3.13. More specifically, the velocity vector map, isotherms and concentration contours for the case examined above at steady state computed from three different domain sizes are contrasted in Figs. 3.11-3.13. Noted that the results predicted from the domain size of 4.5×3.3 m² are in good agreement with that from

the size of $6 \times 4.61 \text{ m}^2$. Thus the computation model with the domain size $4.61 \times 3.3 \text{ m}^2$ is considered to be suitable in predicting the transport processes in the vertical display cabinet in the present study. Hence the domain size $4.61 \times 3.3 \text{ m}^2$ is used in the subsequent computation.

3.2.3 Verification with Published Results

To further verify the proposed solution method, the present results for some limiting cases are compared with the computational data reported in the literature. This is illustrated in Figs. 3.14 and 3.15 by comparing our predicted steady cavity flow pattern and isotherms with that from Chen and Yuan [10] for the case with $Re_b = 18,371$, $Gr_t = 2.7 \times 10^{10}$ and $Ri_t = 0.2$ without considering the mass transfer in the flow for $H = 2.0 \text{ m}$ and $b_j = 0.1 \text{ m}$. Note that our prediction is in qualitative agreement with the results from Chen and Yuan [10]. Moreover, the steady flow, heat and mass transfer for the limiting case of a vertical square enclosure simultaneously subjected to horizontal temperature and concentration differences predicted from the present model is compared with that from Lai [26] in Figs. 3.16-3.18 for a chosen case. The present results for the steady streamlines, isotherms and iso-concentration lines are in good agreement with that of Lai [26].

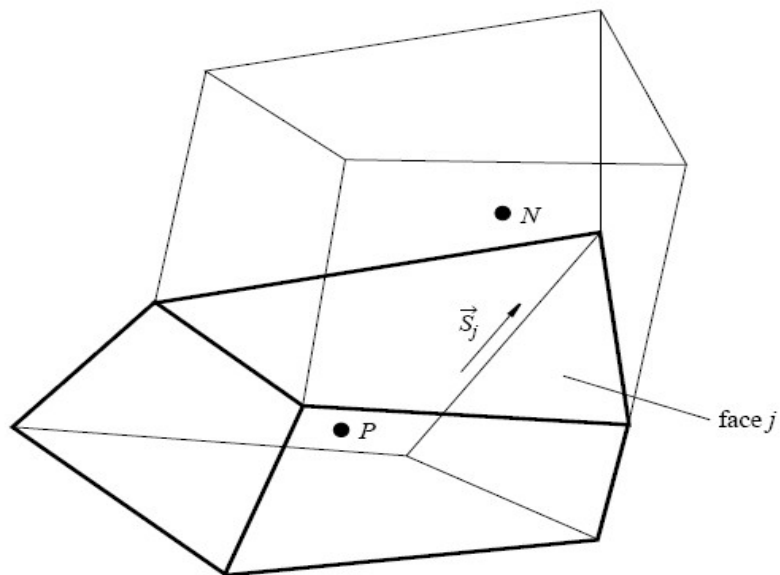


Fig. 3.1 The locations of the centred node P in a typical cell and centred node N in the neighbor cell.

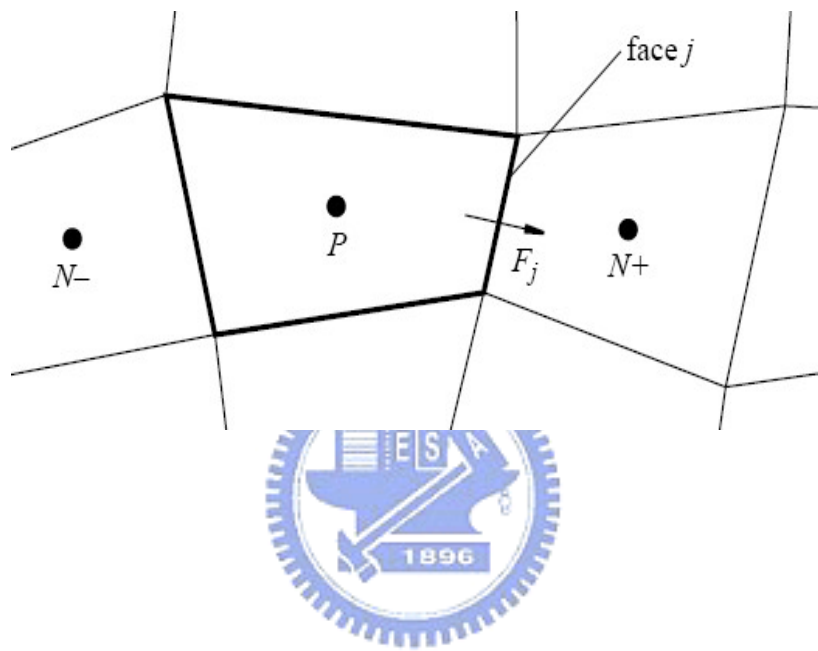


Fig. 3.2 The upwind differencing with node labeling for flux discretization.

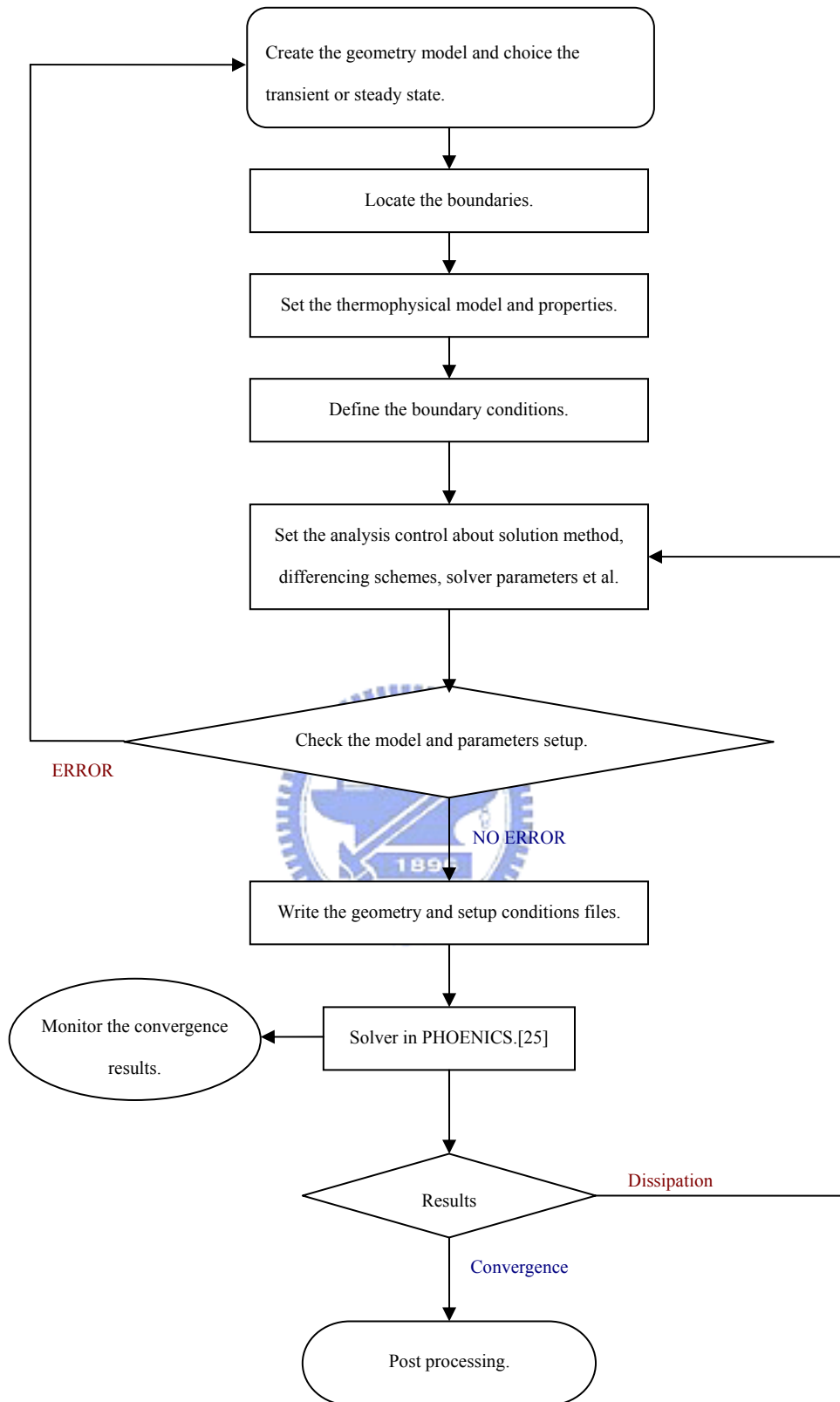


Fig. 3.3 Flow chart for the simulation procedures.

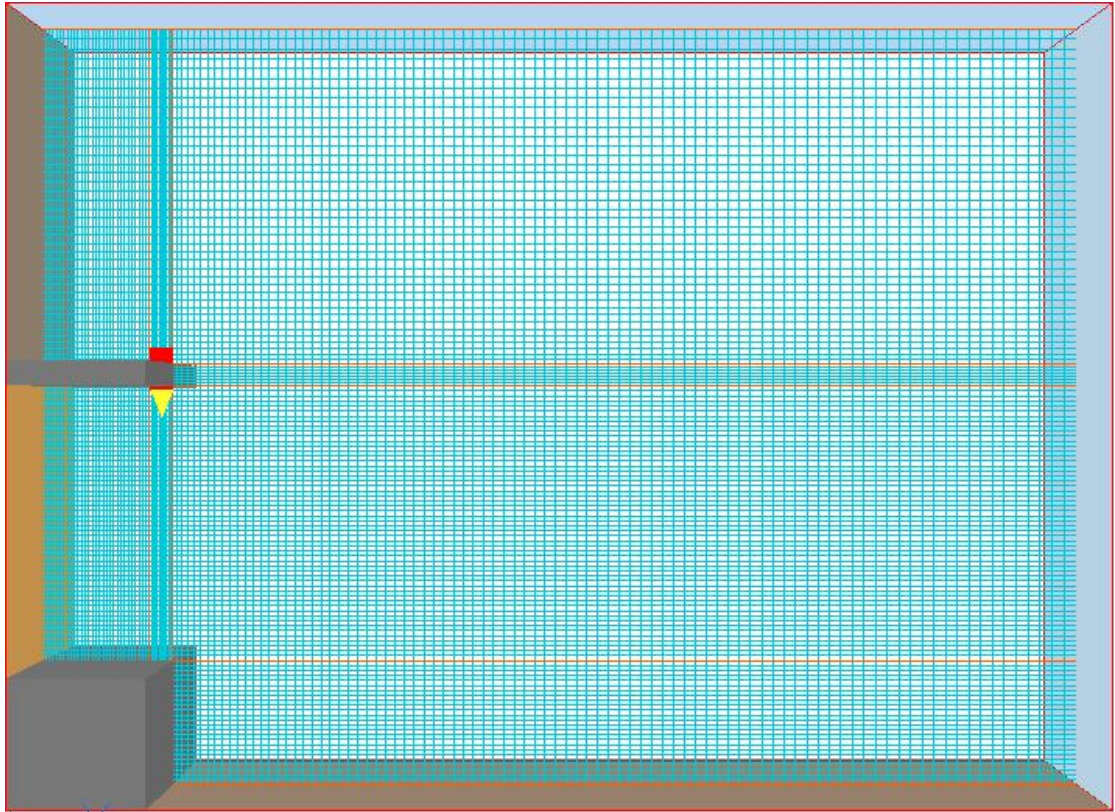


Fig. 3.4 The mesh distribution for the entire computational domain.

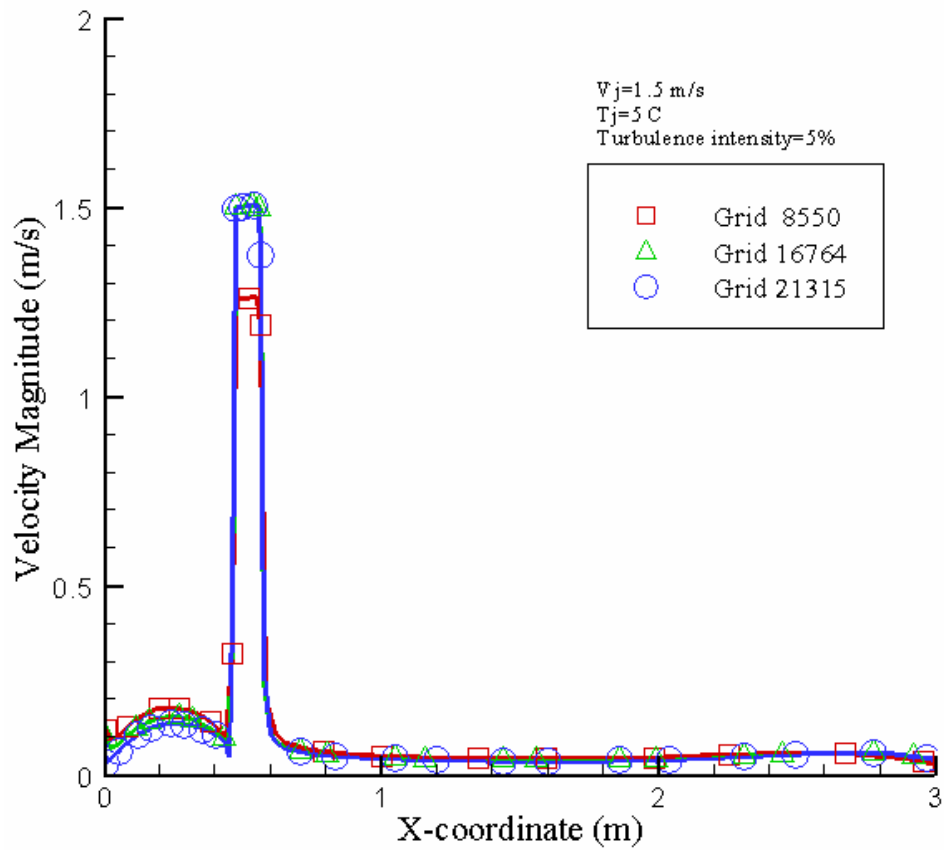


Fig. 3.5 The horizontal variations of the steady velocity magnitude at the selected locations on the line $z = 1.7 \text{ m}$ predicted from three different grids for $b_j = 0.1 \text{ m}$, $V_j = 1.5 \text{ m/s}$, $\Delta T = 20 \text{ }^\circ\text{C}$ and $N = 0$.

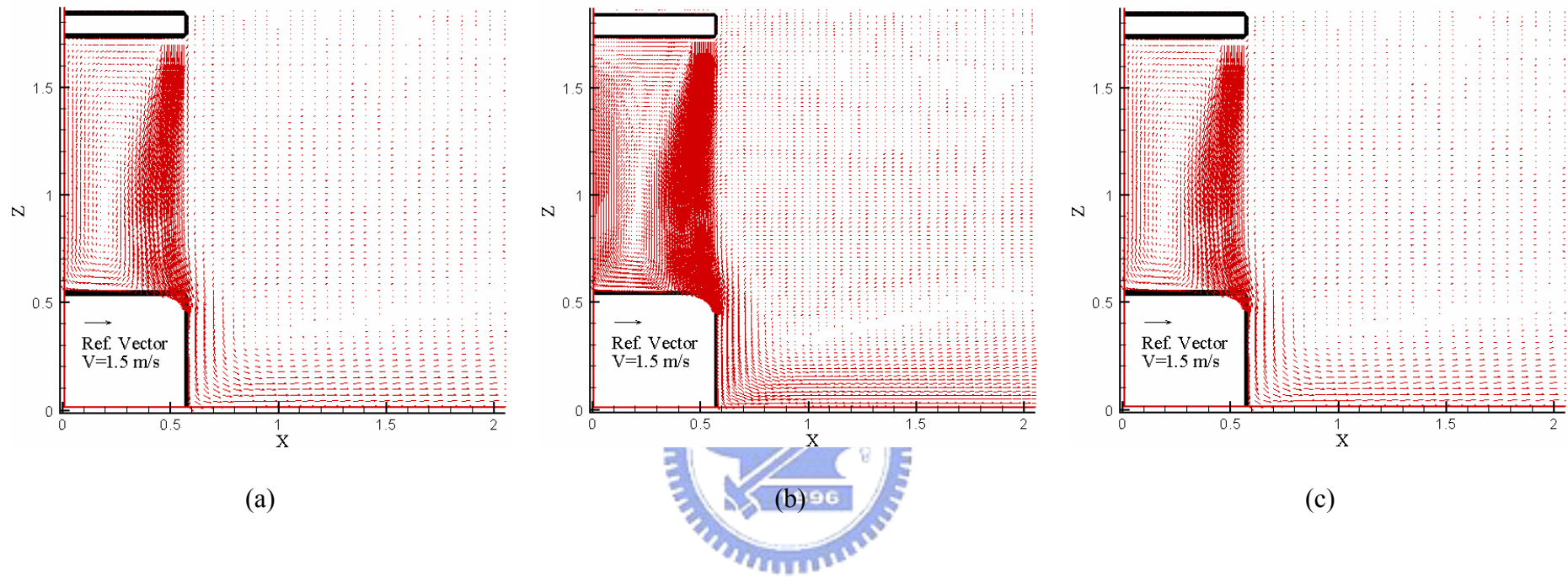


Fig. 3.6 Velocity vector maps at steady state for $b_j = 0.1 \text{ m}$, $Re_b = 9,548$, $Gr_t = 4.61 \times 10^9$, and $Gr_m = 2.94 \times 10^8$ predicted from the grids with (a) 8,550 cells, (b) 21,315 cells and (c) 16,764 cells.

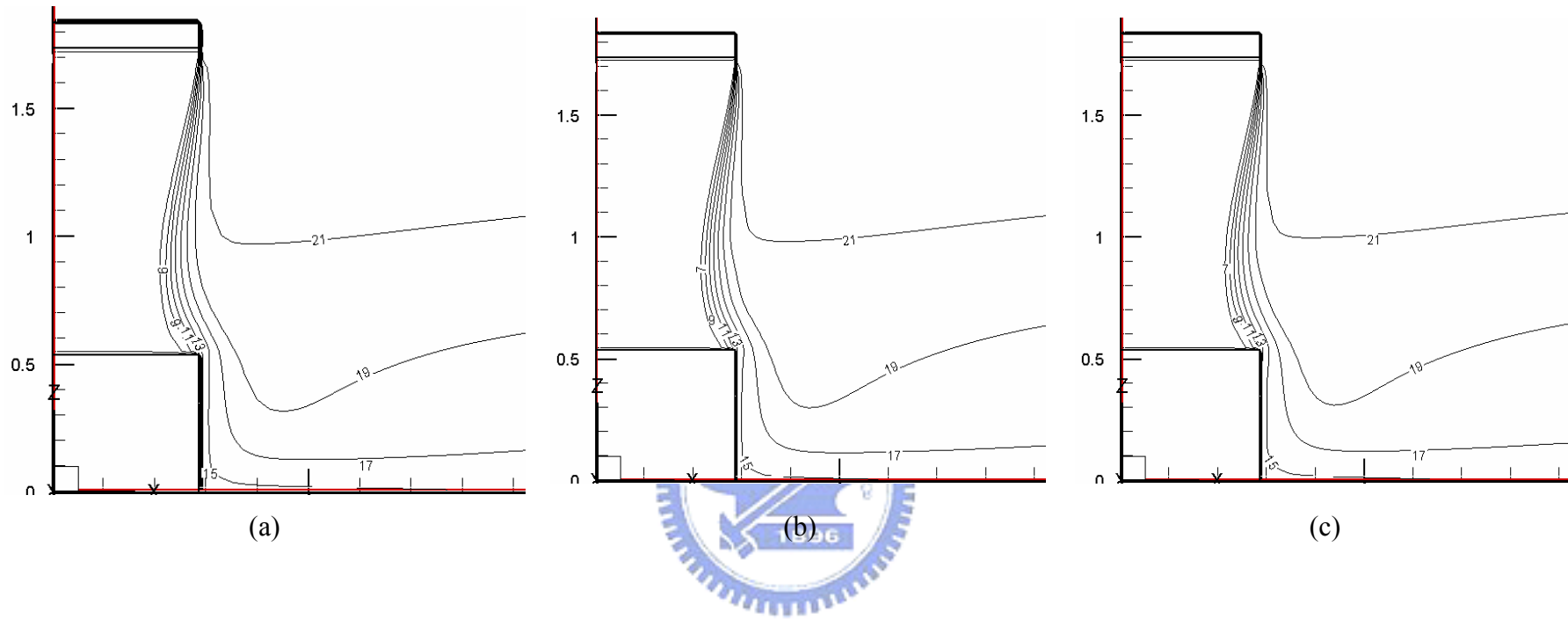


Fig. 3.7 Isotherms at steady state for $b_j = 0.1$ m, $Re_b = 9,548$, $Gr_t = 4.61 \times 10^9$, and $Gr_m = 2.94 \times 10^8$ predicted from the grids with (a) 8,550 cells, (b) 21,315 cells and (c) 16,764 cells.

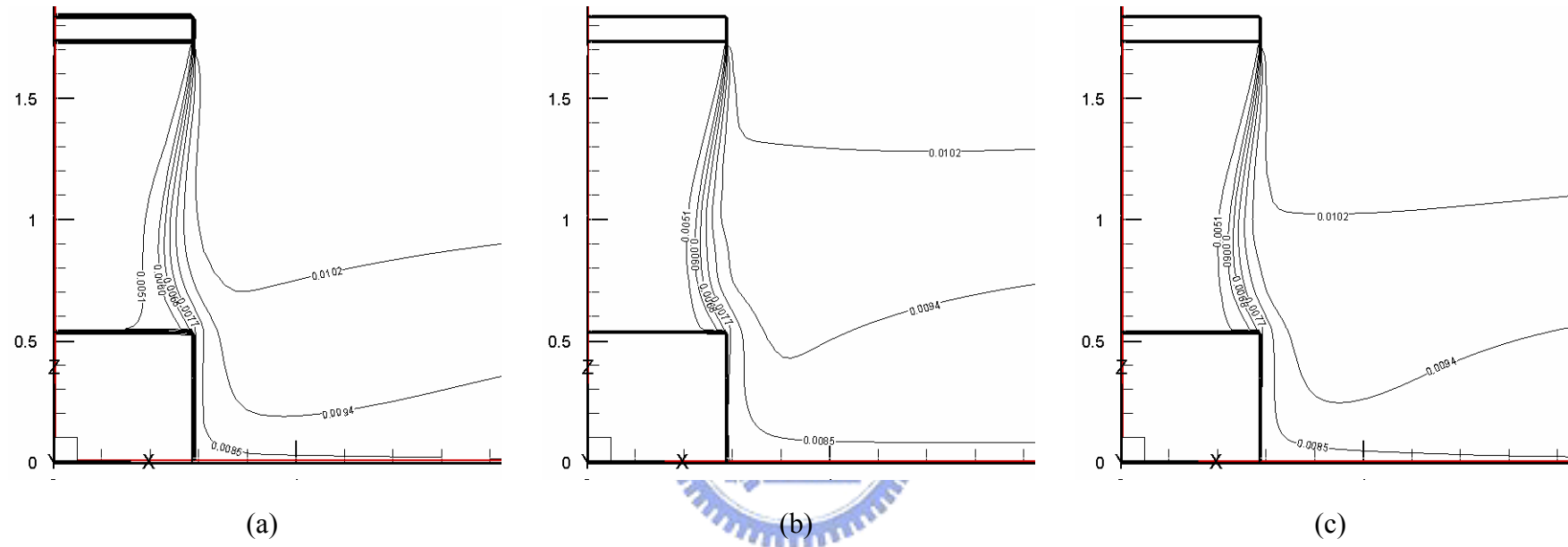
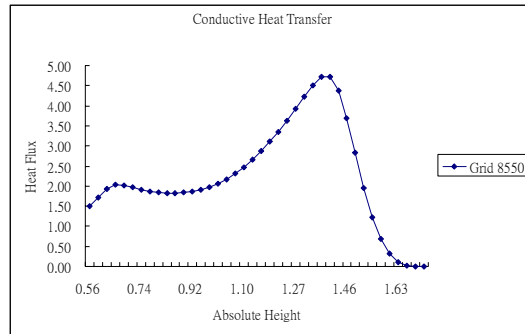
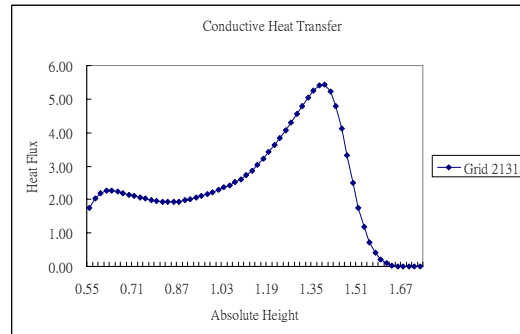


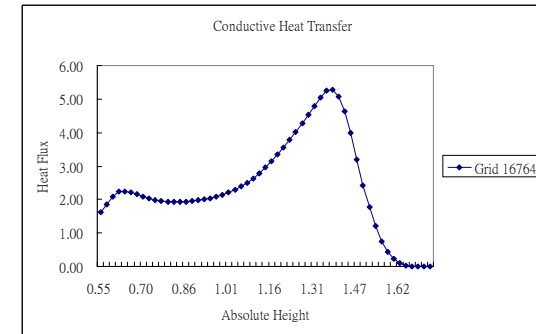
Fig. 3.8 Iso-concentration lines at steady state for $b_j = 0.1$ m, $Re_b = 9,548$, $Gr_t = 4.61 \times 10^9$, and $Gr_m = 2.94 \times 10^8$ predicted from the grids with (a) 8,550 cells, (b) 21,315 cells and (c) 16,764 cells.



(a)



(b)



(c)

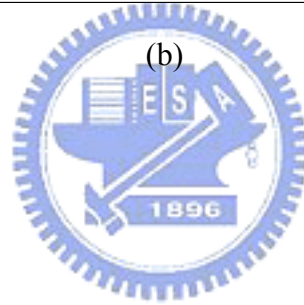
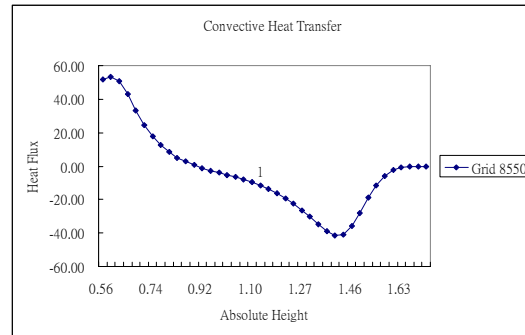
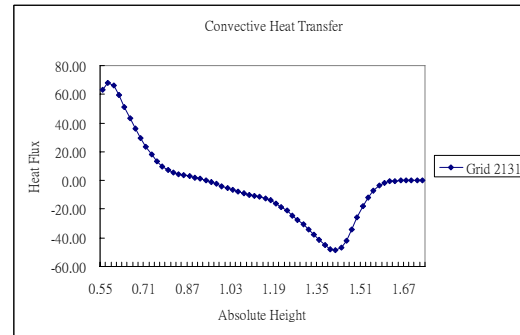


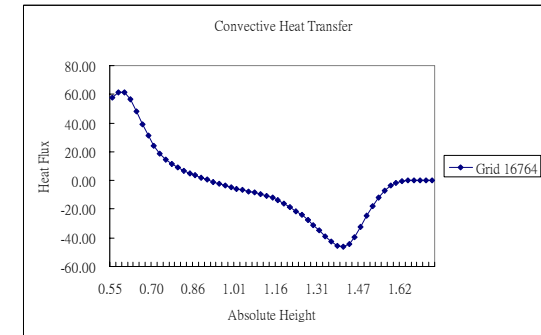
Fig. 3.9 Conduction heat flux at $x = 0.52$ m at steady state for $b_j = 0.1$ m, $Re_b = 9,548$, $Gr_t = 4.61 \times 10^9$, and $Gr_m = 2.94 \times 10^8$ predicted from the grids with (a) 8,550 cells, (b) 21,315 cells and (c) 16,764 cells.



(a)



(b)



(c)

Fig. 3.10 Convection heat flux at $x = 0.52$ m at steady state for $b_j = 0.1$ m, $Re_b = 9,548$, $Gr_t = 4.61 \times 10^9$, and $Gr_m = 2.94 \times 10^8$ predicted from the grids with (a) 8,550 cells, (b) 21,315 cells and (c) 16,764 cells.

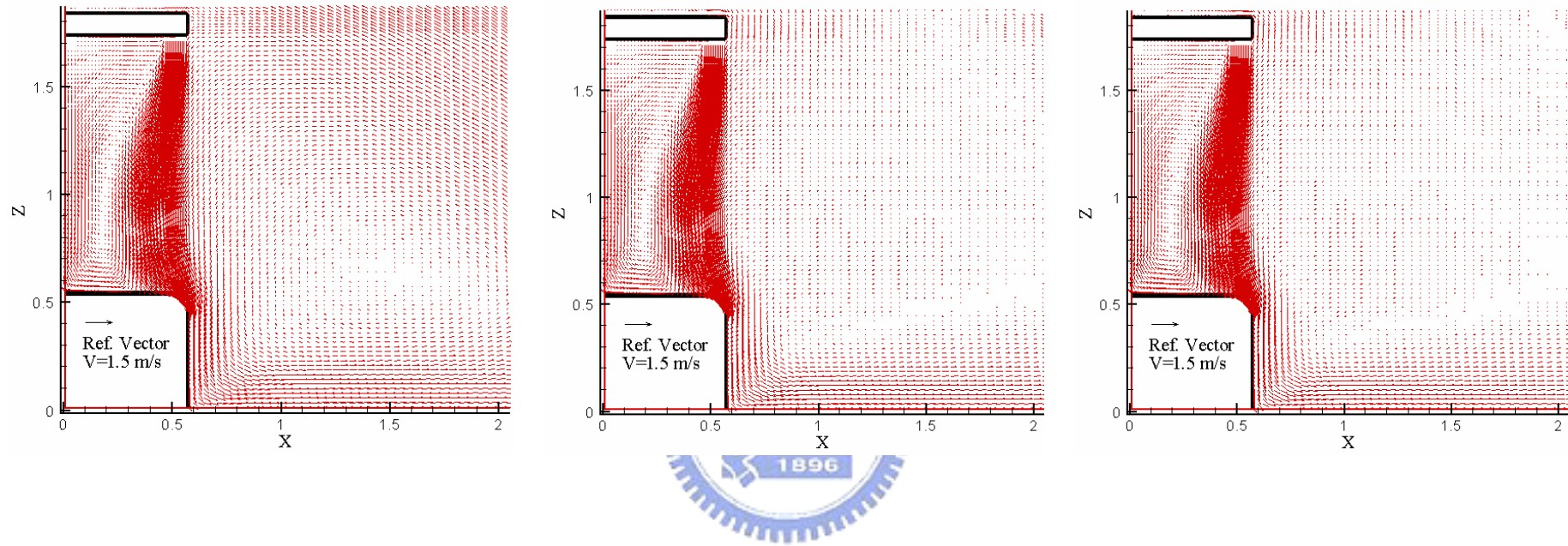


Fig. 3.11 Velocity vector maps at steady state for $b_j = 0.1$ m, $Re_b = 9,548$, $Gr_t = 4.61 \times 10^9$, and $Gr_m = 2.94 \times 10^8$ predicted with the domain size of (a) 3×2.5 m², (b) 6×4.5 m² and (c) 4.61×3.3 m².

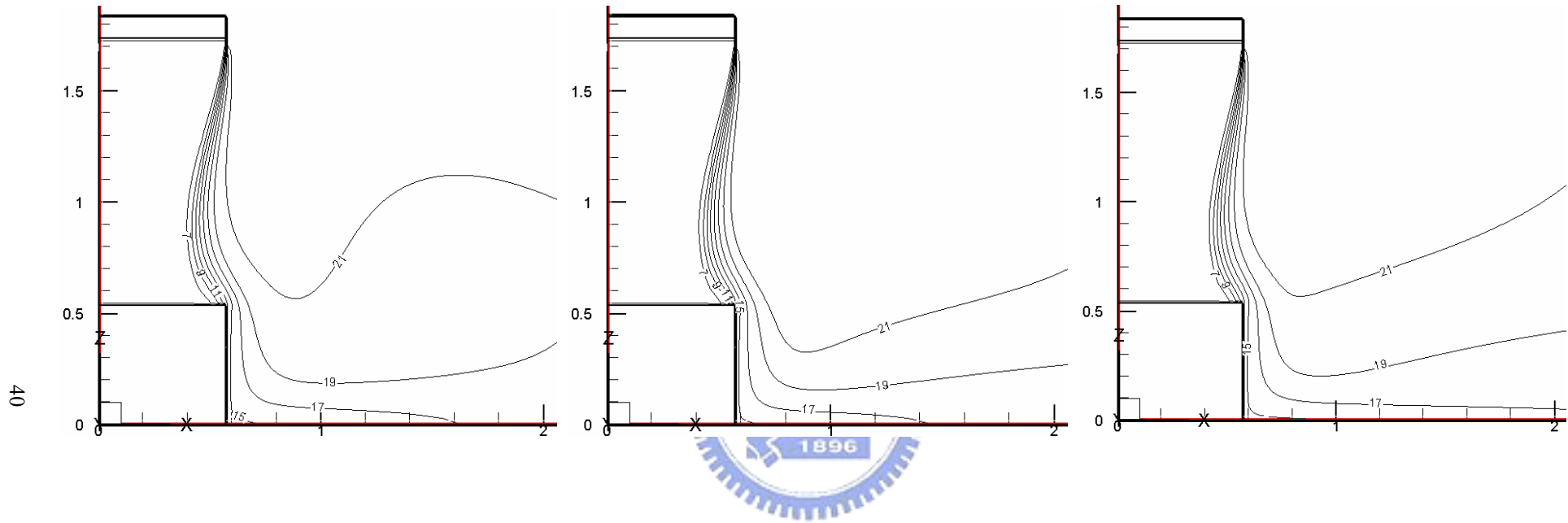


Fig. 3.12 Isotherms at steady state for $b_j = 0.1$ m, $Re_b = 9,548$, $Gr_t = 4.61 \times 10^9$, and $Gr_m = 2.94 \times 10^8$ predicted with the domain size of (a) 3×2.5 m², (b) 6×4.5 m² and (c) 4.61×3.3 m².

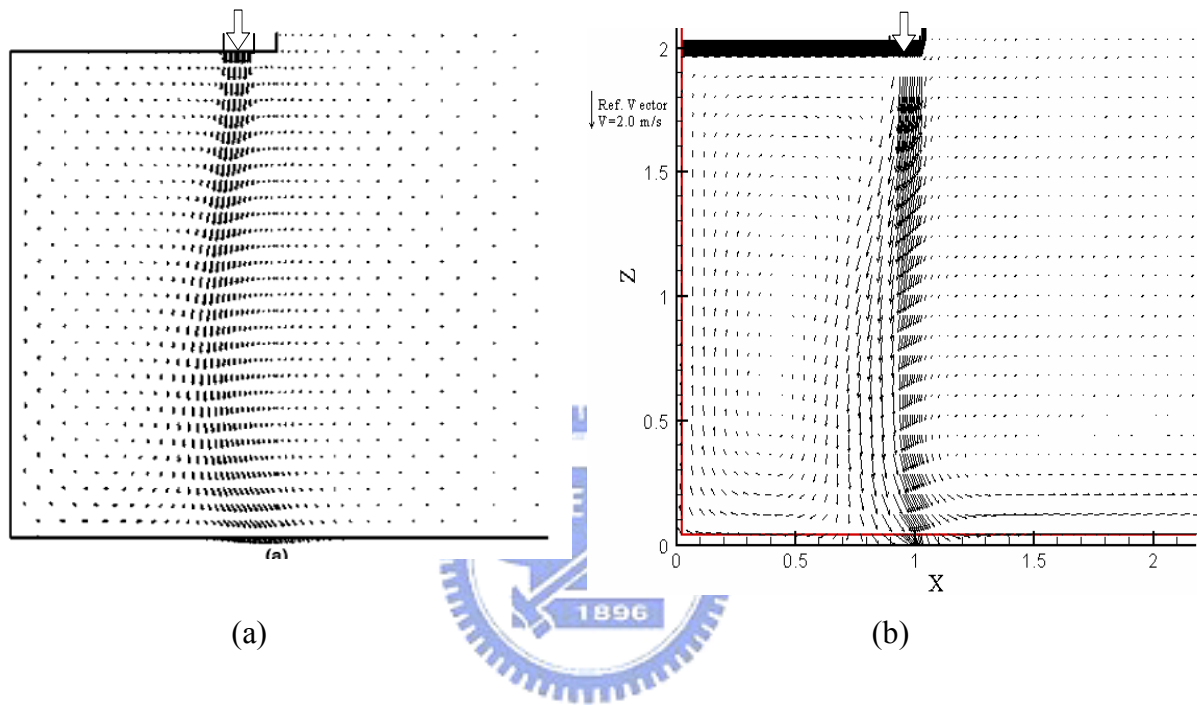


Fig. 3.14 Vector velocity maps in the steady cavity flow for the case with $b_j = 0.1$ m, $H = 2.0$ m, $Re_b = 18,371$, $Gr_t = 2.7 \times 10^{10}$, $Pr = 0.71$ and $N = 0$ predicted from (a) Chen & Yuan (2005) and (b) present study.

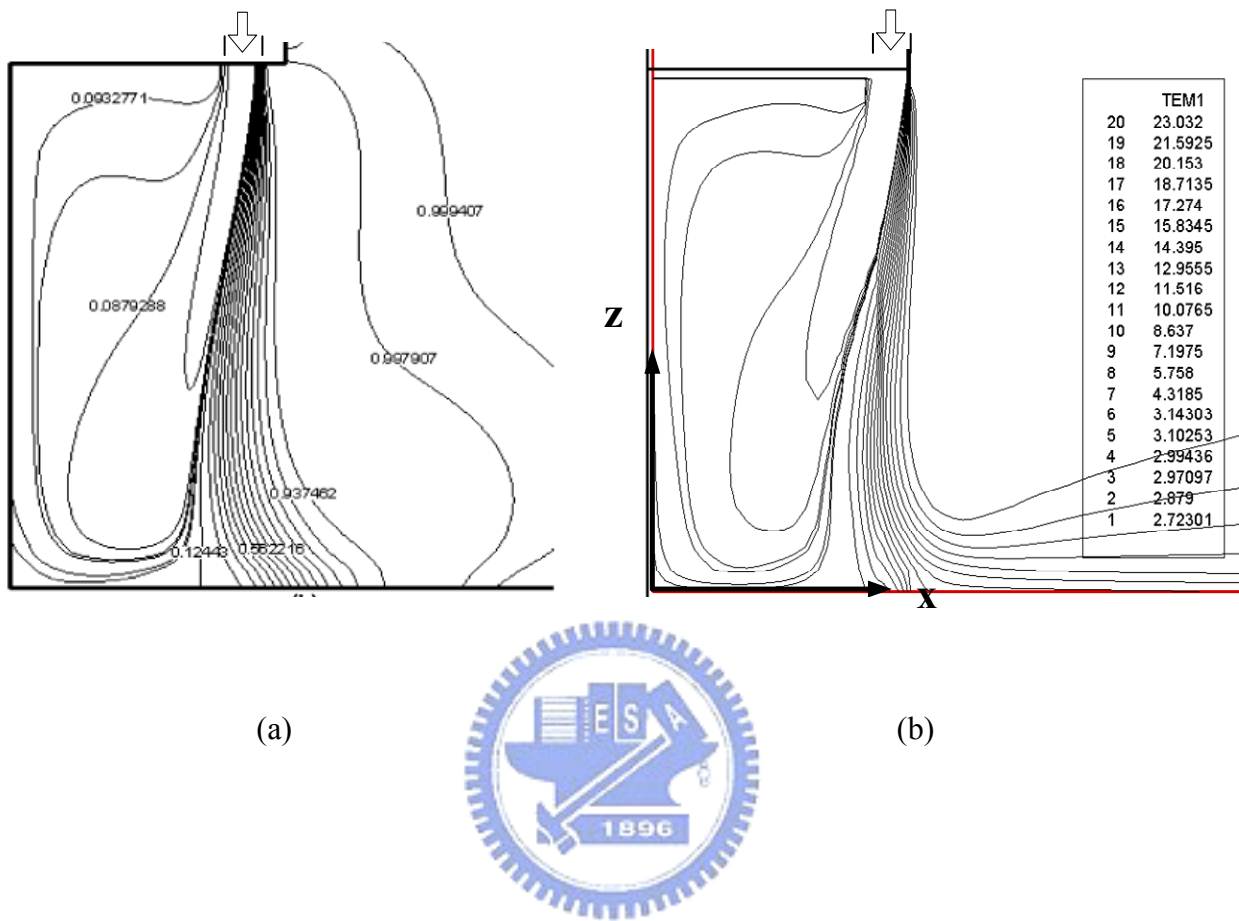


Fig. 3.15 Isotherms in the steady cavity flow for the case with $b_j = 0.1$ m, $H = 2.0$ m, $Re_b = 18,371$, $Gr_t = 2.7 \times 10^{10}$, $Pr = 0.71$ and $N = 0$ predicted from (a) Chen & Yuan (2005) and (b) present study.

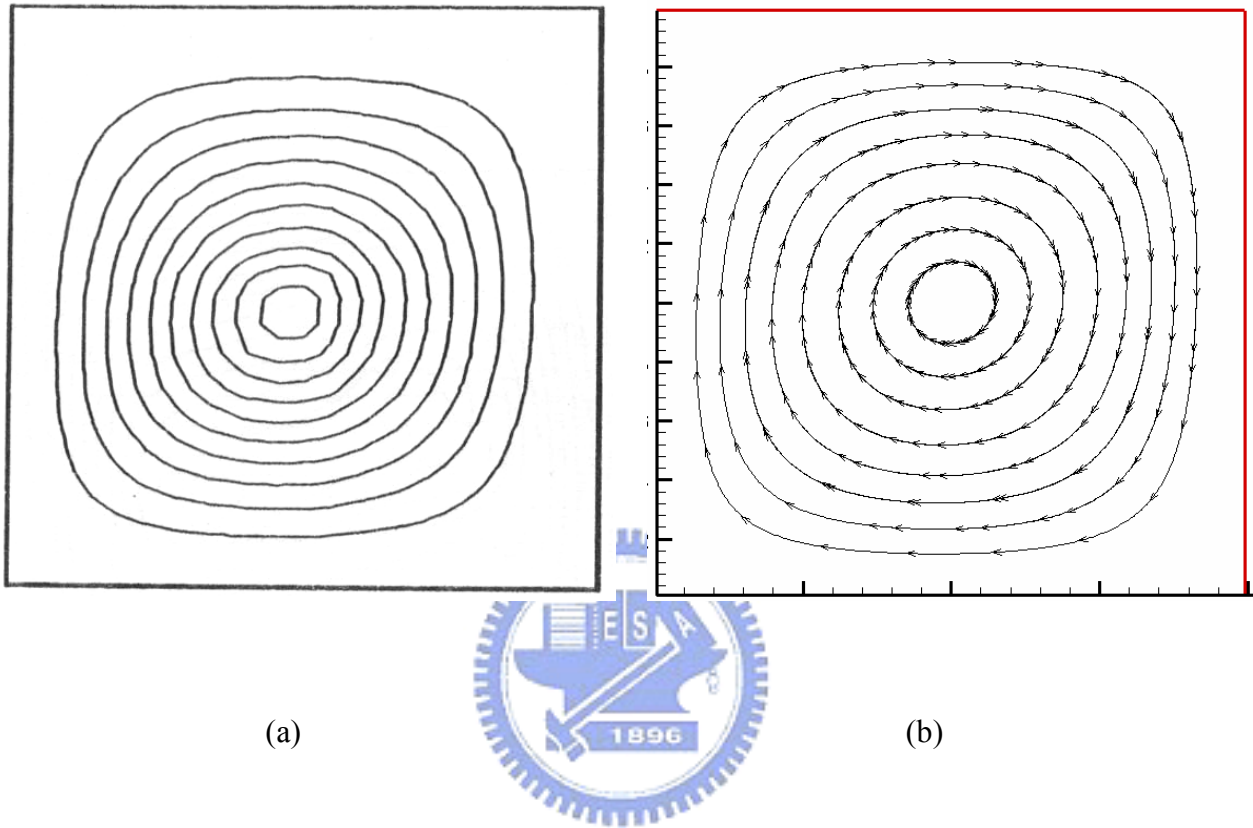


Fig. 3.16 Streamlines in the steady square cavity flow for the case with $H = L = 0.02$ m, $Gr_t = 10^3$, $Gr_m = 1.43 \times 10^3$, $Pr = 0.71$ predicted from (a) Lai (1989) and (b) present study.

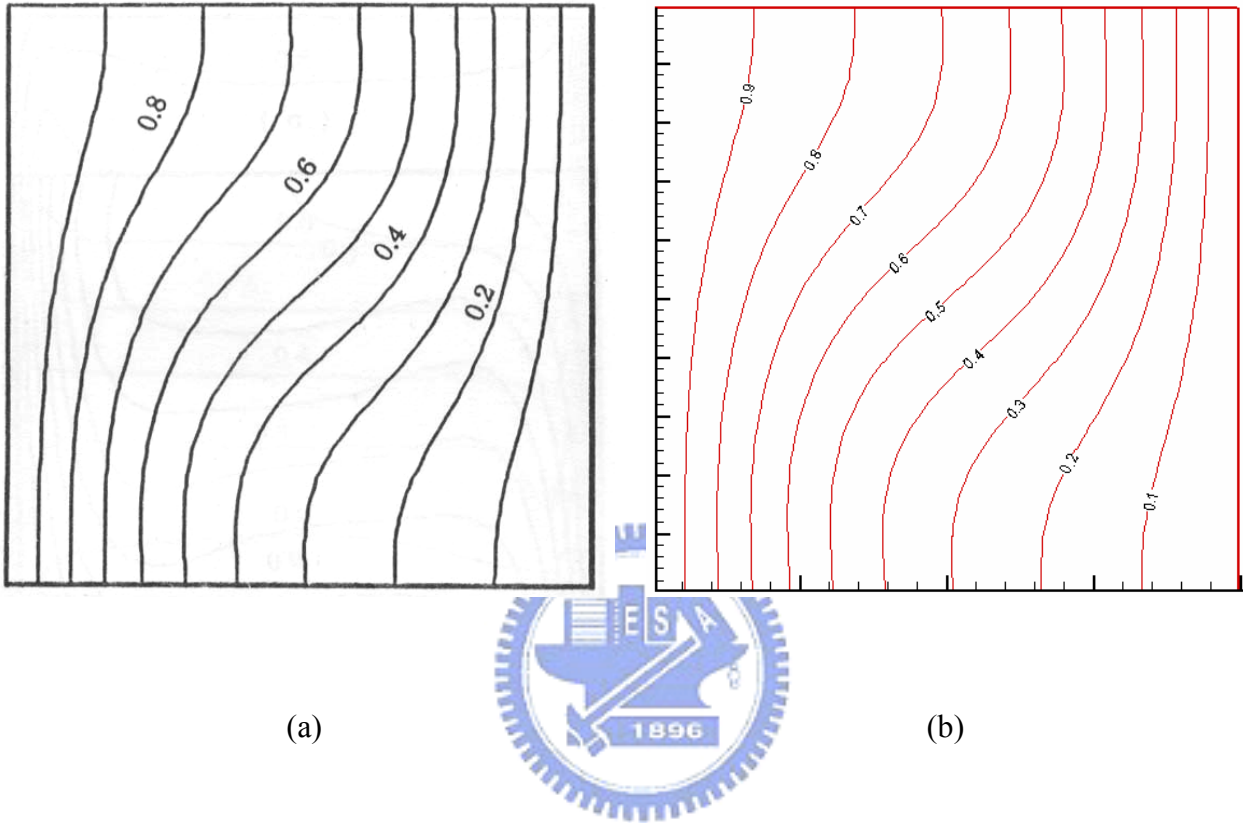


Fig. 3.17 Isotherms in the steady square cavity flow for the case with $H = L = 0.02$ m, $Gr_t = 10^3$, $Gr_m = 1.43 \times 10^3$, $Pr = 0.71$ predicted from (a) Lai (1989) and (b) present study.

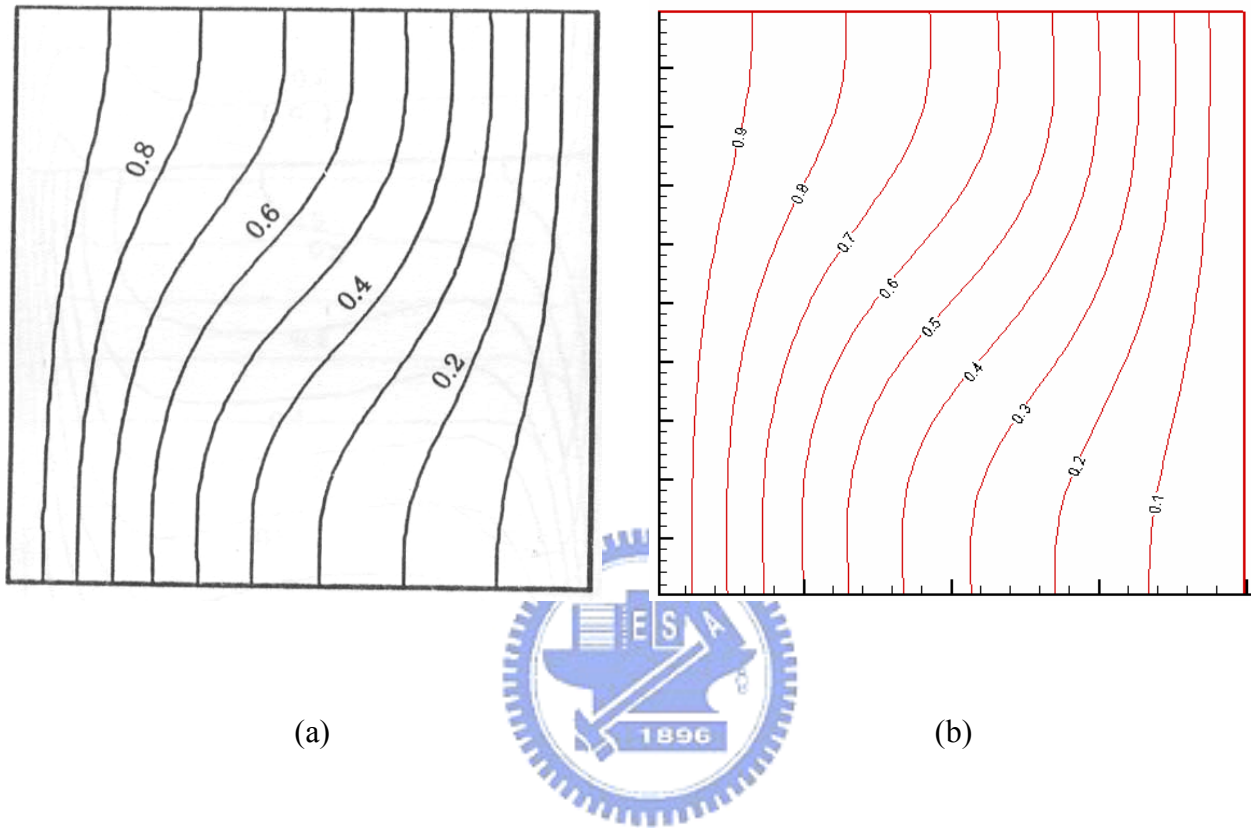


Fig. 3.18 Iso-concentration lines in the steady square cavity flow for the case with $H = L = 0.02$ m, $Gr_t = 10^3$, $Gr_m = 1.43 \times 10^3$, $Pr = 0.71$ predicted from (a) Lai (1989) and (b) present study.

CHAPTER 4

RESULTS AND DISCUSSION

In the present numerical simulation of the transport processes in the open vertical refrigerated display case, computation is carried out mainly for the injection slot width of 0.05, 0.07, 0.1 and 0.12 m at the air discharge grille. The air discharge-to-return grille separation distance H is fixed at 1.20 m and the cabinet depth is fixed at 0.57 m with the injected air velocity ranging from 0.25 to 3.0 m/s. The temperature difference ΔT and mass fraction difference of water vapor Δw_1 between the air discharge and ambient are fixed at 20°C and 0.00701, respectively. The chosen Schmidt number for the air-water vapor mixture is $Sc = \nu / D = 0.6$. The dimensionless groups governing the flow patterns are the jet Reynolds number base on the slot width at the air curtain discharge, thermal and solutal Grashof numbers, and thermal and solutal Richardson numbers (Buoyancy-to-Inertia ratios). They are respectively defined as

$$Re_b = \bar{V}_j b_j / \nu \quad (4.1)$$

$$Gr_t = g \beta_t \cdot \Delta T \cdot H^3 / \nu^2 \quad (4.2)$$

$$Gr_m = g \beta_m \cdot \Delta w_1 \cdot H^3 / \nu^2 \quad (4.3)$$

$$Ri_t = Gr_t / Re_H^2 \quad (4.4)$$

and

$$Ri_m = Gr_m / Re_H^2 \quad (4.5)$$

Here the Reynolds number based on the cavity height H is defined as

$$Re_H = \bar{V}_j H / \nu = Re_b \cdot (H / b_j) \quad (4.6)$$

And for the situation with back panel perforations the perforation Reynolds number is defined as

$$Re_p = \bar{V}_p H \cdot d_p / \nu \quad (4.7)$$

Here \bar{V}_p and d_p are the average air speed at perforations and the back panel perforation density, respectively.

Thus in this study the air curtain discharge Reynolds number Re_b ranges from 1,910 to 9,548 and the thermal and solutal Richardson numbers respectively vary from 0.0879 to 12.7 and from 0.0056 to 0.806. Selected results from the present computation for the combined heat and mass transfer in the open cavity flow (the ratio of solutal buoyancy to thermal buoyancy $N = 0.0637$) are presented here to unravel how the jet Reynolds number, Grashof numbers, Richardson numbers, and the ratio H / b_j affect the flow patterns driven by the interaction of inertia force of the air curtain, and thermal and concentration buoyancy forces in the vertical display cabinet. It should be mentioned that only the results at steady or statistical state will be examined in the following to investigate the long time behavior of the flow.

4.1 Inertia-Driven Recirculating Flow Patterns for Un-cooled Air Curtain

At first, the effects of the initial jet Reynolds number at the air discharge grille on the predicted steady flow pattern for the limiting case in the absence of mass transfer ($\Delta w_1 = 0$) at $b_j = 0.1$ m for an un-cooled air curtain ($Gr_t = 0$) are presented in Fig. 4.1. Thus the open cavity flow is driven by the jet inertia alone. The results clearly show

that a single large recirculating vortex is induced in the vertical cavity by the inertia force of the air curtain for all Re_b . Besides, at $Gr_t = 0$ and $N = 0$ the air curtain moves vertically downwards and the vortex in the cavity has not been cut apart. The predicted vortex flow patterns in the cavity at steady state for the present limiting case affected by the slot width of the air discharge can be illustrated by comparing the results shown in Figs. 4.1 and 4.2 again for $Gr_t = 0$ and $N = 0$. The results indicate that the flow recirculation is stronger for a higher initial jet Reynolds number. Moreover, at the same jet Reynolds number the flow recirculation is stronger for a smaller air curtain width. This is attributed to the higher initial jet speed for a smaller b_j .

4.2 Buoyancy-Driven Recirculating Flow Patterns for Cold Air

Curtain

Next, the recirculating flow in the cavity driven by the jet inertia and thermal buoyancy alone ($Gr_m = 0$) is examined. In an air curtain moving through an open vertical cavity, Chen & Yuan [10] observed that the air curtain bent slightly inward under the simultaneous action of the jet entrainment and the thermal buoyancy in the vertical open area. The open cavity flows resulting from the negatively buoyant jets at different Ri_t in the study of Chen & Yuan [10] are shown in Fig. 4.3 to facilitate the comparison with our predictions. Note that the cold air curtain breaks as the thermal Richardson number increases to 0.32. The flow pattern changes from a single clockwise vortex to a double-vortex structure. Specifically, at the high Richardson number there appear two counter-rotating vortices in the cabinet with one on top of the other. The air curtain becomes relatively wide near the cavity bottom and it loses the strength to prevent the warm, moist air from the surrounding to penetrate into the cavity.

4.3 Effects of Air Curtain Reynolds Number

How the jet Reynolds number at the air discharge grille affects the flow pattern

in the vertical display cabinet studied here is examined next. First, for the limiting case without the temperature and concentration differences between the air curtain and ambient for $\Delta T = 0^\circ\text{C}$ and $\Delta w_1 = 0$ ($Gr_t = 0$ and $Gr_m = 0$), no buoyancy induced flow appears in the cavity for all jet Reynolds numbers as already shown in Figs. 4.1 and 4.2. The flow patterns at steady state are all in the form of single large vortex circulating along the cavity walls and the air curtain. For the simultaneous presence of temperature and concentration differences between the air curtain and ambient with $Gr_t = 4.61 \times 10^9$ and $N = 0.0637$, the results in Fig. 4.4 show that the air curtain bends toward the cavity as it moves downwards and the bending is larger for a lower Re_b . The obviously results from the increasing buoyancy-to-inertia ratio for a reduction in Re_b at fixed Gr_t and Gr_m . Thus the buoyancy forces exhibit stronger effects on the flow. Note that for the low Re_b of 8,275 the air curtain bending is so large that it touches the inner cold vertical plate of the cavity (Fig. 4.4(b)). Under this situation another flow recirculation is induced in the bottom of the cavity. It is also noted that the isotherms and iso-concentration lines also bend significantly toward the cavity a lower Re_b (Figs. 4.5(b) to (e) and Figs. 4.6(b) to (e)). The intrusion of the warm and humid air from the ambient into the cavity is relatively prominent. It is of interest to point out that at the very low Re_b of 1,910 the air jet is deflected toward the cavity immediately after it is discharged from the air injection slot and the intruding air from the ambient dominates the cavity. Similar trends are noted in Figs. 4.7-4.9 and Figs. 4.10-4.12 respectively for smaller jet discharge width of 0.07 and 0.05 m.

4.4 Effects of Richardson Numbers

We proceed to examine how the recirculating flow in the cavity is affected by the thermal and solutal Richardson numbers by inspecting the predicted results for various Re_H at given Gr_t and Gr_m . The results in Figs. 4.4-4.6 clearly indicate that a reduction in the initial jet Reynolds numbers Re_b and hence Re_H causes an earlier

bending of the air curtain and the recirculating flow in the upper region of the cavity occupies a smaller region and is weaker. This is due to the fact that at smaller Re_b and Re_H the strength of the jet inertia is weaker and the air entrain is easier to be deflected by the intruding air from the ambient. The buoyancy effects on the flow are hence weaker for smaller Ri_t and Ri_m . Moreover, the thermal and solutal Richardson numbers for the cases considered here are listed in Table 4.1.

Based on the data from the present prediction for $H = 1.20$ m and for the width of the air curtain discharge varied from 0.05 to 0.12 m, the critical condition for the air curtain to touch the inner bottom corner of the cabinet can be correlated as

$$Re_b \times (H/b_j) = -0.36240201 + 17153.557 \times (Ri_m)^{-1/2} + 88.055002 \times [\ln(Ri_t)] \times (Ri_t)^{1/2} \quad (4.7)$$

The above equation can predict our data with a standard deviation less than 0.009%.

4.5 Effects of H / b_j Ratio

The effects of the ratio between the cavity height and jet width at the air discharge grille on the recirculating flow in the cavity are examined next. According to the definition of the Richardson numbers, $Ri_t = Gr_t / Re_H^2 = (Gr_t / Re_b^2) \cdot (b_j / H)^2$ and $Ri_m = Gr_m / Re_H^2 = (Gr_m / Re_b^2) \cdot (b_j / H)^2$. Thus for given Gr_t , Gr_m and Re_b the Richardson numbers are smaller for a reduction in the air curtain width at the air discharge grille. Hence the effects of the H / b_j on the flow can be inferred by comparing the corresponding results in Figs. 4.4 to 4.6 for $b_j = 0.1$ m with that in Figs. 4.7 to 4.9 for $b_j = 0.07$ m and Figs. 4.10 to 4.12 for $b_j = 0.05$ m for the same Gr_t , Gr_m and Re_b . Note that an increase in the H / b_j ratio reduces the Richardson numbers and hence reduces the buoyancy effects. This can be more clearly seen by comparing the results for the isotherms and iso-concentration lines. Specifically, at a large H / b_j the distortions in the isotherms and iso-concentration lines are less severe to a certain degree.

4.6 Effects of the Air Discharge with an Inclined Angle

The results presented above clearly indicate that the thermal and solutal buoyancies tend to deflect the initially vertically downward moving air curtain toward the cavity core and to induce the intrusion of the warm, moist air from the ambient into the cavity. This apparently results in a significant reduction of the performance of the display cabinet. Based on this observation, we move further to investigate the possibility of retarding the air curtain bending by inclining the jet at the air discharge grille toward the ambient. Results from this investigation are shown in Figs. 4.13 to 4.15 for $b_j = 0.1$ m, in Figs. 4.22 to 4.24 for $b_j = 0.07$ m, and in Figs. 4.31 to 4.33 for $b_j = 0.05$ m for the inclined angle of the jet $\gamma = 5^\circ$. The jet inclined angle is defined as the angle between the jet axis at the discharge grille and a vertically downward line. Comparing the results in Figs. 4.13 to 4.15 with that in Figs. 4.4 to 4.6 for $b_j = 0.1$ m, the results in Figs. 4.22-4.24 with that in Figs. 4.7-4.9 for $b_j = 0.07$ m and the results in Figs. 4.31-4.33 with that in Figs. 4.10-4.12 for $b_j = 0.05$ m clearly reveal that for an inclined jet the bending of the air curtain delays to some degree and the ambient air intrusion into the cavity is weaker. Besides, the buoyancy induced distortions in the isotherms and iso-concentration lines are somewhat reduced. At large inclined angle the delay in the air curtain bending is more significant and the distortions in the isotherms and iso-concentration lines are further reduced, as evident from the results in Figs. 4.16-4.21, Figs. 4.25-4.30 and Figs. 4.34-4.39, for the air injection slot width of 0.1, 0.07 and 0.05m, respectively.

4.7 The Entrainment Factor

As indicated in the literature review, the thermal entrainment factor was proposed by Chen & Yuan [4, 10] and Bhattacharjee & Loth [11] to signify the degree of the ambient warm air entrainment by the air curtain. It is of interest to examine the thermal entrainment factors predicted here for the cases presented above. The results

are shown in Table 4.2. Noted that for the air discharge with and without inclined angle the thermal entrainment factor varies nonmonotonically with the jet Reynolds number Re_b . Especially, an increase in α at decreasing Re_b is somewhat unusual. A close inspection of the recirculating flow patterns for various cases reveals that at a lower Re_b the bending of the air curtain appears earlier and the air curtain curves toward the cold vertical plate of the display case, as discussed in the previous sections. The air curtain then moves along the cold plate for a longer distance. Therefore at the return grille the air curtain can be at a lower temperature, resulting in a higher thermal entrainment factor. According to the unusual variation of α with Re_b , the thermal entrainment factor is not considered to be a proper indication of the air entrainment by the jet when the air curtain bending is severe enough to induce two flow recirculations in the cavity.

4.8 Effect of Air Discharge with Double Air Curtain Design

In actual applications, some manufacturers develop the open vertical display cabinets with double air curtains. It is of interest to explore how the double air curtain affect the flow in the display cabinets. In this investigation the single air jet at the discharge grille is divided into two parts. The inner and outer air jets can be both issued from the discharge grille and are in the same vertically downward direction. The jet width and speed are b_i and V_i for the inner jet and b_o and V_o for the outer jet at the discharge grille. The corresponding jet Reynolds numbers at the discharge grille are Re_{ci} and Re_{co} , respectively. To facilitate the comparison with the predicted results for the single air curtain, here the total width of the two jets, $b_i + b_o$, is chosen to be 0.1 m. Besides, the thermal and solutal Grashof numbers are fixed at the same values as that in Figs. 4.4-4.6.

Figures 4.40-4.42 show the predicted steady flow, isotherms and iso-concentration lines for $b_i = 0.03$ m and $b_o = 0.07$ m at $Re_{ci} = 1,910$ for Re_{co} varied from

1,910 to 7,638. The results clearly indicate that by increasing the Reynolds number of the outer jet the bending of the air curtains is delayed to a significant degree. Besides, the distortions in the isotherm and iso-concentration lines are less pronounced, due to the smaller buoyancy effects. Note that for $Re_{co} \geq 6,365$ only a single air circulation is induced and the air curtains do not directly touch the vertical cold plate of the cavity (Figs. 4.40(d) and (e)). Similar trends are noted in Figs. 4.43-4.45 for Re_{ci} fixed at 3,183 and Re_{co} varied from 1,910 to 6,365.

It is important to understand how the relative magnitudes of Re_{ci} and Re_{co} affect the flow in the cabinet for a fixed value of $(Re_{ci} + Re_{co})$. This is illustrated in Figs. 4.46-4.48 for $Re_{ci} + Re_{co} = 9,548$. Note that the bending of the air curtains and the intrusion of the warm moist air reduce slightly for a higher Re_{ci} and a lower Re_{co} (Fig. 4.46). This is also reflected in the distributions of the isotherms and iso-concentration lines.

We move ahead to examine the effects of the relative magnitudes of the two jet widths at the air discharge grille on the flow in the display case. Figures 4.49-4.54 present the steady velocity vector maps, isotherms and iso-concentration lines for $b_i = b_o = 0.05$ m. Contrasting these results with that in Figs. 4.40-4.45 for $b_i = 0.03$ m and $b_o = 0.07$ m reveals that the intrusion of the warm air from the ambient is slightly weaker for the cabinets with equal widths of the inner and outer jets at the discharge grille. The effects of the jet widths are particularly prominent for the results shown in Fig. 4.43(c) and Fig. 4.52(c). Note that for $b_i = b_o = 0.05$ m only a single flow recirculation is induced in the cavity. But for $b_i = 0.03$ m and $b_o = 0.07$ m there are two flow recirculations in the cavity and the thermal intrusion from the ambient is rather substantial.

The effects of the relative magnitudes of Re_{ci} and Re_{co} on the cavity flow are shown in Figs. 4.55-4.57 for $b_i = b_o = 0.05$ m again for $(Re_{ci} + Re_{co})$ fixed at 9,548.

The results also indicate that the intrusion of the warm air from the ambient is less important when the inner jet is at a higher Reynolds number and outer jet is at a lower Reynolds number.

Furthermore, the results for another set of jet widths with $b_i = 0.07$ m and $b_o = 0.03$ m are shown in Figs. 4.58-4.63. These results, when compared with that in Figs. 4.40-4.45 for $b_i = 0.03$ and $b_o = 0.07$ m, indicate that the air curtain bending is significantly improved when the inner jet width is larger and the outer jet width is smaller. The effects of the jet width are particularly stronger for the cases shown in Figs. 4.40 (c), and 4.58(c) and for the cases in Figs. 4.43(c) and 4.61(c). Note that at $b_i = 0.07$ m and $b_o = 0.03$ m for the same Re_{ci} and Re_{co} only a single flow recirculation is induced in the cavity as indicated in Figs. 4.43(c) and 4.61(c).

Finally, the effects of the relative magnitudes of Re_{ci} and Re_{co} on the cavity flow are illustrated in Figs. 4.64-4.66 for $b_i = 0.07$ m and $b_o = 0.03$ m for $(Re_{ci} + Re_{co}) = 9,548$. Note that the air curtain bending is more significant when the inner jet Reynolds number is substantially higher than the outer jet Reynolds number.

More results are shown in Figs. 4.67-4.102 for a larger total width of the two-curtain design with $b = 0.12$ m and in 4.103-4.120 a smaller total width of 0.07 m. Similar trends are noted.

At this point it is of interest to explore the possibility of reducing the air curtain bending toward the cavity core by inclining the outer jet toward the ambient with the inner jet still in the vertically downward direction. Selected results from this exploration are shown in Figs. 4.121-4.129 for the outer jet inclined at 25° for $b_i = b_o = 0.05$ m. Contrasting these results with the corresponding cases given in Figs. 4.49-4.57 for the outer and inner jets both in the vertically downward direction reveals that some improvement in the air curtain bending can be obtained especially when $(Re_{ci} + Re_{co})$ is at intermediate level (Figs. 4.49 (c) and 4.121 (c)).

4.9 Effect of Back Panel Perforation

As indicated by Navaz et al. [3] and Chen and Yuan [4], the air flow from the back panel perforation as schematically shown in Fig. 4.130 can improve the air flow stability in the cavity and slightly reduces the heat load to the cavity. The results from the present predictions including the air flow moving horizontally into the cavity from the vertical panel of the cavity are shown in Figs. 4.131-4.157 for the cases with single air curtain. Comparing these results with those in Figs. 4.4-4.39 for the cases without back panel perforation discloses that the air flow from the back panel can delay the air curtain bending and hence reduces the intrusion of the warm moist air into the cavity. The effects of the back panel perforation are stronger for a higher Reynolds number of the flow from the perforation and a higher perforation density.



Table 4.1 Variations of Richardson numbers with the jet Reynolds number.

	Air discharge width = 0.12 m		Air discharge width = 0.10 m	
Re_b	Ri_m	Ri_t	Ri_m	Ri_t
9548.06	3.22E-02	5.06E-01	2.24E-02	3.51E-01
8274.98	4.29E-02	6.74E-01	2.98E-02	4.68E-01
6365.37	7.25E-02	1.14E+00	5.04E-02	7.91E-01
5092.30	1.13E-01	1.78E+00	7.87E-02	1.24E+00
3182.69	2.90E-01	4.56E+00	2.02E-01	3.16E+00
1909.61	8.06E-01	1.27E+01	5.60E-01	8.79E+00
	Air discharge width = 0.07 m		Air discharge width = 0.05 m	
Re_b	Ri_m	Ri_t	Ri_m	Ri_t
9548.06	1.10E-02	1.72E-01	5.60E-03	8.79E-02
8274.98	1.46E-02	2.29E-01	7.45E-03	1.17E-01
6365.37	2.47E-02	3.88E-01	1.26E-02	1.98E-01
5092.30	3.86E-02	6.06E-01	1.97E-02	3.09E-01
3182.69	9.87E-02	1.55E+00	5.04E-02	7.91E-01
1909.61	2.74E-01	4.31E+00	1.40E-01	2.20E+00

Table 4.2 Entrainment factors for selected cases with a single air curtain design.

Air discharge width = 0.10 m		Air discharge width = 0.10 m with $\gamma= 5^\circ$	
Reynolds Number Re_b	Entrainment Factor α	Reynolds number Re_b	Entrainment Factor α
9548	0.3535	9548	0.34745
8275	0.33289	8275	0.33143
6365	0.3534	6365	0.3651
5092	0.37195	5092	0.39525
3183	0.3736	3183	0.3961
1910	0.2701	1910	0.30965
Air discharge width = 0.07 m		Air discharge width = 0.07 m with $\gamma= 5^\circ$	
Reynolds Number Re_b	Entrainment Factor α	Reynolds Number Re_b	Entrainment Factor α
9548	0.3592	9548	0.32075
8275	0.359975	8275	0.31828
6365	0.3319	6365	0.331
5092	0.35135	5092	0.36045
3183	0.3779	3183	0.38475
1910	0.2857	1910	0.313815

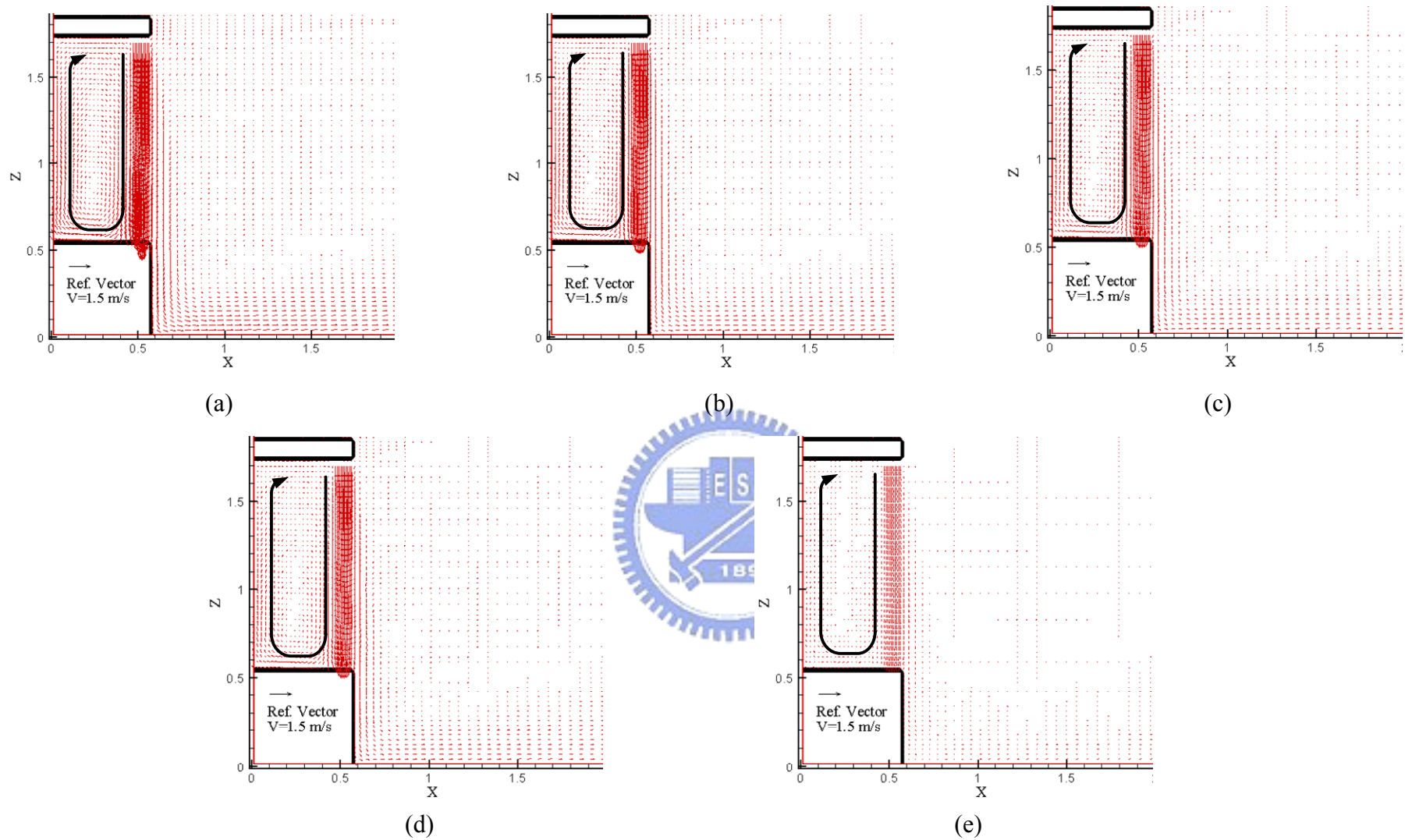


Fig. 4.1 Velocity vector maps for steady cavity flow for $b_j = 0.1$ m, $Gr_t = 0$ ($\Delta T = 0^\circ\text{C}$) and $N = 0$ for $Re_b =$ (a) 9,548 ($V_j = 1.5$ m/s), (b) 6,365 ($V_j = 1.0$ m/s), (c) 5,092 ($V_j = 0.8$ m/s), (d) 3,183 ($V_j = 0.5$ m/s) and (e) 1,910 ($V_j = 0.3$ m/s).

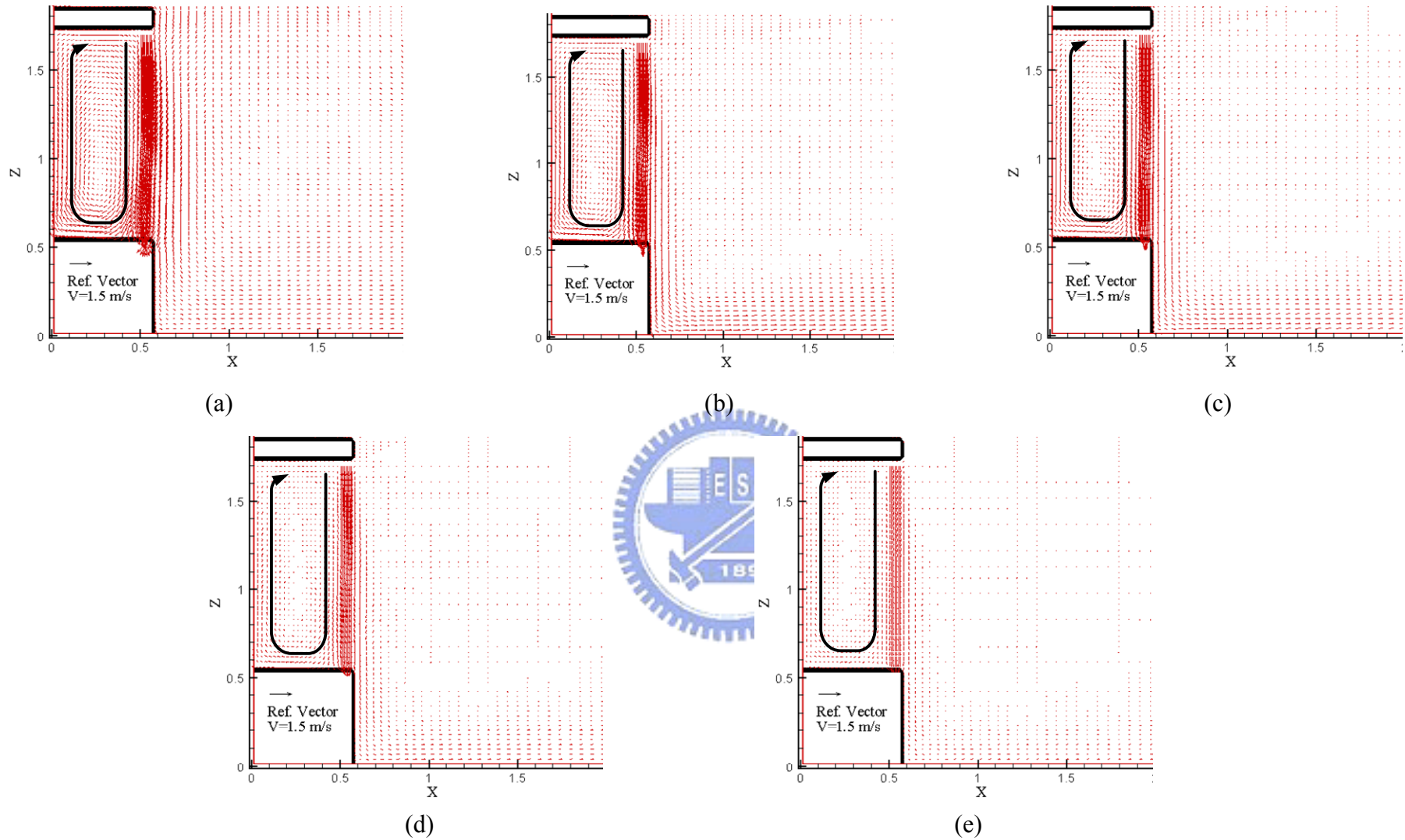


Fig. 4.2 Velocity vector maps for steady cavity flow for $b_j = 0.07$ m, $Gr_t = 0$ ($\Delta T = 0^\circ\text{C}$), and $N = 0$ for $Re_b =$ (a) 9,548 ($V_j = 2.143$ m/s), (b) 6,365 ($V_j = 1.428$ m/s), (c) 5,092 ($V_j = 1.143$ m/s), (d) 3,183 ($V_j = 0.714$ m/s) and (e) 1,910 ($V_j = 0.428$ m/s).

(e)

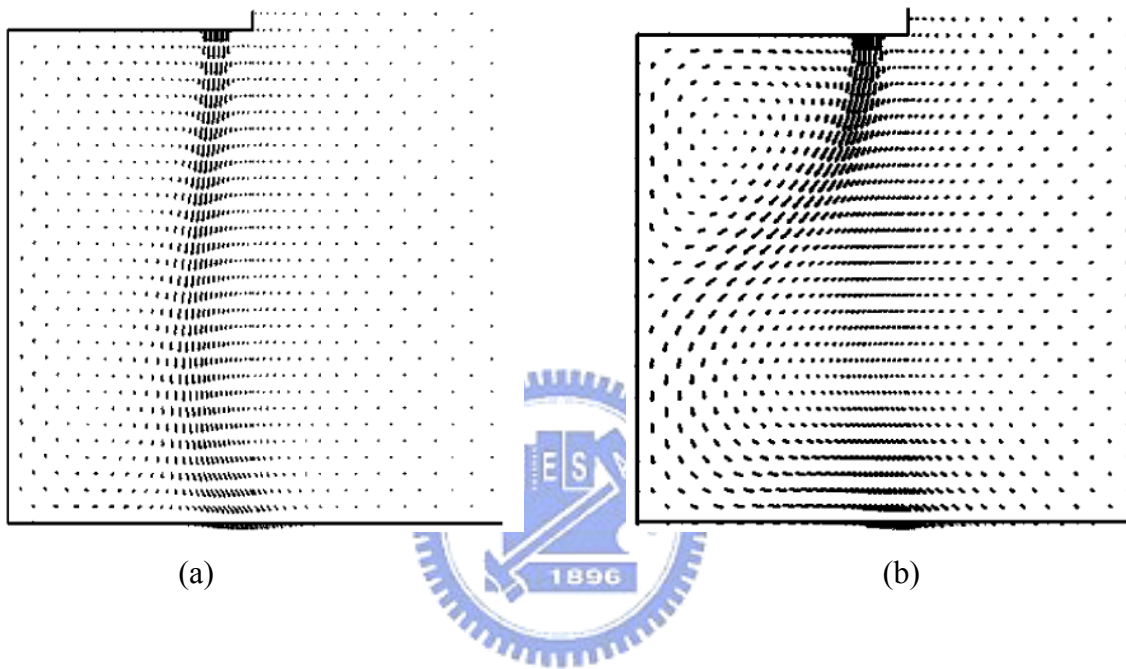


Fig.4.3 Steady recirculating flow pattern from Chen & Yuan [10] for $H / b_j = 20$, $Gr_t = 2.7 \times 10^{10}$ and $N = 0$ for (a) $Ri_t = 0.2$ and (b) $Ri_t = 0.32$.

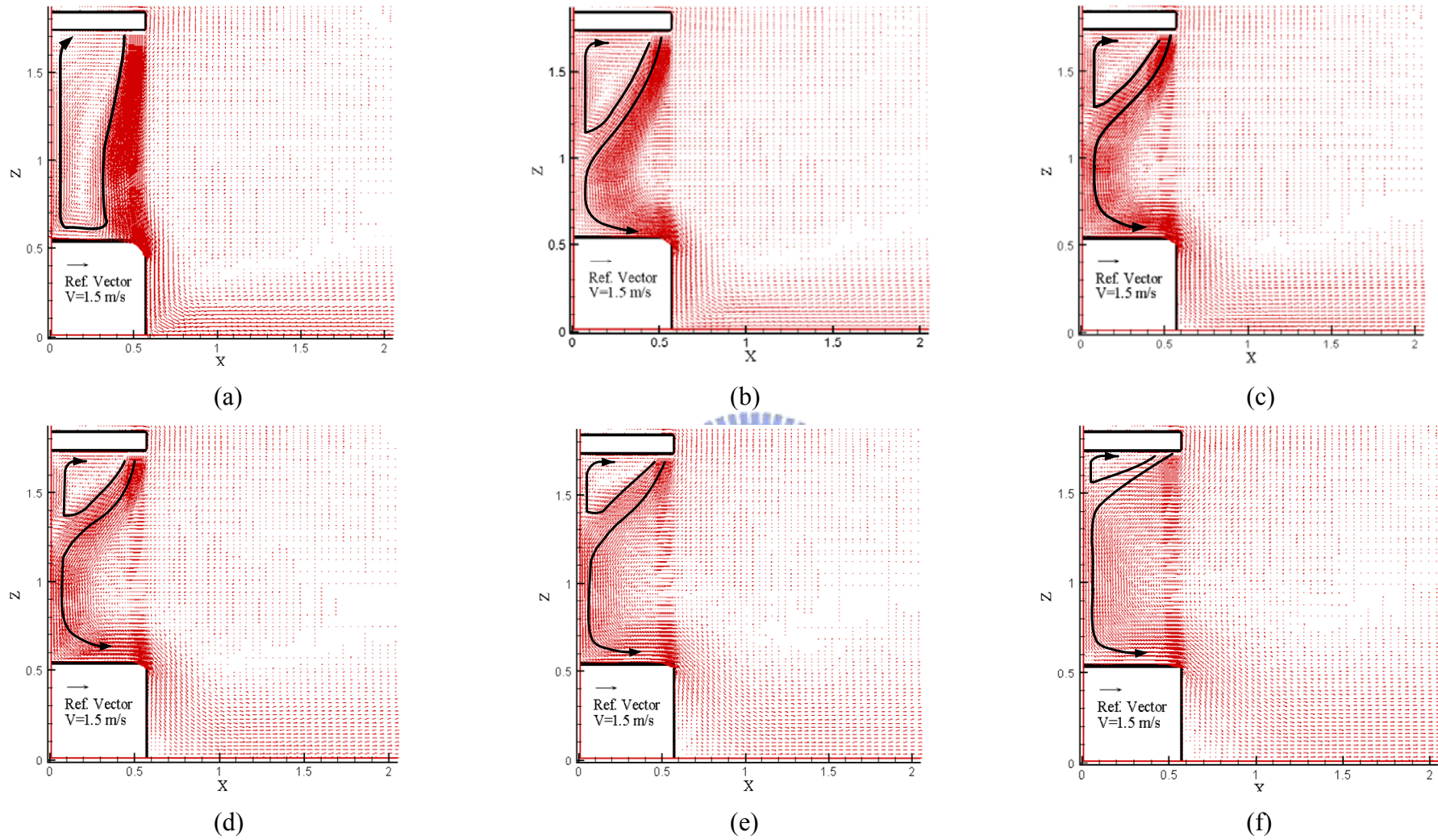


Fig. 4.4 Velocity vector maps for steady cavity flow for $b_j = 0.1$ m, $Gr_t = 4.61 \times 10^9$ ($\Delta T = 20^\circ\text{C}$), and $N = 6.37 \times 10^{-2}$ for $Re_b =$ (a) 9,548 ($V_j = 1.5$ m/s), (b) 8,275 ($V_j = 1.3$ m/s), (c) 6,365 ($V_j = 1.0$ m/s), (d) 5,092 ($V_j = 0.8$ m/s), (e) 3,183 ($V_j = 0.5$ m/s) and (f) 1,910 ($V_j = 0.3$ m/s).

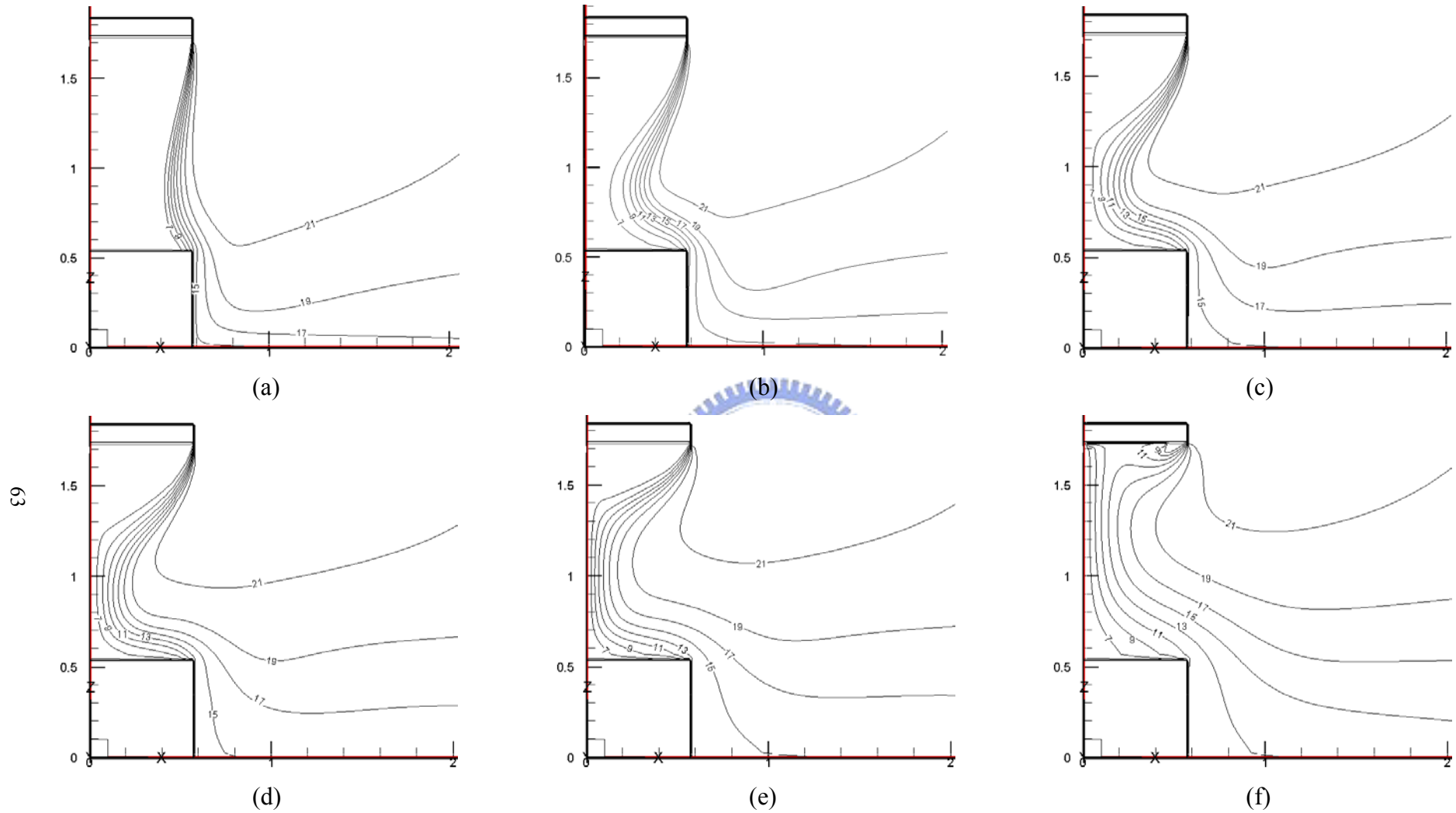


Fig. 4.5 Isotherms in the cavity for steady cavity flow for $b_j = 0.1$ m, $Gr_t = 4.61 \times 10^9$ ($\Delta T = 20^\circ C$), and $N = 6.37 \times 10^{-2}$ for $Re_b =$ (a) 9,548 ($V_j = 1.5$ m/s), (b) 8,275 ($V_j = 1.3$ m/s), (c) 6,365 ($V_j = 1.0$ m/s), (d) 5,092 ($V_j = 0.8$ m/s), (e) 3,183 ($V_j = 0.5$ m/s) and (f) 1,910 ($V_j = 0.3$ m/s).

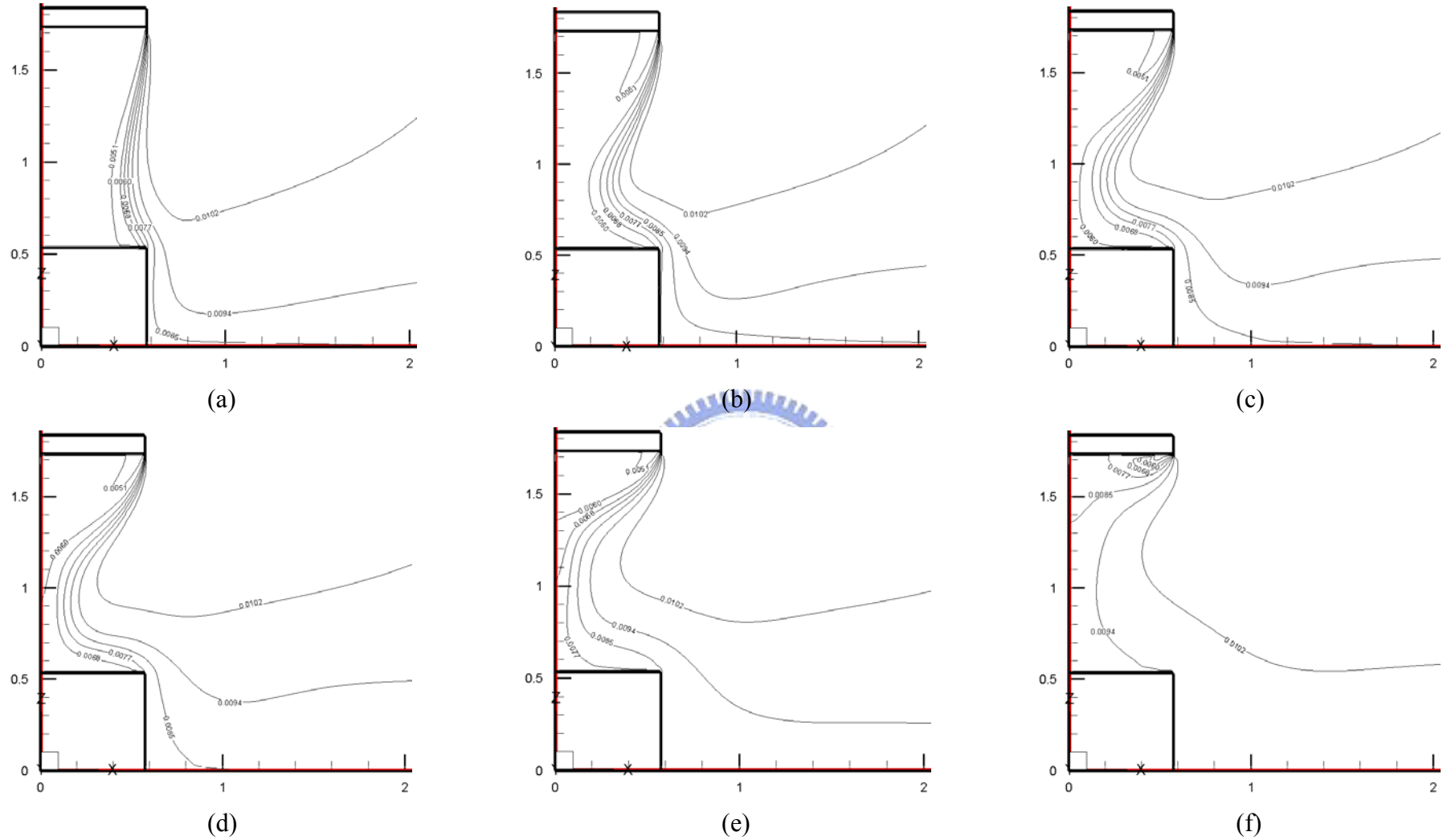


Fig. 4.6 Iso-concentration lines in the cavity for steady cavity flow for $b_j = 0.1$ m, $Gr_t = 4.61 \times 10^9$ ($\Delta T = 20^\circ\text{C}$), and $N = 6.37 \times 10^{-2}$ for $Re_b =$ (a) 9,548 ($V_j = 1.5$ m/s), (b) 8,275 ($V_j = 1.3$ m/s), (c) 6,365 ($V_j = 1.0$ m/s), (d) 5,092 ($V_j = 0.8$ m/s), (e) 3,183 ($V_j = 0.5$ m/s) and (f) 1,910 ($V_j = 0.3$ m/s).

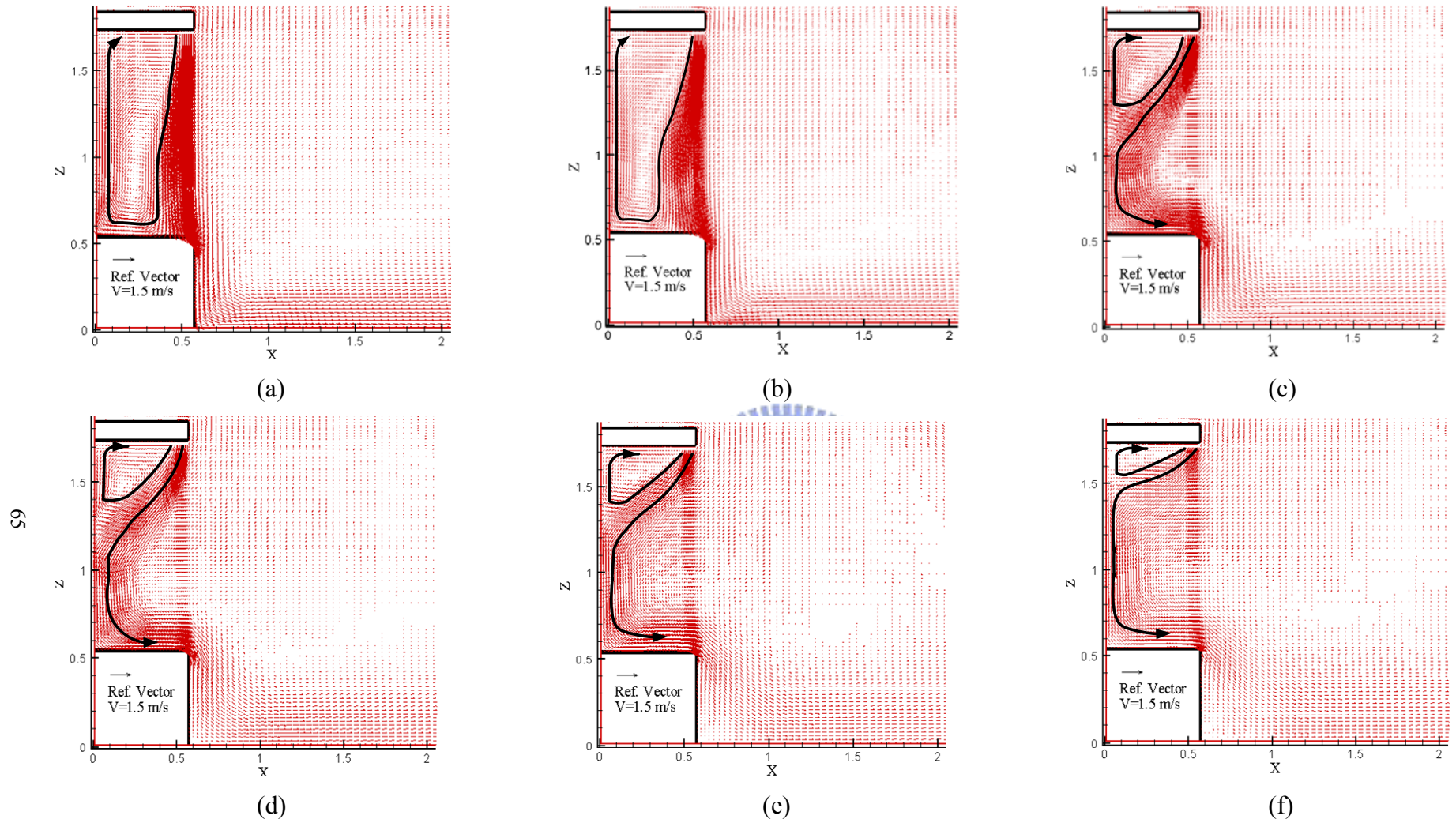


Fig. 4.7 Velocity vector maps for steady cavity flow for $b_j = 0.07$ m, $Gr_t = 4.61 \times 10^9$ ($\Delta T = 20^\circ C$), and $N = 6.37 \times 10^{-2}$ for $Re_b =$ (a) 9,548 ($V_j = 2.143$ m/s), (b) 8,275 ($V_j = 1.857$ m/s), (c) 6,365 ($V_j = 1.428$ m/s), (d) 5,092 ($V_j = 1.143$ m/s), (e) 3,183 ($V_j = 0.714$ m/s) and (f) 1,910 ($V_j = 0.428$ m/s).

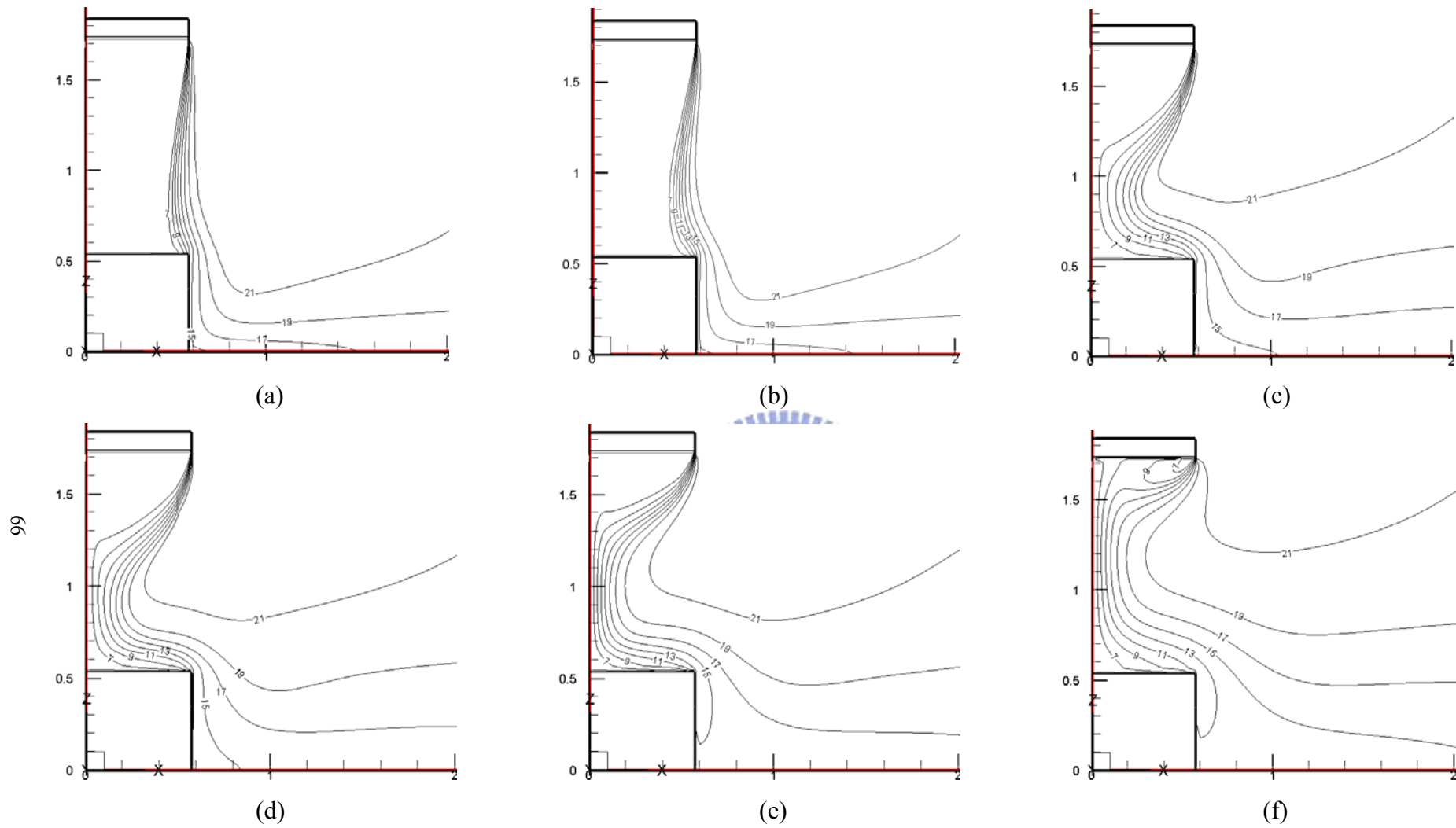


Fig. 4.8 Isotherms in the cavity for steady cavity flow for $b = 0.07$ m, $Gr_t = 4.61 \times 10^9$ ($\Delta T = 20^\circ\text{C}$), and $N = 6.37 \times 10^{-2}$ for $Re_b =$ (a) 9,548 ($V_j = 2.143$ m/s), (b) 8,275 ($V_j = 1.857$ m/s), (c) 6,365 ($V_j = 1.428$ m/s), (d) 5,092 ($V_j = 1.143$ m/s), (e) 3,183 ($V_j = 0.714$ m/s) and (f) 1,910 ($V_j = 0.428$ m/s).

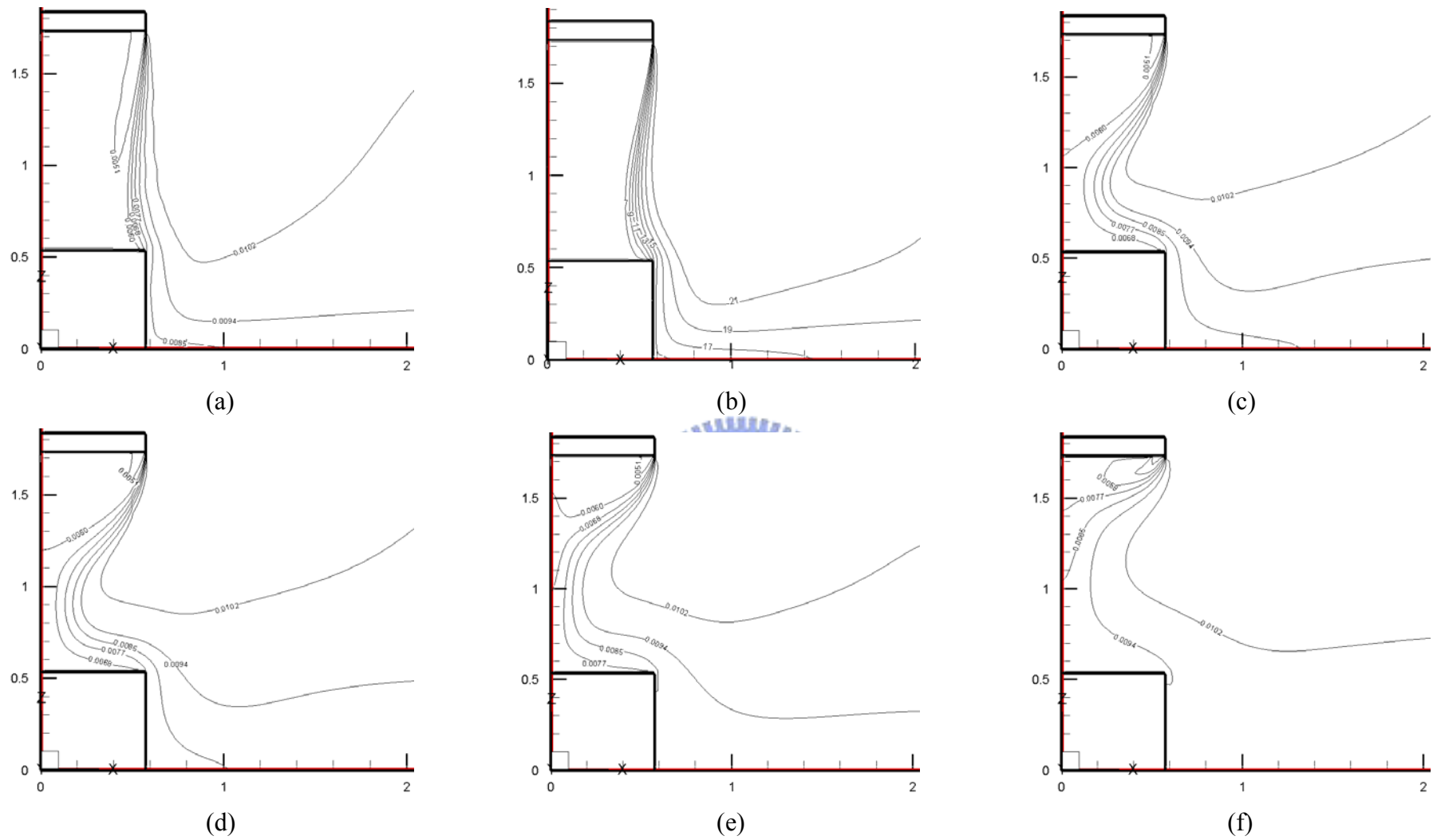


Fig. 4.9 Iso-concentration lines in the cavity for steady cavity flow for $b = 0.07$ m, $Gr_t = 4.61 \times 10^9$ ($\Delta T = 20^\circ\text{C}$), and $N = 6.37 \times 10^{-2}$ for $Re_b =$ (a) 9,548 ($V_j = 2.143$ m/s), (b) 8,275 ($V_j = 1.857$ m/s), (c) 6,365 ($V_j = 1.428$ m/s), (d) 5,092 ($V_j = 1.143$ m/s), (e) 3,183 ($V_j = 0.714$ m/s) and (f) 1,910 ($V_j = 0.428$ m/s).

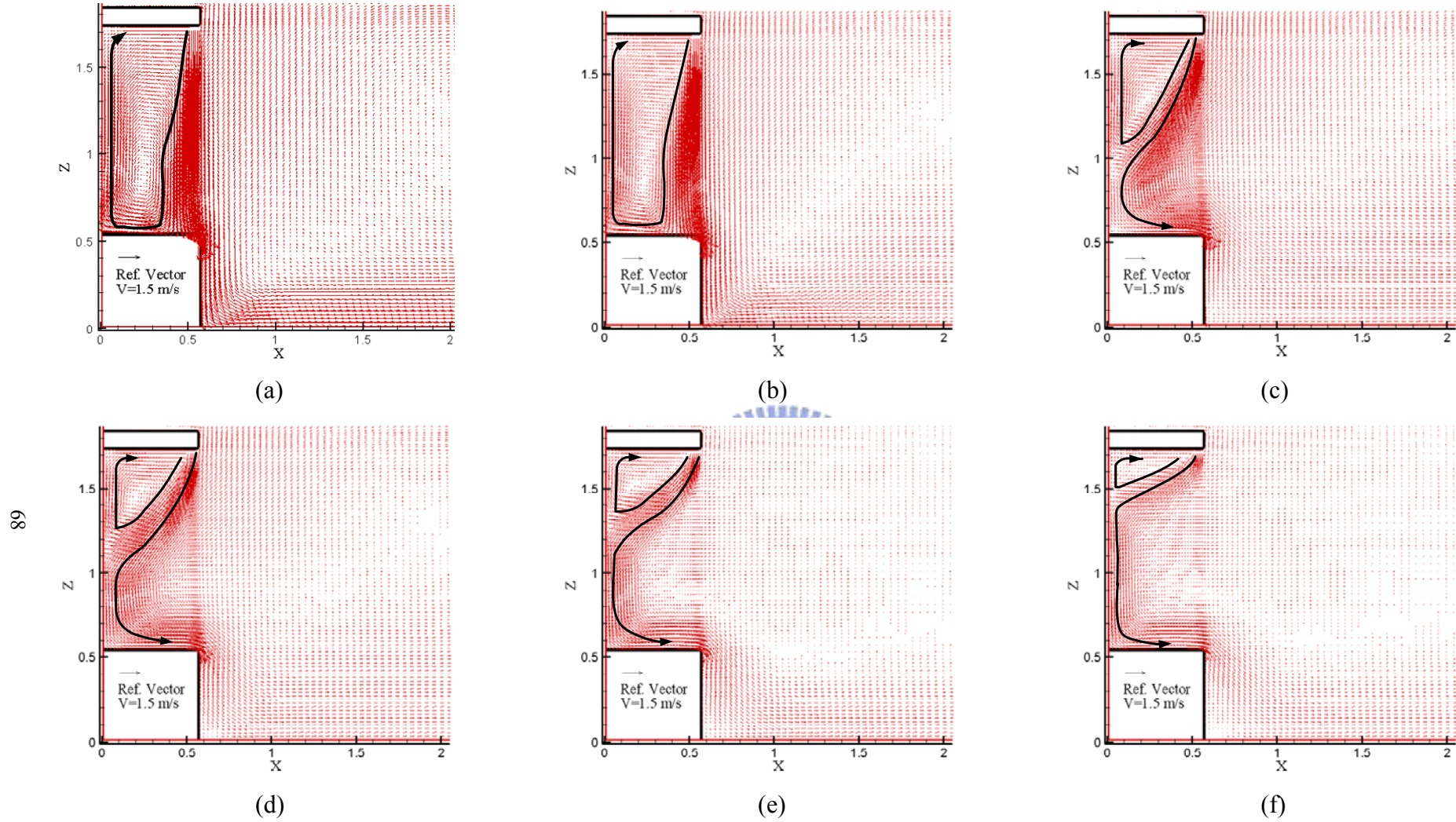


Fig. 4.10 Velocity vector maps for steady cavity flow for $b_j = 0.05$ m, $Gr_t = 4.61 \times 10^9$ ($\Delta T = 20^\circ\text{C}$), and $N = 6.37 \times 10^{-2}$ for $Re_b =$ (a) 9,548 ($V_j = 3$ m/s), (b) 8,275 ($V_j = 2.6$ m/s), (c) 6,365 ($V_j = 2.0$ m/s), (d) 5,092 ($V_j = 1.6$ m/s), (e) 3,183 ($V_j = 1.0$ m/s) and (f) 1,910 ($V_j = 0.6$ m/s).

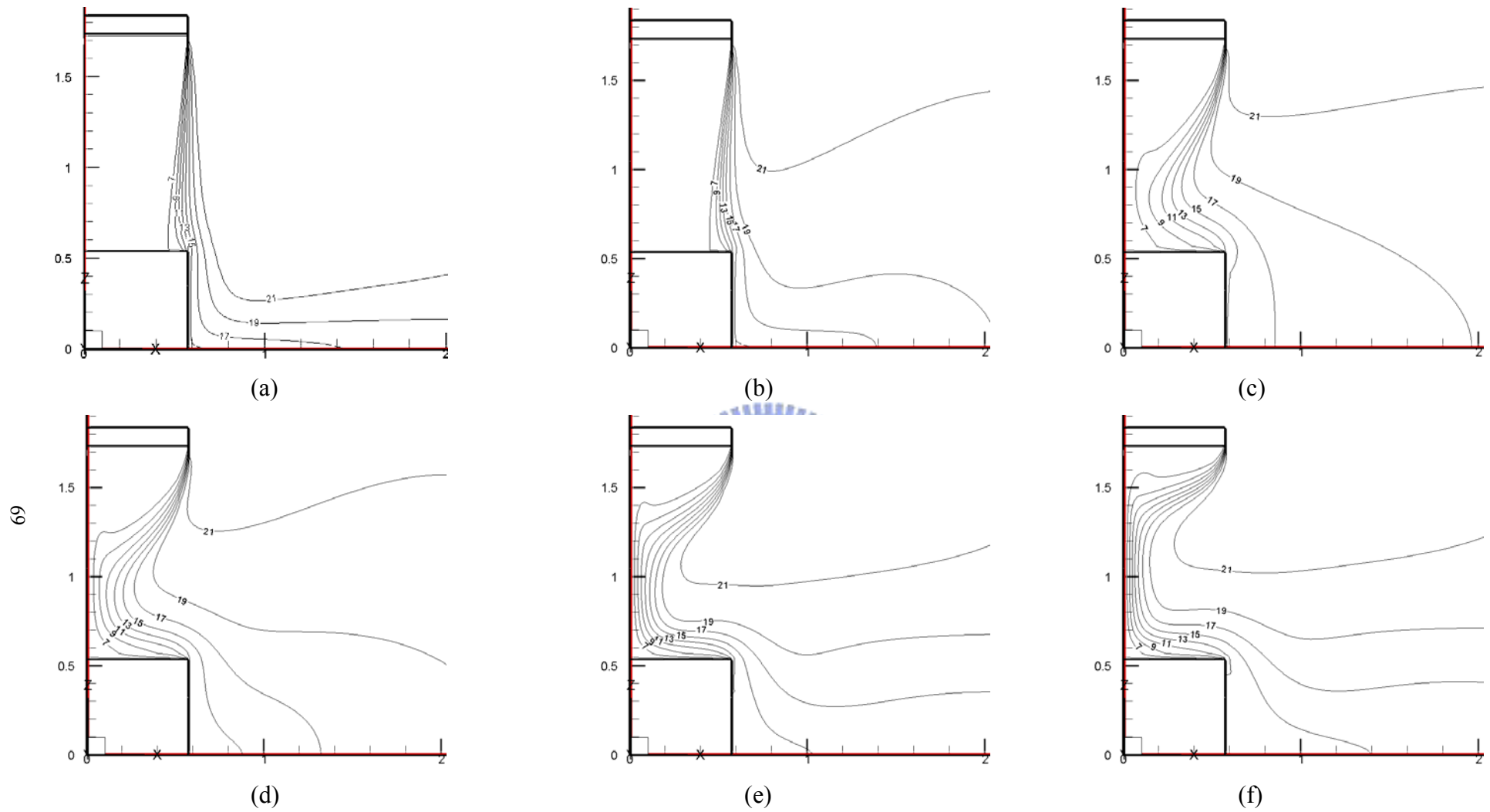


Fig. 4.11 Isotherms in the cavity for steady cavity flow for $b_j = 0.05$ m, $Gr_t = 4.61 \times 10^9$ ($\Delta T = 20^\circ C$), and $N = 6.37 \times 10^{-2}$ for $Re_b =$ (a) 9,548 ($V_j = 3$ m/s), (b) 8,275 ($V_j = 2.6$ m/s), (c) 6,365 ($V_j = 2.0$ m/s), (d) 5,092 ($V_j = 1.6$ m/s), (e) 3,183 ($V_j = 1.0$ m/s) and (f) 1,910 ($V_j = 0.6$ m/s).

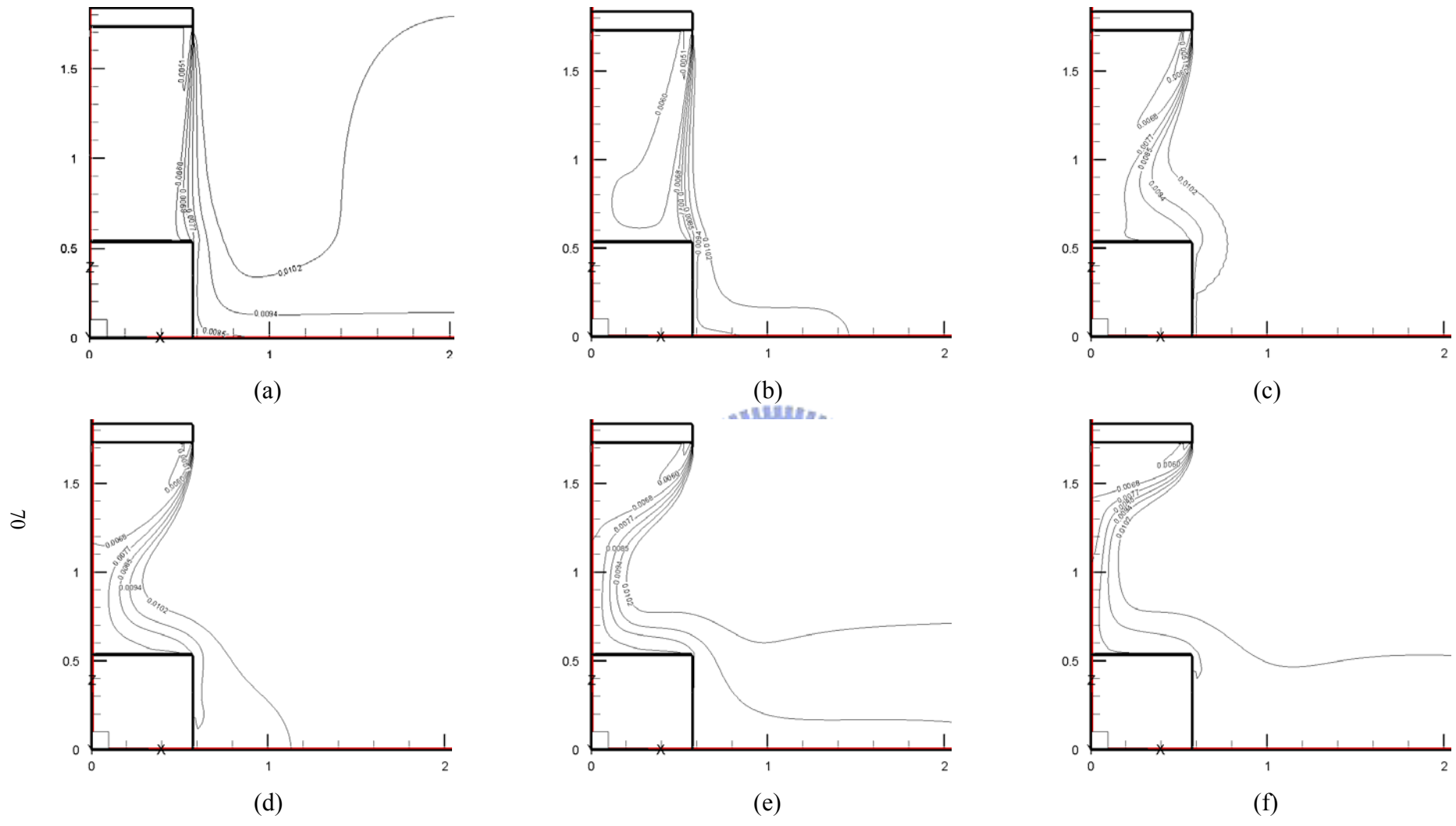


Fig. 4.12 Iso-concentration lines in the cavity for steady cavity flow for $b_j = 0.05$ m, $Gr_t = 4.61 \times 10^9$ ($\Delta T = 20^\circ C$), and $N = 6.37 \times 10^{-2}$ for $Re_b =$ (a) 9,548 ($V_j = 3$ m/s), (b) 8,275 ($V_j = 2.6$ m/s), (c) 6,365 ($V_j = 2.0$ m/s), (d) 5,092 ($V_j = 1.6$ m/s), (e) 3,183 ($V_j = 1.0$ m/s) and (f) 1,910 ($V_j = 0.6$ m/s).

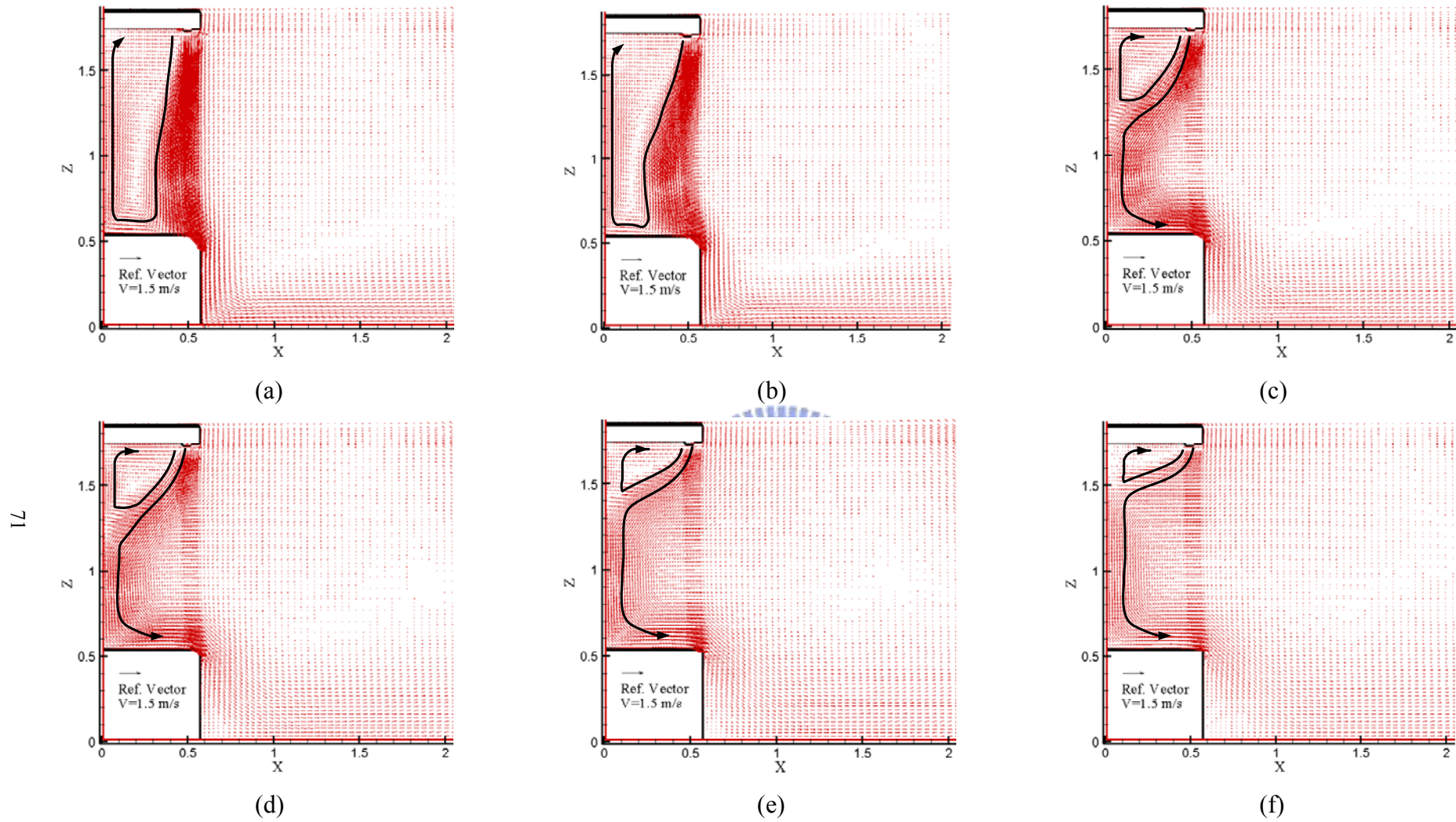


Fig. 4.13 Velocity vector maps for steady cavity flow for $b_j = 0.1$ m, $Gr_t = 4.61 \times 10^9$ ($\Delta T = 20^\circ\text{C}$), and $N = 6.37 \times 10^{-2}$ with a jet inclined angle of 5° for $Re_b =$ (a) 9,548 ($V_j = 1.5$ m/s), (b) 8,275 ($V_j = 1.3$ m/s), (c) 6,365 ($V_j = 1.0$ m/s), (d) 5,092 ($V_j = 0.8$ m/s), (e) 3,183 ($V_j = 0.5$ m/s) and (f) 1,910 ($V_j = 0.3$ m/s).

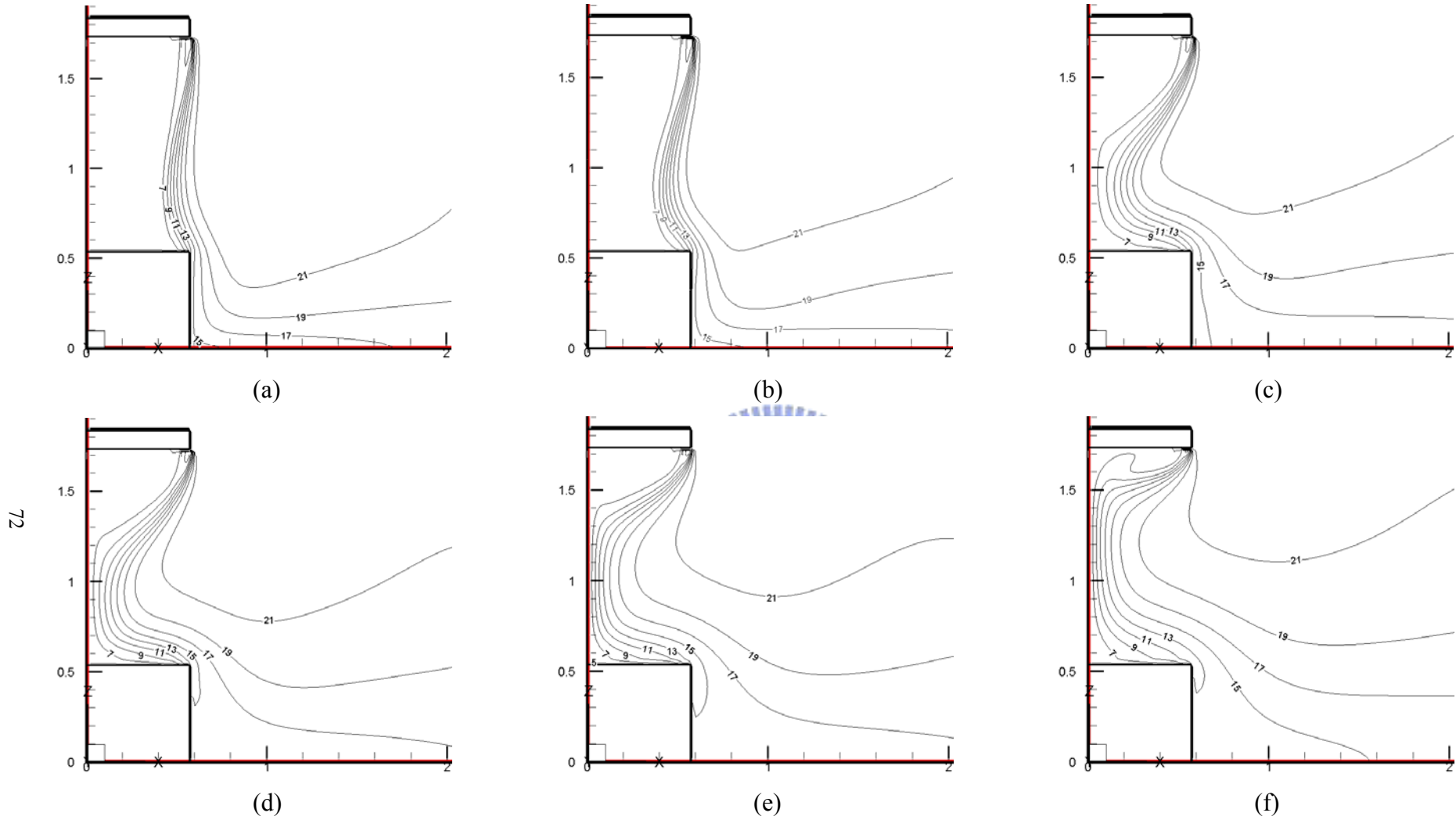


Fig. 4.14 Isotherms for steady cavity flow for $b_j = 0.1$ m, $Gr_t = 4.61 \times 10^9$ ($\Delta T = 20^\circ\text{C}$), and $N = 6.37 \times 10^{-2}$ with a jet inclined angle of 5° for $Re_b =$ (a) 9,548 ($V_j = 1.5$ m/s), (b) 8,275 ($V_j = 1.3$ m/s), (c) 6,365 ($V_j = 1.0$ m/s), (d) 5,092 ($V_j = 0.8$ m/s), (e) 3,183 ($V_j = 0.5$ m/s) and (f) 1,910 ($V_j = 0.3$ m/s).

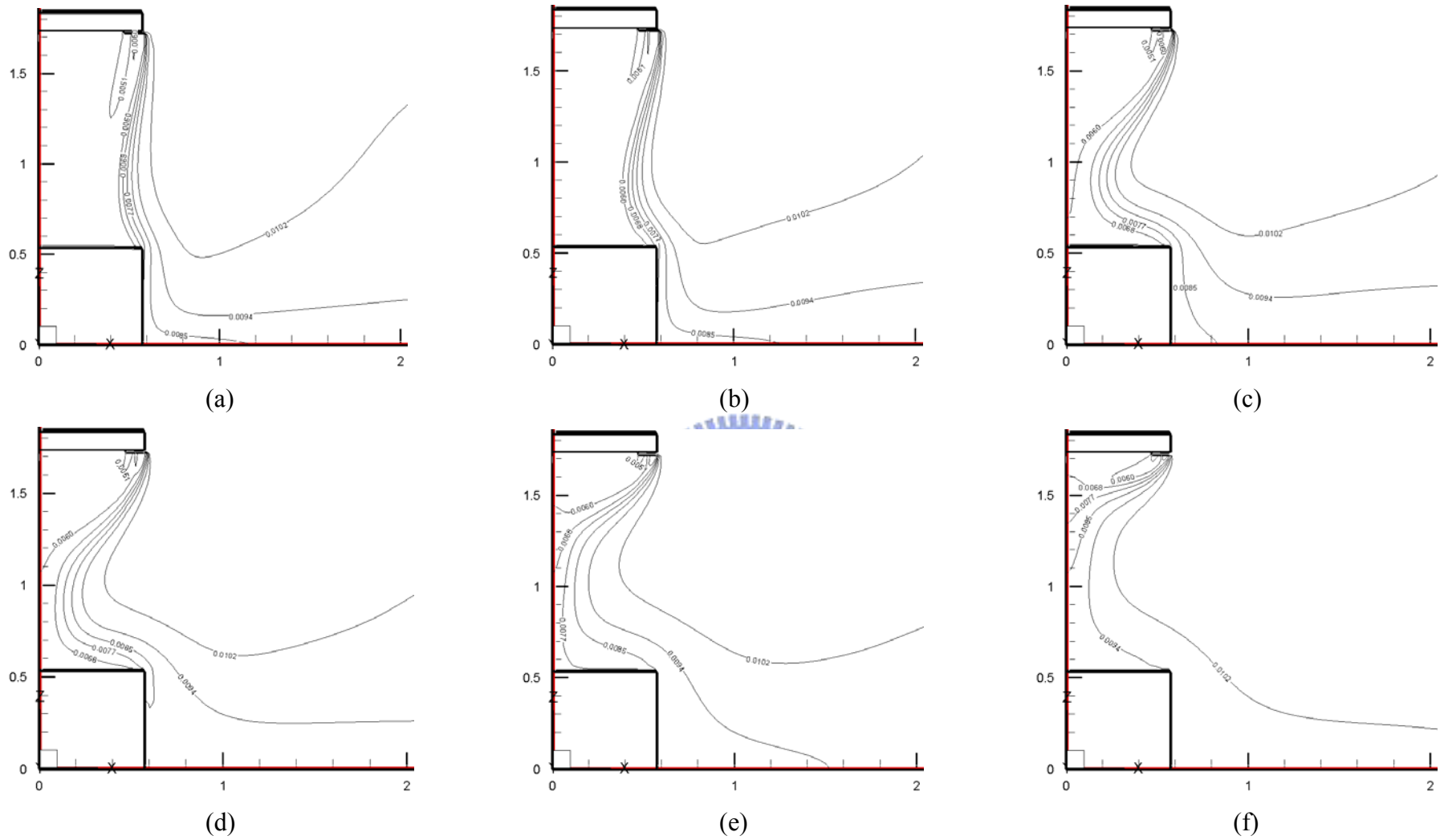


Fig. 4.15 Iso-concentration lines for steady cavity flow for $b_j = 0.1$ m, $Gr_t = 4.61 \times 10^9$ ($\Delta T = 20^\circ\text{C}$), and $N = 6.37 \times 10^{-2}$ with a jet inclined angle of 5° for $Re_b =$ (a) 9,548 ($V_j = 1.5$ m/s), (b) 8,275 ($V_j = 1.3$ m/s), (c) 6,365 ($V_j = 1.0$ m/s), (d) 5,092 ($V_j = 0.8$ m/s), (e) 3,183 ($V_j = 0.5$ m/s) and (f) 1,910 ($V_j = 0.3$ m/s).

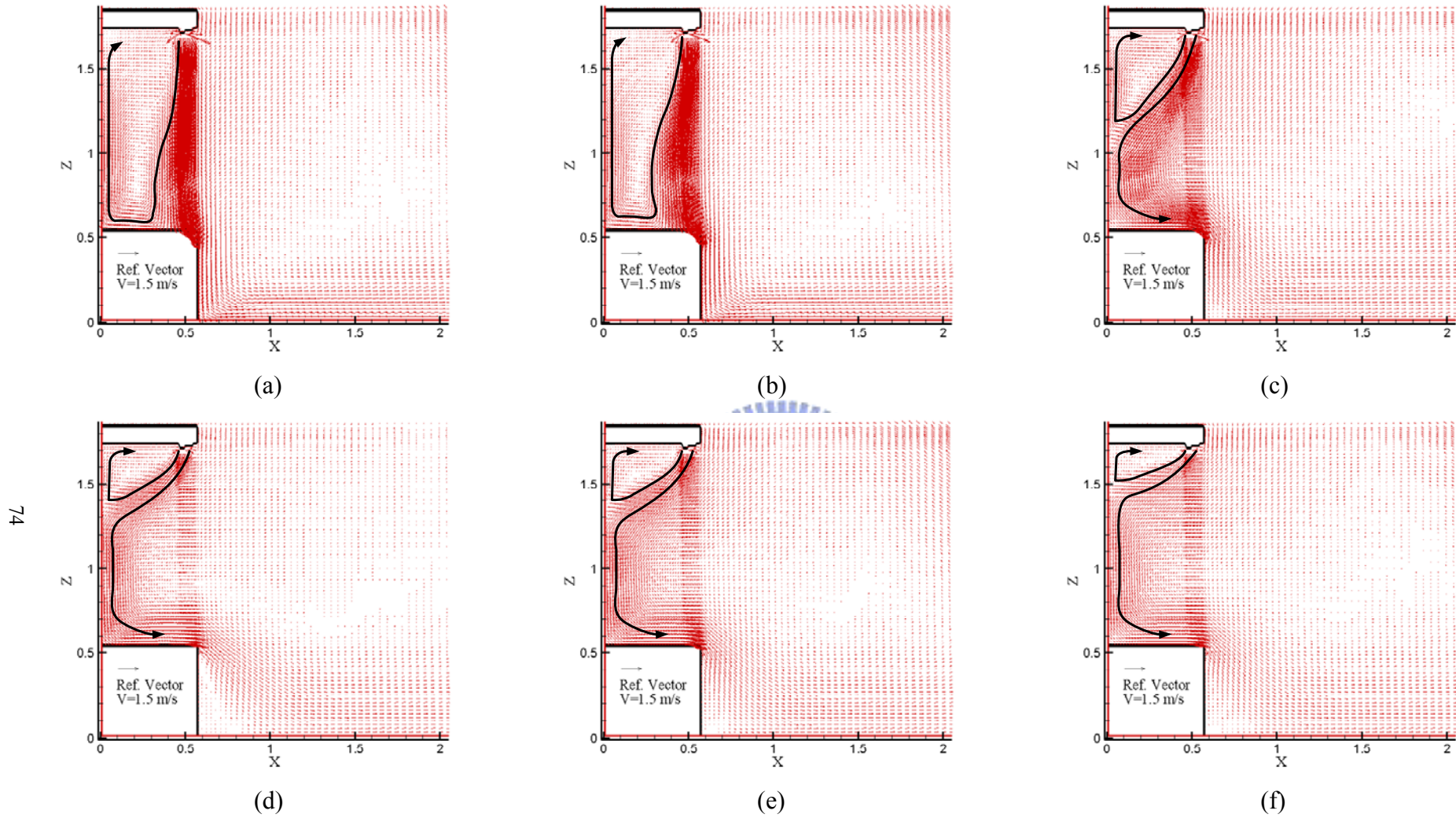


Fig. 4.16 Velocity vector maps for steady cavity flow for $b_j = 0.1$ m, $Gr_t = 4.61 \times 10^9$ ($\Delta T = 20^\circ\text{C}$), and $N = 6.37 \times 10^{-2}$ with a jet inclined angle of 15° for $Re_b =$ (a) 9,548 ($V_j = 1.5$ m/s), (b) 8,275 ($V_j = 1.3$ m/s), (c) 6,365 ($V_j = 1.0$ m/s), (d) 5,092 ($V_j = 0.8$ m/s), (e) 3,183 ($V_j = 0.5$ m/s) and (f) 1,910 ($V_j = 0.3$ m/s).

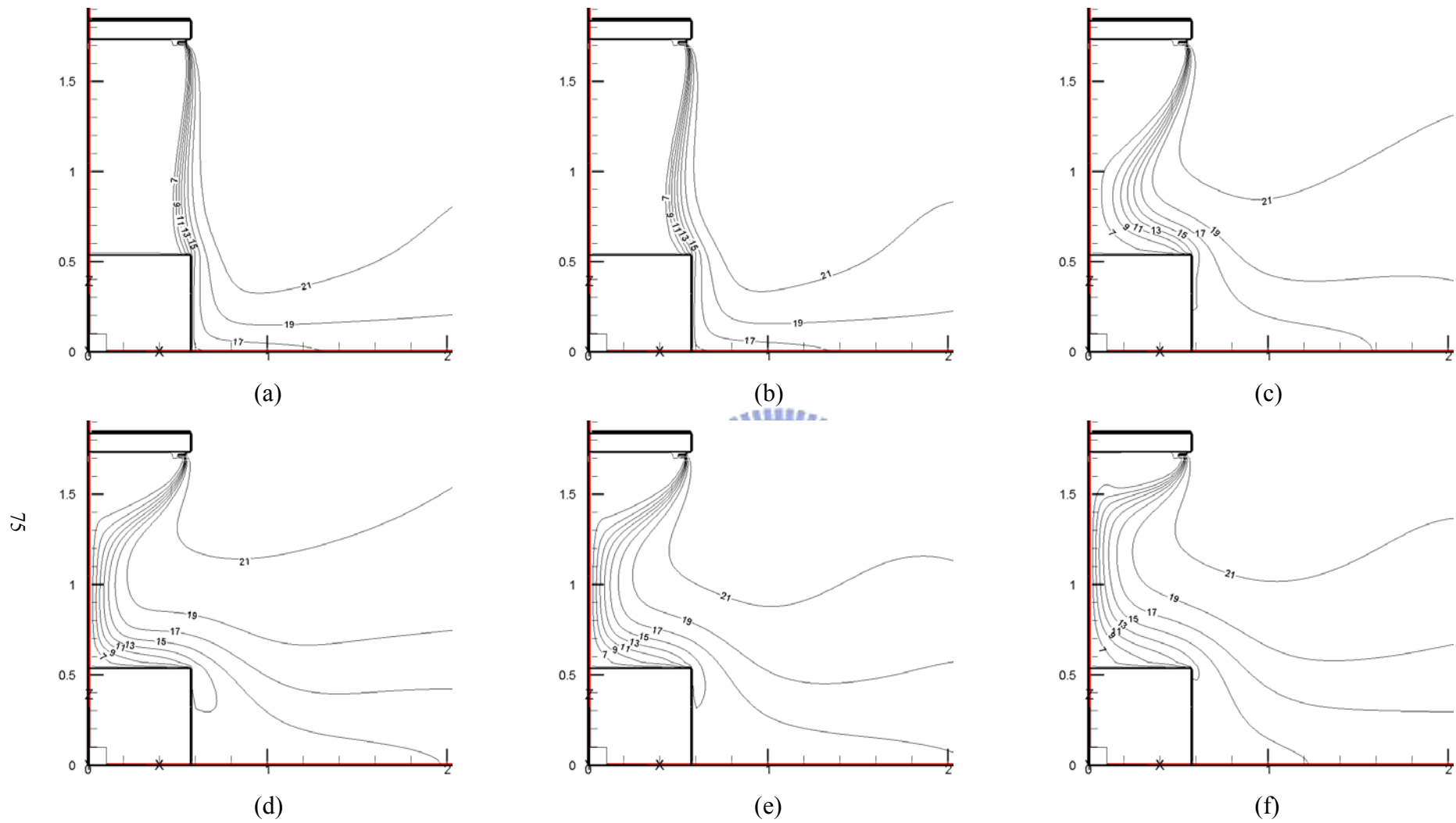


Fig. 4.17 Isotherms for steady cavity flow for $b_j = 0.1$ m, $Gr_t = 4.61 \times 10^9$ ($\Delta T = 20^\circ\text{C}$), and $N = 6.37 \times 10^{-2}$ with a jet inclined angle of 15° for $Re_b =$ (a) 9,548 ($V_j = 1.5$ m/s), (b) 8,275 ($V_j = 1.3$ m/s), (c) 6,365 ($V_j = 1.0$ m/s), (d) 5,092 ($V_j = 0.8$ m/s), (e) 3,183 ($V_j = 0.5$ m/s) and (f) 1,910 ($V_j = 0.3$ m/s).

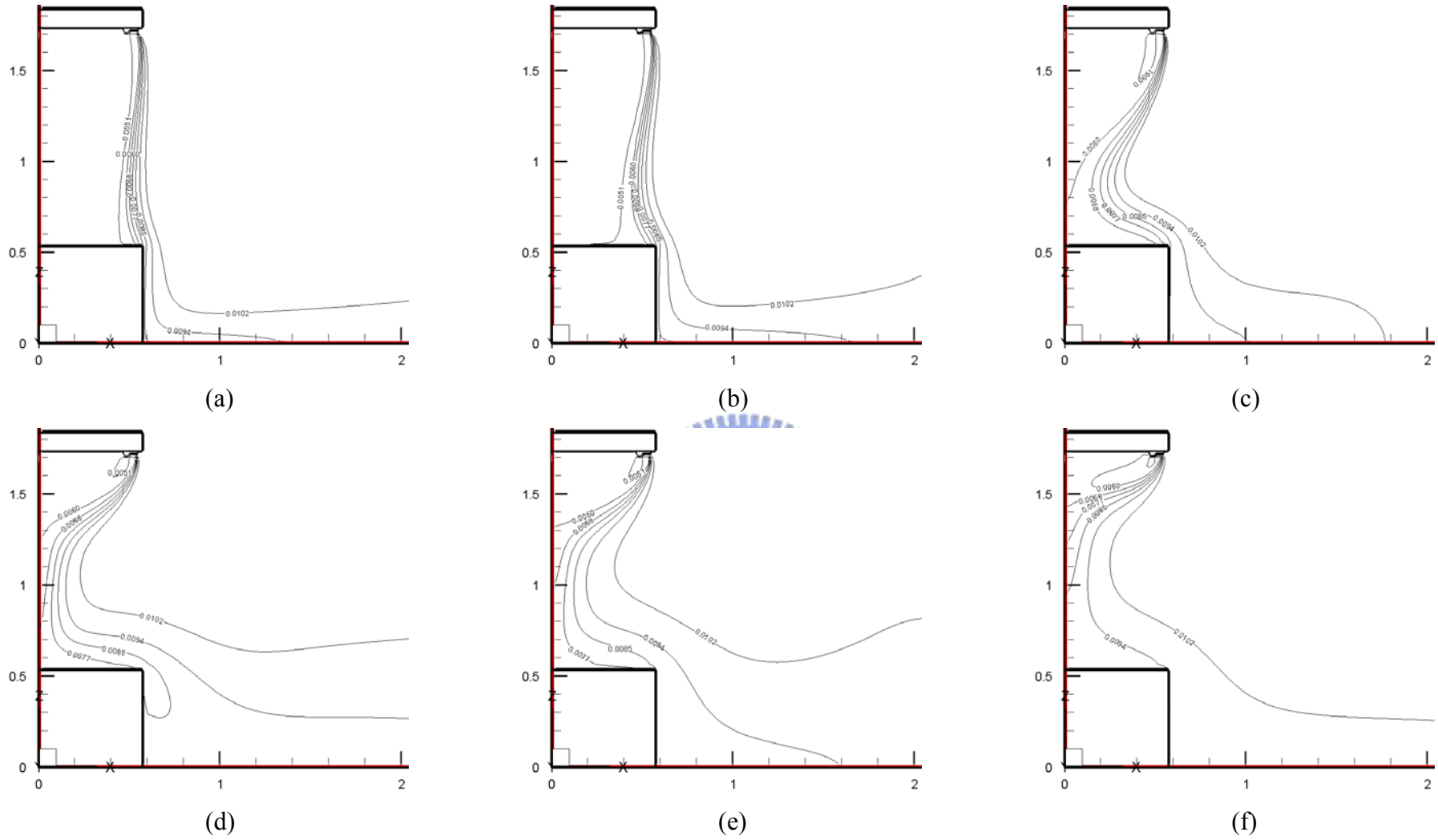


Fig. 4.18 Iso-concentration lines for steady cavity flow for $b_j = 0.1$ m, $Gr_t = 4.61 \times 10^9$ ($\Delta T = 20^\circ\text{C}$), and $N = 6.37 \times 10^{-2}$ with a jet inclined angle of 15° for $Re_b =$ (a) 9,548 ($V_j = 1.5$ m/s), (b) 8,275 ($V_j = 1.3$ m/s), (c) 6,365 ($V_j = 1.0$ m/s), (d) 5,092 ($V_j = 0.8$ m/s), (e) 3,183 ($V_j = 0.5$ m/s) and (f) 1,910 ($V_j = 0.3$ m/s).

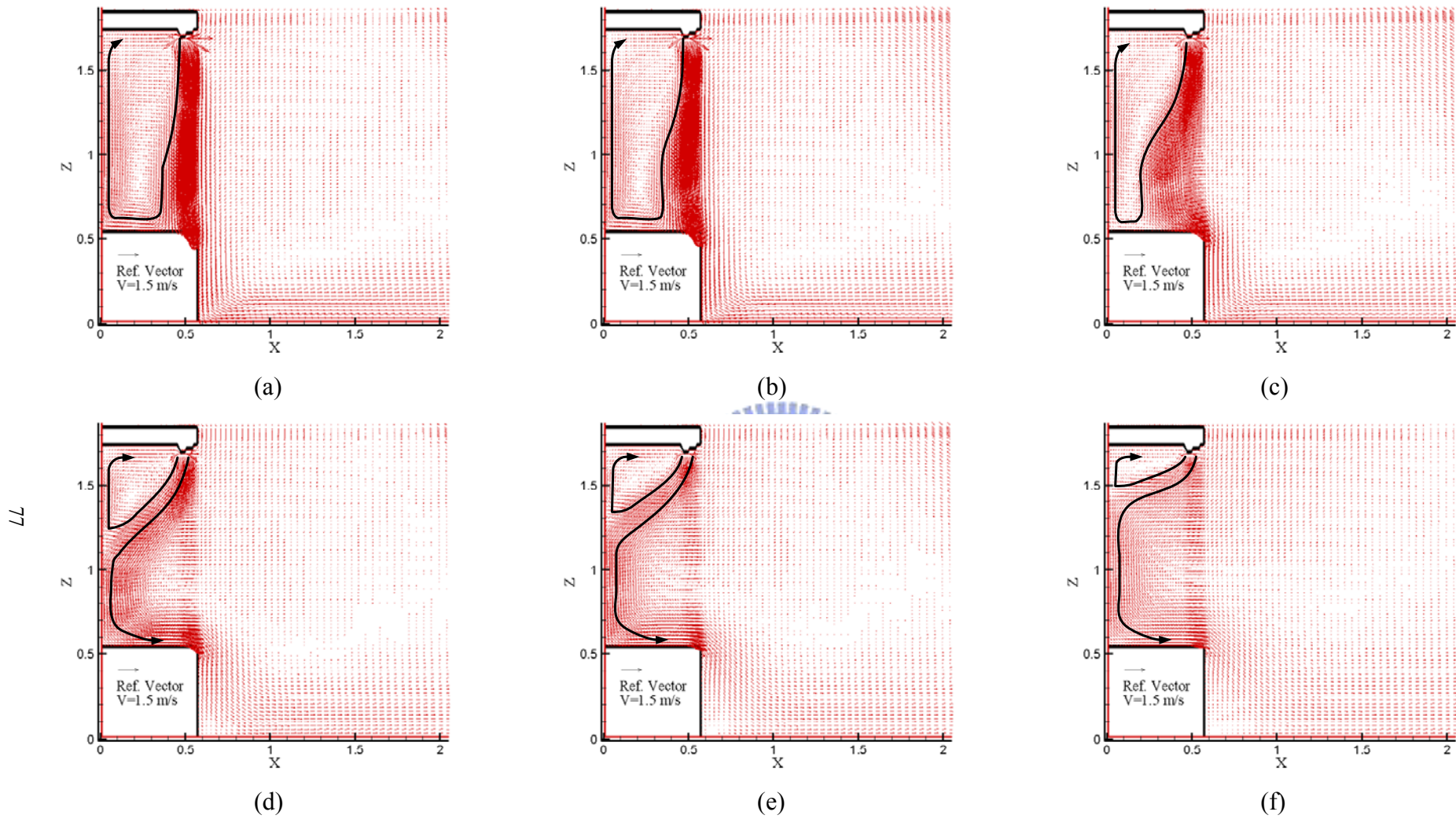


Fig. 4.19 Velocity vector maps for steady cavity flow for $b_j = 0.1 \text{ m}$, $Gr_t = 4.61 \times 10^9$ ($\Delta T = 20^\circ\text{C}$), and $N = 6.37 \times 10^{-2}$ with a jet inclined angle of 25° for $Re_b =$ (a) 9,548 ($V_j = 1.5 \text{ m/s}$), (b) 8,275 ($V_j = 1.3 \text{ m/s}$), (c) 6,365 ($V_j = 1.0 \text{ m/s}$), (d) 5,092 ($V_j = 0.8 \text{ m/s}$), (e) 3,183 ($V_j = 0.5 \text{ m/s}$) and (f) 1,910 ($V_j = 0.3 \text{ m/s}$).

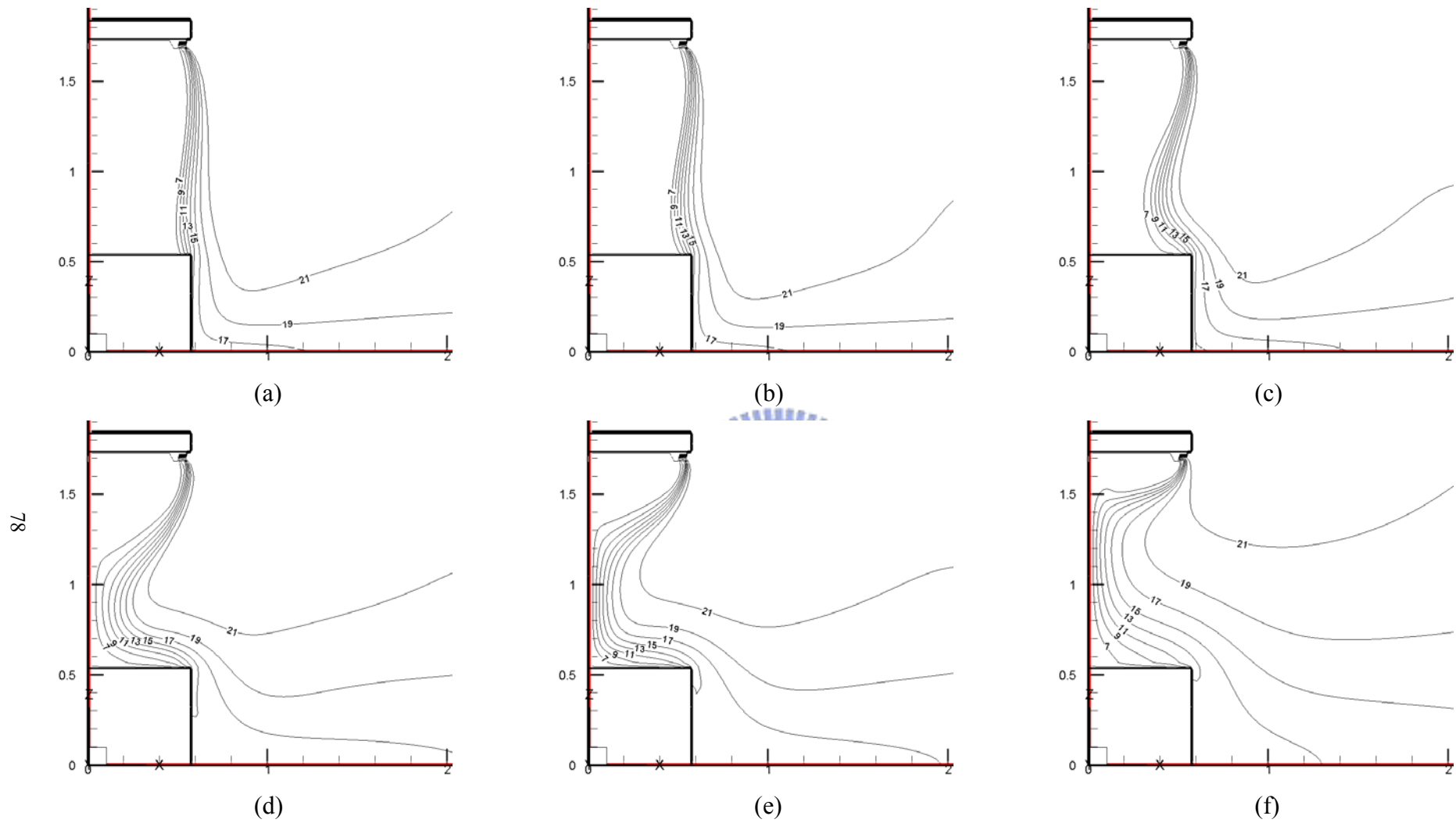


Fig. 4.20 Isotherms for steady cavity flow for $b_j = 0.1$ m, $Gr_t = 4.61 \times 10^9$ ($\Delta T = 20^\circ\text{C}$), and $N = 6.37 \times 10^{-2}$ with a jet inclined angle of 25° for $Re_b =$ (a) 9,548 ($V_j = 1.5$ m/s), (b) 8,275 ($V_j = 1.3$ m/s), (c) 6,365 ($V_j = 1.0$ m/s), (d) 5,092 ($V_j = 0.8$ m/s), (e) 3,183 ($V_j = 0.5$ m/s) and (f) 1,910 ($V_j = 0.3$ m/s).

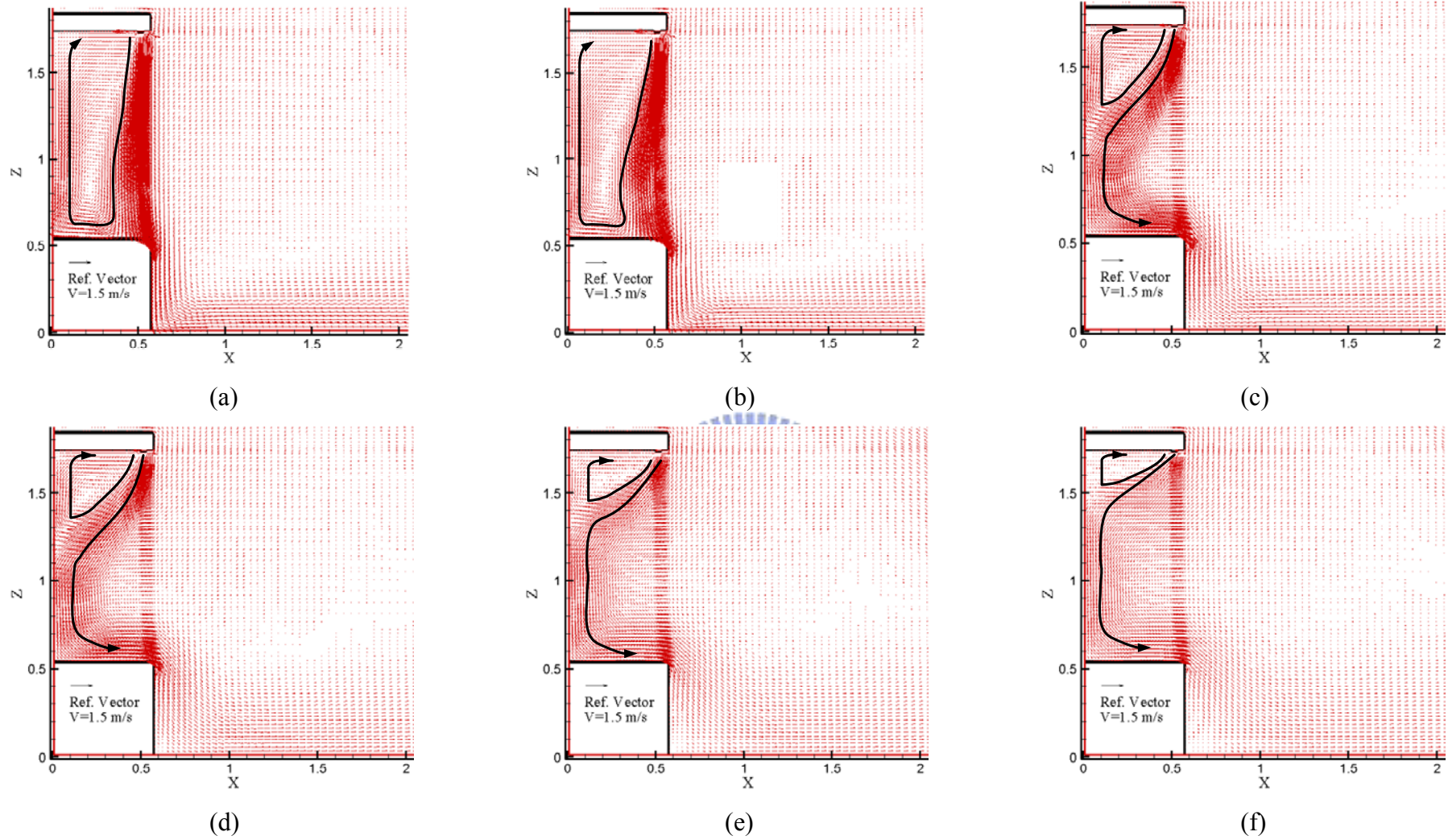


Fig. 4.22 Velocity vector maps for steady cavity flow for $b_j = 0.07$ m, $Gr_t = 4.61 \times 10^9$ ($\Delta T = 20^\circ\text{C}$), and $N = 6.37 \times 10^{-2}$ with a jet inclined angle of 5° for $Re_b =$ (a) 9,548 ($V_j = 2.143$ m/s), (b) 8,275 ($V_j = 1.857$ m/s), (c) 6,365 ($V_j = 1.428$ m/s), (d) 5,092 ($V_j = 1.143$ m/s), (e) 3,183 ($V_j = 0.714$ m/s) and (f) 1,910 ($V_j = 0.428$ m/s).

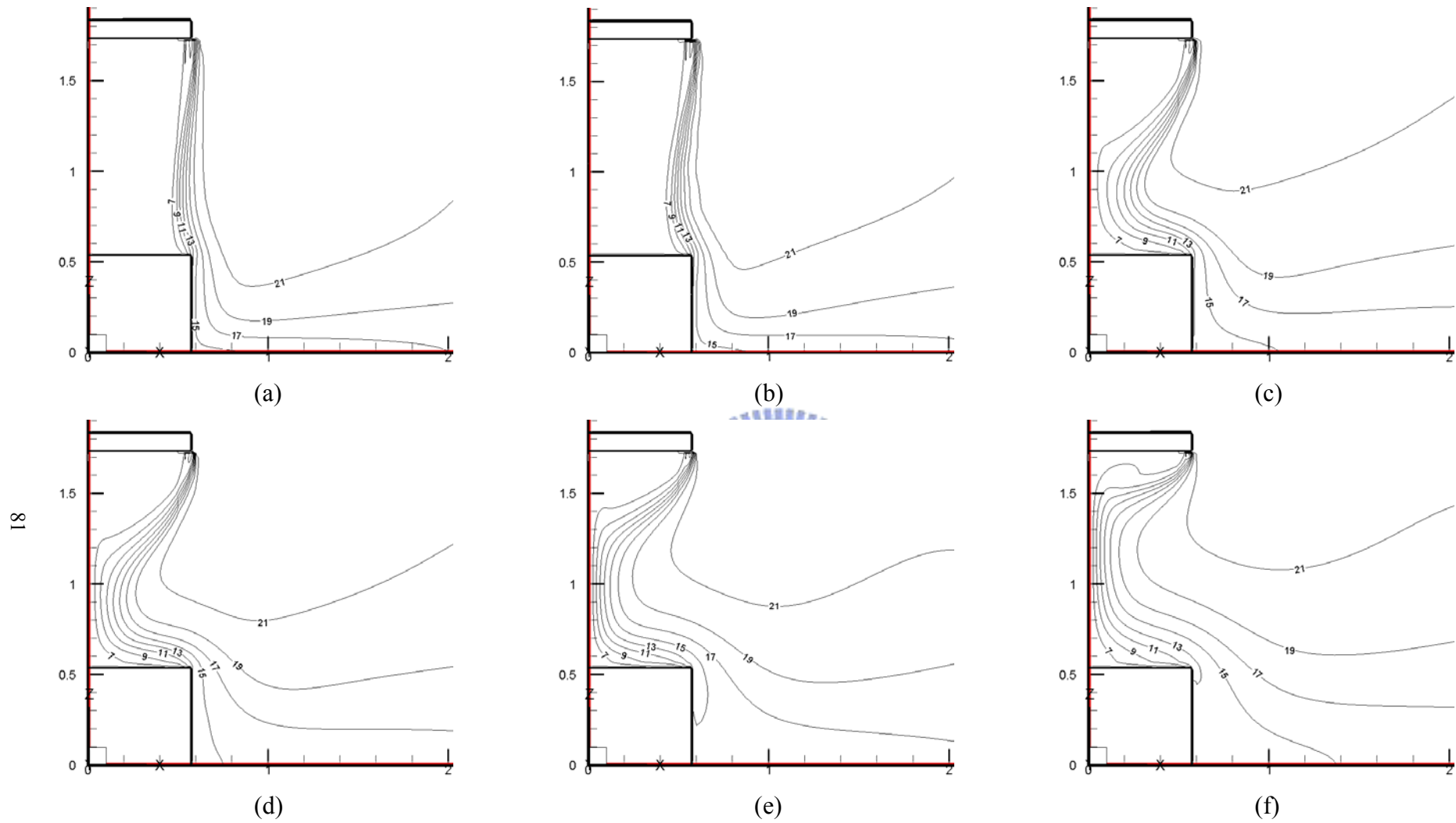


Fig. 4.23 Isotherms for steady cavity flow for $b_j = 0.07$ m, $Gr_t = 4.61 \times 10^9$ ($\Delta T = 20^\circ\text{C}$), and $N = 6.37 \times 10^{-2}$ with a jet inclined angle of 5° for $Re_b =$ (a) 9,548 ($V_j = 2.143$ m/s), (b) 6,365 ($V_j = 1.428$ m/s), (c) 5,092 ($V_j = 1.143$ m/s), (d) 3,183 ($V_j = 0.714$ m/s) and (e) 1,910 ($V_j = 0.428$ m/s).

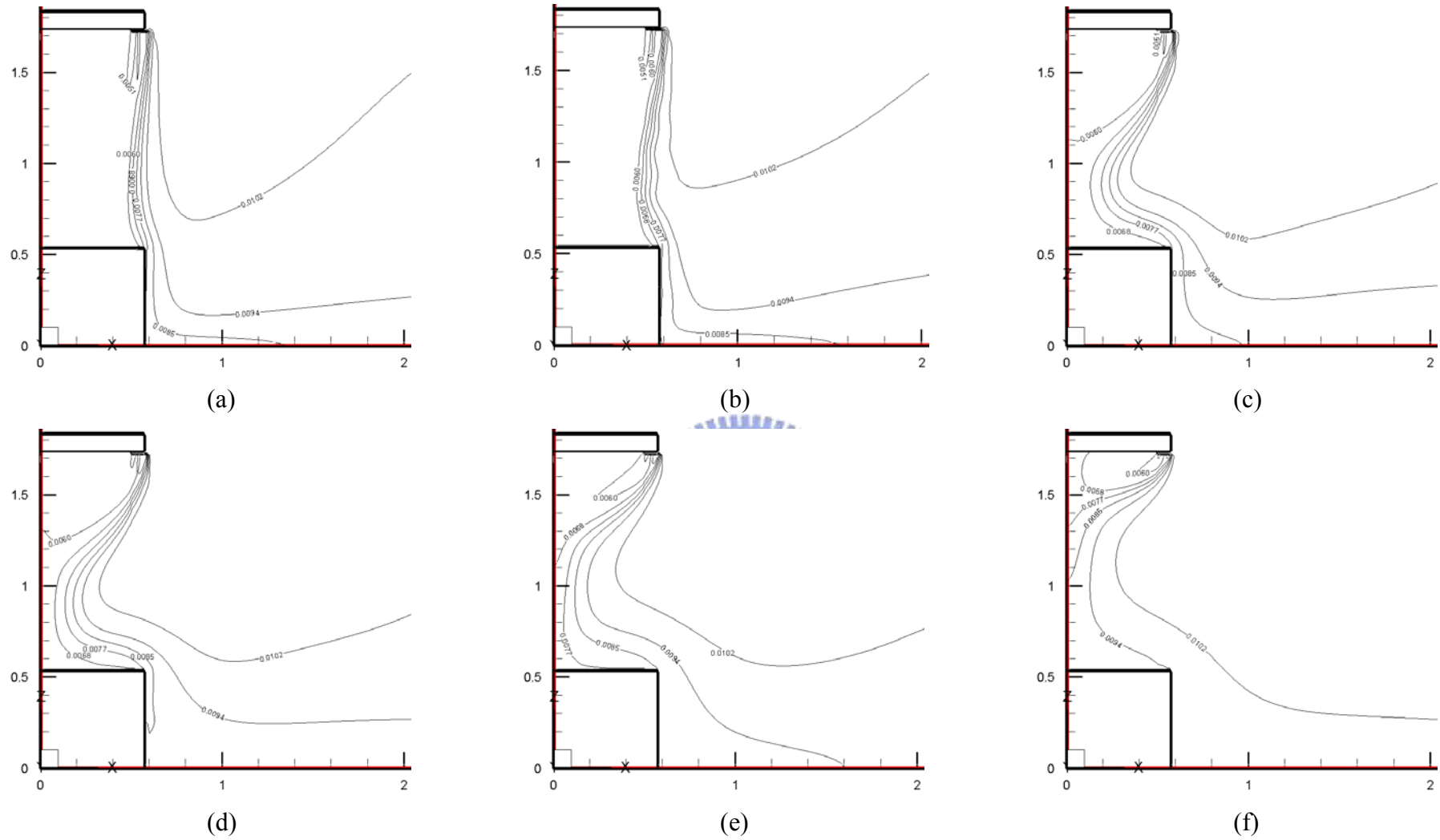


Fig. 4.24 Iso-concentration lines for steady cavity flow for $b_j = 0.07$ m, $Gr_t = 4.61 \times 10^9$ ($\Delta T = 20^\circ\text{C}$), and $N = 6.37 \times 10^{-2}$ with a jet inclined angle of 5° for $Re_b =$ (a) 9,548 ($V_j = 2.143$ m/s), (b) 6,365 ($V_j = 1.428$ m/s), (c) 5,092 ($V_j = 1.143$ m/s), (d) 3,183 ($V_j = 0.714$ m/s) and (e) 1,910 ($V_j = 0.428$ m/s)

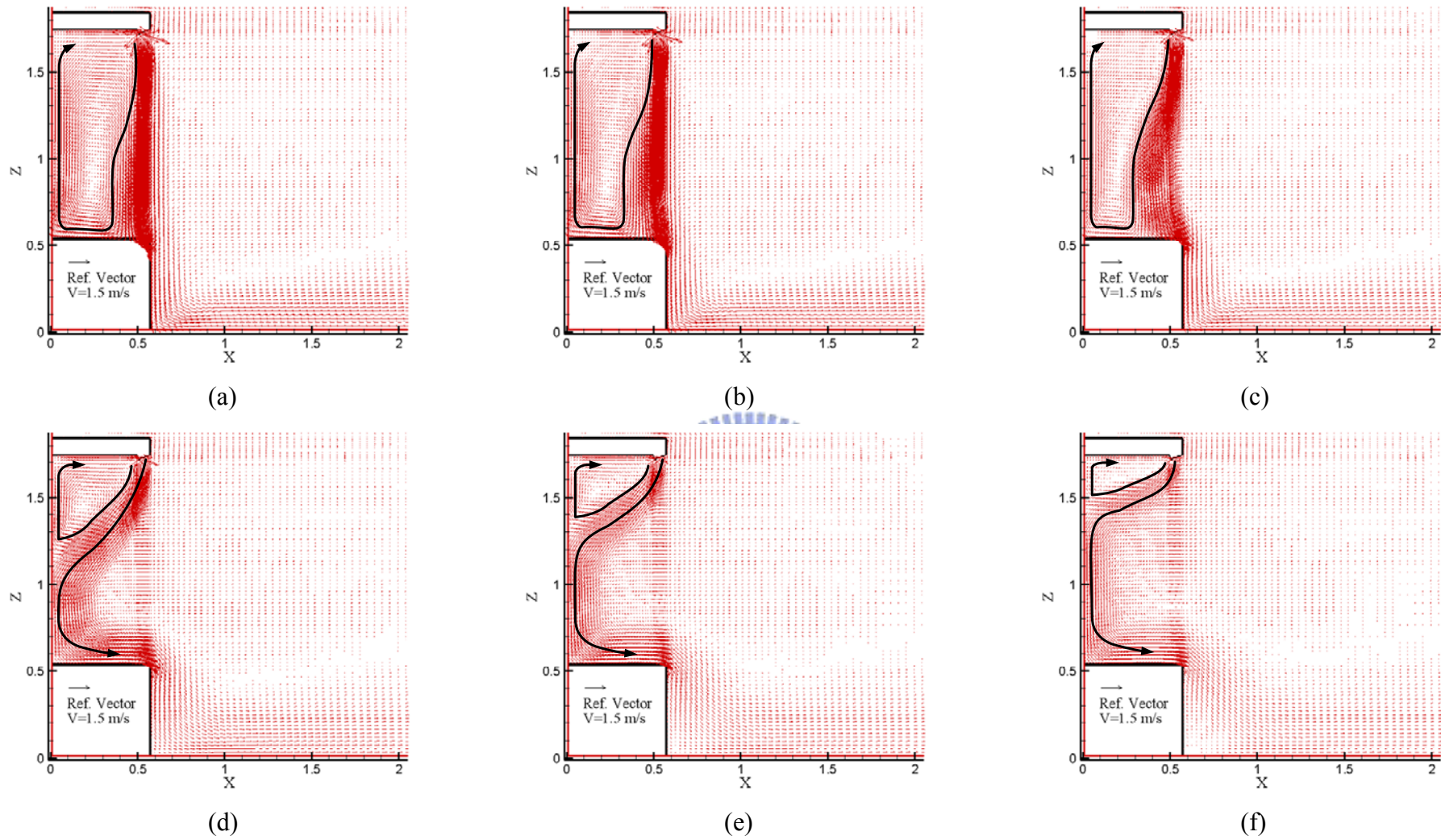


Fig. 4.25 Velocity vector maps for steady cavity flow for $b_j = 0.07$ m, $Gr_t = 4.61 \times 10^9$ ($\Delta T = 20^\circ\text{C}$), and $N = 6.37 \times 10^{-2}$ with a jet inclined angle of 15° for $Re_b =$ (a) 9,548 ($V_j = 2.142$ m/s), (b) 8,275 ($V_j = 1.857$ m/s), (c) 6,365 ($V_j = 1.428$ m/s), (d) 5,092 ($V_j = 1.142$ m/s), (e) 3,183 ($V_j = 0.714$ m/s) and (f) 1,910 ($V_j = 0.428$ m/s).

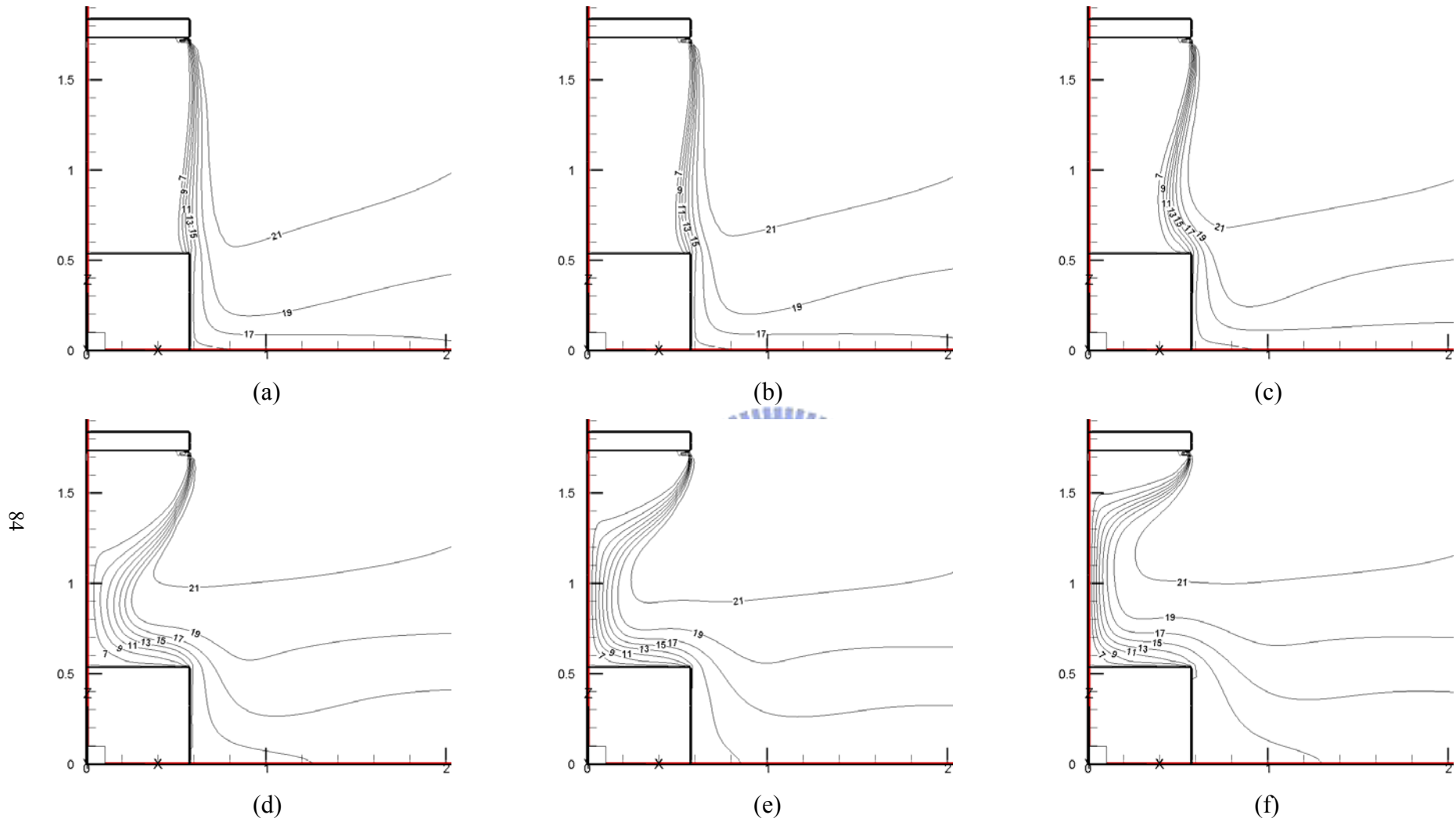


Fig. 4.26 Isotherms for steady cavity flow for $b_j = 0.07$ m, $Gr_t = 4.61 \times 10^9$ ($\Delta T = 20^\circ\text{C}$), and $N = 6.37 \times 10^{-2}$ with a jet inclined angle of 15° for $Re_b =$ (a) 9,548 ($V_j = 2.142$ m/s), (b) 8,275 ($V_j = 1.857$ m/s), (c) 6,365 ($V_j = 1.428$ m/s), (d) 5,092 ($V_j = 1.142$ m/s), (e) 3,183 ($V_j = 0.714$ m/s) and (f) 1,910 ($V_j = 0.428$ m/s).

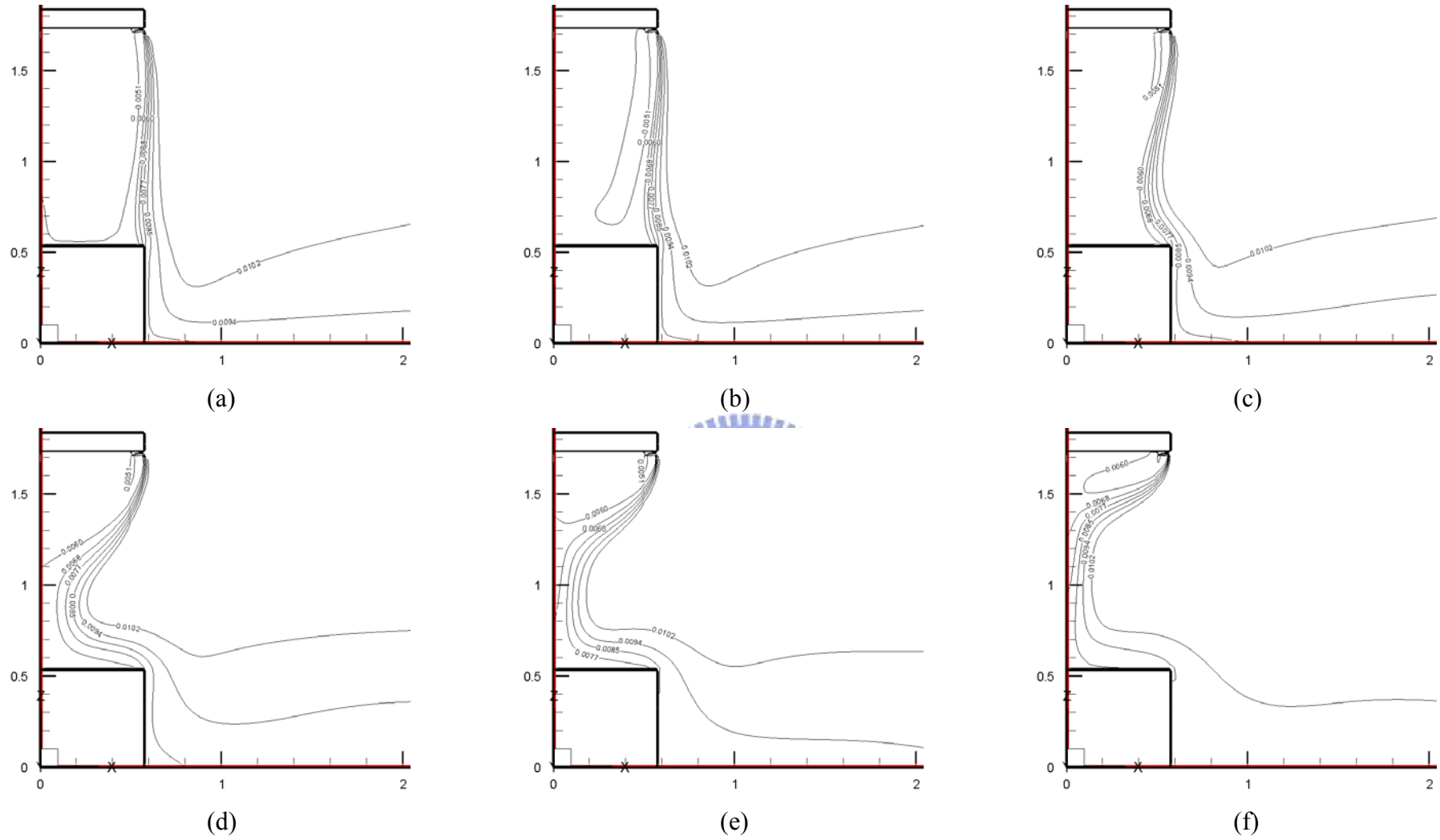


Fig. 4.27 Iso-concentration lines for steady cavity flow for $b_j = 0.07$ m, $Gr_t = 4.61 \times 10^9$ ($\Delta T = 20^\circ\text{C}$), and $N = 6.37 \times 10^{-2}$ with a jet inclined angle of 15° for $Re_b =$ (a) 9,548 ($V_j = 2.142$ m/s), (b) 8,275 ($V_j = 1.857$ m/s), (c) 6,365 ($V_j = 1.428$ m/s), (d) 5,092 ($V_j = 1.142$ m/s), (e) 3,183 ($V_j = 0.714$ m/s) and (f) 1,910 ($V_j = 0.428$ m/s).

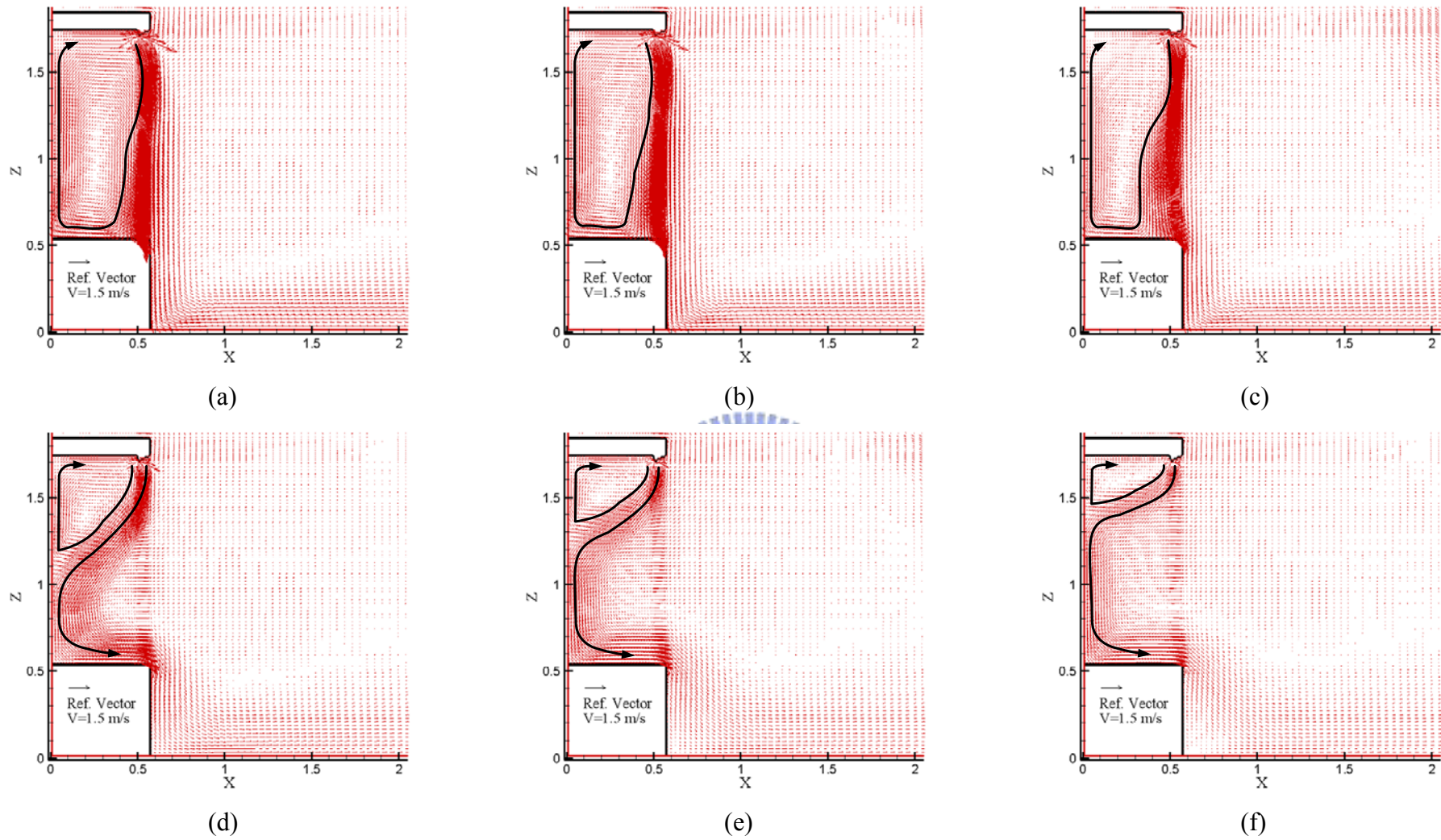


Fig. 4.28 Velocity vector maps for steady cavity flow for $b_j = 0.07$ m, $Gr_t = 4.61 \times 10^9$ ($\Delta T = 20^\circ\text{C}$), and $N = 6.37 \times 10^{-2}$ with a jet inclined angle of 25° for $Re_b =$ (a) 9,548 ($V_j = 2.142$ m/s), (b) 8,275 ($V_j = 1.857$ m/s), (c) 6,365 ($V_j = 1.428$ m/s), (d) 5,092 ($V_j = 1.142$ m/s), (e) 3,183 ($V_j = 0.714$ m/s) and (f) 1,910 ($V_j = 0.428$ m/s).

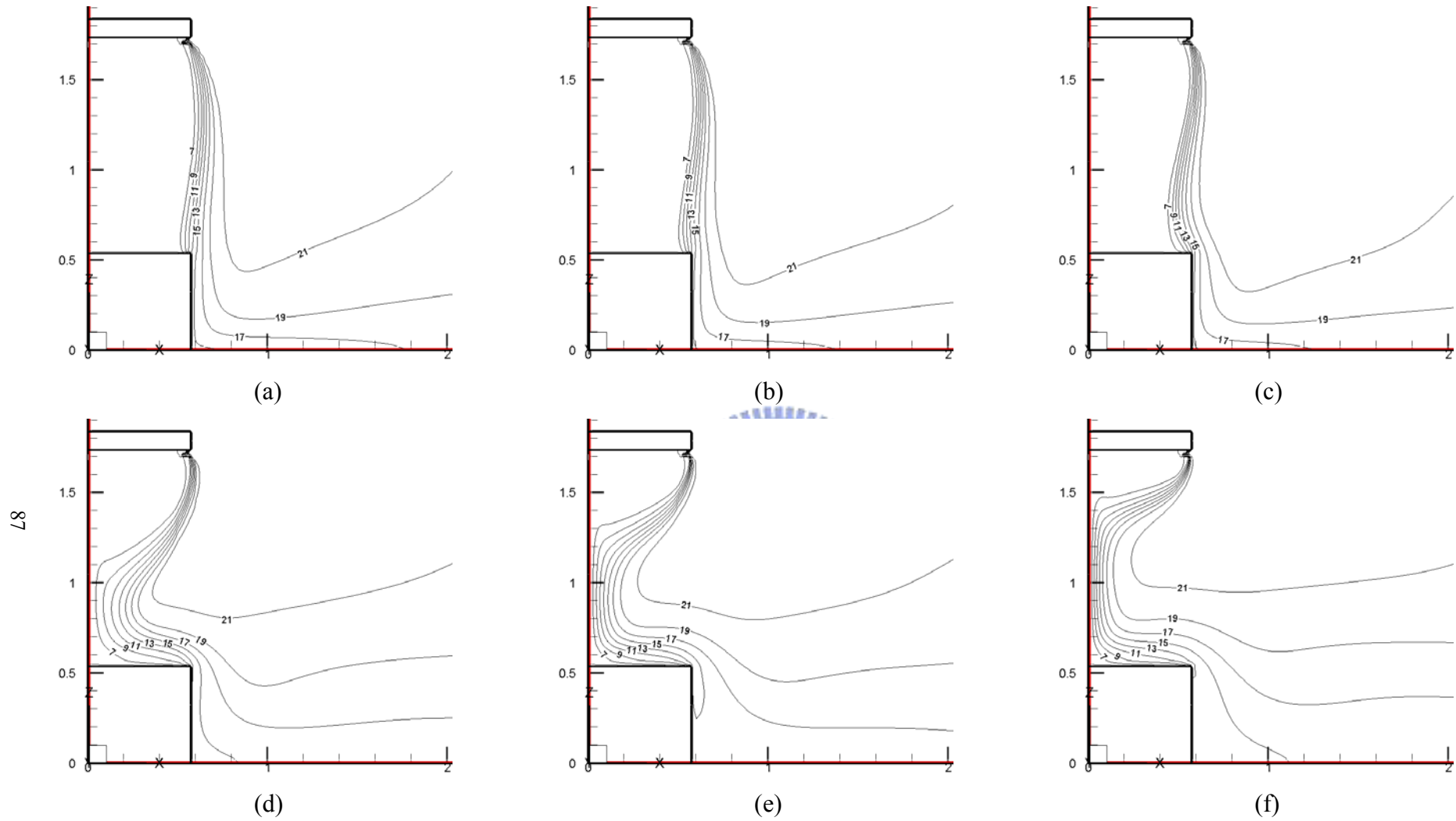


Fig. 4.29 Isotherms for steady cavity flow for $b_j = 0.07$ m, $Gr_t = 4.61 \times 10^9$ ($\Delta T = 20^\circ C$), and $N = 6.37 \times 10^{-2}$ with a jet inclined angle of 25° for $Re_b =$ (a) 9,548 ($V_j = 2.142$ m/s), (b) 8,275 ($V_j = 1.857$ m/s), (c) 6,365 ($V_j = 1.428$ m/s), (d) 5,092 ($V_j = 1.142$ m/s), (e) 3,183 ($V_j = 0.714$ m/s) and (f) 1,910 ($V_j = 0.428$ m/s).

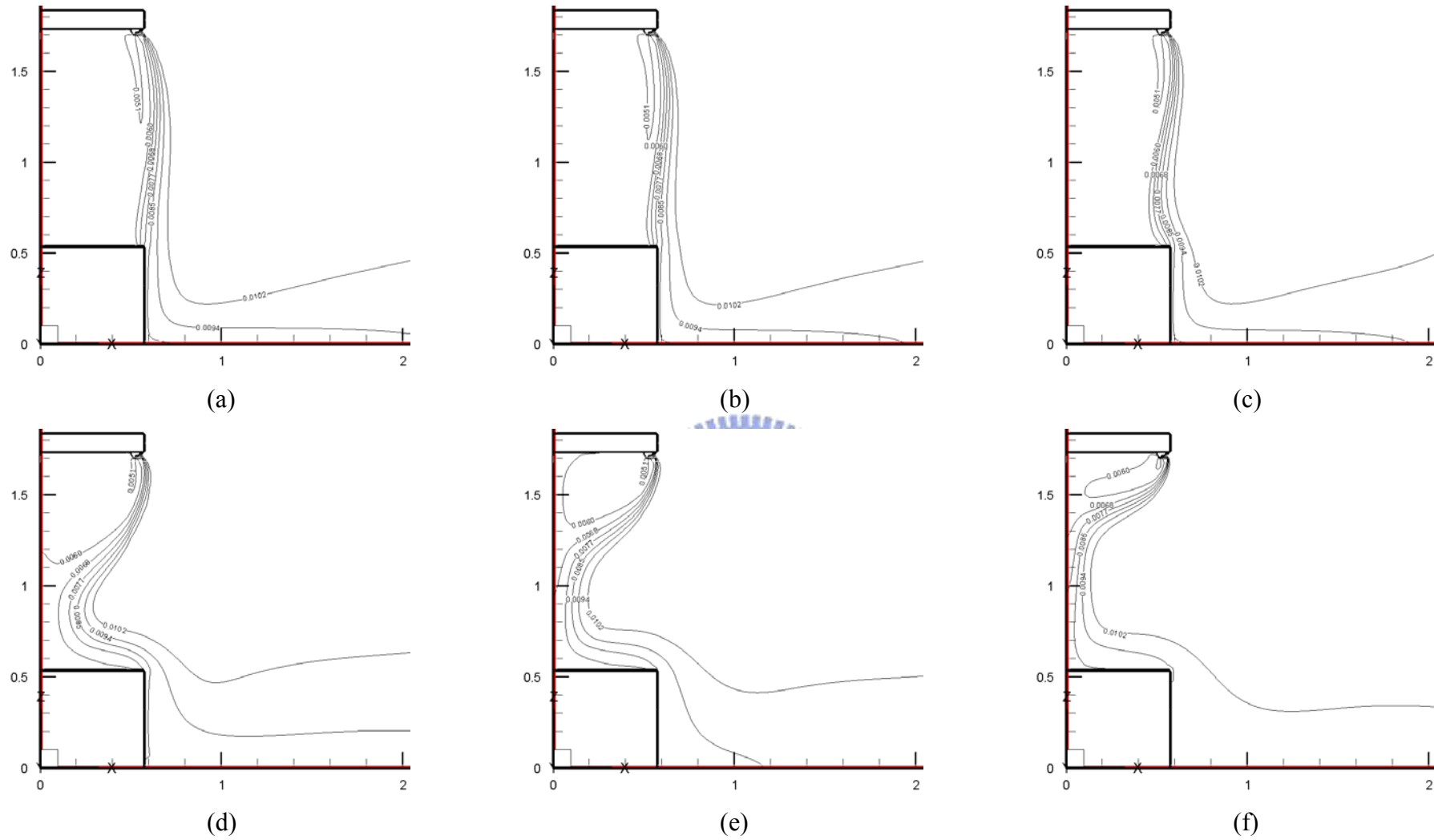


Fig. 4.30 Iso-concentration lines for steady cavity flow for $b_j = 0.07$ m, $Gr_t = 4.61 \times 10^9$ ($\Delta T = 20^\circ\text{C}$), and $N = 6.37 \times 10^{-2}$ with a jet inclined angle of 25° for $Re_b =$ (a) 9,548 ($V_j = 2.142$ m/s), (b) 8,275 ($V_j = 1.857$ m/s), (c) 6,365 ($V_j = 1.428$ m/s), (d) 5,092 ($V_j = 1.142$ m/s), (e) 3,183 ($V_j = 0.714$ m/s) and (f) 1,910 ($V_j = 0.428$ m/s).

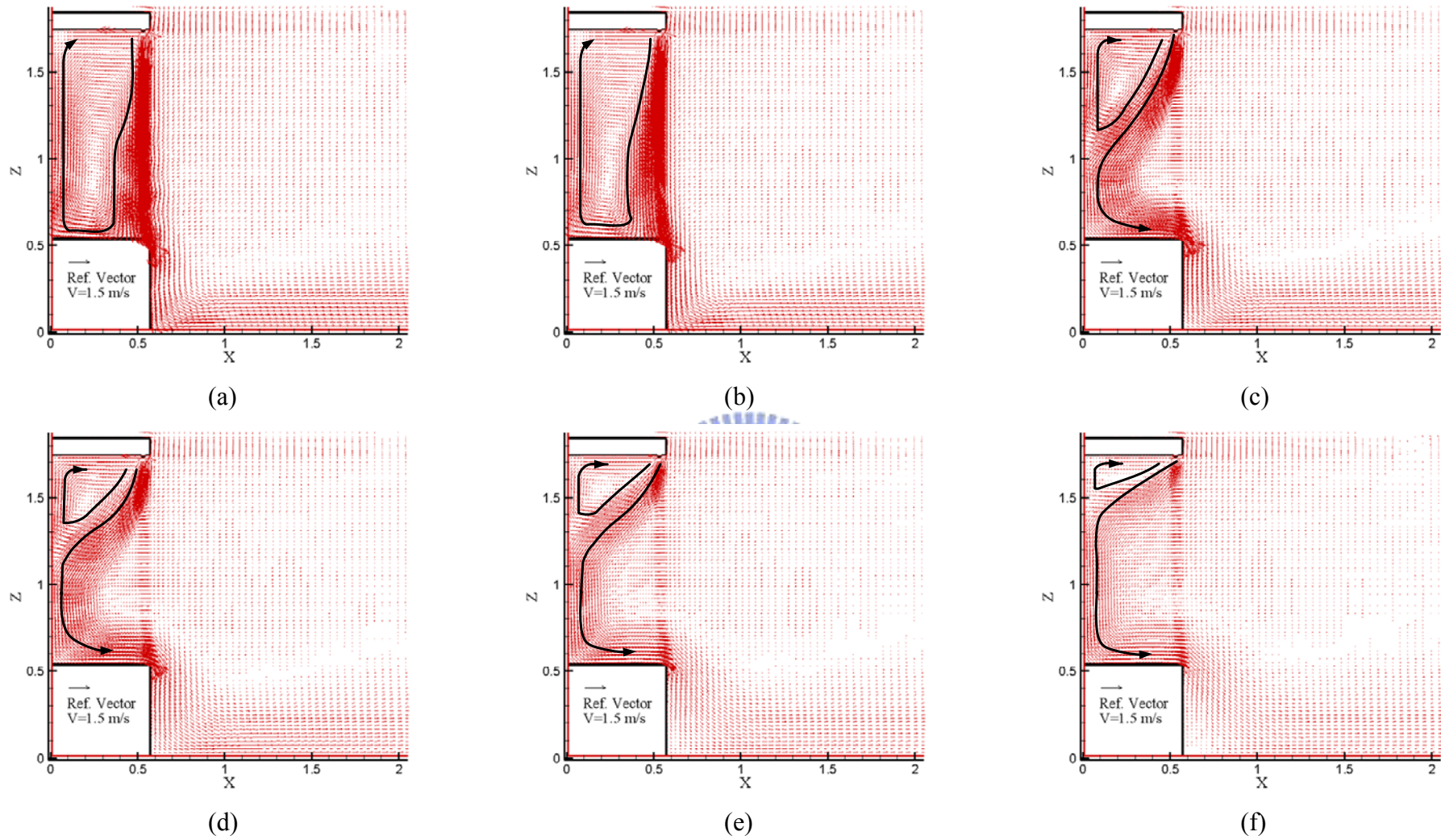


Fig. 4.31 Velocity vector maps for steady cavity flow for $b_j = 0.05$ m, $Gr_t = 4.61 \times 10^9$ ($\Delta T = 20^\circ\text{C}$), and $N = 6.37 \times 10^{-2}$ with a jet inclined angle of 5° for $Re_b =$ (a) 9,548 ($V_j = 3$ m/s), (b) 8,275 ($V_j = 2.6$ m/s), (c) 6,365 ($V_j = 2.0$ m/s), (d) 5,092 ($V_j = 1.6$ m/s), (e) 3,183 ($V_j = 1.0$ m/s) and (f) 1,910 ($V_j = 0.6$ m/s).

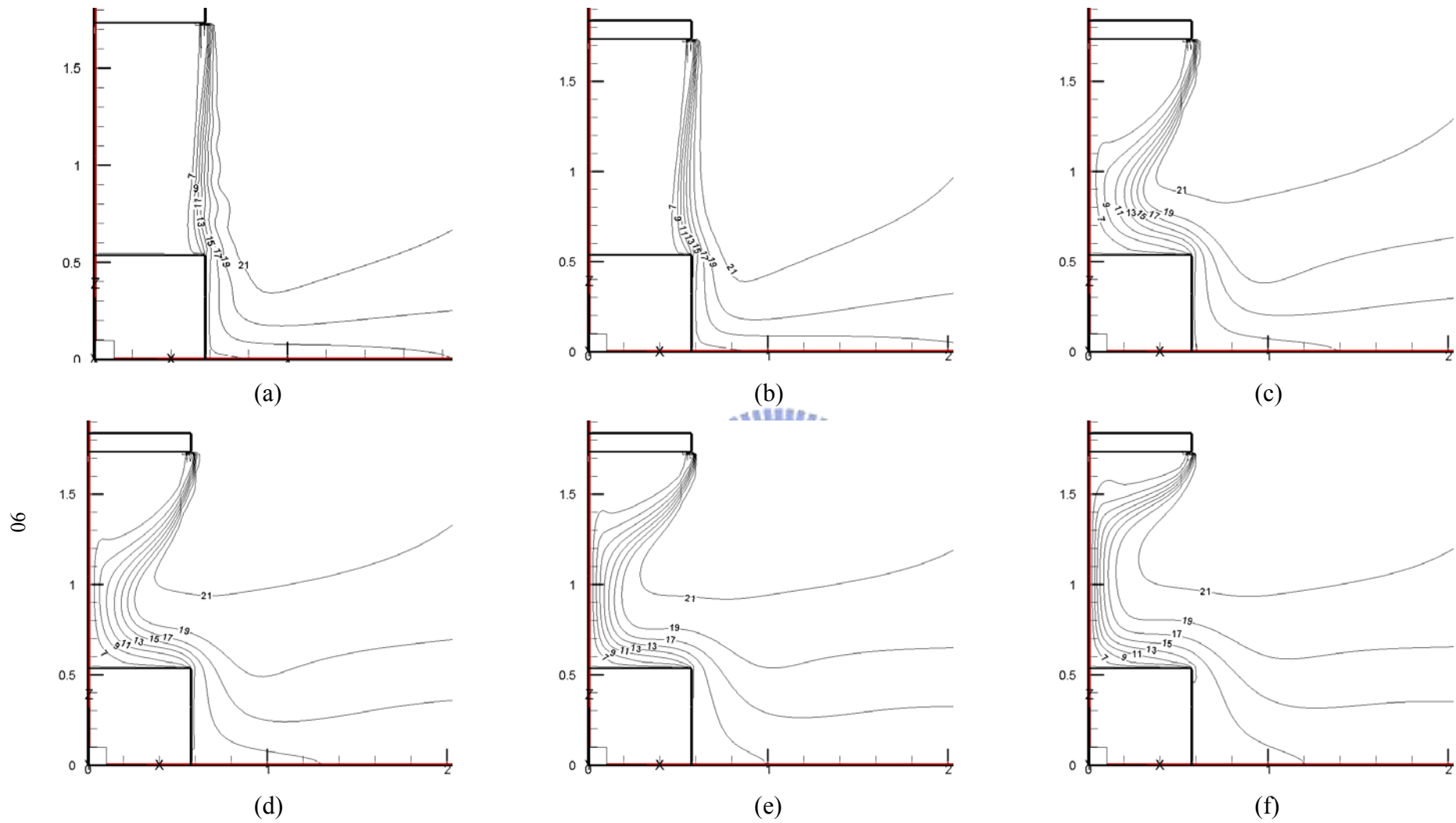


Fig. 4.32 Isotherms for steady cavity flow for $b_j = 0.05$ m, $Gr_t = 4.61 \times 10^9$ ($\Delta T = 20^\circ\text{C}$), and $N = 6.37 \times 10^{-2}$ with a jet inclined angle of 5° for $Re_b =$ (a) 9,548 ($V_j = 3$ m/s), (b) 8,275 ($V_j = 2.6$ m/s), (c) 6,365 ($V_j = 2.0$ m/s), (d) 5,092 ($V_j = 1.6$ m/s), (e) 3,183 ($V_j = 1.0$ m/s) and (f) 1,910 ($V_j = 0.6$ m/s).

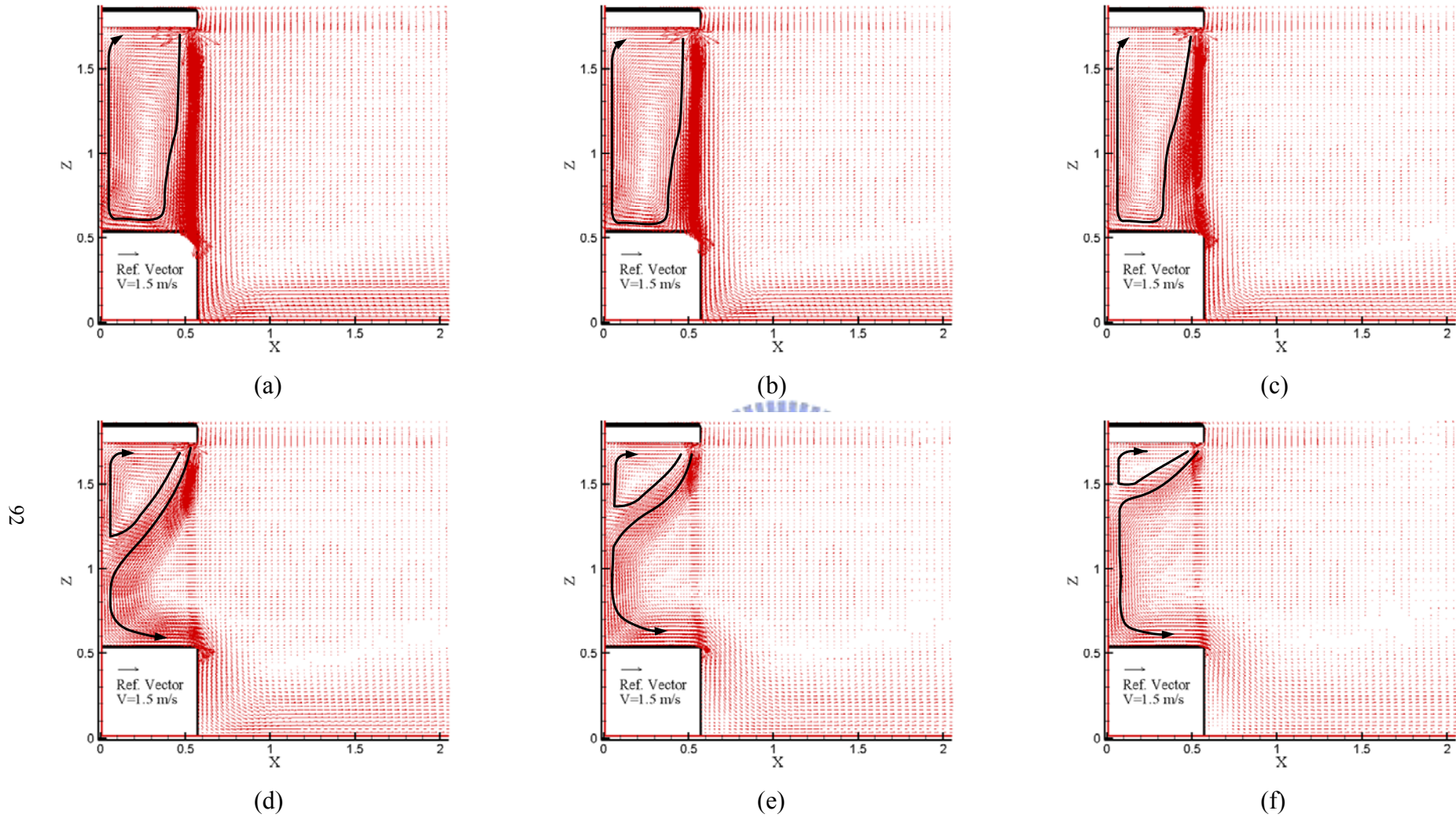


Fig. 4.34 Velocity vector maps for steady cavity flow for $b_j = 0.05$ m, $Gr_t = 4.61 \times 10^9$ ($\Delta T = 20^\circ\text{C}$), and $N = 6.37 \times 10^{-2}$ with a jet inclined angle of 15° for $Re_b =$ (a) 9,548 ($V_j = 3$ m/s), (b) 8,275 ($V_j = 2.6$ m/s), (c) 6,365 ($V_j = 2.0$ m/s), (d) 5,092 ($V_j = 1.6$ m/s), (e) 3,183 ($V_j = 1.0$ m/s) and (f) 1,910 ($V_j = 0.6$ m/s).

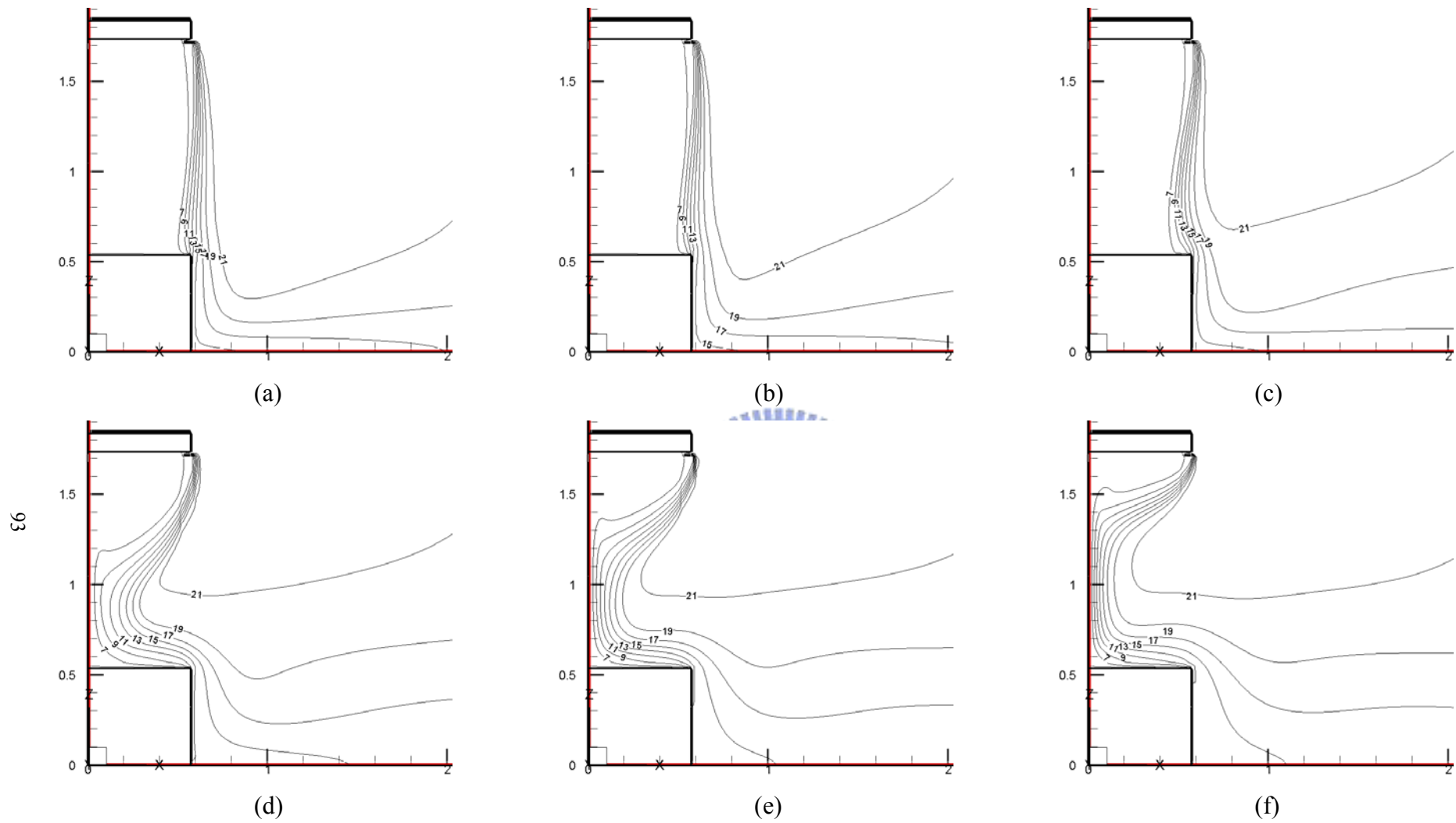


Fig. 4.35 Isotherms for steady cavity flow for $b_j = 0.05$ m, $Gr_t = 4.61 \times 10^9$ ($\Delta T = 20^\circ\text{C}$), and $N = 6.37 \times 10^{-2}$ with a jet inclined angle of 15° for $Re_b =$ (a) 9,548 ($V_j = 3$ m/s), (b) 8,275 ($V_j = 2.6$ m/s), (c) 6,365 ($V_j = 2.0$ m/s), (d) 5,092 ($V_j = 1.6$ m/s), (e) 3,183 ($V_j = 1.0$ m/s) and (f) 1,910 ($V_j = 0.6$ m/s).

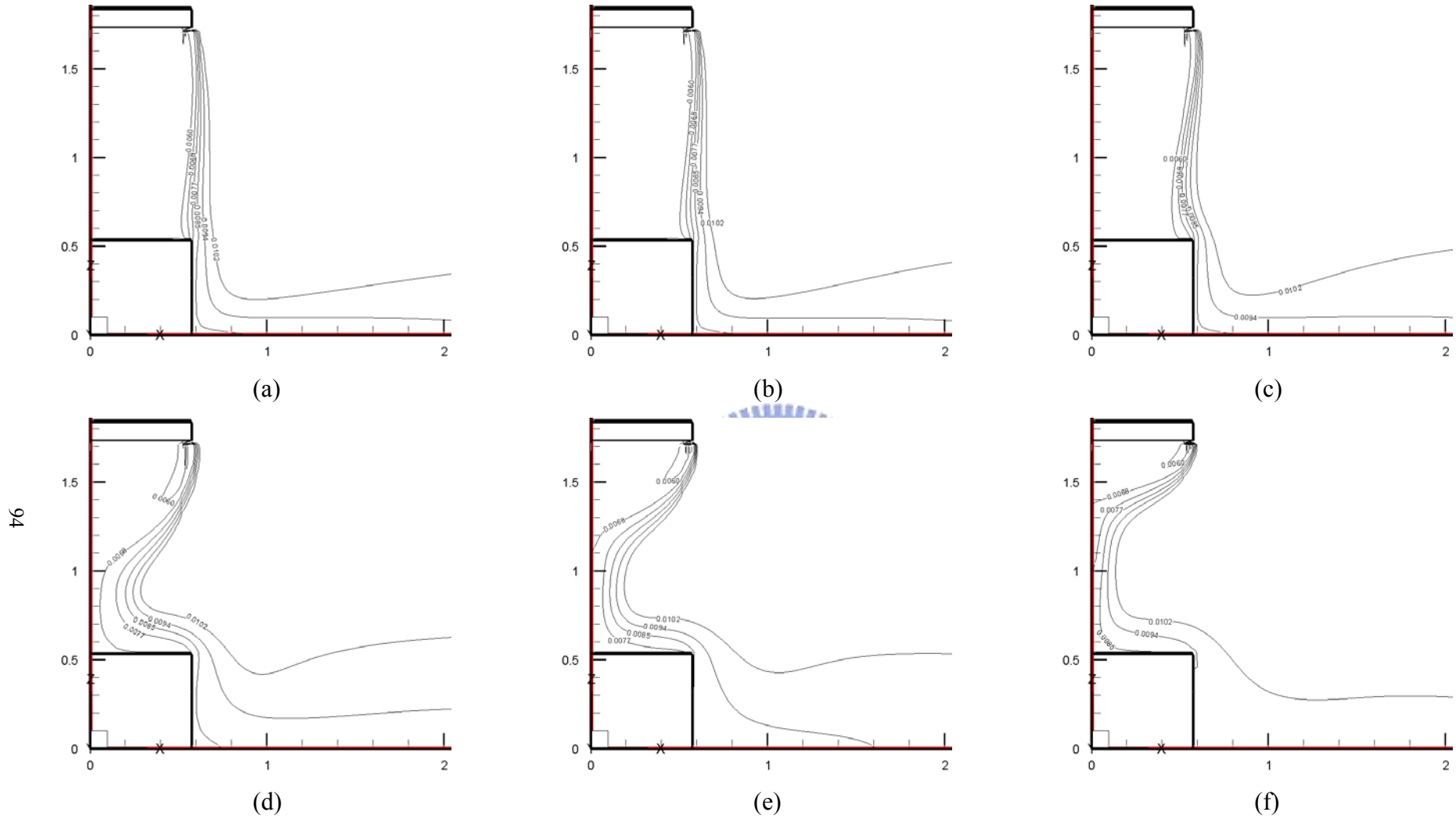


Fig. 4.36 Iso-concentration lines for steady cavity flow for $b_j = 0.05$ m, $Gr_t = 4.61 \times 10^9$ ($\Delta T = 20^\circ\text{C}$), and $N = 6.37 \times 10^{-2}$ with a jet inclined angle of 15° for $Re_b =$ (a) 9,548 ($V_j = 3$ m/s), (b) 8,275 ($V_j = 2.6$ m/s), (c) 6,365 ($V_j = 2.0$ m/s), (d) 5,092 ($V_j = 1.6$ m/s), (e) 3,183 ($V_j = 1.0$ m/s) and (f) 1,910 ($V_j = 0.6$ m/s).

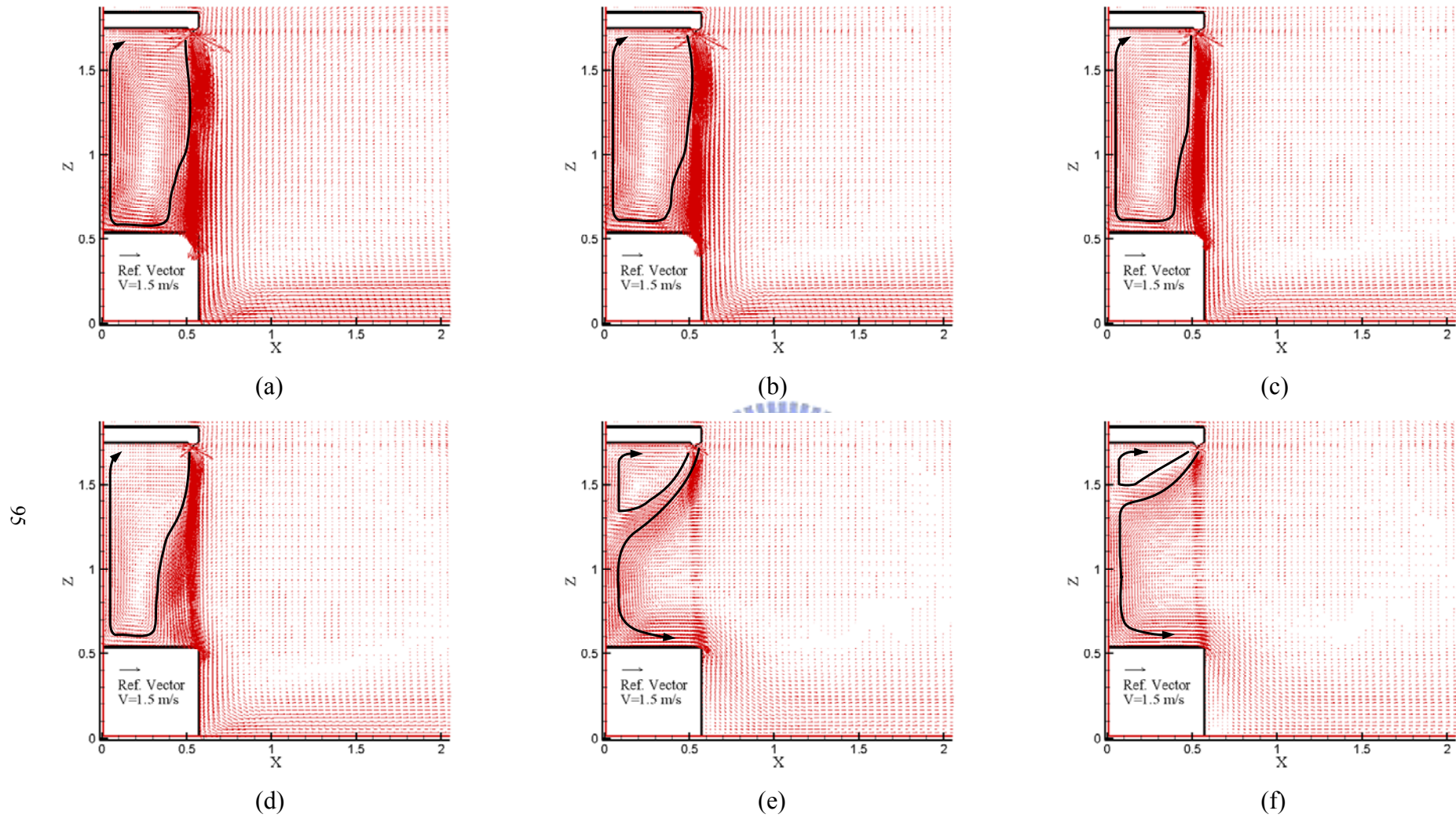


Fig. 4.37 Velocity vector maps for steady cavity flow for $b_j = 0.05$ m, $Gr_t = 4.61 \times 10^9$ ($\Delta T = 20^\circ\text{C}$), and $N = 6.37 \times 10^{-2}$ with a jet inclined angle of 25° for $Re_b =$ (a) 9,548 ($V_j = 3$ m/s), (b) 8,275 ($V_j = 2.6$ m/s), (c) 6,365 ($V_j = 2.0$ m/s), (d) 5,092 ($V_j = 1.6$ m/s), (e) 3,183 ($V_j = 1.0$ m/s) and (f) 1,910 ($V_j = 0.6$ m/s).

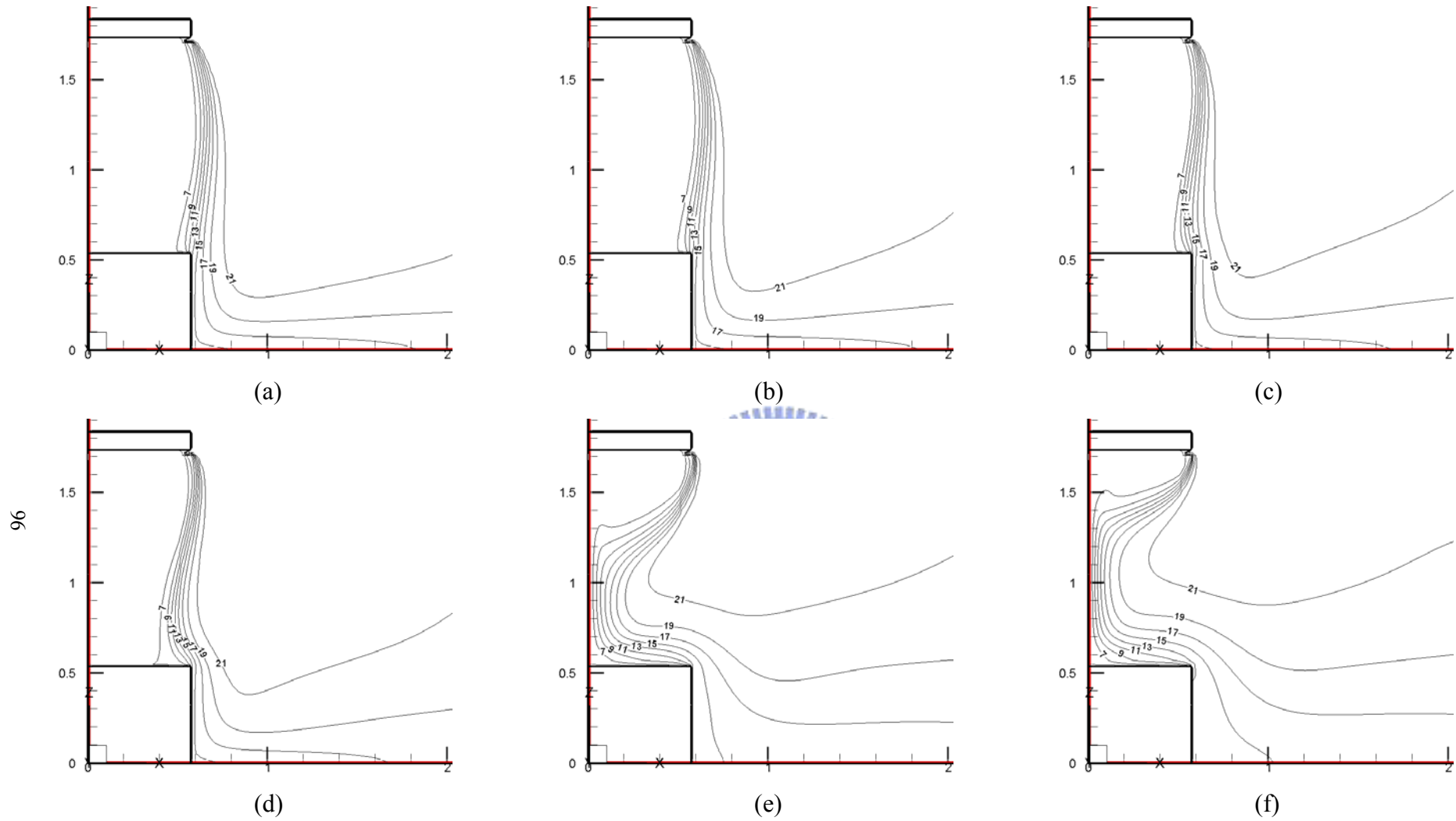


Fig. 4.38 Isotherms for steady cavity flow for $b_j = 0.05$ m, $Gr_t = 4.61 \times 10^9$ ($\Delta T = 20^\circ\text{C}$), and $N = 6.37 \times 10^{-2}$ with a jet inclined angle of 25° for $Re_b =$ (a) 9,548 ($V_j = 3$ m/s), (b) 8,275 ($V_j = 2.6$ m/s), (c) 6,365 ($V_j = 2.0$ m/s), (d) 5,092 ($V_j = 1.6$ m/s), (e) 3,183 ($V_j = 1.0$ m/s) and (f) 1,910 ($V_j = 0.6$ m/s).

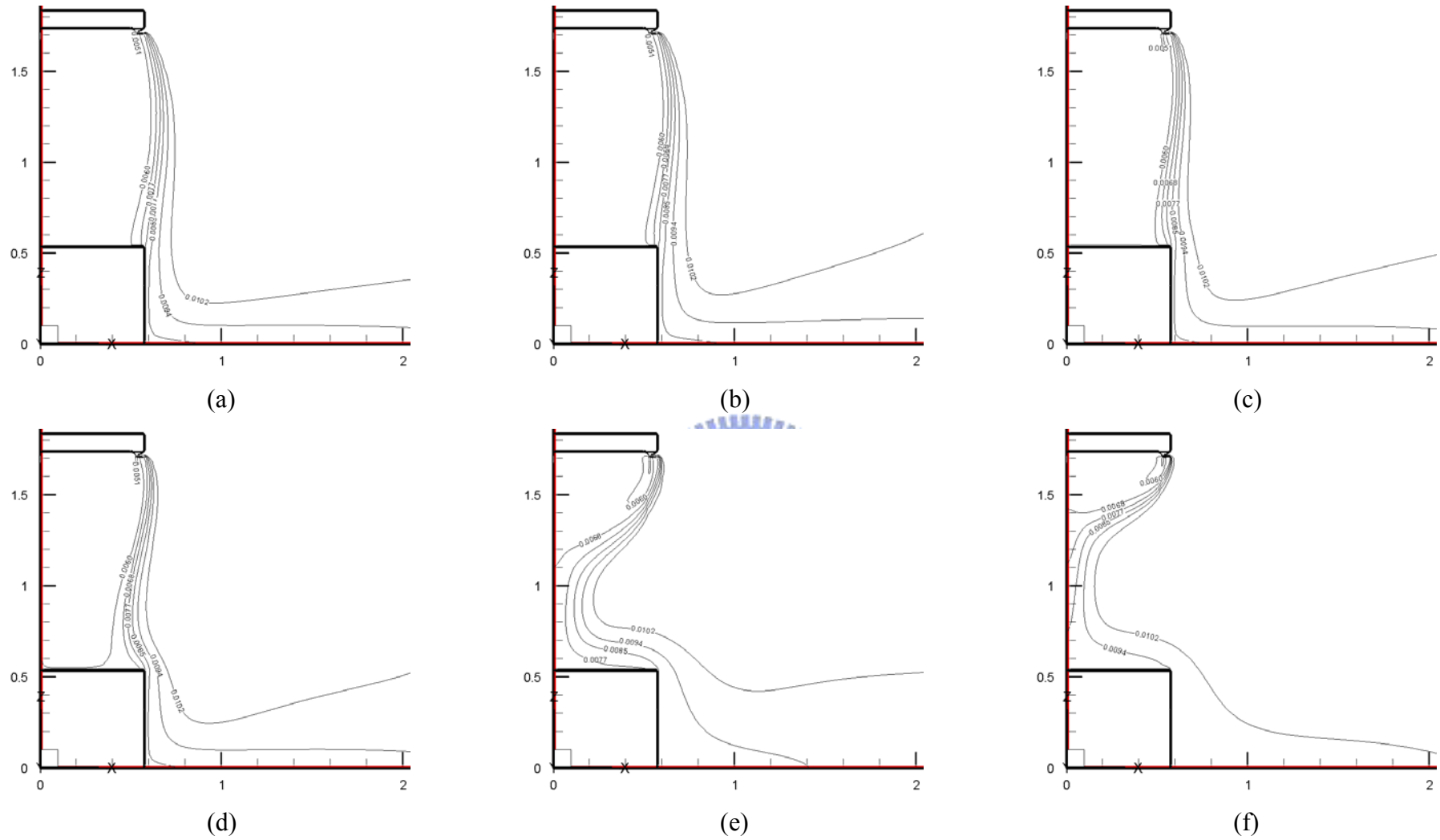


Fig. 4.39 Iso-concentration lines for steady cavity flow for $b_j = 0.05$ m, $Gr_t = 4.61 \times 10^9$ ($\Delta T = 20^\circ\text{C}$), and $N = 6.37 \times 10^{-2}$ with a jet inclined angle of 25° for $Re_b =$ (a) 9,548 ($V_j = 3$ m/s), (b) 8,275 ($V_j = 2.6$ m/s), (c) 6,365 ($V_j = 2.0$ m/s), (d) 5,092 ($V_j = 1.6$ m/s), (e) 3,183 ($V_j = 1.0$ m/s) and (f) 1,910 ($V_j = 0.6$ m/s).

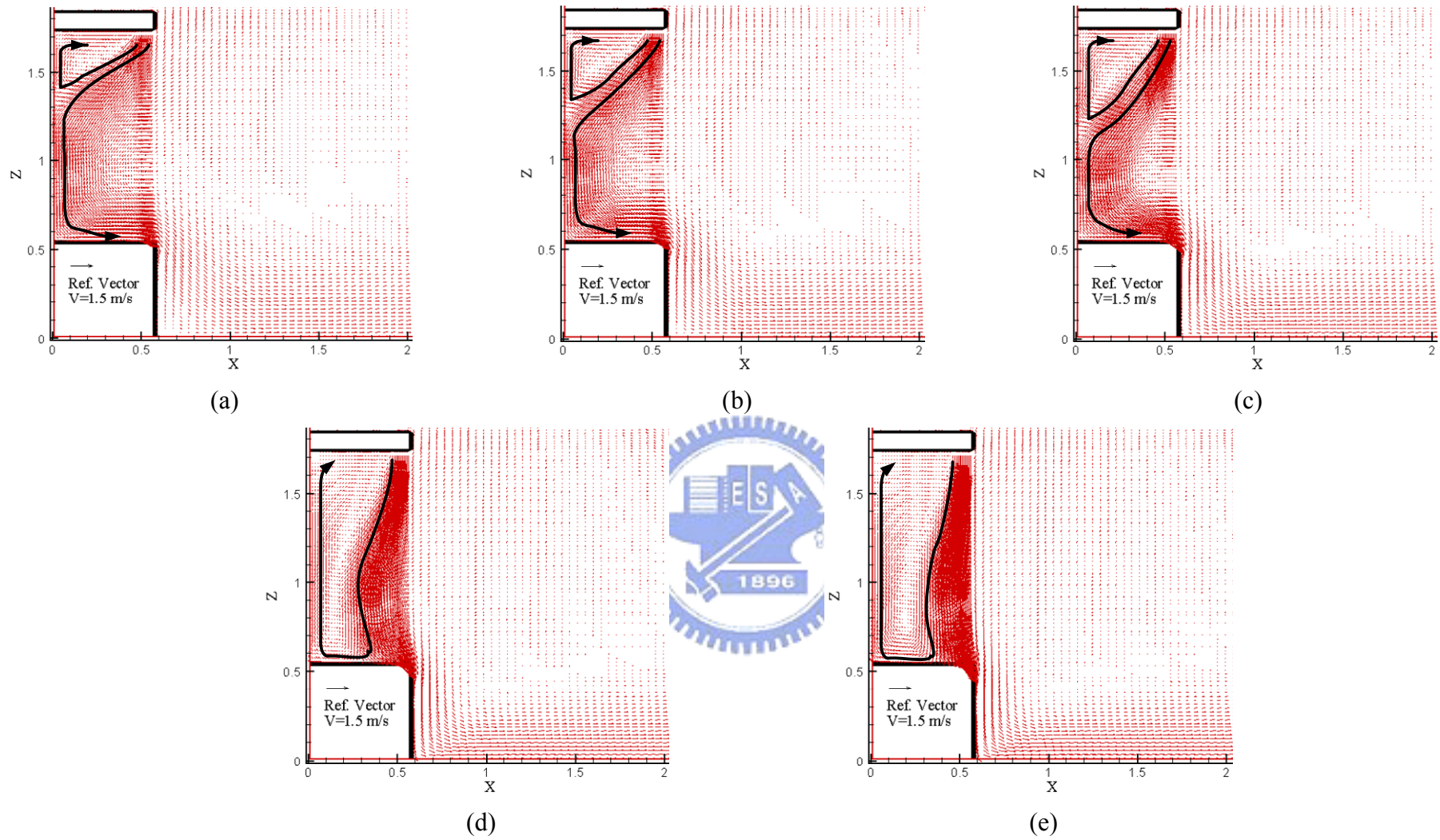


Fig. 4.40 Velocity vector maps for steady cavity flow for a double air curtain design with $b_i = 0.03$ m, $b_o = 0.07$ m, $Gr_i = 4.61 \times 10^9$ ($\Delta T = 20^\circ\text{C}$), and $N = 6.37 \times 10^{-2}$ for $Re_{ci} = 1,910$ and $Re_{co} =$ (a) 1,910, (b) 3,183, (c) 5,092, (d) 6,365 and (e) 7,638.

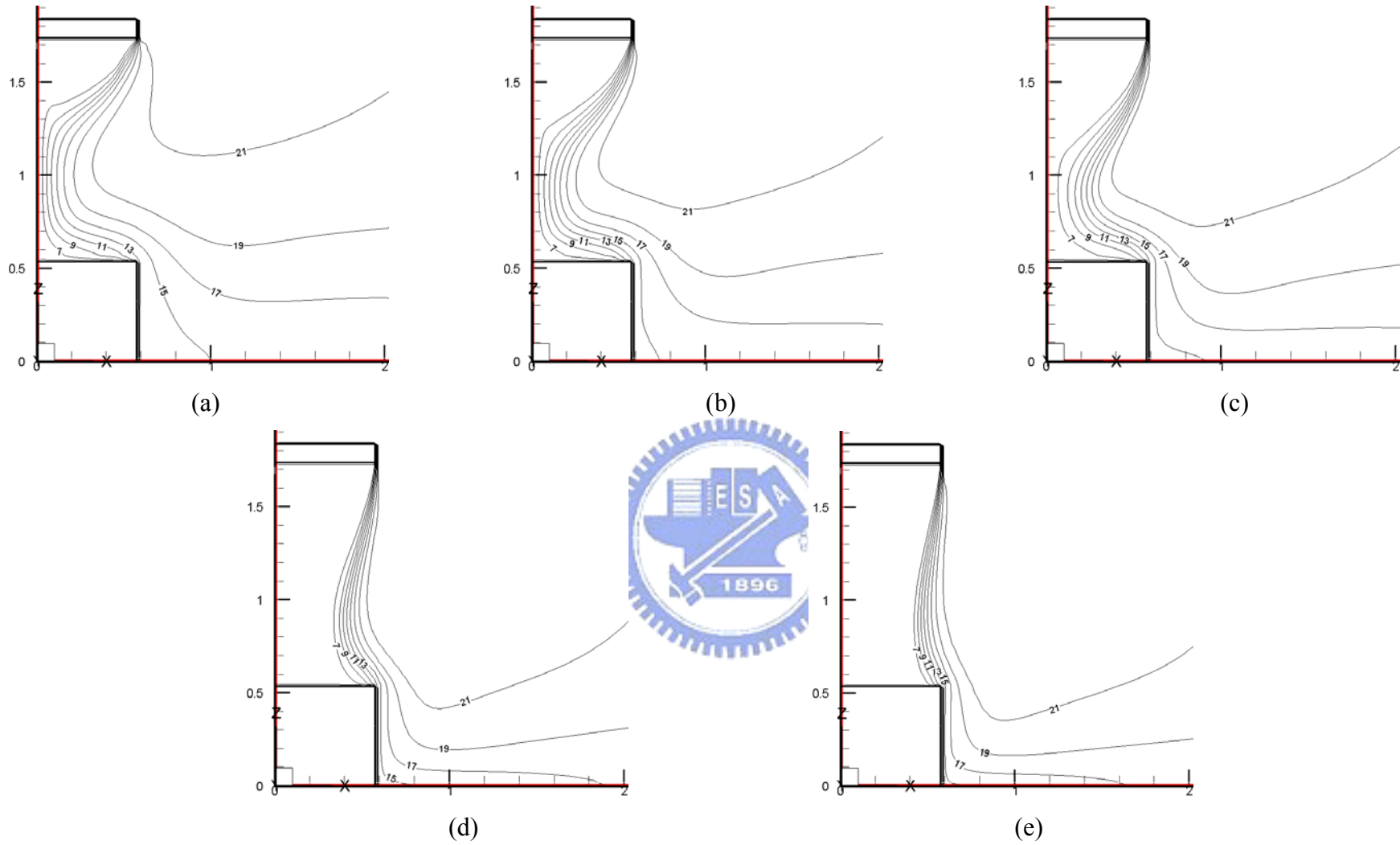


Fig. 4.41 Isotherms for steady cavity flow for a double air curtain design with $b_i = 0.03$ m, $b_o = 0.07$ m, $Gr_t = 4.61 \times 10^9$ ($\Delta T = 20^\circ\text{C}$), and $N = 6.37 \times 10^{-2}$ for $Re_{ci} = 1,910$ and $Re_{co} =$ (a) 1,910, (b) 3,183, (c) 5,092, (d) 6,365 and (e) 7,638.

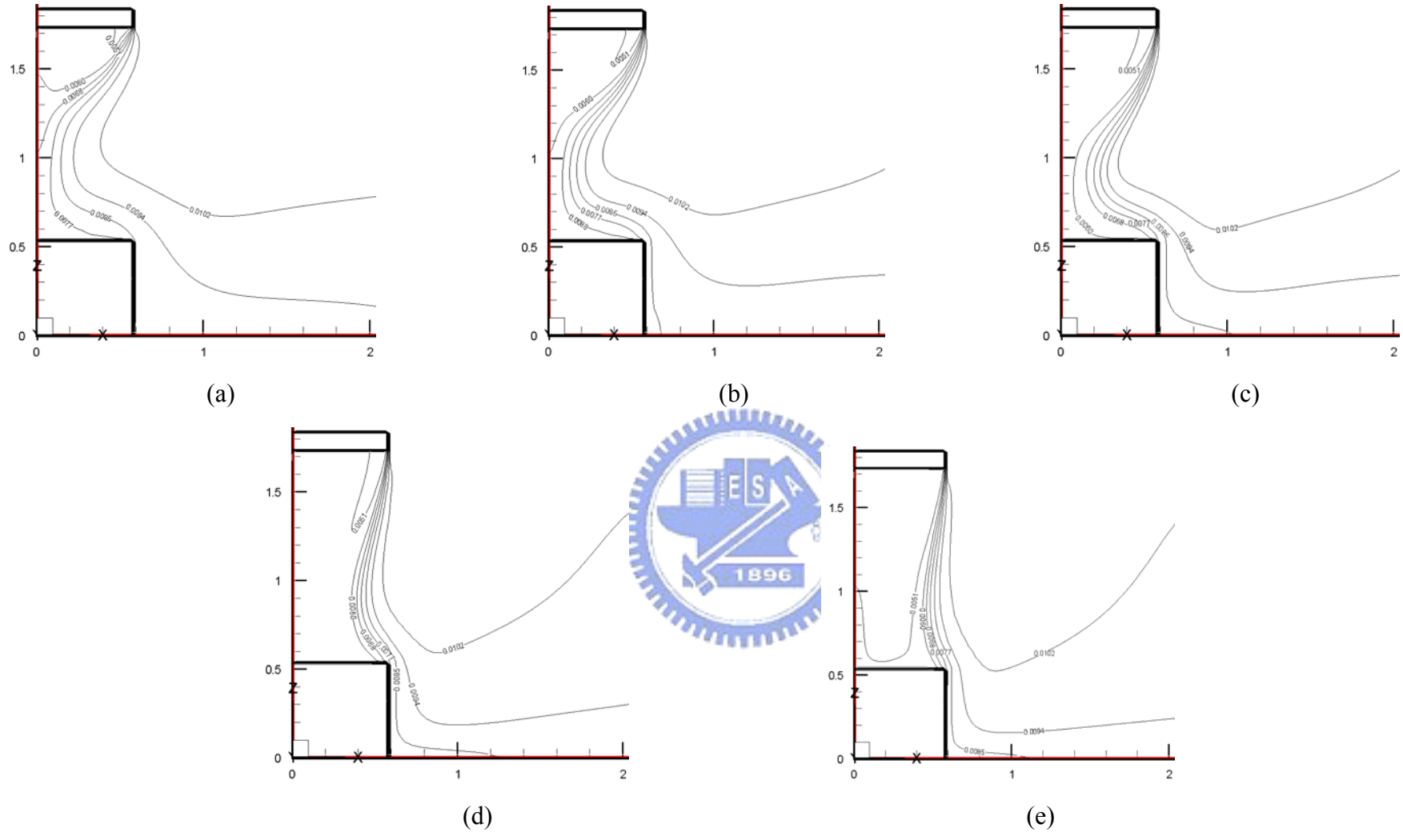


Fig. 4.42 Iso-concentration lines for steady cavity flow for a double air curtain design with $b_i = 0.03$ m, $b_o = 0.07$ m, $Gr_i = 4.61 \times 10^9$ ($\Delta T = 20^\circ C$), and $N = 6.37 \times 10^{-2}$ for $Re_{ci} = 1,910$ and $Re_{co} =$ (a) 1,910, (b) 3,183, (c) 5,092, (d) 6,365 and (e) 7,638.

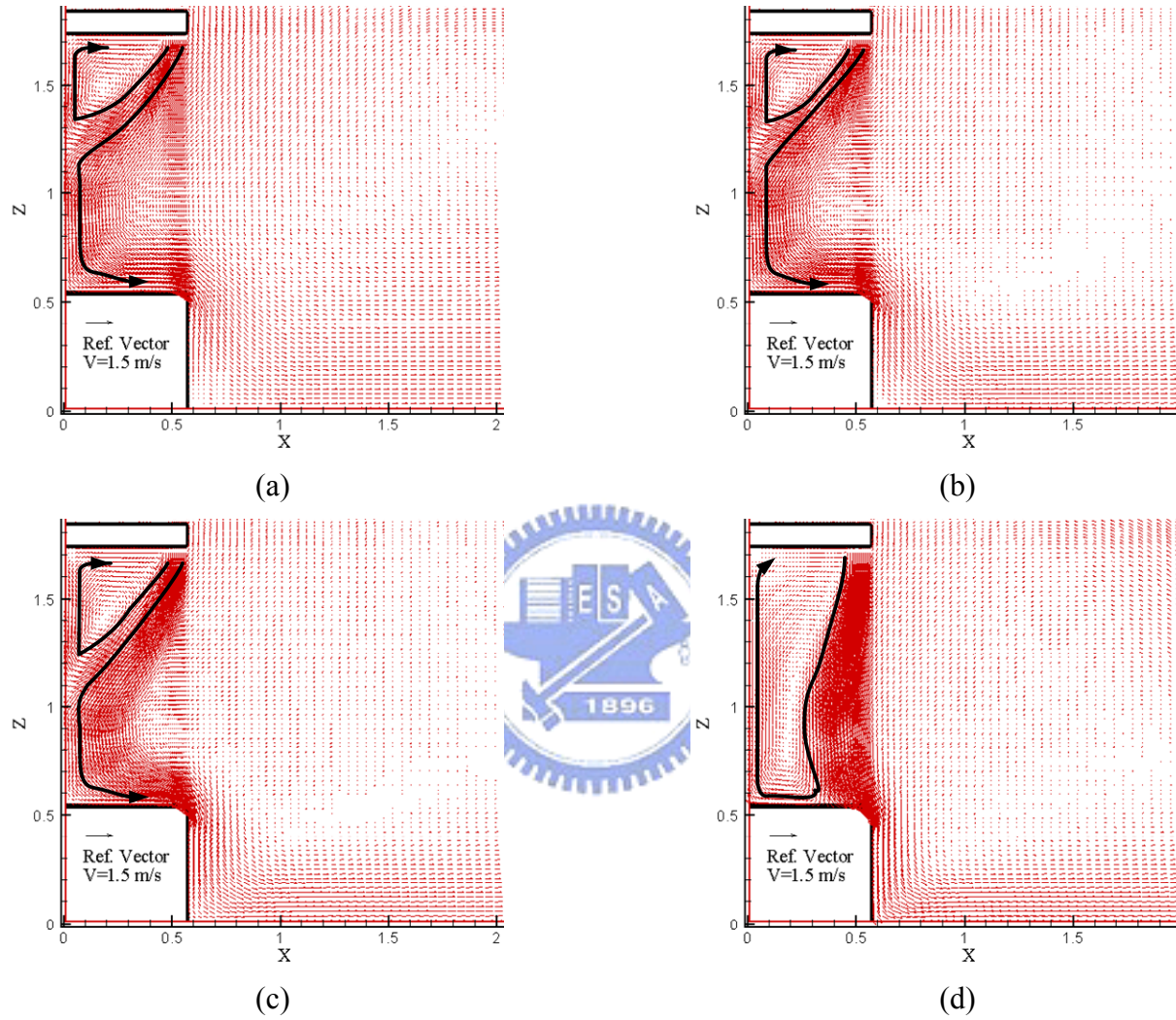


Fig. 4.43 Velocity vector maps for steady cavity flow for a double air curtain design with $b_i = 0.03$ m, $b_o = 0.07$ m, $Gr_t = 4.61 \times 10^9$ ($\Delta T = 20^\circ\text{C}$), and $N = 6.37 \times 10^{-2}$ for $Re_{ci} = 3,183$ and $Re_{co} =$ (a) 1,910, (b) 3,183, (c) 5,092, and (d) 6,365.

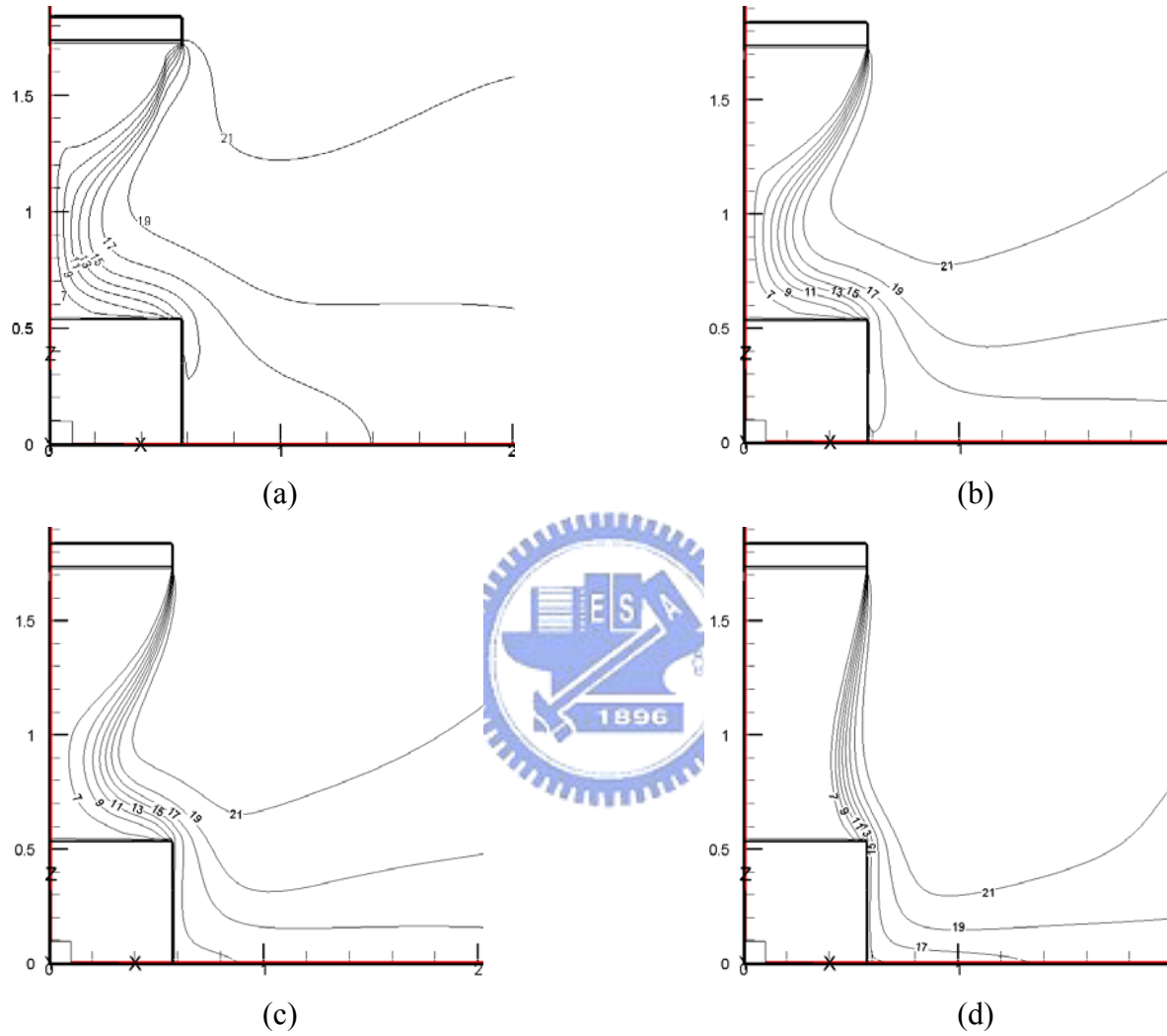


Fig. 4.44 Isotherms for steady cavity flow for a double air curtain design with $b_i = 0.03$ m, $b_o = 0.07$ m, $Gr_t = 4.61 \times 10^9$ ($\Delta T = 20^\circ\text{C}$), and $N = 6.37 \times 10^{-2}$ for $Re_{ci} = 3,183$ and $Re_{co} =$ (a) 1,910, (b) 3,183, (c) 5,092, and (d) 6,365.

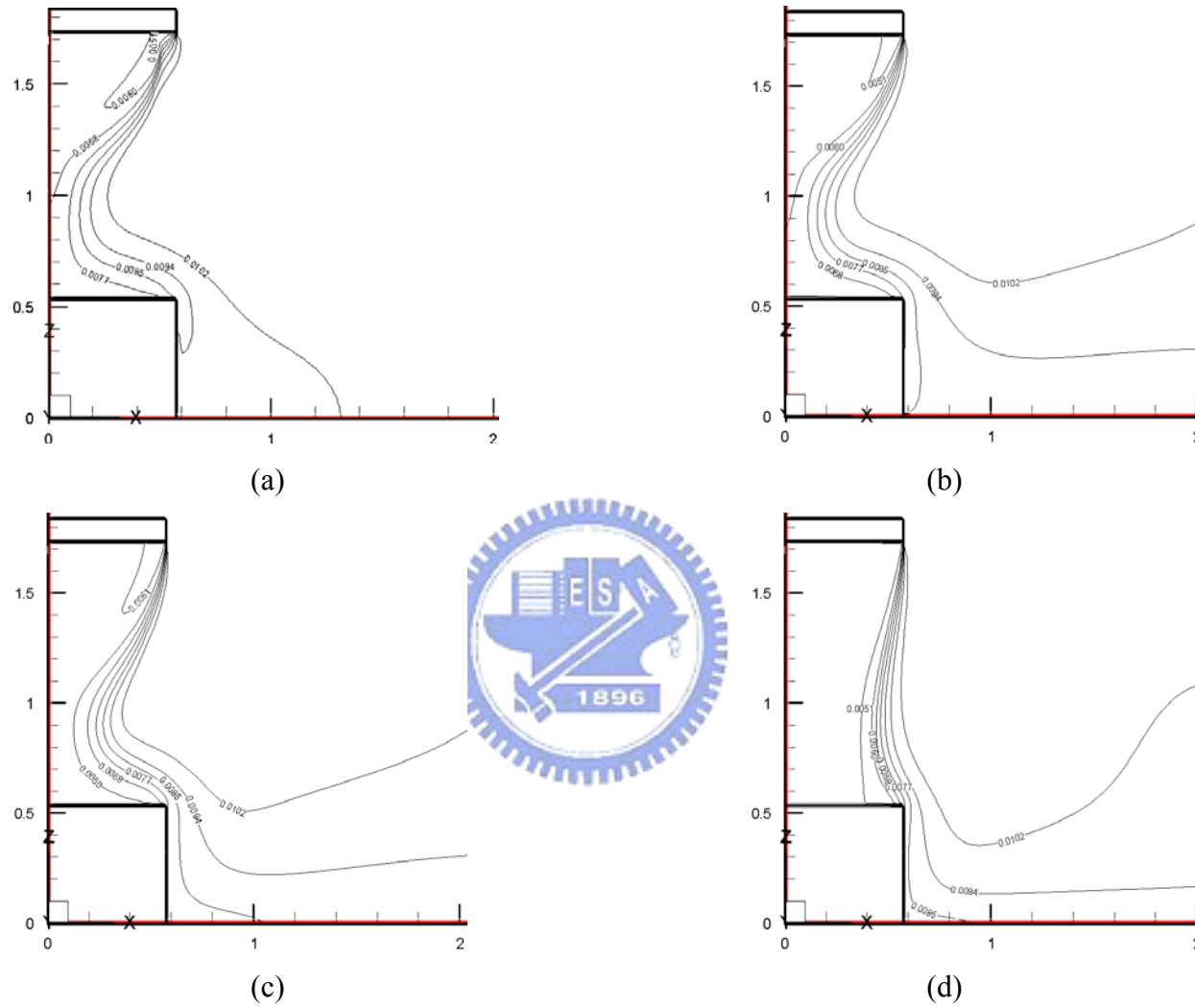


Fig. 4.45 Iso-concentration lines for steady cavity flow for a double air curtain design with $b_i = 0.03$ m, $b_o = 0.07$ m, $Gr_t = 4.61 \times 10^9$ ($\Delta T = 20^\circ\text{C}$), and $N = 6.37 \times 10^{-2}$ for $Re_{ci} = 3,183$ and $Re_{co} =$ (a) 1,910, (b) 3,183, (c) 5,092, and (d) 6,365.

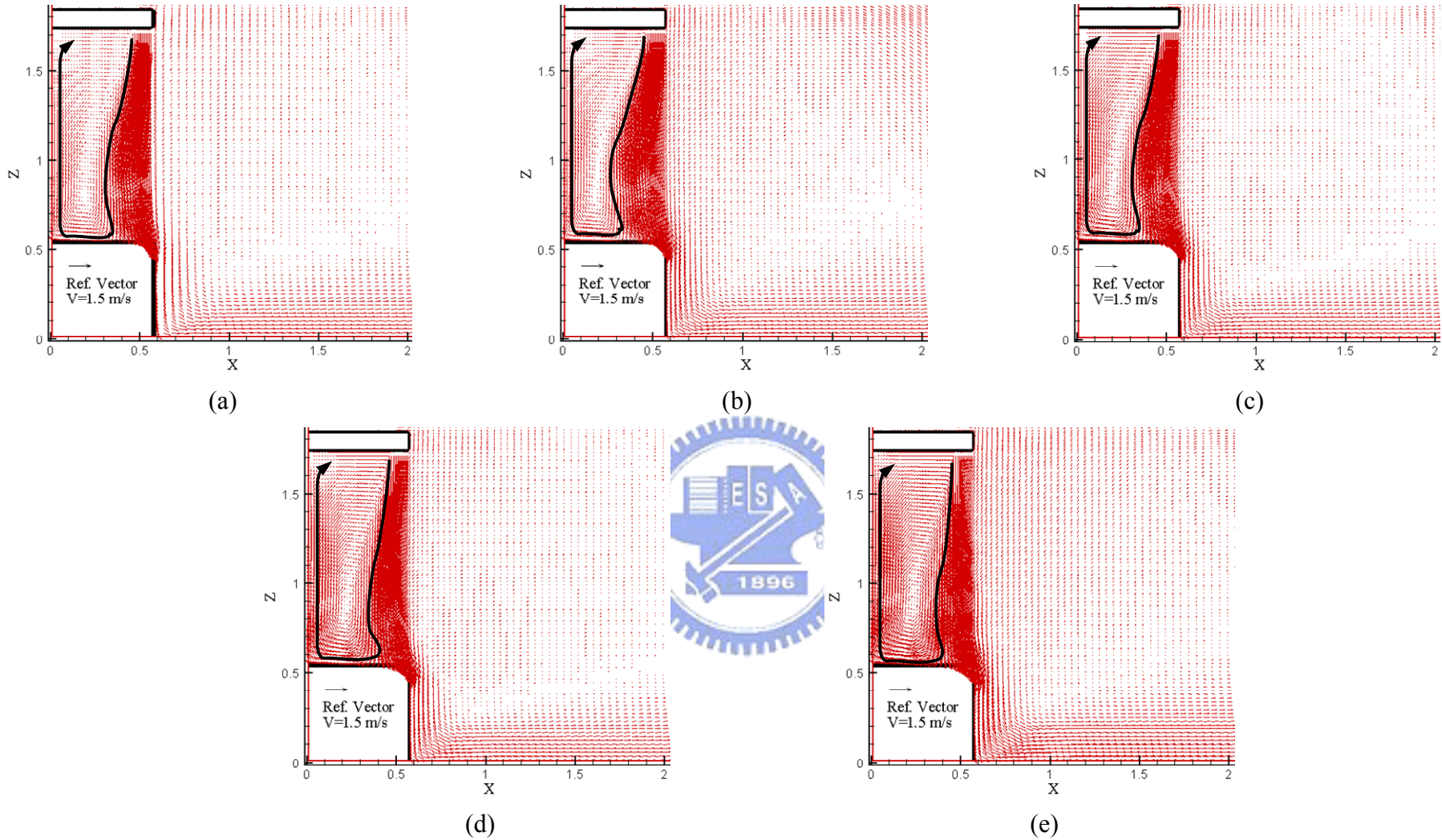


Fig. 4.46 Velocity vector maps for steady cavity flow for a double air curtain design with $b_i = 0.03$ m, $b_o = 0.07$ m, $Gr_t = 4.61 \times 10^9$ ($\Delta T = 20^\circ\text{C}$), and $N = 6.37 \times 10^{-2}$ for (a) $Re_{ci} = 1,910$ and $Re_{co} = 7,638$, (b) $Re_{ci} = 3,183$ and $Re_{co} = 6,365$, (c) $Re_{ci} = 5,092$ and $Re_{co} = 4,456$, (d) $Re_{ci} = 6,365$ and $Re_{co} = 3,183$, (e) $Re_{ci} = 7,638$ and $Re_{co} = 1,910$.

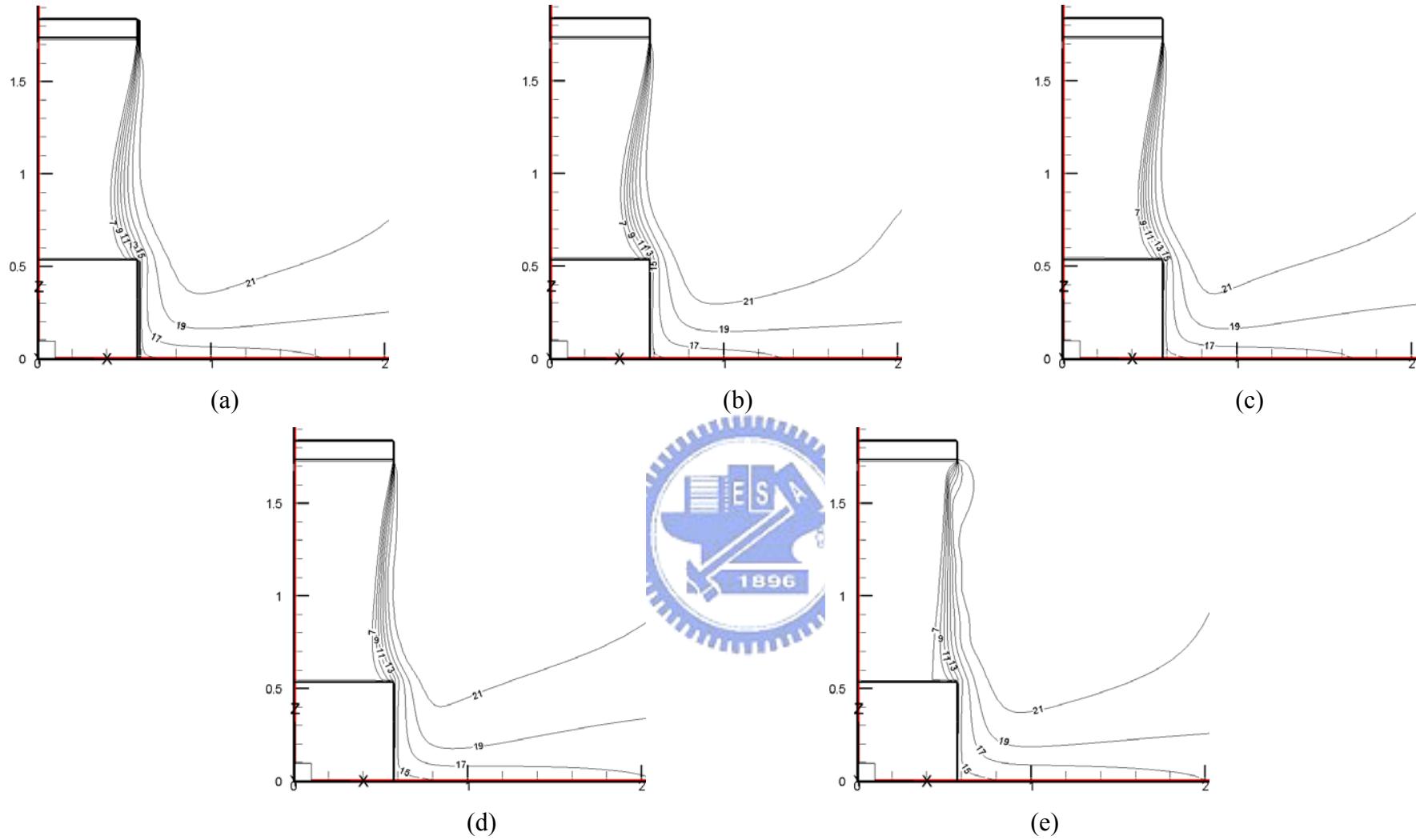


Fig. 4.47 Isotherms for steady cavity flow for a double air curtain design with $b_i = 0.03$ m, $b_o = 0.07$ m, $Gr_t = 4.61 \times 10^9$ ($\Delta T = 20^\circ\text{C}$), and $N = 6.37 \times 10^{-2}$ for (a) $Re_{ci} = 1,910$ and $Re_{co} = 7,638$, (b) $Re_{ci} = 3,183$ and $Re_{co} = 6,365$, (c) $Re_{ci} = 5,092$ and $Re_{co} = 4,456$, (d) $Re_{ci} = 6,365$ and $Re_{co} = 3,183$, (e) $Re_{ci} = 7,638$ and $Re_{co} = 1,910$.

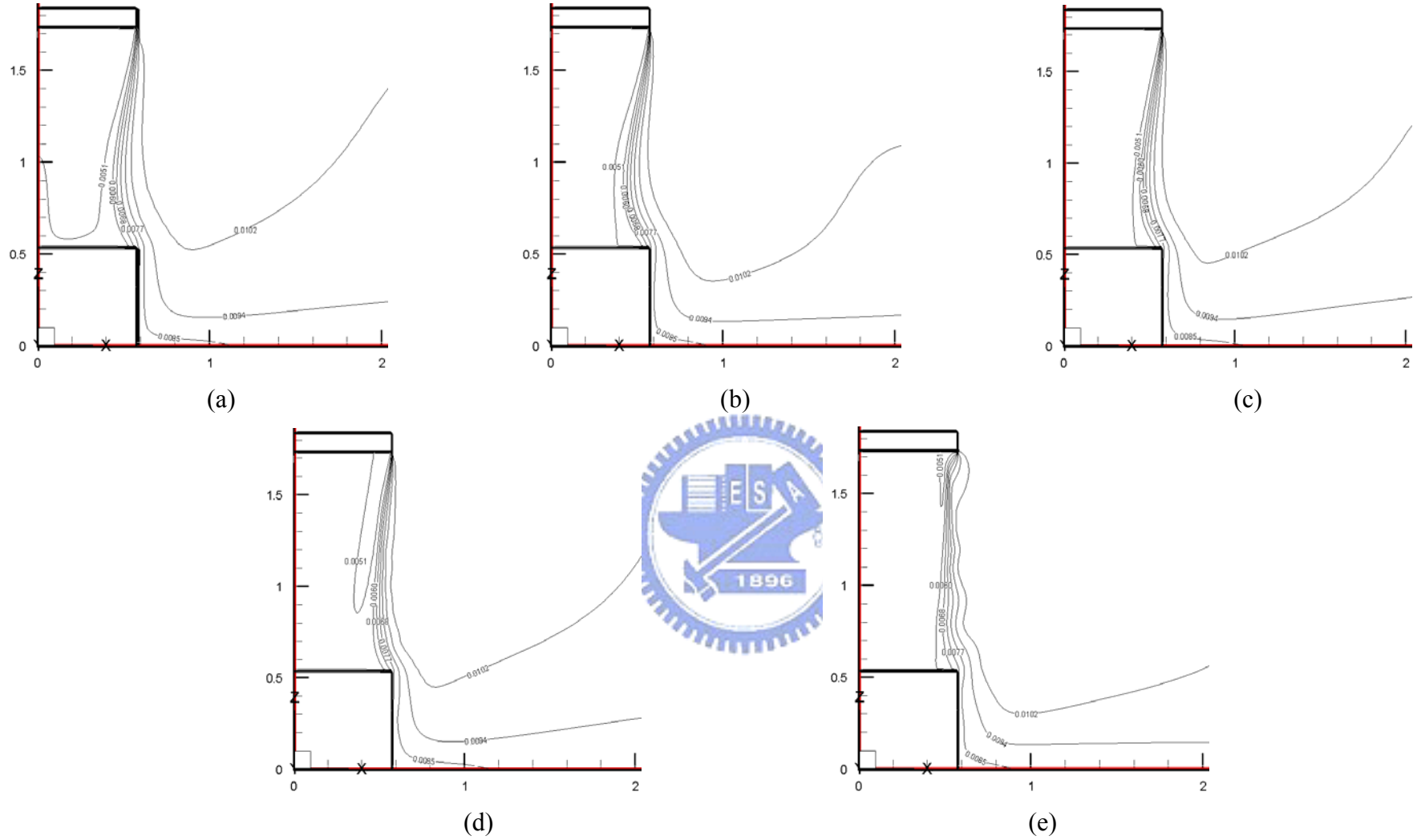


Fig. 4.48 Iso-concentration lines for steady cavity flow for a double air curtain design with $b_i = 0.03$ m, $b_o = 0.07$ m, $Gr_t = 4.61 \times 10^9$ ($\Delta T = 20^\circ\text{C}$), and $N = 6.37 \times 10^{-2}$ for (a) $Re_{ci} = 1,910$ and $Re_{co} = 7,638$, (b) $Re_{ci} = 3,183$ and $Re_{co} = 6,365$, (c) $Re_{ci} = 5,092$ and $Re_{co} = 4,456$, (d) $Re_{ci} = 6,365$ and $Re_{co} = 3,183$, (e) $Re_{ci} = 7,638$ and $Re_{co} = 1,910$.

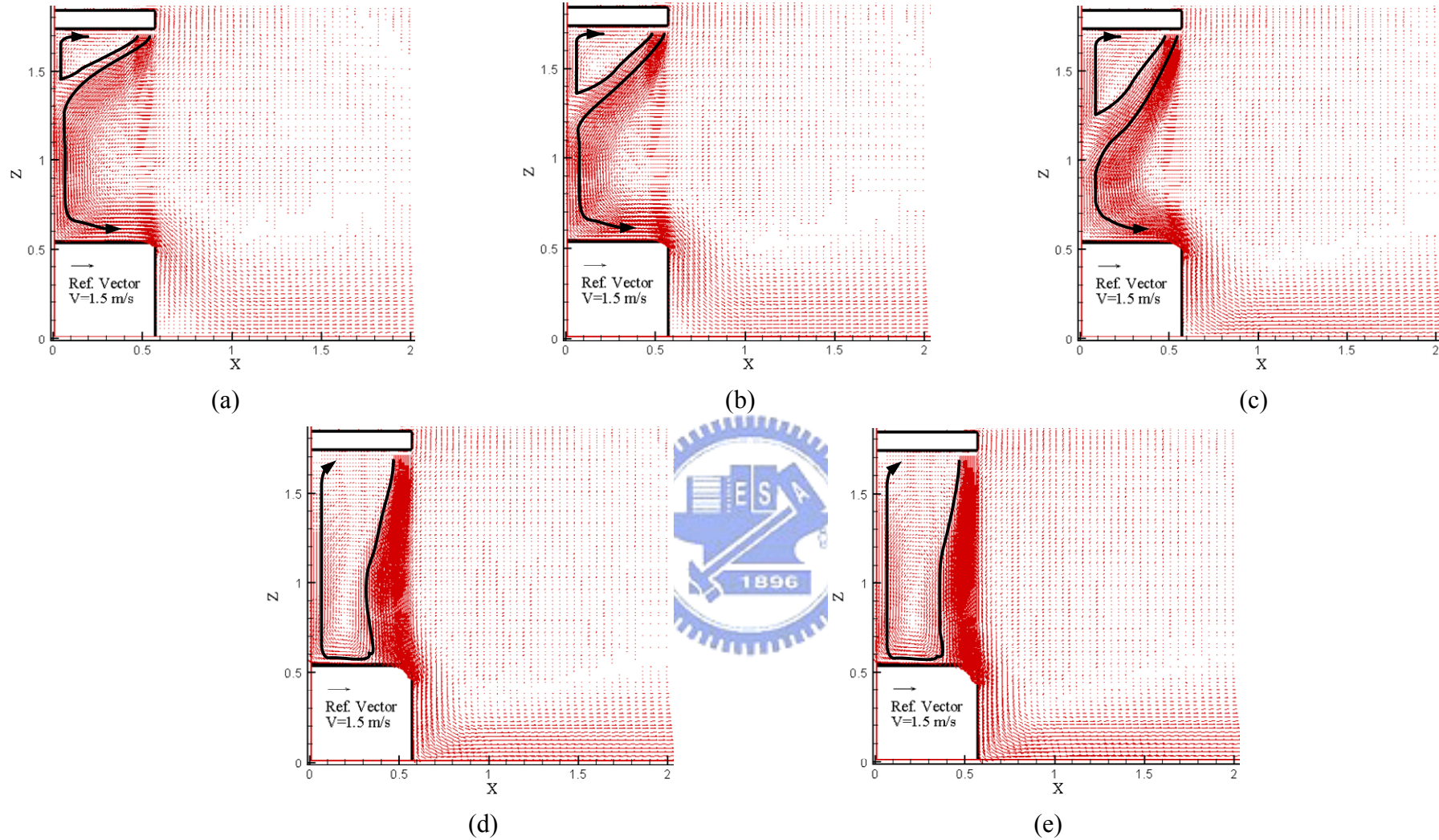


Fig. 4.49 Velocity vector maps for steady cavity flow for a double air curtain design with $b_i = 0.05$ m, $b_o = 0.05$ m, $Gr_t = 4.61 \times 10^9$ ($\Delta T = 20^\circ\text{C}$), and $N = 6.37 \times 10^{-2}$ for $Re_{ci} = 1,910$ and $Re_{co} =$ (a) 1,910, (b) 3,183, (c) 5,092, (d) 6,365 and (e) 7,638.

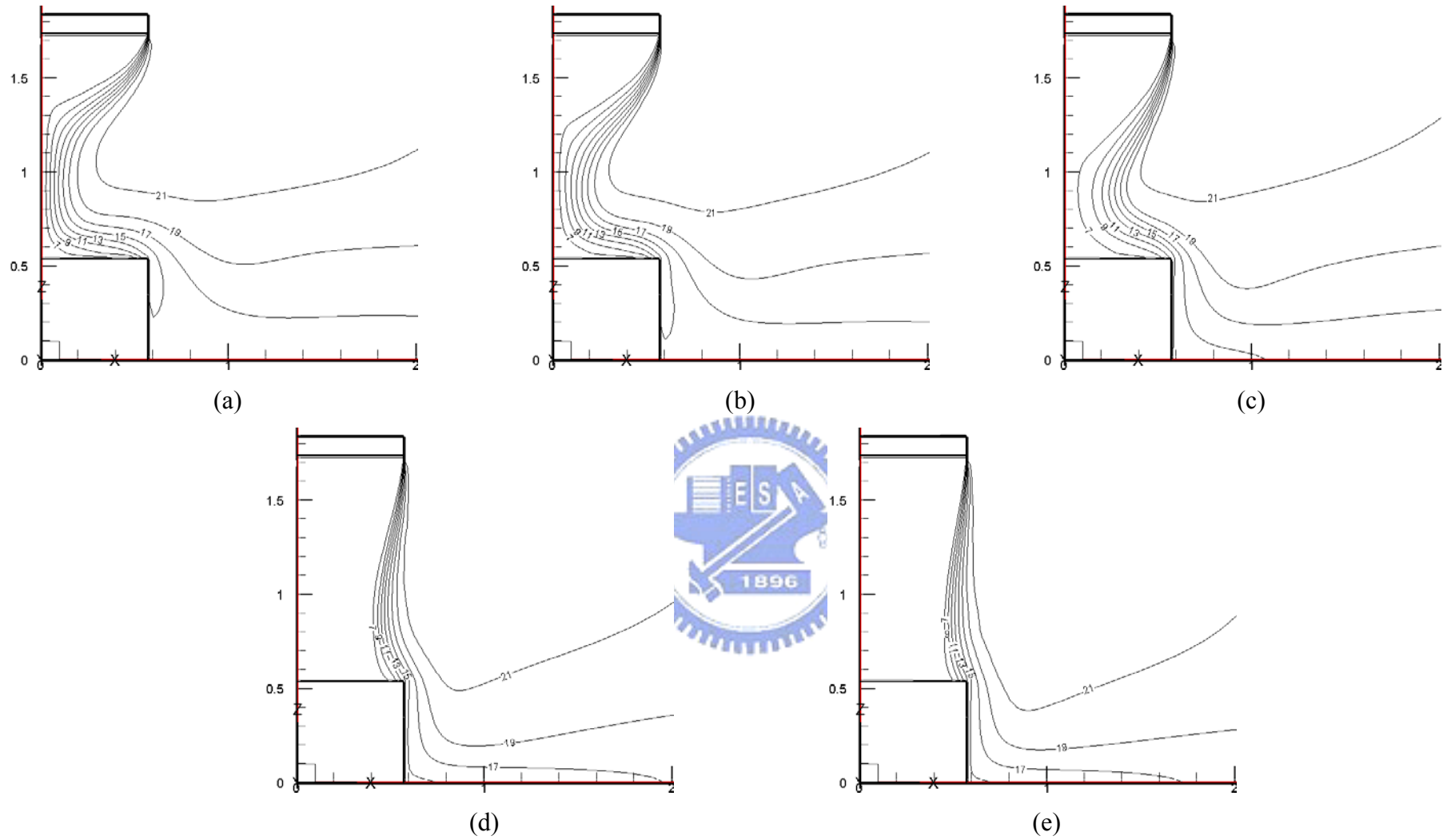


Fig. 4.50 Isotherms for steady cavity flow for a double air curtain design with $b_i = 0.05$ m, $b_o = 0.05$ m, $Gr_t = 4.61 \times 10^9$ ($\Delta T = 20^\circ\text{C}$), and $N = 6.37 \times 10^{-2}$ for $Re_{ci} = 1,910$ and $Re_{co} =$ (a) 1,910, (b) 3,183, (c) 5,092, (d) 6,365 and (e) 7,638.

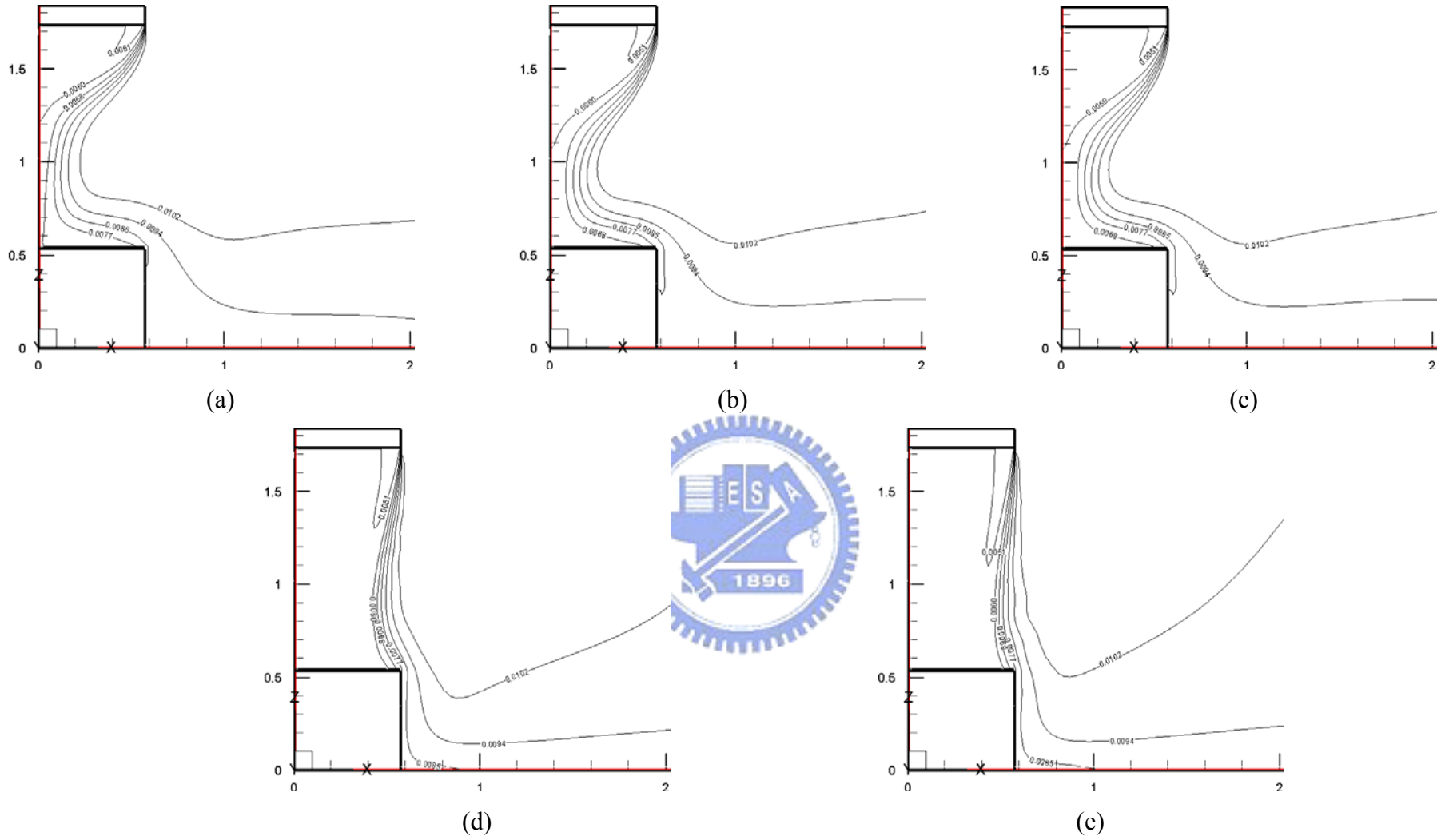


Fig. 4.51 Iso-concentration lines for steady cavity flow for a double air curtain design with $b_i = 0.05$ m, $b_o = 0.05$ m, $Gr_i = 4.61 \times 10^9$ ($\Delta T = 20^\circ\text{C}$), and $N = 6.37 \times 10^{-2}$ for $Re_{ci} = 1,910$ and $Re_{co} =$ (a) 1,910, (b) 3,183, (c) 5,092, (d) 6,365 and (e) 7,638.

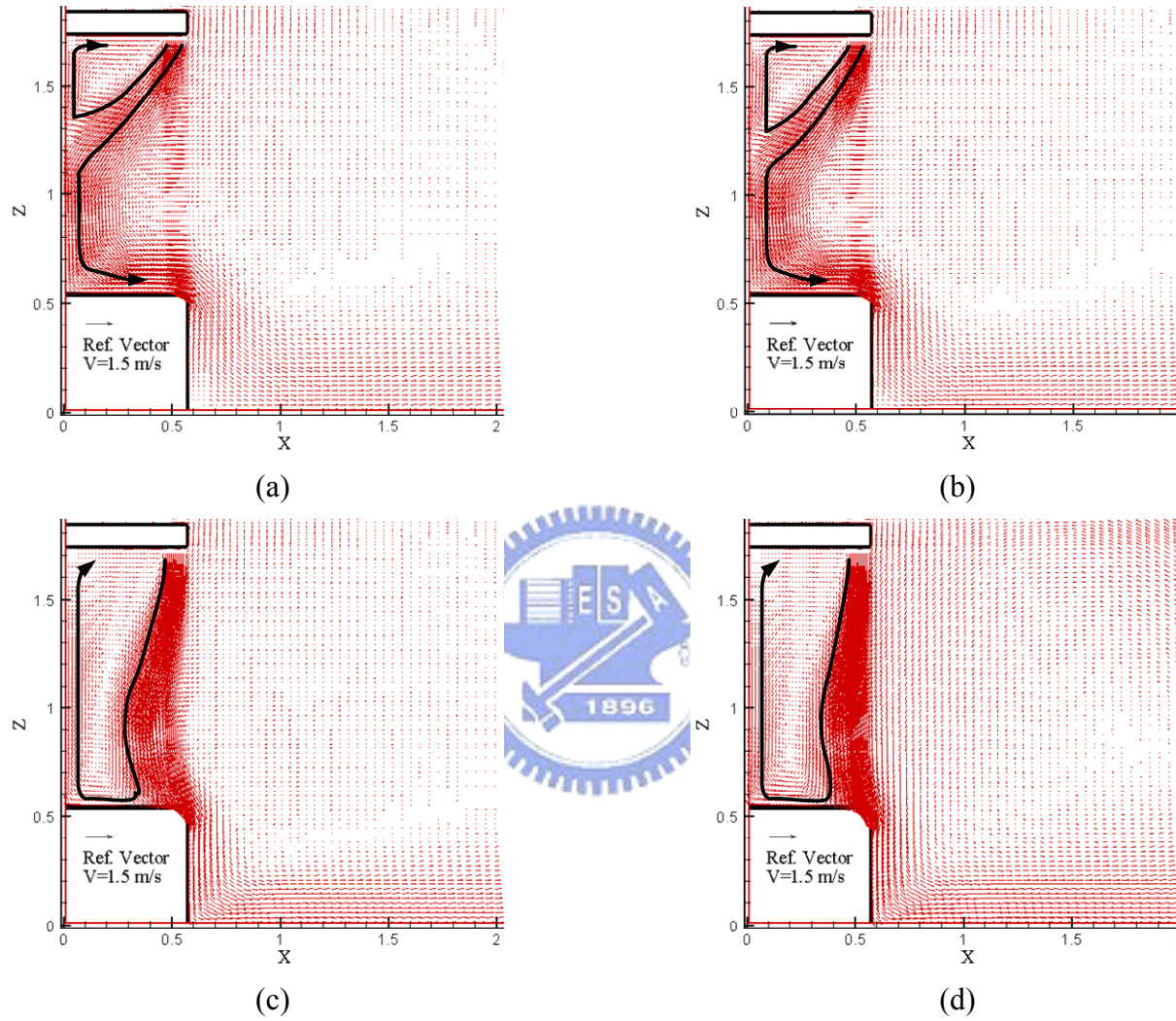


Fig. 4.52 Velocity vector maps for steady cavity flow for a double air curtain design with $b_i = 0.05$ m, $b_o = 0.05$ m, $Gr_t = 4.61 \times 10^9$ ($\Delta T = 20^\circ\text{C}$), and $N = 6.37 \times 10^{-2}$ for $Re_{ci} = 3,183$ and $Re_{co} =$ (a) 1,910, (b) 3,183, (c) 5,092, and (d) 6,365.

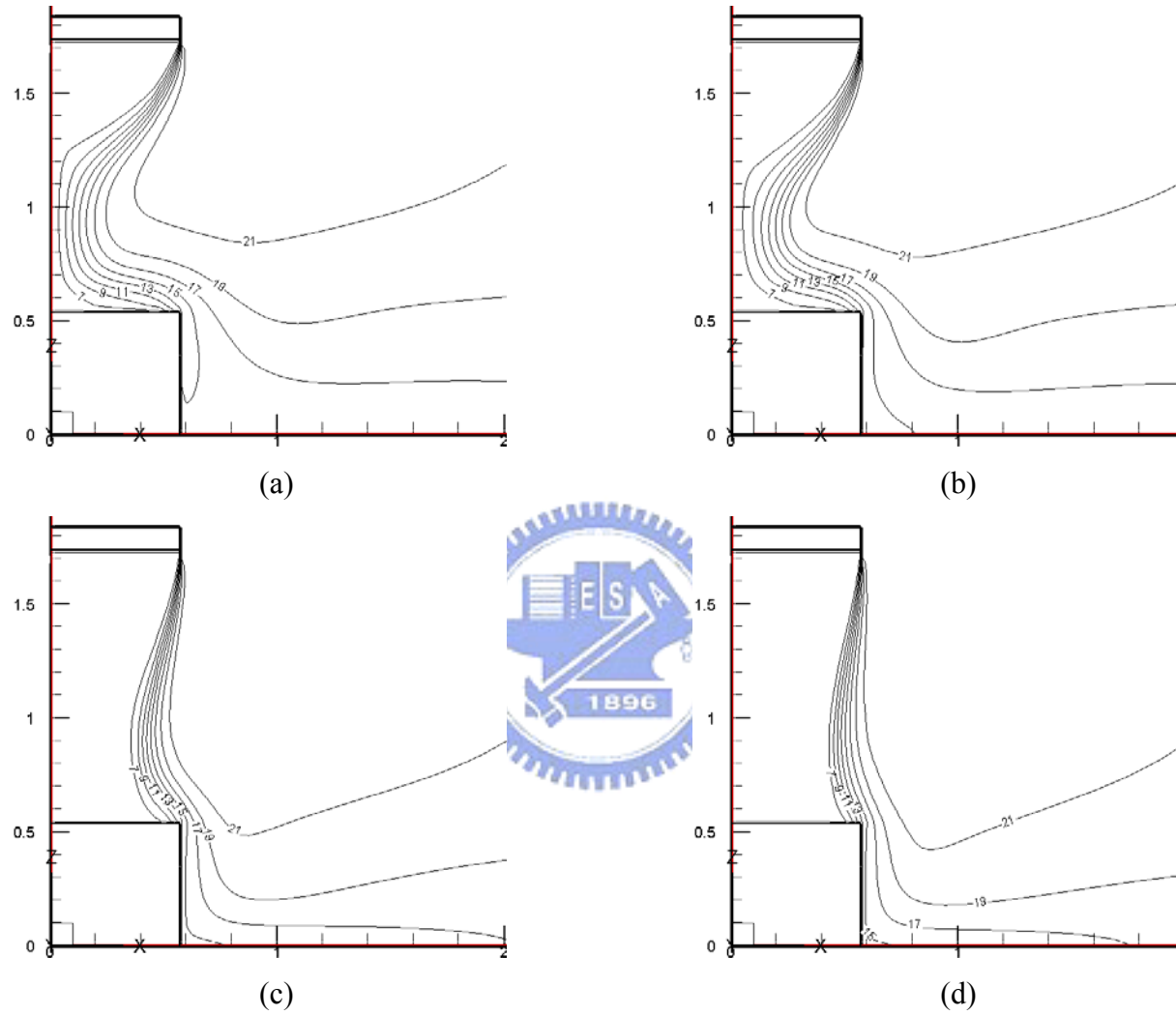


Fig. 4.53 Isotherms for steady cavity flow for a double air curtain design with $b_i = 0.05$ m, $b_o = 0.05$ m, $Gr_t = 4.61 \times 10^9$ ($\Delta T = 20^\circ\text{C}$), and $N = 6.37 \times 10^{-2}$ for $Re_{ci} = 3,183$ and $Re_{co} =$ (a) 1,910, (b) 3,183, (c) 5,092, and (d) 6,365.

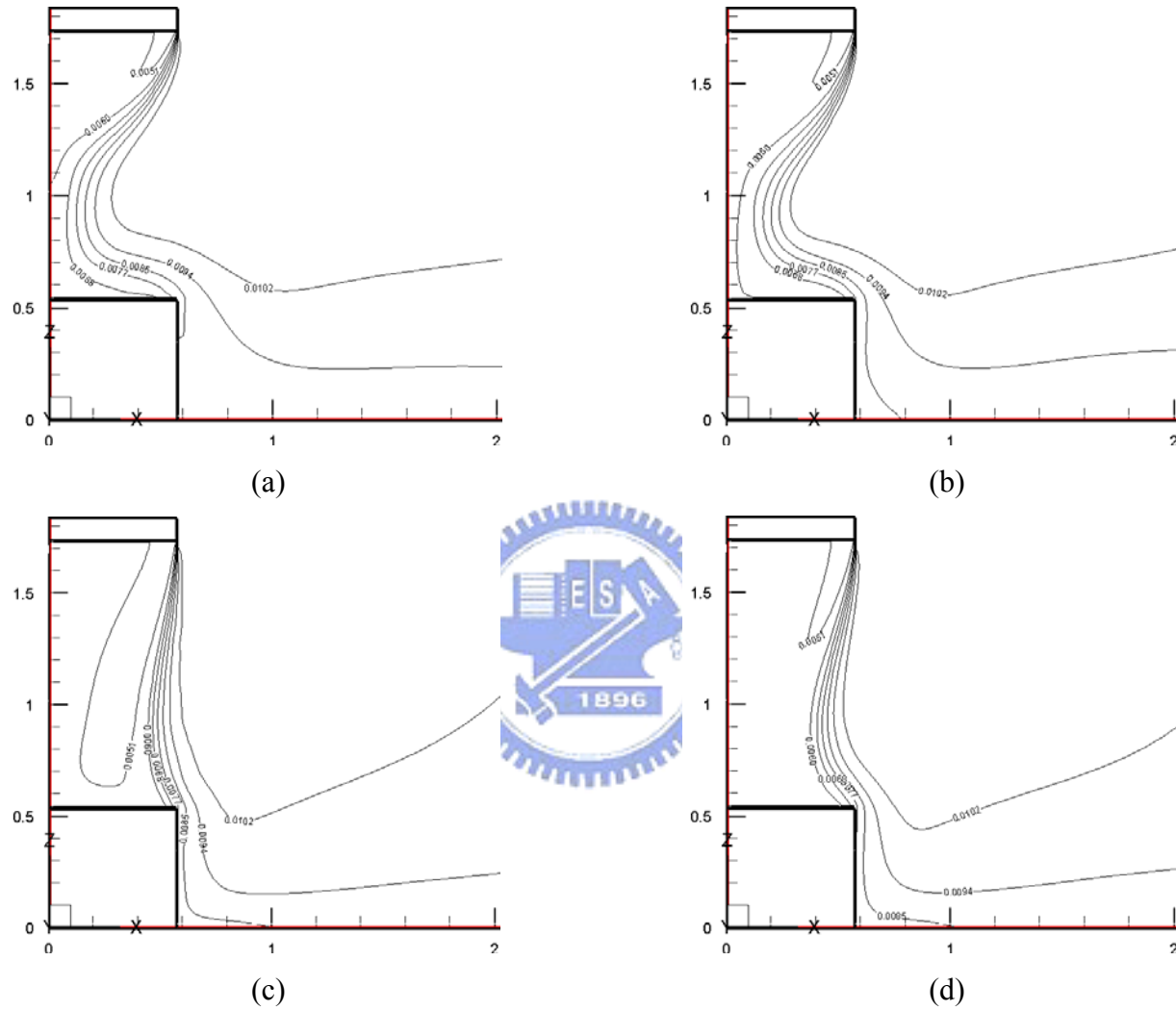


Fig. 4.54 Iso-concentration lines for steady cavity flow for a double air curtain design with $b_i = 0.05$ m, $b_o = 0.05$ m, $Gr_t = 4.61 \times 10^9$ ($\Delta T = 20^\circ\text{C}$), and $N = 6.37 \times 10^{-2}$ for $Re_{ci} = 3,183$ and $Re_{co} =$ (a) 1,910, (b) 3,183, (c) 5,092, and (d) 6,365.

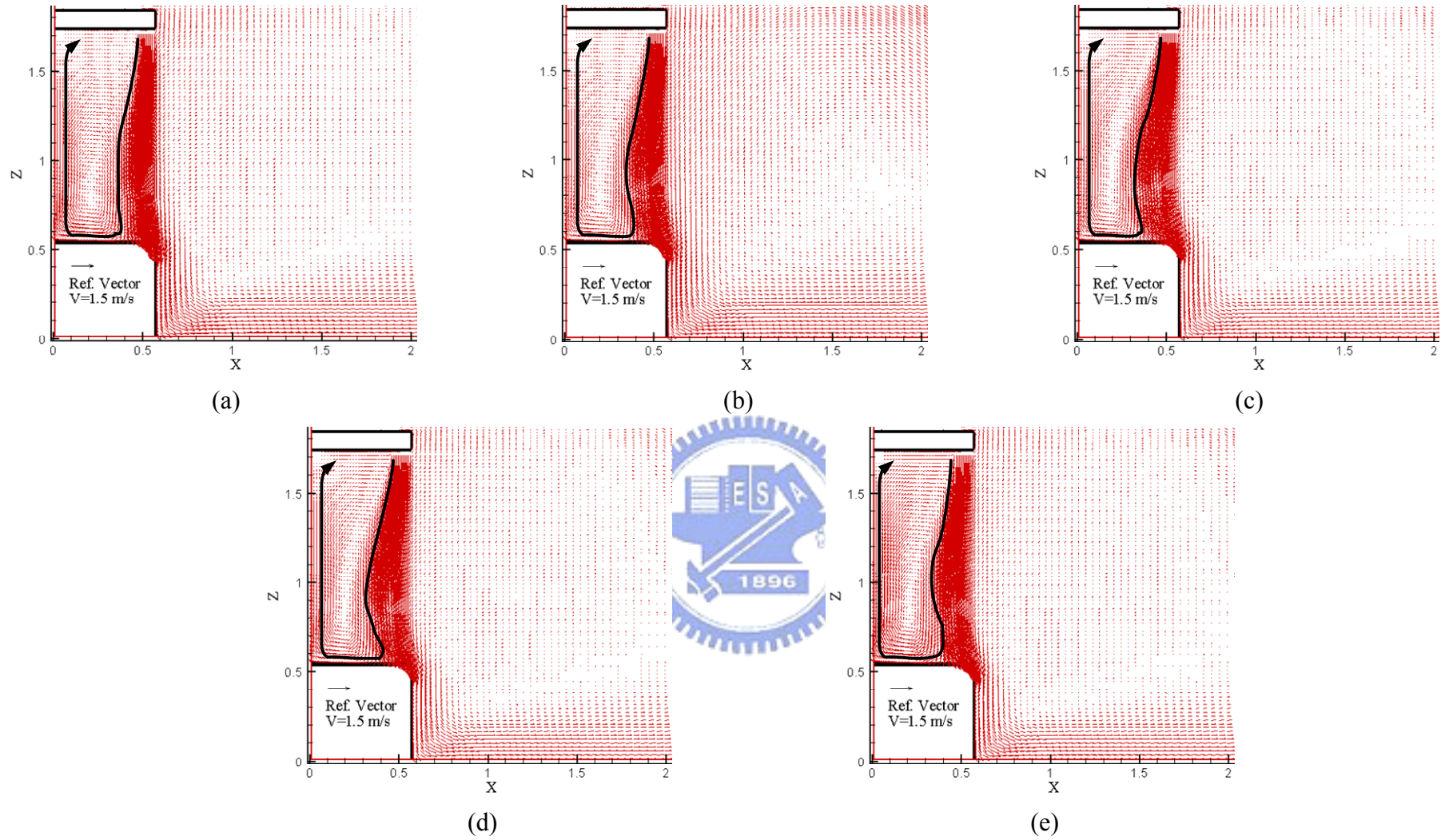


Fig. 4.55 Velocity vector maps for steady cavity flow for a double air curtain design with $b_i = 0.05$ m, $b_o = 0.05$ m, $Gr_t = 4.61 \times 10^9$ ($\Delta T = 20^\circ\text{C}$), and $N = 6.37 \times 10^{-2}$ for (a) $Re_{ci} = 1,910$ and $Re_{co} = 7,638$, (b) $Re_{ci} = 3,183$ and $Re_{co} = 6,365$, (c) $Re_{ci} = 5,092$ and $Re_{co} = 4,456$, (d) $Re_{ci} = 6,365$ and $Re_{co} = 3,183$, (e) $Re_{ci} = 7,638$ and $Re_{co} = 1,910$.

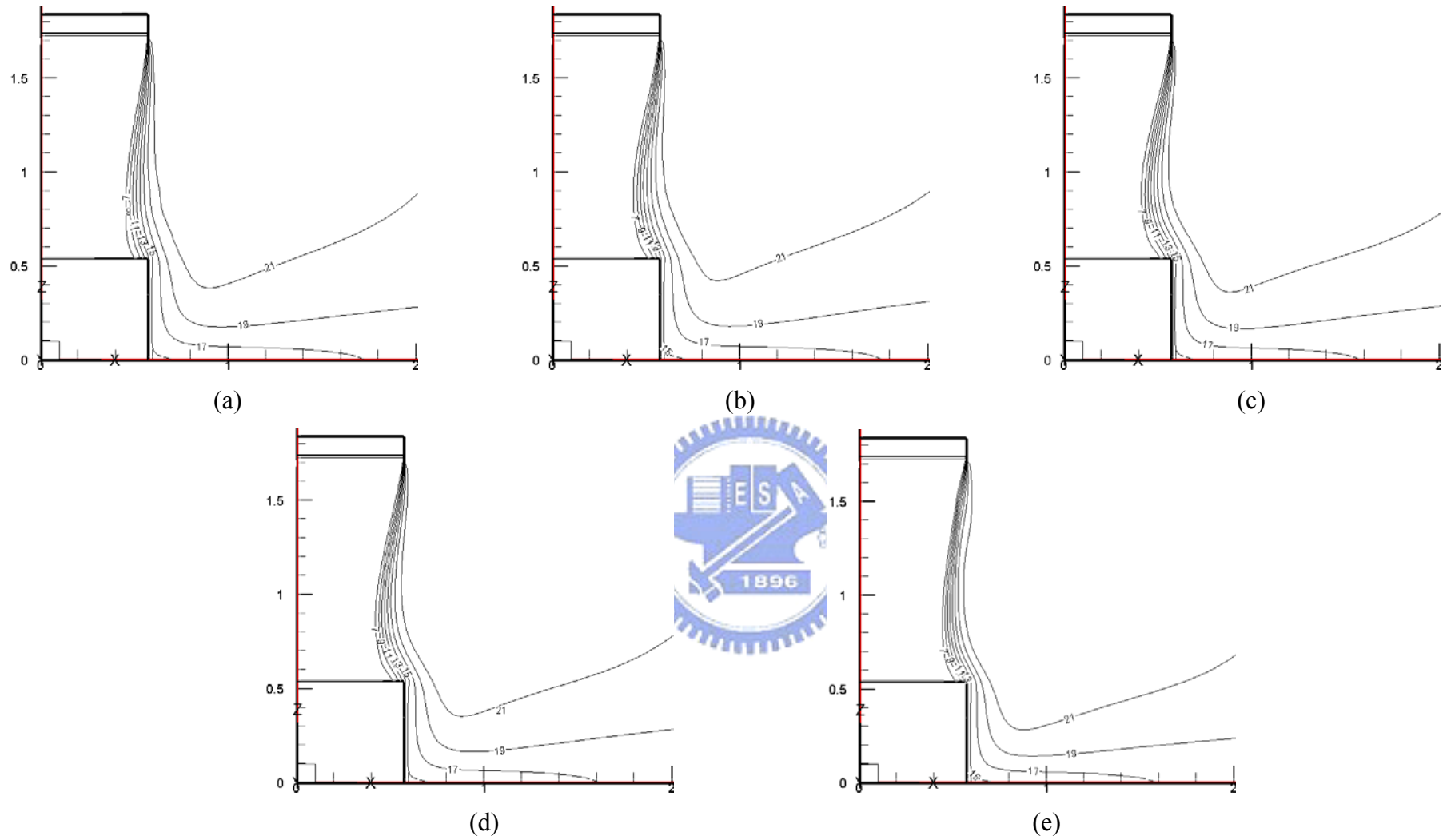


Fig. 4.56 Isotherms for steady cavity flow for a double air curtain design with $b_i = 0.05$ m, $b_o = 0.05$ m, $Gr_t = 4.61 \times 10^9$ ($\Delta T = 20^\circ\text{C}$), and $N = 6.37 \times 10^{-2}$ for (a) $Re_{ci} = 1,910$ and $Re_{co} = 7,638$, (b) $Re_{ci} = 3,183$ and $Re_{co} = 6,365$, (c) $Re_{ci} = 5,092$ and $Re_{co} = 4,456$, (d) $Re_{ci} = 6,365$ and $Re_{co} = 3,183$, (e) $Re_{ci} = 7,638$ and $Re_{co} = 1,910$.

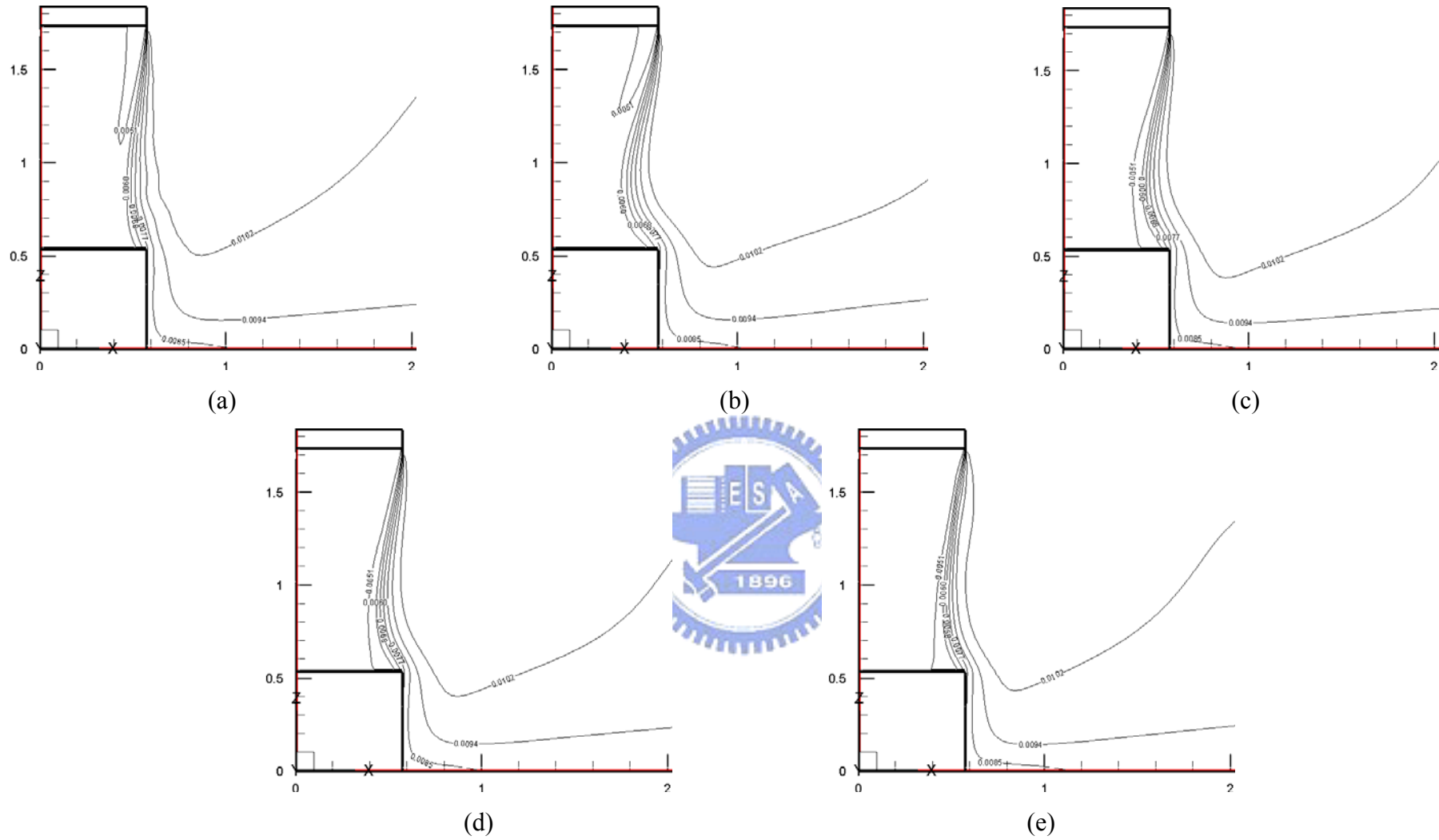


Fig. 4.57 Iso-concentration lines for steady cavity flow for a double air curtain design with $b_i = 0.05$ m, $b_o = 0.05$ m, $Gr_t = 4.61 \times 10^9$ ($\Delta T = 20^\circ\text{C}$), and $N = 6.37 \times 10^{-2}$ for (a) $Re_{ci} = 1,910$ and $Re_{co} = 7,638$, (b) $Re_{ci} = 3,183$ and $Re_{co} = 6,365$, (c) $Re_{ci} = 5,092$ and $Re_{co} = 4,456$, (d) $Re_{ci} = 6,365$ and $Re_{co} = 3,183$, (e) $Re_{ci} = 7,638$ and $Re_{co} = 1,910$.

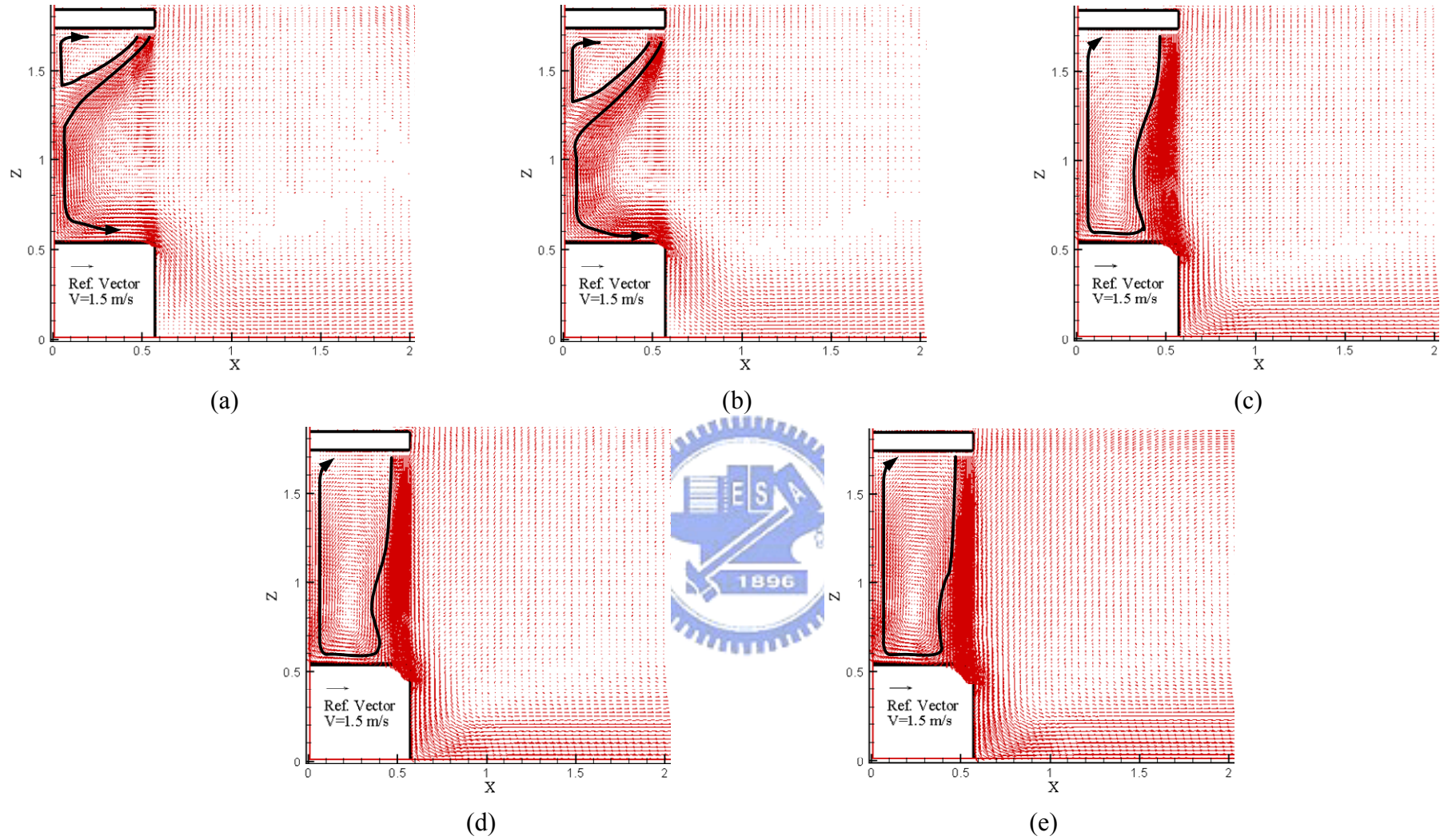


Fig. 4.58 Velocity vector maps for steady cavity flow for a double air curtain design with $b_i = 0.07$ m, $b_o = 0.03$ m, $Gr_t = 4.61 \times 10^9$ ($\Delta T = 20^\circ\text{C}$), and $N = 6.37 \times 10^{-2}$ for $Re_{ci} = 1,910$ and $Re_{co} =$ (a) 1,910, (b) 3,183, (c) 5,092, (d) 6,365 and (e) 7,638.

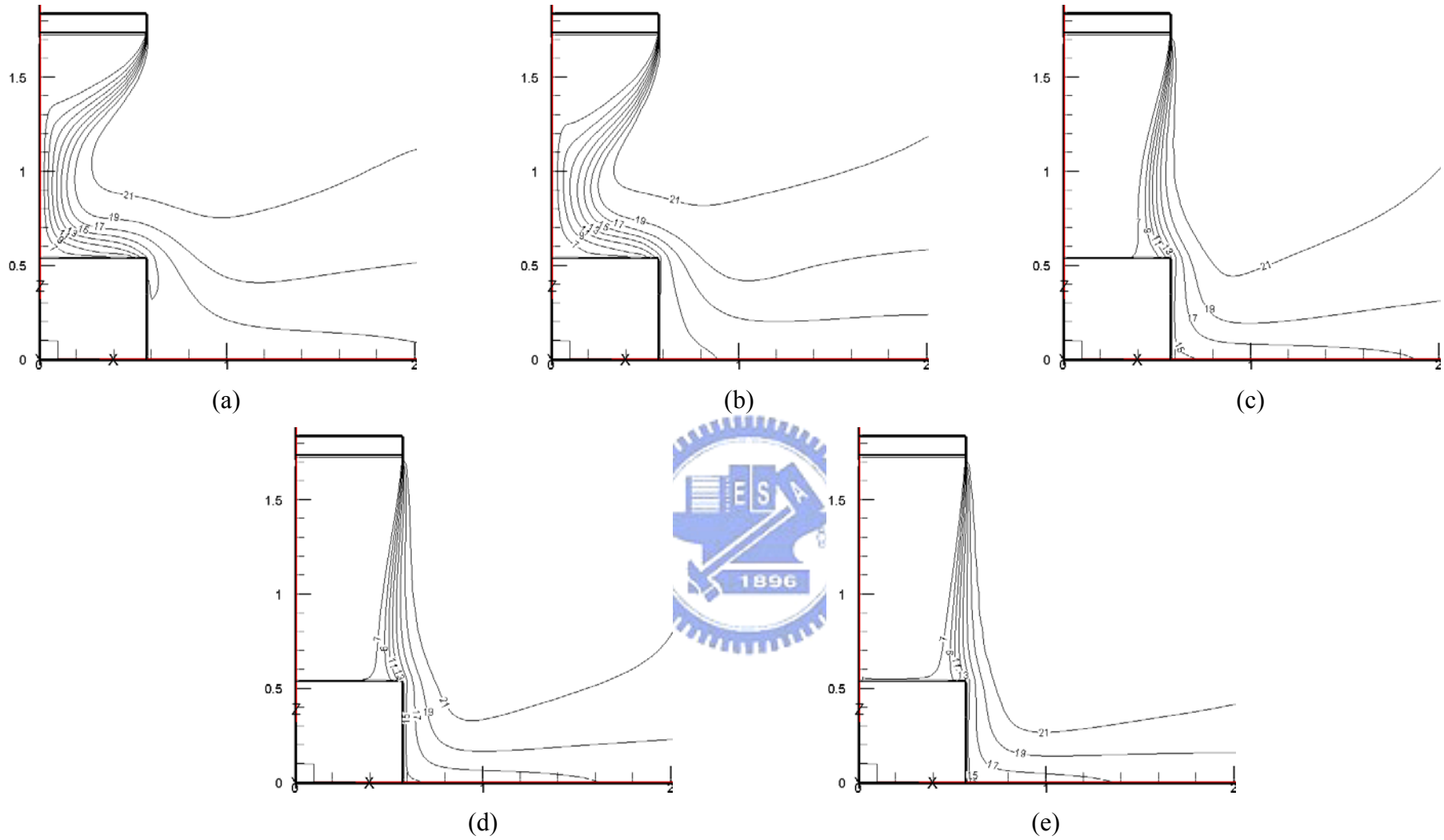


Fig. 4.59 Isotherms for steady cavity flow for a double air curtain design with $b_i = 0.07$ m, $b_o = 0.03$ m, $Gr_t = 4.61 \times 10^9$ ($\Delta T = 20^\circ\text{C}$), and $N = 6.37 \times 10^{-2}$ for $Re_{ci} = 1,910$ and $Re_{co} =$ (a) 1,910, (b) 3,183, (c) 5,092, (d) 6,365 and (e) 7,638.

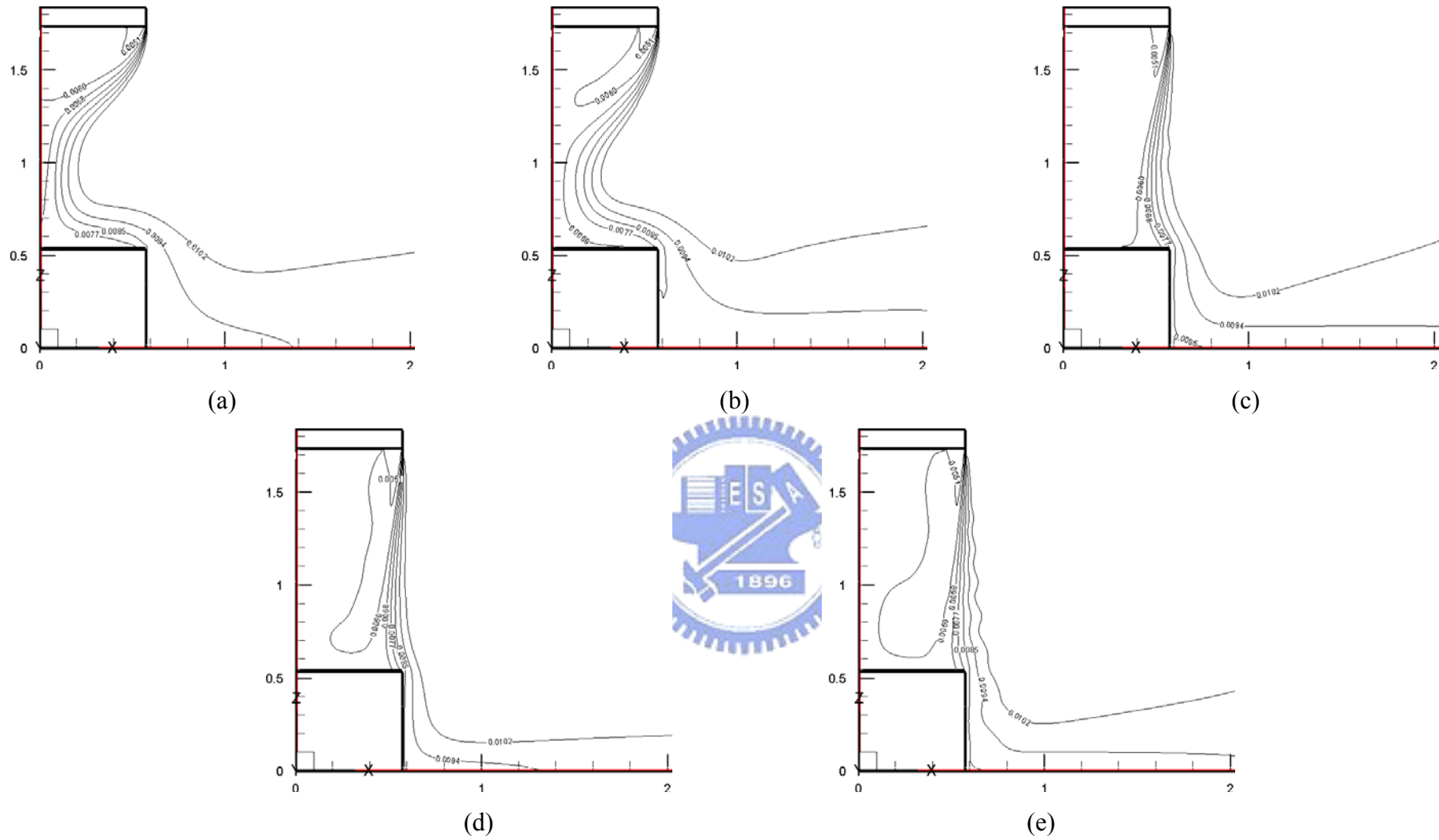


Fig. 4.60 Iso-concentration lines for steady cavity flow for a double air curtain design with $b_i = 0.07$ m, $b_o = 0.03$ m, $Gr_i = 4.61 \times 10^9$ ($\Delta T = 20^\circ\text{C}$), and $N = 6.37 \times 10^{-2}$ for $Re_{ci} = 1,910$ and $Re_{co} =$ (a) 1,910, (b) 3,183, (c) 5,092, (d) 6,365 and (e) 7,638.

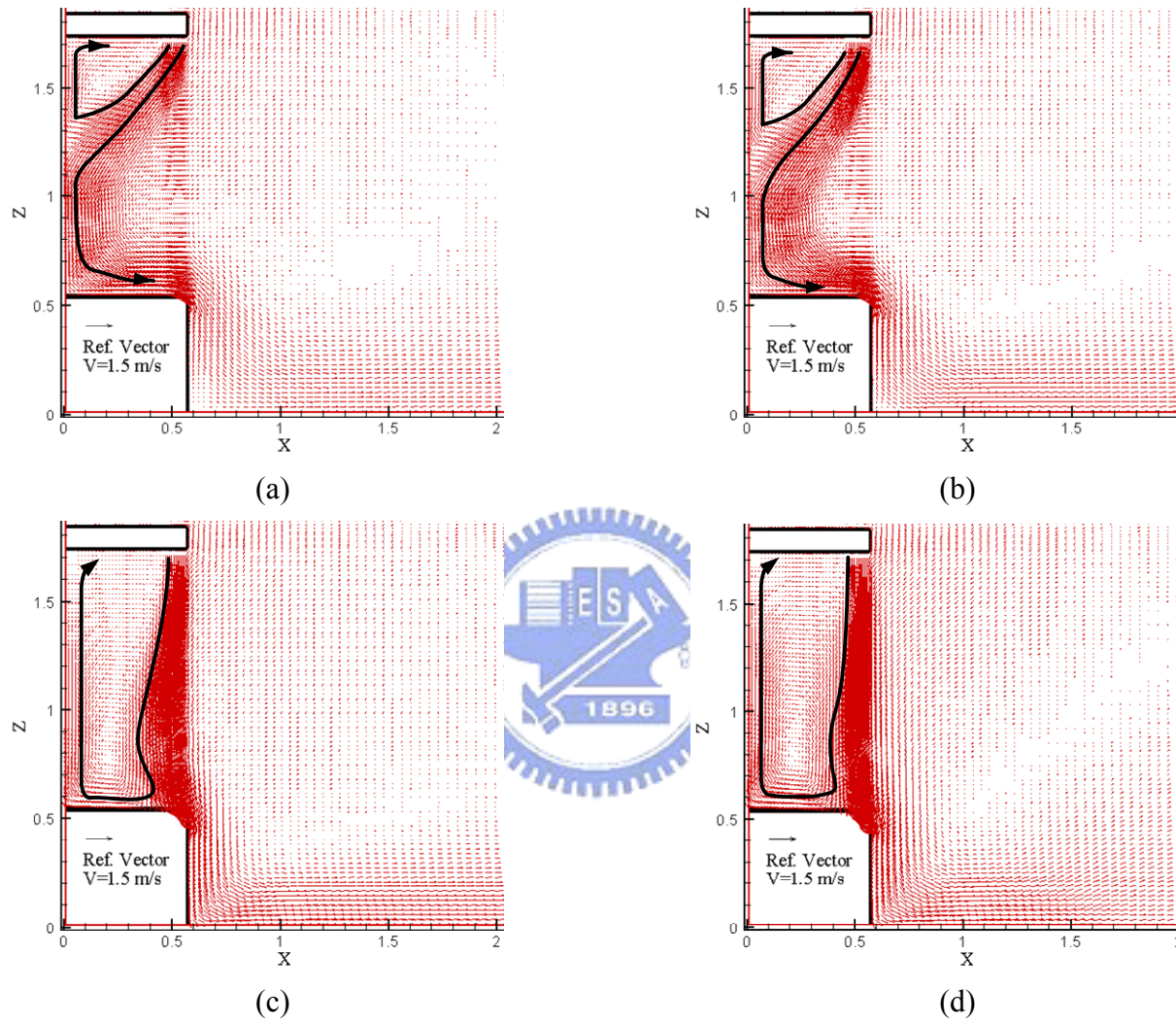


Fig. 4.61 Velocity vector maps for steady cavity flow for a double air curtain design with $b_i = 0.07$ m, $b_o = 0.03$ m, $Gr_t = 4.61 \times 10^9$ ($\Delta T = 20^\circ\text{C}$), and $N = 6.37 \times 10^{-2}$ for $Re_{ci} = 3,183$ and $Re_{co} =$ (a) 1,910, (b) 3,183, (c) 5,092, and (d) 6,365.

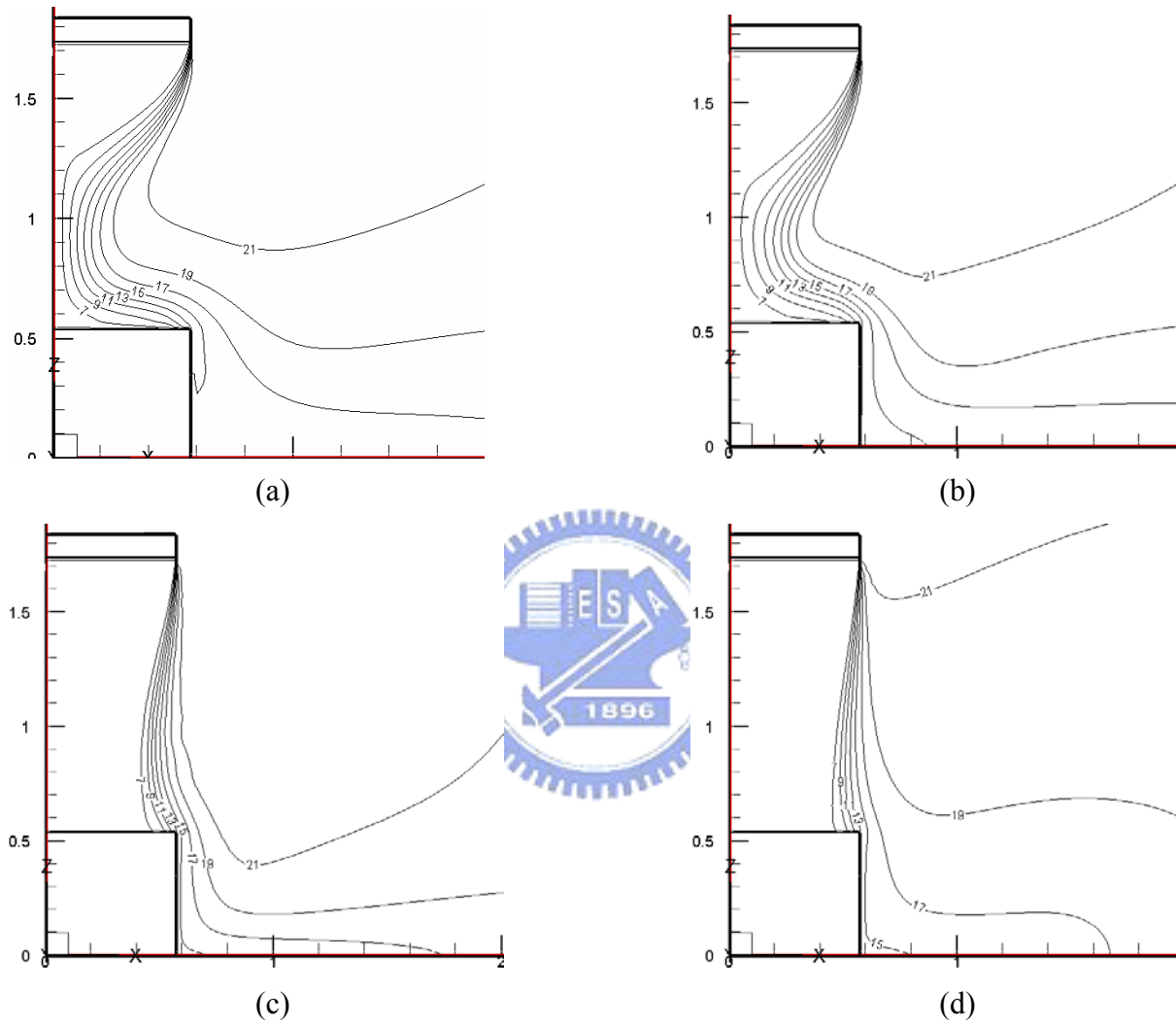


Fig. 4.62 Isotherms for steady cavity flow for a double air curtain design with $b_i = 0.07$ m, $b_o = 0.03$ m, $Gr_t = 4.61 \times 10^9$ ($\Delta T = 20^\circ\text{C}$), and $N = 6.37 \times 10^{-2}$ for $Re_{ci} = 3,183$ and $Re_{co} =$ (a) 1,910, (b) 3,183, (c) 5,092, and (d) 6,365.

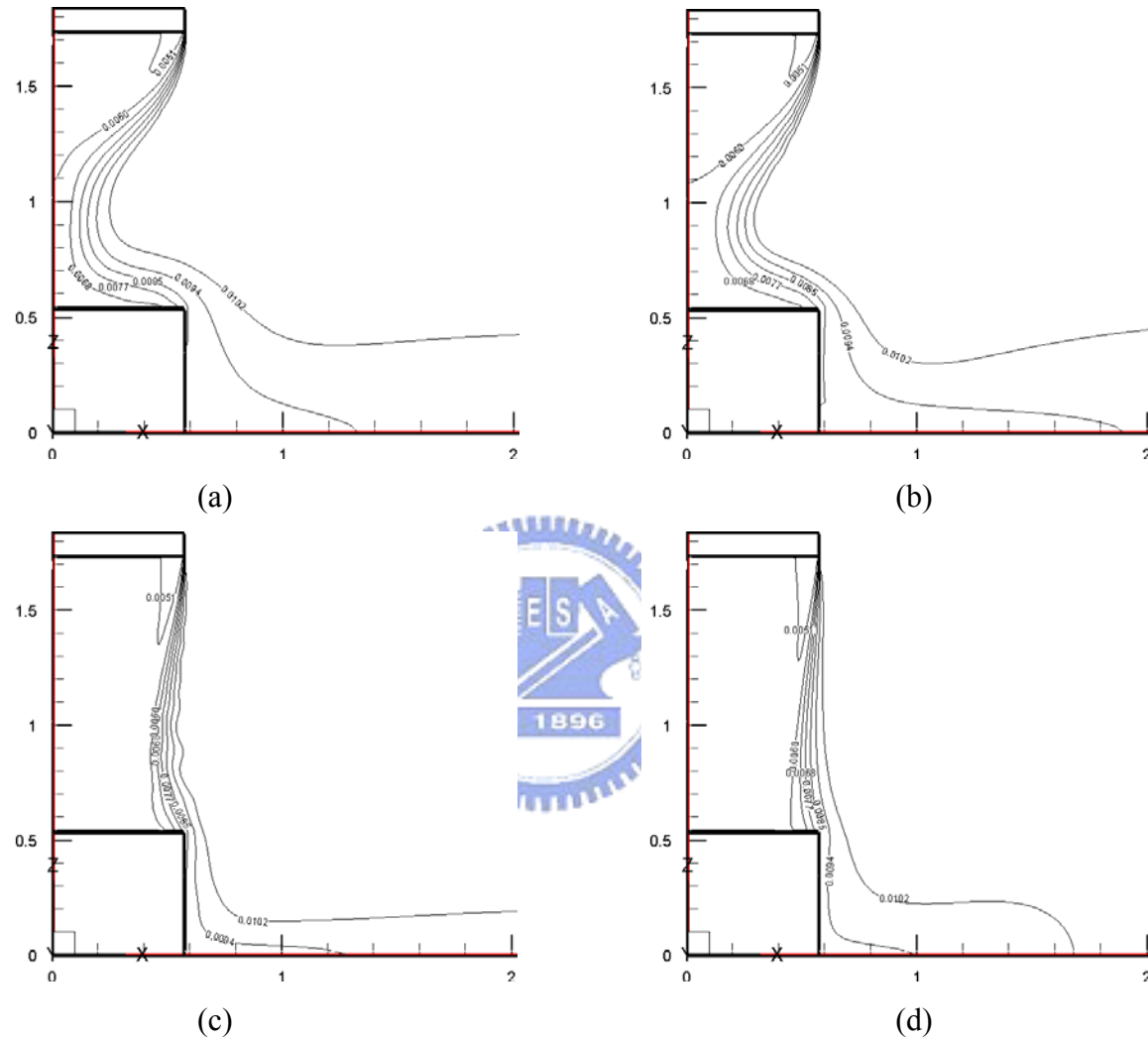


Fig. 4.63 Iso-concentration lines for steady cavity flow for a double air curtain design with $b_i = 0.07$ m, $b_o = 0.03$ m, $Gr_i = 4.61 \times 10^9$ ($\Delta T = 20^\circ\text{C}$), and $N = 6.37 \times 10^{-2}$ for $Re_{ci} = 3,183$ and $Re_{co} =$ (a) 1,910, (b) 3,183, (c) 5,092, and (d) 6,365.

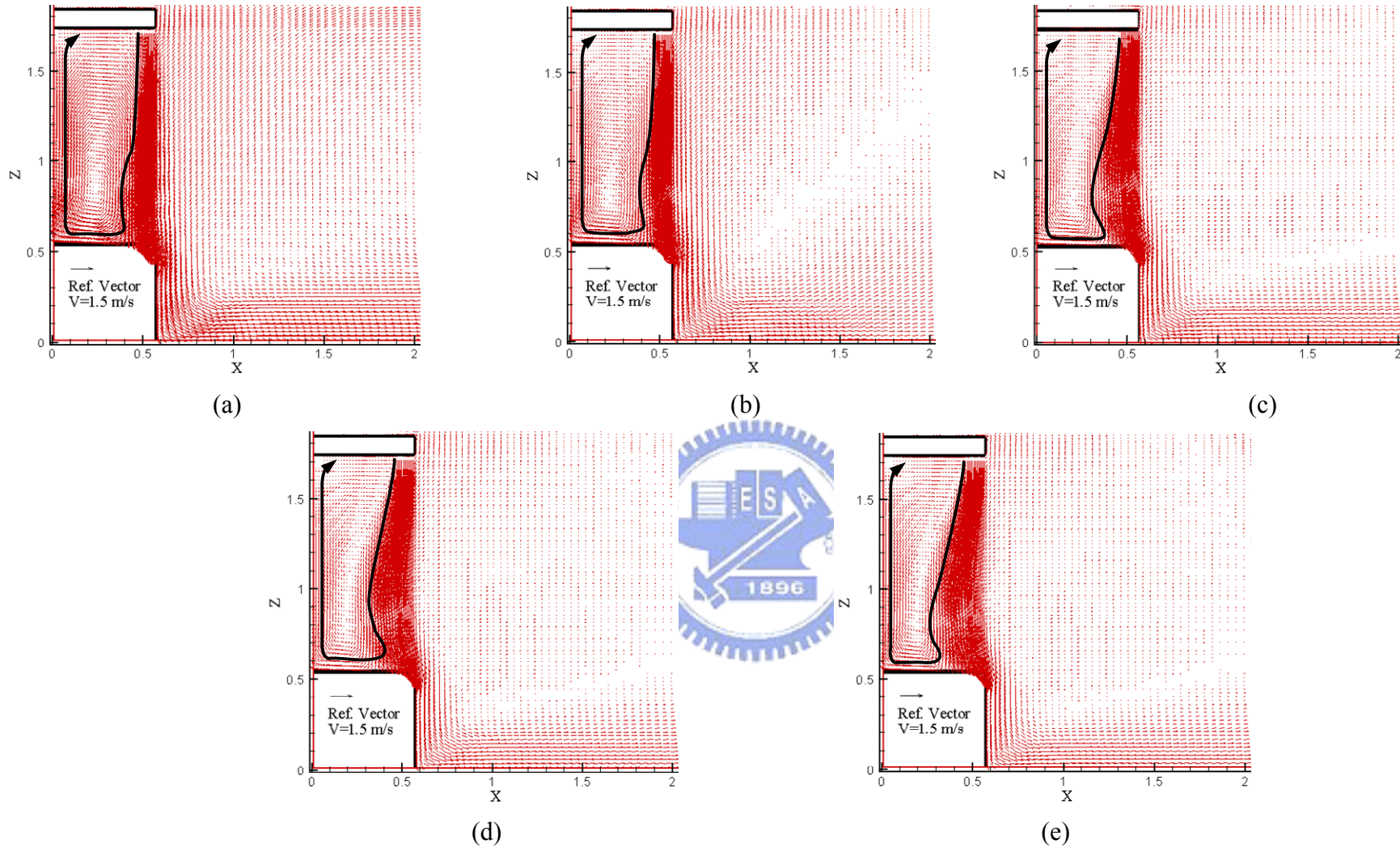


Fig. 4.64 Velocity vector maps for steady cavity flow for a double air curtain design with $b_i = 0.07$ m, $b_o = 0.03$ m, $Gr_t = 4.61 \times 10^9$ ($\Delta T = 20^\circ\text{C}$), and $N = 6.37 \times 10^{-2}$ for (a) $Re_{ci} = 1,910$ and $Re_{co} = 7,638$, (b) $Re_{ci} = 3,183$ and $Re_{co} = 6,365$, (c) $Re_{ci} = 5,092$ and $Re_{co} = 4,456$, (d) $Re_{ci} = 6,365$ and $Re_{co} = 3,183$, (e) $Re_{ci} = 7,638$ and $Re_{co} = 1,910$.

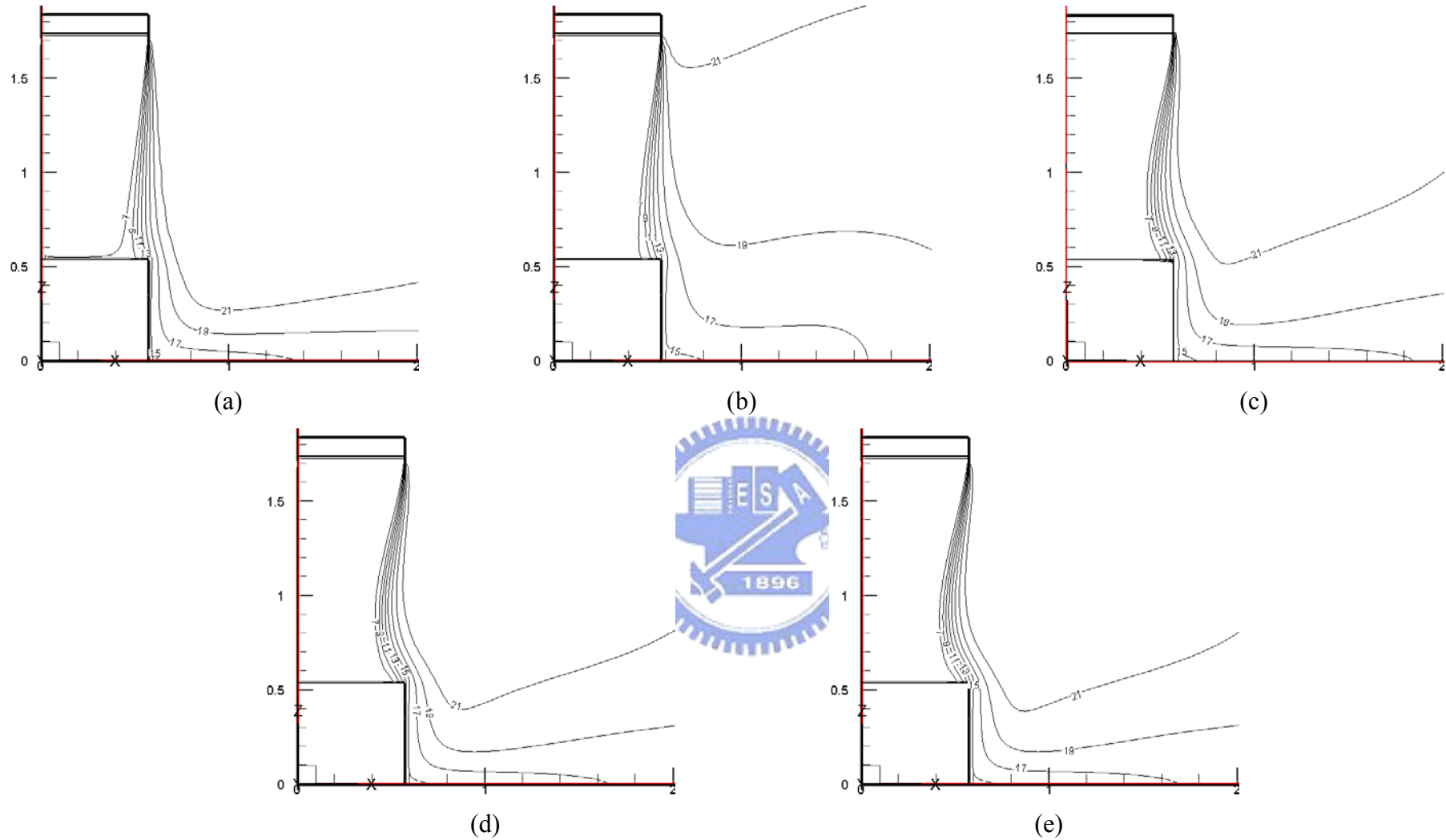


Fig. 4.65 Isotherms for steady cavity flow for a double air curtain design with $b_i = 0.07$ m, $b_o = 0.03$ m, $Gr_t = 4.61 \times 10^9$ ($\Delta T = 20^\circ\text{C}$), and $N = 6.37 \times 10^{-2}$ for (a) $Re_{ci} = 1,910$ and $Re_{co} = 7,638$, (b) $Re_{ci} = 3,183$ and $Re_{co} = 6,365$, (c) $Re_{ci} = 5,092$ and $Re_{co} = 4,456$, (d) $Re_{ci} = 6,365$ and $Re_{co} = 3,183$, (e) $Re_{ci} = 7,638$ and $Re_{co} = 1,910$.

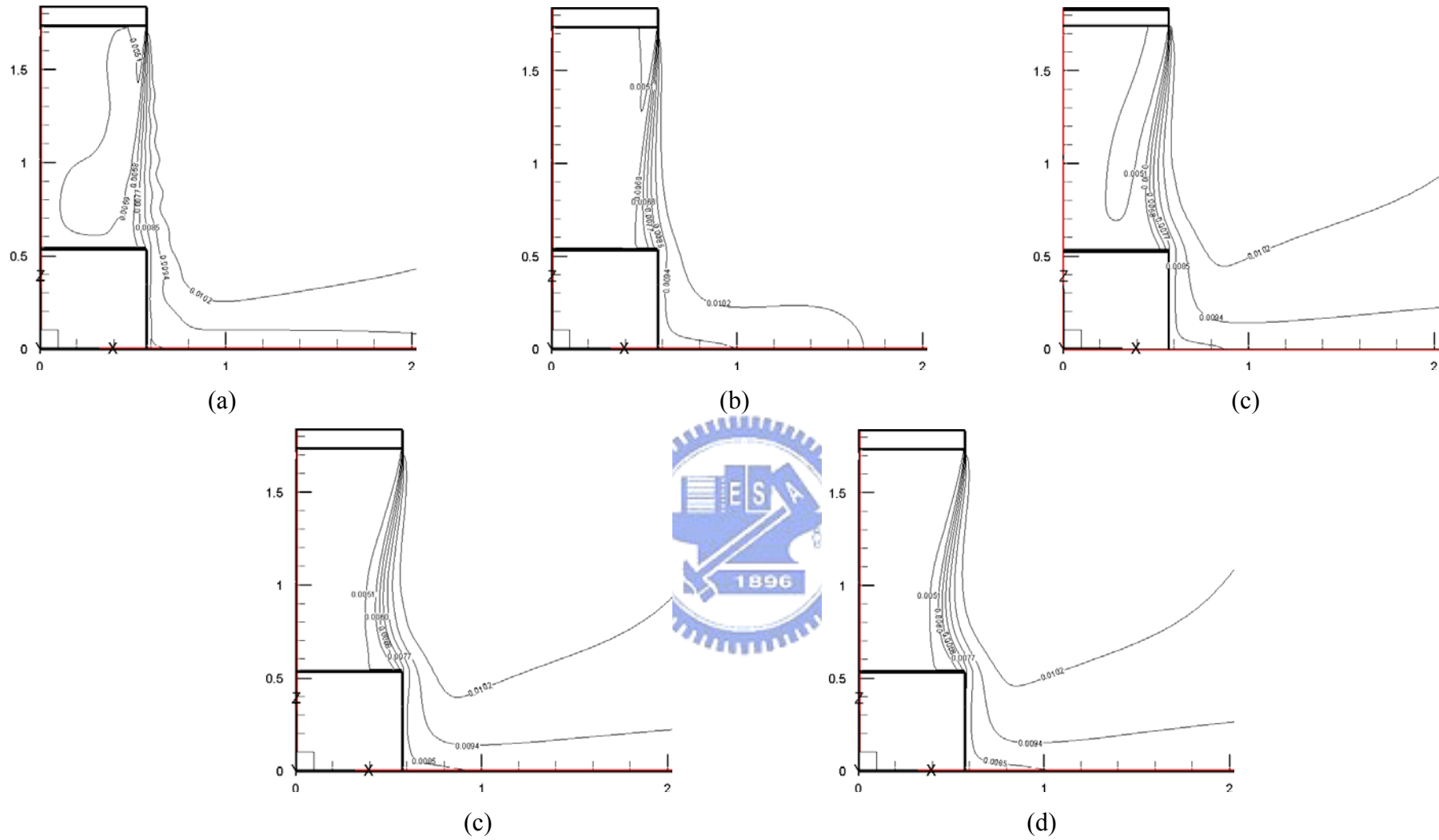


Fig. 4.66 Iso-concentration lines for steady cavity flow for a double air curtain design with $b_i = 0.07$ m, $b_o = 0.03$ m, $Gr_t = 4.61 \times 10^9$ ($\Delta T = 20^\circ\text{C}$), and $N = 6.37 \times 10^{-2}$ for (a) $Re_{ci} = 1,910$ and $Re_{co} = 7,638$, (b) $Re_{ci} = 3,183$ and $Re_{co} = 6,365$, (c) $Re_{ci} = 5,092$ and $Re_{co} = 4,456$, (d) $Re_{ci} = 6,365$ and $Re_{co} = 3,183$, (e) $Re_{ci} = 7,638$ and $Re_{co} = 1,910$.

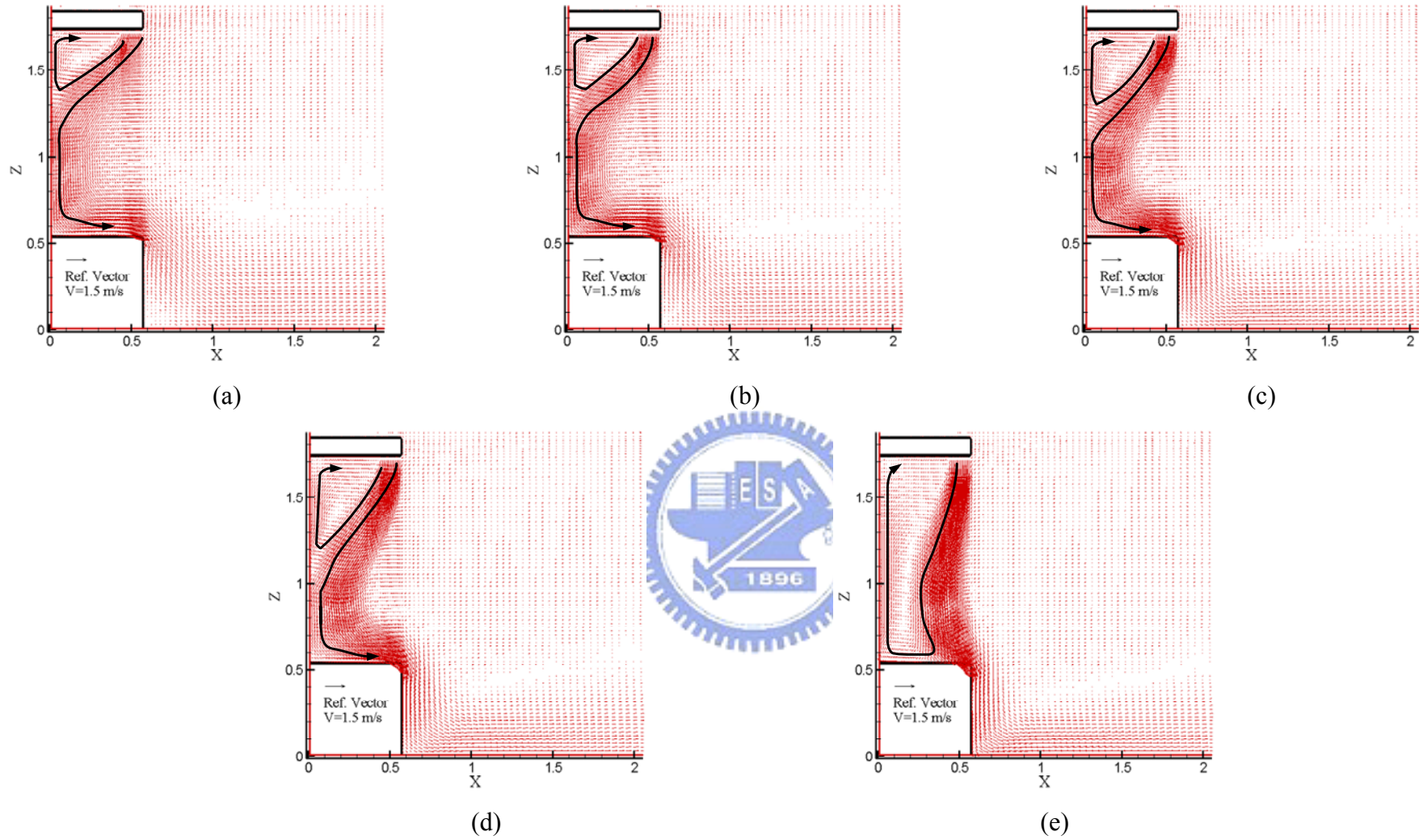


Fig. 4.67 Velocity vector maps for steady cavity flow for a double air curtain design with $b_i = 0.03$ m, $b_o = 0.09$ m, $Gr_t = 4.61 \times 10^9$ ($\Delta T = 20^\circ\text{C}$), and $N = 6.37 \times 10^{-2}$ for $Re_{ci} = 1,910$ and $Re_{co} =$ (a) 1,910, (b) 3,183, (c) 5,092, (d) 6,365 and (e) 7,638.

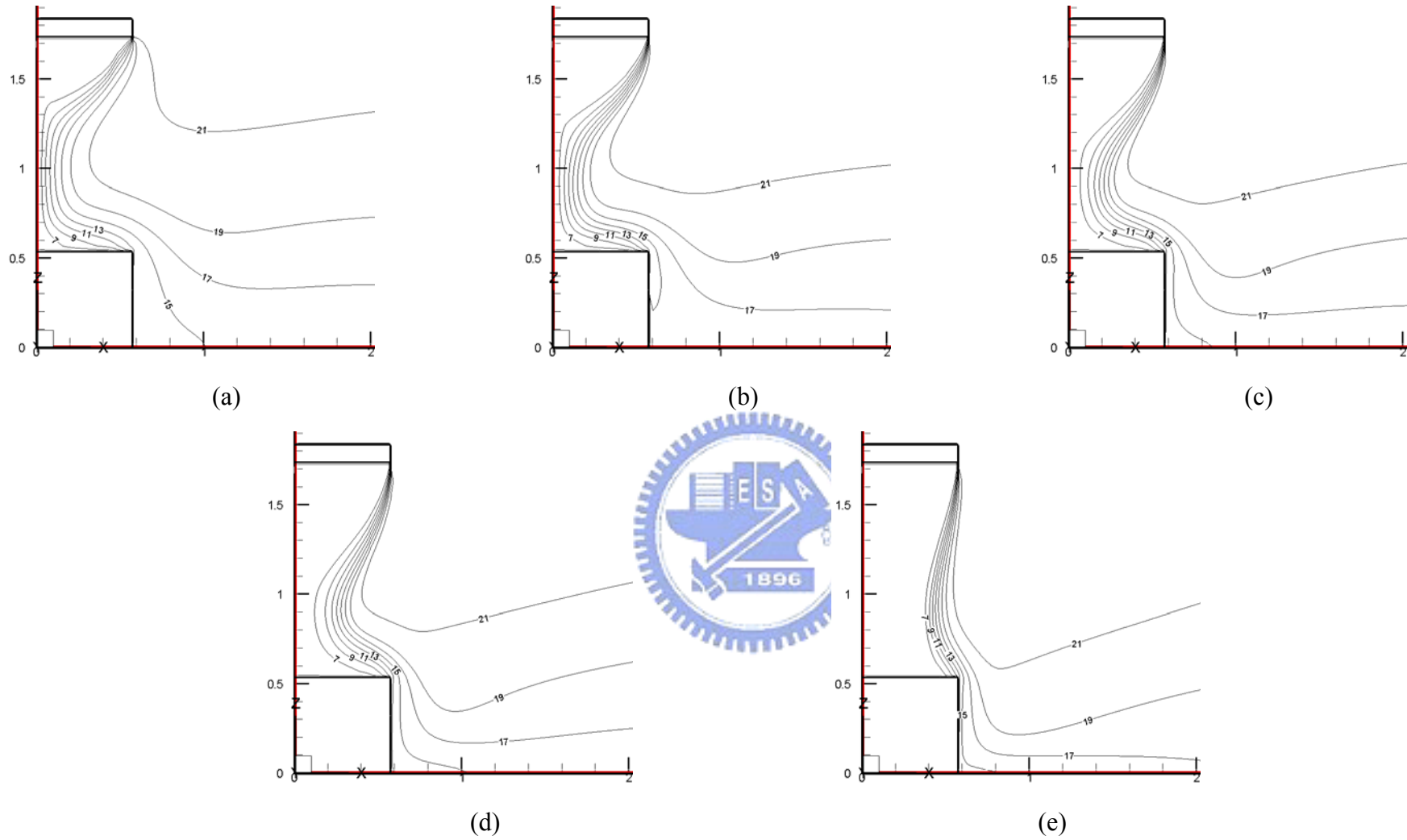


Fig. 4.68 Isotherms for steady cavity flow for a double air curtain design with $b_i = 0.03$ m, $b_o = 0.09$ m, $Gr_t = 4.61 \times 10^9$ ($\Delta T = 20^\circ\text{C}$), and $N = 6.37 \times 10^{-2}$ for $Re_{ci} = 1,910$ and $Re_{co} =$ (a) 1,910, (b) 3,183, (c) 5,092, (d) 6,365 and (e) 7,638.

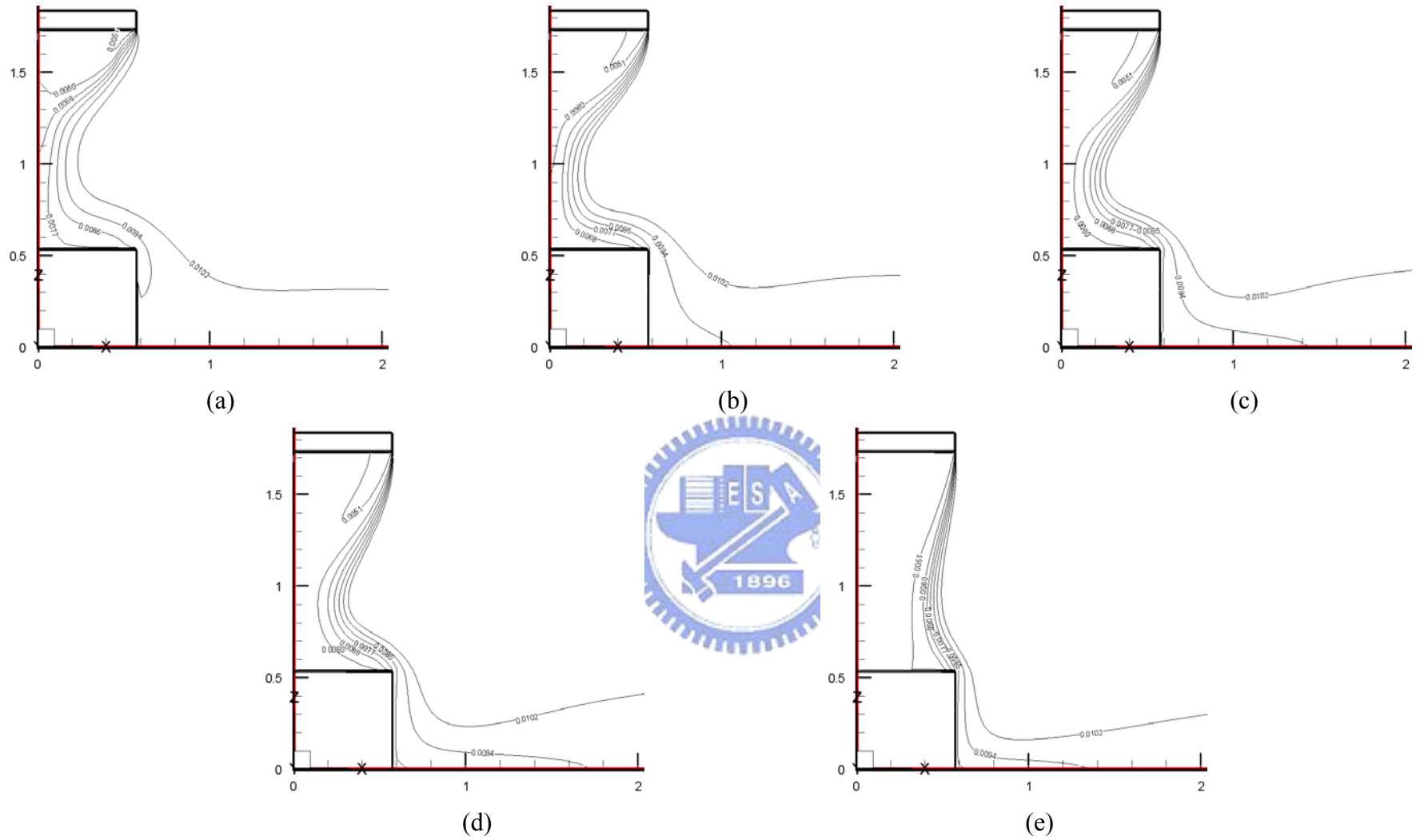


Fig. 4.69 Iso-concentration lines for steady cavity flow for a double air curtain design with $b_i = 0.03$ m, $b_o = 0.09$ m, $Gr_i = 4.61 \times 10^9$ ($\Delta T = 20^\circ\text{C}$), and $N = 6.37 \times 10^{-2}$ for $Re_{ci} = 1,910$ and $Re_{co} =$ (a) 1,910, (b) 3,183, (c) 5,092, (d) 6,365 and (e) 7,638.

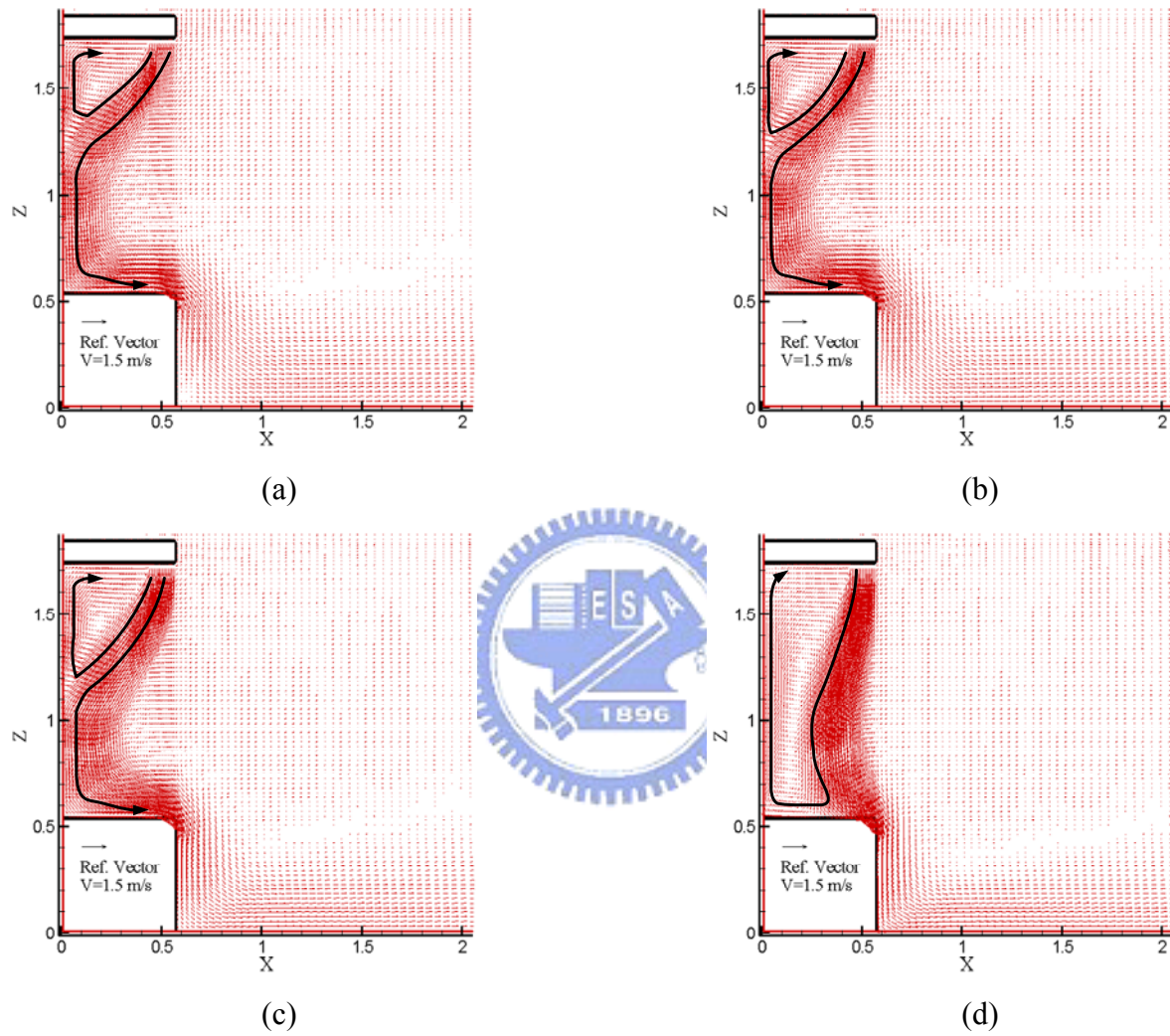


Fig. 4.70 Velocity vector maps for steady cavity flow for a double air curtain design with $b_i = 0.03$ m, $b_o = 0.09$ m, $Gr_t = 4.61 \times 10^9$ ($\Delta T = 20^\circ\text{C}$), and $N = 6.37 \times 10^{-2}$ for $Re_{ci} = 3,183$ and $Re_{co} =$ (a) 1,910, (b) 3,183, (c) 5,092, and (d) 6,365.

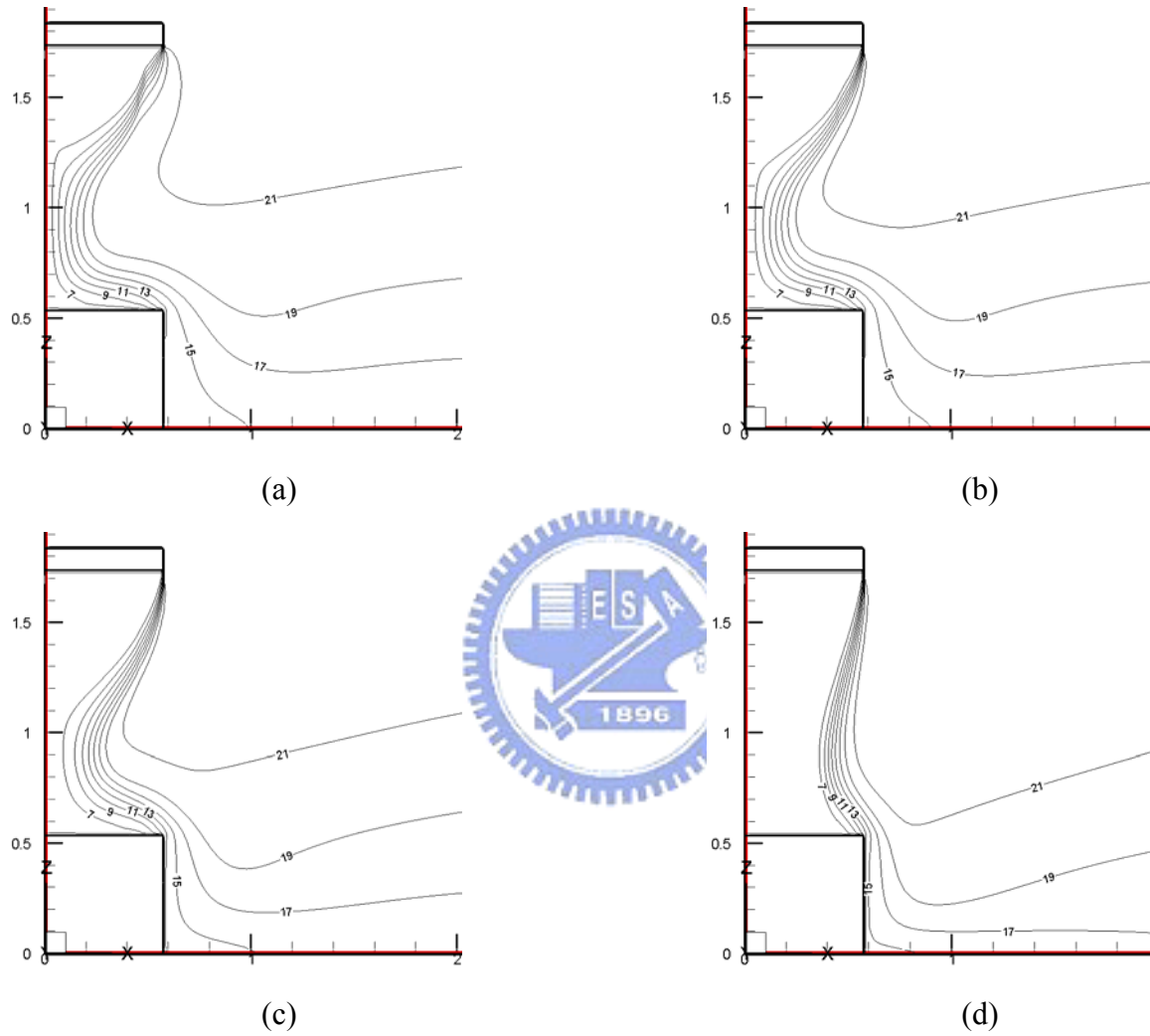


Fig. 4.71 Isotherms for steady cavity flow for a double air curtain design with $b_i = 0.03$ m, $b_o = 0.09$ m, $Gr_t = 4.61 \times 10^9$ ($\Delta T = 20^\circ\text{C}$), and $N = 6.37 \times 10^{-2}$ for $Re_{ci} = 3,183$ and $Re_{co} =$ (a) 1,910, (b) 3,183, (c) 5,092, and (d) 6,365.

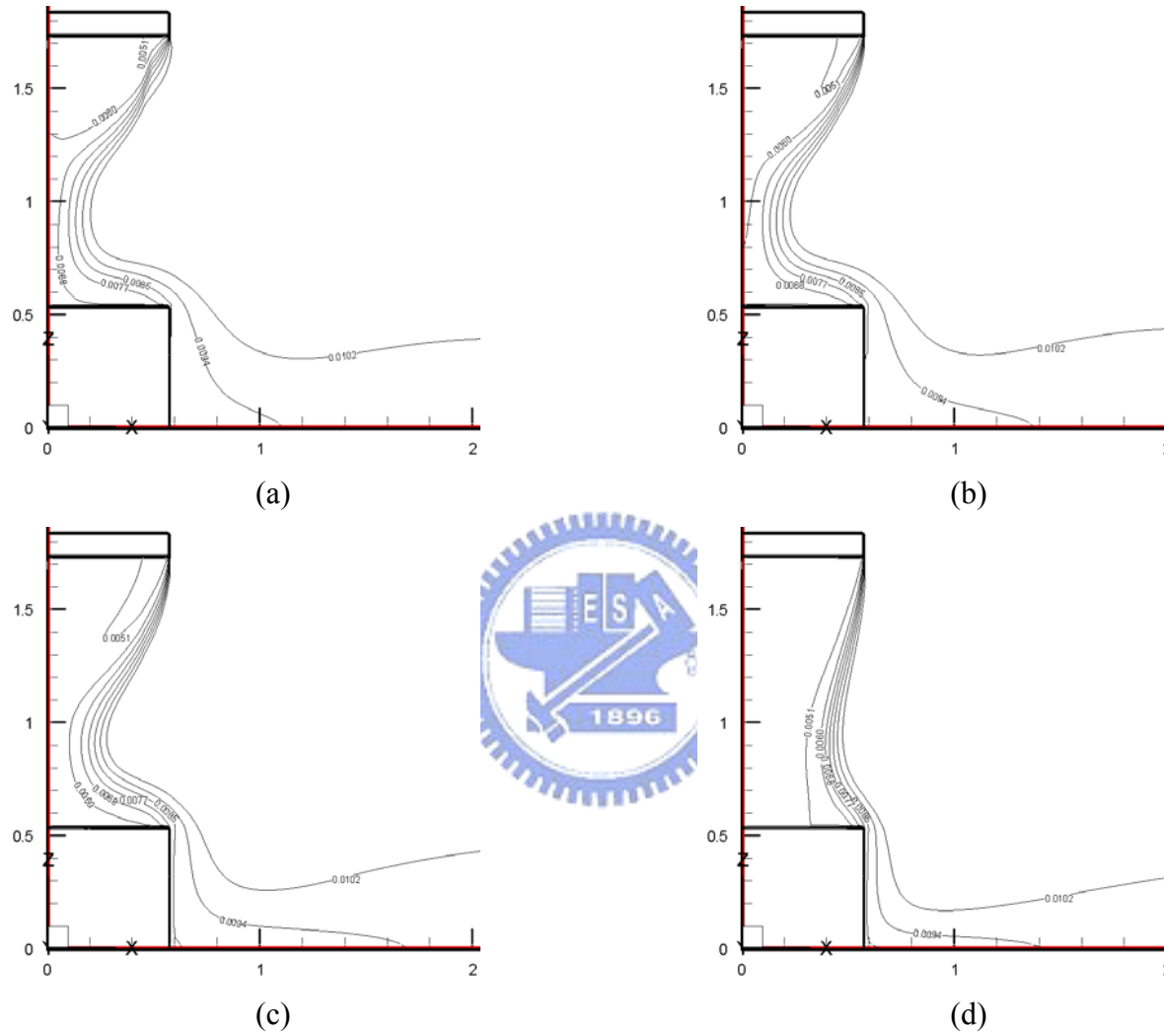


Fig. 4.72 Iso-concentration lines for steady cavity flow for a double air curtain design with $b_i = 0.03$ m, $b_o = 0.09$ m, $Gr_t = 4.61 \times 10^9$ ($\Delta T = 20^\circ\text{C}$), and $N = 6.37 \times 10^{-2}$ for $Re_{ci} = 3,183$ and $Re_{co} =$ (a) 1,910, (b) 3,183, (c) 5,092, and (d) 6,365.

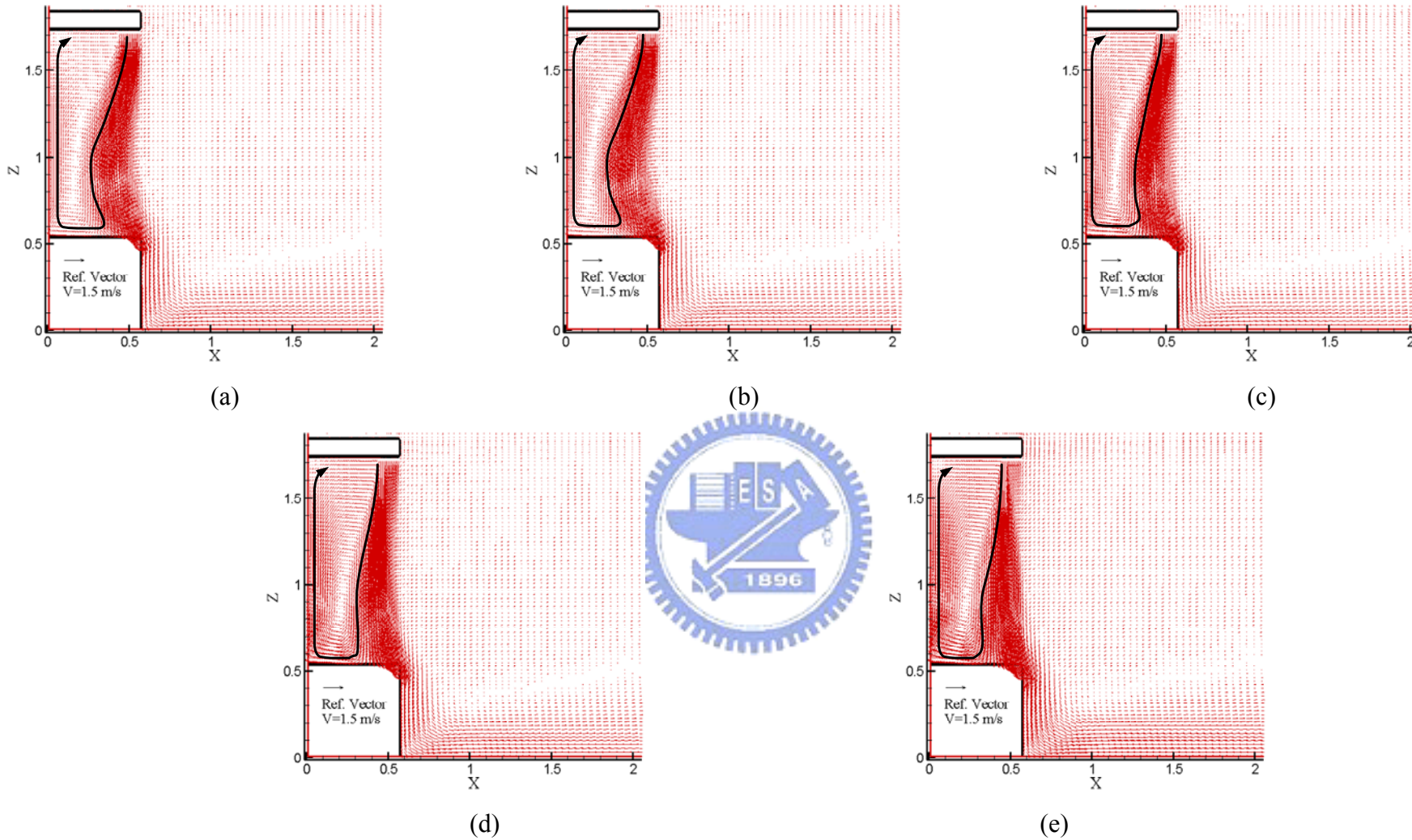


Fig. 4.73 Velocity vector maps for steady cavity flow for a double air curtain design with $b_i = 0.03$ m, $b_o = 0.09$ m, $Gr_t = 4.61 \times 10^9$ ($\Delta T = 20^\circ\text{C}$), and $N = 6.37 \times 10^{-2}$ for (a) $Re_{ci} = 1,910$ and $Re_{co} = 7,638$, (b) $Re_{ci} = 3,183$ and $Re_{co} = 6,365$, (c) $Re_{ci} = 5,092$ and $Re_{co} = 4,456$, (d) $Re_{ci} = 6,365$ and $Re_{co} = 3,183$, (e) $Re_{ci} = 7,638$ and $Re_{co} = 1,910$.

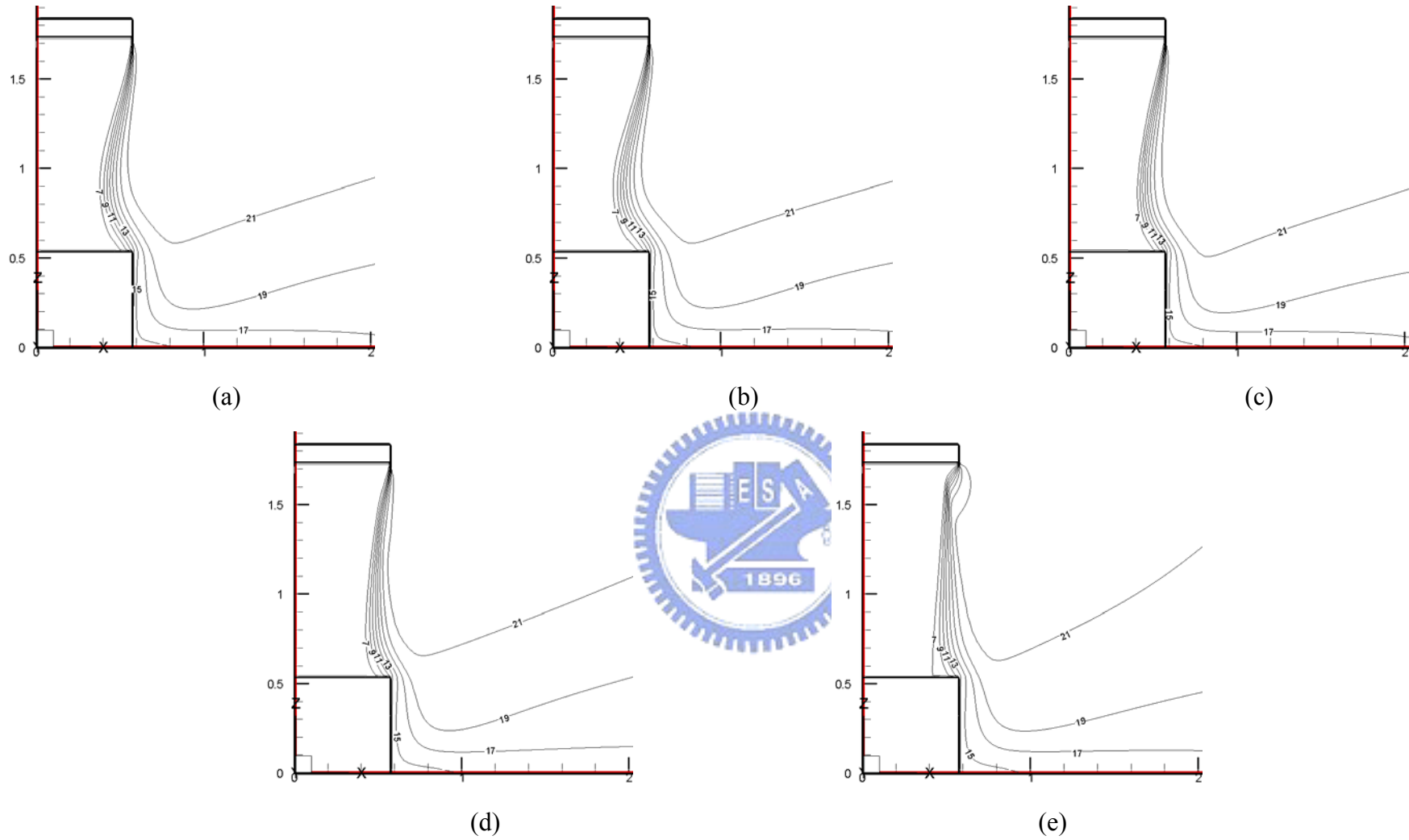


Fig. 4.74 Isotherms for steady cavity flow for a double air curtain design with $b_i = 0.03$ m, $b_o = 0.09$ m, $Gr_t = 4.61 \times 10^9$ ($\Delta T = 20^\circ\text{C}$), and $N = 6.37 \times 10^{-2}$ for (a) $Re_{ci} = 1,910$ and $Re_{co} = 7,638$, (b) $Re_{ci} = 3,183$ and $Re_{co} = 6,365$, (c) $Re_{ci} = 5,092$ and $Re_{co} = 4,456$, (d) $Re_{ci} = 6,365$ and $Re_{co} = 3,183$, (e) $Re_{ci} = 7,638$ and $Re_{co} = 1,910$.

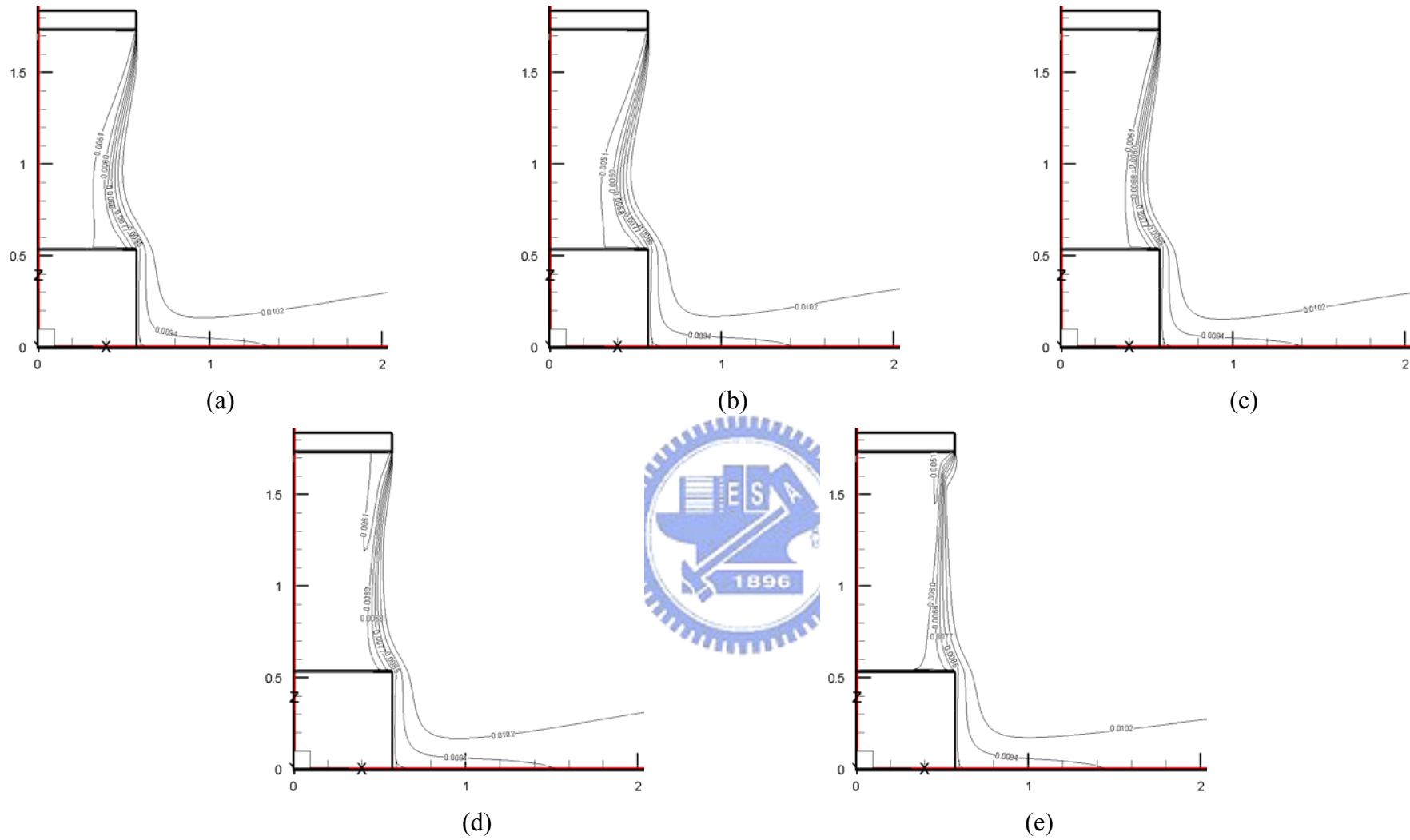


Fig. 4.75 Iso-concentration lines for steady cavity flow for a double air curtain design with $b_i = 0.03$ m, $b_o = 0.09$ m, $Gr_t = 4.61 \times 10^9$ ($\Delta T = 20^\circ\text{C}$), and $N = 6.37 \times 10^{-2}$ for (a) $Re_{ci} = 1,910$ and $Re_{co} = 7,638$, (b) $Re_{ci} = 3,183$ and $Re_{co} = 6,365$, (c) $Re_{ci} = 5,092$ and $Re_{co} = 4,456$, (d) $Re_{ci} = 6,365$ and $Re_{co} = 3,183$, (e) $Re_{ci} = 7,638$ and $Re_{co} = 1,910$.

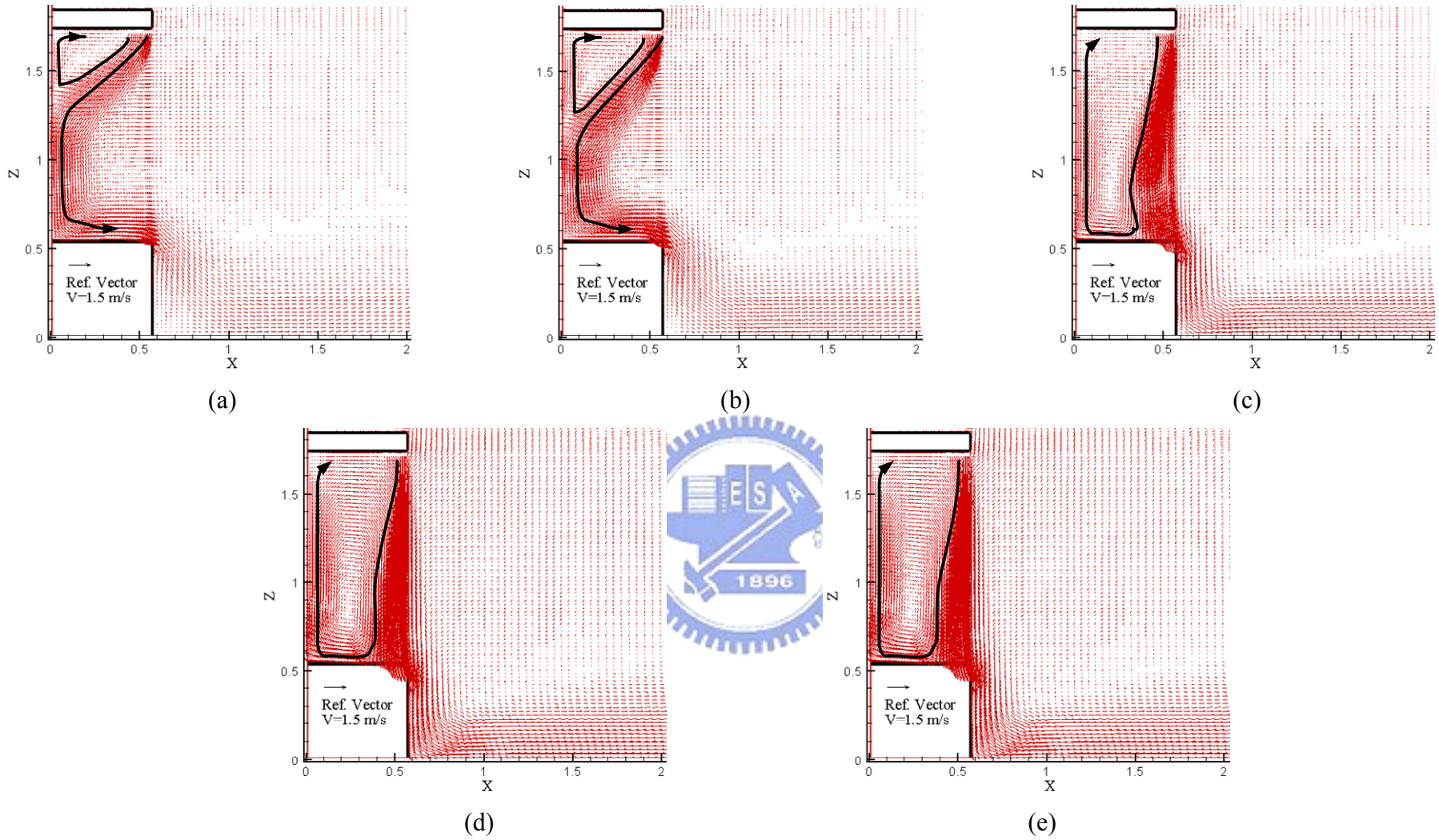


Fig. 4.76 Velocity vector maps for steady cavity flow for a double air curtain design with $b_i = 0.09$ m, $b_o = 0.03$ m, $Gr_t = 4.61 \times 10^9$ ($\Delta T = 20^\circ\text{C}$), and $N = 6.37 \times 10^{-2}$ for $Re_{ci} = 1,910$ and $Re_{co} =$ (a) 1,910, (b) 3,183, (c) 5,092, (d) 6,365 and (e) 7,638.

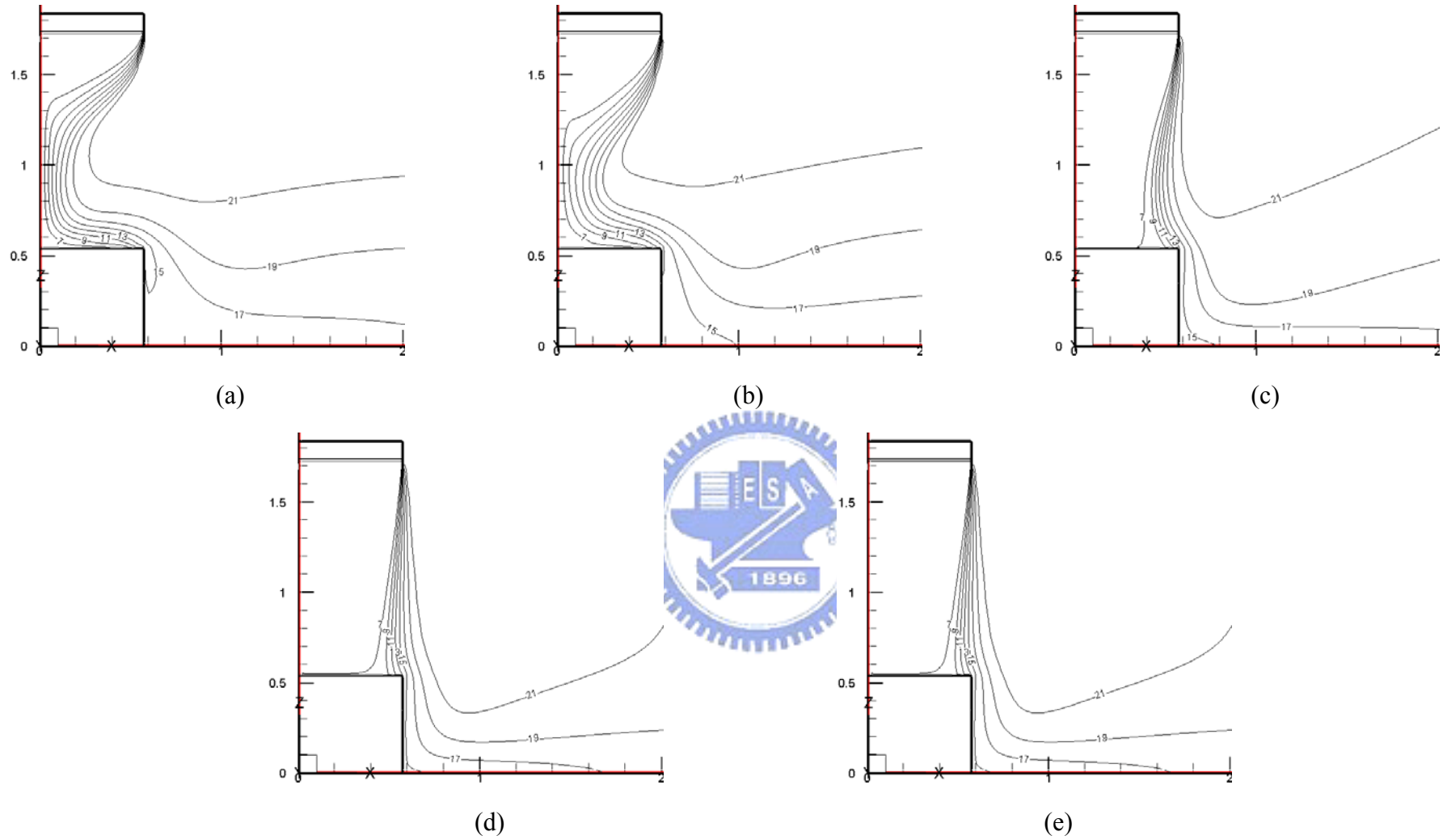


Fig. 4.77 Isotherms for steady cavity flow for a double air curtain design with $b_i = 0.09$ m, $b_o = 0.03$ m, $Gr_t = 4.61 \times 10^9$ ($\Delta T = 20^\circ\text{C}$), and $N = 6.37 \times 10^{-2}$ for $Re_{ci} = 1,910$ and $Re_{co} =$ (a) 1,910, (b) 3,183, (c) 5,092, (d) 6,365 and (e) 7,638.

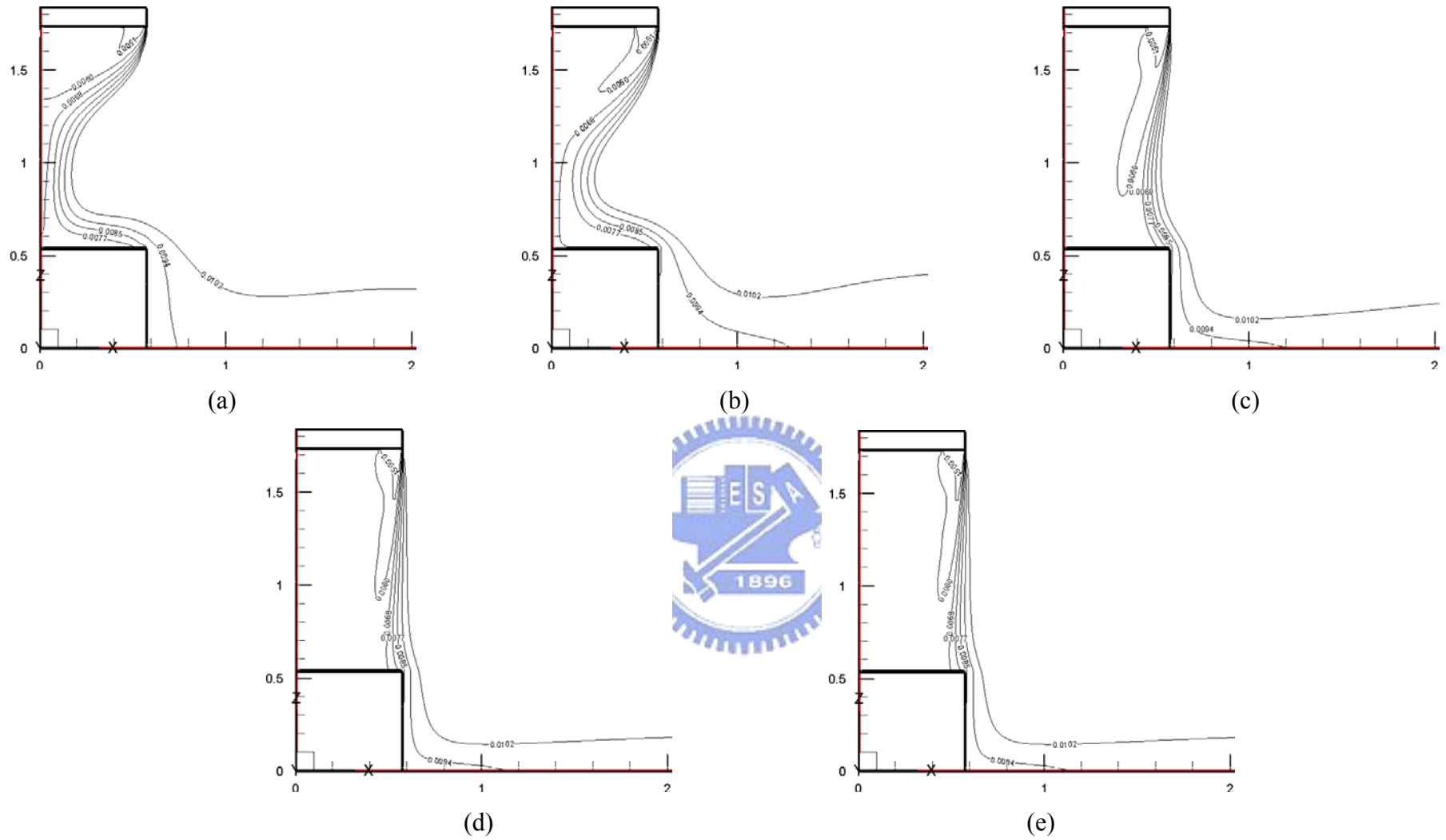


Fig. 4.78 Iso-concentration lines for steady cavity flow for a double air curtain design with $b_i = 0.09$ m, $b_o = 0.03$ m, $Gr_i = 4.61 \times 10^9$ ($\Delta T = 20^\circ\text{C}$), and $N = 6.37 \times 10^{-2}$ for $Re_{ci} = 1,910$ and $Re_{co} =$ (a) 1,910, (b) 3,183, (c) 5,092, (d) 6,365 and (e) 7,638.

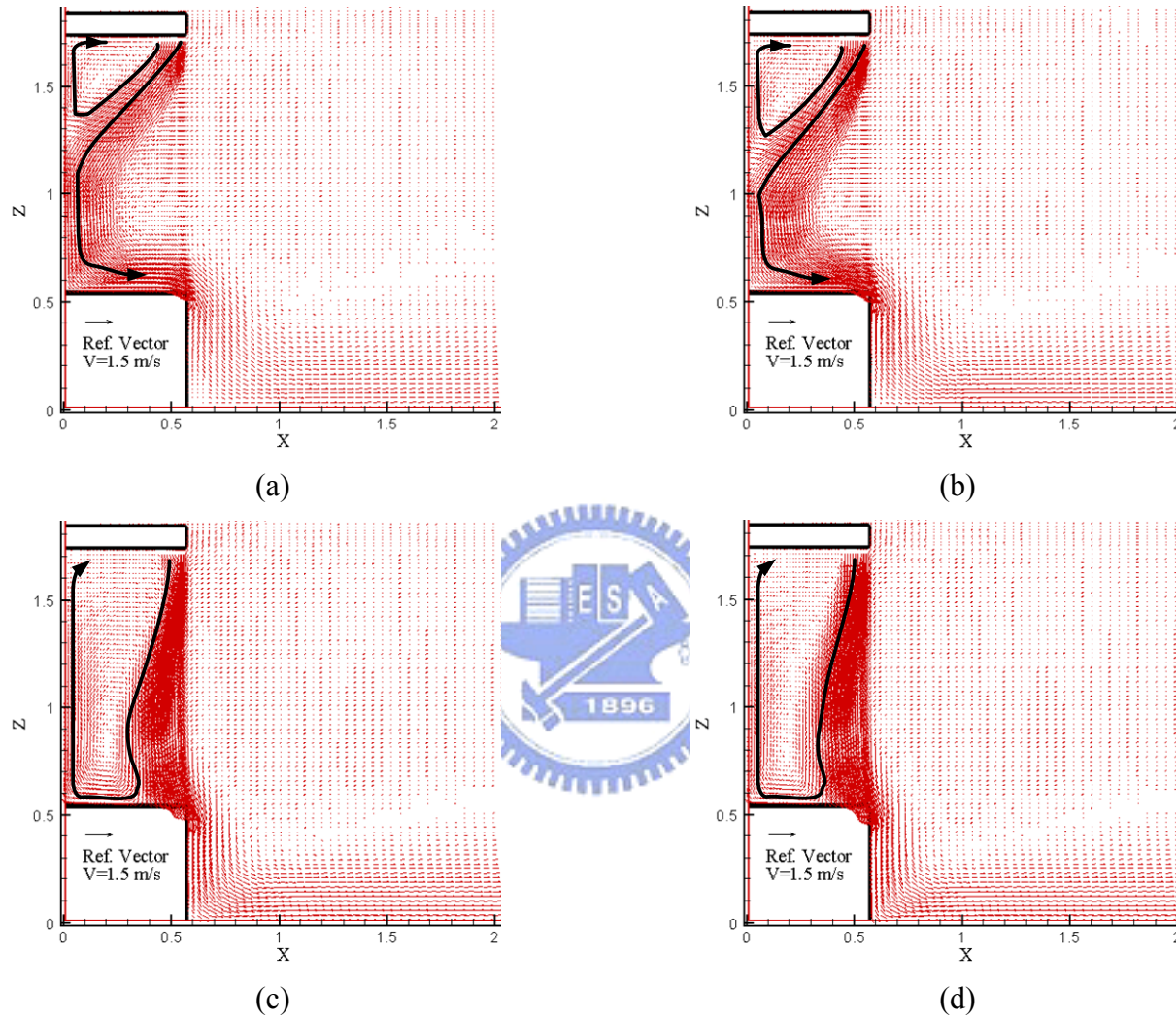


Fig. 4.79 Velocity vector maps for steady cavity flow for a double air curtain design with $b_i = 0.09$ m, $b_o = 0.03$ m, $Gr_t = 4.61 \times 10^9$ ($\Delta T = 20^\circ\text{C}$), and $N = 6.37 \times 10^{-2}$ for $Re_{ci} = 3,183$ and $Re_{co} =$ (a) 1,910, (b) 3,183, (c) 5,092, and (d) 6,365.

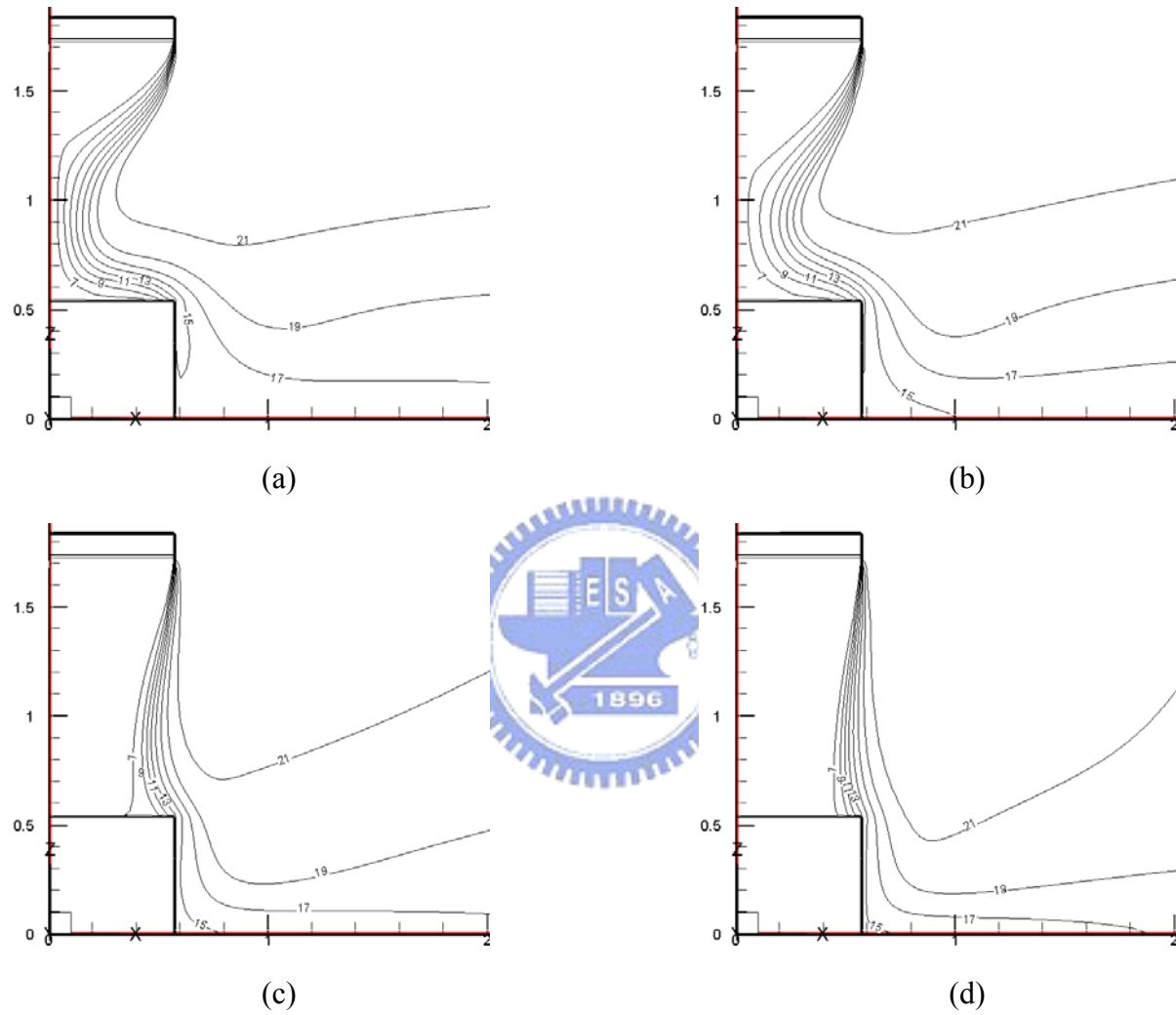


Fig. 4.80 Isotherms for steady cavity flow for a double air curtain design with $b_i = 0.09$ m, $b_o = 0.03$ m, $Gr_t = 4.61 \times 10^9$ ($\Delta T = 20^\circ\text{C}$), and $N = 6.37 \times 10^{-2}$ for $Re_{ci} = 3,183$ and $Re_{co} =$ (a) 1,910, (b) 3,183, (c) 5,092, and (d) 6,365.

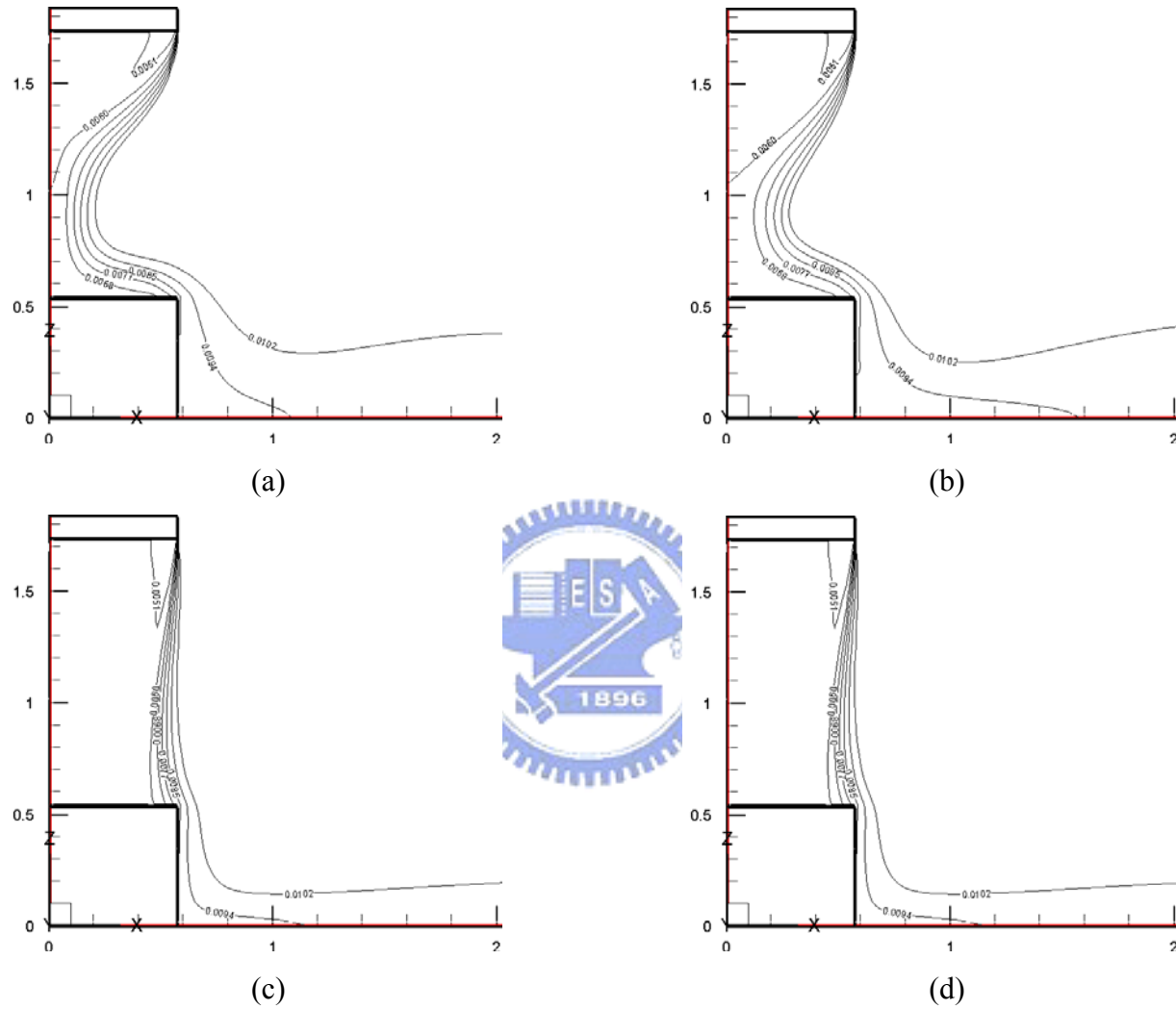


Fig. 4.81 Iso-concentration lines for steady cavity flow for a double air curtain design with $b_i = 0.09$ m, $b_o = 0.03$ m, $Gr_t = 4.61 \times 10^9$ ($\Delta T = 20^\circ\text{C}$), and $N = 6.37 \times 10^{-2}$ for $Re_{ci} = 3,183$ and $Re_{co} =$ (a) 1,910, (b) 3,183, (c) 5,092, and (d) 6,365.

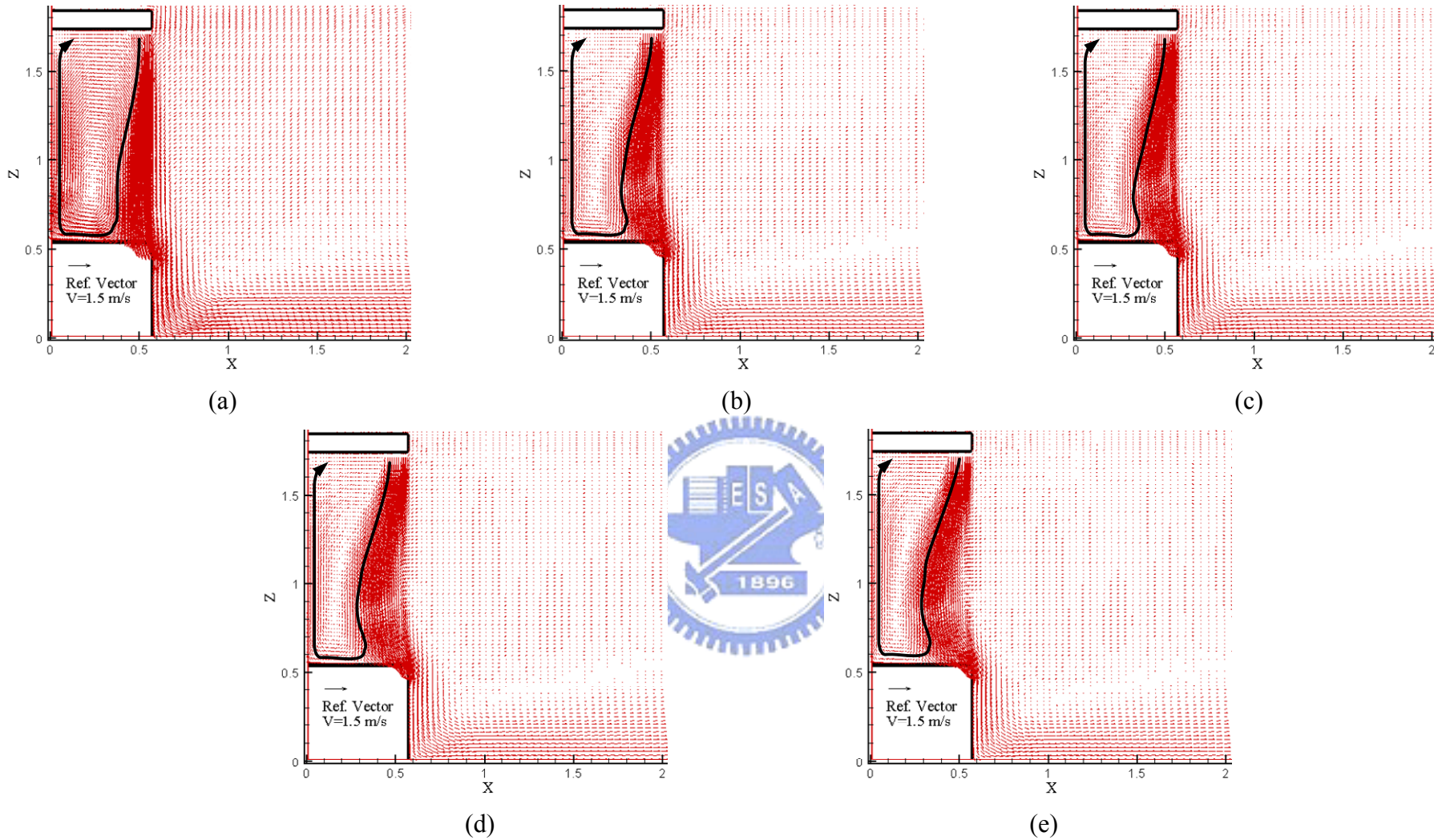


Fig. 4.82 Velocity vector maps for steady cavity flow for a double air curtain design with $b_i = 0.09$ m, $b_o = 0.03$ m, $Gr_t = 4.61 \times 10^9$ ($\Delta T = 20^\circ\text{C}$), and $N = 6.37 \times 10^{-2}$ for (a) $Re_{ci} = 1,910$ and $Re_{co} = 7,638$, (b) $Re_{ci} = 3,183$ and $Re_{co} = 6,365$, (c) $Re_{ci} = 5,092$ and $Re_{co} = 4,456$, (d) $Re_{ci} = 6,365$ and $Re_{co} = 3,183$, (e) $Re_{ci} = 7,638$ and $Re_{co} = 1,910$.

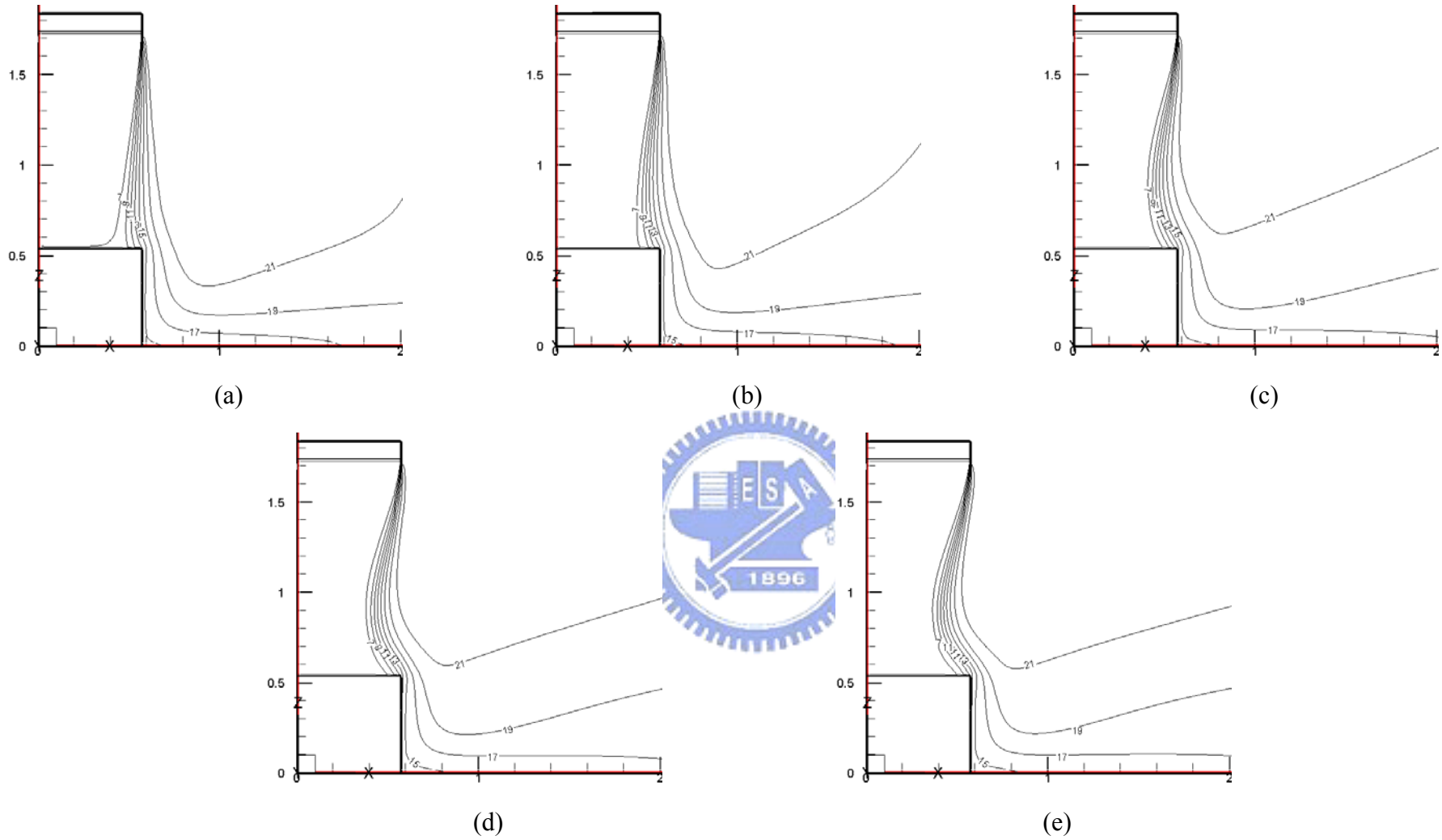


Fig. 4.83 Isotherms for steady cavity flow for a double air curtain design with $b_i = 0.09$ m, $b_o = 0.03$ m, $Gr_t = 4.61 \times 10^9$ ($\Delta T = 20^\circ\text{C}$), and $N = 6.37 \times 10^{-2}$ for (a) $Re_{ci} = 1,910$ and $Re_{co} = 7,638$, (b) $Re_{ci} = 3,183$ and $Re_{co} = 6,365$, (c) $Re_{ci} = 5,092$ and $Re_{co} = 4,456$, (d) $Re_{ci} = 6,365$ and $Re_{co} = 3,183$, (e) $Re_{ci} = 7,638$ and $Re_{co} = 1,910$.

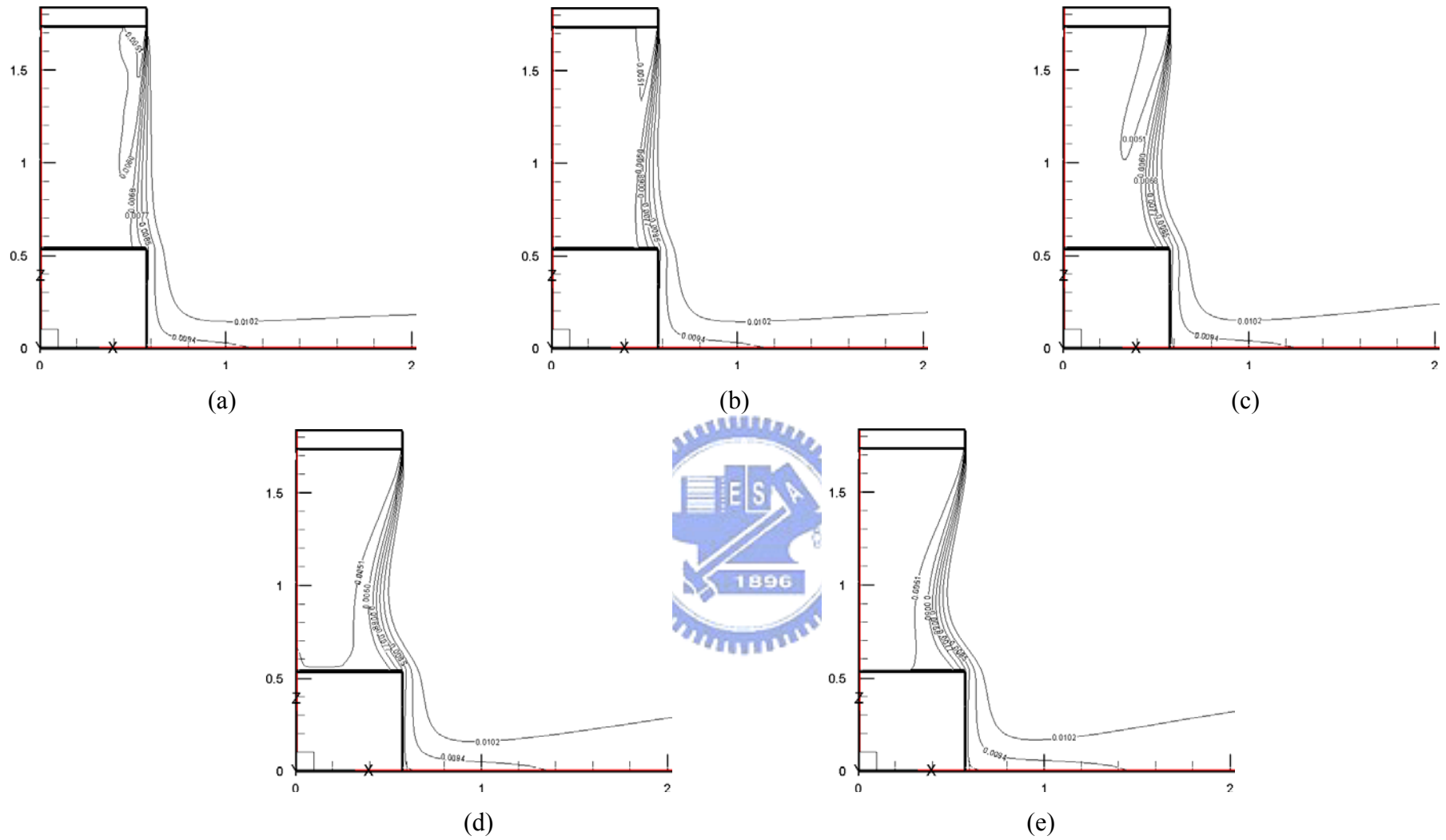


Fig. 4.84 Iso-concentration lines for steady cavity flow for a double air curtain design with $b_i = 0.09$ m, $b_o = 0.03$ m, $Gr_t = 4.61 \times 10^9$ ($\Delta T = 20^\circ\text{C}$), and $N = 6.37 \times 10^{-2}$ for (a) $Re_{ci} = 1,910$ and $Re_{co} = 7,638$, (b) $Re_{ci} = 3,183$ and $Re_{co} = 6,365$, (c) $Re_{ci} = 5,092$ and $Re_{co} = 4,456$, (d) $Re_{ci} = 6,365$ and $Re_{co} = 3,183$, (e) $Re_{ci} = 7,638$ and $Re_{co} = 1,910$.

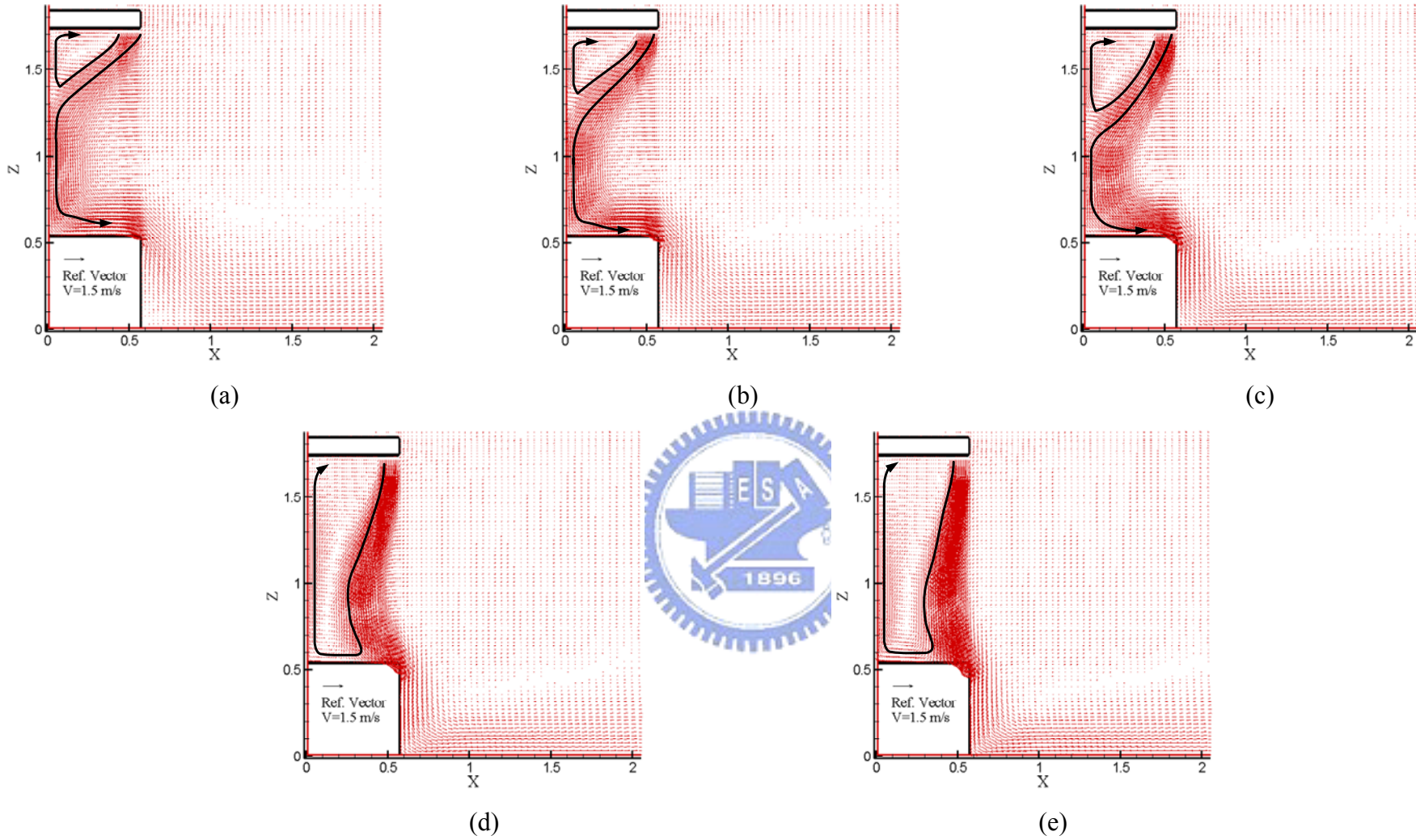


Fig. 4.85 Velocity vector maps for steady cavity flow for a double air curtain design with $b_i = 0.05$ m, $b_o = 0.07$ m, $Gr_t = 4.61 \times 10^9$ ($\Delta T = 20^\circ\text{C}$), and $N = 6.37 \times 10^{-2}$ for $Re_{ci} = 1,910$ and $Re_{co} =$ (a) 1,910, (b) 3,183, (c) 5,092, (d) 6,365 and (e) 7,638.

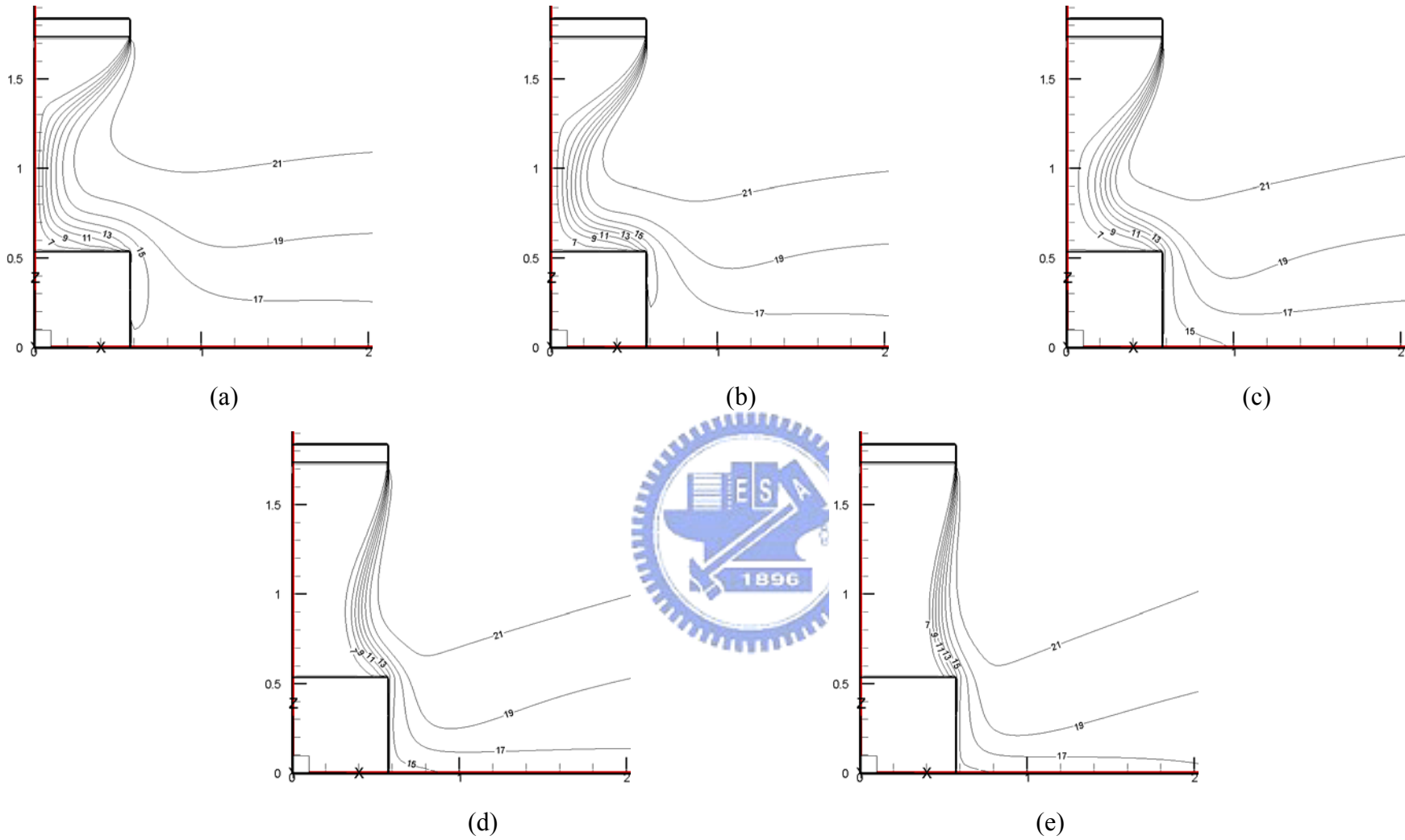


Fig. 4.86 Isotherms for steady cavity flow for a double air curtain design with $b_i = 0.05$ m, $b_o = 0.07$ m, $Gr_t = 4.61 \times 10^9$ ($\Delta T = 20^\circ\text{C}$), and $N = 6.37 \times 10^{-2}$ for $Re_{ci} = 1,910$ and $Re_{co} =$ (a) 1,910, (b) 3,183, (c) 5,092, (d) 6,365 and (e) 7,638.

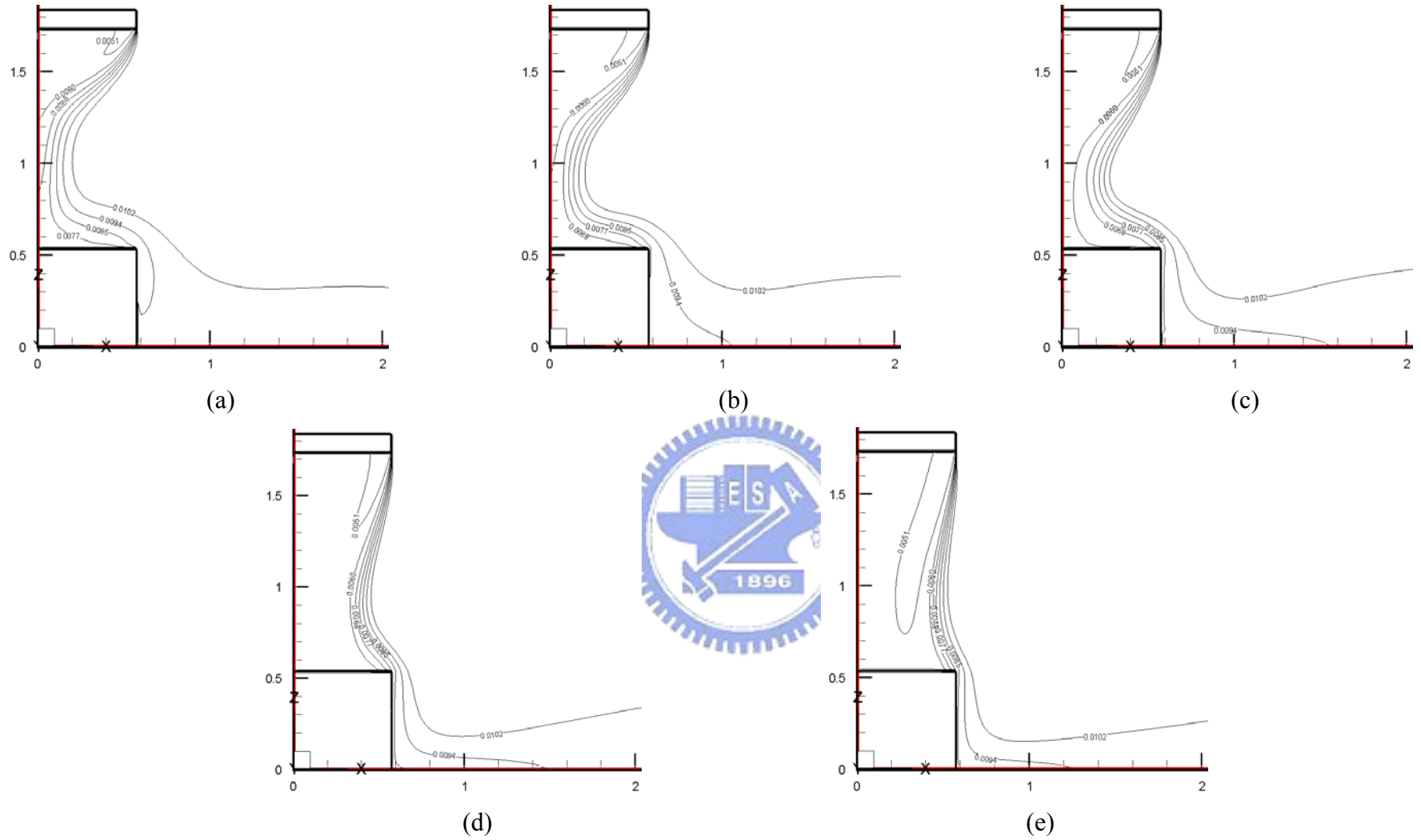


Fig. 4.87 Iso-concentration lines for steady cavity flow for a double air curtain design with $b_i = 0.05$ m, $b_o = 0.07$ m, $Gr_i = 4.61 \times 10^9$ ($\Delta T = 20^\circ\text{C}$), and $N = 6.37 \times 10^{-2}$ for $Re_{ci} = 1,910$ and $Re_{co} =$ (a) 1,910, (b) 3,183, (c) 5,092, (d) 6,365 and (e) 7,638.

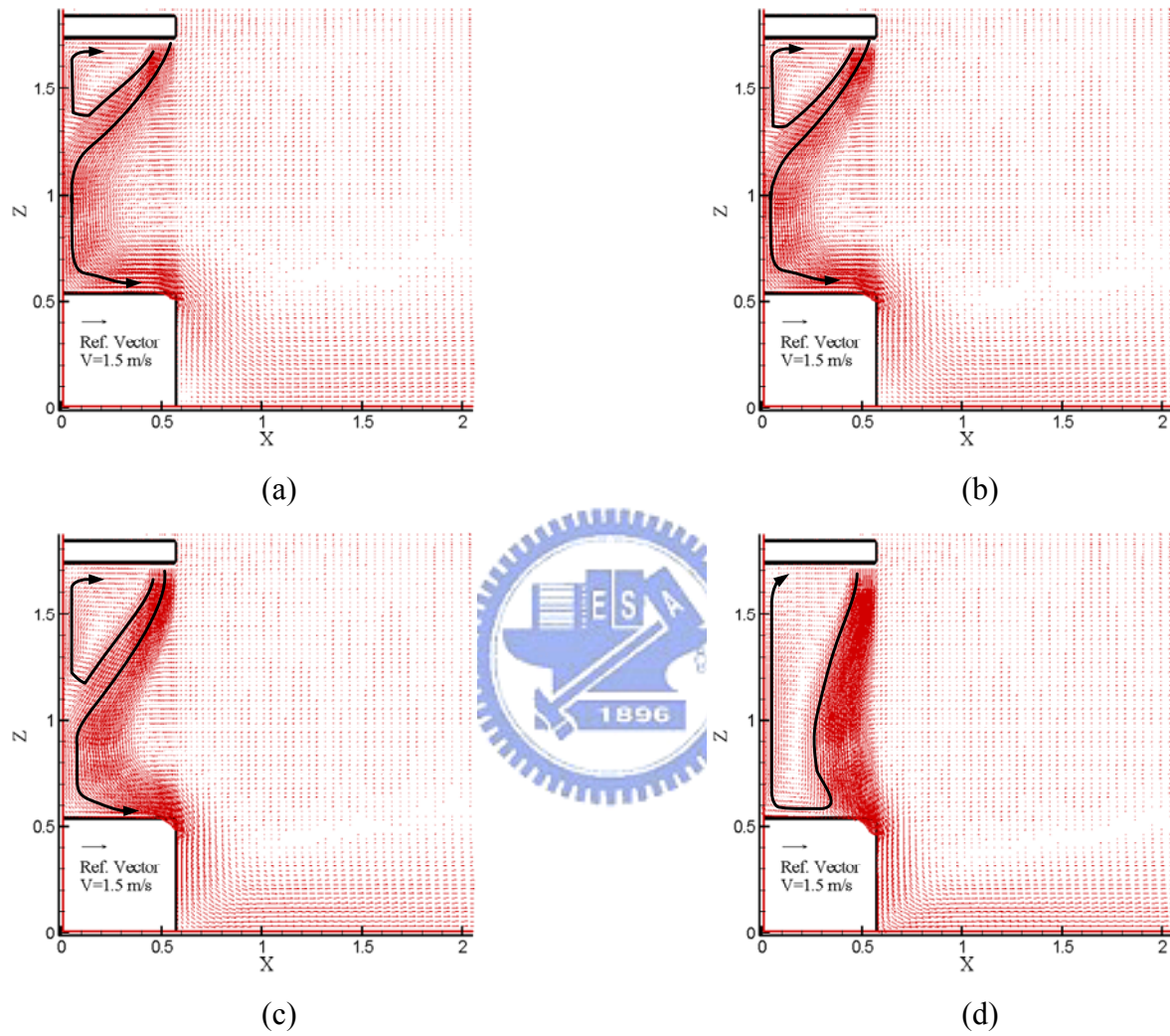


Fig. 4.88 Velocity vector maps for steady cavity flow for a double air curtain design with $b_i = 0.05$ m, $b_o = 0.07$ m, $Gr_t = 4.61 \times 10^9$ ($\Delta T = 20^\circ\text{C}$), and $N = 6.37 \times 10^{-2}$ for $Re_{ci} = 3,183$ and $Re_{co} =$ (a) 1,910, (b) 3,183, (c) 5,092, and (d) 6,365.

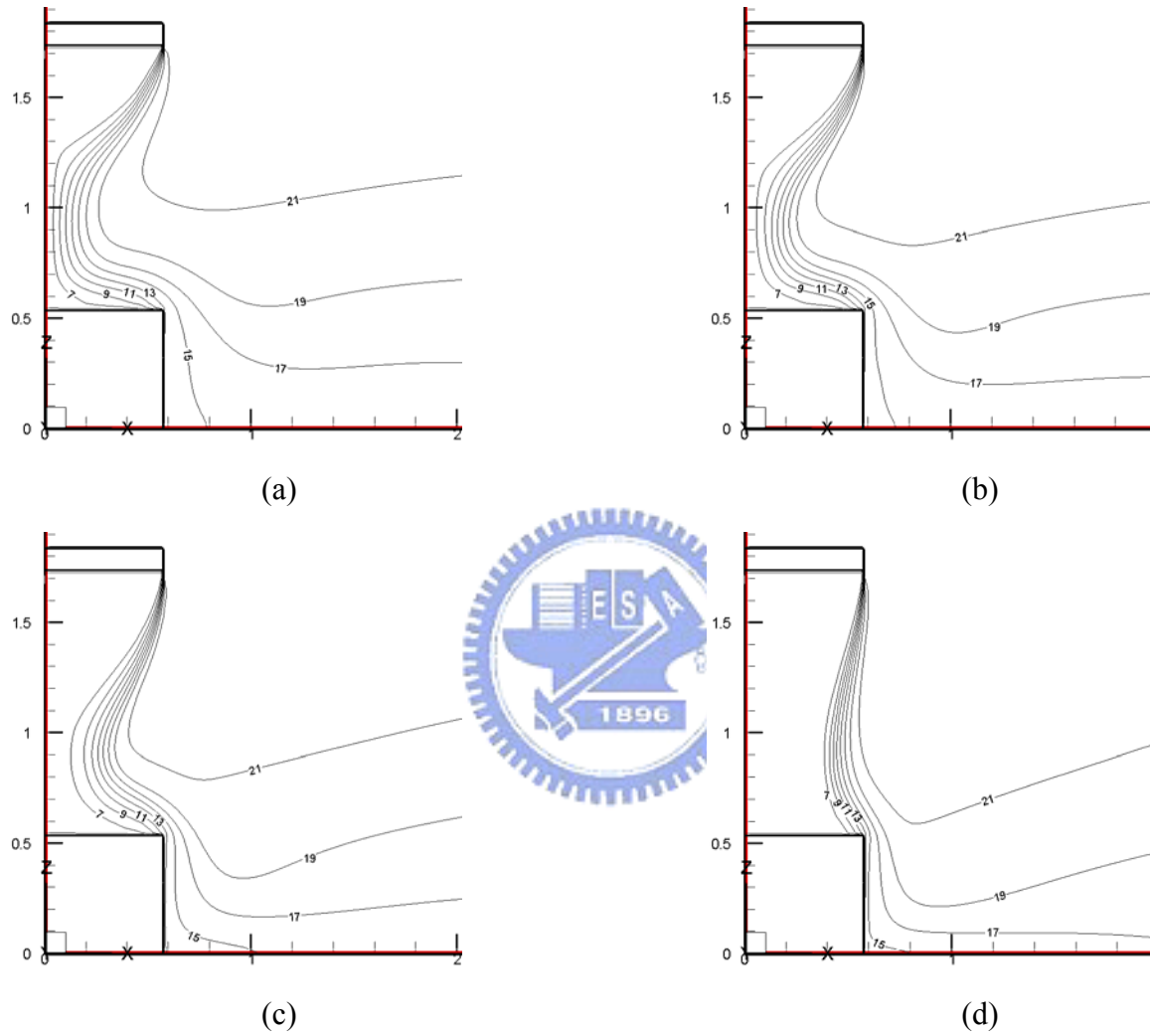


Fig. 4.89 Isotherms for steady cavity flow for a double air curtain design with $b_i = 0.05$ m, $b_o = 0.07$ m, $Gr_t = 4.61 \times 10^9$ ($\Delta T = 20^\circ\text{C}$), and $N = 6.37 \times 10^{-2}$ for $Re_{ci} = 3,183$ and $Re_{co} =$ (a) 1,910, (b) 3,183, (c) 5,092, and (d) 6,365.

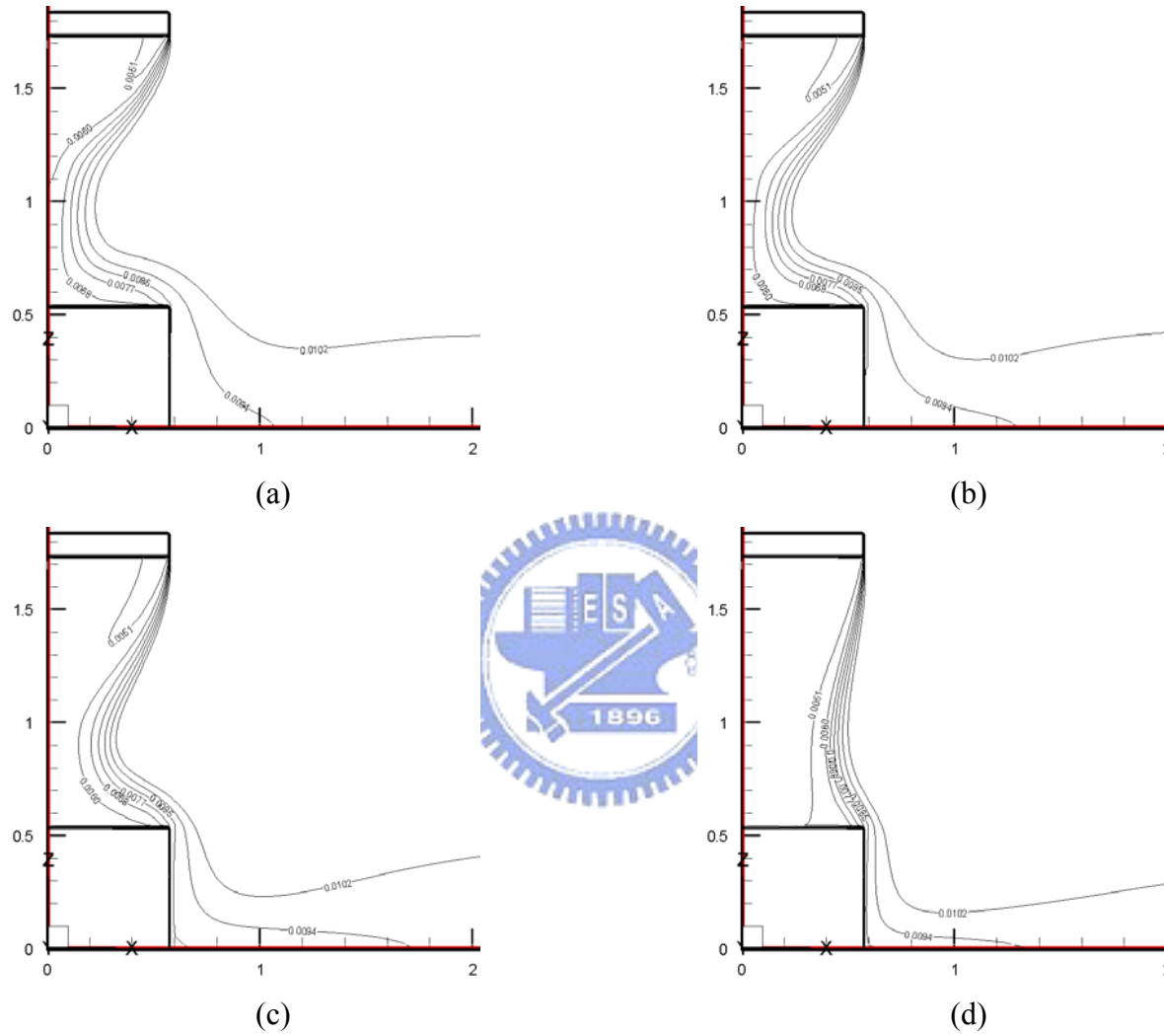


Fig. 4.90 Iso-concentration lines for steady cavity flow for a double air curtain design with $b_i = 0.05$ m, $b_o = 0.07$ m, $Gr_t = 4.61 \times 10^9$ ($\Delta T = 20^\circ\text{C}$), and $N = 6.37 \times 10^{-2}$ for $Re_{ci} = 3,183$ and $Re_{co} =$ (a) 1,910, (b) 3,183, (c) 5,092, and (d) 6,365.

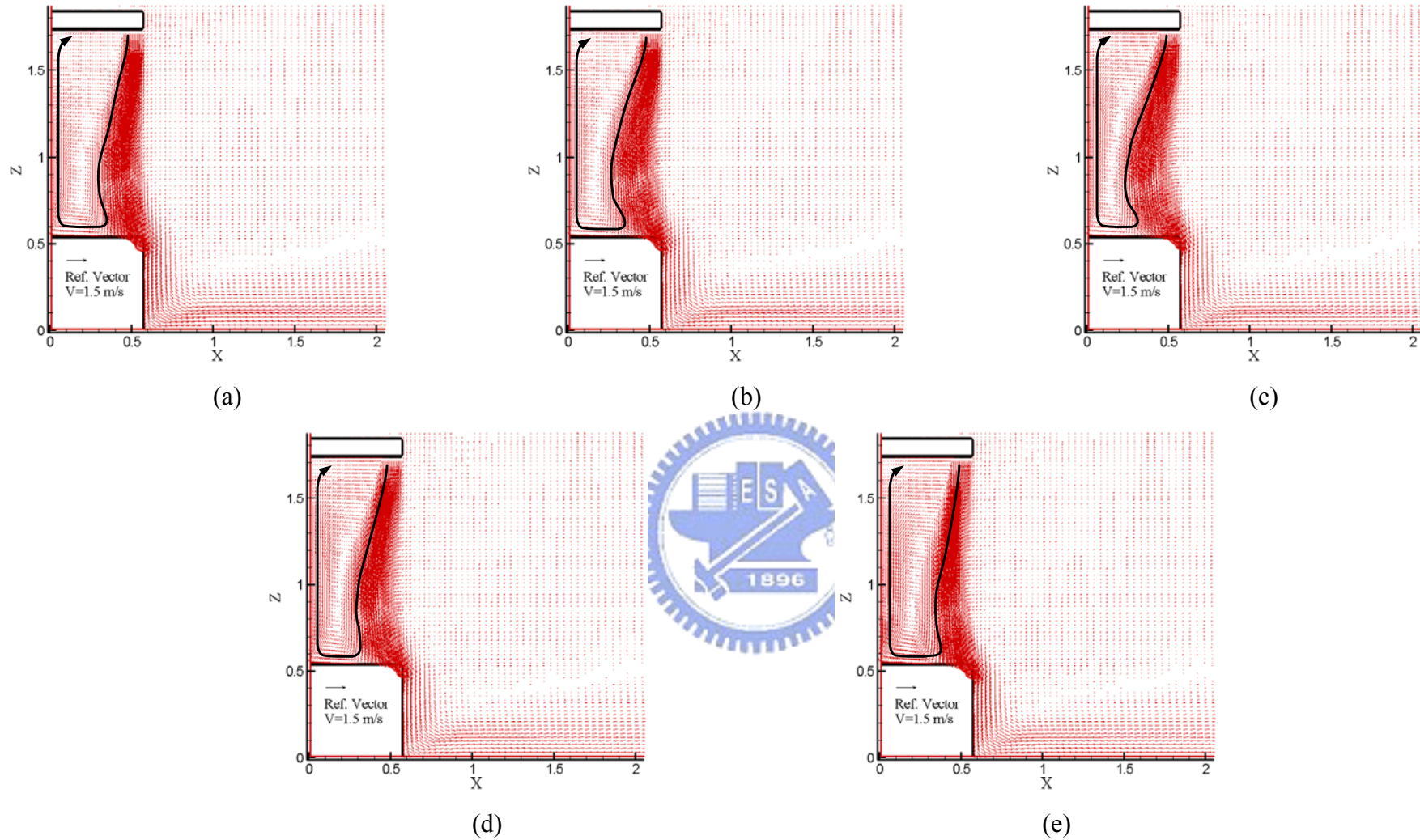


Fig. 4.91 Velocity vector maps for steady cavity flow for a double air curtain design with $b_i = 0.05$ m, $b_o = 0.07$ m, $Gr_t = 4.61 \times 10^9$ ($\Delta T = 20^\circ\text{C}$), and $N = 6.37 \times 10^{-2}$ for (a) $Re_{ci} = 1,910$ and $Re_{co} = 7,638$, (b) $Re_{ci} = 3,183$ and $Re_{co} = 6,365$, (c) $Re_{ci} = 5,092$ and $Re_{co} = 4,456$, (d) $Re_{ci} = 6,365$ and $Re_{co} = 3,183$, (e) $Re_{ci} = 7,638$ and $Re_{co} = 1,910$.

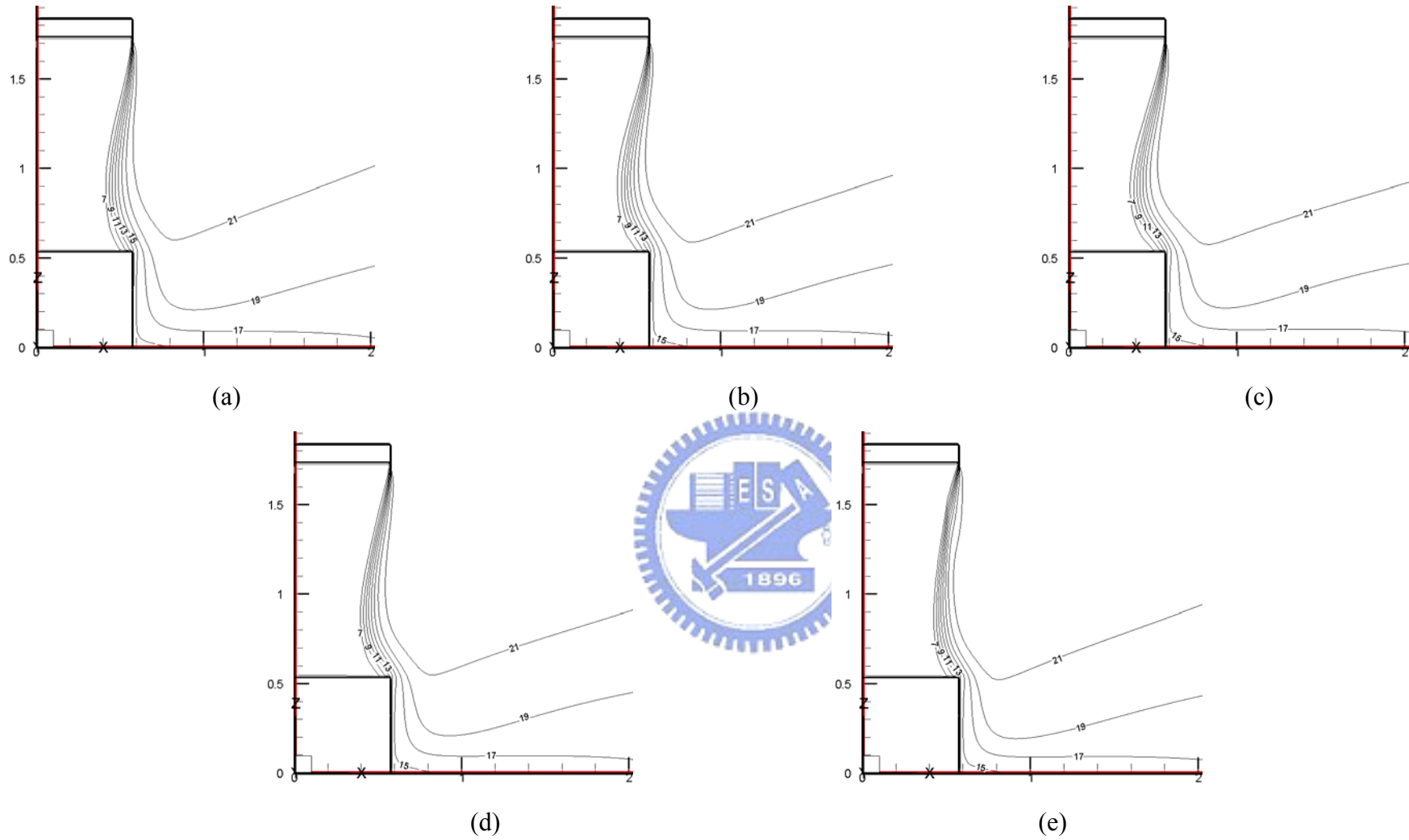


Fig. 4.92 Isotherms for steady cavity flow for a double air curtain design with $b_i = 0.05$ m, $b_o = 0.07$ m, $Gr_t = 4.61 \times 10^9$ ($\Delta T = 20^\circ\text{C}$), and $N = 6.37 \times 10^{-2}$ for (a) $Re_{ci} = 1,910$ and $Re_{co} = 7,638$, (b) $Re_{ci} = 3,183$ and $Re_{co} = 6,365$, (c) $Re_{ci} = 5,092$ and $Re_{co} = 4,456$, (d) $Re_{ci} = 6,365$ and $Re_{co} = 3,183$, (e) $Re_{ci} = 7,638$ and $Re_{co} = 1,910$.

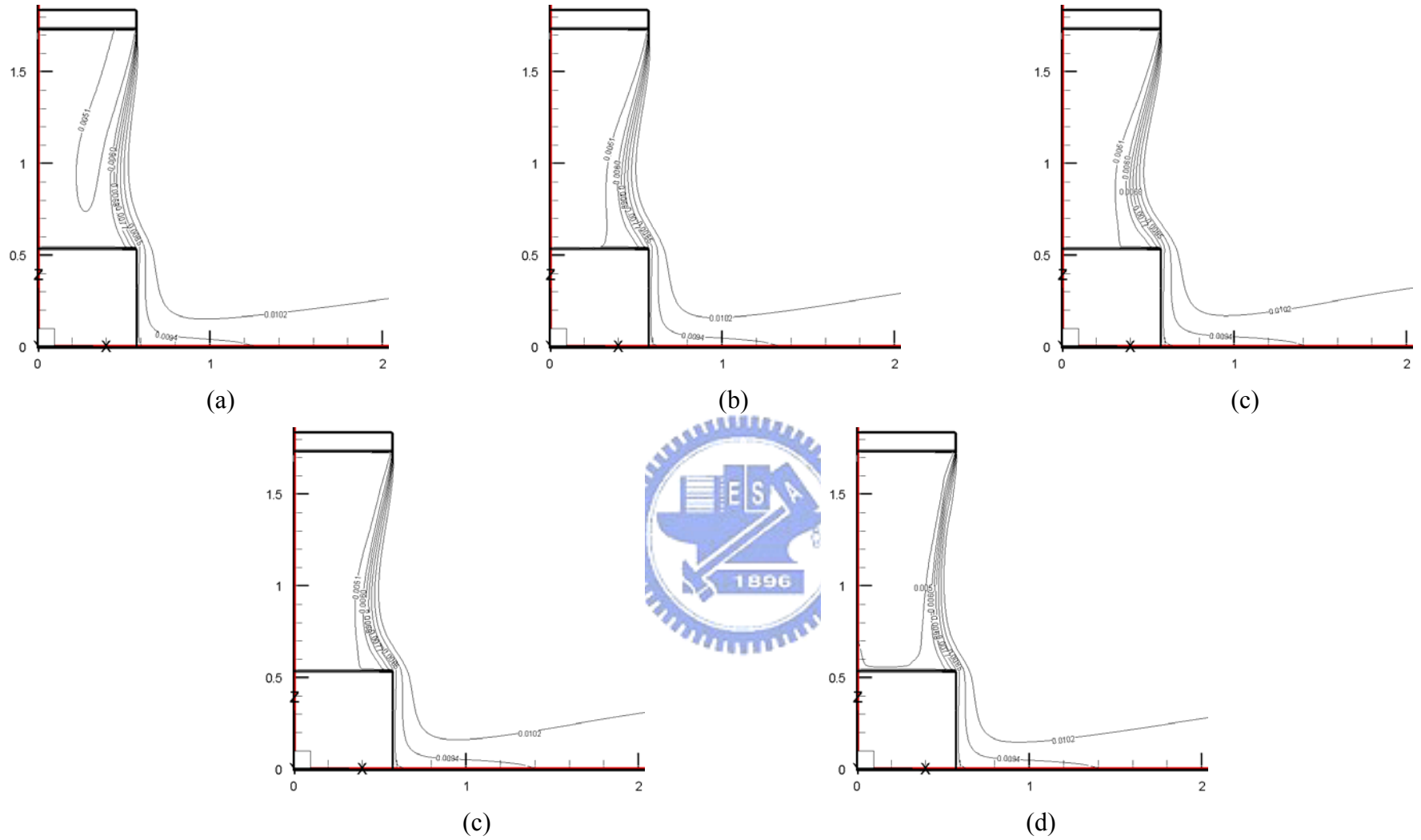


Fig. 4.93 Iso-concentration lines for steady cavity flow for a double air curtain design with $b_i = 0.05$ m, $b_o = 0.07$ m, $Gr_t = 4.61 \times 10^9$ ($\Delta T = 20^\circ\text{C}$), and $N = 6.37 \times 10^{-2}$ for (a) $Re_{ci} = 1,910$ and $Re_{co} = 7,638$, (b) $Re_{ci} = 3,183$ and $Re_{co} = 6,365$, (c) $Re_{ci} = 5,092$ and $Re_{co} = 4,456$, (d) $Re_{ci} = 6,365$ and $Re_{co} = 3,183$, (e) $Re_{ci} = 7,638$ and $Re_{co} = 1,910$.

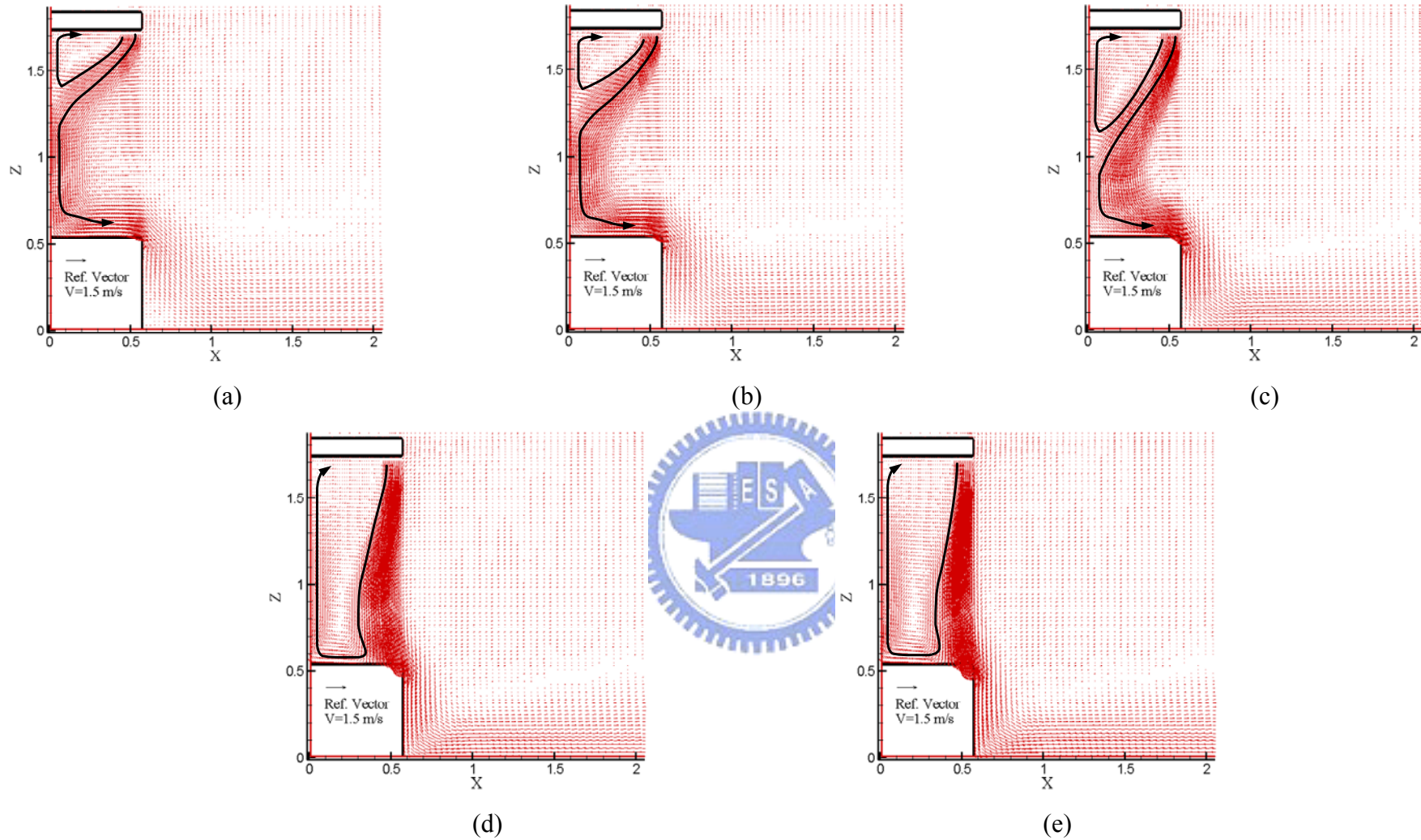


Fig. 4.94 Velocity vector maps for steady cavity flow for a double air curtain design with $b_i = 0.07$ m, $b_o = 0.05$ m, $Gr_t = 4.61 \times 10^9$ ($\Delta T = 20^\circ\text{C}$), and $N = 6.37 \times 10^{-2}$ for $Re_{ci} = 1,910$ and $Re_{co} =$ (a) 1,910, (b) 3,183, (c) 5,092, (d) 6,365 and (e) 7,638.

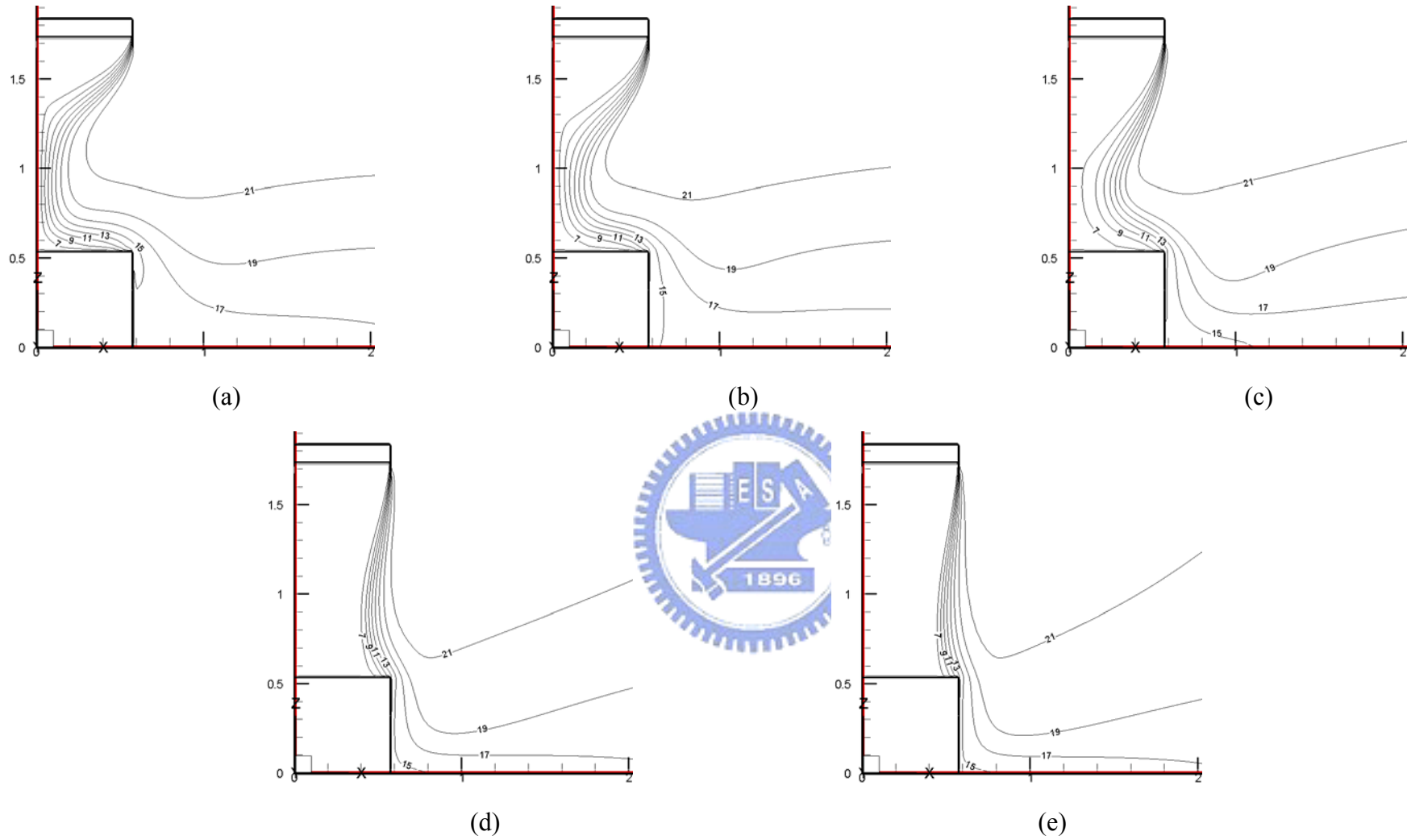


Fig. 4.95 Isotherms for steady cavity flow for a double air curtain design with $b_i = 0.07$ m, $b_o = 0.05$ m, $Gr_t = 4.61 \times 10^9$ ($\Delta T = 20^\circ\text{C}$), and $N = 6.37 \times 10^{-2}$ for $Re_{ci} = 1,910$ and $Re_{co} =$ (a) 1,910, (b) 3,183, (c) 5,092, (d) 6,365 and (e) 7,638.

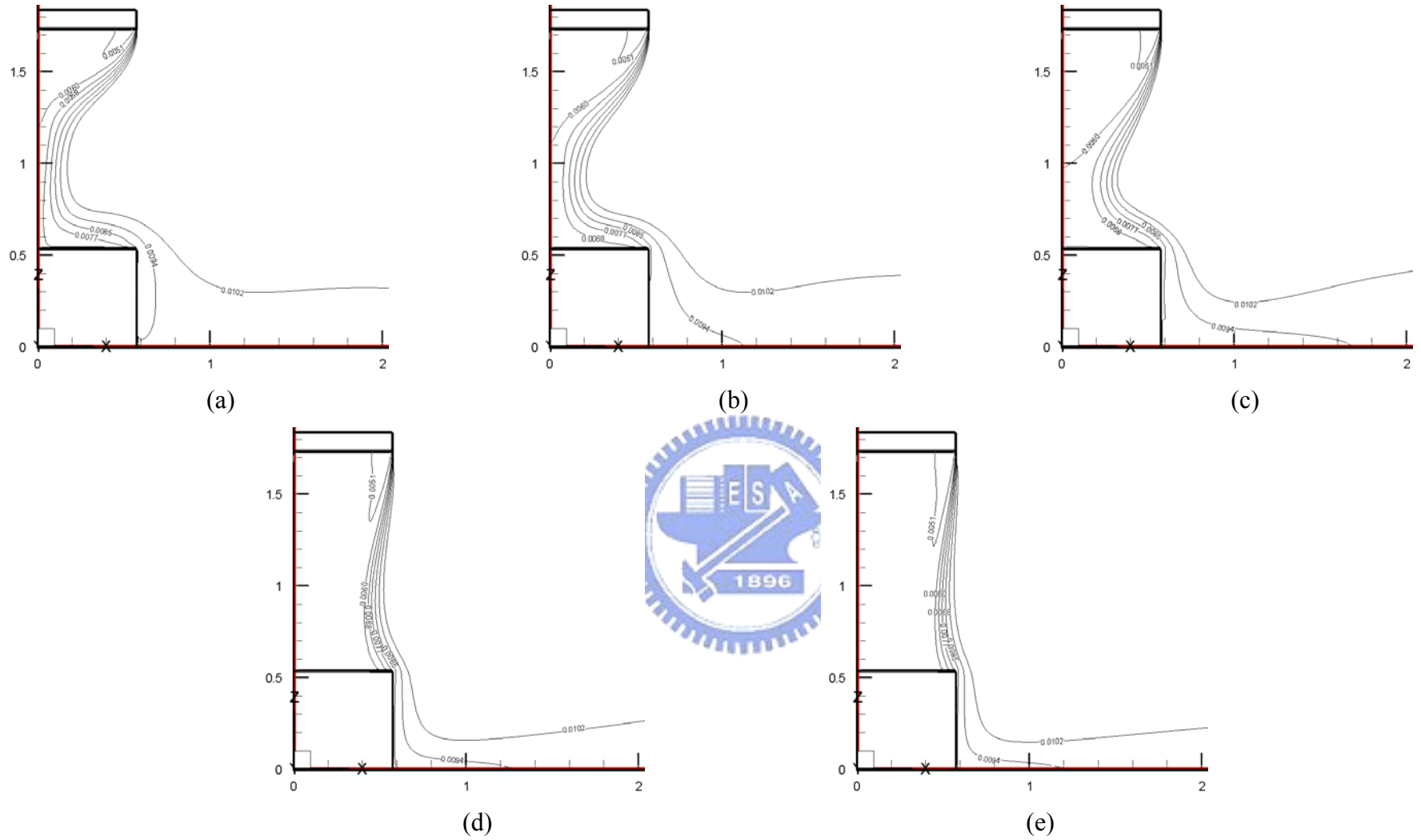


Fig. 4.96 Iso-concentration lines for steady cavity flow for a double air curtain design with $b_i = 0.07$ m, $b_o = 0.05$ m, $Gr_i = 4.61 \times 10^9$ ($\Delta T = 20^\circ\text{C}$), and $N = 6.37 \times 10^{-2}$ for $Re_{ci} = 1,910$ and $Re_{co} =$ (a) 1,910, (b) 3,183, (c) 5,092, (d) 6,365 and (e) 7,638.

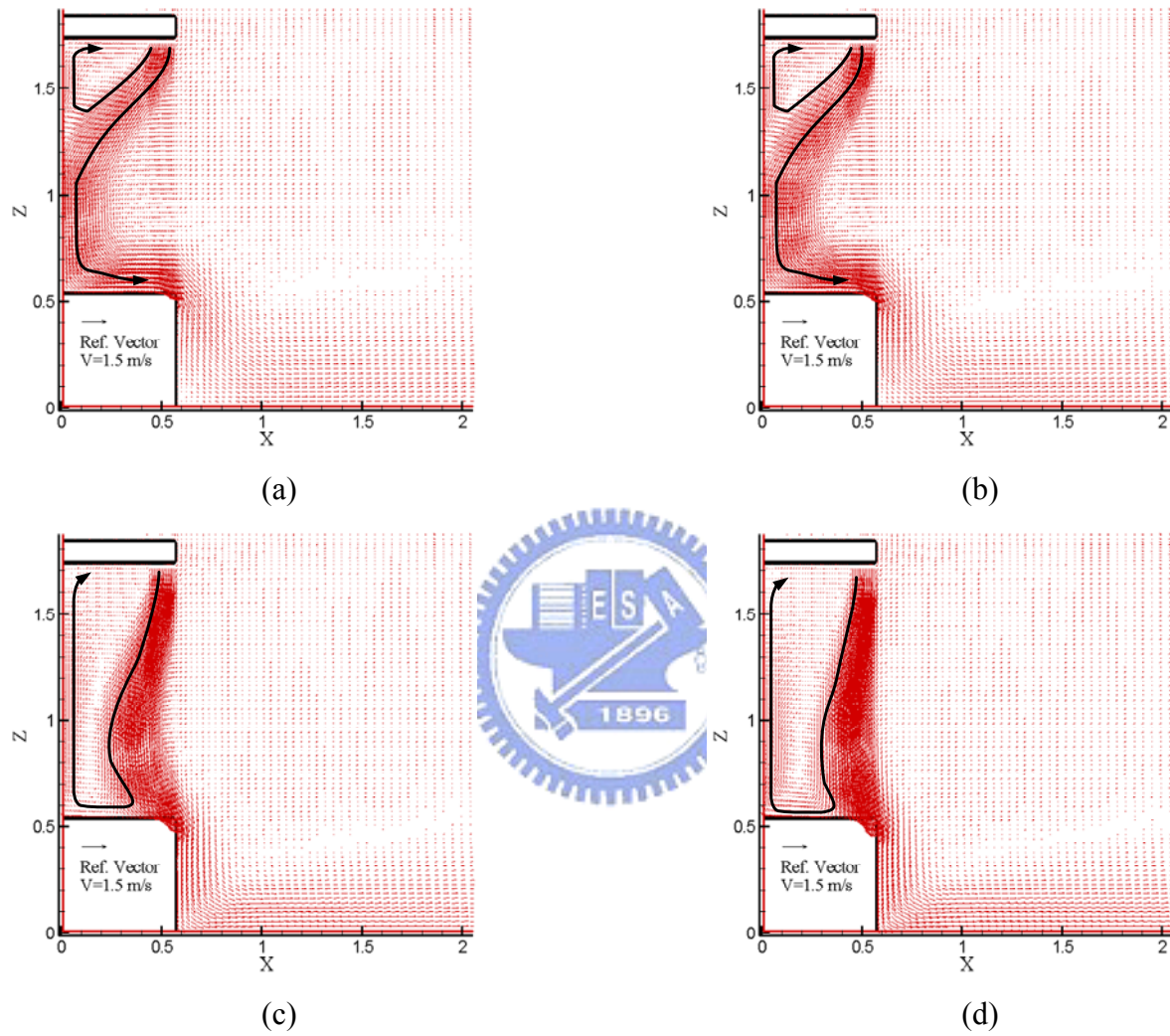


Fig. 4.97 Velocity vector maps for steady cavity flow for a double air curtain design with $b_i = 0.07$ m, $b_o = 0.05$ m, $Gr_t = 4.61 \times 10^9$ ($\Delta T = 20^\circ\text{C}$), and $N = 6.37 \times 10^{-2}$ for $Re_{ci} = 3,183$ and $Re_{co} =$ (a) 1,910, (b) 3,183, (c) 5,092, and (d) 6,365.

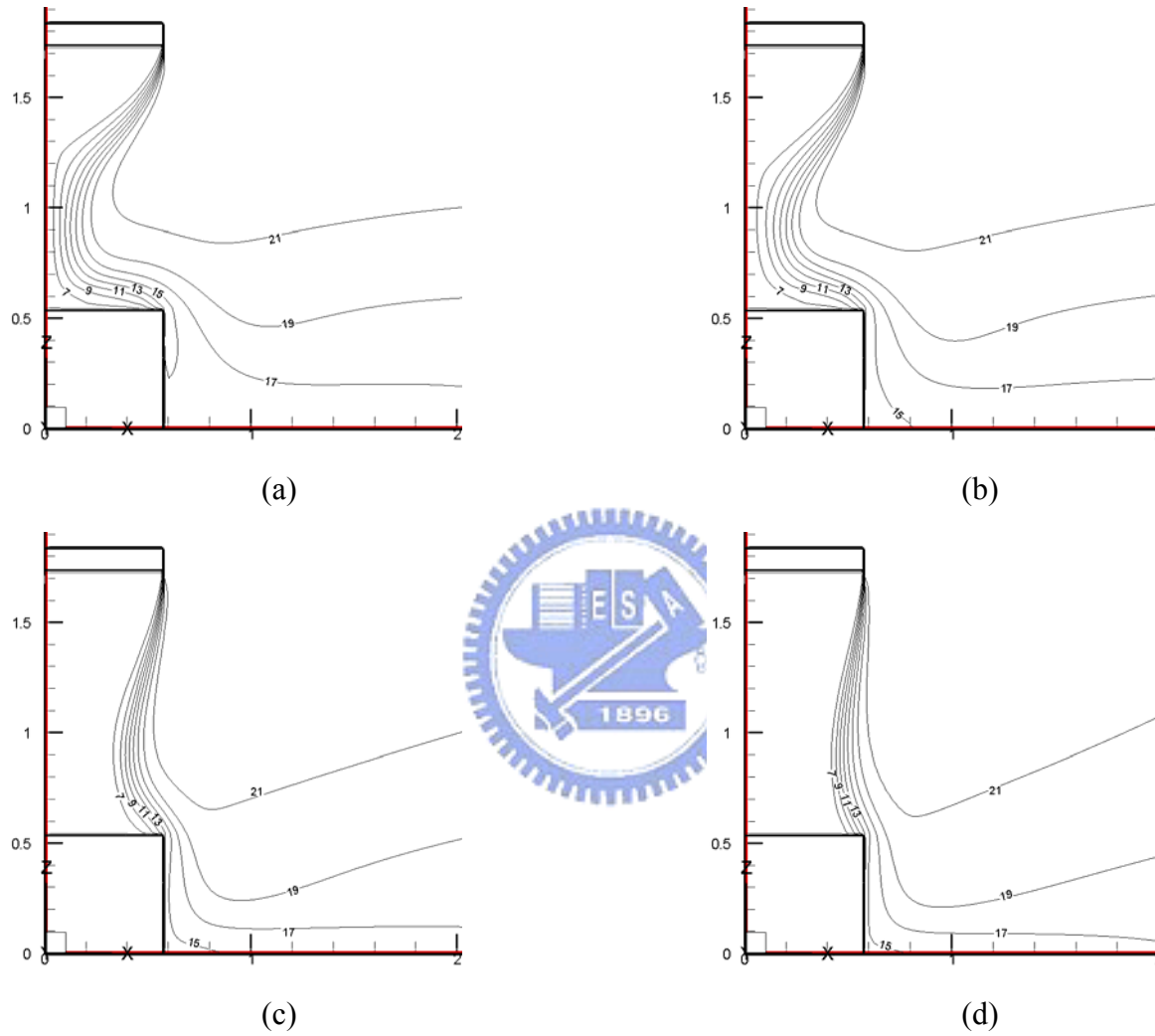


Fig. 4.98 Isotherms for steady cavity flow for a double air curtain design with $b_i = 0.07$ m, $b_o = 0.05$ m, $Gr_t = 4.61 \times 10^9$ ($\Delta T = 20^\circ\text{C}$), and $N = 6.37 \times 10^{-2}$ for $Re_{ci} = 3,183$ and $Re_{co} =$ (a) 1,910, (b) 3,183, (c) 5,092, and (d) 6,365.

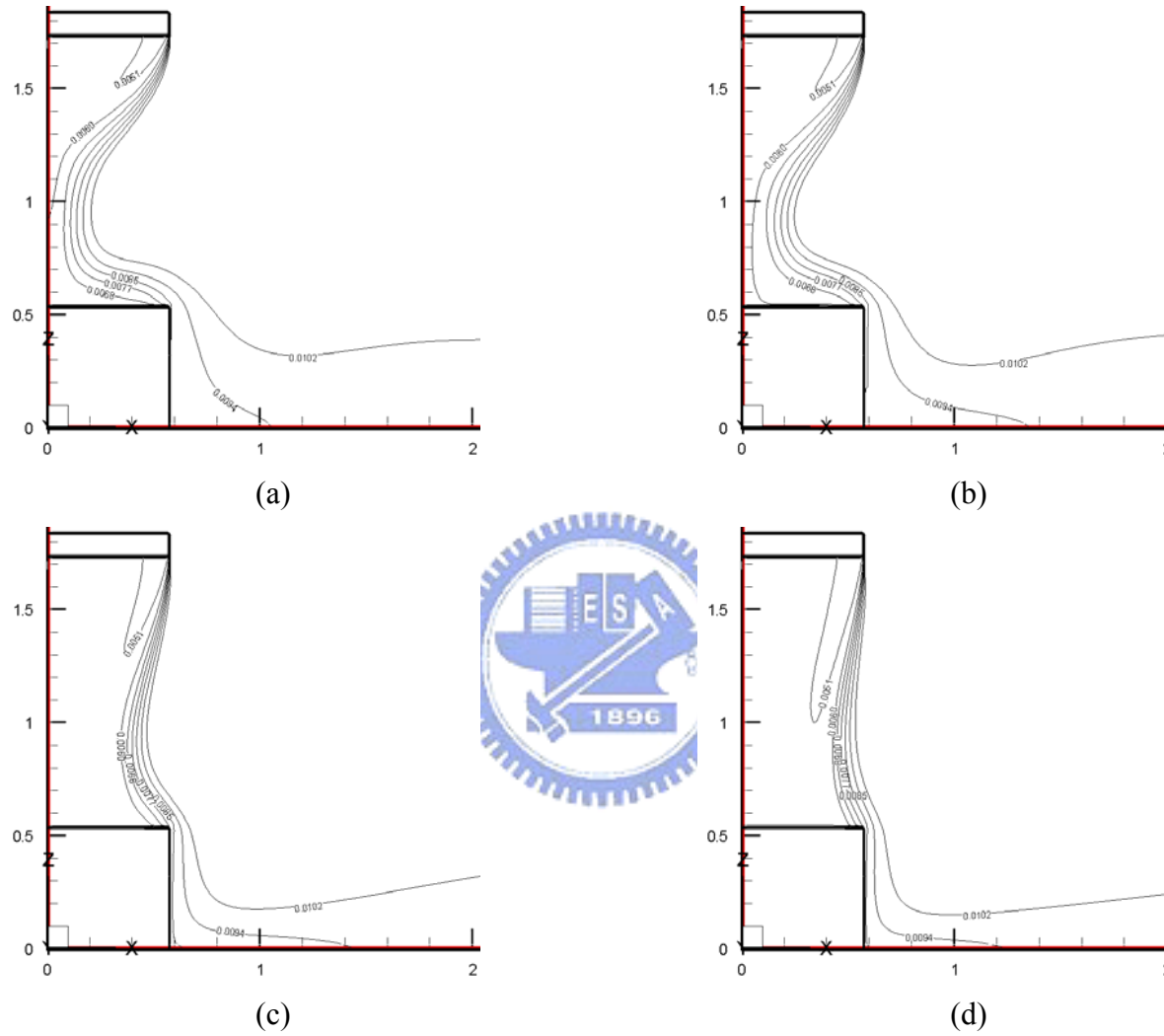


Fig. 4.99 Iso-concentration lines for steady cavity flow for a double air curtain design with $b_i = 0.07$ m, $b_o = 0.05$ m, $Gr_t = 4.61 \times 10^9$ ($\Delta T = 20^\circ\text{C}$), and $N = 6.37 \times 10^{-2}$ for $Re_{ci} = 3,183$ and $Re_{co} =$ (a) 1,910, (b) 3,183, (c) 5,092, and (d) 6,365.

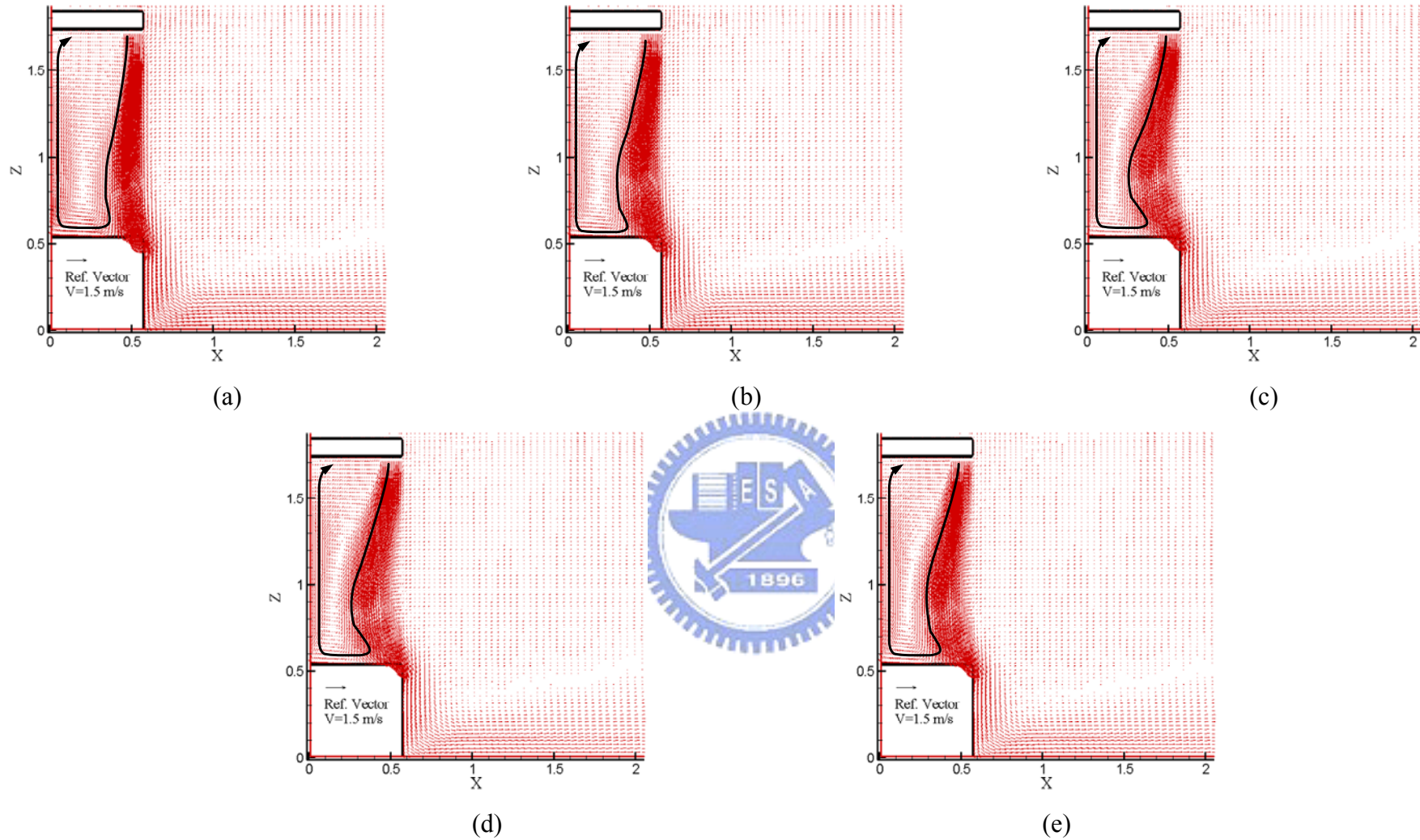


Fig. 4.100 Velocity vector maps for steady cavity flow for a double air curtain design with $b_i = 0.07$ m, $b_o = 0.05$ m, $Gr_t = 4.61 \times 10^9$ ($\Delta T = 20^\circ\text{C}$), and $N = 6.37 \times 10^{-2}$ for (a) $Re_{ci} = 1,910$ and $Re_{co} = 7,638$, (b) $Re_{ci} = 3,183$ and $Re_{co} = 6,365$, (c) $Re_{ci} = 5,092$ and $Re_{co} = 4,456$, (d) $Re_{ci} = 6,365$ and $Re_{co} = 3,183$, (e) $Re_{ci} = 7,638$ and $Re_{co} = 1,910$.

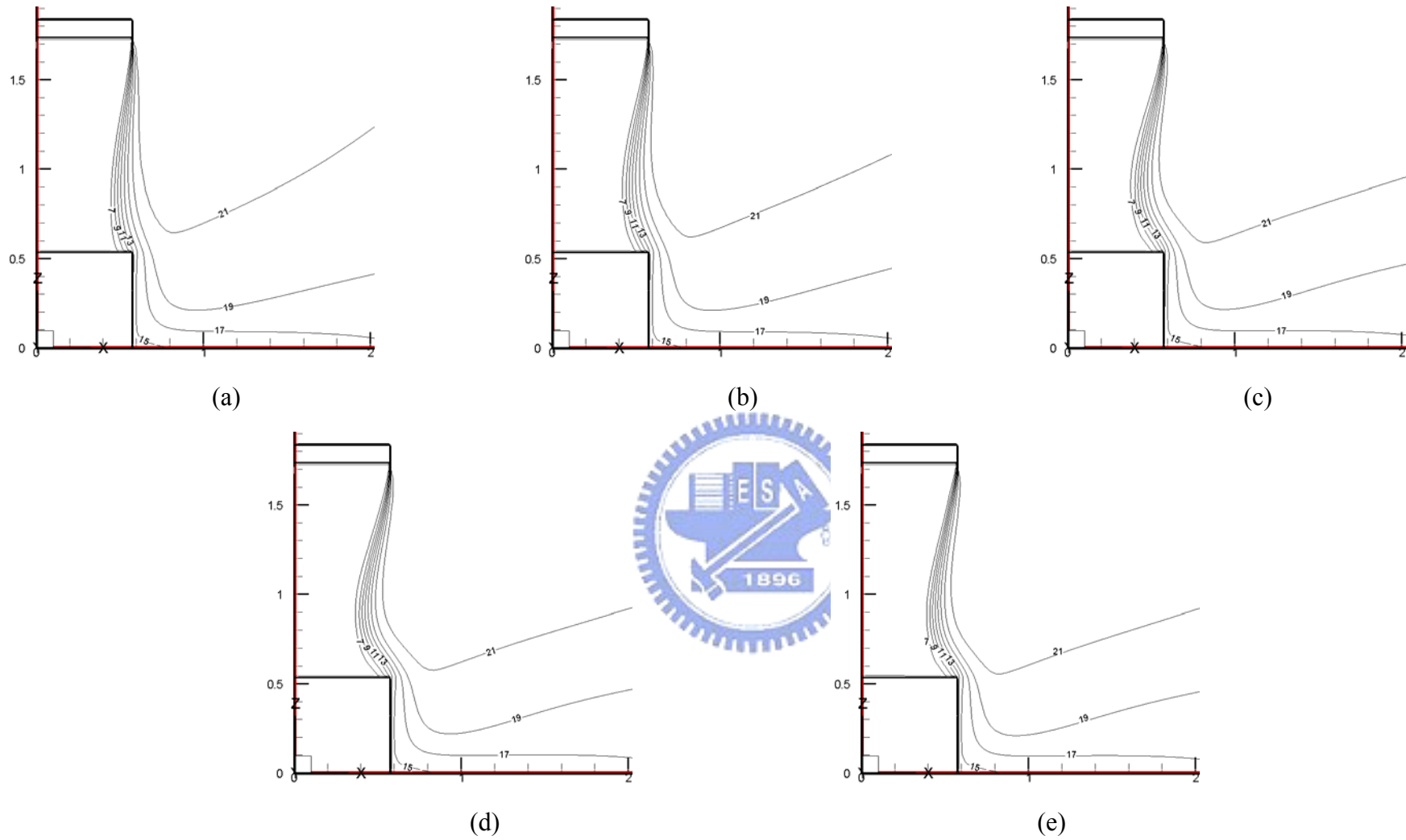


Fig. 4.101 Isotherms for steady cavity flow for a double air curtain design with $b_i = 0.07$ m, $b_o = 0.05$ m, $Gr_t = 4.61 \times 10^9$ ($\Delta T = 20^\circ\text{C}$), and $N = 6.37 \times 10^{-2}$ for (a) $Re_{ci} = 1,910$ and $Re_{co} = 7,638$, (b) $Re_{ci} = 3,183$ and $Re_{co} = 6,365$, (c) $Re_{ci} = 5,092$ and $Re_{co} = 4,456$, (d) $Re_{ci} = 6,365$ and $Re_{co} = 3,183$, (e) $Re_{ci} = 7,638$ and $Re_{co} = 1,910$.

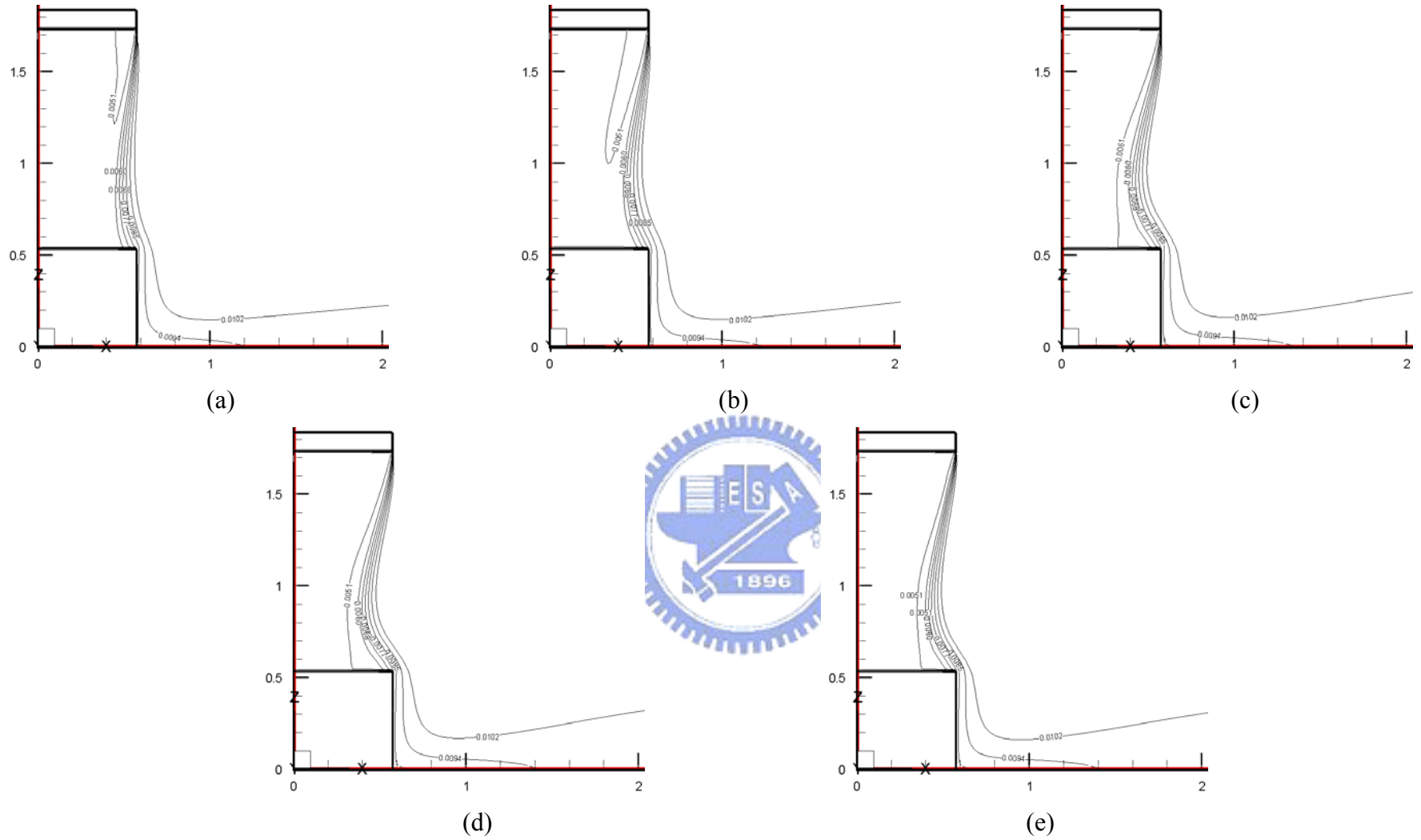


Fig. 4.102 Iso-concentration lines for steady cavity flow for a double air curtain design with $b_i = 0.07$ m, $b_o = 0.05$ m, $Gr_t = 4.61 \times 10^9$ ($\Delta T = 20^\circ\text{C}$), and $N = 6.37 \times 10^{-2}$ for (a) $Re_{ci} = 1,910$ and $Re_{co} = 7,638$, (b) $Re_{ci} = 3,183$ and $Re_{co} = 6,365$, (c) $Re_{ci} = 5,092$ and $Re_{co} = 4,456$, (d) $Re_{ci} = 6,365$ and $Re_{co} = 3,183$, (e) $Re_{ci} = 7,638$ and $Re_{co} = 1,910$.

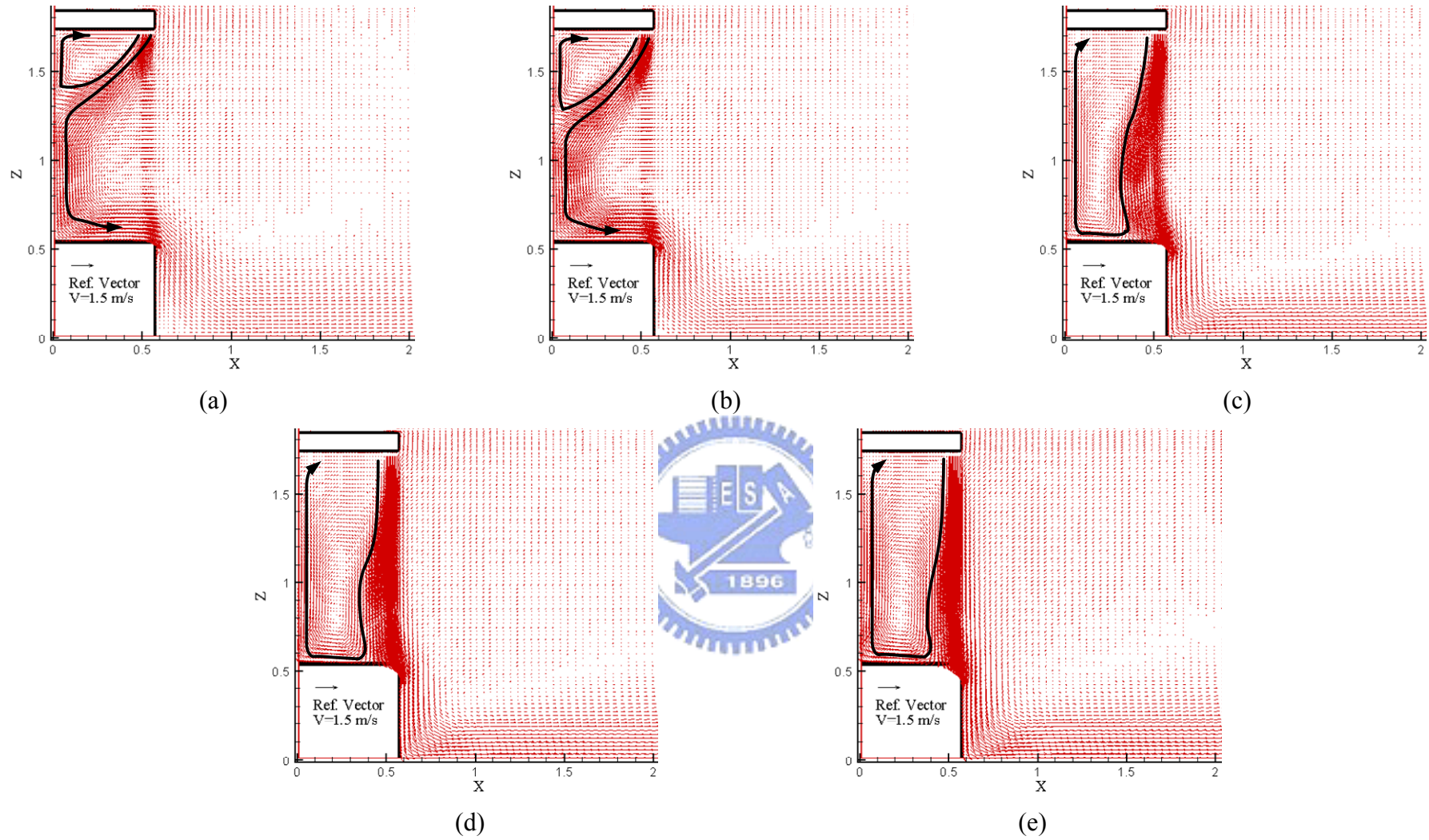


Fig. 4.103 Velocity vector maps for steady cavity flow for a double air curtain design with $b_i = 0.03$ m, $b_o = 0.04$ m, $Gr_i = 4.61 \times 10^9$ ($\Delta T = 20^\circ\text{C}$), and $N = 6.37 \times 10^{-2}$ for $Re_{ci} = 1,910$ and $Re_{co} =$ (a) 1,910, (b) 3,183, (c) 5,092, (d) 6,365 and (e) 7,638.

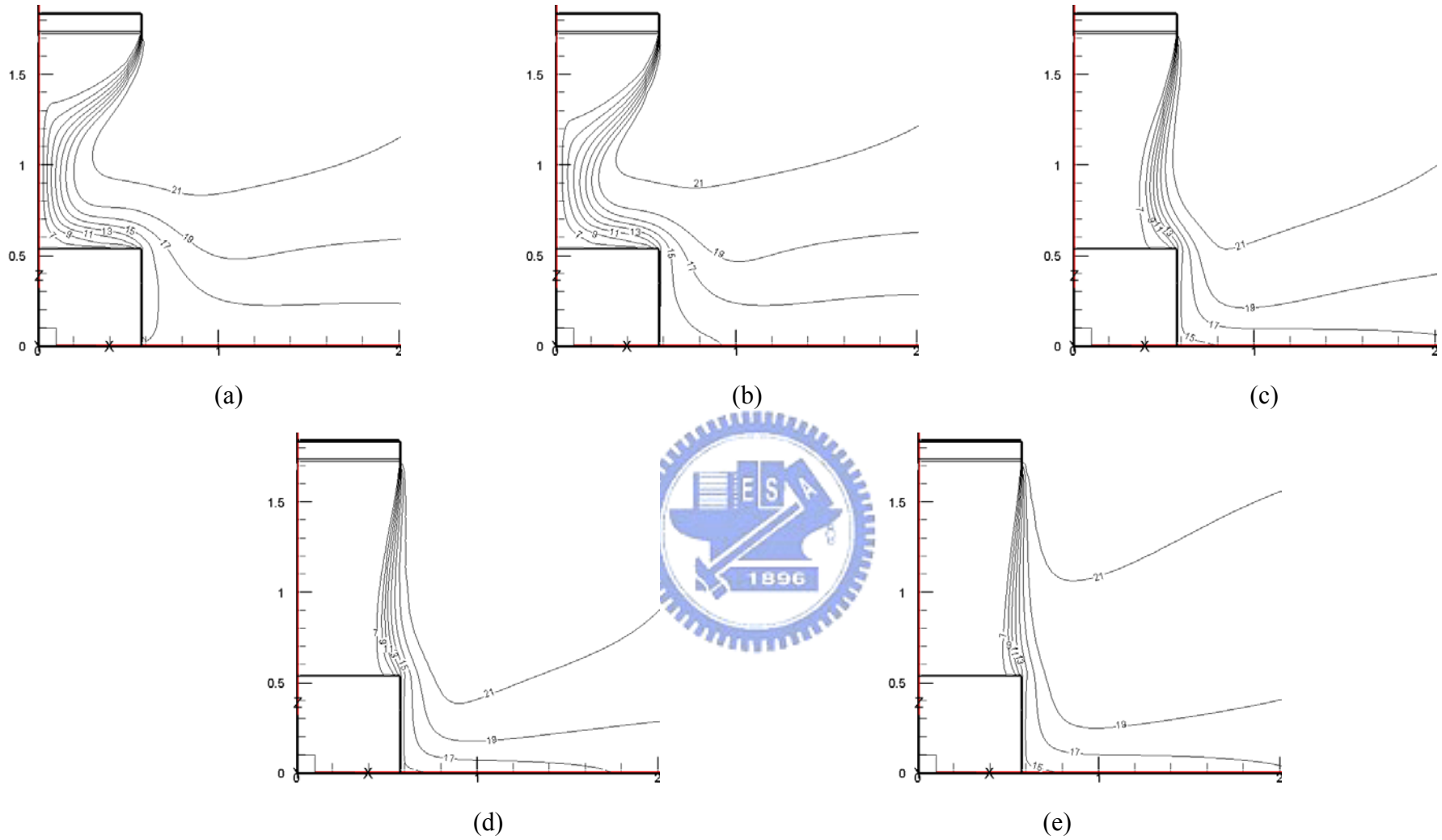


Fig. 4.104 Isotherms for steady cavity flow for a double air curtain design with $b_i = 0.03$ m, $b_o = 0.04$ m, $Gr_t = 4.61 \times 10^9$ ($\Delta T = 20^\circ\text{C}$), and $N = 6.37 \times 10^{-2}$ for $Re_{ci} = 1,910$ and $Re_{co} =$ (a) 1,910, (b) 3,183, (c) 5,092, (d) 6,365 and (e) 7,638.

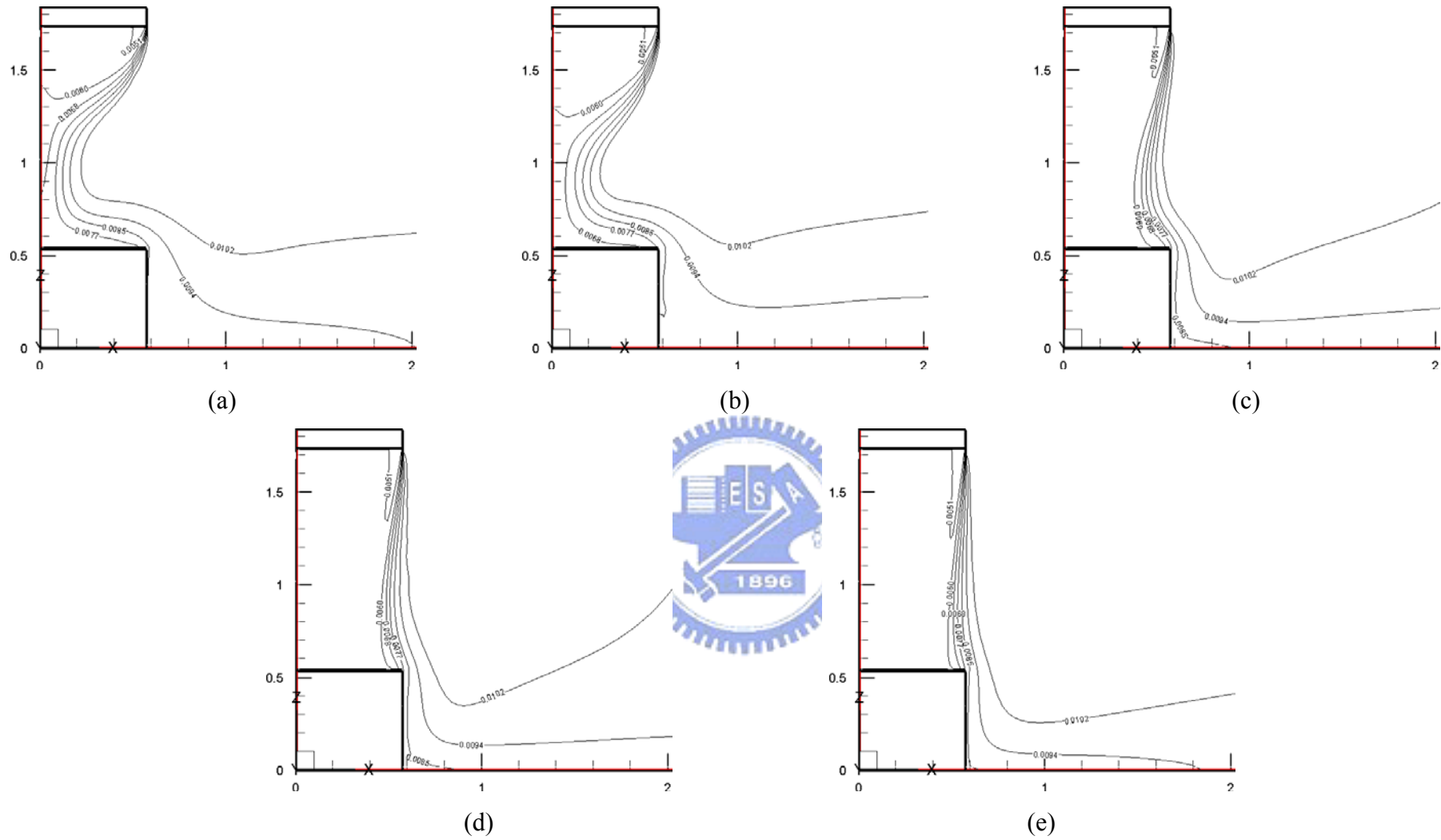


Fig. 4.105 Iso-concentration lines for steady cavity flow for a double air curtain design with $b_i = 0.03$ m, $b_o = 0.04$ m, $Gr_t = 4.61 \times 10^9$ ($\Delta T = 20^\circ\text{C}$), and $N = 6.37 \times 10^{-2}$ for $Re_{ci} = 1,910$ and $Re_{co} =$ (a) 1,910, (b) 3,183, (c) 5,092, (d) 6,365 and (e) 7,638.

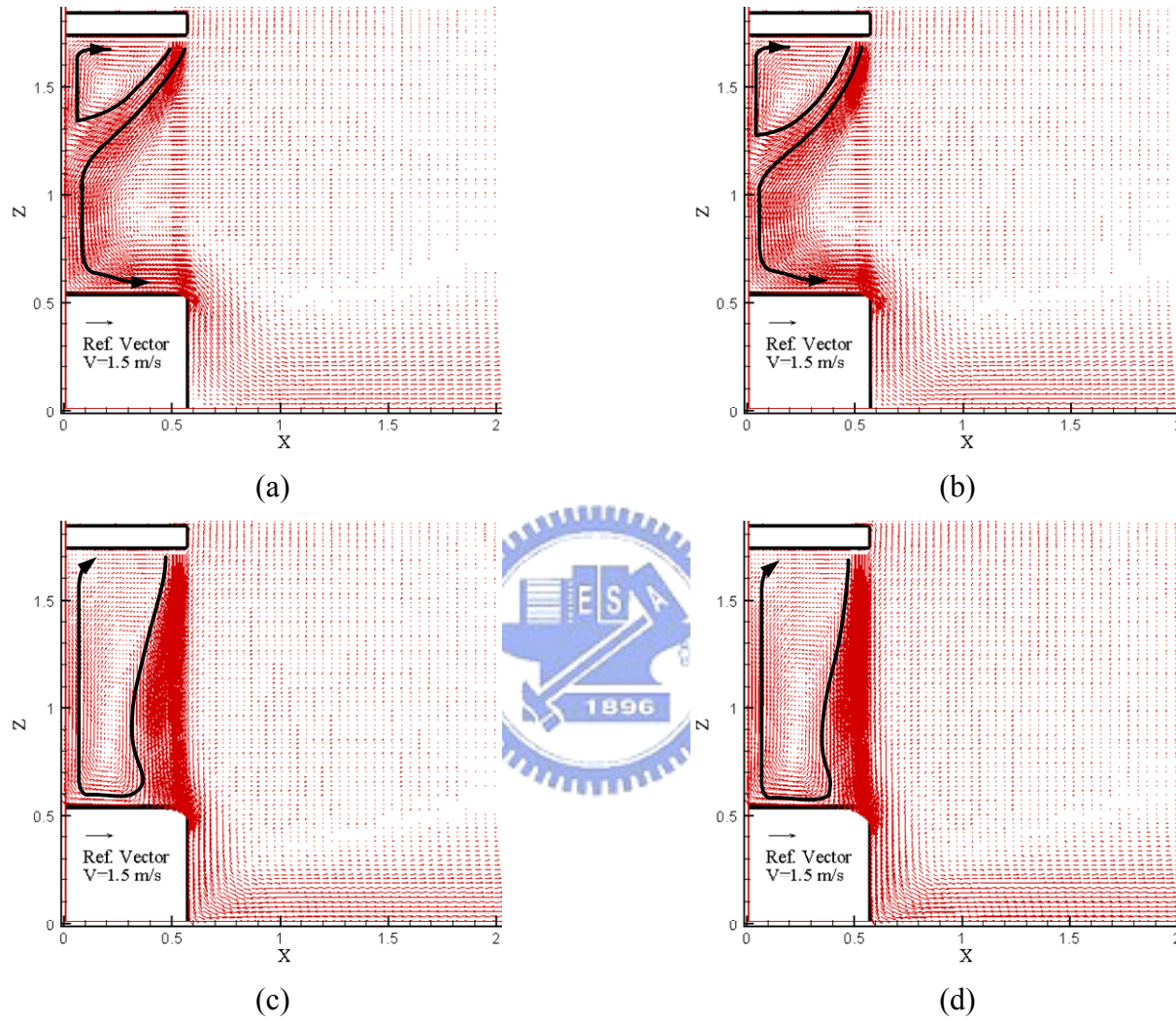


Fig. 4.106 Velocity vector maps for steady cavity flow for a double air curtain design with $b_i = 0.03$ m, $b_o = 0.04$ m, $Gr_t = 4.61 \times 10^9$ ($\Delta T = 20^\circ\text{C}$), and $N = 6.37 \times 10^{-2}$ for $Re_{ci} = 3,183$ and $Re_{co} =$ (a) 1,910, (b) 3,183, (c) 5,092, and (d) 6,365.

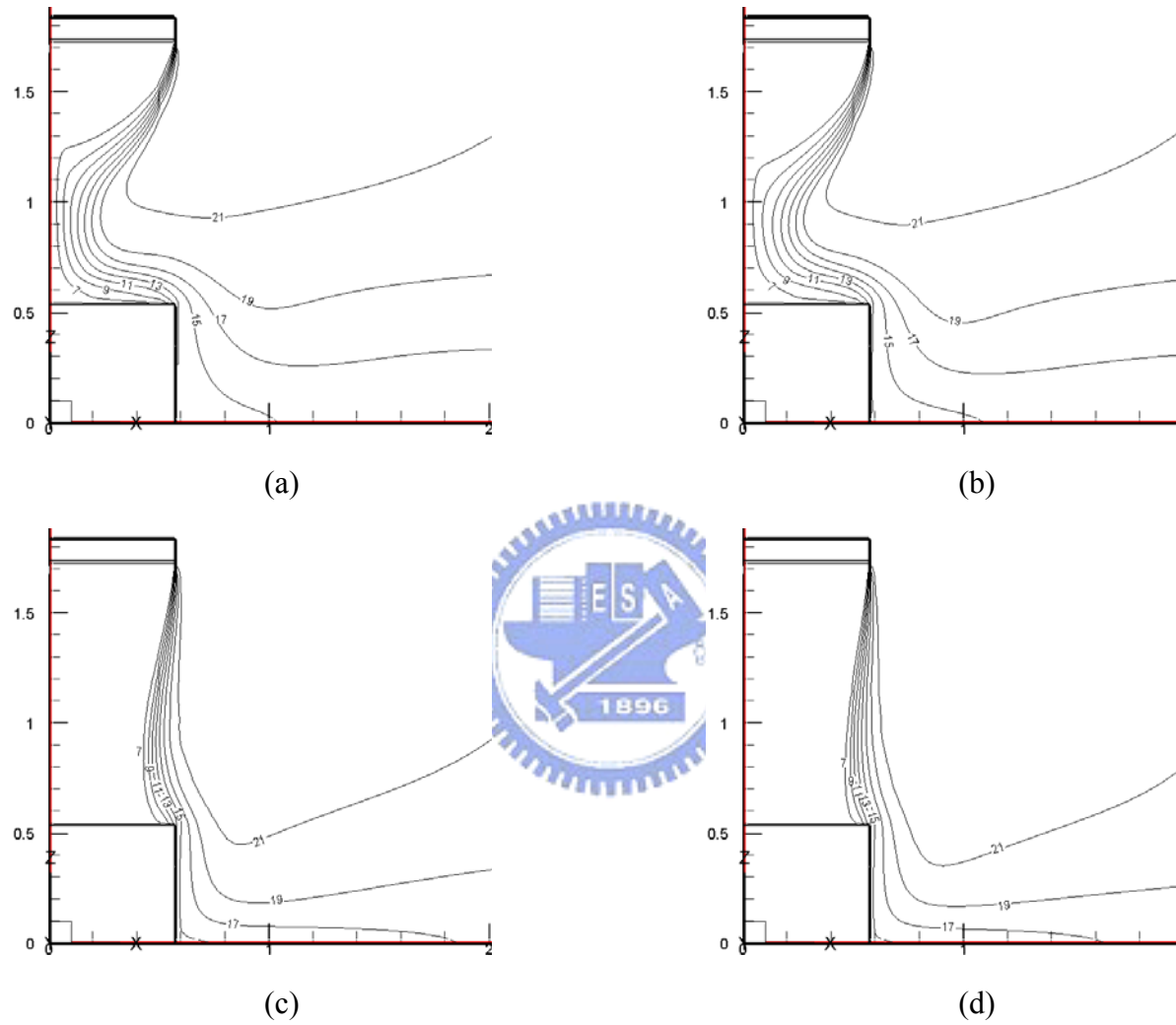


Fig. 4.107 Isotherms for steady cavity flow for a double air curtain design with $b_i = 0.03$ m, $b_o = 0.04$ m, $Gr_t = 4.61 \times 10^9$ ($\Delta T = 20^\circ\text{C}$), and $N = 6.37 \times 10^{-2}$ for $Re_{ci} = 3,183$ and $Re_{co} =$ (a) 1,910, (b) 3,183, (c) 5,092, and (d) 6,365.

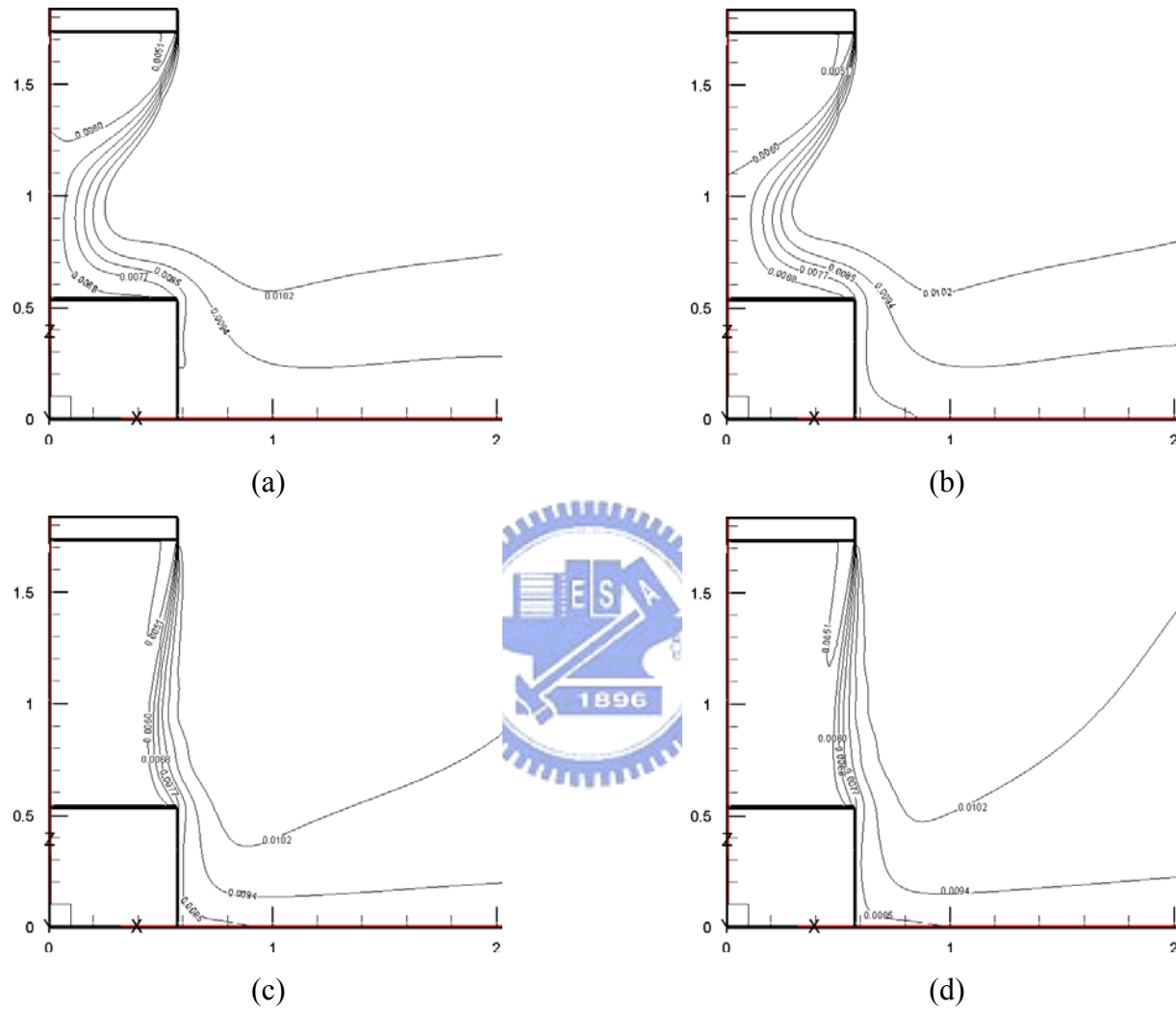


Fig. 4.108 Iso-concentration lines for steady cavity flow for a double air curtain design with $b_i = 0.03$ m, $b_o = 0.04$ m, $Gr_t = 4.61 \times 10^9$ ($\Delta T = 20^\circ\text{C}$), and $N = 6.37 \times 10^{-2}$ for $Re_{ci} = 3,183$ and $Re_{co} =$ (a) 1,910, (b) 3,183, (c) 5,092, and (d) 6,365.

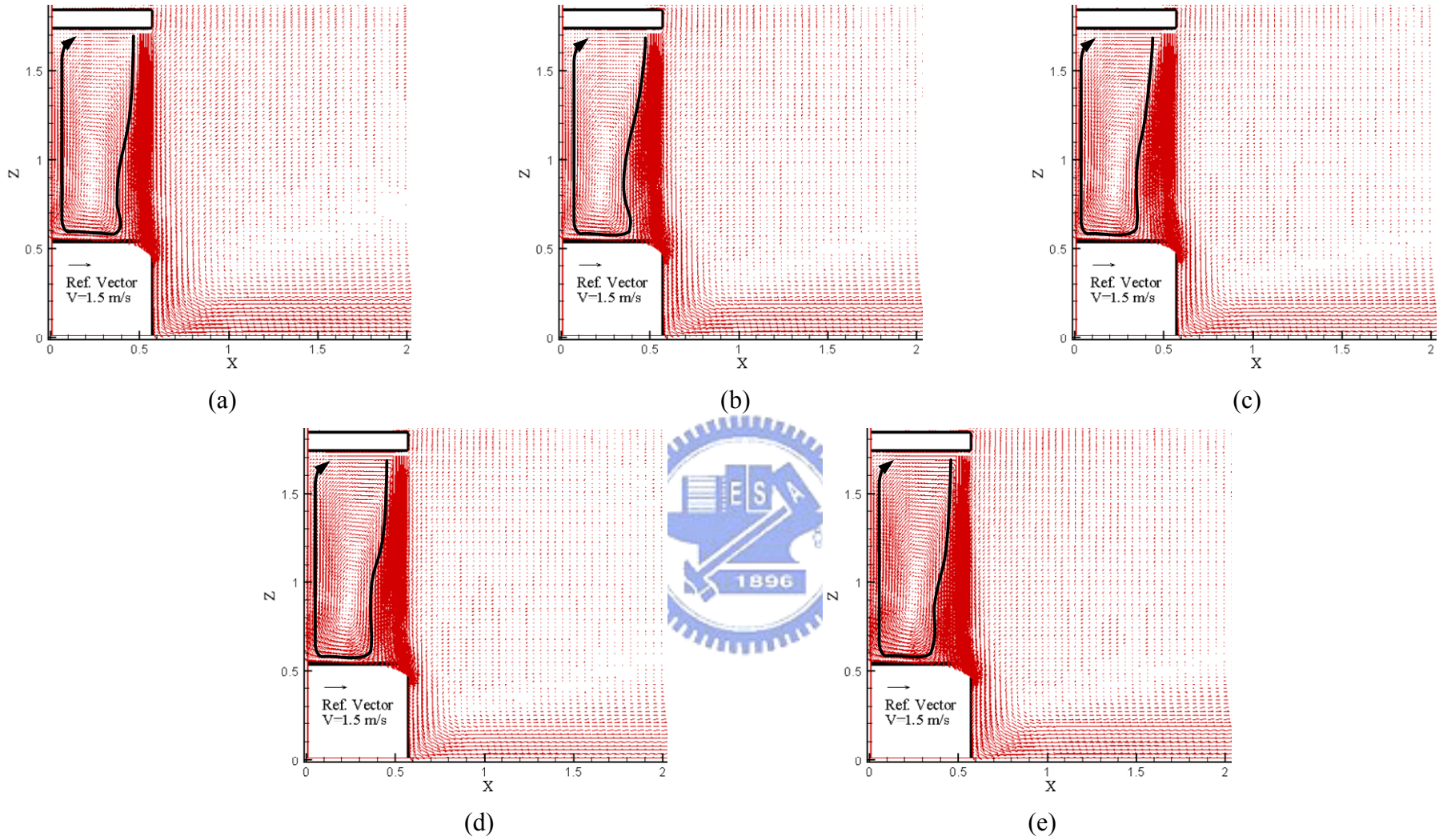


Fig. 4.109 Velocity vector maps for steady cavity flow for a double air curtain design with $b_i = 0.03$ m, $b_o = 0.04$ m, $Gr_t = 4.61 \times 10^9$ ($\Delta T = 20^\circ\text{C}$), and $N = 6.37 \times 10^{-2}$ for (a) $Re_{ci} = 1,910$ and $Re_{co} = 7,638$, (b) $Re_{ci} = 3,183$ and $Re_{co} = 6,365$, (c) $Re_{ci} = 5,092$ and $Re_{co} = 4,456$, (d) $Re_{ci} = 6,365$ and $Re_{co} = 3,183$, (e) $Re_{ci} = 7,638$ and $Re_{co} = 1,910$.

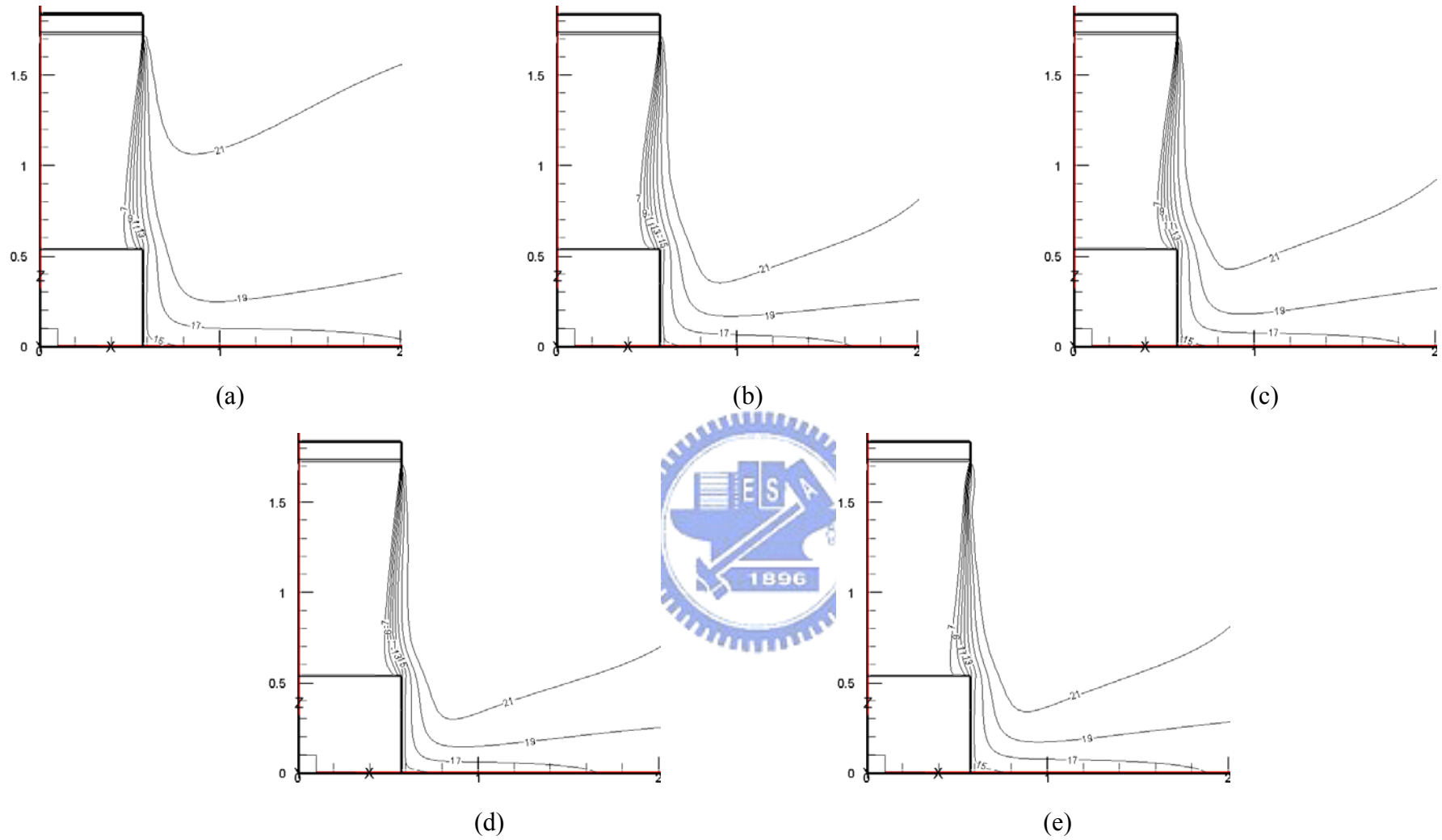


Fig. 4.110 Isotherms for steady cavity flow for a double air curtain design with $b_i = 0.03$ m, $b_o = 0.04$ m, $Gr_t = 4.61 \times 10^9$ ($\Delta T = 20^\circ\text{C}$), and $N = 6.37 \times 10^{-2}$ for (a) $Re_{ci} = 1,910$ and $Re_{co} = 7,638$, (b) $Re_{ci} = 3,183$ and $Re_{co} = 6,365$, (c) $Re_{ci} = 5,092$ and $Re_{co} = 4,456$, (d) $Re_{ci} = 6,365$ and $Re_{co} = 3,183$, (e) $Re_{ci} = 7,638$ and $Re_{co} = 1,910$.

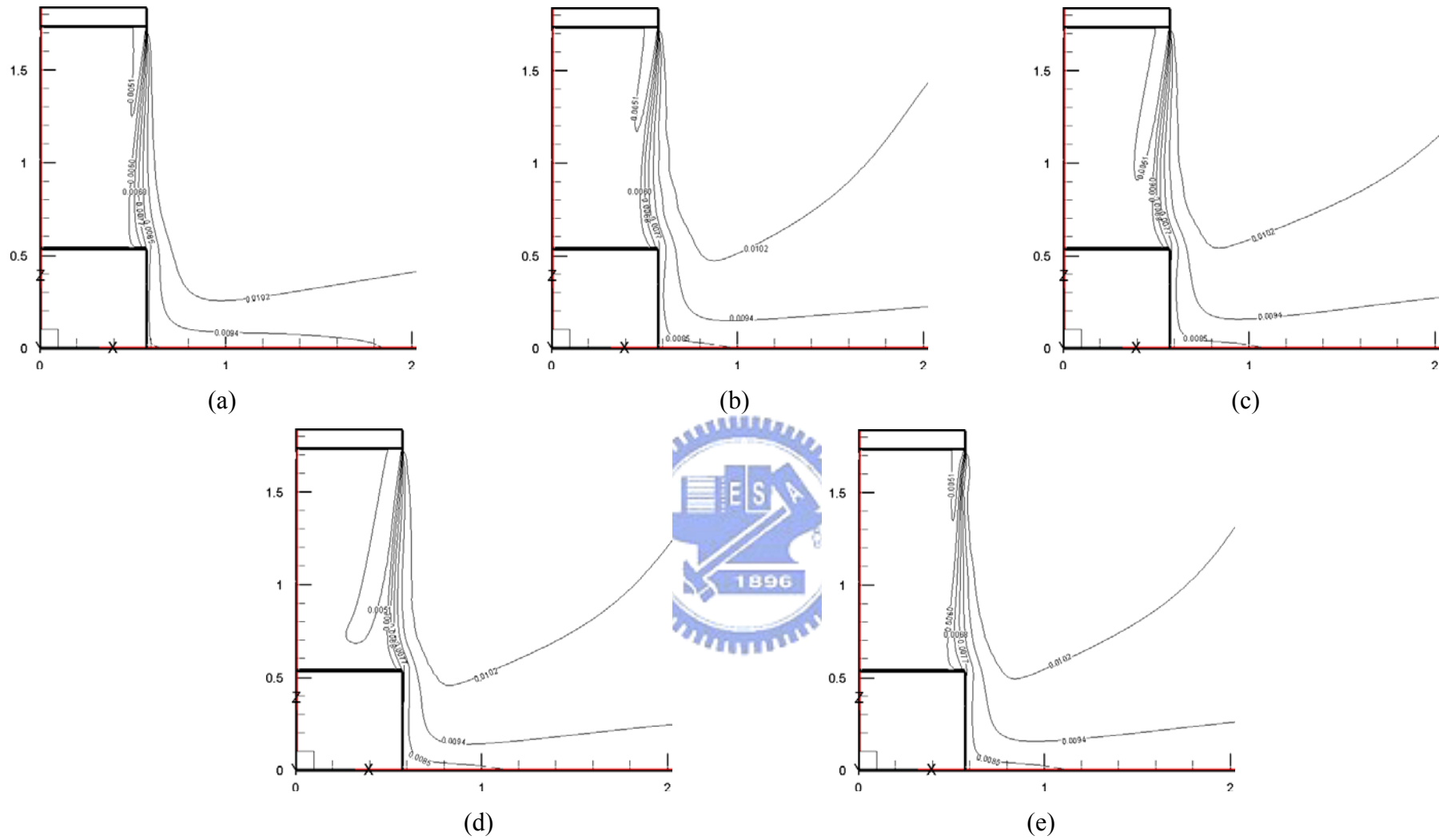


Fig. 4.111 Iso-concentration lines for steady cavity flow for a double air curtain design with $b_i = 0.03$ m, $b_o = 0.04$ m, $Gr_t = 4.61 \times 10^9$ ($\Delta T = 20^\circ\text{C}$), and $N = 6.37 \times 10^{-2}$ for (a) $Re_{ci} = 1,910$ and $Re_{co} = 7,638$, (b) $Re_{ci} = 3,183$ and $Re_{co} = 6,365$, (c) $Re_{ci} = 5,092$ and $Re_{co} = 4,456$, (d) $Re_{ci} = 6,365$ and $Re_{co} = 3,183$, (e) $Re_{ci} = 7,638$ and $Re_{co} = 1,910$.

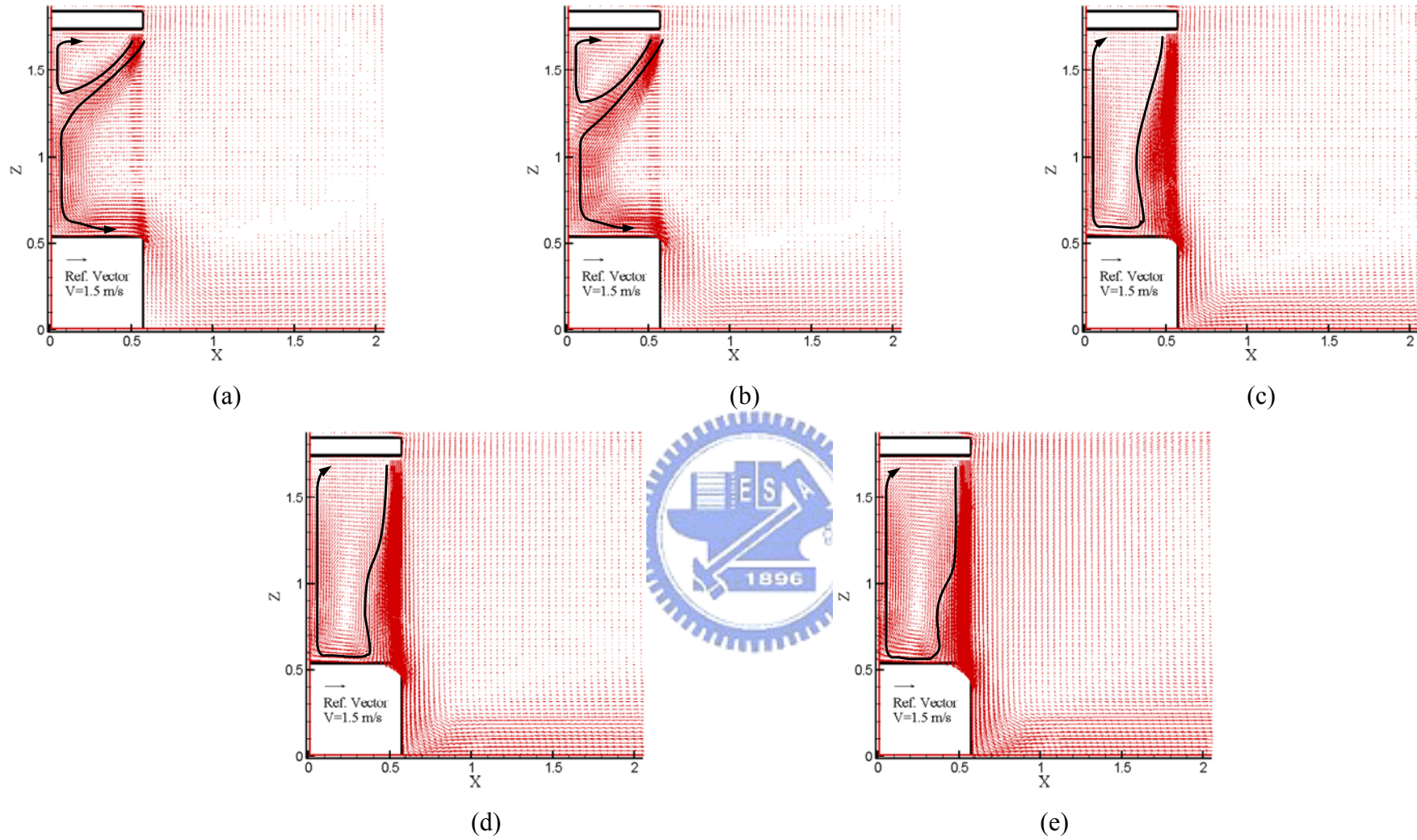


Fig. 4.112 Velocity vector maps for steady cavity flow for a double air curtain design with $b_i = 0.04$ m, $b_o = 0.03$ m, $Gr_i = 4.61 \times 10^9$ ($\Delta T = 20^\circ\text{C}$), and $N = 6.37 \times 10^{-2}$ for $Re_{ci} = 1,910$ and $Re_{co} =$ (a) 1,910, (b) 3,183, (c) 5,092, (d) 6,365 and (e) 7,638.

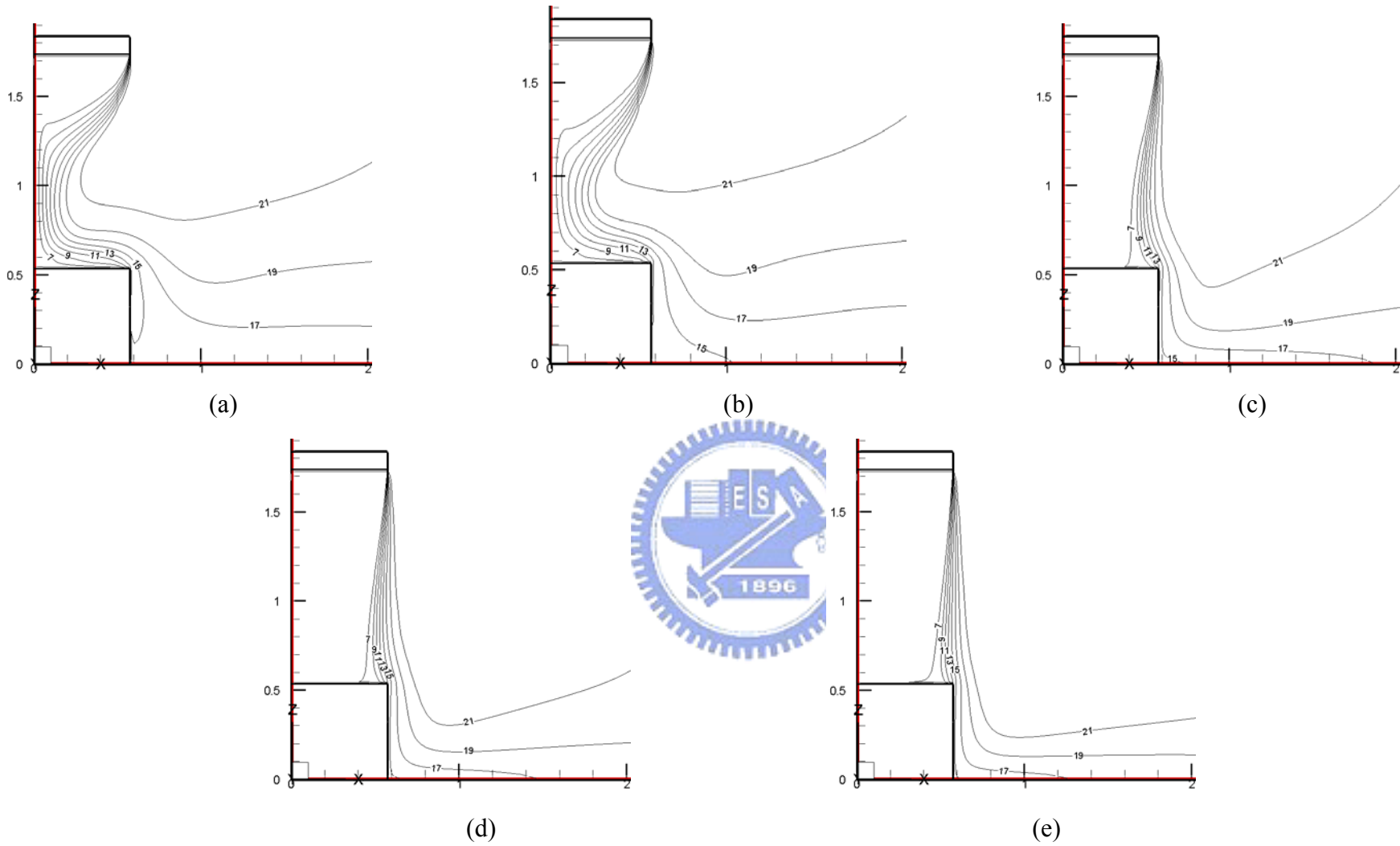


Fig. 4.113 Isotherms for steady cavity flow for a double air curtain design with $b_i = 0.04$ m, $b_o = 0.03$ m, $Gr_t = 4.61 \times 10^9$ ($\Delta T = 20^\circ\text{C}$), and $N = 6.37 \times 10^{-2}$ for $Re_{ci} = 1,910$ and $Re_{co} =$ (a) 1,910, (b) 3,183, (c) 5,092, (d) 6,365 and (e) 7,638.

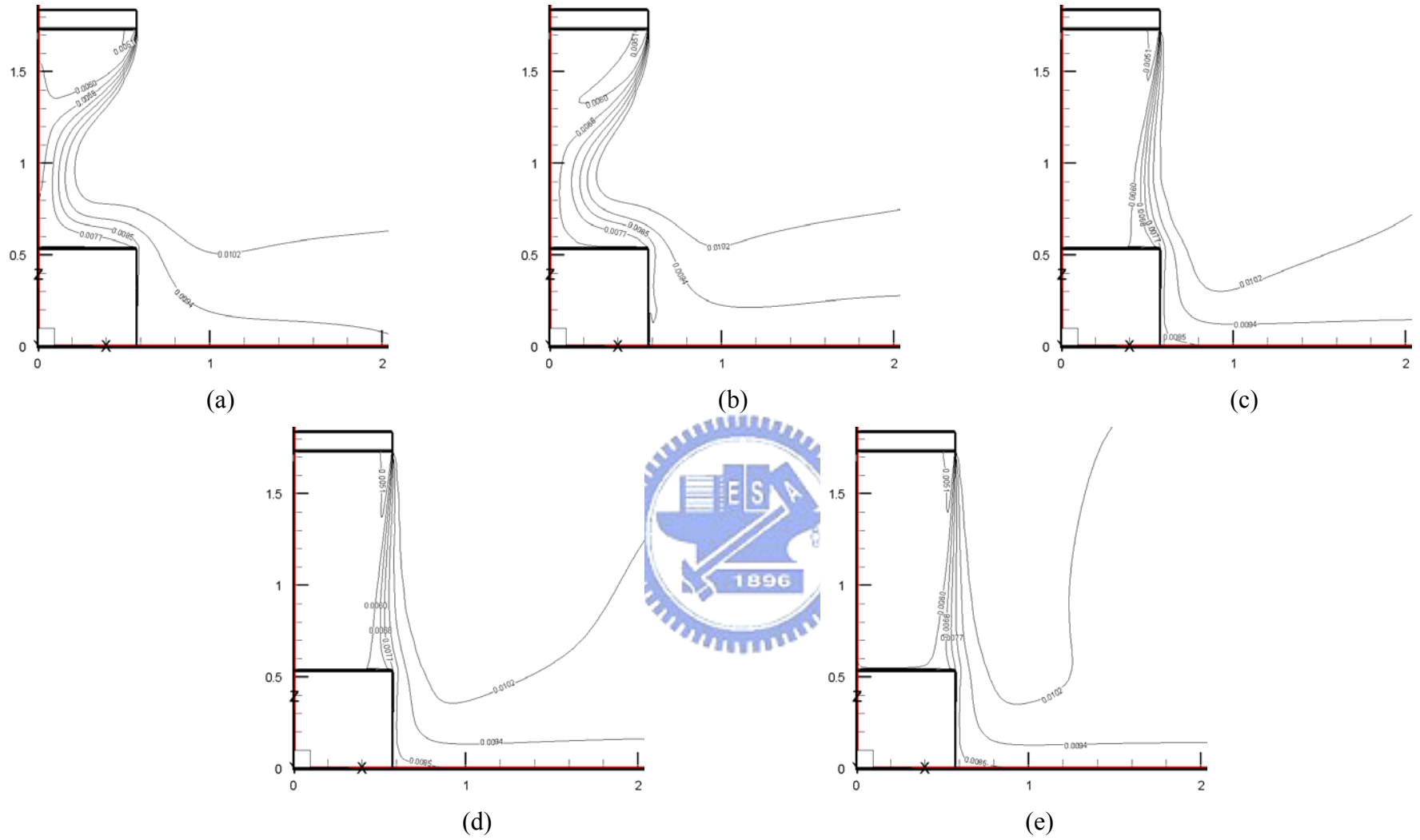


Fig. 4.114 Iso-concentration lines for steady cavity flow for a double air curtain design with $b_i = 0.04$ m, $b_o = 0.03$ m, $Gr_t = 4.61 \times 10^9$ ($\Delta T = 20^\circ\text{C}$), and $N = 6.37 \times 10^{-2}$ for $Re_{ci} = 1,910$ and $Re_{co} =$ (a) 1,910, (b) 3,183, (c) 5,092, (d) 6,365 and (e) 7,638.

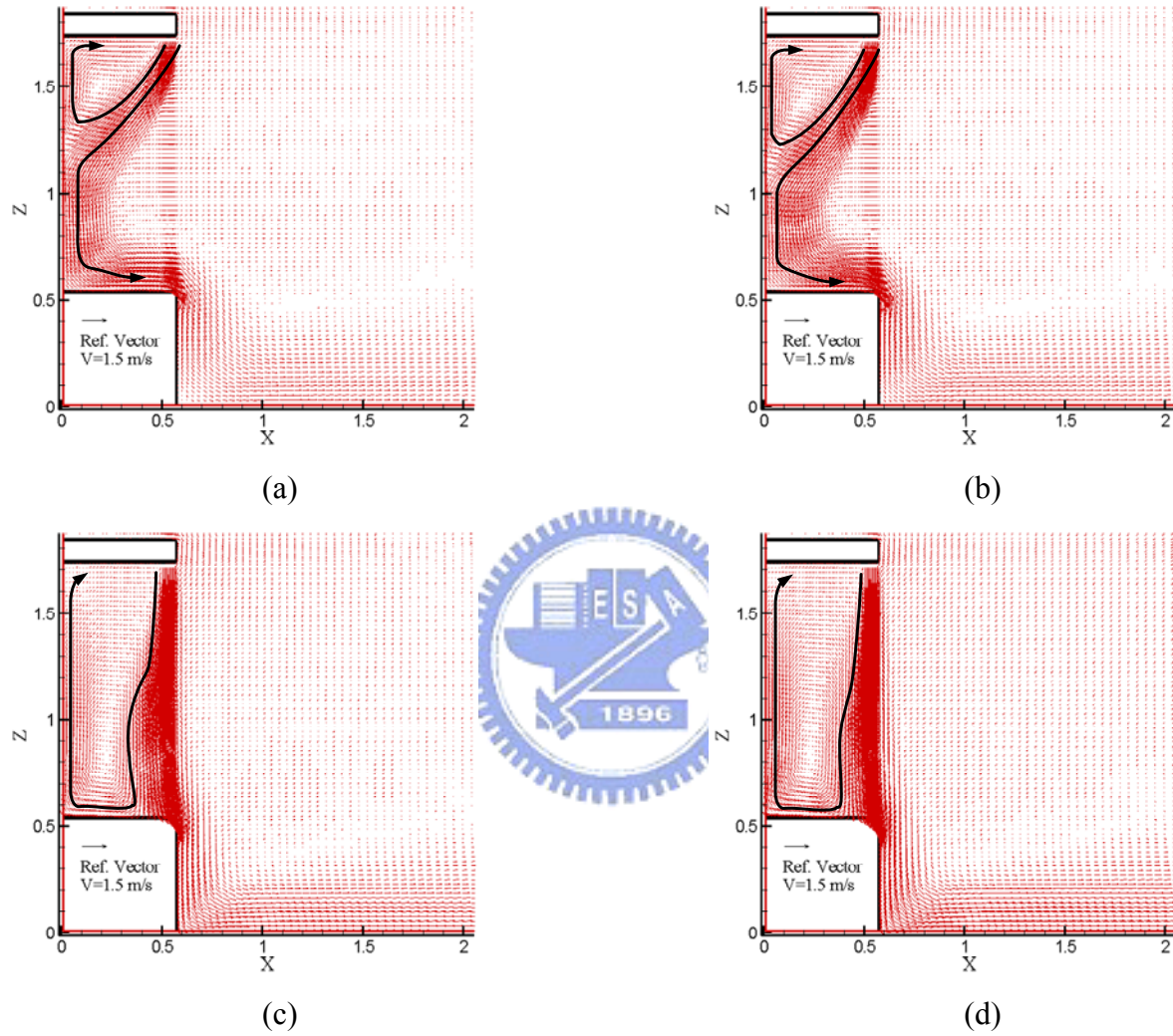


Fig. 4.115 Velocity vector maps for steady cavity flow for a double air curtain design with $b_i = 0.04 \text{ m}$, $b_o = 0.03 \text{ m}$, $Gr_t = 4.61 \times 10^9$ ($\Delta T = 20^\circ\text{C}$), and $N = 6.37 \times 10^{-2}$ for $Re_{ci} = 3,183$ and $Re_{co} =$ (a) 1,910, (b) 3,183, (c) 5,092, and (d) 6,365.

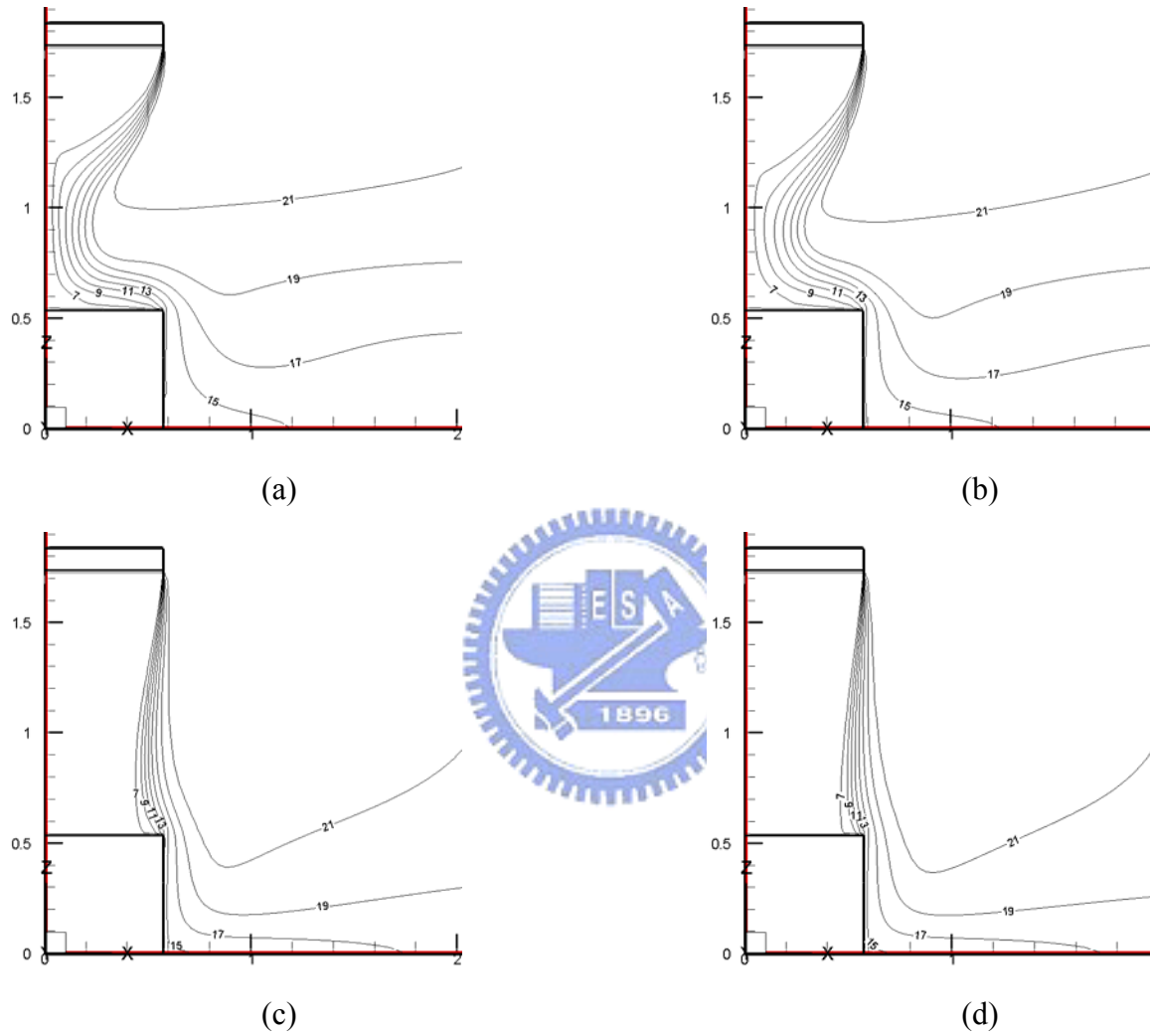
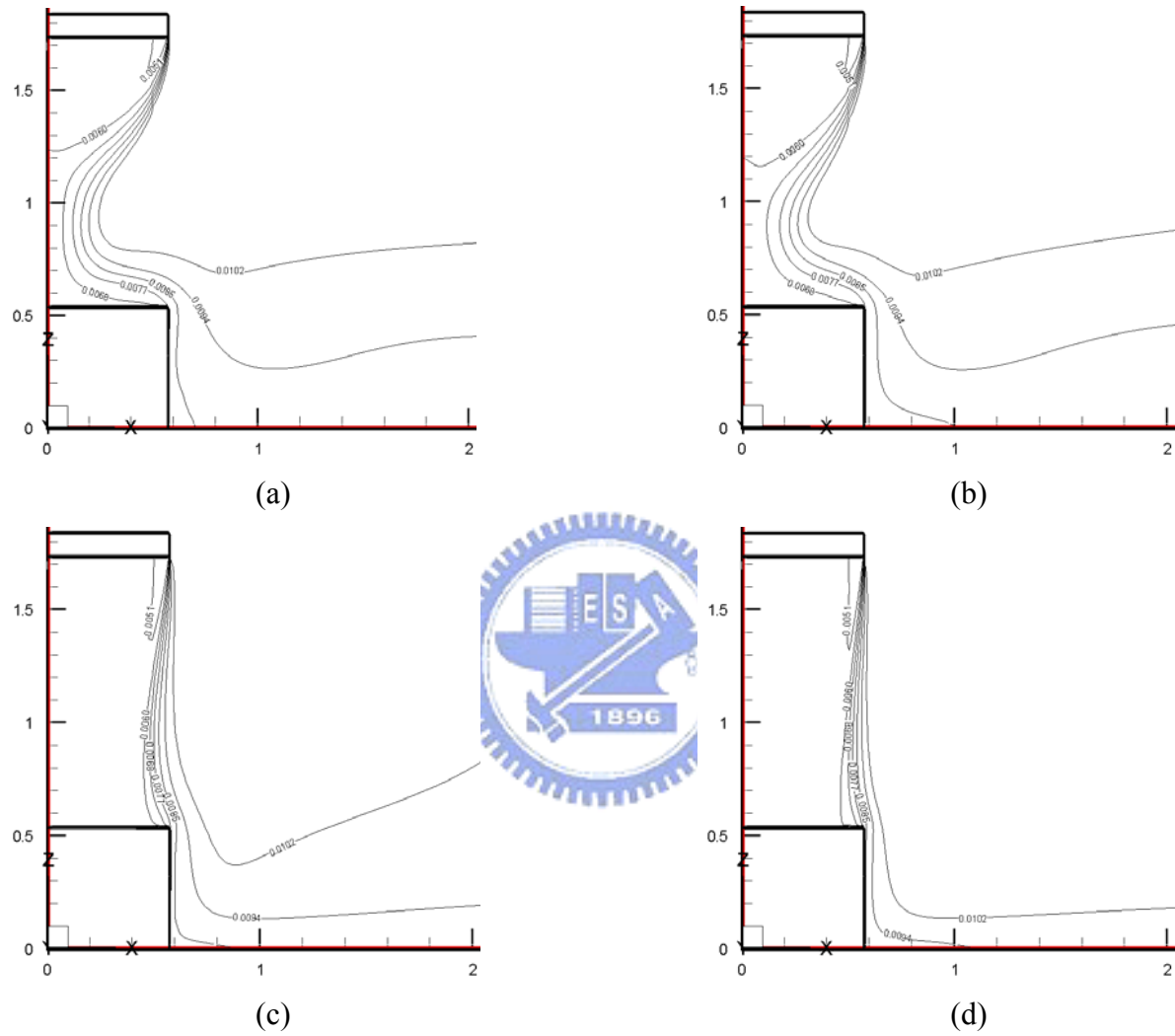


Fig. 4.116 Isotherms for steady cavity flow for a double air curtain design with $b_i = 0.04$ m, $b_o = 0.03$ m, $Gr_t = 4.61 \times 10^9$ ($\Delta T = 20^\circ\text{C}$), and $N = 6.37 \times 10^{-2}$ for $Re_{ci} = 3,183$ and $Re_{co} =$ (a) 1,910, (b) 3,183, (c) 5,092, and (d) 6,365.



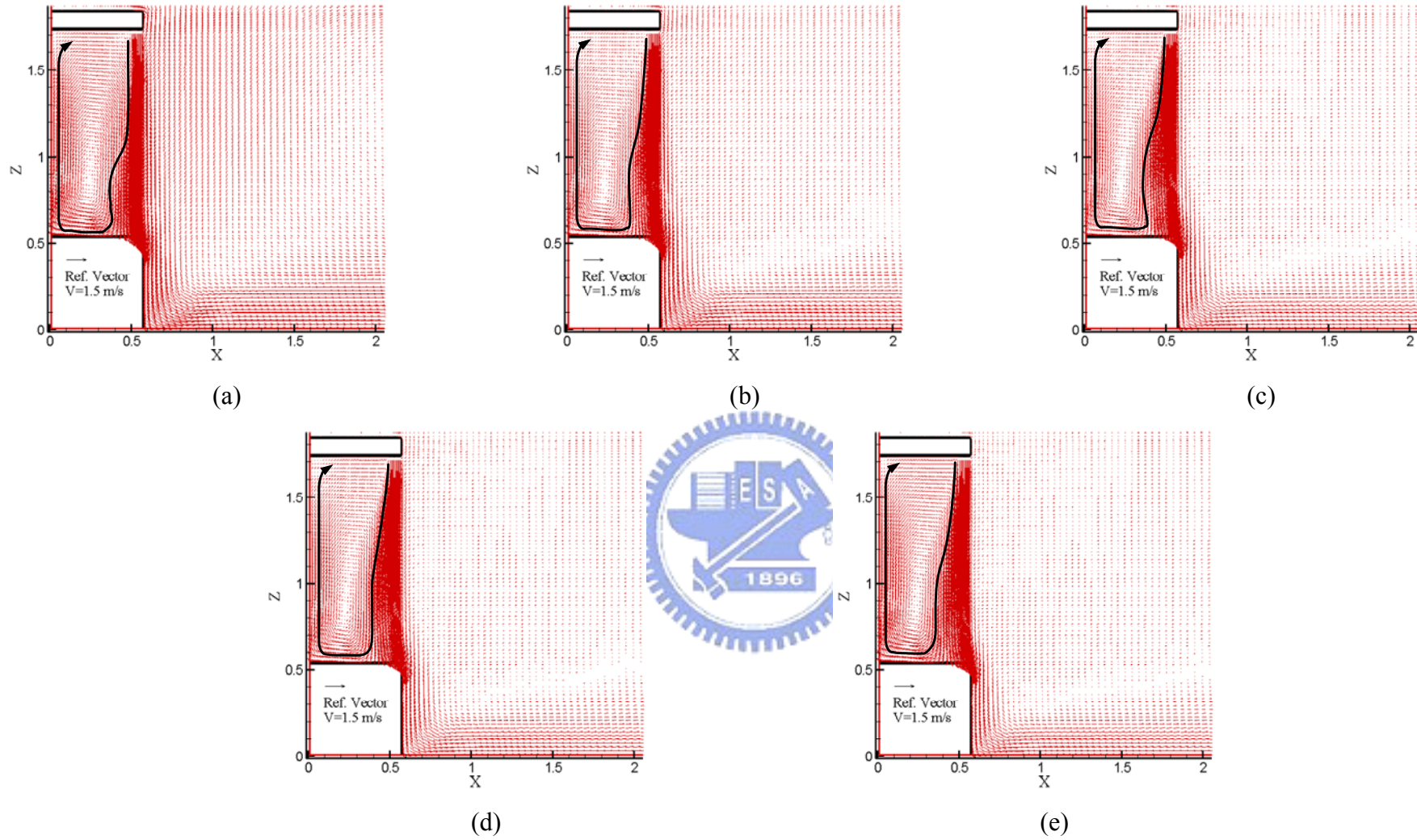


Fig. 4.118 Velocity vector maps for steady cavity flow for a double air curtain design with $b_i = 0.04$ m, $b_o = 0.03$ m, $Gr_t = 4.61 \times 10^9$ ($\Delta T = 20^\circ\text{C}$), and $N = 6.37 \times 10^{-2}$ for (a) $Re_{ci} = 1,910$ and $Re_{co} = 7,638$, (b) $Re_{ci} = 3,183$ and $Re_{co} = 6,365$, (c) $Re_{ci} = 5,092$ and $Re_{co} = 4,456$, (d) $Re_{ci} = 6,365$ and $Re_{co} = 3,183$, (e) $Re_{ci} = 7,638$ and $Re_{co} = 1,910$.

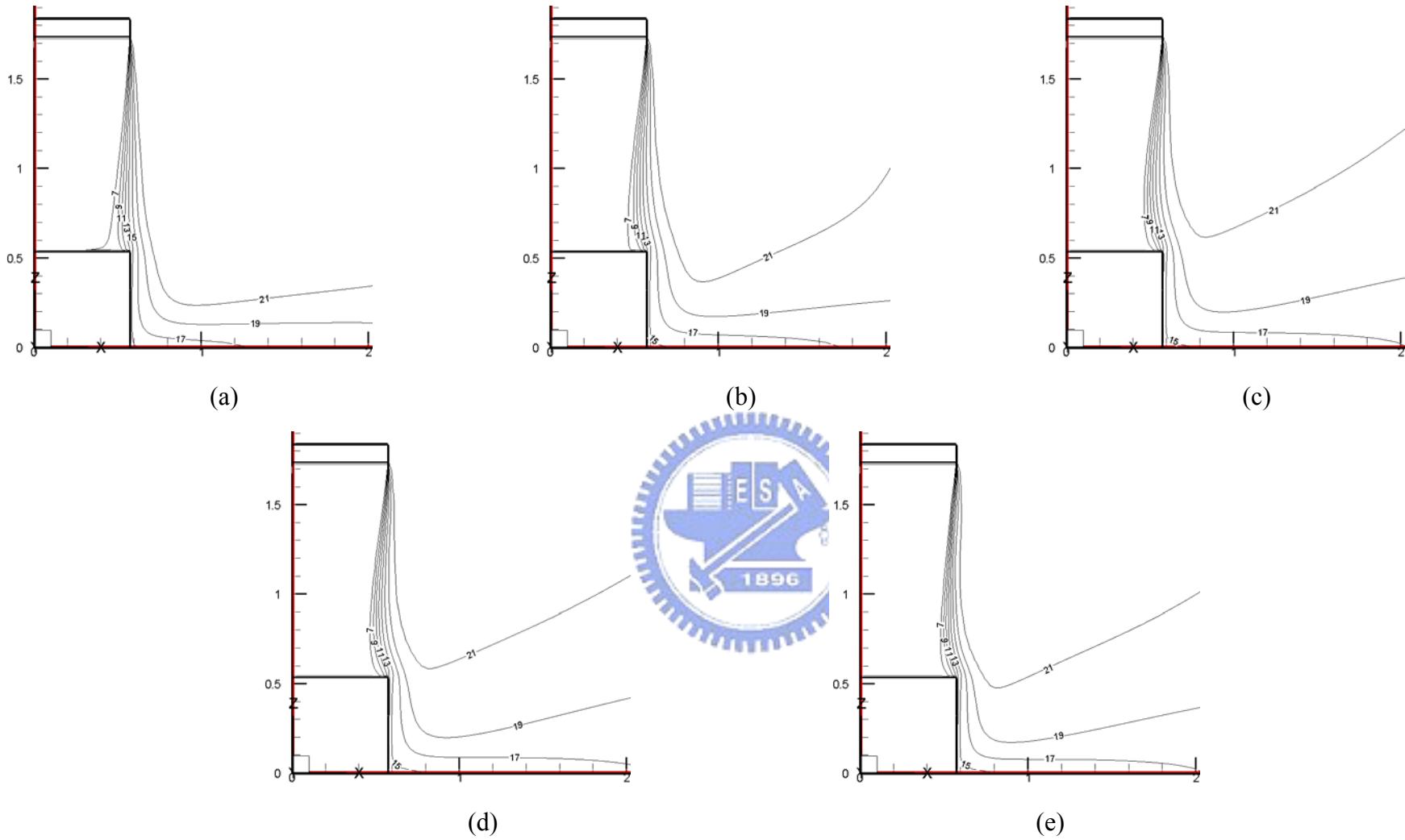


Fig. 4.119 Isotherms for steady cavity flow for a double air curtain design with $b_i = 0.04$ m, $b_o = 0.03$ m, $Gr_t = 4.61 \times 10^9$ ($\Delta T = 20^\circ\text{C}$), and $N = 6.37 \times 10^{-2}$ for (a) $Re_{ci} = 1,910$ and $Re_{co} = 7,638$, (b) $Re_{ci} = 3,183$ and $Re_{co} = 6,365$, (c) $Re_{ci} = 5,092$ and $Re_{co} = 4,456$, (d) $Re_{ci} = 6,365$ and $Re_{co} = 3,183$, (e) $Re_{ci} = 7,638$ and $Re_{co} = 1,910$.

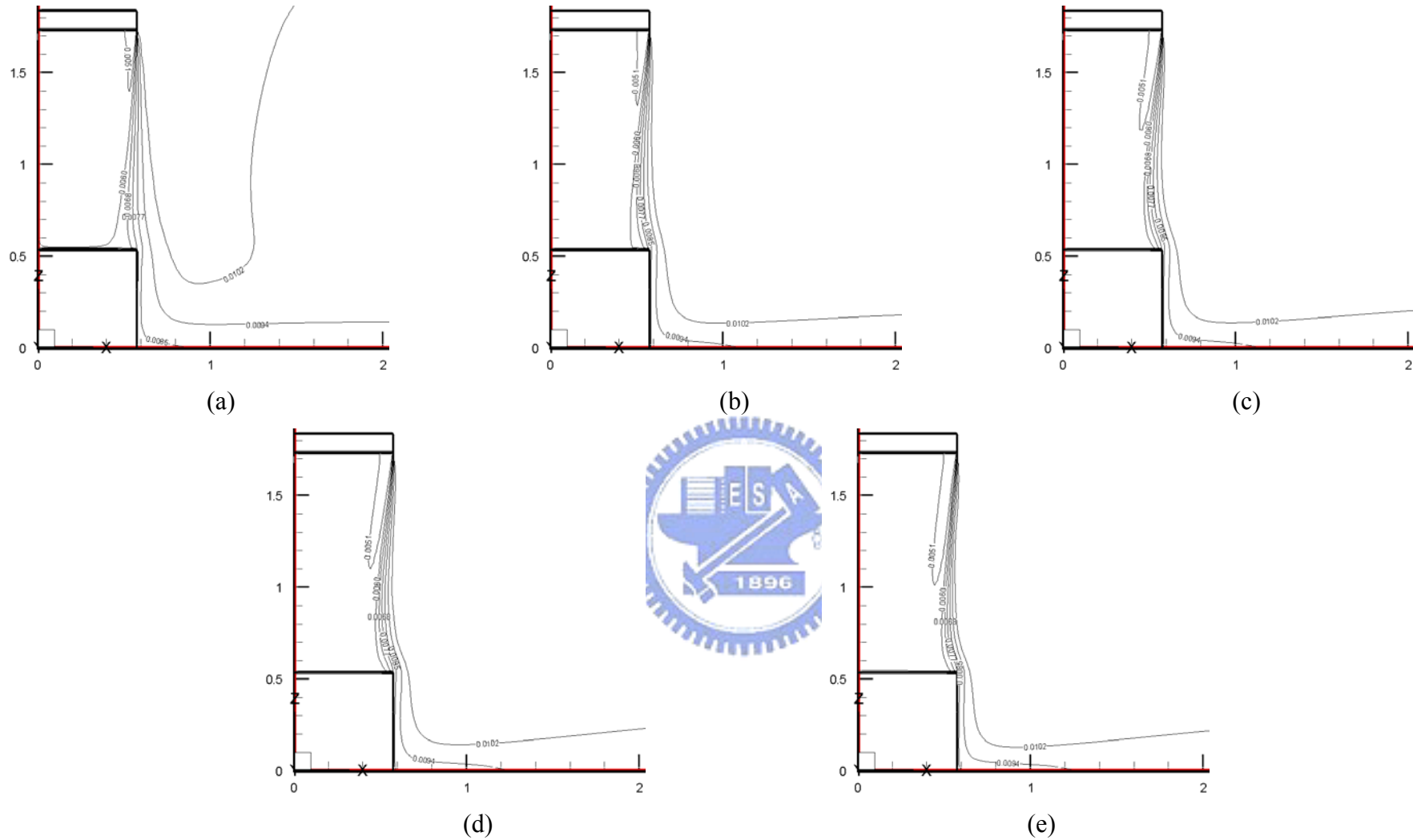


Fig. 4.120 Iso-concentration lines for steady cavity flow for a double air curtain design with $b_i = 0.04$ m, $b_o = 0.03$ m, $Gr_t = 4.61 \times 10^9$ ($\Delta T = 20^\circ\text{C}$), and $N = 6.37 \times 10^{-2}$ for (a) $Re_{ci} = 1,910$ and $Re_{co} = 7,638$, (b) $Re_{ci} = 3,183$ and $Re_{co} = 6,365$, (c) $Re_{ci} = 5,092$ and $Re_{co} = 4,456$, (d) $Re_{ci} = 6,365$ and $Re_{co} = 3,183$, (e) $Re_{ci} = 7,638$ and $Re_{co} = 1,910$.

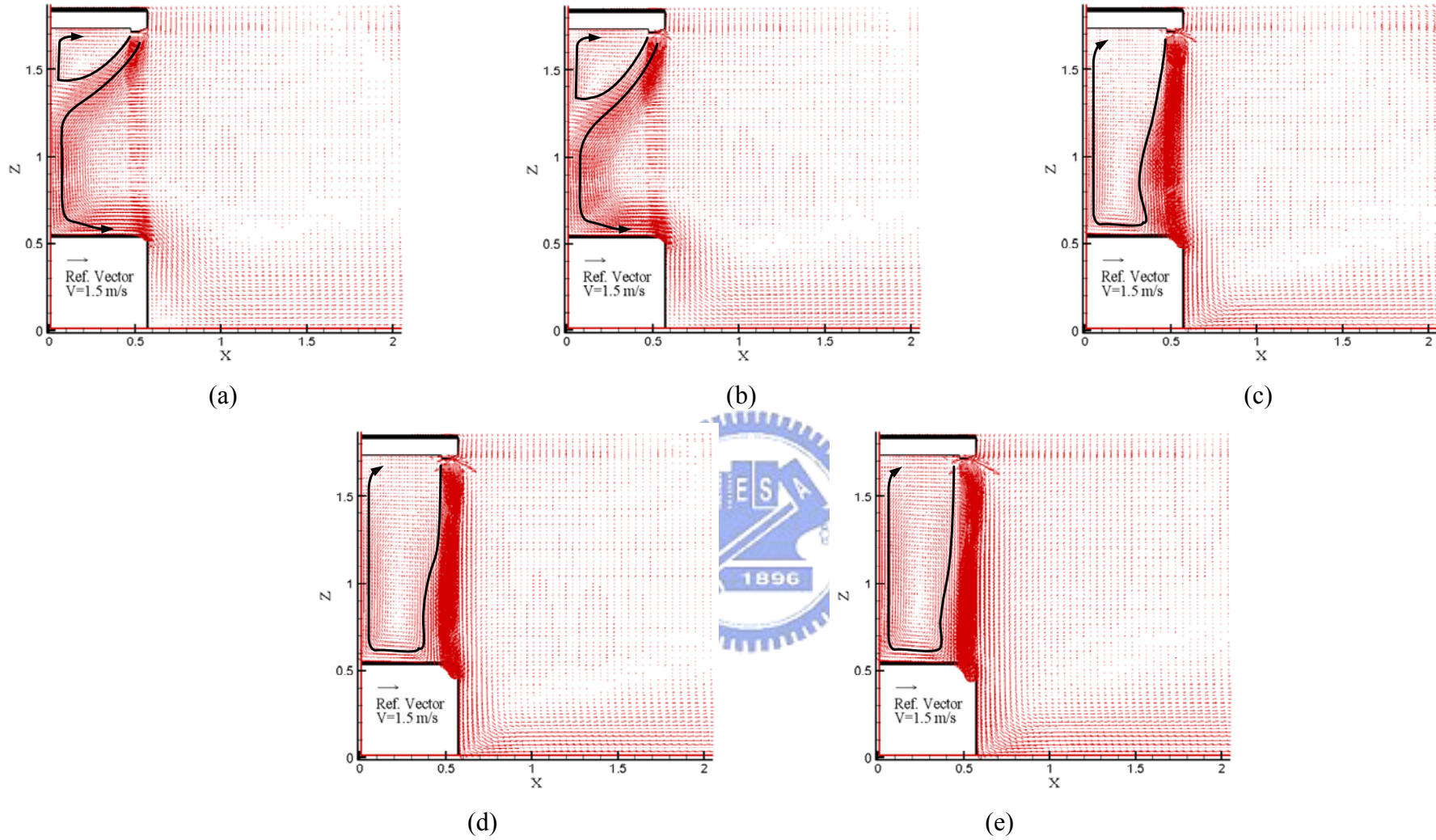


Fig. 4.121 Velocity vector maps for steady cavity flow for a double air curtain design with $b_i = 0.05$ m, and $b_o = 0.05$ m, $Gr_t = 4.61 \times 10^9$ ($\Delta T = 20^\circ C$), and $N = 6.37 \times 10^{-2}$ with a outer curtain inclined angle of 25° for $Re_{ci} = 1,910$ and $Re_{co} =$ (a) 1,910, (b) 3,183, (c) 5,092, (d) 6,365 and (e) 7,638.

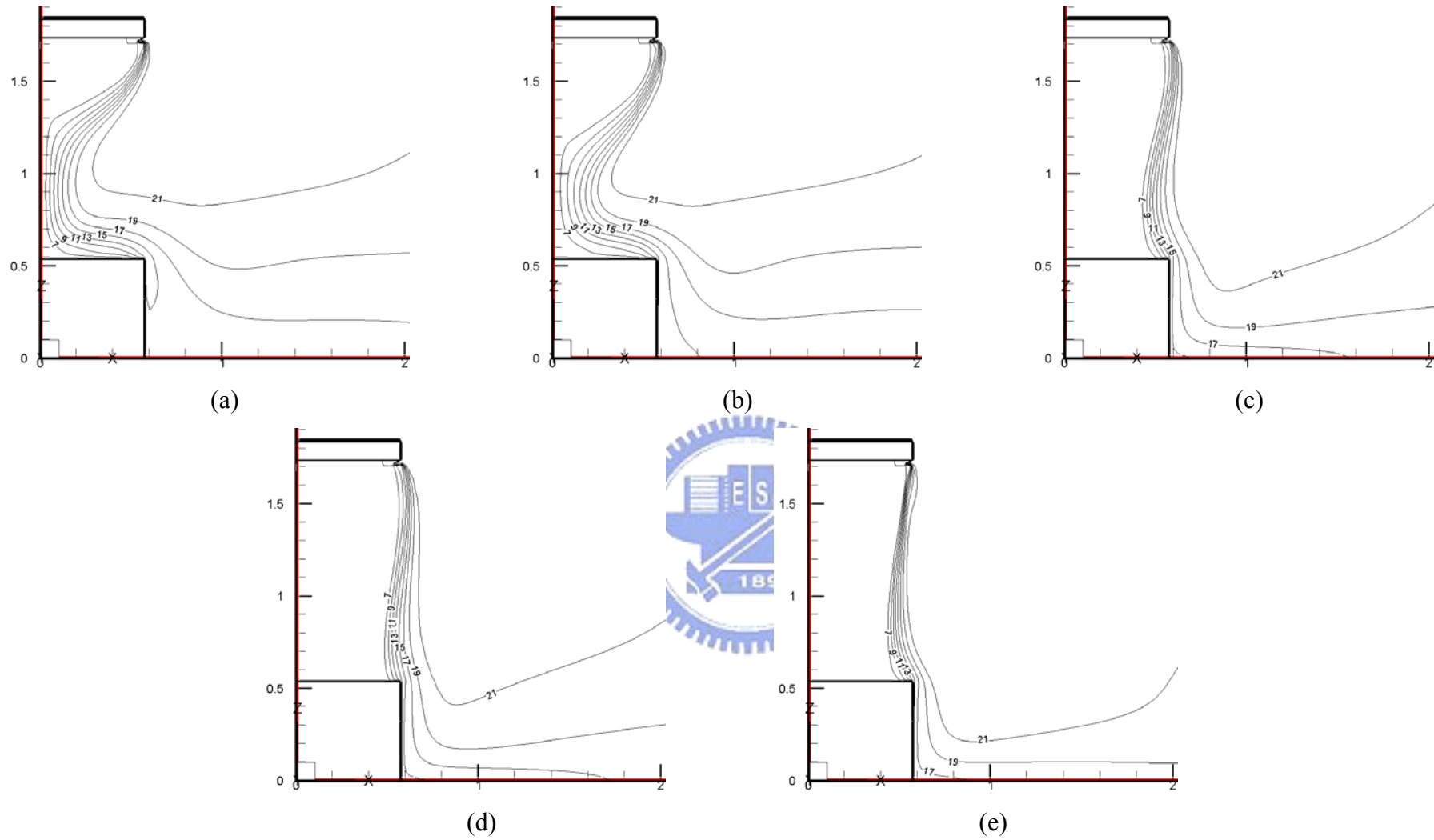


Fig. 4.122 Isotherms for steady cavity flow for a double air curtain design with $b_i = 0.05$ m, and $b_o = 0.05$ m, $Gr_t = 4.61 \times 10^9$ ($\Delta T = 20$ °C), and $N = 6.37 \times 10^{-2}$ with a outer curtain inclined angle of 25° for $Re_{ci} = 1,910$ and $Re_{co} =$ (a) 1,910, (b) 3,183, (c) 5,092, (d) 6,365 and (e) 7,638.

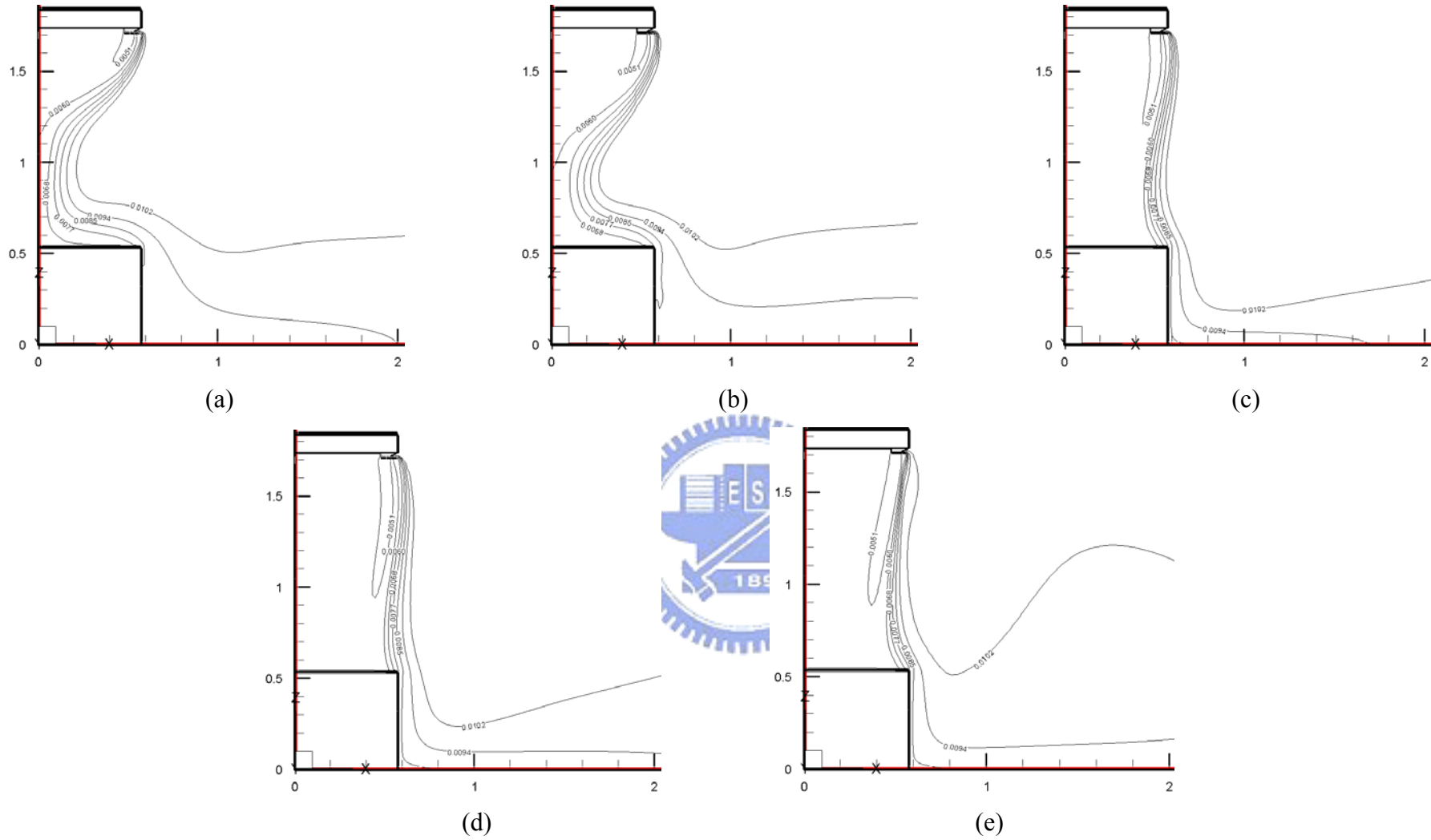


Fig. 4.123 Iso-concentration lines for steady cavity flow for a double air curtain design with $b_i = 0.05$ m, and $b_o = 0.05$ m, $Gr_t = 4.61 \times 10^9$ ($\Delta T = 20^\circ C$), and $N = 6.37 \times 10^{-2}$ with a outer curtain inclined angle of 25° for $Re_{ci} = 3,183$ and $Re_{co} =$ (a) 1,910, (b) 3,183, (c) 5,092, (d) 6,365 and (e) 7,638.

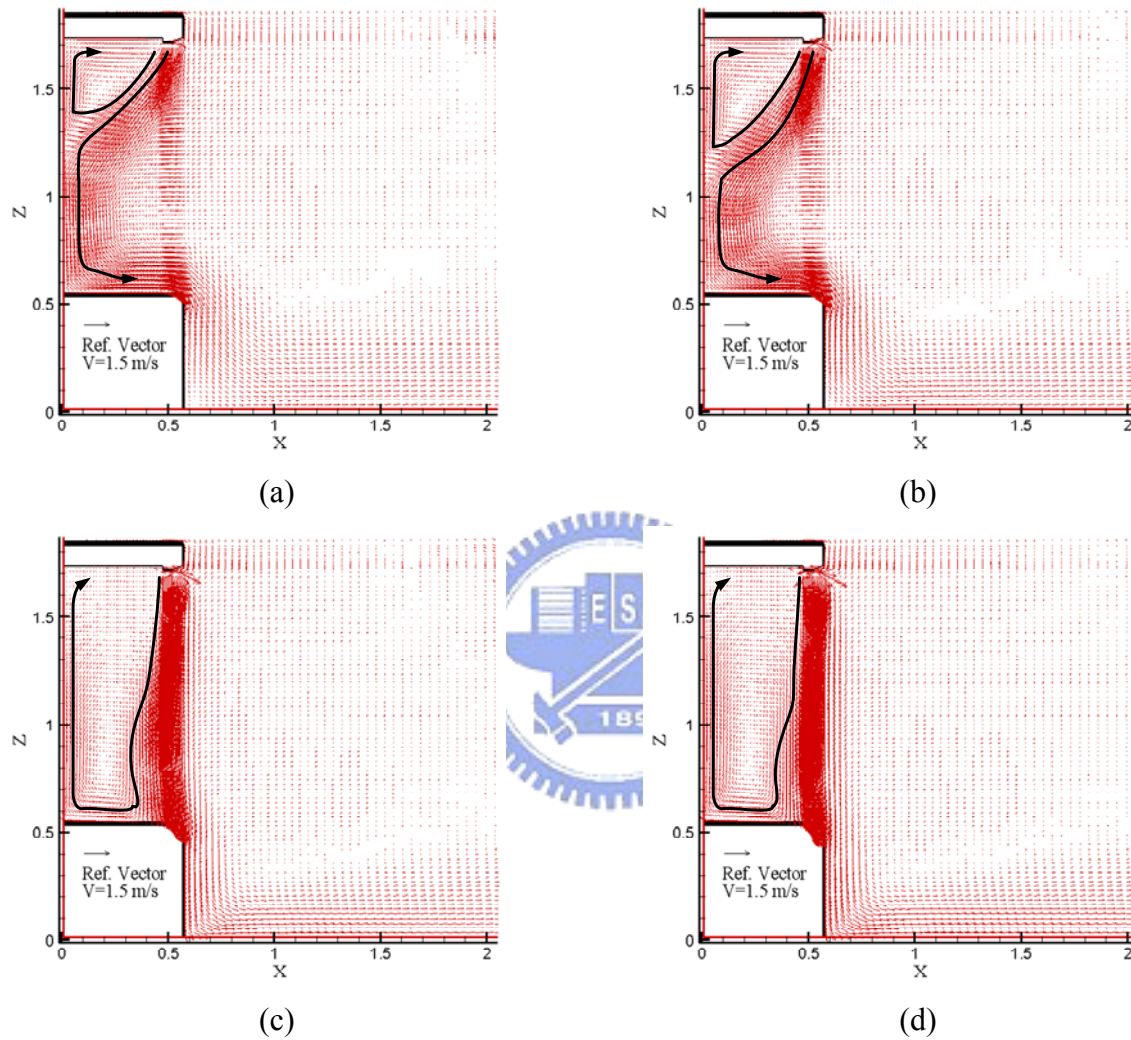


Fig. 4.124 Velocity vector maps for steady cavity flow for a double air curtain design with $b_i = 0.05$ m, and $b_o = 0.05$ m, $Gr_t = 4.61 \times 10^9$ ($\Delta T = 20^\circ\text{C}$), and $N = 6.37 \times 10^{-2}$ with a outer curtain inclined angle of 25° for $Re_{ci} = 3,183$ and $Re_{co} =$ (a) 1,910, (b) 3,183, (c) 5,092, and (d) 6,365.

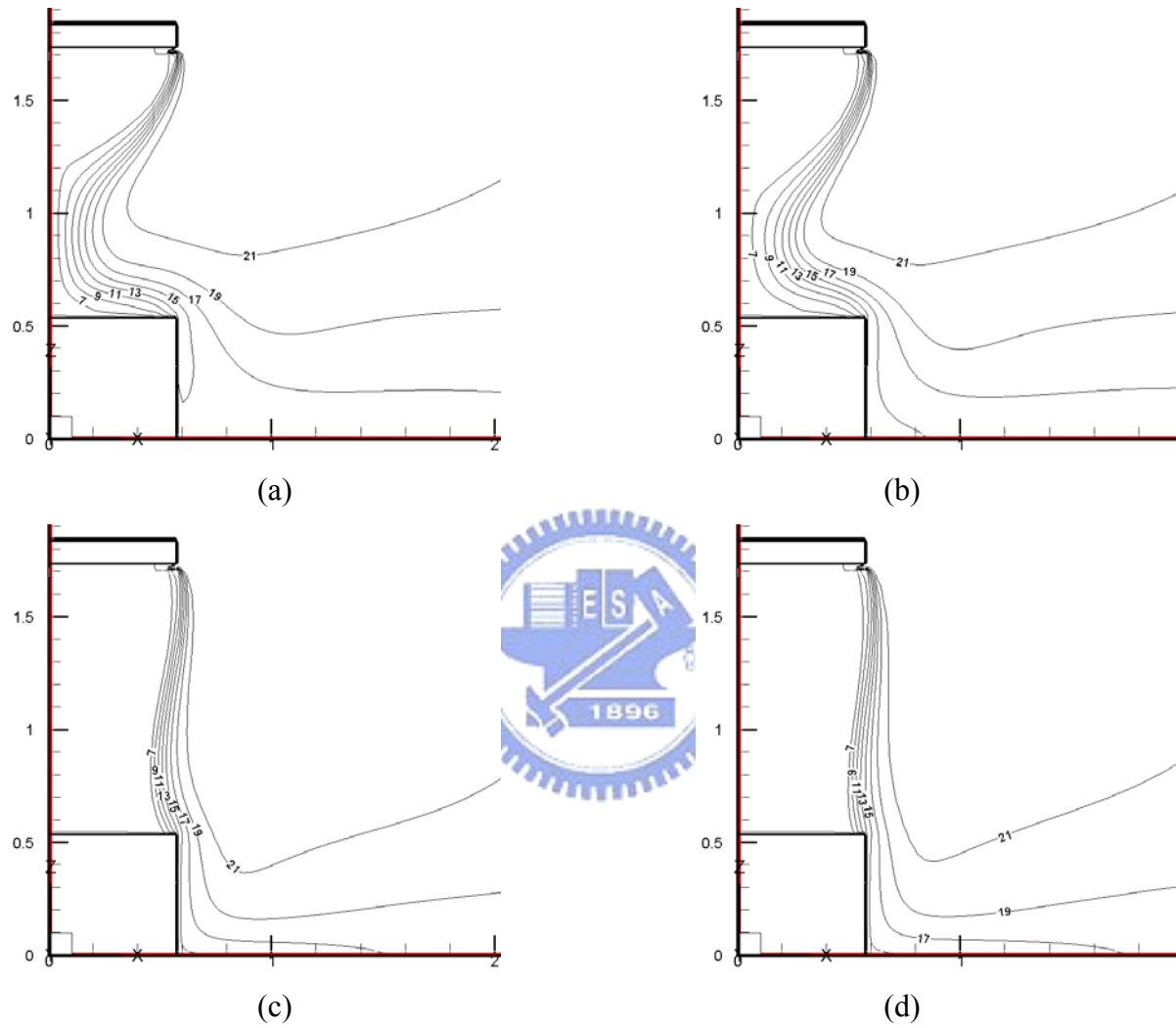


Fig. 4.125 Isotherms for steady cavity flow for a double air curtain design with $b_i = 0.05$ m, and $b_o = 0.05$ m, $Gr_t = 4.61 \times 10^9$ ($\Delta T = 20$ °C), and $N = 6.37 \times 10^{-2}$ with a outer curtain inclined angle of 25° for $Re_{ci} = 3,183$ and $Re_{co} =$ (a) 1,910, (b) 3,183, (c) 5,092, and (d) 6,365.

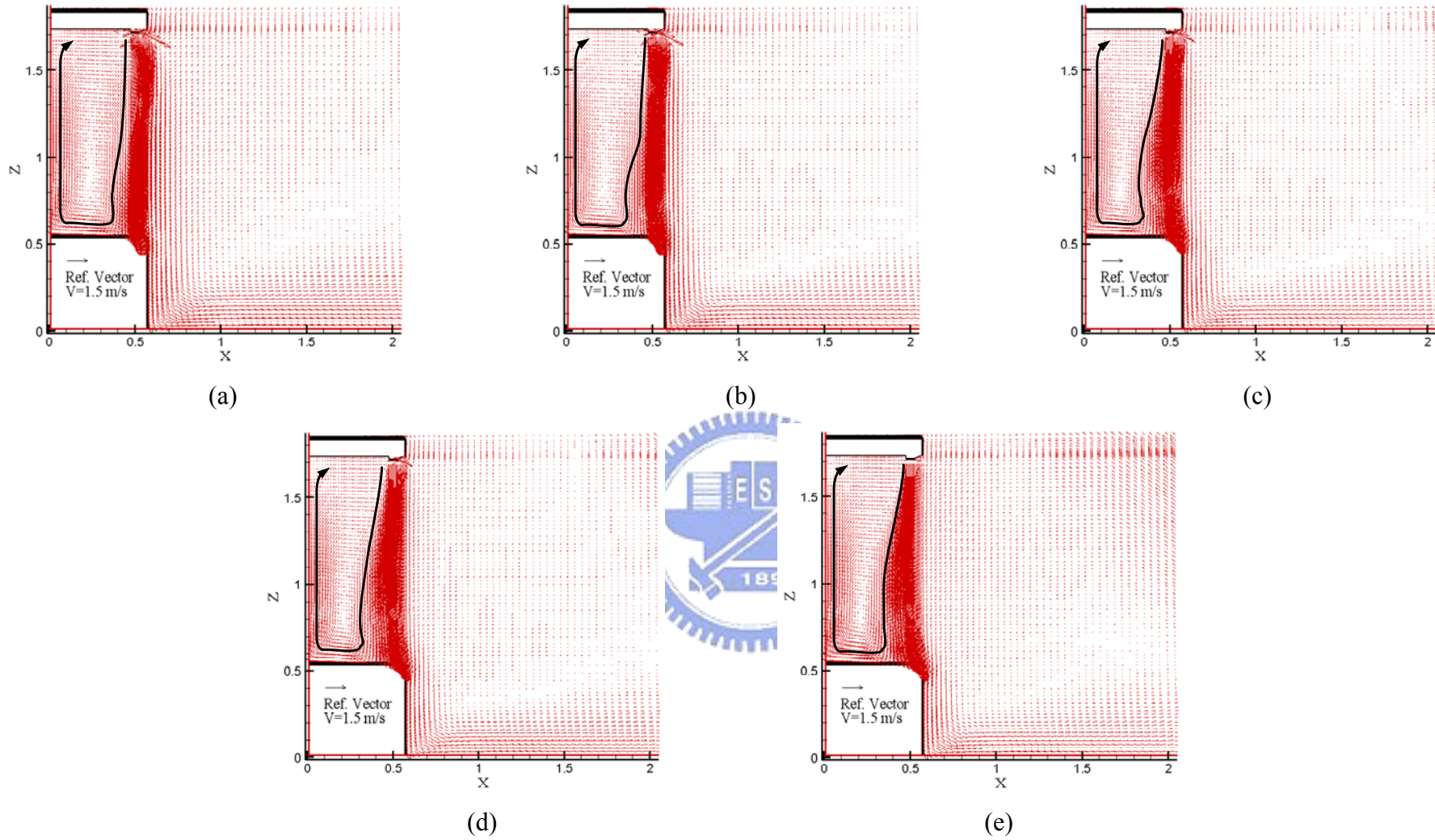


Fig. 4.127 Velocity vector maps for steady cavity flow for a double air curtain design with $b_i = 0.05$ m, and $b_o = 0.05$ m, $Gr_t = 4.61 \times 10^9$ ($\Delta T = 20^\circ\text{C}$), and $N = 6.37 \times 10^{-2}$ with a outer curtain inclined angle of 25° for (a) $Re_{ci} = 1,910$ and $Re_{co} = 7,638$, (b) $Re_{ci} = 3,183$ and $Re_{co} = 6,365$, (c) $Re_{ci} = 5,092$ and $Re_{co} = 4,456$, (d) $Re_{ci} = 6,365$ and $Re_{co} = 3,183$, (e) $Re_{ci} = 7,638$ and $Re_{co} = 1,910$.

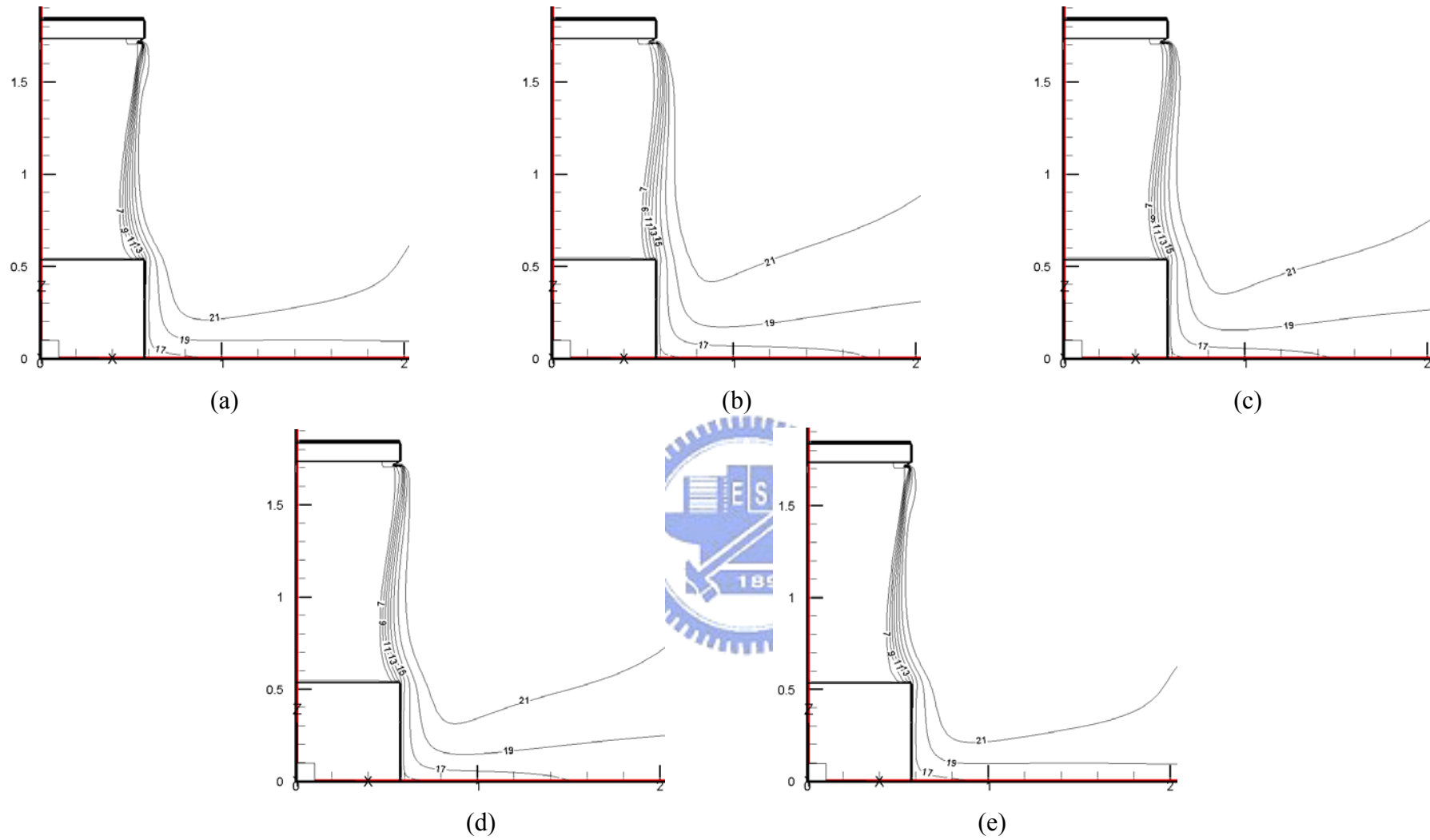


Fig. 4.128 Isotherms for steady cavity flow for a double air curtain design with $b_i = 0.05$ m, and $b_o = 0.05$ m, $Gr_t = 4.61 \times 10^9$ ($\Delta T = 20$ °C), and $N = 6.37 \times 10^{-2}$ with a outer curtain inclined angle of 25° for (a) $Re_{ci} = 1,910$ and $Re_{co} = 7,638$, (b) $Re_{ci} = 3,183$ and $Re_{co} = 6,365$, (c) $Re_{ci} = 5,092$ and $Re_{co} = 4,456$, (d) $Re_{ci} = 6,365$ and $Re_{co} = 3,183$, (e) $Re_{ci} = 7,638$ and $Re_{co} = 1,910$.

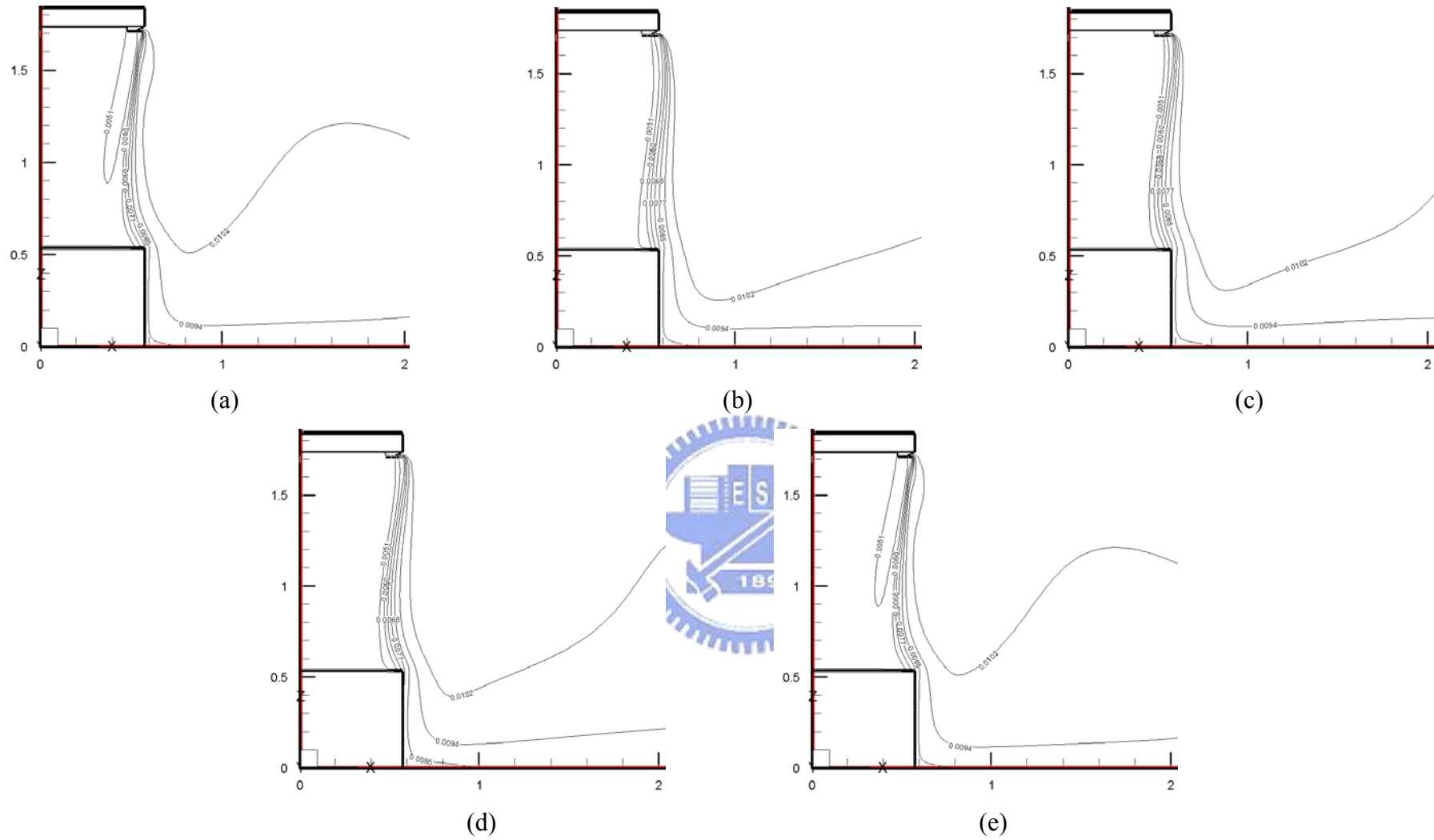


Fig. 4.129 Iso-concentration lines for steady cavity flow for a double air curtain design with $b_i = 0.05$ m, and $b_o = 0.05$ m, $Gr_t = 4.61 \times 10^9$ ($\Delta T = 20^\circ\text{C}$), and $N = 6.37 \times 10^{-2}$ with a outer curtain inclined angle of 25° for (a) $Re_{ci} = 1,910$ and $Re_{co} = 7,638$, (b) $Re_{ci} = 3,183$ and $Re_{co} = 6,365$, (c) $Re_{ci} = 5,092$ and $Re_{co} = 4,456$, (d) $Re_{ci} = 6,365$ and $Re_{co} = 3,183$, (e) $Re_{ci} = 7,638$ and $Re_{co} = 1,910$.

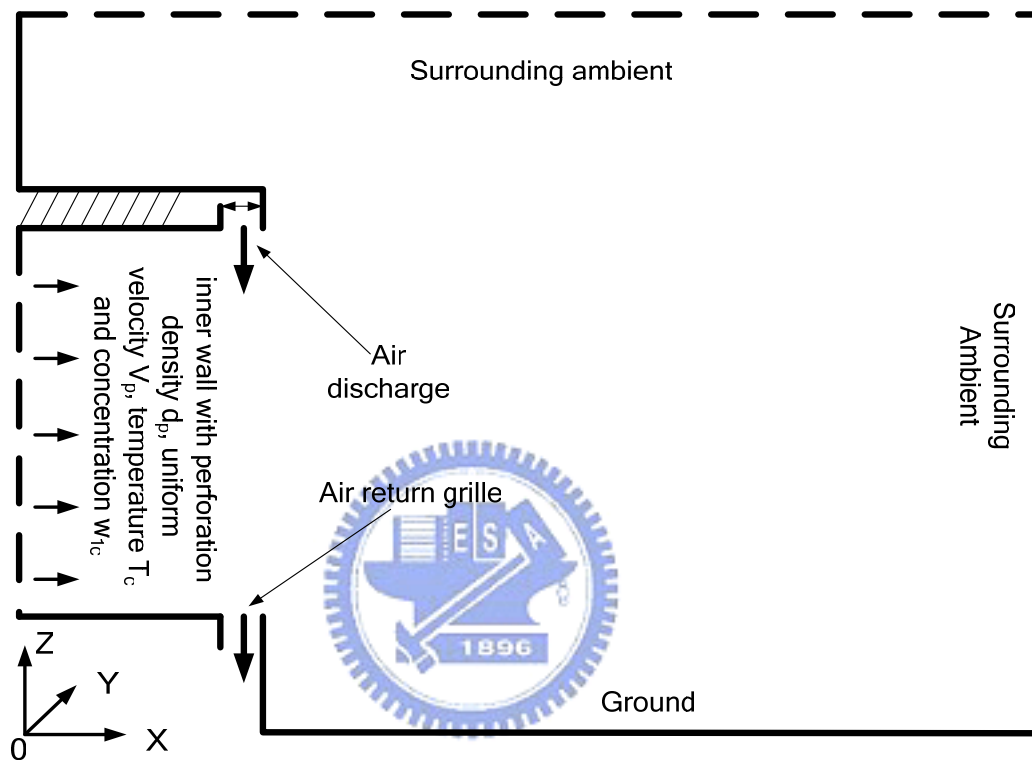


Fig. 4.130 Schematic diagram of an open vertical cavity with back panel perforation.

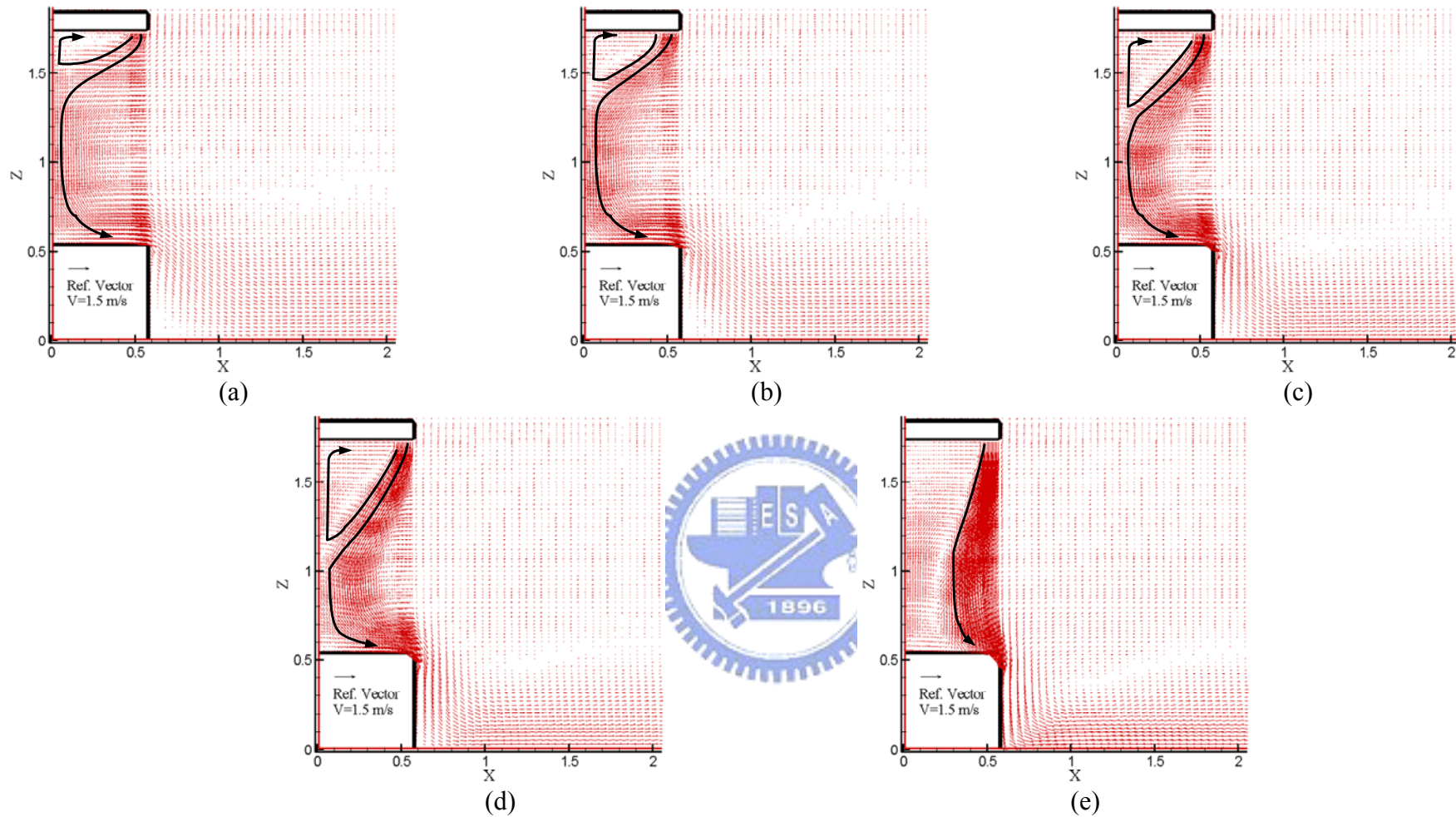


Fig. 4.131 Velocity vector maps for steady cavity flow for a single air curtain design with perforation density of 35% for $b_j = 0.1$ m, $Gr_t = 4.61 \times 10^9$ ($\Delta T = 20^\circ\text{C}$), and $N = 6.37 \times 10^{-2}$ for $Re_p = 1,910$ and $Re_b =$ (a) 1,910, (b) 3,183, (c) 5,092, (d) 6,365, and (e) 9,548.

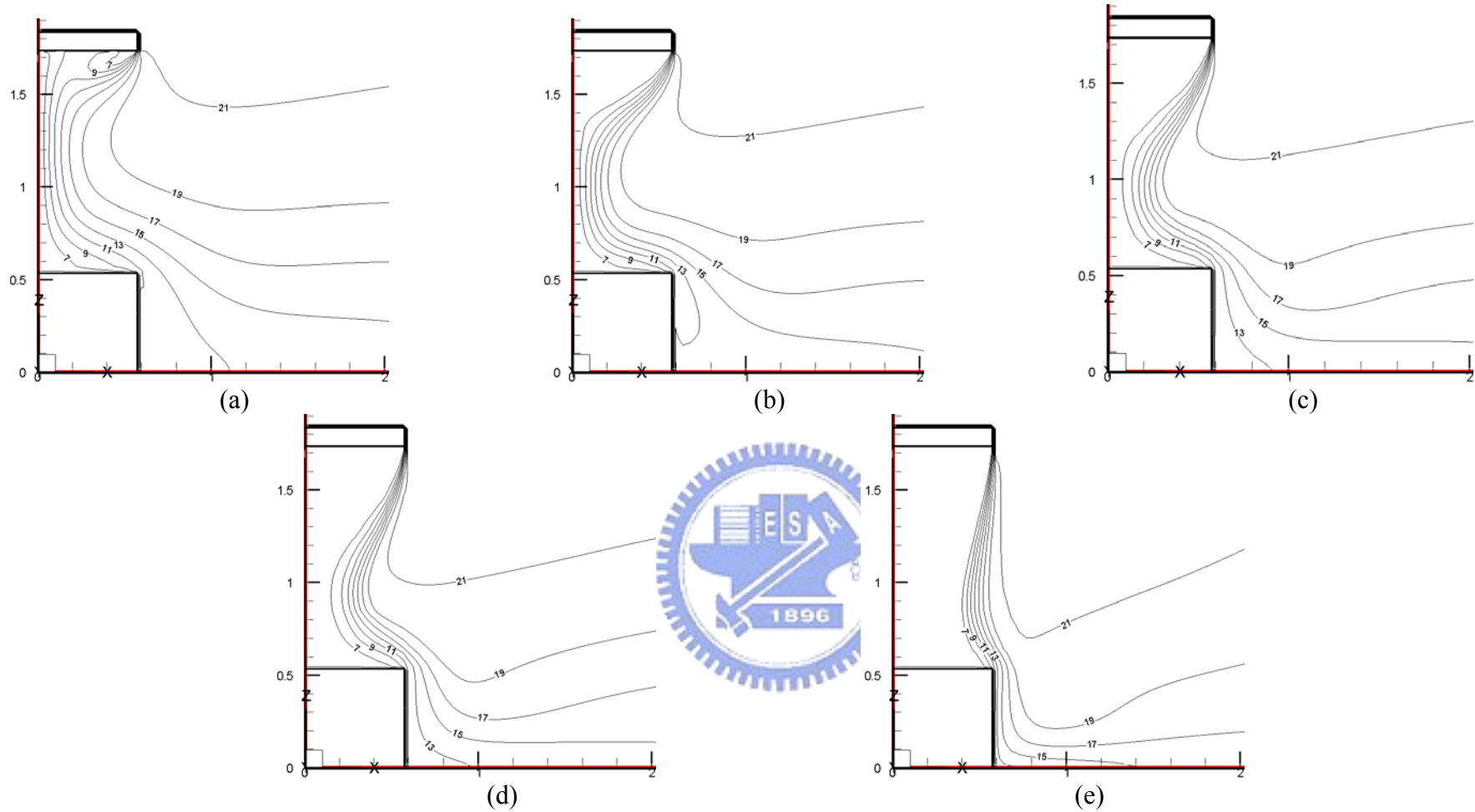


Fig. 4.132 Isotherms for steady cavity flow for a single air curtain design with perforation density of 35% for $b_j = 0.1$ m, $Gr_t = 4.61 \times 10^9$ ($\Delta T = 20^\circ\text{C}$), and $N = 6.37 \times 10^{-2}$ for $Re_p = 1,910$ and $Re_b =$ (a) 1,910, (b) 3,183, (c) 5,092, (d) 6,365, and (e) 9,548.

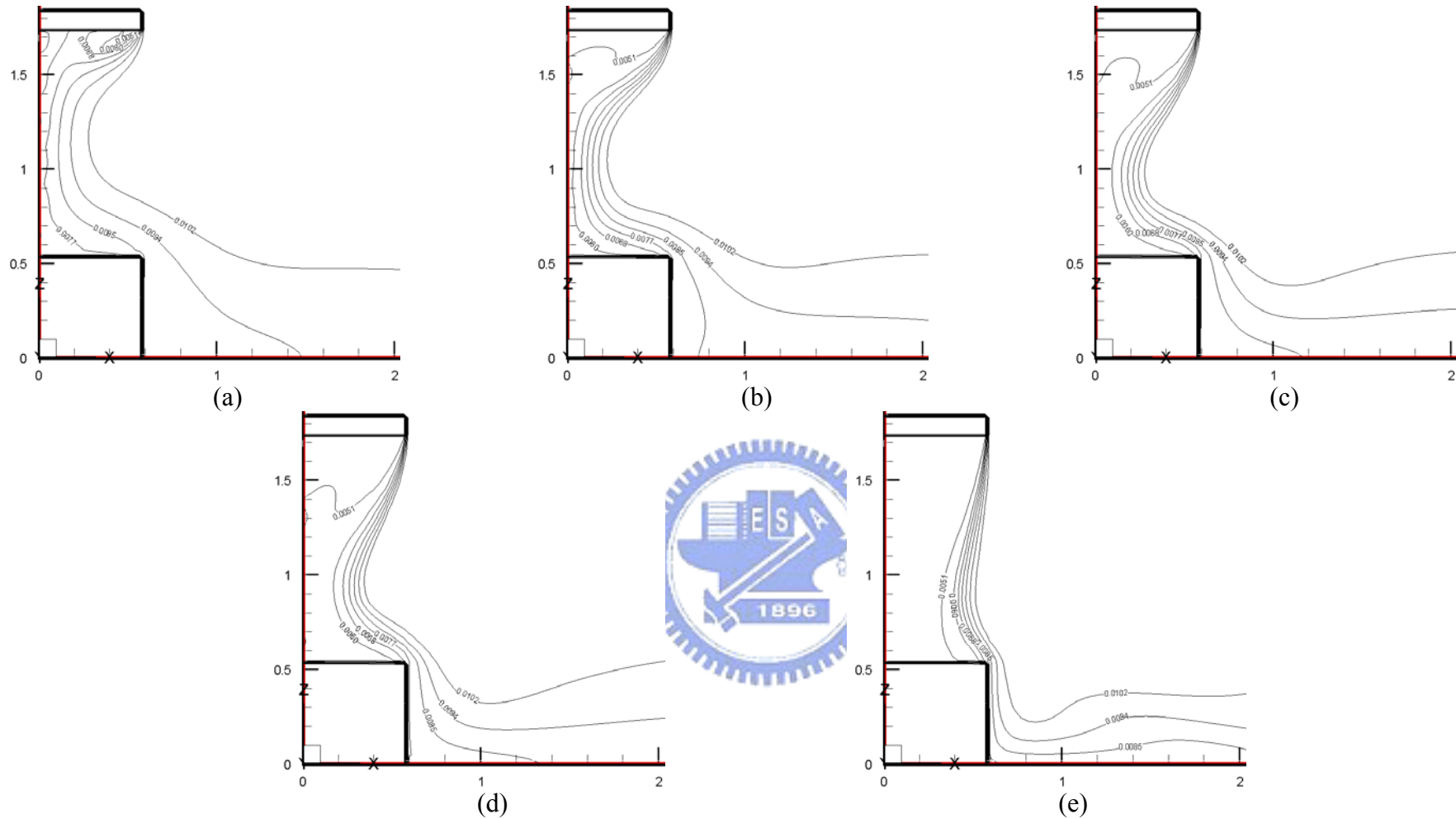


Fig. 4.133 Iso-concentration lines for steady cavity flow for a single air curtain design with perforation density of 35% for $b_j = 0.1$ m, $Gr_t = 4.61 \times 10^9$ ($\Delta T = 20^\circ\text{C}$), and $N = 6.37 \times 10^{-2}$ for $Re_p = 1,910$ and $Re_b =$ (a) 1,910, (b) 3,183, (c) 5,092, (d) 6,365, and (e) 9,548.

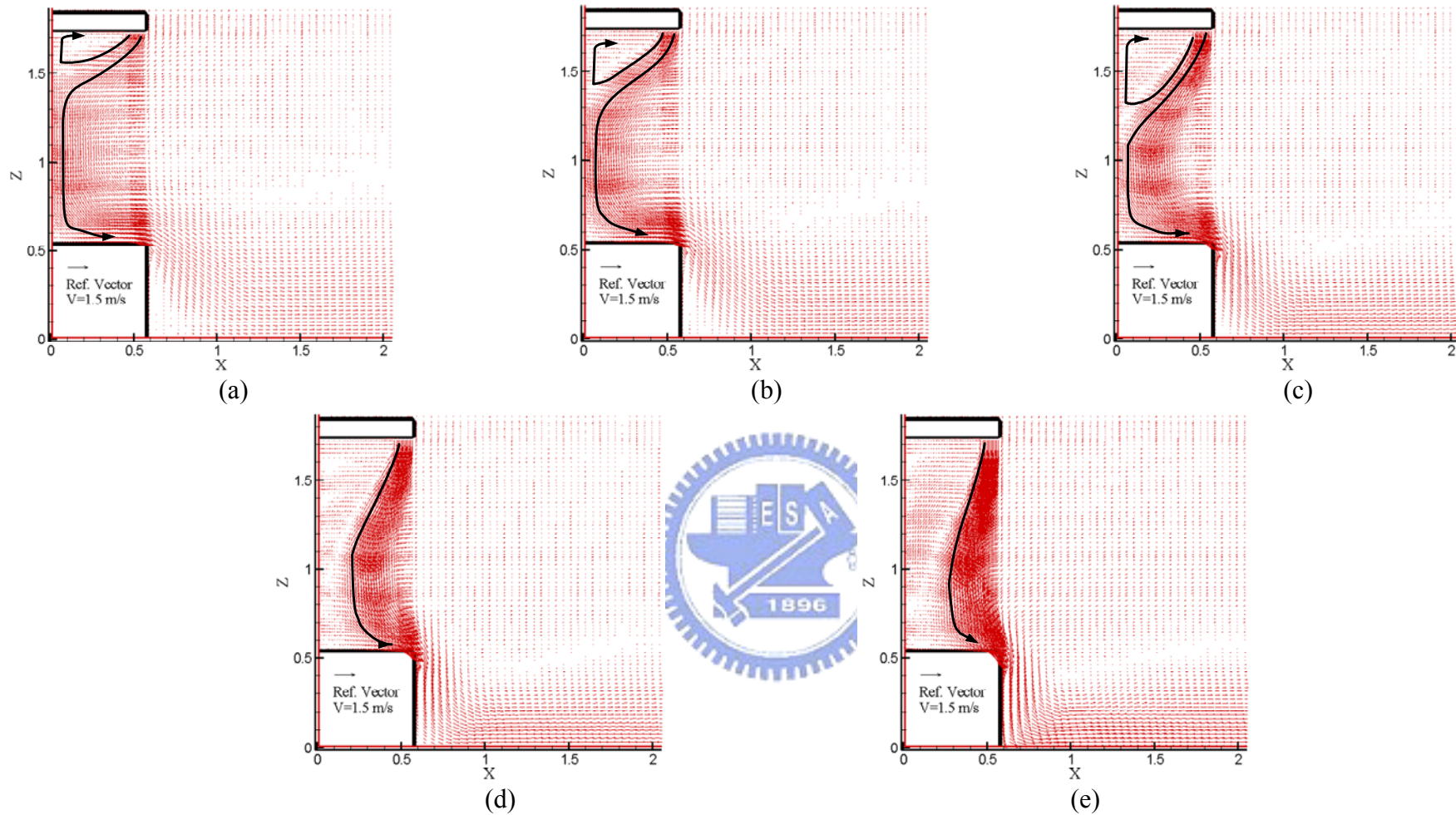


Fig. 4.134 Velocity vector maps for steady cavity flow for a single air curtain design with perforation density of 35% for $b_j = 0.1$ m, $Gr_t = 4.61 \times 10^9$ ($\Delta T = 20^\circ\text{C}$), and $N = 6.37 \times 10^{-2}$ for $Re_p = 3,183$ and $Re_b =$ (a) 1,910, (b) 3,183, (c) 5,092, (d) 6,365, and (e) 9,548.

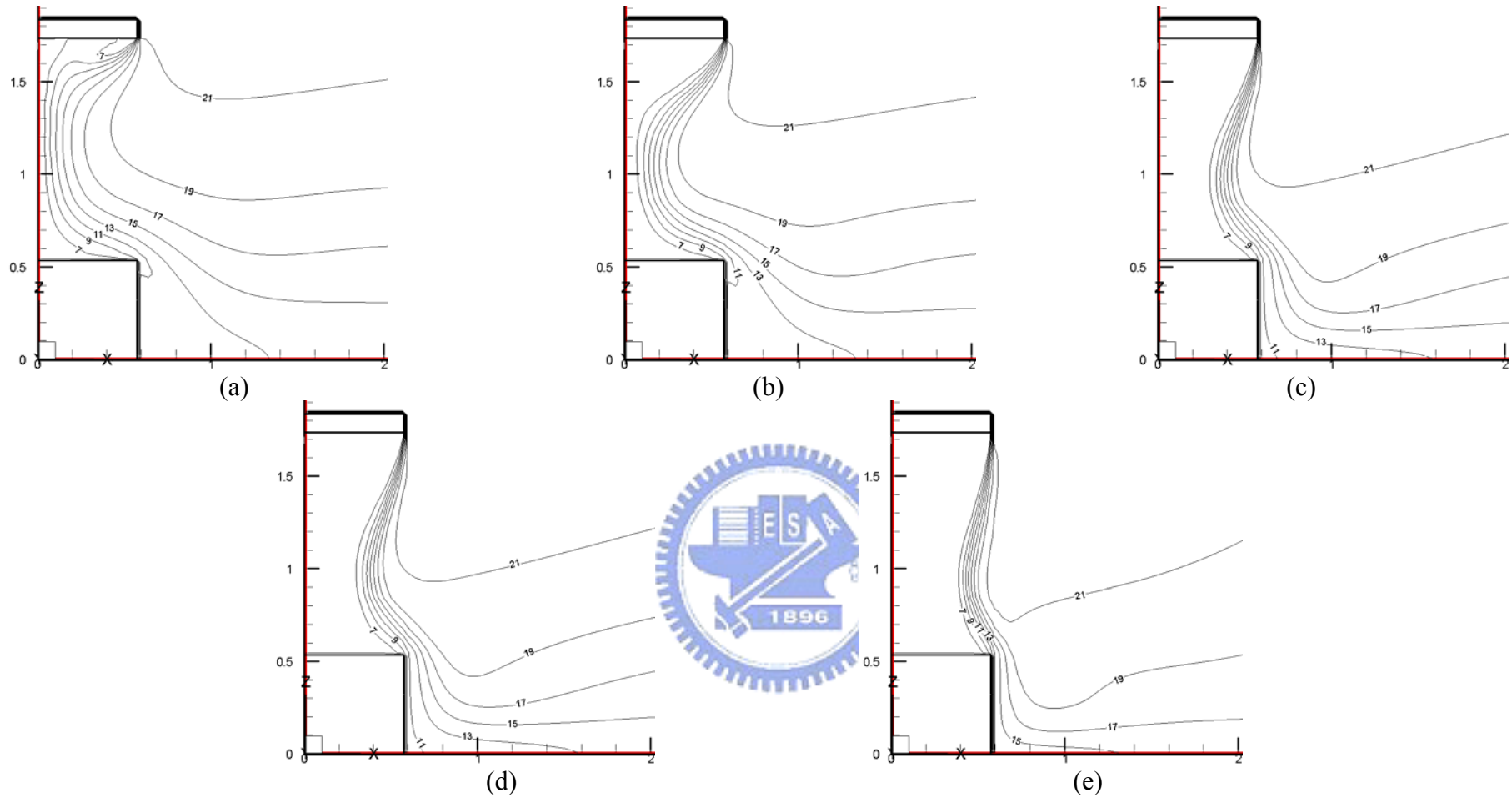


Fig. 4.135 Isotherms for steady cavity flow for a single air curtain design with perforation density of 35% for $b_j = 0.1$ m, $Gr_t = 4.61 \times 10^9$ ($\Delta T = 20^\circ\text{C}$), and $N = 6.37 \times 10^{-2}$ for $Re_p = 3,183$ and $Re_b =$ (a) 1,910 (b) 3,183, (c) 5,092, (d) 6,365, and (e) 9,548.

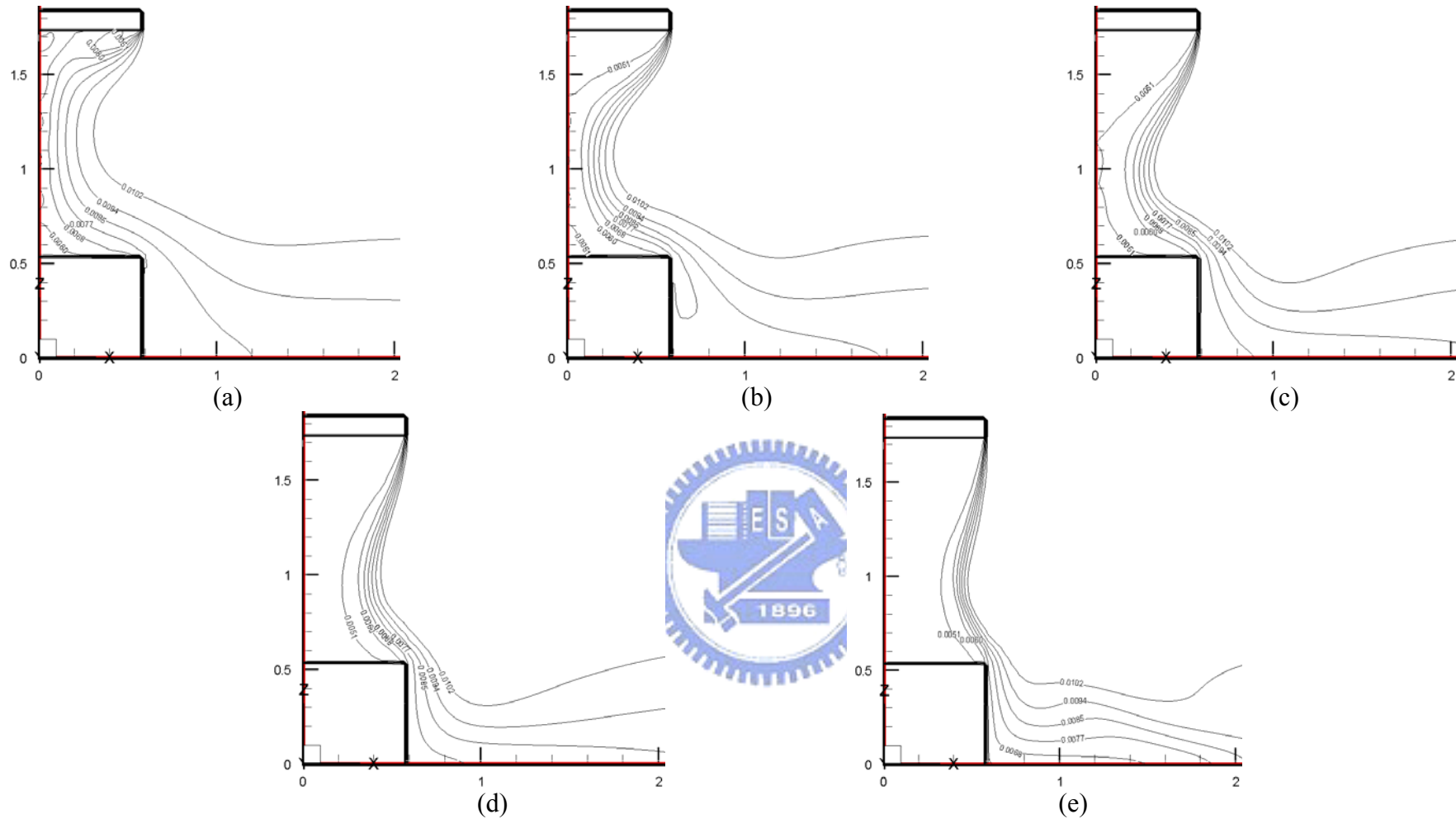


Fig. 4.136 Iso-concentration lines for steady cavity flow for a single air curtain design with perforation density of 35% for $b_j = 0.1$ m, $Gr_t = 4.61 \times 10^9$ ($\Delta T = 20^\circ\text{C}$), and $N = 6.37 \times 10^{-2}$ for $Re_p = 3,183$ and $Re_b =$ (a) 1,910, (b) 3,183, (c) 5,092, (d) 6,365, and (e) 9,548.

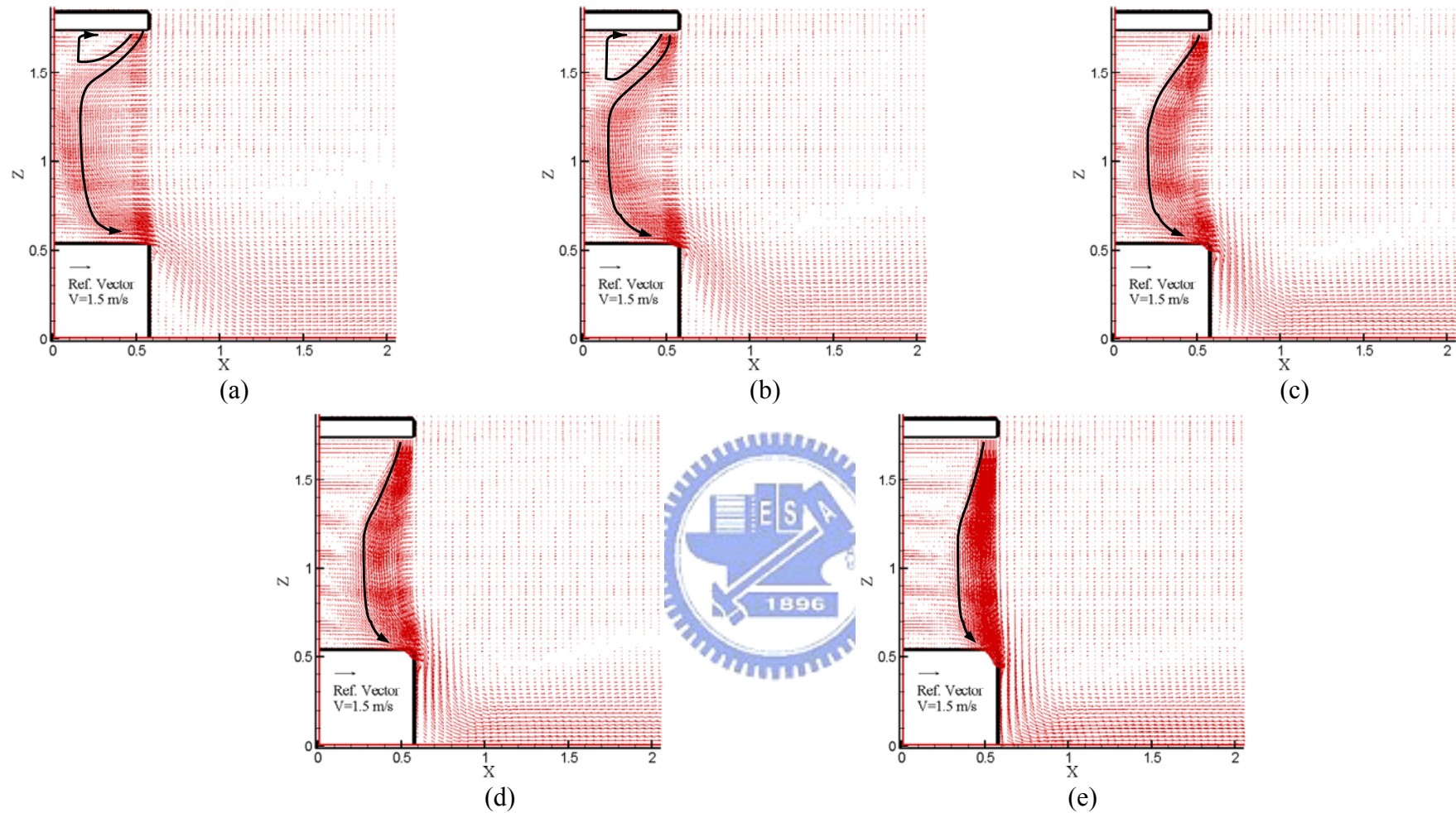


Fig. 4.137 Velocity vector maps for steady cavity flow for a single air curtain design with perforation density of 35% for $b_j = 0.1$ m, $Gr_t = 4.61 \times 10^9$ ($\Delta T = 20^\circ\text{C}$), and $N = 6.37 \times 10^{-2}$ for $Re_p = 5,092$ and $Re_b =$ (a) 1,910, (b) 3,183, (c) 5,092, (d) 6,365, and (e) 9,548.

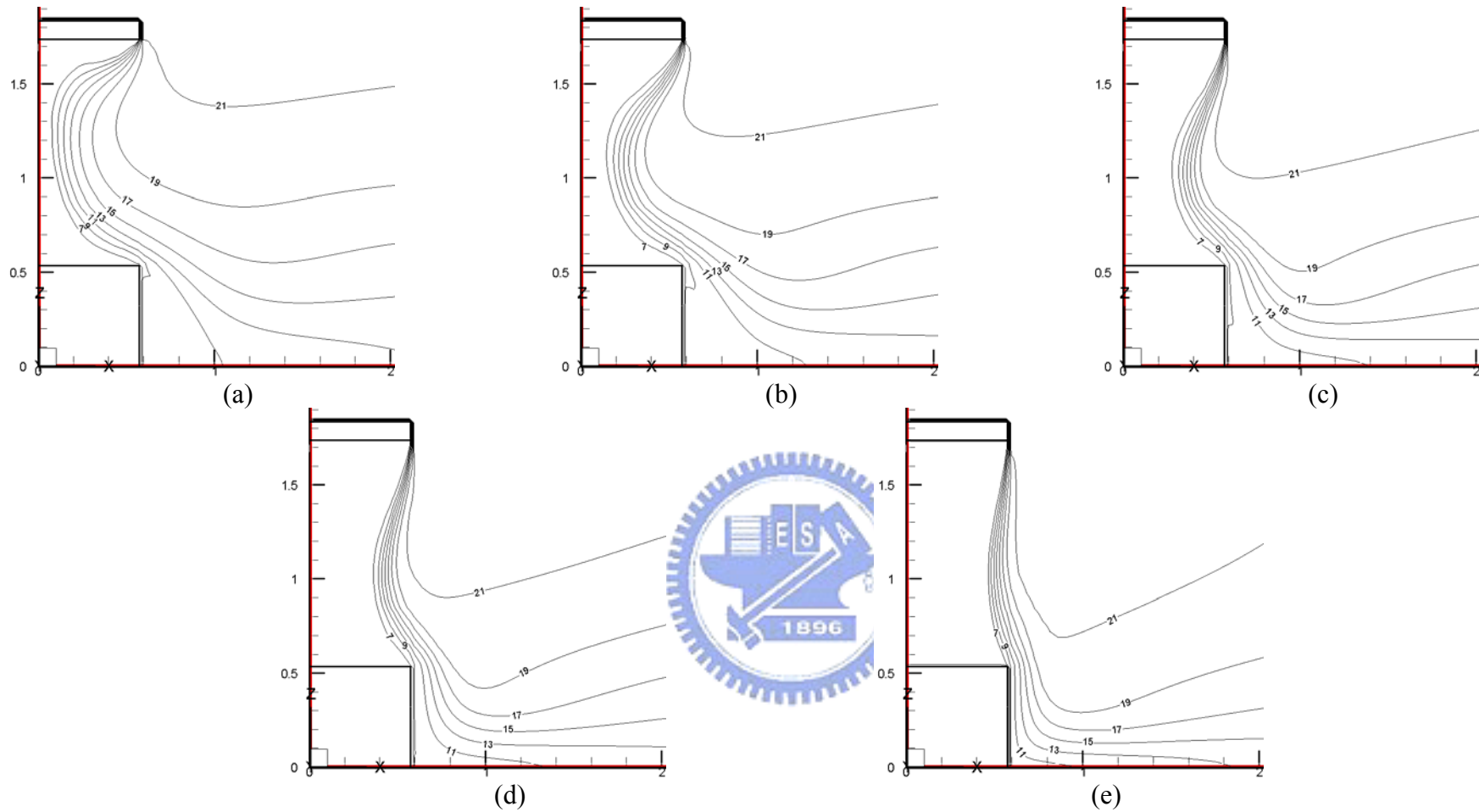


Fig. 4.138 Isotherms for steady cavity flow for a single air curtain design with perforation density of 35% for $b_j = 0.1$ m, $Gr_t = 4.61 \times 10^9$ ($\Delta T = 20^\circ\text{C}$), and $N = 6.37 \times 10^{-2}$ for $Re_p = 5,092$ and $Re_b =$ (a) 1,910 (b) 3,183, (c) 5,092, (d) 6,365, and (e) 9,548.

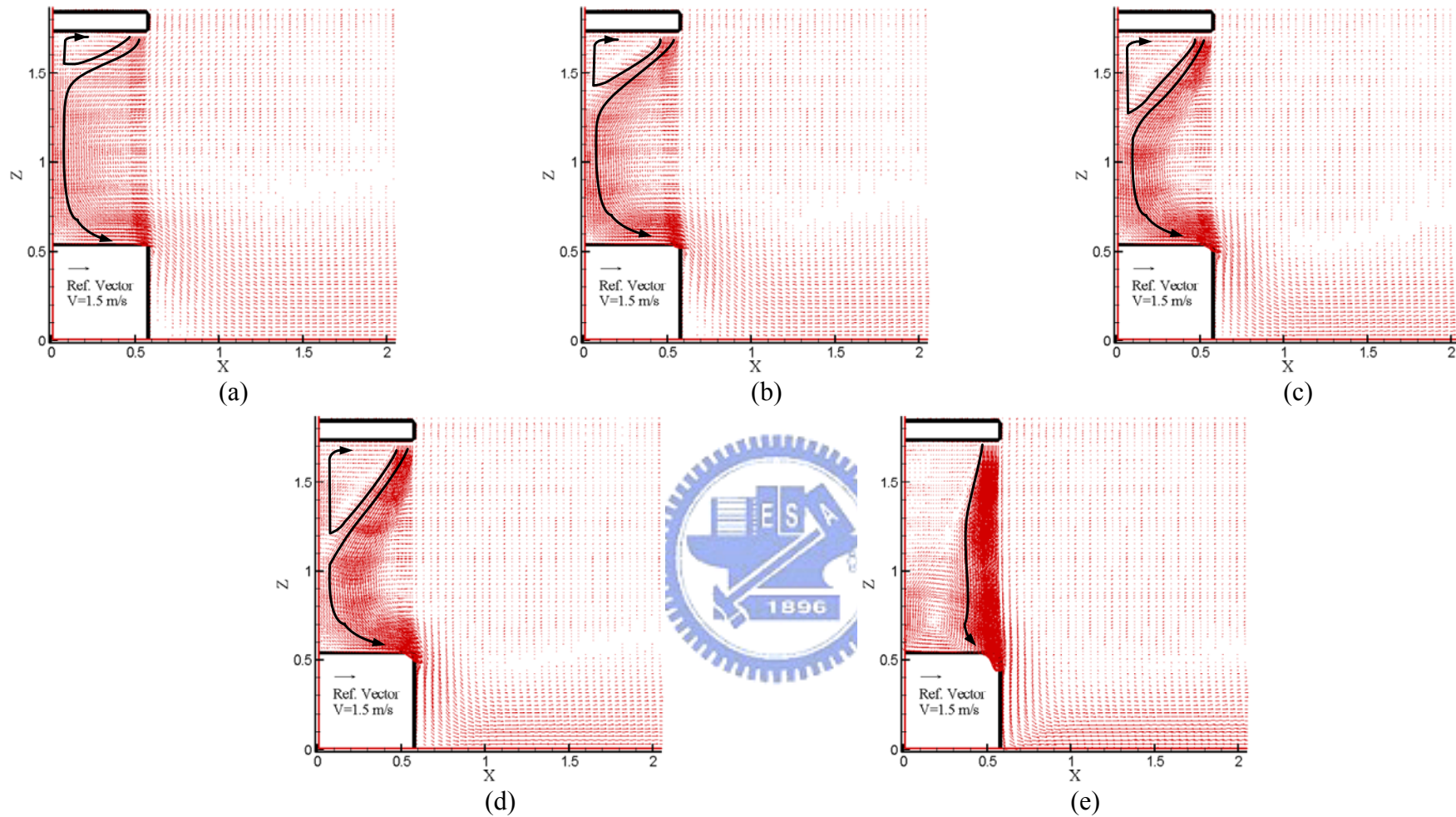


Fig. 4.140 Velocity vector maps for steady cavity flow for a single air curtain design with perforation density of 25% for $b_j = 0.1$ m, $Gr_t = 4.61 \times 10^9$ ($\Delta T = 20^\circ\text{C}$), and $N = 6.37 \times 10^{-2}$ for $Re_p = 1,910$ and $Re_b =$ (a) 1,910, (b) 3,183, (c) 5,092, (d) 6,365, and (e) 9,548.

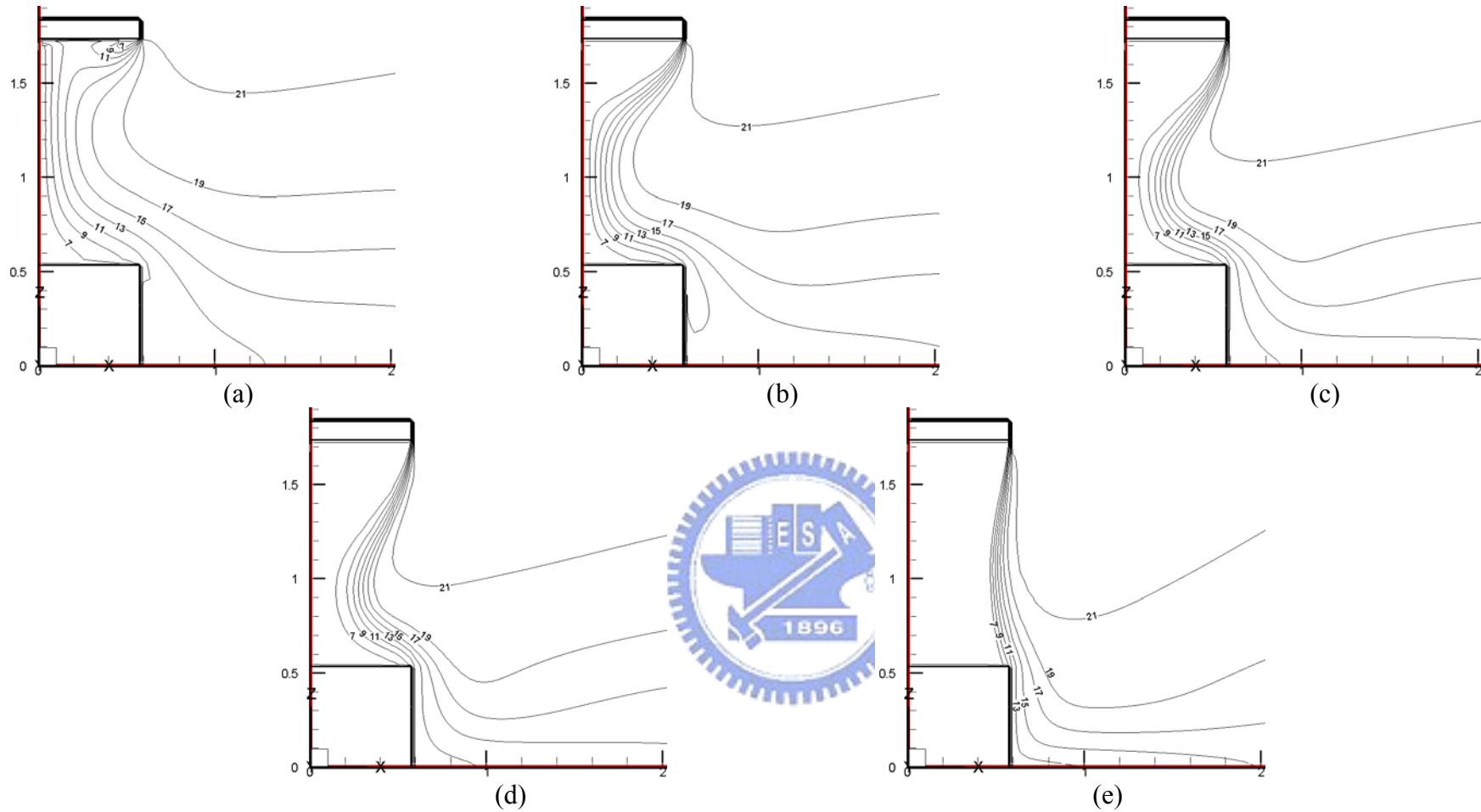


Fig. 4.141 Isotherms for steady cavity flow for a single air curtain design with perforation density of 25% for $b_j = 0.1$ m, $Gr_t = 4.61 \times 10^9$ ($\Delta T = 20^\circ\text{C}$), and $N = 6.37 \times 10^{-2}$ for $Re_p = 1,910$ and $Re_b =$ (a) 1,910, (b) 3,183, (c) 5,092, (d) 6,365, and (e) 9,548.

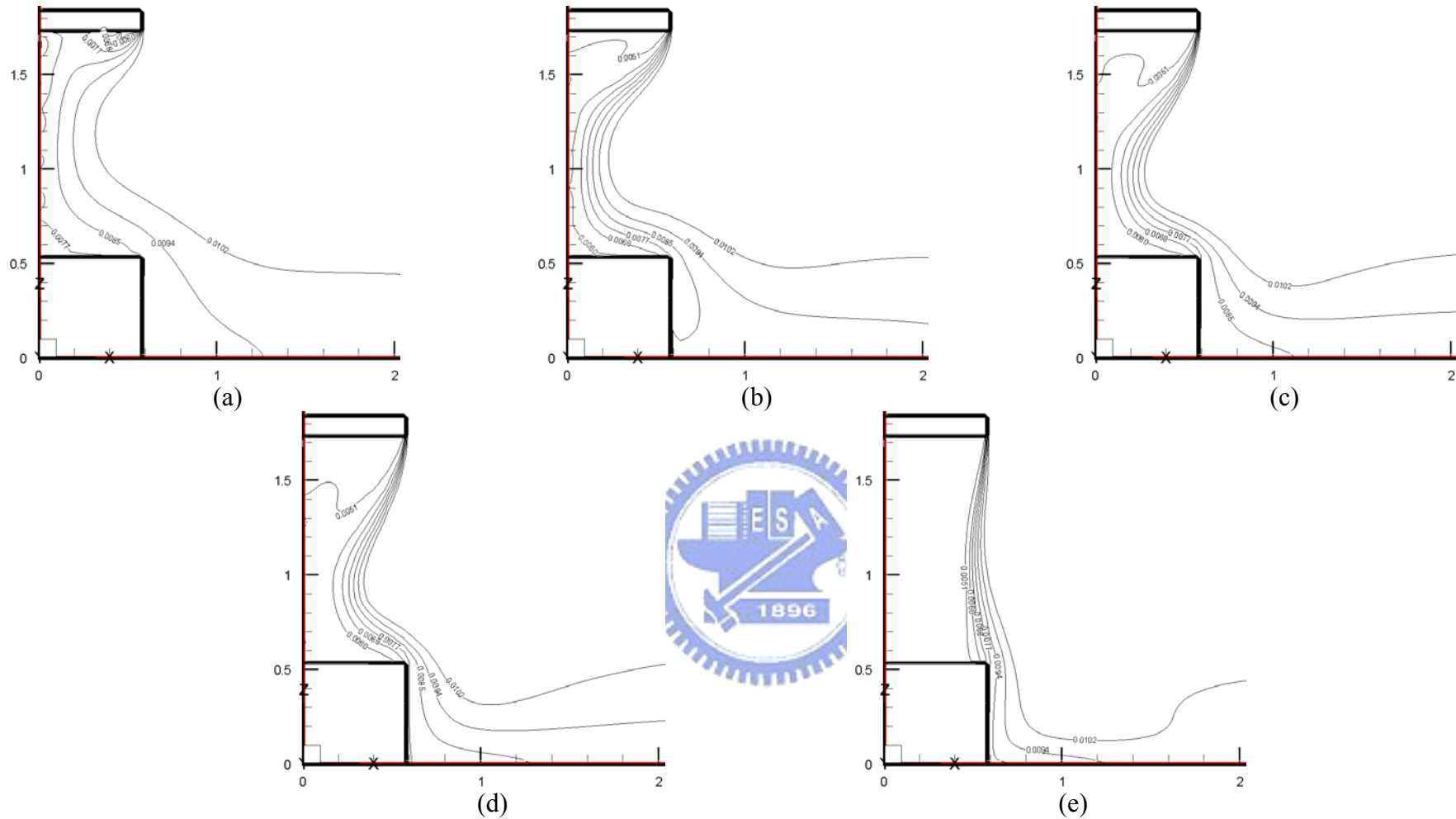


Fig. 4.142 Iso-concentration lines for steady cavity flow for a single air curtain design with perforation density of 25% for $b_j = 0.1$ m, $Gr_t = 4.61 \times 10^9$ ($\Delta T = 20^\circ\text{C}$), and $N = 6.37 \times 10^{-2}$ for $Re_p = 1,910$ and $Re_b =$ (a) 1,910, (b) 3,183, (c) 5,092, (d) 6,365, and (e) 9,548.

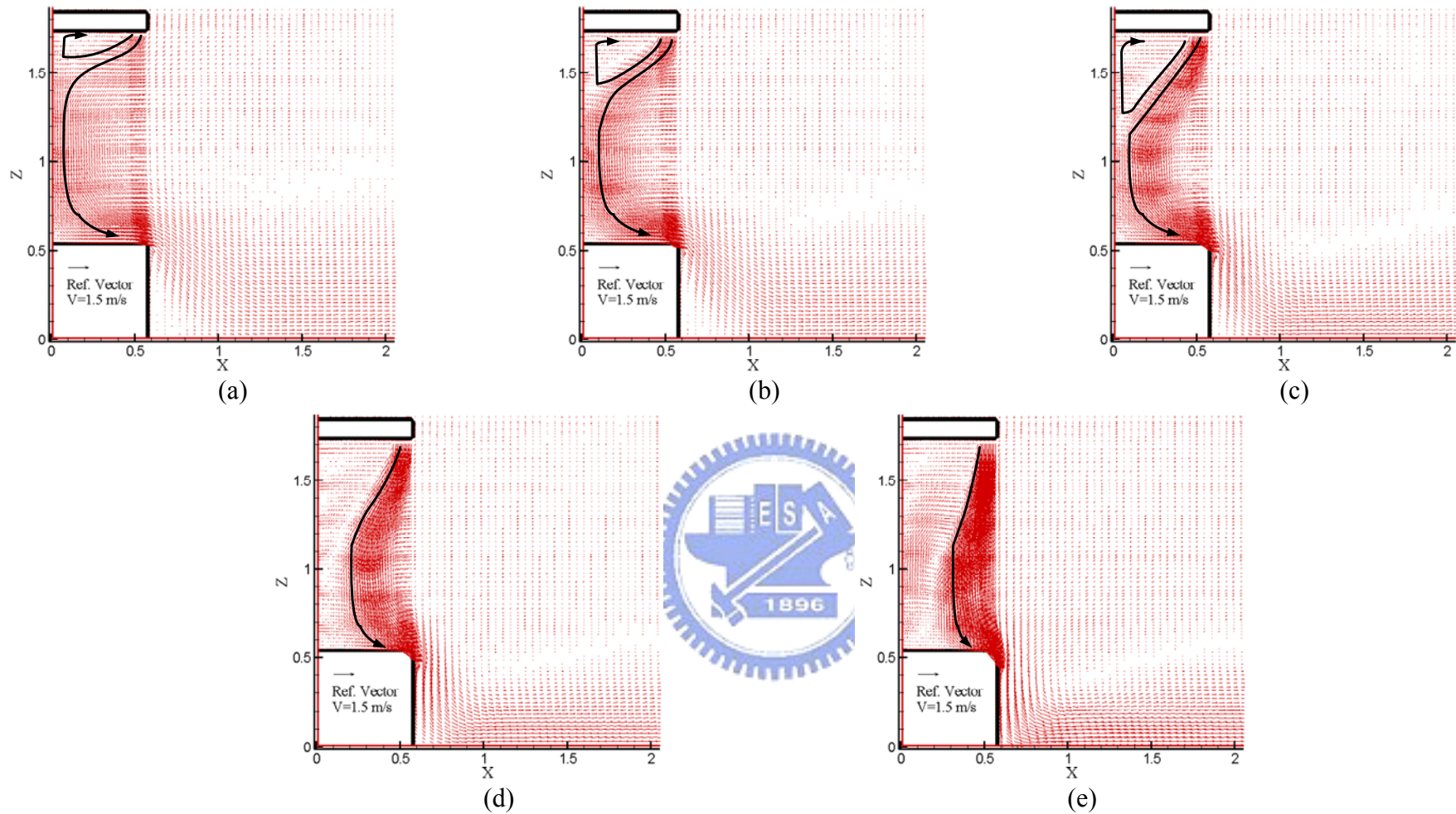


Fig. 4.143 Velocity vector maps for steady cavity flow for a single air curtain design with perforation density of 25% for $b_j = 0.1$ m, $Gr_t = 4.61 \times 10^9$ ($\Delta T = 20^\circ\text{C}$), and $N = 6.37 \times 10^{-2}$ for $Re_p = 3,183$ and $Re_b =$ (a) 1,910, (b) 3,183, (c) 5,092, (d) 6,365, and (e) 9,548.

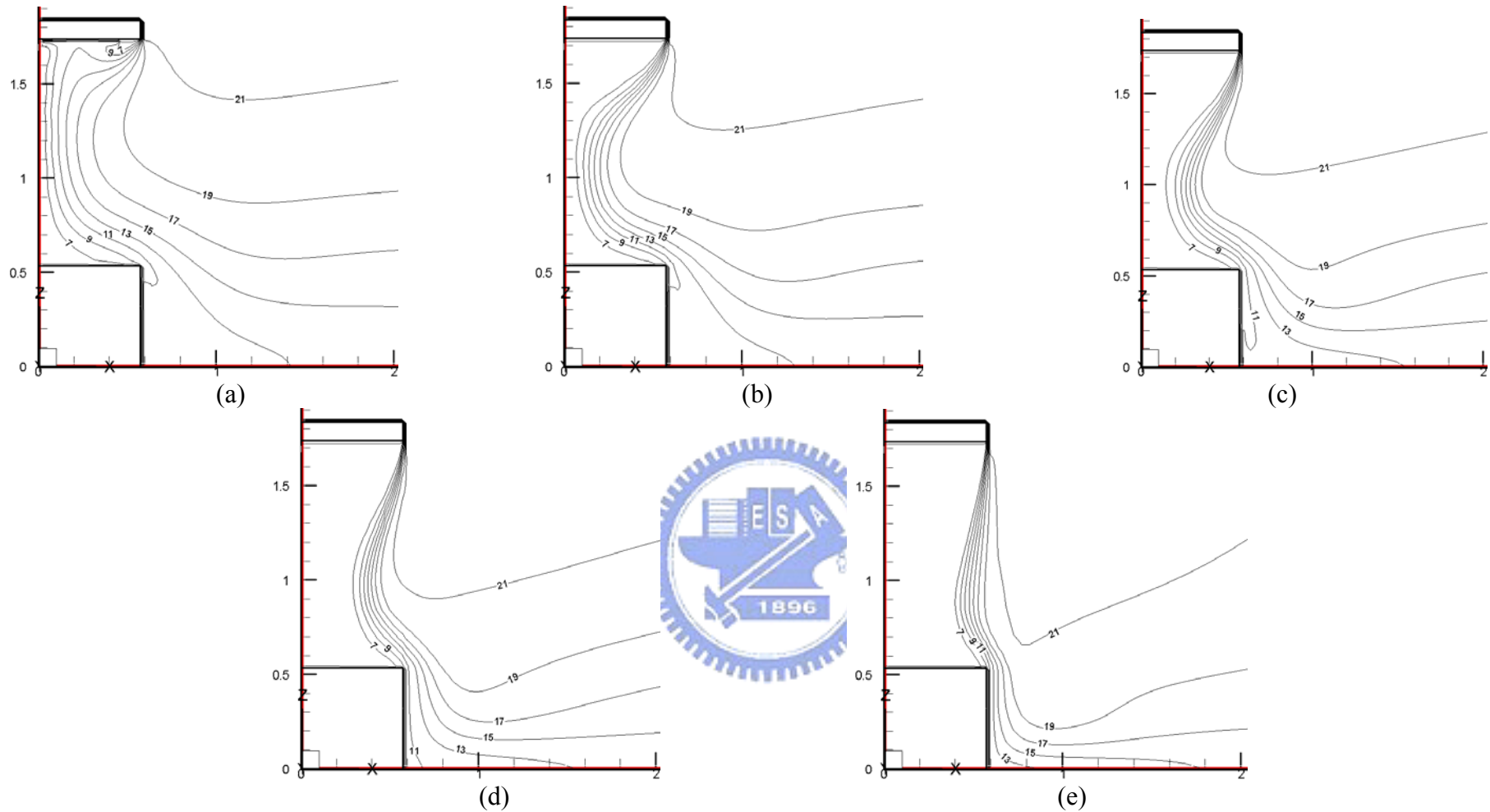


Fig. 4.144 Isotherms for steady cavity flow for a single air curtain design with perforation density of 25% for $b_j = 0.1$ m, $Gr_t = 4.61 \times 10^9$ ($\Delta T = 20^\circ\text{C}$), and $N = 6.37 \times 10^{-2}$ for $Re_p = 3,183$ and $Re_b =$ (a) 1,910 (b) 3,183, (c) 5,092, (d) 6,365, and (e) 9,548.

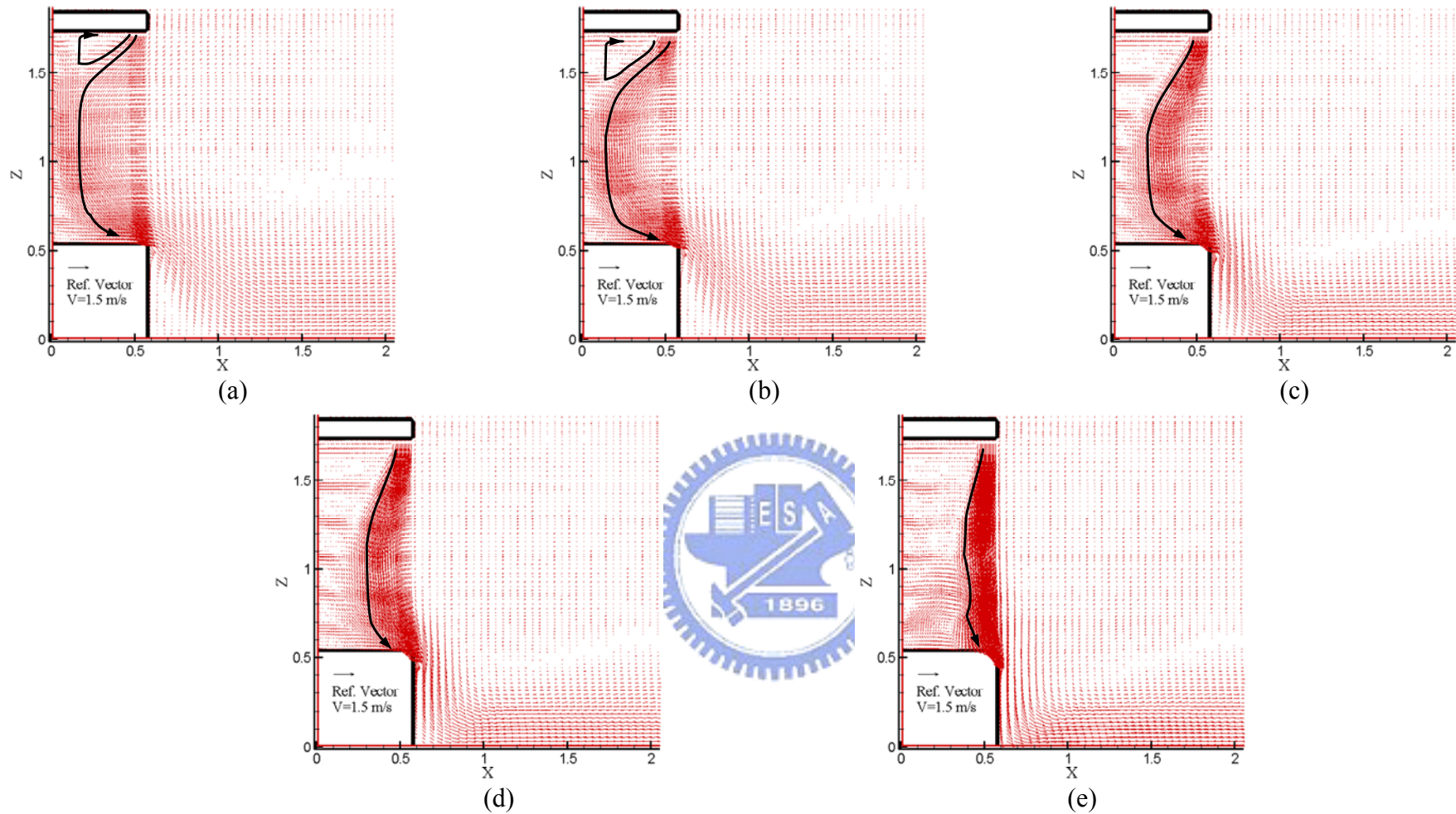


Fig. 4.146 Velocity vector maps for steady cavity flow for a single air curtain design with perforation density of 25% for $b_j = 0.1$ m, $Gr_t = 4.61 \times 10^9$ ($\Delta T = 20^\circ\text{C}$), and $N = 6.37 \times 10^{-2}$ for $Re_p = 5,092$ and $Re_b =$ (a) 1,910, (b) 3,183, (c) 5,092, (d) 6,365, and (e) 9,548.

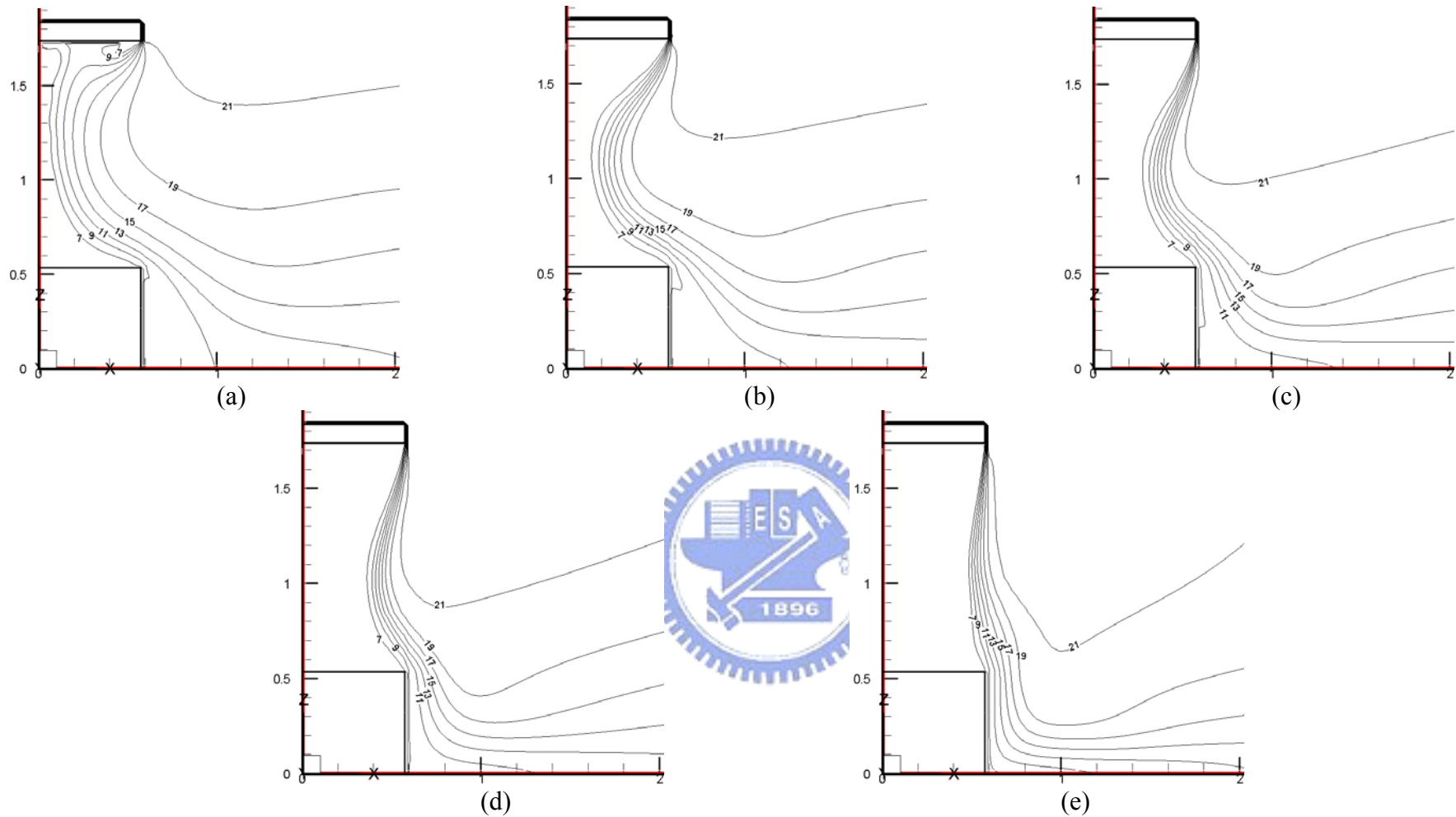


Fig. 4.147 Isotherms for steady cavity flow for a single air curtain design with perforation density of 25% for $b_j = 0.1$ m, $Gr_t = 4.61 \times 10^9$ ($\Delta T = 20^\circ\text{C}$), and $N = 6.37 \times 10^{-2}$ for $Re_p = 5,092$ and $Re_b =$ (a) 1,910 (b) 3,183, (c) 5,092, (d) 6,365, and (e) 9,548.

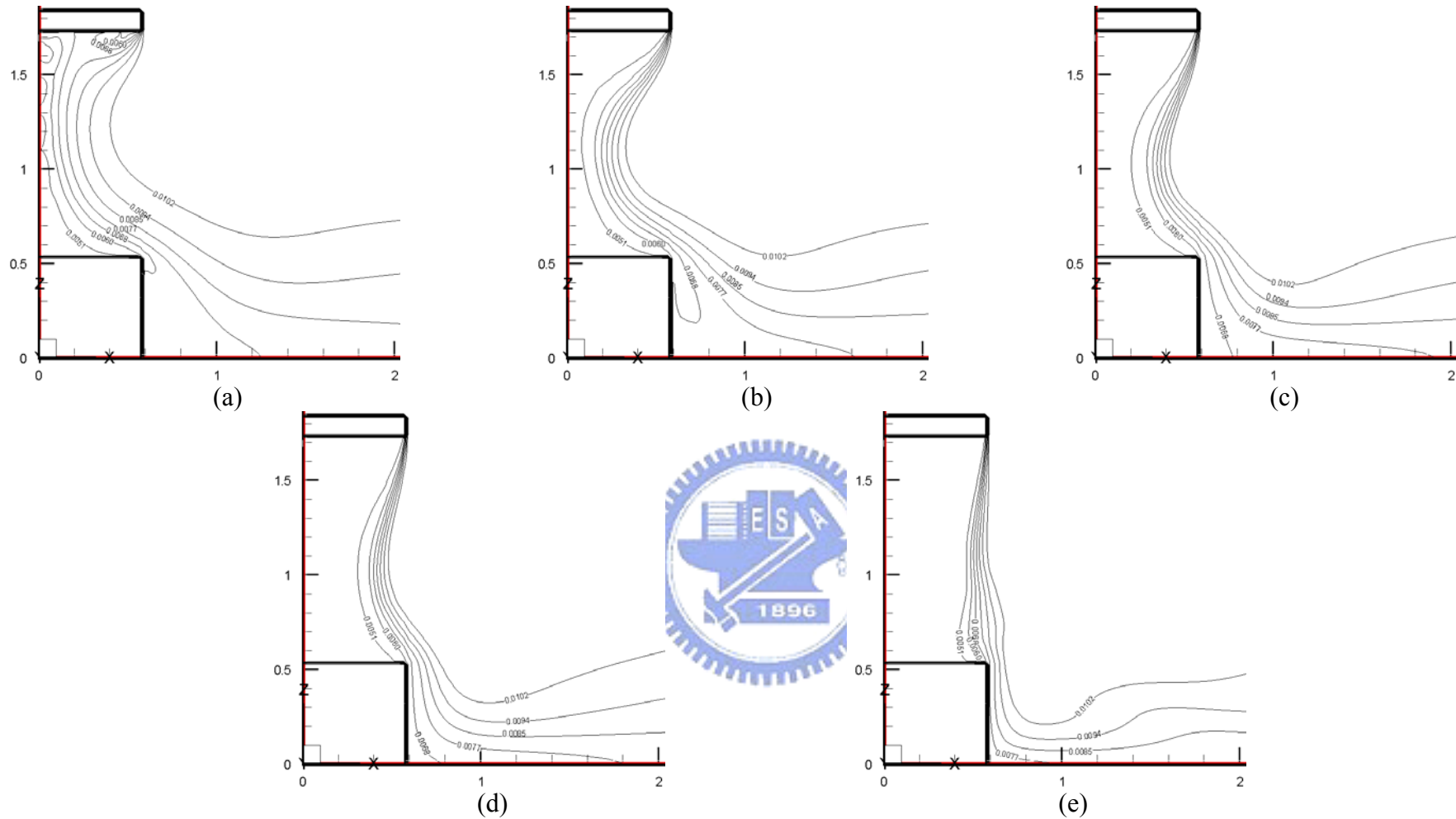


Fig. 4.148 Iso-concentration lines for steady cavity flow for a single air curtain design with perforation density of 25% for $b_j = 0.1$ m, $Gr_t = 4.61 \times 10^9$ ($\Delta T = 20^\circ\text{C}$), and $N = 6.37 \times 10^{-2}$ for $Re_p = 5,092$ and $Re_b =$ (a) 1,910, (b) 3,183, (c) 5,092, (d) 6,365, and (e) 9,548.

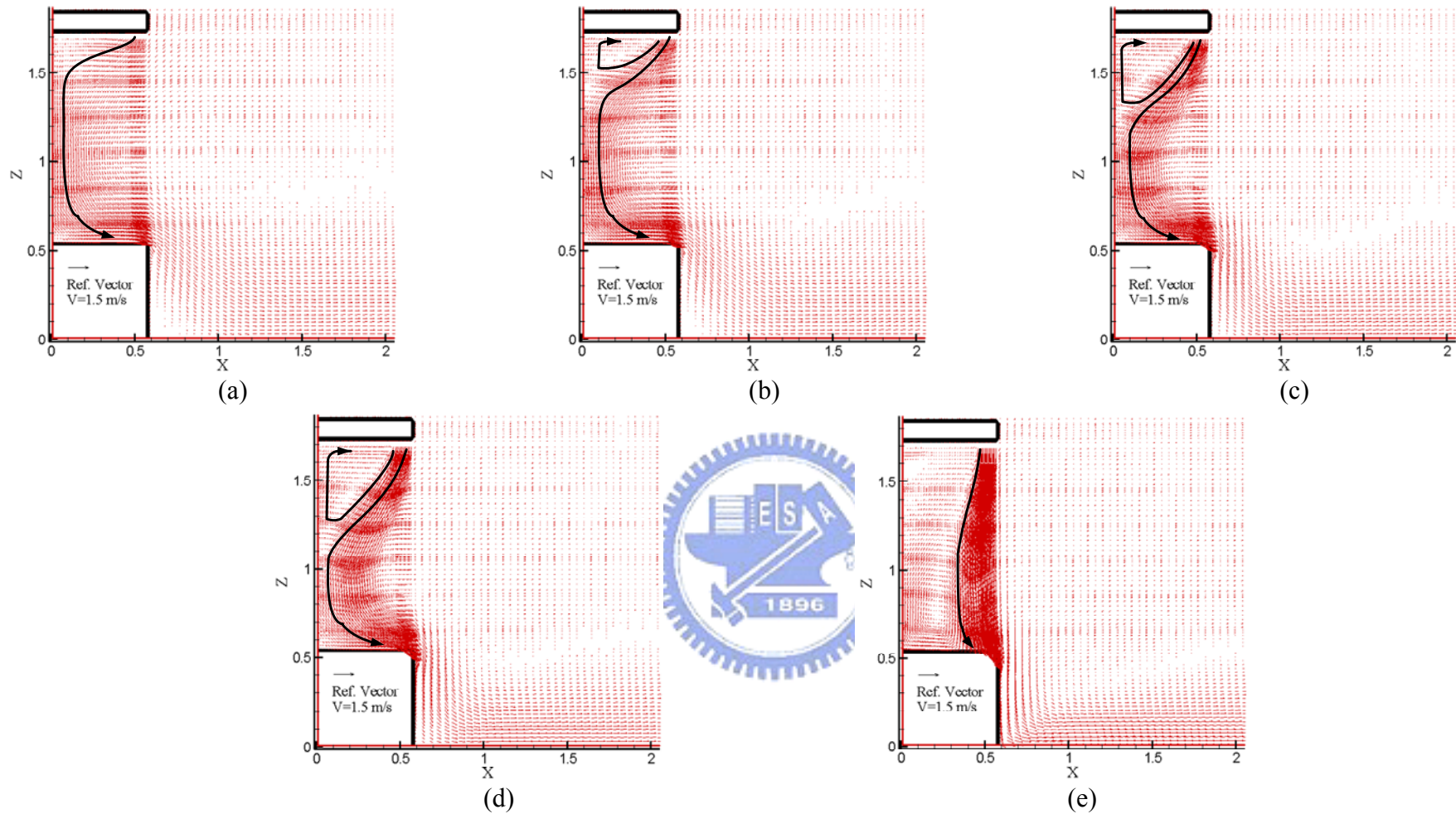


Fig. 4.149 Velocity vector maps for steady cavity flow for a single air curtain design with perforation density of 15% for $b_j = 0.1$ m, $Gr_t = 4.61 \times 10^9$ ($\Delta T = 20^\circ\text{C}$), and $N = 6.37 \times 10^{-2}$ for $Re_p = 1,910$ and $Re_b =$ (a) 1,910, (b) 3,183, (c) 5,092, (d) 6,365, and (e) 9,548.

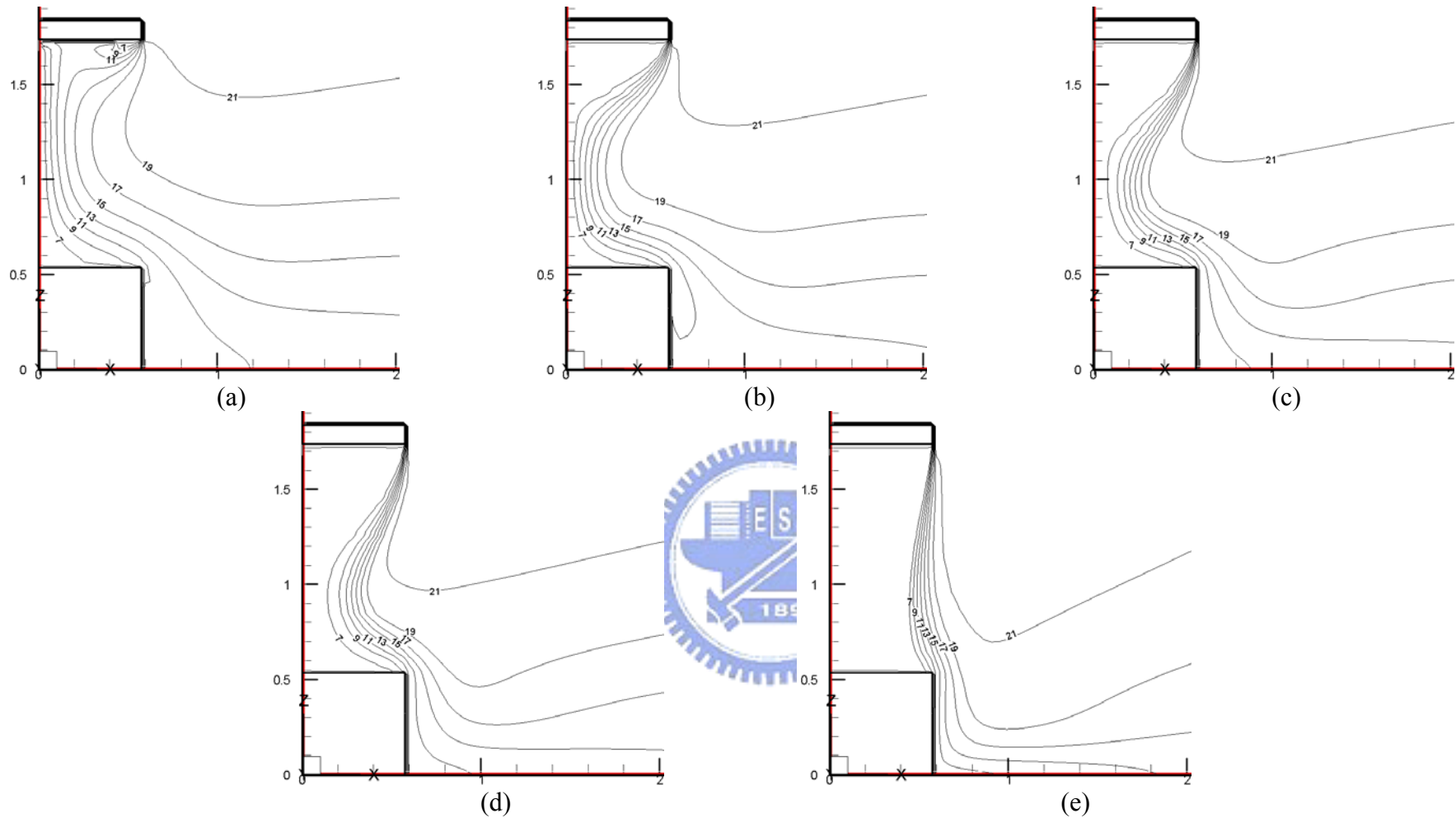


Fig. 4.150 Isotherms for steady cavity flow for a single air curtain design with perforation density of 15% for $b_j = 0.1$ m, $Gr_t = 4.61 \times 10^9$ ($\Delta T = 20^\circ\text{C}$), and $N = 6.37 \times 10^{-2}$ for $Re_p = 1,910$ and $Re_b =$ (a) 1,910, (b) 3,183, (c) 5,092, (d) 6,365, and (e) 9,548.

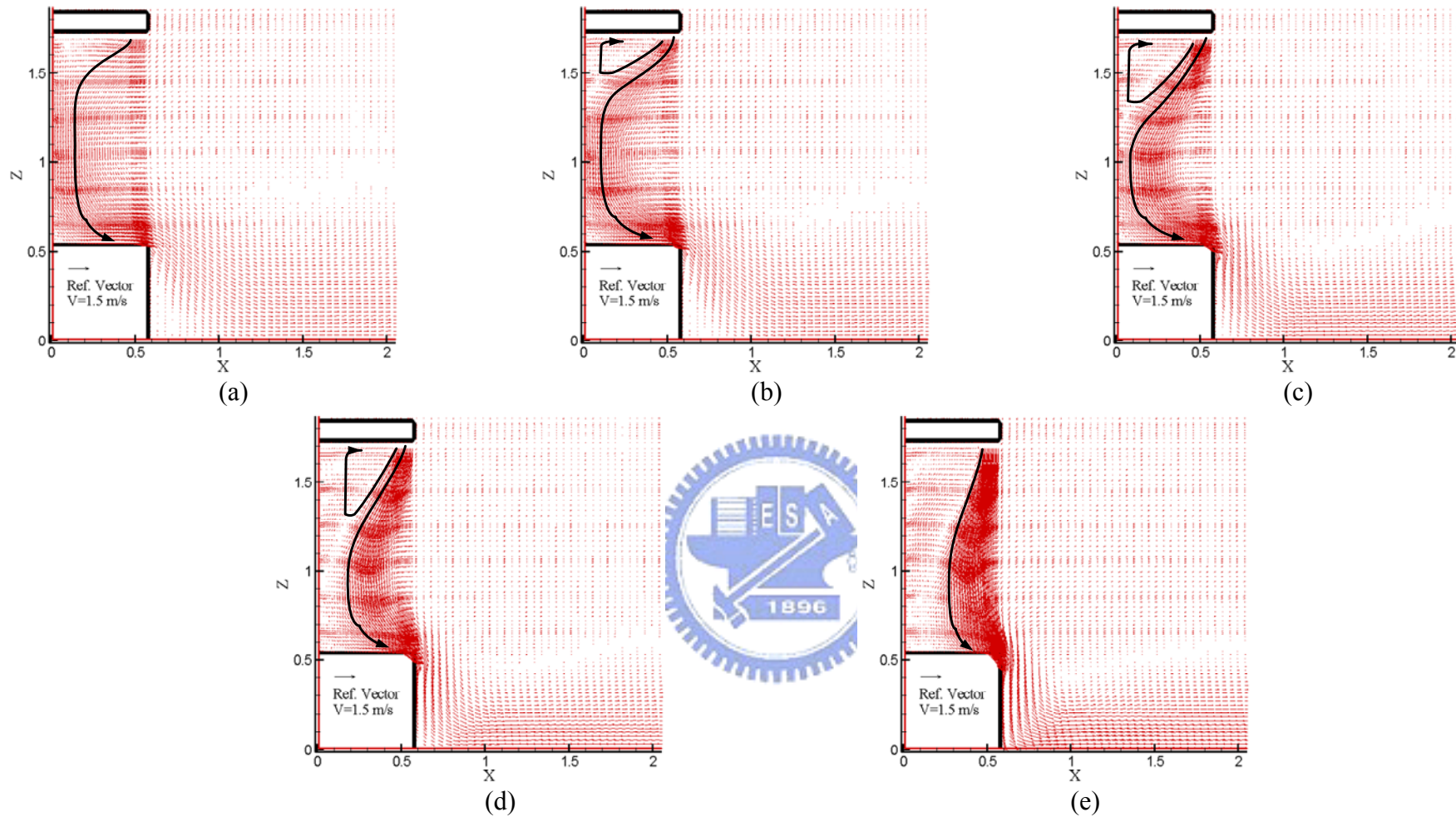


Fig. 4.152 Velocity vector maps for steady cavity flow for a single air curtain design with perforation density of 15% for $b_j = 0.1$ m, $Gr_t = 4.61 \times 10^9$ ($\Delta T = 20^\circ\text{C}$), and $N = 6.37 \times 10^{-2}$ for $Re_p = 3,183$ and $Re_b =$ (a) 1,910, (b) 3,183, (c) 5,092, (d) 6,365, and (e) 9,548.

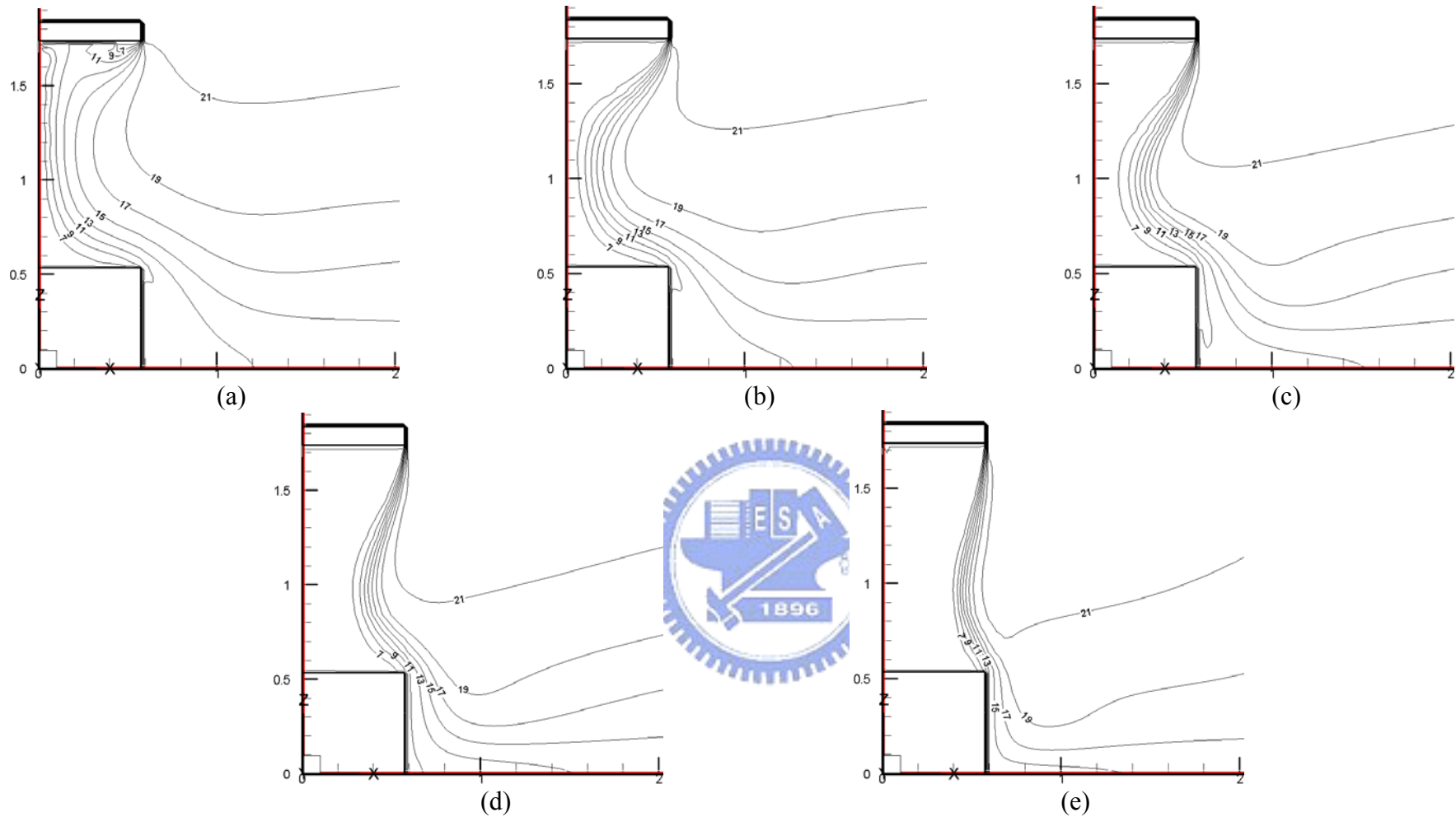


Fig. 4.153 Isotherms for steady cavity flow for a single air curtain design with perforation density of 15% for $b_j = 0.1$ m, $Gr_t = 4.61 \times 10^9$ ($\Delta T = 20^\circ\text{C}$), and $N = 6.37 \times 10^{-2}$ for $Re_p = 3,183$ and $Re_b =$ (a) 1,910 (b) 3,183, (c) 5,092, (d) 6,365, and (e) 9,548.

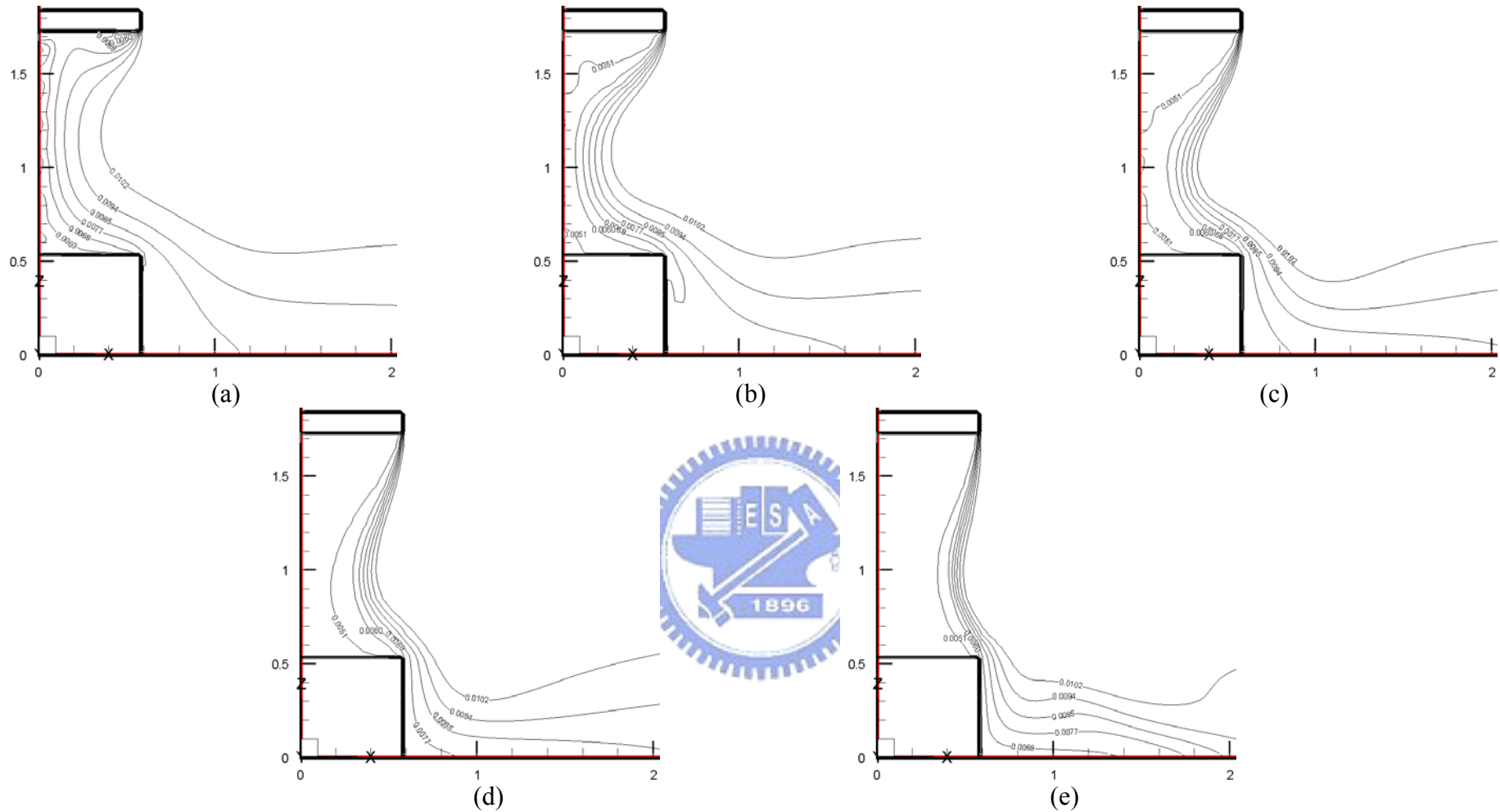


Fig. 4.154 Iso-concentration lines for steady cavity flow for a single air curtain design with perforation density of 15% for $b_j = 0.1$ m, $Gr_t = 4.61 \times 10^9$ ($\Delta T = 20^\circ C$), and $N = 6.37 \times 10^{-2}$ for $Re_p = 3,183$ and $Re_b =$ (a) 1,910, (b) 3,183, (c) 5,092, (d) 6,365, and (e) 9,548.

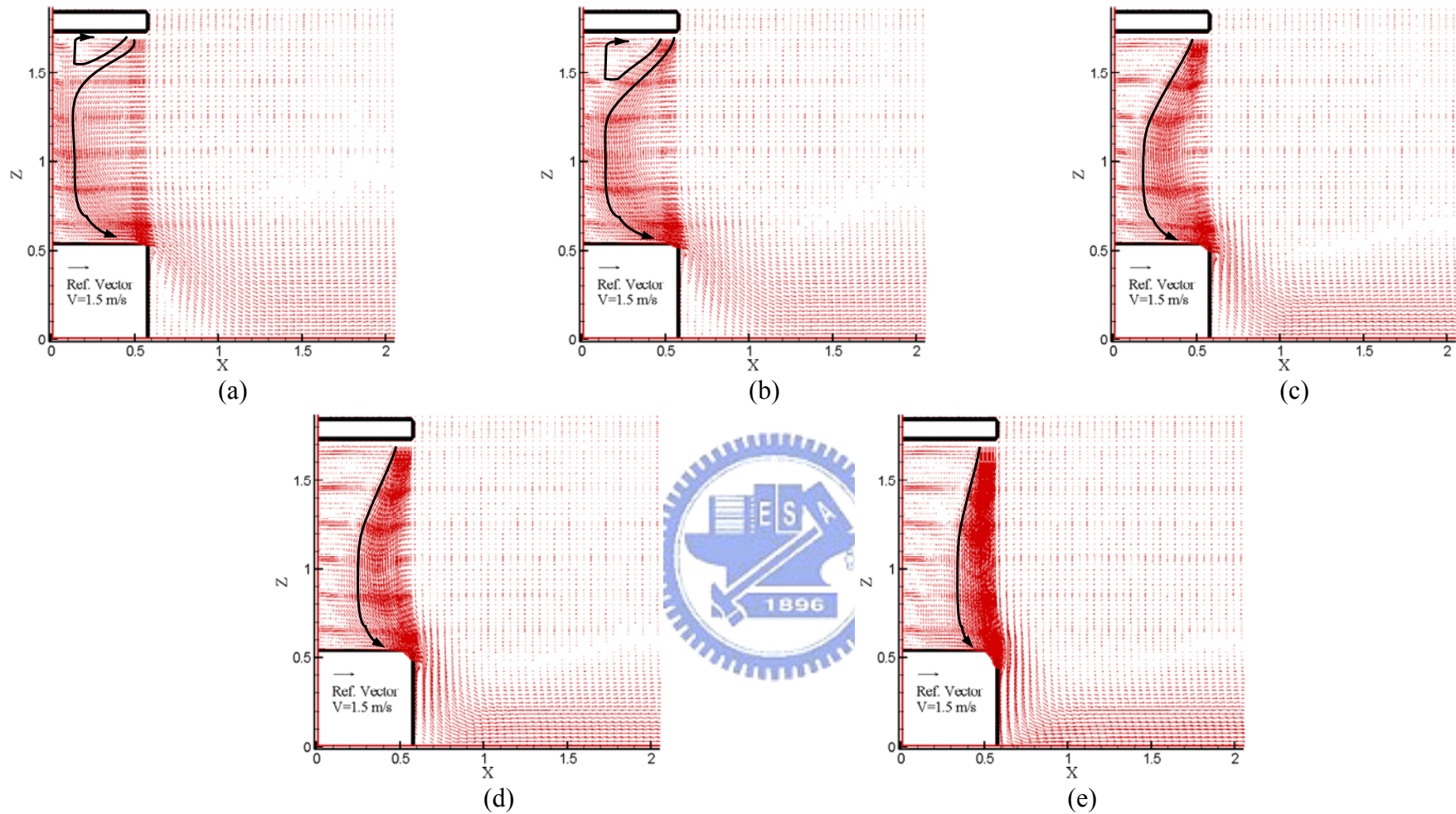


Fig. 4.155 Velocity vector maps for steady cavity flow for a single air curtain design with perforation density of 15% for $b_j = 0.1$ m, $Gr_t = 4.61 \times 10^9$ ($\Delta T = 20^\circ\text{C}$), and $N = 6.37 \times 10^{-2}$ for $Re_p = 5,092$ and $Re_b =$ (a) 1,910, (b) 3,183, (c) 5,092, (d) 6,365, and (e) 9,548.

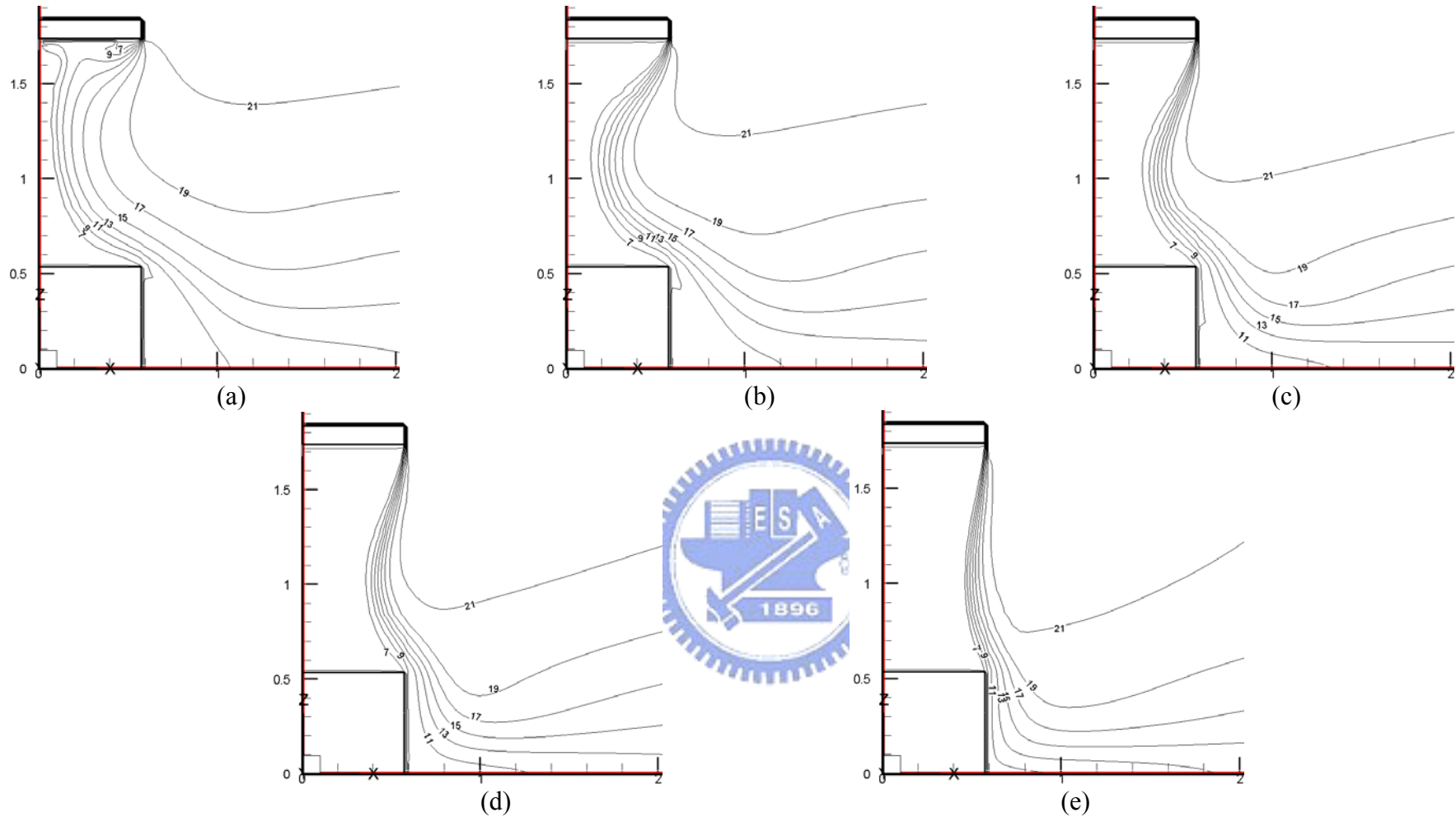


Fig. 4.156 Isotherms for steady cavity flow for a single air curtain design with perforation density of 15% for $b_j = 0.1$ m, $Gr_t = 4.61 \times 10^9$ ($\Delta T = 20^\circ\text{C}$), and $N = 6.37 \times 10^{-2}$ for $Re_p = 5,092$ and $Re_b =$ (a) 1,910 (b) 3,183, (c) 5,092, (d) 6,365, and (e) 9,548.

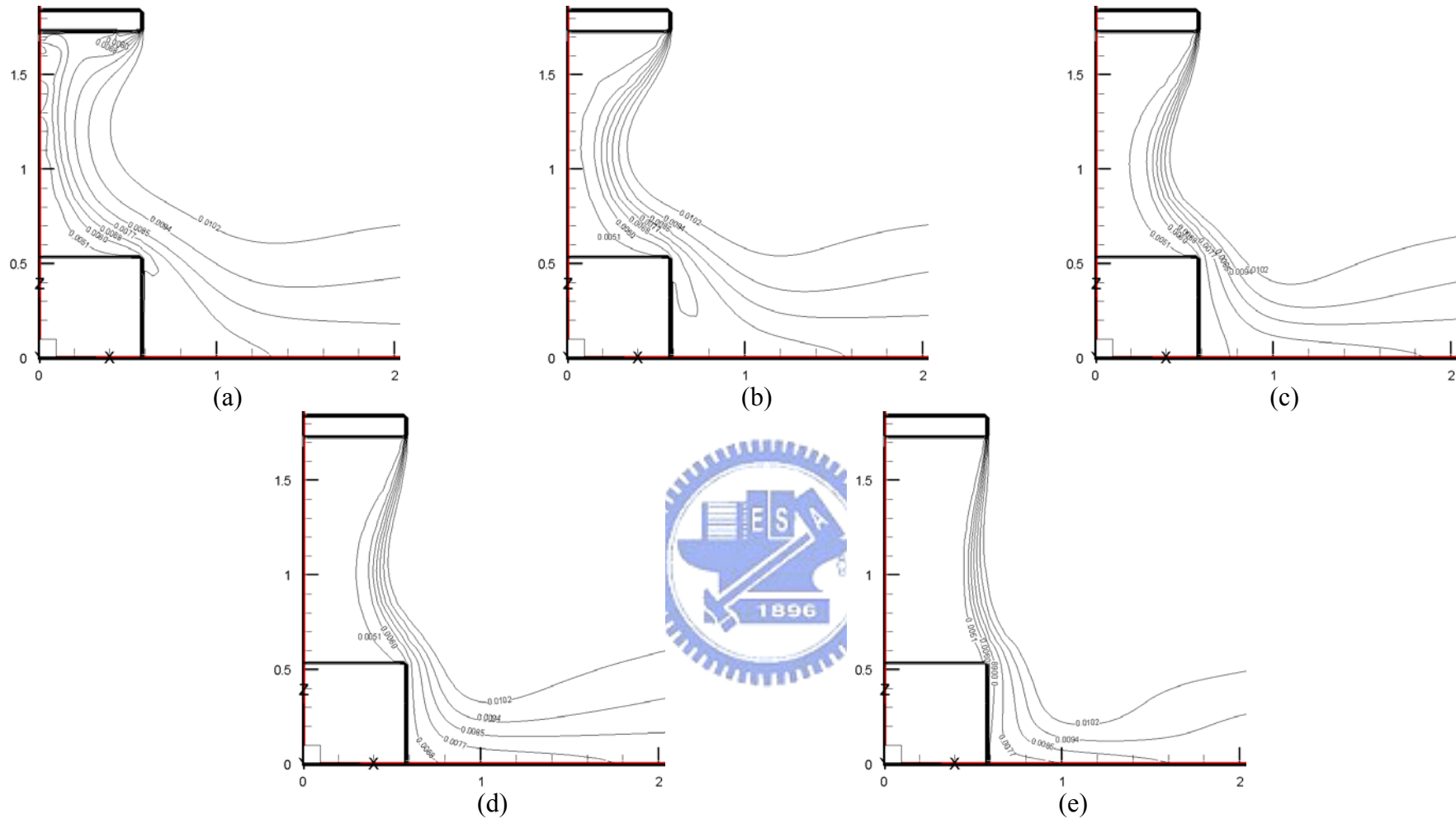


Fig. 4.157 Iso-concentration lines for steady cavity flow for a single air curtain design with perforation density of 15% for $b_j = 0.1$ m, $Gr_t = 4.61 \times 10^9$ ($\Delta T = 20^\circ\text{C}$), and $N = 6.37 \times 10^{-2}$ for $Re_p = 5,092$ and $Re_b =$ (a) 1,910, (b) 3,183, (c) 5,092, (d) 6,365, and (e) 9,548.

CHAPTER 5

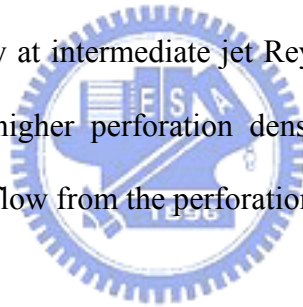
CONCLUDING REMARKS

In the present study a numerical simulation has been carried out to explore the transport processes in a vertical open refrigerated display cabinet including the momentum, heat and mass transfer effects. Computations were performed for the jet speed at the air discharge grille varying from 0.25 to 3.0 m/s and injection slot width ranging from 0.05 to 0.12 m for fixed air discharge-to-return grille separation distance of 1.20 m, cabinet depth of 0.57 m, and air discharge- ambient temperature difference of 20 °C corresponding to $T_j = 5^\circ\text{C}$ and $T_{\text{amb}} = 25^\circ\text{C}$. The relative humidities at the air discharge and ambient are respectively fixed at 90% and 60%. Effects of the jet speed at the air discharge grille, slot width of the discharge jet, buoyancy-to-inertia ratios, and inclined angle of the discharge jet on the flow, thermal and solutal characteristics in the display cabinet were examined in detail. Moreover, the cabinet flow affected by the arrangement of a double-air curtain design and by the back panel perforation is inspected. The major results obtained here can be summarized as follows.

- (1). In the absence of the buoyancy effects the flow in the cabinet is in the form of a single large flow recirculation driven by the entrainment of the air curtain.
- (2). For the buoyancy-to-inertia ratios (Richardson numbers) exceeding certain levels, the bending of the air curtain toward the cabinet core and the intrusion of the warm moist air into the cabinet occur. The air curtain bending and the warm air intrusion become more prominent at higher Richardson numbers and there are two flow recirculations induced in the cabinet.
- (3). A reduction in the width of the injection slot causes a decrease in the Richardson numbers for a fixed Reynolds number, which then results in a milder air curtain

bending and warm air intrusion.

- (4). Inclining the air curtain at the discharge grille slightly toward the ambient can reduce the air curtain bending and warm air intrusion.
- (5). In a double air curtain design the air curtain bending and warm air intrusion can be improved by a larger inner jet width and a smaller outer jet width at the discharge grille for a fixed total width of two jets. However, the relative magnitudes of the inner and outer jet Reynolds numbers produce nonmonotonic influences on the performance of the cabinet. Besides, inclining the outer air jet toward the ambient can delay the air curtain bending and reduce the warm air intrusion into the cabinet.
- (6). The air flow from the back panel perforation can improve the performance of the display cabinet especially at intermediate jet Reynolds numbers. The effects are more pronounced at a higher perforation density of the panel and a higher Reynolds number of the flow from the perforation.



REFERENCES

- [1] G. Cortella, M. Manzan, and G. Comini, CFD simulation of refrigerated display cabinets, *International Journal of Refrigeration* 24 (2001) 250-260
- [2] H. K. Navaz, R. Faramarzi, M. Gharib, D. Dabiri, and D. Modarress, The application of advanced methods in analyzing the performance of the air curtain in a refrigerated display case, *ASME Journal of Fluid Engineering* 124 (2002) 756-764
- [3] H. K. Navaz, B. S. Henderson, R. Faramarzi, A. Pourmovahed, and F. Taugwalder, Jet entrainment rate in air curtain of open refrigerated display cases, *International Journal of Refrigeration* 28 (2005) 267-275
- [4] Y.G. Chen and X. L. Yuan, Experimental study of the performance of single-band air curtain for a multi-deck refrigerated display cabinet, *Journal of Food Engineering* 69 (2005) 261-267
- [5] Y. T. Ge and S. A. Tassou, Simulation of the performance of single jet air curtains for vertical refrigerated display cabinets, *Applied Thermal Engineering* 21 (2001) 201-219
- [6] G. Cortella, CFD-aided retail cabinets design, *Computers and electronics in agriculture* 34 (2002) 43-66
- [7] R. Faramarzi, Efficient display case refrigeration, *ASHRAE Journal* 41(11) (1999) 46-54
- [8] R. Faramarzi and M. Woodworth, Colder temperatures in Display Cases, *ASHRAE Journal* 39(12) (1997) 35-39
- [9] R. Faramarzi and M. Woodworth, The case of the cool case, *Engineered System* 15(5) (1998) 72-77
- [10] Y.G. Chen and X. L. Yuan, Simulation of a cavity insulated by a vertical single

- band cold air curtain, *Energy conversion & Management* 46 (2005) 1745-1756
- [11] P. Bhattacharjee and E. Loth, Entrainment by a refrigerated air curtain down a wall, *ASME Journal of Fluid Engineering* 126 (2004) 871-879
- [12] R. Faramarzi and K. Kemp, Comparing Older and Newer refrigerated display cases, *ASHRAE Journal* 41(8) (1999) 45-49
- [13] R. H. Howell, N. Q. Van, and C. E. Smith, Heat and moisture transfer through turbulent recirculated plane air curtains, *ASHRAE Transactions* 82(1) (1976) 191-205
- [14] R. H. Howell, Effects of store relative humidity on refrigerated display case performance, *ASHRAE Transactions* 99 (1993) 667-678
- [15] R. H. Howell and M. Shibata, Optimum heat transfer through turbulent recirculated plan air curtain, *ASHRAE Transactions* 89 (1980) 188-200
- [16] J. Cui and S. Wang, Application of CFD in evaluation and energy-efficient design of air curtains for horizontal refrigerated display cases, *International Journal of Thermal Sciences* 43 (2004) 993-1002
- [17] M. Axell and P. Fahlen, Design criteria for energy efficient vertical air curtains in display cabinets, 21th International Congress of Refrigeration 2003, Washington, D.C., ICR0284
- [18] N. Q. Van, and R. H. Howell, Influence of initial turbulence intensity on the development of plane air-curtain jets, *ASHRAE Transactions* 82(1) (1976) 208-228
- [19] S. Besbes, H. Mhiri, S. E. Golli, G. L. Palec, and P. Bournot, Numerical study of a heated cavity insulated by a horizontal laminar jet, *Energy Conversion & Management* 42 (2001) 1417-1435
- [20] R. I. Loerke and H. M. Nagib, Control of free stream turbulence by means of

honeycomb: A balance between suppression and generation, ASME Journal of Fluid Engineering 98(1) (1976) 342-353

- [21] Y. Wu, G. Xie, Z. Chen, L. Niu, and D. Sun., An investigation on flowing patterns of the airflow and its characteristics of heat and mass transfer in an island open display cabinet with goods, Applied Thermal Engineering 24 (2004) 1945-1957
- [22] H. Mhiri, S.E. Golli, A. Berthon, G. L. Palec, and P. Bournot, Numerical study of the thermal and aerodynamic insulation of a cavity with a vertical downstream air jet, International Communications in Heat and Mass Transfer 25 (1998) 919-928
- [23] B. E. Launder and D. B. Spalding, The numerical computation of turbulent flows, Comput. Methods Appl. Mech. Eng. 1974(3) 269-289
- [24] S. V. Patankar and D. B. Spalding, A calculation procedure for heat, mass and momentum transfer in three-dimensional parabolic flow, International Journal of Heat and Mass Transfer 15 (1972) 1787-1806
- [25] Concentration Heat and Momentum Limited, PHOENICS 3.5, Bakery House (2003)
- [26] W. T. Lai, Natural heat and mass transfer in a rectangular enclosure, Ph.D. thesis, University of Minnesota, 1989